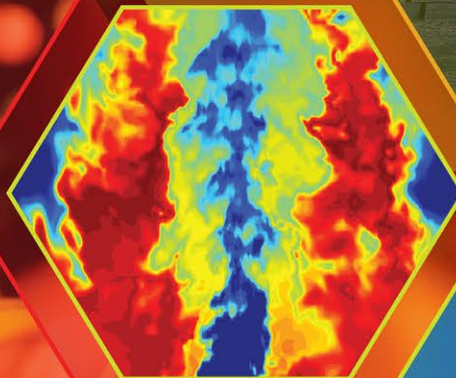


TNF2016

THIRTEENTH INTERNATIONAL
WORKSHOP ON MEASUREMENT
& COMPUTATION OF
TURBULENT FLAMES

JULY 28-30 | SEOUL, KOREA



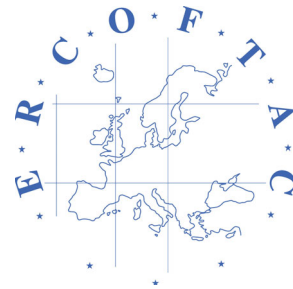
blank

JULY 28-30 | SEOUL, KOREA

TNF2016

THIRTEENTH INTERNATIONAL
WORKSHOP ON MEASUREMENT &
COMPUTATION OF TURBULENT FLAMES

SPONSORS



TECHNISCHE
UNIVERSITÄT
DARMSTADT



SFB/Transregio 150
Turbulente, chemisch reagierende
Mehrphasenströmungen in Wandnähe

TNF13 Workshop Proceedings – Table of Contents

Summary	6
List of Participants	14
Agenda	18
Update on Stratified Flames	
<i>Andreas Kempf and Fabian Proch</i>	
Summary	20
Presentation Slides – TUD Flames	21
Presentation Slides – Cambridge Flames.....	34
Sydney Piloted Flame Comparisons	
<i>Benoît Fiorina</i>	
Summary	50
Presentation Slides	52
Influence of Pilot Parameters	
<i>Thibault F. Guiberti</i>	
Summary	96
Presentation Slides	97
Progress Variable and Regime indicators	
<i>Robert Barlow, Christian Hasse, Matthias Ihme</i>	
Summary	106
Presentation Slides – Progress Variable for Experiments.....	109
Presentation Slides – Regime Identification and Characterization	122
Presentation Slides – Progress Variable and Combustion Regime.....	134
Piloted DME Jet Flames	
<i>Andreas Kronenburg</i>	
Summary	150
Presentation Slides	151
Turbulent Counterflow Flames	
<i>Jonathan Frank, Steve Pope, Peter Lindstedt</i>	
Summary	178
Presentation Slides	180

TNF13 Workshop Proceedings – Table of Contents

Flame-Wall Interaction

Andreas Dreizler and Johannes Janicka

Summary	214
Presentation Slides – Experiments	218
Presentation Slides – Simulations.....	246

New Burners and Flames

Wolfgang Meier

Summary	272
Presentation Slides	273

Experiments and Simulations at Elevated Pressure

William Roberts, Hong Im, Gaetano Magnotti, Joe Oefelein, Jonathan Frank

Summary	284
Presentation Slides – KAUST Experiments.....	285
Presentation Slides – KAUST Simulations	302
Presentation Slides – Sandia	310

Key Challenges and Priorities

Johannes Janicka

Presentation Slides	324
---------------------------	-----

Poster Abstracts

List of Poster Titles and Authors	330
Two-Page Poster Abstracts	334

SUMMARY

Thirteenth Workshop on Measurement and Computation of Turbulent Flames (TNF13)

July 28-30, Seoul, Korea

R. Barlow, A. Dreizler, B. Fiorina, J. Frank, C. Hasse,
M. Ihme, H. Im, J. Janicka, A. Kempf, A. Kronenburg,
A. Masri, W. Meier, J. Oefelein, F. Proch, W. Roberts

INTRODUCTION

The TNF Workshop series was initiated in 1996 to address validation of RANS based models for turbulent nonpremixed flames and partially-premixed flames where combustion occurs mainly in a diffusion flame mode. The emphasis has been on fundamental issues of turbulence-chemistry interactions in flames that are relatively simple in terms of both geometry and chemistry. Although the TNF acronym has been retained, the word *nonpremixed* has been dropped from the title, and our scope has expanded (since TNF9 Montreal, 2008) to address three challenges:

- Development and validation of modeling approaches which are accurate over a broad range of combustion modes and regimes (nonpremixed, partially-premixed, stratified, and fully premixed).
- Extension of quantitative validation work to include more complex fuels (beyond CH₄) and fuel mixtures that are of practical interest.
- Establishment of a more complete framework for verification and validation of combustion LES, including quality assessment of calculations, as well as development of approaches for quantitative comparisons of multidimensional and time-resolved data from experiments and simulations.

Our overall goal is to accelerate the development of advanced combustion models that are soundly based in fundamental science, rigorously tested against experiments, and capable of predicting flame behavior over a wide range of conditions. One of the most useful functions of this workshop series has been to provide a framework for collaborative comparisons of measured and modeled results. Such comparisons are most informative when multiple modeling approaches are represented and when there has been early communication and cooperation regarding how the calculations should be carried out and what results should be compared. Experience has shown that comparisons on new target flames can generate significant new insights, but also many new questions. These questions motivate further research, both computational and experimental, and subsequent rounds of model comparisons. Another important function of the workshop series is to provide overviews of new work on established target cases, as well as new burner configurations and emerging topics that are relevant to our overall goals and may attract a critical mass of people interested in collaboratively investigating the new burner or research topic.

Previous workshops were held in Naples, Italy (1996), Heppenheim, Germany (1997), Boulder, Colorado (1998), Darmstadt, Germany (1999), Delft, The Netherlands (2000), Sapporo, Japan (2002), Chicago, Illinois (2004), Heidelberg, Germany (2006), Montreal, Canada (2008), Beijing, China (2010), Darmstadt, Germany (2012), and Pleasanton, California (2014). Proceedings and summaries of all the workshops are available at <http://www.sandia.gov/TNF>.

TNF12 was attended by 101 researchers from 13 countries. The main sessions topics were:

- Update on Stratified Flames
- Sydney Partially-Premixed Jet Flame Comparisons
- Progress Variable and Regime Indicators in Partially-Premixed Flames
- Update on DME Flames
- Counterflow Flames
- Flame-Wall Interaction
- New Burners and Flames
- Experiments and Simulations at Elevated Pressure

The complete TNF13 Proceedings are available for download in pdf format from www.sandia.gov/TNF. The pdf file includes the list of participants, workshop agenda, summary abstracts of technical sessions, presentation slides, and two-page abstracts of the 41 contributed posters.

The sections that follow briefly outline the presentations and key points of discussion. Comments and conclusions given here are based on the perspectives of the authors and do not necessarily represent consensus opinions of the workshop participants. This summary does not attempt to address all topics discussed at the workshop or to define all the terms, acronyms, or references. Readers are encouraged to consult the complete TNF13 Proceedings and also the Proceedings of previous TNF Workshops, because each workshop builds upon what has been done before.

PLANNING

The 2018 TNF Workshop will be held in Dublin, Ireland prior to the 37th Combustion Symposium. It is likely that the schedules of the TNF, ISF, and PTF Workshops will overlap on July 27-28, 2018 (Friday and Saturday). The respective organizers are coordinating on venue and agendas to minimize conflicts and complications for the participants.

Key challenges and research priorities to be addressed before TNF14 are outlined at the end of this summary. Early coordination to select target cases, define ground rules for model comparisons, and establish priorities for collaborative experimental and computational work is strongly encouraged. Regular communication among members of the organizing committee and key contributors is also strongly encouraged. Suggestions for new topics should be communicated to the TNF Organizing Committee.

ACKNOWLEDGMENTS

The work of all the session coordinators and contributors is gratefully acknowledged. Sponsorship funds were provided by ANSYS, Continuum Lasers, Edgewave, ERCOFTAC, La Vision, Sirah Lasers, and TU Darmstadt through the SFB/Transregio 150 Project. These contributions allowed significant reduction of the registration fees for university faculty, postdocs, and students. Support for the TNF web site has been provided by the U. S. Department of Energy, Office of Basic Energy Sciences, Division of Chemical Sciences, Geosciences, and Biosciences. Sandia National Laboratories is a multi-mission laboratory managed and operated by Sandia Corporation, a wholly owned subsidiary of Lockheed Martin Corporation, for the U.S. Department of Energy's National Nuclear Security Administration under contract DE-AC04-94AL85000.

HIGHLIGHTS OF PRESENTATIONS AND DISCUSSIONS

Each section that follows was condensed from a session summary in the complete proceedings.

IMPORTANT NOTE ON USE OF THIS MATERIAL

Results in this and other TNF Workshop proceedings are contributed in the spirit of open scientific collaboration. Some results represent completed work, while others are from work in progress. Readers should keep this in mind when reviewing these materials.

It would be inappropriate to quote or reference specific results from these proceedings without first checking with the individual author(s) for permission and for the latest information on results and references.

Update on Stratified Flames

Coordinators: Andreas Kempf, Fabian Proch

This was the fourth TNF Workshop to consider stratified combustion as a focus topic. The objective of the session was an update on new simulation results and new experimental data for the stratified burners investigated at Darmstadt University and Cambridge University (with Sandia National Laboratories). Both are co-annular burners with relatively simple geometries, and both sets of experiments were designed to isolate effects of mixture stratification of on turbulent methane flame structure and provide test cases for combustion models. The session included an overview of the geometry and experimental conditions for these two burners, a review of previous comparisons, and results from new simulations completed since the comparisons at the 2014 workshop.

A broad conclusion regarding these flames is that good predictions are achieved by combustion models that treat the stratified flame as an ensemble of homogeneous premixed flames of different mixture fractions. This was not necessarily expected at the outset. The important conclusion that mildly stratified flames can be modeled as premixed flames was also supported by the recently published conditional analysis of the Cambridge flames. Although effects of stratification are present in the experimental results and can be isolated by multiple conditioning methods, the effects on overall scalar structure and flame propagation are minor.

Sydney Partially-Premixed Flame Comparisons

Coordinator: Benoît Fiorina

The objective of the session was to compare recent simulations of the Sydney piloted burner. The burner geometry consists of two concentric tubes surrounded by a pilot annulus. It is centered in a wind tunnel supplying a co-flowing air stream. A set of experimental data has been provided by Sydney University and Sandia. In the configuration studied in the workshop, the central tube is fed with fuel whereas air is flowing through the outer tube. The air co-flow velocity is fixed at 15 m/s. The central pipe can be recessed upstream of the burner exit plane, varying therefore the mixing between fuel and air. For sufficiently large recession distance (L_r) of the inner tube with respect to the burner exit plane, the mixture is nearly homogeneous at the burner exit, while intermediate recession distances lead to equivalence-ratio inhomogeneities. This experimental configuration, conducive to multiple flame structures, is extremely interesting for model validation. It is indeed representative of practical combustion chambers, which may exhibit strong equivalence ratio heterogeneities, promoting the development of mixed combustion regimes. The Sydney burner constitutes a challenging target for turbulent combustion models, which have in general their own flame affinity.

This session provided: 1) An overview of the burner configuration and flame features; 2) An overview of the modeling approaches and simulation parameters used by the different groups; 3) A discussion of specifications for the inflow boundary conditions, including information on pre-

calculated inflows from nonreacting LES by the Princeton group; 4) Comparison of measured and predicted mean and rms profiles of velocity and selected scalars; and 5) Preliminary observations regarding tendencies of different flamelet modeling approaches. Results from a comprehensive parametric experimental study of the effects of pilot flame parameters on the stability of piloted turbulent CNG and LPG jet flames on the Sydney inhomogeneous burner were also presented.

Except for the first radial profiles close to the burner exit, significant differences are observed between simulations and experiments. In particular, most of the computations do not capture the mixing between fuel and air, which makes the analysis of the combustion model difficult. A very large scattering is observed for CO, for which the production rate is very sensitive to the combustion regime. Analysis and conclusions have to be conducted with great care as most of numerical data are preliminary. This exercise is however very promising, mainly for two reasons. First, the configuration is challenging and should break the models, especially regarding the prediction of CO formation. Second, as many groups are involved in the comparison, results can be conditioned by the type of model. For instance, it is possible to verify if several simulations conducted with turbulent combustion model dedicated to premixed flames will draw similar conclusions.

To go further into the analysis, most of the numerical results have to be consolidated. In particular, an improvement of the mixture fraction field is mandatory prior analyzing the turbulent combustion model impact. Ideally, mesh independency studies for mixing and velocity under non-reactive conditions should be conducted. To limit differences between computational set-up, groups should use the same prescription of boundary conditions. Complimentary velocity and mixture fraction measurements on cold configurations would be, in this context, very useful.

Progress Variable and Regime Indicators in Partially Premixed Flames

Coordinators: Robert Barlow, Christian Hasse, Matthias Ihme

This session consisted of three parts, all related progress variable definitions, combustion regime indicators, and the connections between experiments and modeling on these topics. The first part considered alternative definitions of progress variable in the context of Raman/Rayleigh experiments in partially-premixed methane flames. Results on the joint statistics of progress variable and mixture fraction in the Sydney piloted jet flames were presented as examples of a possible additional basis for comparing measured and modeled result in the future.

The second part introduced a novel approach to extract information on the local combustion regime, chemical explosive mode, and heat release rate from 1D Raman/Rayleigh measurements. An important point is that this approach avoids the need to measure 3D gradients, which are used in most definitions of regime indicators in the computational literature.

The third part considered progress variable definitions in the context of modeling. The possibility to optimize a progress variable definition to maximize signal to noise ratio in results Raman/Rayleigh experiments was also introduced. Various combustion regime indicators from the literature were reviewed. A combustion model compliance indicator was introduced, with an example application of flamelet model assignment in LES of the Sydney piloted flame.

Update on DME Flames

Coordinator: Andreas Kronenburg

A series of piloted partially-premixed jet flames of dimethyl ether (25 volume percent DME in air) was introduced at TNF11 to extend experiment/model comparisons to more complex fuels than methane. This session reviewed the available experimental data on these flames and key points from modelling contributions at TNF12. Results from three new modeling contributions were presented, including RANS/multi-environment-PDF of flame DME-F, LES/PDF of flame DME-D, and LES/MMC of flames DME-D and DME-F. New measurements have now extended the parameter

range of the original flame series: DME flame G' has a reduced pilot velocity to increase localized extinction.

New auto-ignition DME experiments of the Sydney group are now available. The fuel jet consists of DME/air mixtures varying from pure DME to a DME-to-air ratio of 1:7. The jet is surrounded by a hot co-flow with temperatures ranging from 1200K to 1500K. The experimental campaign includes lift-off height graphs, simultaneous OH and CH₂O PLIF, temporal evolution and statistics of the flame base and ignition kernels, and simultaneous acoustic and chemiluminescence data. First RANS-PDF computations show strong dependencies on the chemical mechanism during ignition events.

Goals for TNF14 should comprise computations of the entire piloted jet flame series (Sandia DME D-G') with focus on the accurate prediction of the degree of localized extinction, in particular in flames G and potentially G'. We should also seek clarification of the predictions' dependencies on the chemical mechanisms. This may include the need for a quantitative comparison of formaldehyde as this is the measured species with the most pronounced differences for all flame and flow conditions.

Counterflow Flames

Coordinator: Jonathan Frank

The session on turbulent counterflow flames extended experimental and computational studies from TNF12 using the two burner designs from Yale University and Darmstadt/Imperial College. New work addressed several issues identified at TNF12. LES (Sandia) of internal flow dynamics in the Yale burner addressed the need for detailed treatment of boundary conditions. LES/PDF parametric studies (Cornell) of partially-premixed methane flames showed excellent agreement with experiments.

Influences of chemistry on combustion regime transitions were investigated (Imperial College) by varying the fuel (CH₄, DME, ETOH) and upper nozzle equivalence ratio (0.2-1.0). Fuel chemistry effects influenced the conditional velocity statistics, and the impact of fuel chemistry on fluid state probabilities indicated an approximate scaling with Da number. Simulations (Duisburg-Essen) of lean premixed CH₄ counterflow flames ($\Phi=0.8, 0.9$) in the reactant-vs-reactant configuration of the Darmstadt/Imperial College burner were extended from TNF12 using both LES/FDF calculations and moment methods.

Goals for TNF14 should include more contributors with different modeling approaches, testing models across different modes of combustion using the counterflow geometry, and using simulations of internal flow to specify boundary conditions at the nozzle exits. A comparison of the two existing internal flow simulations of the Yale burner geometry would be useful. Goals should also include more detailed analysis of conditional statistics using experiments and high-fidelity simulations that focus on the inter-nozzle region. This effort could include additional fuels and flame conditions and sufficiently long simulation times to study the temporal evolution of localized extinction and re-ignition.

Flame Wall Interaction

Coordinators: Andreas Dreizler, Johannes Janicka

Flame-wall interaction (FWI) has been identified as a highly relevant process. However, FWI has received comparatively little attention within the scientific community. Based on issues discussed at TNF12, the objective of the FWI-session at TNF13 was twofold: to introduce a new benchmark configuration that is available as a TNF target flame; and to show the progress made in simulating the physical processes associated with near-wall reactive flows and identify important shortcomings of modeling flame-wall interactions to steer future efforts.

The new target case is a side-wall quenching (SWQ) configuration. Recent measurements regarding the thermochemical state, reaction rates, and velocity boundary layers were presented. For the example of stoichiometric methane-air flames, by comparison with most recent DNS data, it could be shown that diffusion rather than low temperature reactions cause significant deviations within the thermochemical state compared to unbounded flames.

Simulations of FWI by several groups were presented, including works of SINTEF (Trondheim, A. Gruber), UMich (Michigan, V. Raman), EM2C (Paris, O. Gicquel), UniBW (Munich, M. Pfitzner) and TUD (Darmstadt, J. Janicka).

New Burners and Flames

Coordinator: Wolfgang Meier

Two burners were presented in this session: The first one was a dual swirl gas turbine model combustor for partially premixed flames that was developed by KIT and DLR within the collaborative research center SFB606. This dual swirl burner was operated with methane and air at thermal powers of typically 25 kW. Raman multispecies and temperature measurements as well as PIV velocity measurements have been performed for two cases: (1) A stable flame with $P_{th} = 22.5$ kW, $\phi = 0.63$ and air split ratio between outer and inner swirler of 1.6; (2) an oscillating flame with $P_{th} = 25.0$ kW, $\phi = 0.70$ and air split ratio of 1.6. The second burner was the industrial gas turbine swirl burner G30 DLE from the Siemens SGT-100 turbine that was investigated in a high-pressure test rig and included here as part of the introduction to the challenges of experiments and simulations at elevated pressure. Experimental data on this burner is currently available only to cooperation partners of Siemens.

Experiments and Simulations at Elevated Pressure

Coordinator: Bill Roberts, Hong Im, Joe Oefelein

The intent of this session was to introduce key issues and challenges associated with model validation efforts for combustion at elevated pressure. The session started with an overview of a few existing high pressure facilities designed for studying canonical flames, followed by the description of the new KAUST facilities that will be available for international collaboration. An overview of challenges and opportunities for temperature and major species measurements in high pressure flames at the KAUST facility was also presented. To guide the experimental effort, large eddy simulations (LES) capabilities have been developed by the KAUST group in collaboration with University of Rome, and initial simulations at various pressure conditions have been conducted. Based on scaling, increasing Re with pressure, while maintaining Da approximately constant, is proposed as a first set of parametric studies for the TNF community.

The Sandia group focused on challenges and progress in modeling turbulent combustion processes at elevated pressure, including simulation of multiphase and supercritical fuel injection and mixing with real-fluid thermodynamics and transport, use of UQ methods to optimize chemical models for simulations, and simulation of auto-ignition dynamics. Recent developments in quantitative imaging of turbulent mixing dynamics in high-pressure fuel injection systems were also reviewed.

KEY CHALLENGES AND PRIORITIES

In the area of stratified combustion it would be desirable to develop a burner configuration that achieves higher levels of stratification (higher local mixture fraction gradients) and higher levels of turbulence than in the TU Darmstadt and Cambridge/Sandia cases considered so far.

An important related challenge is to extend work that has been done in measurement and modeling of highly turbulent premixed flames (e.g., Sydney PPJB). High-turbulence and high-Ka premixed flames were prominent on the agenda of the Premixed Turbulent Flames (PTF) Workshop, so the

topic was dropped from TNF13 to avoid conflicts. Coordination with the PTF organizers may facilitate a broader community effort in this area.

The Sydney piloted inhomogeneous jet flames attracted many modeling efforts, but because most of the computational results were preliminary, more work will be needed to allow for detailed comparisons. On the experimental side, velocity measurements (nonreacting and reacting) are needed at flow conditions matching those of the scalar experiments. On the simulation side, there are needs to consolidate the treatment of boundary conditions, improve mixture fraction predictions, demonstrate mesh independence, and improve CO predictions. Application of conditional averaging should also be done in a coordinated way to achieve better physical understanding.

Regime identification and regime-independent modeling will be important topics for TNF14. Further work on development of regime indicators for simulations and experiments should prove beneficial for understanding of multi-regime combustion.

Development of target cases that combine features of high turbulence, high mixture-fraction gradients, and regime crossing should be considered. Important objectives in this context would be to avoid high sensitivity to boundary conditions (such as with piloted flames near blowoff) and include features relevant to practical combustors, while keeping geometric complexity within the reach of most academic codes.

It is important to continue working with fuels more complex than methane. Goals for TNF14 should comprise computations of the entire piloted DME jet flame series (Sandia DME D-G') with focus on the accurate prediction of the degree of localized extinction. We should also seek clarification of the predictions' dependencies on the chemical mechanisms. This may include the need for a quantitative comparison of formaldehyde, as this is the measured species with the most pronounced differences for all flame and flow conditions. Quantitative LIF of formaldehyde remains a challenge. Direct measurements of intermediate species by Raman scattering have proven difficult, but important progress has been made, and such data may still allow for more detailed comparisons. Modeling of recently measured DME jet flames in hot coflow (Sydney) should be considered as possible focus topics for TNF14.

For counterflow flames the goals for TNF14 should include more contributors with different modeling approaches, testing models across different modes of combustion using the counterflow geometry, and using simulations of internal flow to specify boundary conditions at the nozzle exits. A comparison of the two existing internal flow simulations of the Yale burner geometry would be useful. Goals should also include more detailed analysis of conditional statistics using experiments and high-fidelity simulations that focus on the inter-nozzle region. This effort could include additional fuels and flame conditions and sufficiently long simulation times to study the temporal evolution of localized extinction and re-ignition.

The side-wall-quench (SWQ) flame is proposed as a future TNF target configuration. Priorities for experimental work are to measure more scalars, measure wall temperature and heat transfer, and conduct parametric variation of such things as wall temperature, surface coatings, fuel, and effusion cooling.

Other challenging topics that are important for the overall TNF goals but were not included as main topics at TNF13 are: quality metrics and uncertainty quantification in LES; analysis and comparison of multi-dimensional data from experiments and simulations; and hot coflow flames, specifically cases where the mechanism of stabilization transitions between auto-ignition and flame propagation.

blank

TNF 2016 Participants

Last name	First Name	Title	Affiliation	email
Angelberger	Christian	Dr.	IFP Energies Nouvelles	christian.angelberger@ifpen.fr
Arndt	Christoph	Mr.	German Aerospace Center (DLR)	christoph.arndt@dlr.de
Attili	Antonio	Dr.	KAUST	antonio.attili@kaust.edu.sa
Bai	Yun	Mr.	Zhejiang University	baiyucuilv@zju.edu.cn
Barlow	Robert	Dr.	Sandia National Laboratories	barlow@sandia.gov
Blanquart	Guillaume	Prof.	Caltech	g.blanquart@caltech.edu
Boehm	Benjamin	Dr.	Darmstadt Technical University	bboehm@ekt.tu-darmstadt.de
Boxx	Isaac	Dr.	German Aerospace Center	isaac.boxx@dlr.de
Boyette	Wesley	Mr.	KAUST	wesley.boyette@kaust.edu.sa
Cailler	Melody	Ms.	EM2C	melody.cailler@ecp.fr
Casey	Tiernan	Dr.	Sandia National Laboratories	tcasey@sandia.gov
Chen	Jackie	Dr.	Sandia National Laboratories	jhchen@sandia.gov
Chen	Jyh-Yuan	Prof.	UC Berkeley	j_y_chen@berkeley.edu
Chong	Shao Teng	Mr.	University of Michigan	stchong@umich.edu
Ciottoli	Pietro Paolo	Dr.	Sapienza Univ. Rome	pietropaolo.ciottoli@uniroma1.it
Cleary	Matthew	Dr.	University of Sydney	m.cleary@sydney.edu.au
Cutcher	Hugh	Mr.	University of Sydney	hcut6115@uni.sydney.edu.au
Dally	Bassam	Prof.	University of Adelaide	bassam.dally@adelaide.edu.au
di Mare	Francesca	Prof.	TU-Darmstadt/DLR Cologne	francesca.dimare@dlr.de
Dibble	Robert	Prof.	KAUST	robert.dibble@kaust.edu.sa
Dreizler	Andreas	Prof.	Darmstadt Technical University	office@ekt.tu-darmstadt.de
Dunn	Matthew	Dr.	The University of Sydney	matthew.dunn@sydney.edu.au
Eggels	Ruud	Dr.	Rolls-Royce Deutschland	ruud.eggels@rolls-royce.com
Fievet	Romain	Mr.	University of Michigan	fievetromain@gmail.com
Fiorina	Benoit	Prof.	Centralesupelec	benoit.fiorina@centralesupelec.fr
Frank	Jonathan	Dr.	Sandia National Laboratories	jhfrank@sandia.gov
Fuest	Frederik	Dr.	LaVision GmbH	frederik.fuest@gmail.com
Galindo	Sebastian	Mr.	The University of Sydney	sgal8842@uni.sydney.edu.au
Geyer	Dirk	Dr.	HAD Darmstadt	dirk.geyer@h-da.de
Giusti	Andrea	Dr.	University of Cambridge	ag813@cam.ac.uk
Gordon	Robert	Dr.	University of Melbourne	robert.gordon@unimelb.edu.au
Guiberti	Thibault	Dr.	The University of Sydney, Australia	thibault.guiberti@kaust.edu.sa
Hampp	Fabian	Mr.	Imperial College London	f.hampp11@imperial.ac.uk
Han	Wang	Mr.	University of Michigan	WHAN@PKU.EDU.CN
Hassanally	Malik	Mr.	University of Michigan	malik.hassanally@gmail.com
Hasse	Christian	Prof.	TU Freiberg	christian.hasse@iec.tu-freiberg.de
Hawkes	Evatt	Prof.	University of New South Wales	evatt.hawkes@unsw.edu.au
Hernandez Peres	Francisco	Dr.	KAUST	francisco.hernandezperez.1@kaust.edu.sa
Hewson	John	Dr.	Sandia National Laboratories	jchewso@sandia.gov
Hochgreb	Simone	Prof.	University of Cambridge	simone.hochgreb@eng.cam.ac.uk
Ihme	Matthias	Prof.	Stanford University	mihme@stanford.edu
Im	Hong	Prof.	KAUST	hong.im@kaust.edu.sa
Janicka	Johannes	Prof.	Darmstadt Technical University	office@ekt.tu-darmstadt.de
Jeon	Sangtae	Mr.	Hanyang University	jist1004@hanyang.ac.kr

TNF 2016 Participants

Last name	First Name	Title	Affiliation	email
Ji	Hyunggeun	Mr.	Hanyang University	hehy@hanyang.ac.kr
Ji	Weiqi	Mr.	Tsinghua University	jwq14@mails.tsinghua.edu.cn
Jones	William	Prof.	Imperial College London	w.jones@imperial.ac.uk
Kempf	Andreas	Prof.	Universität Duisburg-Essen	andreas.kempf@uni-due.de
Kim	Jaehyeon	Mr.	Hanyang University	kjh6781@gmail.com
Kim	Namsu	Mr.	Hanyang University	realk@hanyang.ac.kr
Kim	Yongmo	Prof.	Hanyang University	ymkim@hanyang.ac.kr
Kleinheinz	Konstantin	Mr.	RWTH Aachen University	k.kleinheinz@itv.rwth-aachen.de
Klimenko	Alex	Dr.	The University of Queensland	klimenko@mech.uq.edu.au
Kronenburg	Andreas	Prof.	University of Stuttgart	kronenburg@itv.uni-stuttgart.de
Lee	Bok Jik	Dr.	KAUST	bokjik.lee@kaust.edu.sa
Lee	Myoungkyu	Dr.	University of Texas at Austin	mk@ices.utexas.edu
Li	Tao	Mr.	Imperial College London	t.li13@imperial.ac.uk
Li	Zhongshan	Dr.	Lund University	zhongshan.li@forbrf.lth.se
Lindstedt	Peter	Prof.	Imperial College London	p.lindstedt@imperial.ac.uk
Lu	Zhen	Mr.	Tsinghua University	luz11@mails.tsinghua.edu.cn
Luo	Kun	Prof.	Zhejiang University	zjulk@zju.edu.cn
Macfarlane	Andrew	Mr.	The University of Sydney	amac7548@uni.sydney.edu.au
Maghbouli	Amin	Mr.	Politecnico di Milano	amin.maghbouli@gmail.com
Magnotti	Gaetano	Dr.	Sandia National Laboratories	gmagnet@sandia.gov
Masri	Assaad	Prof.	The University of Sydney	assaad.masri@sydney.edu.au
Meier	Wolfgang	Dr.	DLR-Stuttgart	wolfgang.meier@dlr.de
Mueller	Hagen	Mr.	Bundeswehr University Munich	hagen.mueller@unibw.de
Mueller	Michael	Prof.	Princeton University	muellerm@princeton.edu
Naik	Chitral	Dr.	ANSYS Inc.	chitral.naik@ansys.com
Najm	Habib	Dr.	Sandia National Laboratories	hnnajm@sandia.gov
Navarro-Martinez	Salvador	Dr.	Imperial College London	s.navarro@imperial.ac.uk
Oh	Seungtaek	Mr.	Hanyang University	ost816@naver.com
Park	Sangwoon	Mr.	Hanyang University	avenue-84@hanmail.net
Perry	Bruce	Mr.	Princeton University	baperry@princeton.edu
Pfitzner	Michael	Prof.	Bundeswehr University Munich	michael.pfitzner@unibw.de
Pitsch	Heinz	Prof.	RWTH Aachen University	office@itv.rwth-aachen.de
Pope	Stephen	Prof.	Cornell University	s.b.pope@cornell.edu
Popp	Sebastian	Mr.	TU Bergakademie Freiberg	sebastian.popp@iec.tu-freiberg.de
Prause	Juliane	Ms.	German Aerospace Center	juliane.prause@dlr.de
Proch	Fabian	Mr.	Universität Duisburg-Essen	fabian.proch@uni-due.de
Raman	Venkat	Prof.	The University of Michigan	ramanvr@umich.edu
Ren	Zhuyin	Prof.	Tsinghua University	zhuyinren@tsinghua.edu.cn
Richardson	Edward	Dr.	University of Southampton	e.s.richardson@soton.ac.uk
Rieth	Martin	Mr.	Universität Duisburg-Essen	martin.rieth@uni-due.de
Roberts	William	Prof.	KAUST	william.roberts@kaust.edu.sa
Roekaerts	Dirk	Prof.	Delft University of Technology	d.j.e.m.roekaerts@tudelft.nl
Salehi	Fatemeh	Dr.	University of New South Wales	fatemeh.salehi@sydney.edu.au
Sellmann	Johannes	Mr.	University of Duisburg-Essen	johannes.sellmann@uni-due.de

TNF 2016 Participants

Last name	First Name	Title	Affiliation	email
Sesha Giri	Krishna	Dr.	KAUST	krishna.seshagiri@kaust.edu.sa
Stein	Oliver	Dr.	ITV, University of Stuttgart	o.stein@itv.uni-stuttgart.de
Sutton	Jeffrey	Prof.	Ohio State University	sutton.235@osu.edu
Tong	Chenning	Prof.	Clemson University	ctong@clermson.edu
Varna	Achinta	Mr.	University of New South Wales	a.varna@unsw.edu.au
Wandel	Andrew	Dr.	University of Southern Queensland	andrew.wandel@usq.edu.au
Wang	Haifeng	Prof.	Purdue University	haifeng@purdue.edu
Wang	Haiou	Dr.	University of New South Wales	haiou.wang@unsw.edu.au
Wang	Ping	Prof.	Jiangsu University	pingwang@ujs.edu.cn
Wlokas	Irenaeus	Dr.	University of Duisburg-Essen	i.wlokas@uni-due.de
Xie	Wenwen	Ms.	Tsinghua University	jmm15@mails.tsinghua.edu.cn
Yang	Yue	Prof.	Peking University	yyg@pku.edu.cn
Zhou	Hau	Mr.	Tsinghua University	zhouhua12@mails.tsinghua.edu.cn

blank



TNF2016 Workshop – Agenda

Incheon, Korea, 28 – 30 July 2016

Thursday, July 28:

- 16:00 – 17:00 Registration (Baum Foyer) and Poster Setup
- 17:00 – 18:00 Poster Session with refreshments (Baum Hall B)
- 18:00 – 19:00 *Buffet Dinner (Baum Hall A)*
- 19:00 – 21:00 Poster Session with refreshments (Baum Hall B)

Friday, July 29:

Breakfast Buffet in the Platz Restaurant

- 8:30 – 8:45 Introduction and Announcements (Baum Hall C)
(Rob Barlow)
- 8:45 – 9:30 Update on Stratified Flames
(Coordinator: Andreas Kempf)
- 9:30 – 11:00 Sydney Partially-Premixed Flame Comparisons
(Coordinator: Benoît Fiorina)
- 11:00 – 11:30 *Coffee Break (Poster Session)*
- 11:30 – 13:00 Progress Variable and Regime Indicators in Partially
Premixed Flames
(Coordinators: Rob Barlow, Christian Hasse, and Matthias Ihme)
- 13:00 – 14:00 *Lunch Buffet (Baum Hall A)*
- 14:00 – 14:45 Update on DME Flames
(Coordinator: Andreas Kronenburg)
- 14:45 – 15:45 Counterflow Flames
(Coordinator: Jonathan Frank)
- 15:45 – 16:15 *Coffee Break (Poster Session)*
- 16:15 – 18:00 Flame Wall Interactions
(Coordinators: Andreas Dreizler and Johannes Janicka)
- 18:30 – 19:30 *Buffet Dinner (Baum Hall A)*
- 19:30 – 21:30 Poster Session with refreshments (Baum Hall B)



TNF2016 Workshop – Agenda

Incheon, Korea, 28 – 30 July 2016

Saturday, July 30: (Checkout time is 11:00)

Breakfast buffet in the Platz

- | | |
|---------------|---|
| 9:00 – 9:30 | New Burners and Flames
(Coordinator: Wolfgang Meier) |
| 9:30 – 10:30 | Experiments and Simulations at Elevated Pressure
(Coordinators: Bill Roberts, Hong Im, Joe Oefelein) |
| 10:30 – 11:00 | <i>Coffee Break (Poster Session)</i> |
| 11:00 – 12:00 | Discussion on Key Challenges and Priorities
(Coordinators: Andreas Dreizler, Benoit Fiorina) |
| 12:00 – 12:15 | Action Items and Planning
(Coordinator: Rob Barlow) |
| 12:15 | Adjourn and Remove Posters |
| 12:30 – 13:30 | <i>Lunch Buffet (Baum Hall A)</i> |
| 14:00 | <i>Buses depart for the Symposium venue</i> |

Update on stratified flames

Coordinators: Andreas Kempf and Fabian Proch

The objective of the session was an update on new simulation results and new experimental data for the stratified burners investigated at Darmstadt University and Cambridge University (with Sandia National Laboratories), respectively.

The Darmstadt stratified burner (TSF) has been a TNF target flame since 2010, it consists of three 5-mm-staged concentric tubes placed in a laminar co-flow. Burnt gases exit from the central tube (pilot) to stabilize the flame. A joint Combustion and Flame paper on the burner has been published in 2015 with comparisons of simulation results from five different groups against the measurement data, one key finding was that the effect of heat loss needs to be included into the combustion model to obtain the correct flame propagation speed. A broad conclusion from this joint paper was that: "... good predictions are achieved by combustion models that treat the stratified flame as an ensemble of homogeneous premixed flames of different mixture fractions. Even though the level of stratification investigated here must be considered to be mild, the good results achieved with this approach were not necessarily expected from the outset, giving an evidence that mildly stratified flames can be modeled as a premixed flame." The effect of heat loss was further investigated by the group of Janicka at the TU Darmstadt, they showed that including not only the cooling of the pilot but additionally also the heating up of the inner stream in the simulation reduces the lift-off height and influences the results. The group around Dreizler and Geyer in Darmstadt presented new measurements for the TSF burner with 20% hydrogen addition to the methane fuel for different levels of stratification and shear. New simulation results for the TSF were presented from Zhenjiang University, who used a combination of a presumed filtered density function (FDF) and reaction-diffusion manifold (REDIM) chemistry, the results were in agreement with the ones previously obtained by other groups.

The Cambridge/Sandia burner (SwB) has been a TNF target flame since 2012, it also consists of three concentric tubes in a laminar co-flow, but the center tube is sealed with a ceramic cap, and the flame is stabilized by recirculation of combustion products downstream of this central bluff body. The heat loss effect is smaller than for the TSF burner so that the flame propagation speed can be captured well by adiabatic combustion models. Nevertheless, there is a small effect of heat loss in the region next to the bluff body, as shown by the group of Fiorina at the EM2C Laboratories Paris. The group of Hochgreb at the Cambridge University presented comparisons of measurement data against the LES results from the Kempf group at Duisburg-Essen University. They compared the flame-shape in the burner-mid section from experiment and LES and found a good qualitative agreement. Furthermore, they presented comparisons of equivalence ratio PDFs conditioned on the height above the burner from experiment and LES, the shapes were very similar for the premixed case SwB1, larger deviations occurred for the stratified cases SwB5 and SwB9. Recently published analysis from Cambridge and Sandia showed that, when conditioned on the local equivalence ratio, major species mass fractions over temperature in the stratified flames (both non-swirling and swirling) are well approximated by laminar premixed flames and show only minor differences from the premixed turbulent flame. The group of Jones at the Imperial College London presented new simulation results for most of the measured cases with LES and a stochastic fields combustion model, the obtained results were in agreement with the ones previously presented by other groups. The group of Kempf from Duisburg-Essen University also presented new simulation results for the premixed case SwB1, where all the relevant scales have been resolved on a 0.1 mm grid with a total number of 1.6 billion cells. They found that the results agreed well with the measurements, and presented a detailed analysis of the turbulent flame structure with PDFs and JPDFs, where a conditioning on the height above the burner and the progress of the reaction was necessary to achieve meaningful statistics – the reason being the very strong evolution of flame wrinkling in flow direction.

Update on Stratified Flames

Andreas Kempf
Fabian Proch

University of Duisburg-Essen

with

Benoît Fiorina
CentraleSupélec
University of Paris Saclay
EM2C - CNRS

Outline

Darmstadt Turbulent Stratified Flame (TFS)

Burner setup and flame structure

New heat loss analysis

New measurements

New simulations compared to former results

Cambridge stratified flame series (SwB)

Burner setup and flame structure

Heat loss effect

Conditioned flame structure

Comparison spatial PDFs simulation vs. experiment

New simulations

Comparison to former results

Further presentation by Fabian Proch

Darmstadt turbulent stratified flame (TSF)

TU Darmstadt: G. Kuenne, A. Ketelheun, A. Avdic, J. Janicka, D. Geyer, A. Dreizler, F. di Mare

ITV Aachen: P. Trisjono, K. Kleinheinz, S. Kang, H. Pitsch

Lund University: E. Alenius, C. Duwig

EM2C Paris: R. Mercier, B. Fiorina, M. Cailler

Jiangsu University: P. Wang, C. Wang, Z. He

KIT Karlsruhe: G. Steinhilber, U. Maas

Duisburg-Essen University: F. Proch, F. Cavallo Marincola, A. M. Kempf

Burner setup

Central methane/air pilot for flame stabilization

Two co-annular streams with varying equivalence ratio

Co-flow of air

Temperature/Species: Raman/Rayleigh, Kuenne et al.
CNF 2012

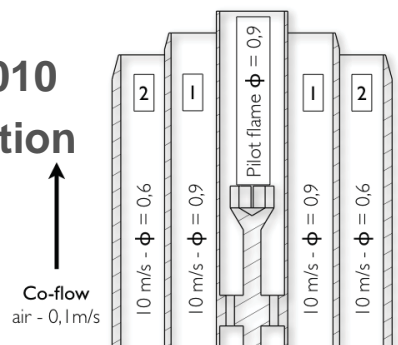
Velocity: PIV/LDV, Seffrin et al. CNF 2010

Heat loss important for flame propagation

Pilot wall temperature of 750 K

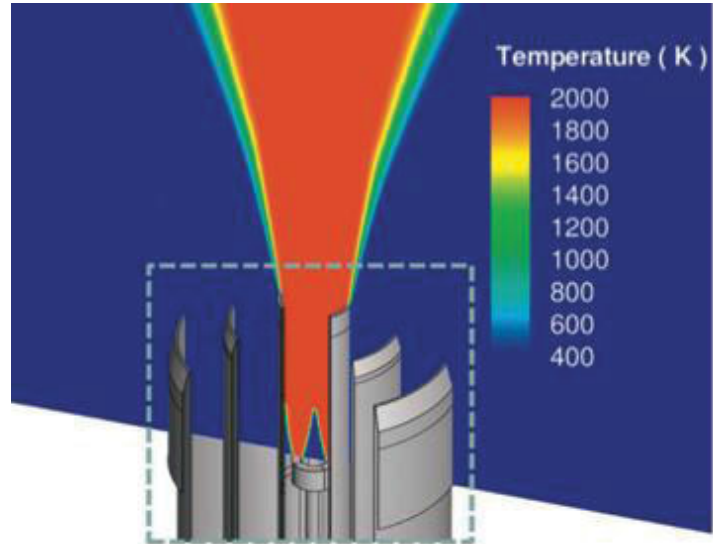
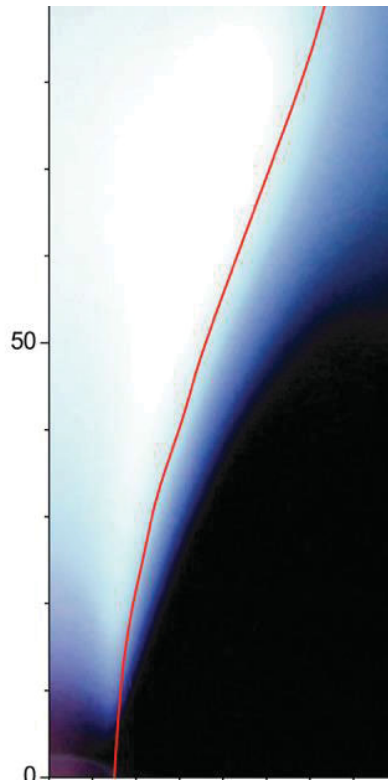
Stratification ratio of 1.5

Sheared cases measured (not shown)

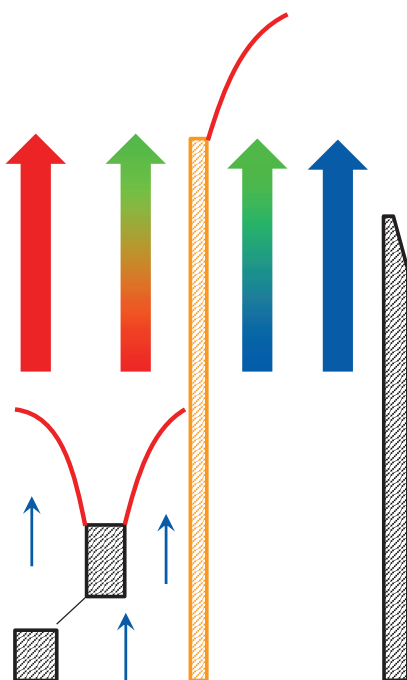


Case	ϕ_p	v_p (m s ⁻¹)	Dh_p (mm)	ϕ_1	v_1 (m s ⁻¹)	Dh_1 (mm)	Re_1	ϕ_2	v_2 (m s ⁻¹)	Dh_2 (mm)	Re_2
TSF-A-i1	0.9	1	14.8	0	10	20.0	13,800	0	10	20.0	13,300
TSF-A-r	0.9	1	14.8	0.9	10	20.0	13,800	0.6	10	20.0	13,300

Flame photography + LES temperature field by Kuenne et al., CNF 2012



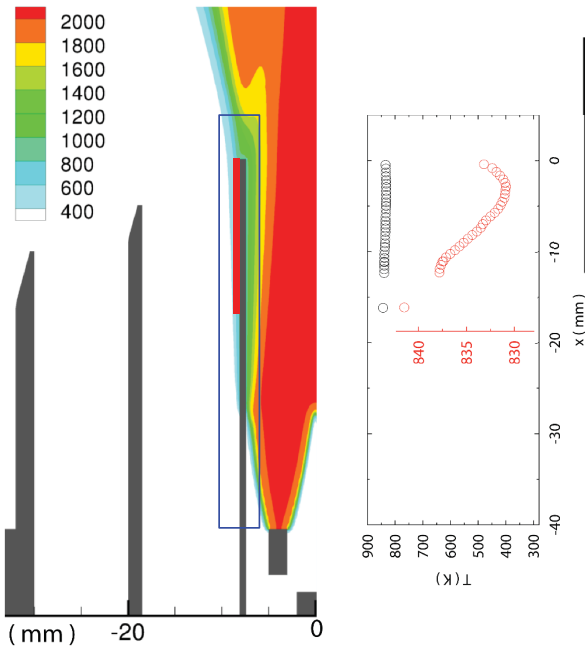
5



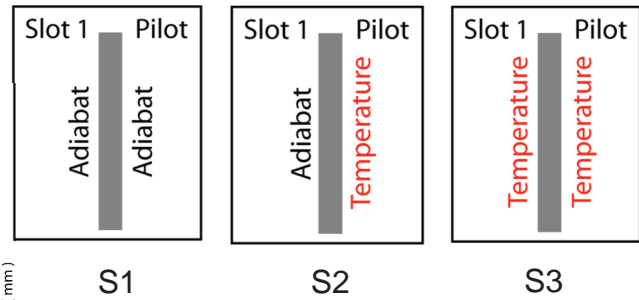
- 2014 **Measurements of the wall temperature**
- $T_i \approx T_o \approx 840\text{ K}$
 - Preheating likely, included in this work
- 2012 **First temperature measurements**
- $T < T_{eq}$
 - Inclusion of heat losses inside the pilot (joint paper from TNF groups)
- 2010 **End of design phase**
- heat transfer was thought to be negligible

6

Phosphor measurements

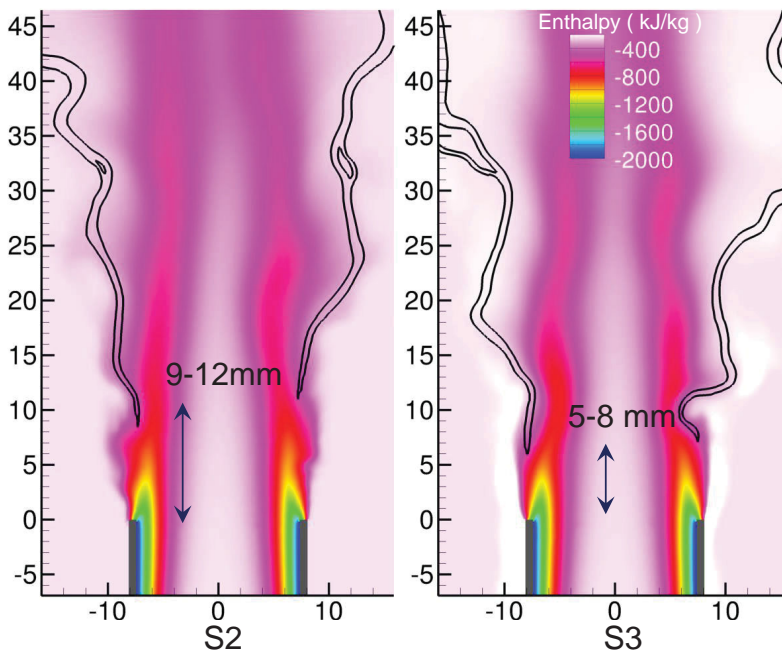


Simulations conducted



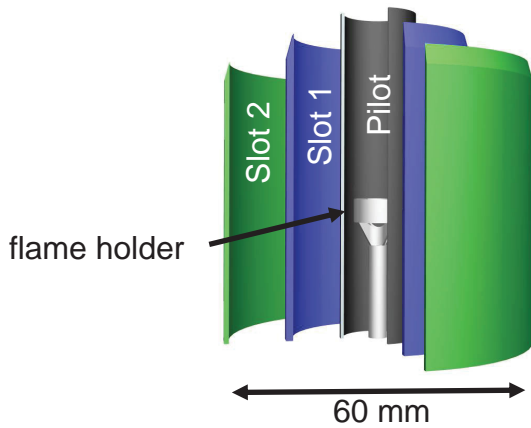
7

Influence thermal BCs, G. Kuenne et al.



Enthalpy loss
gets countered
by the preheating
→ reduced lift-off

8



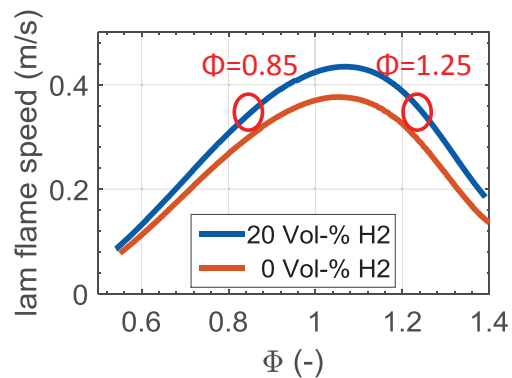
Methane Hydrogen Flame:

Fuel composition:

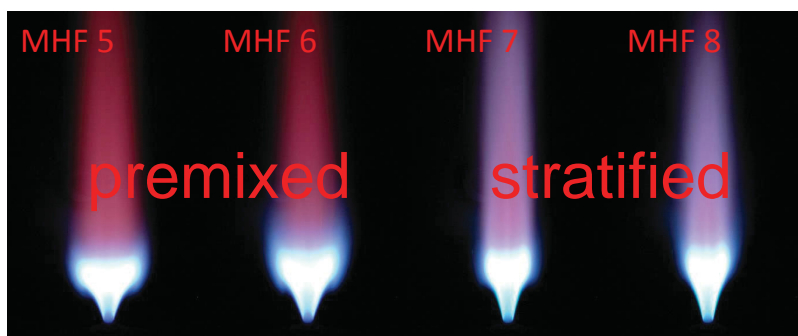
- 80 Vol-% CH₄
- 20 Vol-% H₂

Selection of Φ in terms of laminar flame speed:

$$S_{\text{lam}_\Phi \text{ slot1}} = S_{\text{lam_mean}_\Phi (\text{slot1,slot2})}$$



9



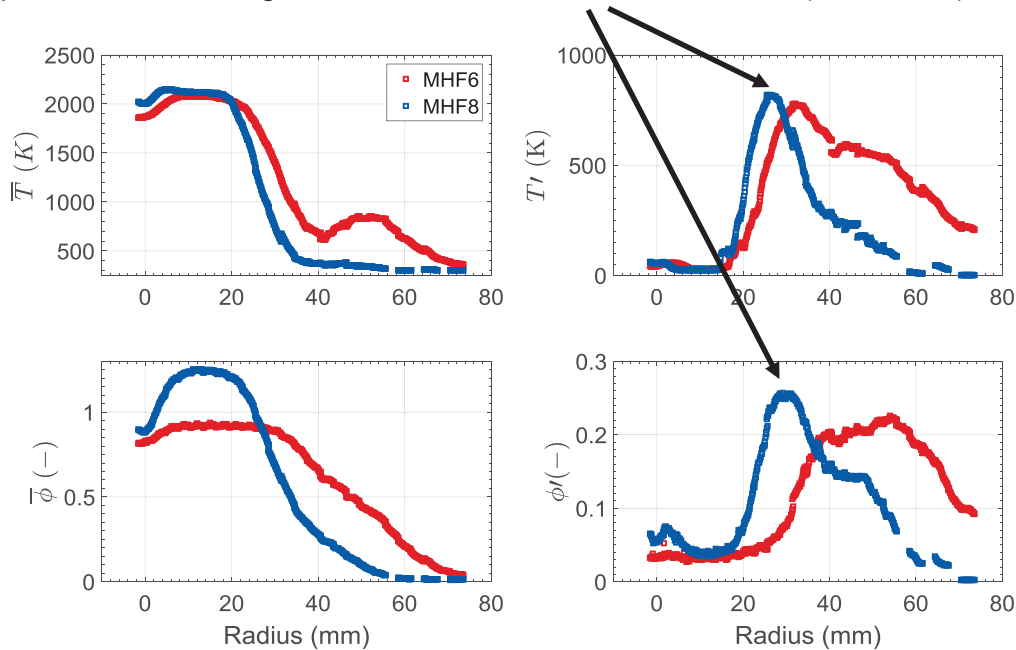
P: $\Phi=0.7$	1m/s						
S1: $\Phi=0.85$	10m/s	S1: $\Phi=0.85$	10m/s	S1: $\Phi=1.25$	10m/s	S1: $\Phi=1.25$	10m/s
S2: $\Phi=0.85$	10m/s	S2: $\Phi=0.85$	15m/s	S2: $\Phi=0.45$	10m/s	S2: $\Phi=0.45$	15m/s
71 kW		94 kW		61 kW		73 kW	

no shear shear

- Measured points:
 - Radial profiles at: $z = 7, 15, 30, 45, 60, 70, 80, 100$ mm above pilot
 - High resolution at intersection of flame brush and mixing layer at $z = 75$ mm, 40000 samples

10

Approx. location of high resolution measurements in MHF8 ($r = 29$ mm)



11

Presumed FDF + REDIM chemistry

1. Reaction-Diffusion Manifold (REDIM)

1. Reduces detailed chemical kinetics to low-dimensional reaction/diffusion manifold in composition space
2. Accounts for coupling of reaction and diffusion
3. Flamelet model and slow manifold concept as limiting cases
4. Applicable to non-premixed, partially premixed, premixed flames

$$\text{ILDIM: } \frac{\partial \psi}{\partial t} = F(\psi)$$

$$\text{REDIM: } \frac{\partial \psi}{\partial t} = (1 - \psi_{\theta} \psi_{\theta}^+) \left\{ F(\psi) + \frac{D}{\rho} \chi_{\theta} \psi_{\theta\theta} \chi_{\theta} \right\}$$

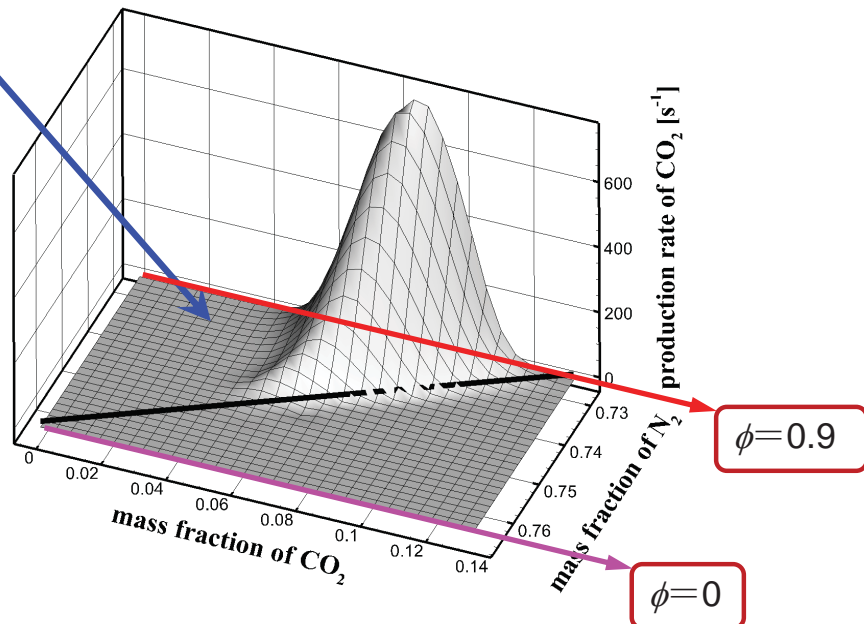
[V. Bykov, U. Maas, Proc. Combust. Inst. 32 (2009) 561-568.]

12

2D REDIM table generated for Darmstadt TSF

$$\phi \in [0, 0.9]$$

N₂ and CO₂
variation region



13

2. REDIM table combined with presumed PDF

- momentum
- mass
- species transport

Transport equations for N₂, CO₂ mass fraction:

$$\frac{\partial \bar{\rho} \tilde{Y}_\alpha}{\partial t} + \frac{\partial}{\partial x} (\bar{\rho} \tilde{u}_i \tilde{Y}_\alpha) + \frac{\partial}{\partial x_i} (\bar{\rho} u_i \tilde{Y}_\alpha - \bar{\rho} \tilde{u}_i \tilde{Y}_\alpha) = \frac{\partial}{\partial x_i} (\bar{\rho} \tilde{D} \frac{\partial \tilde{Y}_\alpha}{\partial x_i}) + \bar{\rho} \tilde{\omega}_\alpha$$

where $\alpha = 1, 2$ represents N₂ and CO₂, respectively.

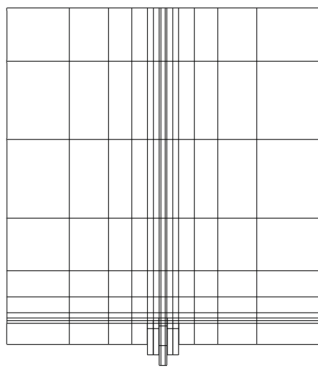
Estimate variance via:

$$\tilde{Y}_\alpha'^2 \approx \frac{C}{4} \left[(\tilde{Y}_{\alpha,n} - \tilde{Y}_{\alpha,s})^2 + (\tilde{Y}_{\alpha,w} - \tilde{Y}_{\alpha,e})^2 + (\tilde{Y}_{\alpha,u} - \tilde{Y}_{\alpha,l})^2 \right]$$

\tilde{Y}_α and $\tilde{Y}_\alpha'^2$ are used to determine Clipped Gaussian PDF

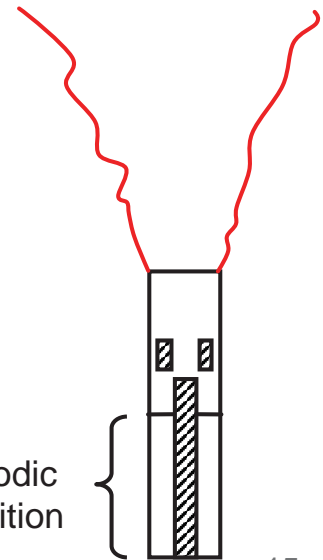
14

multi-block structured grid



LESOCC2C code (originally from W. Rodi group in KIT)
multi-block structured, body-fit grid, with local refinement
2nd order accuracy
Low-Mach number N-S equation

Wall : no-slip, adiabatic, W-W wall function
Inlet : periodic condition
Outlet : convective condition



15

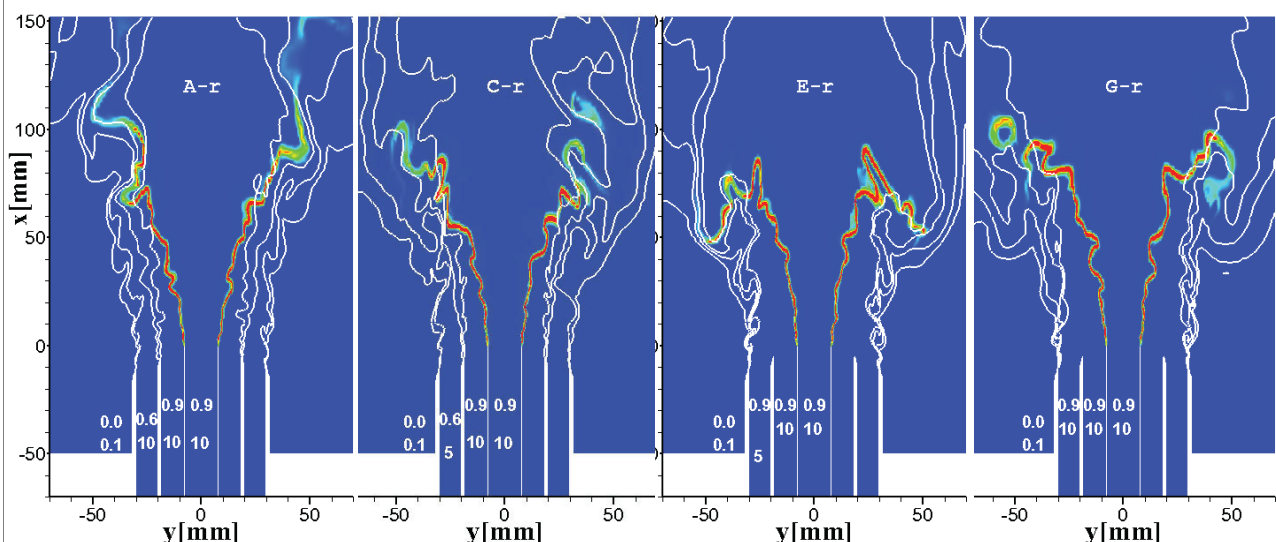
New simulations, P. Wang et al.

A-r (stratified, no shear)

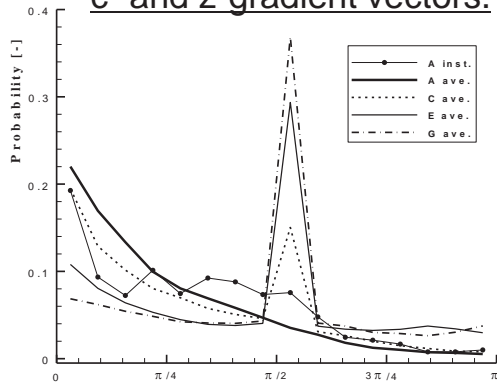
C-r (stratified, shear)

E-r (no stratified, shear)

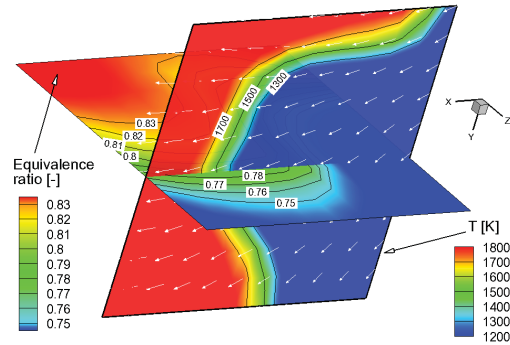
G-r (no stratified, no shear)



Pdf of alignment angle between
c- and z-gradient vectors.

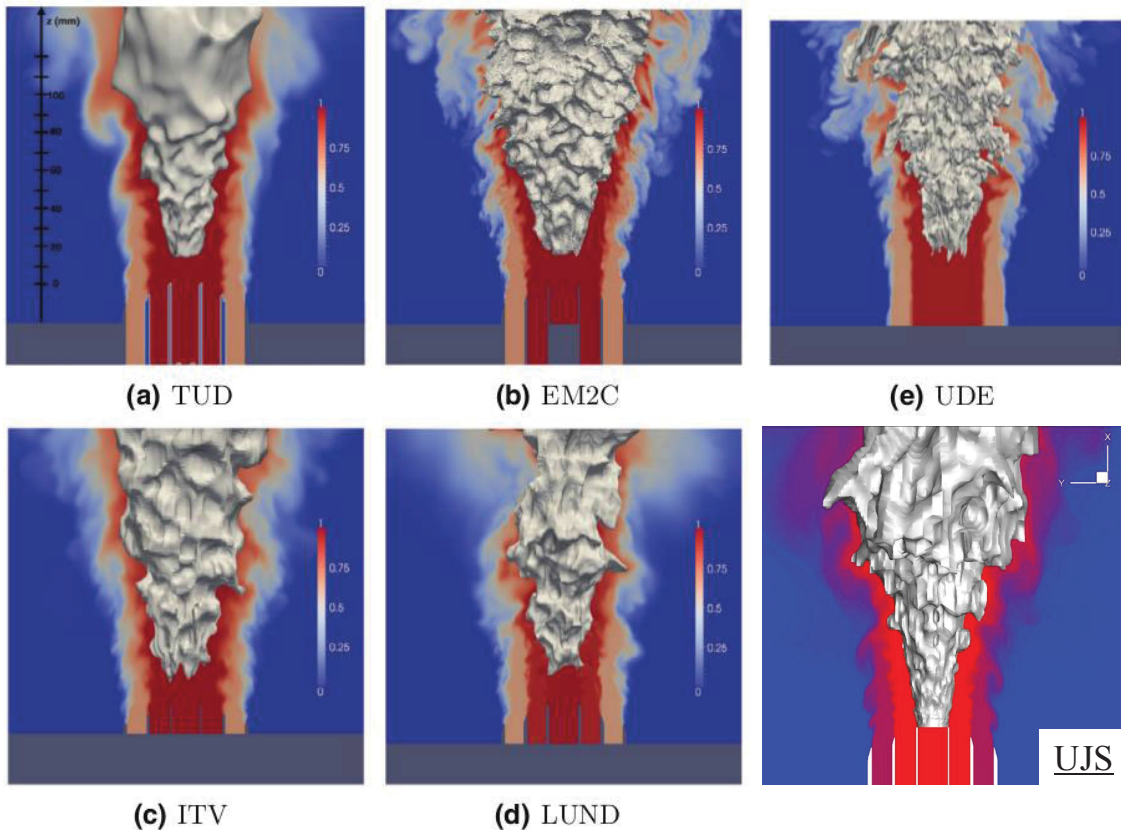


A snapshot of T and ϕ contour.



17

Simulation results – Flame structure

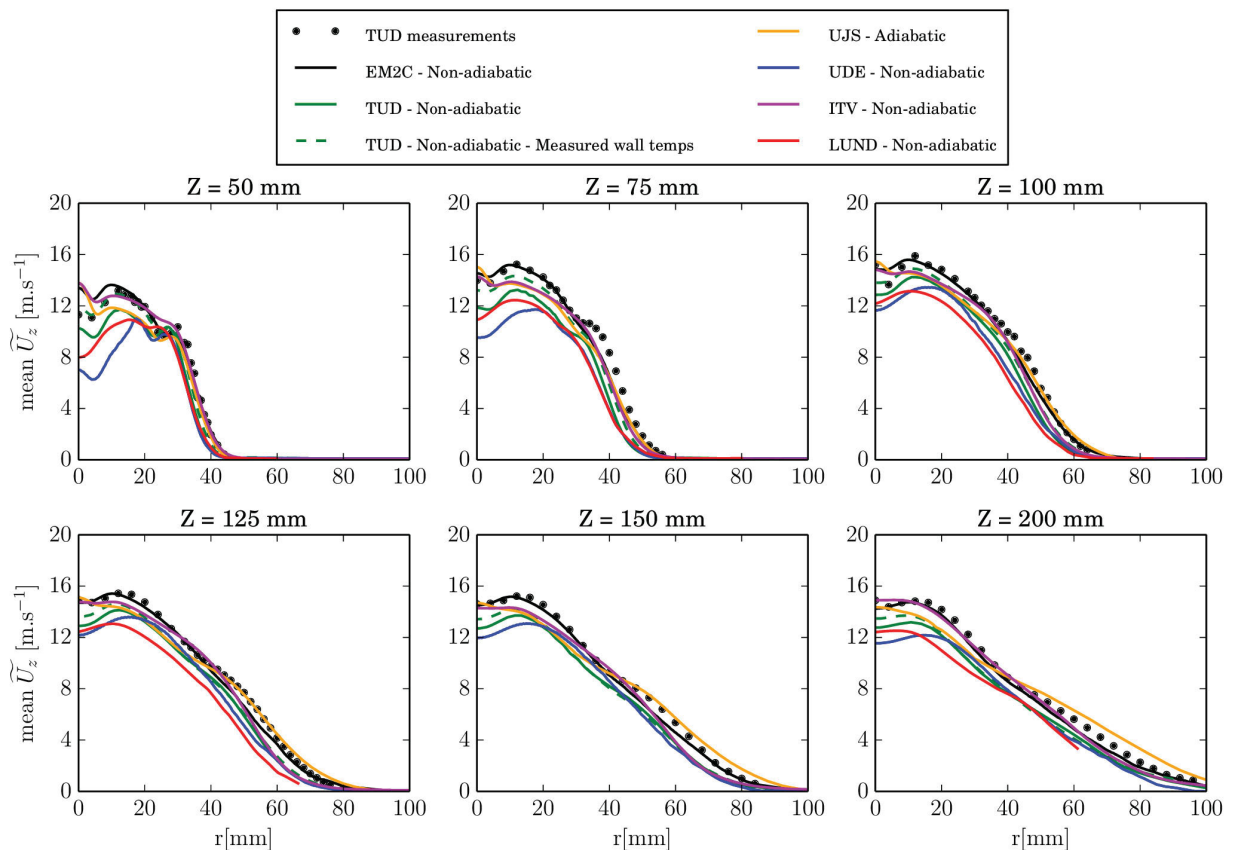


18

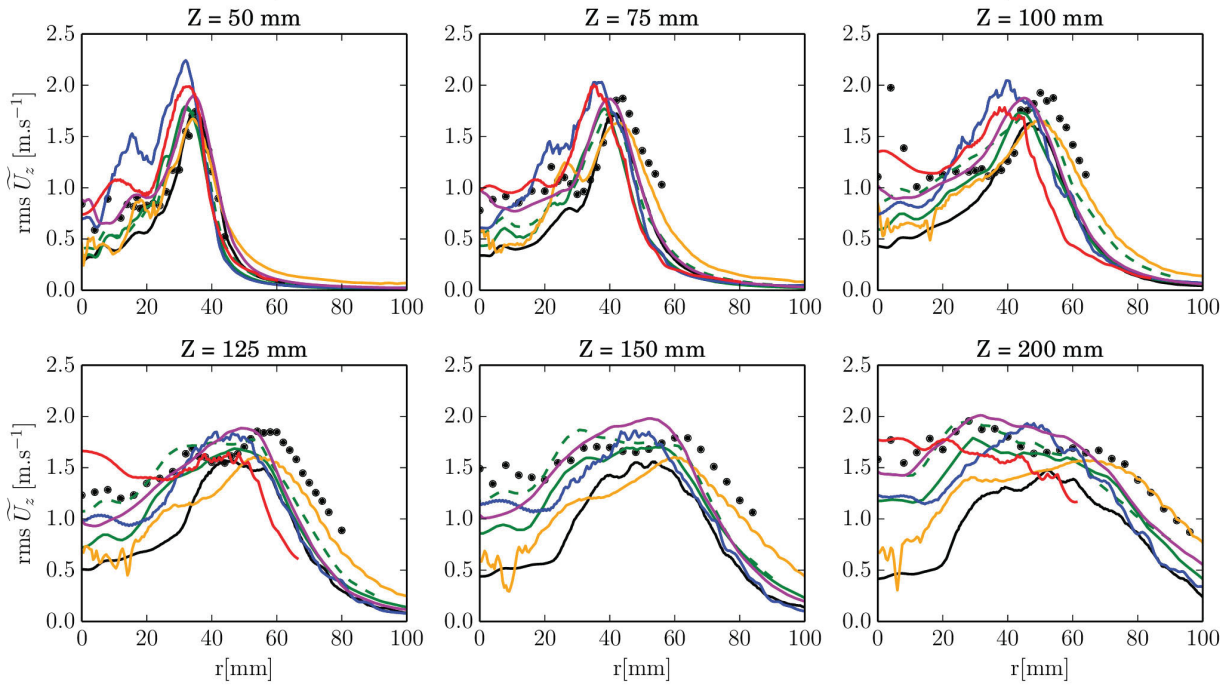
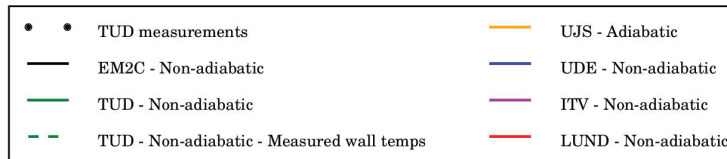
Simulation number	Computational domain	Number of control volume (M)	Flame resolution Δ_x/δ_l	Combustion model
TUD	Pilot, slot 1 and slot 2: $z_- = -120$ mm Coflow: $z_- = -40$ mm Outlet: $z_+ = 600$ mm	6.5	0.4 - 4.4	ATF-FGM ($2 < F < 15$)
EM2C	Slot 1 and slot 2: $z_- = -120$ mm Coflow and pilot: $z_- = -20$ mm Outlet: $z_+ = 1100$ mm	5.4	3	F-TACLES ($\Delta = 10\delta_l$)
ITV	Slot 1 and slot 2: $z_- = -15$ mm Coflow and pilot: $z_- = -15$ mm Outlet: $z_+ = 1100$ mm	3.1	2.3	Coupled G-eq / C
LUND	Pilot, coflow: $z_- = -20$ mm Slot 1 and slot 2: $z_- = -20$ mm Outlet: $z_+ = 1200$ mm	2.9	0.96	No model
UDE	Pilot, coflow: $z_- = -20$ mm Slot 1 and slot 2: $z_- = -20$ mm Outlet: $z_+ = 220$ mm	110	1.0	FSD

19

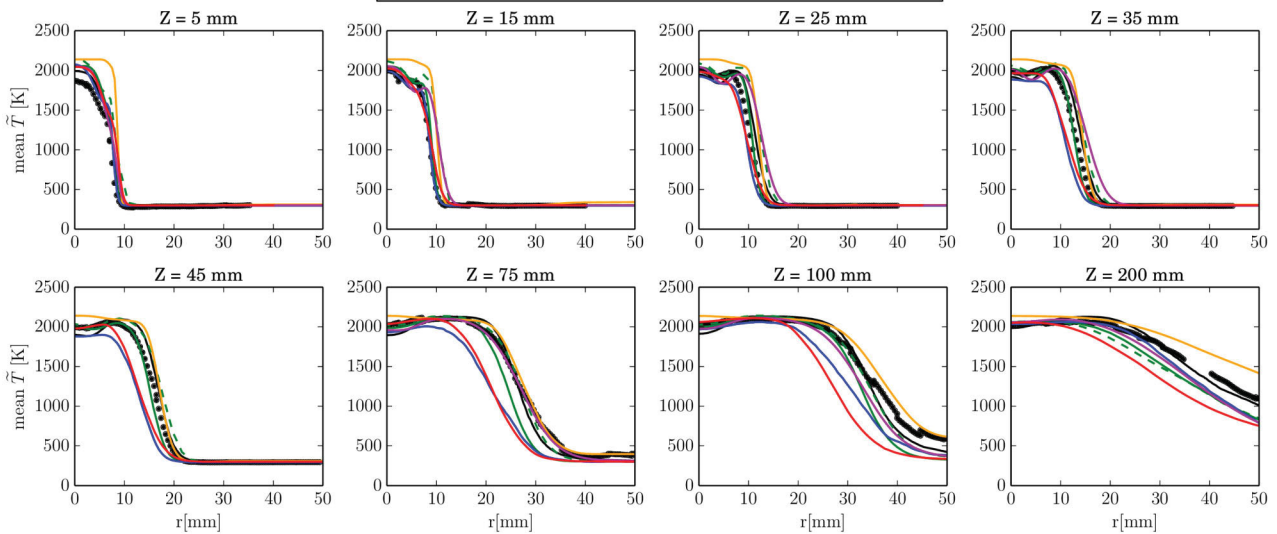
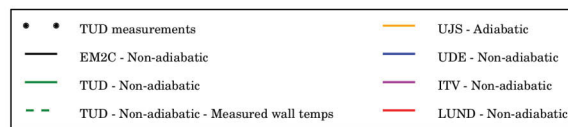
Simulation results – Axial velocity mean

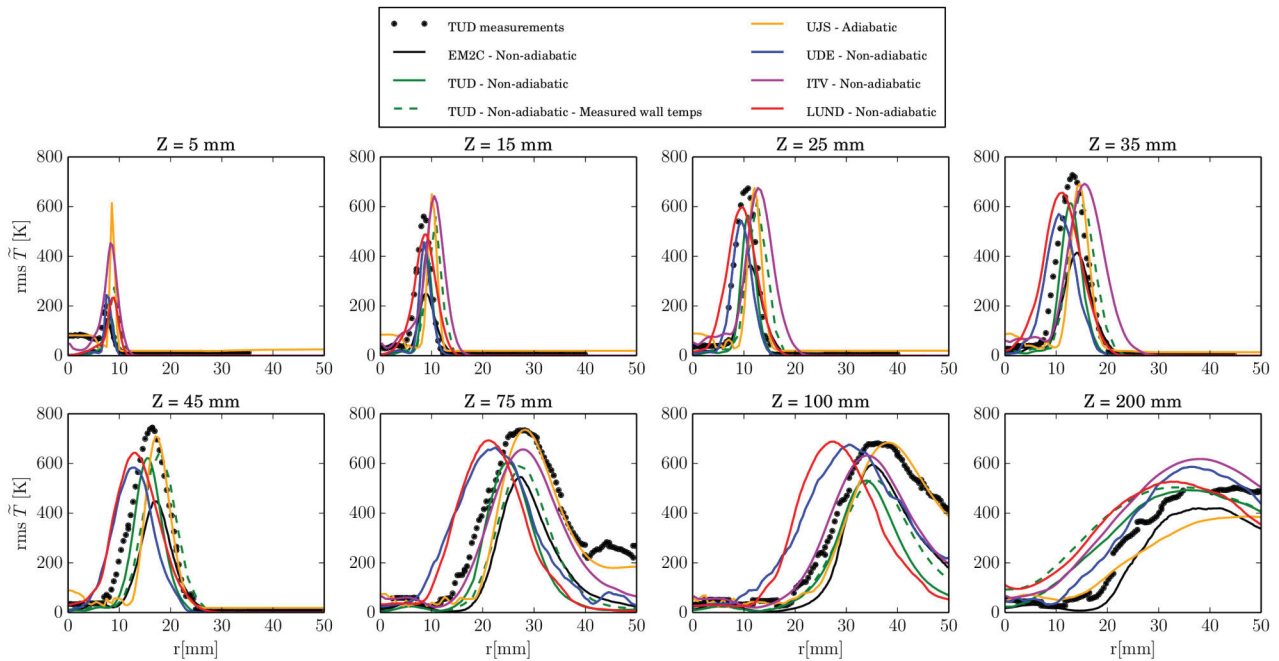


Simulation results – Axial velocity rms



Simulation results – Temperature mean





23

Combustion and Flame 162 (2015) 4264–4282

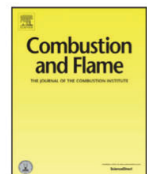


ELSEVIER

Contents lists available at ScienceDirect

Combustion and Flame

journal homepage: www.elsevier.com/locate/combustflame



Challenging modeling strategies for LES of non-adiabatic turbulent stratified combustion



B. Fiorina^{a,*}, R. Mercier^a, G. Kuenne^{b,c}, A. Ketelheun^{b,c}, A. Avdić^{b,d}, J. Janicka^{b,c}, D. Geyer^e,
A. Dreizler^{b,c}, E. Alenius^f, C. Duwig^{f,j}, P. Trisjono^g, K. Kleinheinz^g, S. Kang^h, H. Pitsch^g, F. Prochⁱ,
F. Cavallo Marincolaⁱ, A. Kempfⁱ

^aLaboratoire EM2C, CNRS, CentraleSupélec, Grande Voie des Vignes, Châtenay-Malabry 92290, France

^bInstitute of Energy and Power Plant Technology, TU Darmstadt, Jovanka-Bontschits-Strasse 2, Darmstadt 64287, Germany

^cDarmstadt Graduate School of Energy Science and Engineering, TU Darmstadt, Jovanka-Bontschits-Strasse 2, Darmstadt 64287, Germany

^dGraduate School of Computational Engineering, TU Darmstadt, Dolivostrasse 15, Darmstadt 64293, Germany

^eThermodynamik, Hochschule Darmstadt, Haardtring 100, Darmstadt 64295, Germany

^fDivision of Fluid Mechanics, Department of Energy Sciences, Lund University, Lund SE 22100, Sweden

^gInstitute for Combustion Technology, RWTH Aachen University, Templergraben 64, Aachen 52056, Germany

^hDepartment of Mechanical Engineering, Sogang University, Sinsu-dong, Mapu-gu, Seoul 121-742, Republic of Korea

ⁱInstitute for Combustion and Gasdynamics (IVG), Chair for Fluid Dynamics, University of Duisburg-Essen, Carl-Benz Strasse 199, Duisburg 47048, Germany

^jDepartment of Mechanics, Royal Institute of Technology, SE 10044 Stockholm, Sweden

24

Experimental:

F. Seffrin, F. Fuest, D.A. Geyer, Combust. Flame 157 (2010) 384-396.

B. Böhm, J.K. Frank, A. Dreizler, Proc. Combust. Inst. 33 (2011) 1583-1590.

G. Kuenne, F. Seffrin, F. Fuest, T. Stahler, A. Ketelheun, D. Geyer, J. Janicka, A. Dreizler, Combust. Flame 159 (2012) 2669-2689.

Numerical:

G. Kuenne, F. Seffrin, F. Fuest, T. Stahler, A. Ketelheun, D. Geyer, J. Janicka, A. Dreizler, Combust. Flame 159 (2012) 2669-2689.

F. Cavallo Marincola, T. Ma, A. Kempf, Proc. Combust. Inst. 34 (1) (2013) 1307–1315.

A. Ketelheun, G. Kuenne, J. Janicka, Flow Turbul. Combust. 91 (2013) 867–893.

P. Trisjono, K. Kleinheinz, H. Pitsch, S. Kang, Flow Turbul. Combust. 92 (1-2) (2014) 201–235.

R. Mercier, P. Auzillon, V. Moureau, N. Darabiha, O. Gicquel, D. Veynante, B. Fiorina, Flow Turbul. Combust. 93 (2) (2014) 349–381.

G. Kuenne, M. Euler, A. Ketelheun, A. Avdić, A. Dreizler, J. Janicka, Z. Phys. Chem. 229 (2015) 643-662.

B. Fiorina, R. Mercier, G. Kuenne, A. Ketelheun, A. Avdić, J. Janicka, D. Geyer, A. Dreizler, E. Alenius, C. Duwig, P. Trisjono, K. Kleinheinz, S. Kang, H. Pitsch, F. Proch, F. Cavallo Marincola, A. M. Kempf, Combust. Flame 162 (2015) 4264-4282.

A. Avdić, G. Kuenne, F. di Mare, J. Janicka, Combust. Flame (2016), in press, doi:10.1016/j.combustflame.2016.06.015

Cambridge stratified flame series (SwB)

Cambridge/Sandia: M. Sweeney, S. Hochgreb, M. Dunn, R. Barlow

EM2C Paris: R. Mercier, B. Fiorina

CORIA-CNRS INSA Rouen: S. Nambully, P. Domingo, L. Vervisch

Imperial College London: S. Navarro Martinez, T. Brauner, W. P. Jones, A. J. Marquis

Hanyang University: S. Jeon, T. Kim, Y. Kim

Duisburg-Essen University: F. Proch, A. Kempf

Smaller than TSF burner

Simplified geometry compared to TSF (no chamfer)

Central bluff-body: Flame stabilization by recirculation

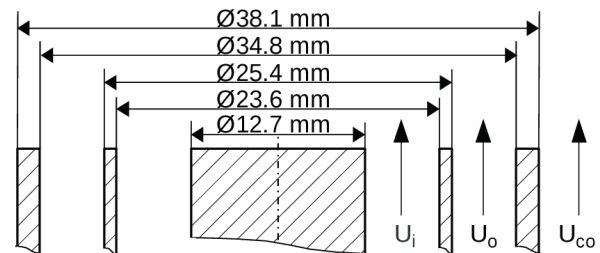
Temperature/Species: Raman/Rayleigh, Sweeney et al. CNF 2012

Velocity: PIV/LDA, Zhou et al. CNF 2013

Stratification ratio up to 3

Shear

Also swirled configurations



Case	U_i (m/s)	U_o (m/s)	U_{co} (m/s)	T (K)	ϕ_i (-)	ϕ_o (-)	ϕ_{co} (-)
SwB1	8.31	18.7	0.4	295	0.75	0.75	0
SwB5	8.31	18.7	0.4	295	1.0	0.5	0
SwB9	8.31	18.7	0.4	295	1.125	0.375	0

27

Flame structure experiment

Figures by Sweeney et al. CNF 2012, comparison by Kamal et al. CNF 2015

SwB1



SwB5



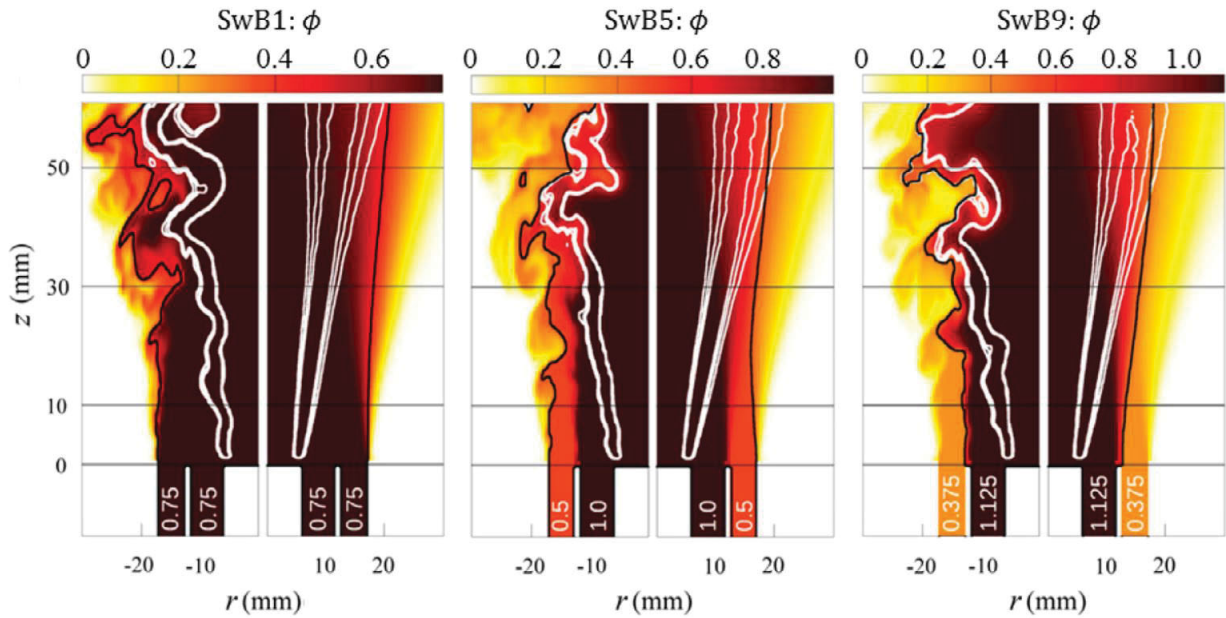
SwB9



28

Flame structure simulation

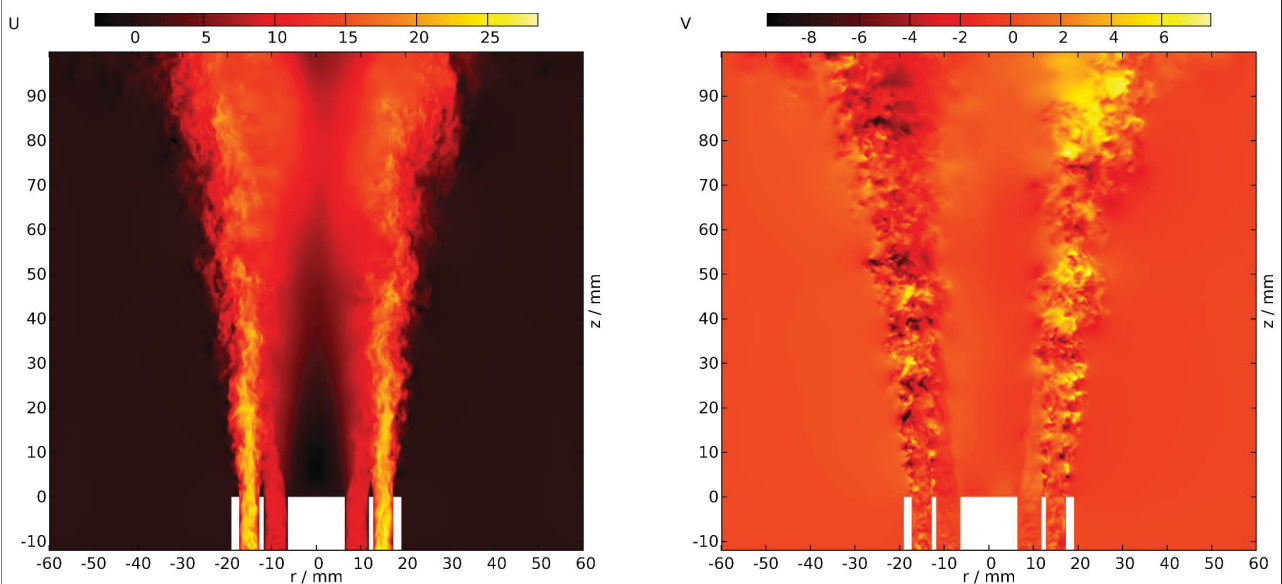
Figures by Proch&Kempf CNF 2014, comparison by Kamal et al. CNF 2015



29

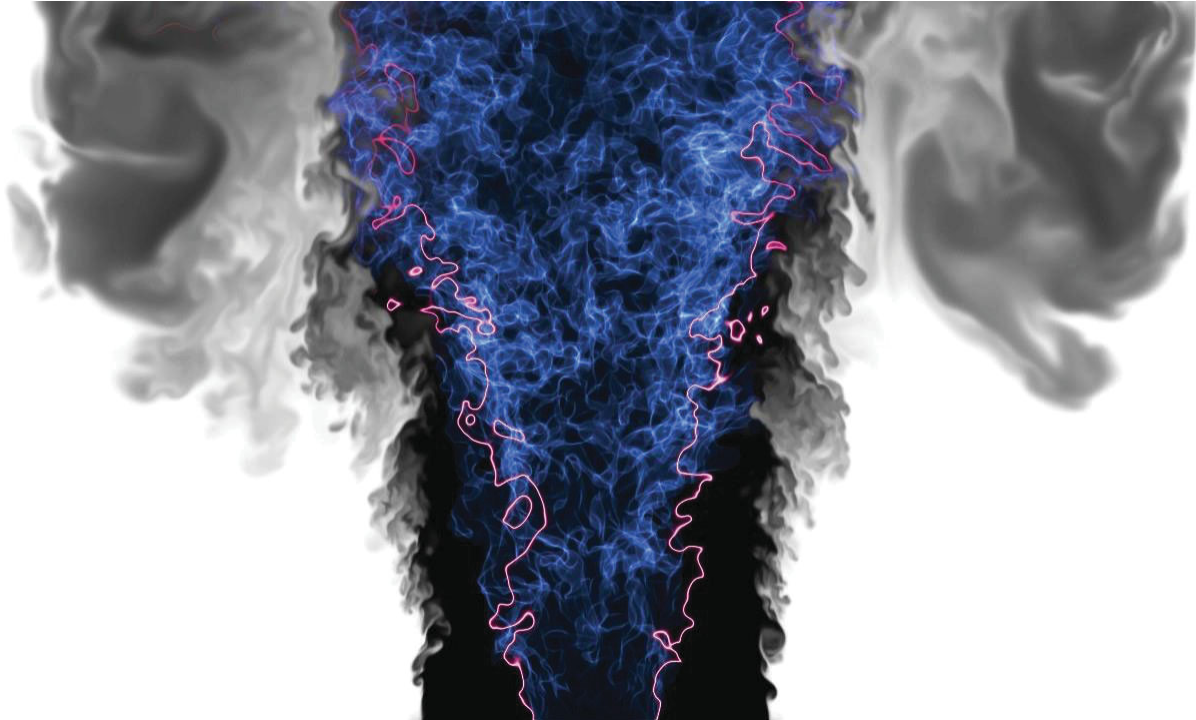
Axial and radial velocity component

SwB1: Flame-resolved PFGM simulation by Proch et al., submitted to CNF



30

SwB1: Flame-resolved PFGM simulation by Proch et al., submitted to CNF

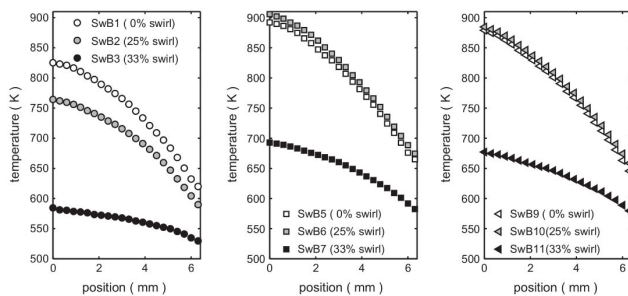


31

Effect of Heat Losses

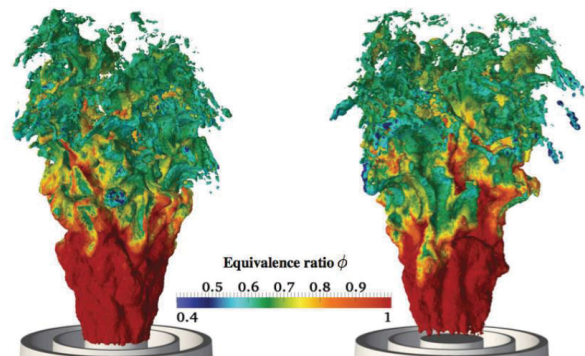
Effect of heat loss much smaller than for TSF
 Very moderate effect on flame position and dynamics
 Peak temperature is affected (Mercier et al., PCI 2015)
 Measurements available (Euler et al., CNF 2014)

Measurements by Euler et al.:



LES by Mercier et al., SwB5:

← adiabatic | non-adiabatic →



32

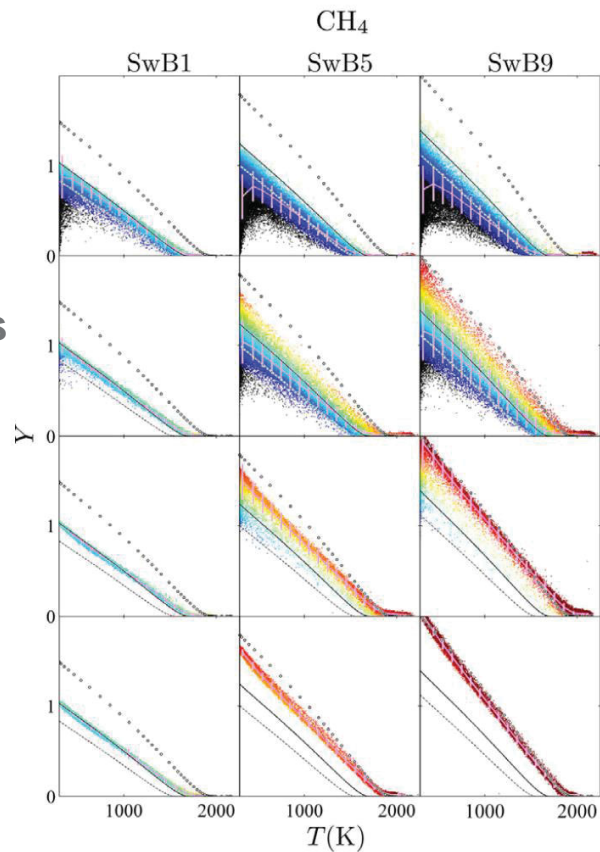
Local flame structure CH₄ unconditioned

Kamal et al. investigated local flame structure by conditional statistics (CNF 2015 + CNF 2016)

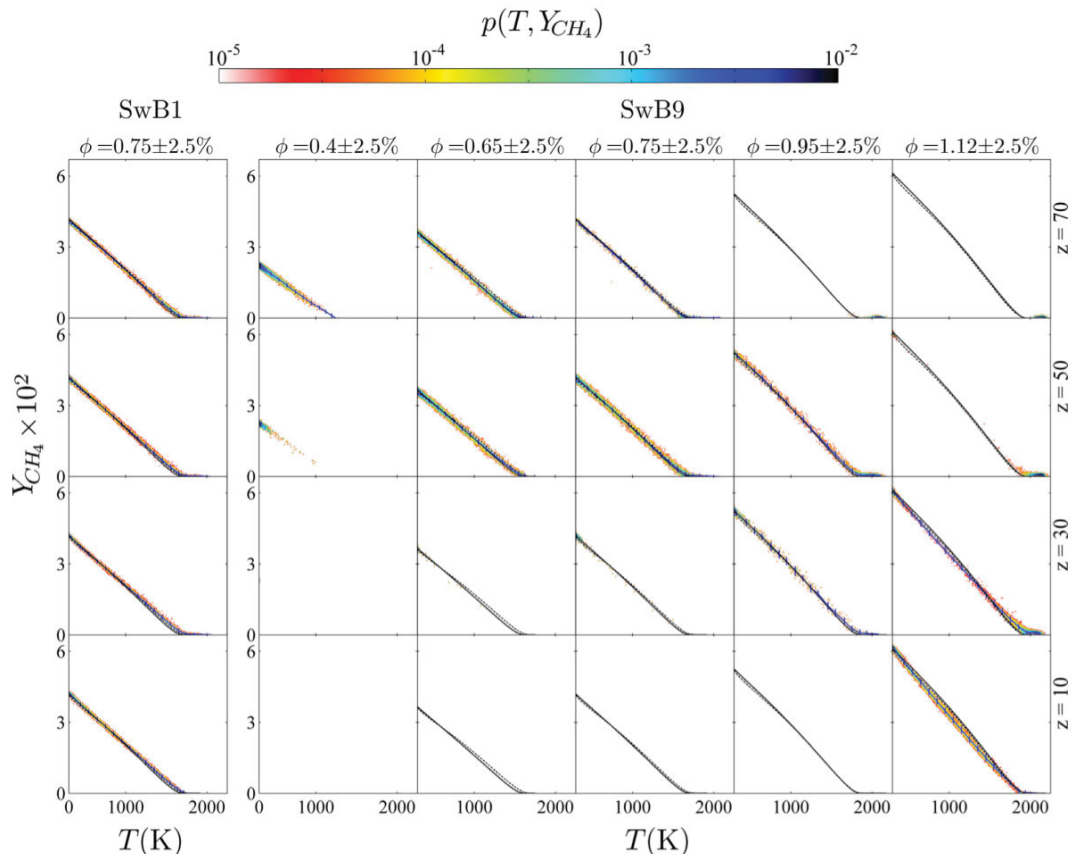
They investigated scatter plots of major species mass fraction vs. temperature

The unconditioned plots show large scatter

If the plots are conditioned on the local equivalence ratio, good agreement with laminar flame results with small scatter



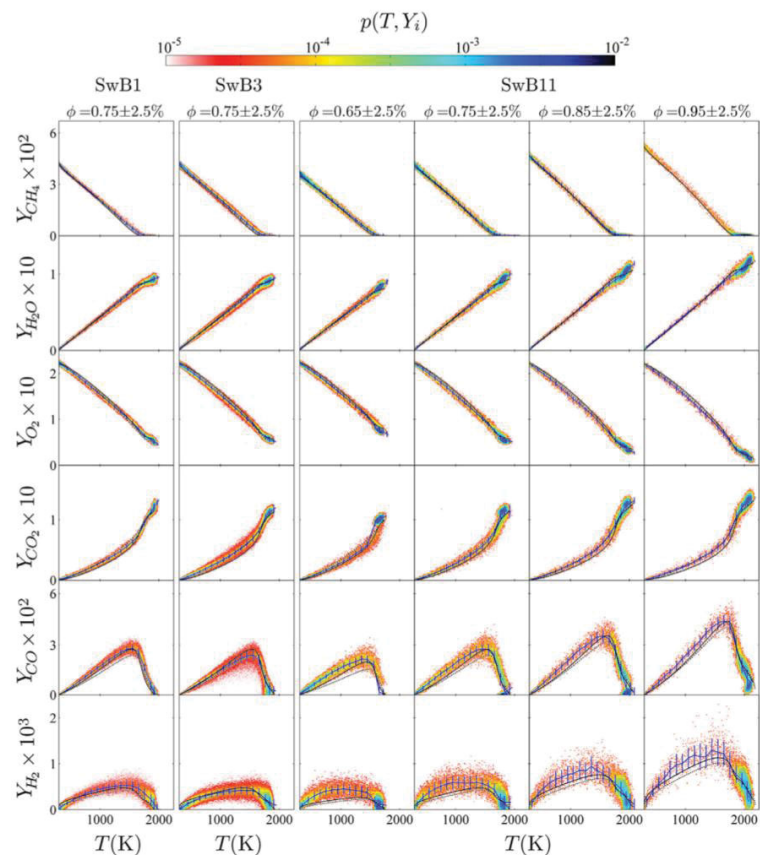
Local flame structure CH₄ conditioned



Local flame structure swirled case

This also applied for swirled cases, deviations are a bit larger due to larger local equivalence ratio gradients

This potentially explains why the stratified flame structure can be recovered well by an ensemble of premixed flamelets with different equivalence ratios



Comparison of PDFs

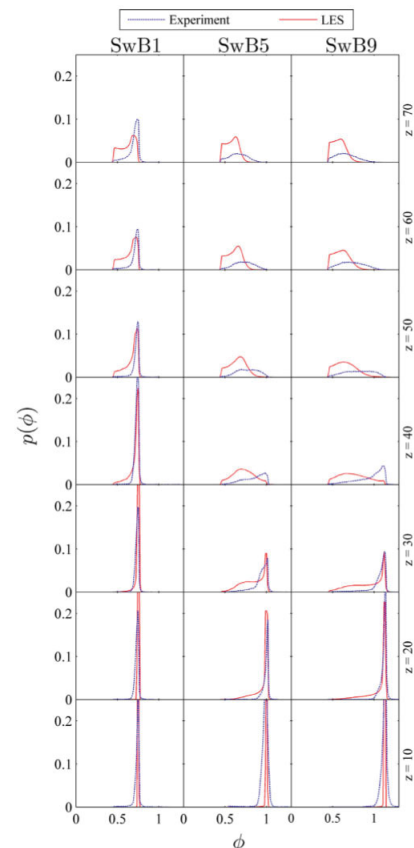
How to compare simulation and experiment beyond temporal statistics?

Kamal et al. (CNF 2015) presented comparison of equivalence ratio PDFs conditioned on burner distance

LES results from Proch&Kempf (CNF 2014)

Similar PDF shapes, especially for premixed case SwB1

More deviations for stratified cases, PDFs from experiment are broader in near-burner region



W P Jones

Department of Mechanical Engineering

Imperial College London

Exhibition Road

London SW7 2AZ

TNF

28-30 July 2016

Stochastic Field Solution Method

UNIVERSITÄT
DUISBURG
ESSEN

Offen im Denken

Represent PDF by N stochastic fields

Ito formulation

$\xi_\alpha^n(\mathbf{x}, t)$ is advanced from t to $t + dt$ according to:

$$\begin{aligned} \bar{\rho} d \xi_\alpha^n = & -\bar{\rho} \tilde{u}_i \frac{\partial \xi_\alpha^n}{\partial x_i} dt + \frac{\partial}{\partial x_i} \left[\left(\frac{\mu}{\sigma} + \frac{\mu_{sgs}}{\sigma_{sgs}} \right) \frac{\partial \xi_\alpha^n}{\partial x_i} \right] dt \\ & + \left(2 \bar{\rho} \frac{\mu_{sgs}}{\sigma_{sgs}} \right)^{1/2} \frac{\partial \xi_\alpha^n}{\partial x_i} dW_i^n(t) - 0.5 C_d \bar{\rho} \tau_{sgs}^{-1} (\xi_\alpha^n - \tilde{\phi}_\alpha^n) dt + \bar{\rho} \dot{\omega}_\alpha^n (\xi_\alpha^n) dt \end{aligned}$$

where $1 \leq n \leq N$, $dW_i^n \approx \eta_i^n \sqrt{dt}$

and η_i^n is a $[-1, +1]$ dichotomic vector

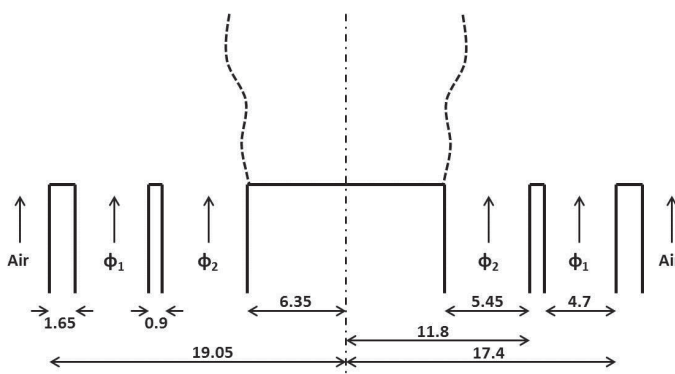
Simulated Flames

- Auto-ignition – Hydrogen and n-heptane
 - Lifted flames : Cabre - Hydrogen & methane
 - Forced ignition: methane,
 - Local extinction – Sandia Flames D, E & F
 - Premixed swirl burner (Darmstadt)
 - Darmstadt stratified flame
 - Lean burn (natural gas) industrial combustor
 - Premixed baffle stabilised flame
 - Cambridge/Sandia stratified flames
 - Methanol Spray flames
 - Axisymmetric swirl combustor
 - FAUGA Combustor,
 - Sector combustor
 - Genrig combustor
- } Kerosene spray

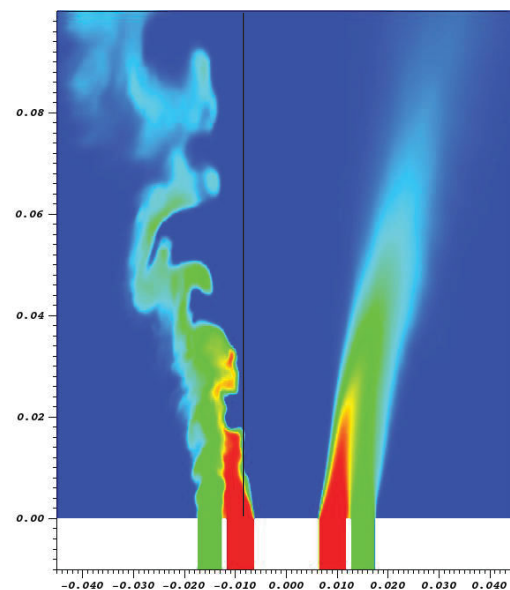
© Imperial College London

Stratified Premixed Turbulent Flames

- The Cambridge Stratified Swirl Burner



U_i (m/s)	U_o (m/s)	U_{co} (m/s)	Λ (mm)	Re_i	Re_o	ϕ_g
8.7	18.7	0.4	1.9	6000	11500	0.75



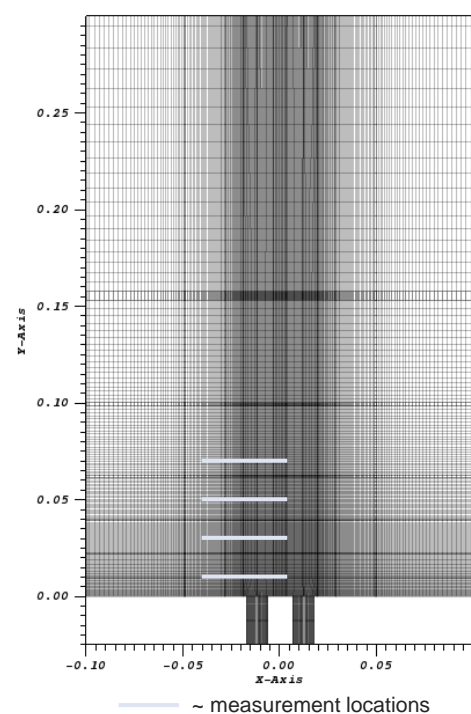
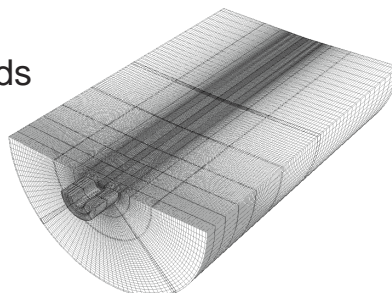
Cambridge Stratified Swirl Burner

Flame	SR = ϕ_2 / ϕ_1	Swirl Flow Ratio
SwB1	0.75/0.75 = 1.0	0.00
SwB2	0.75/0.75 = 1.0	0.25
SwB3	0.75/0.75 = 1.0	0.33
SwB5	1.00/0.50 = 2.0	0.00
SwB6	1.00/0.50 = 2.0	0.25
SwB7	1.00/0.50 = 2.0	0.33
SwB9	1.13/0.38 = 3.0	0.00
SwB10	1.13/0.38 = 3.0	0.25
SwB11	1.13/0.38 = 3.0	0.33

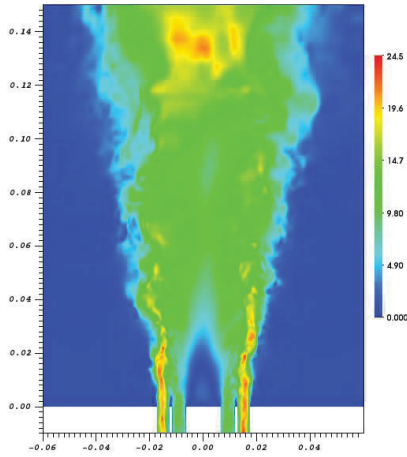
Brauner, T., Jones, W.P., and Marquis, A.J., LES of a Stratified Swirl Burner using a Sub-Grid PDF Approach, Flow, Turbulence and Combustion. 96, 965-985 (2016)

Computational Setup

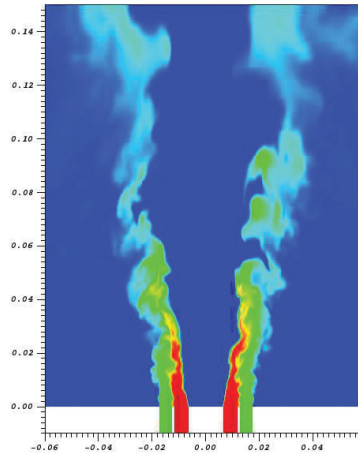
- BOFFIN-LES
- 13.5M cells & 610 blocks
3.7M cells & 163 blocks
0.8M cells & 27 blocks
- Synthetic turbulence generation
- Dynamic Smagorinsky model
- Constant Prandtl/Schmidt number = 0.7
- Reduced GRI 3.0 with 19 species and 15 reactions
- 8 stochastic fields



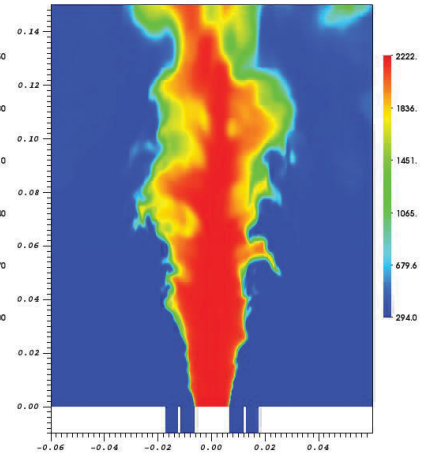
Velocity Magnitude



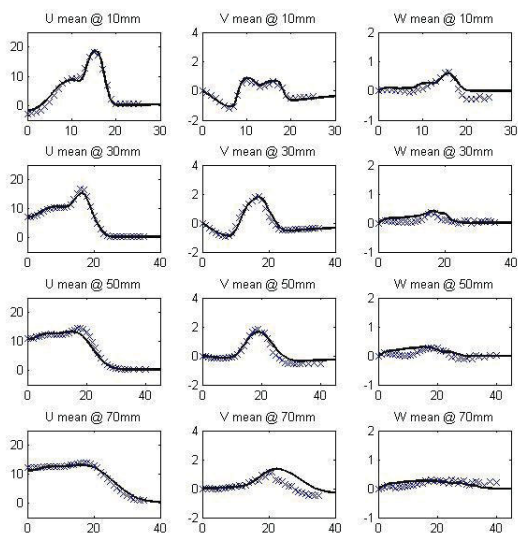
Methane



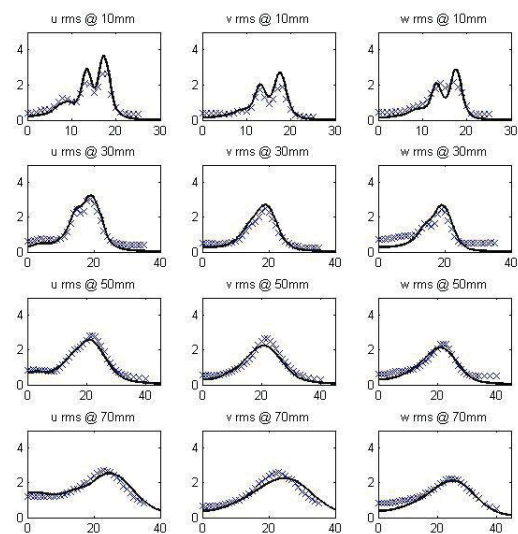
Temperature



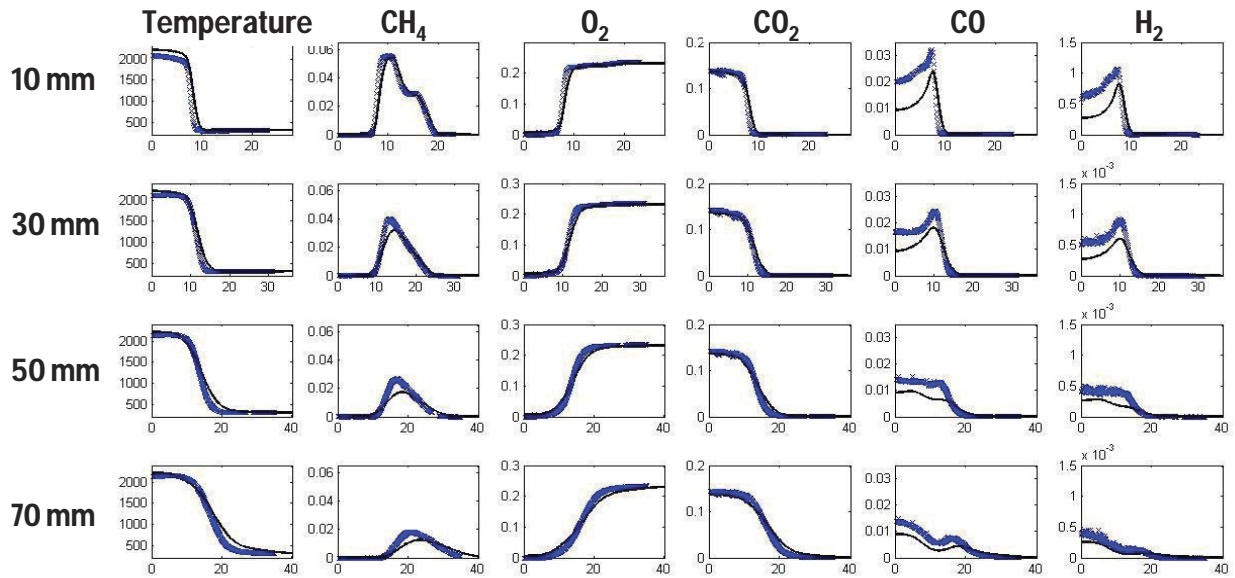
Mean Velocities



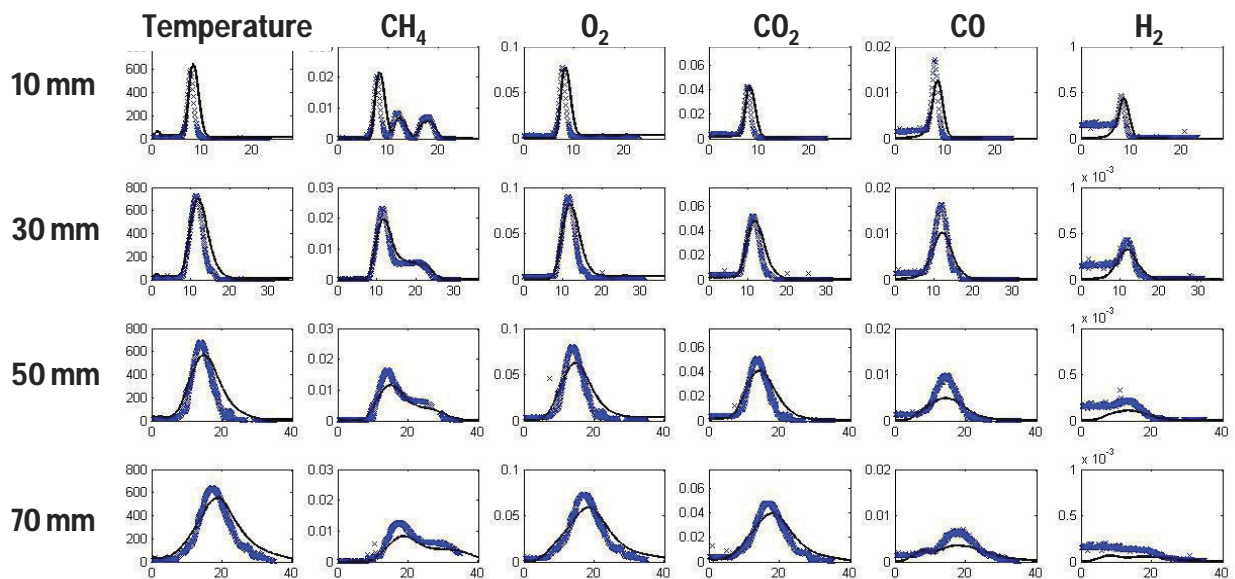
RMS Velocities



Results – SwB5 Scalars - Mean

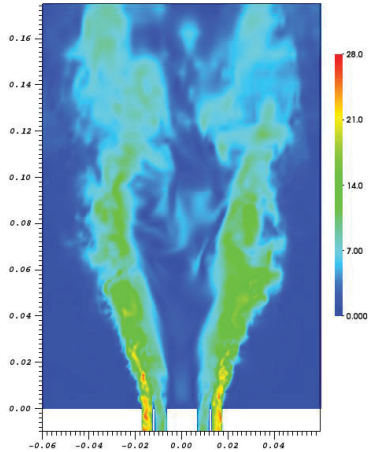


Results – SwB5 Scalars - RMS

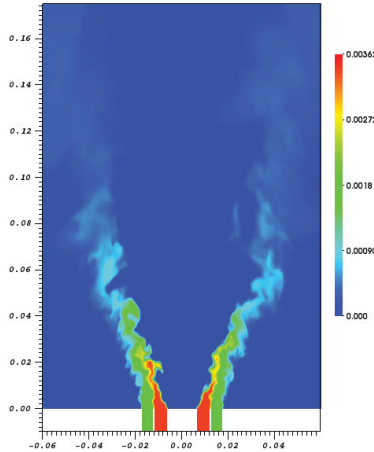


Results - SwB7

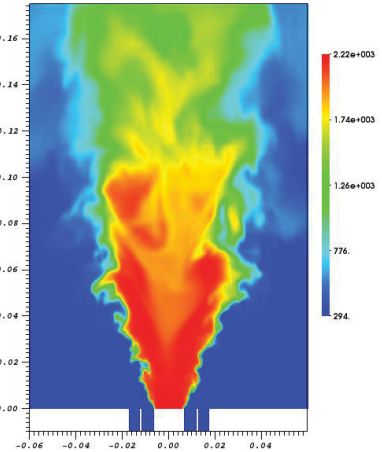
Velocity Magnitude



Methane

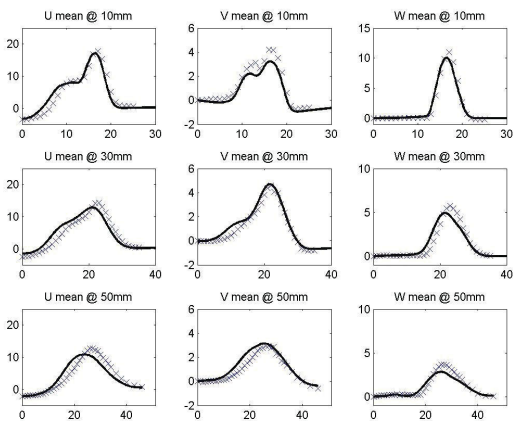


Temperature

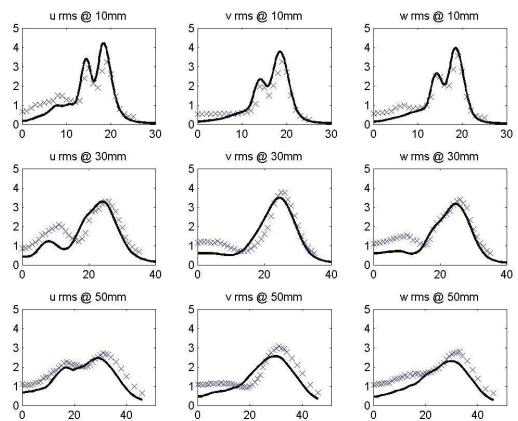


Results – SwB7 Velocities

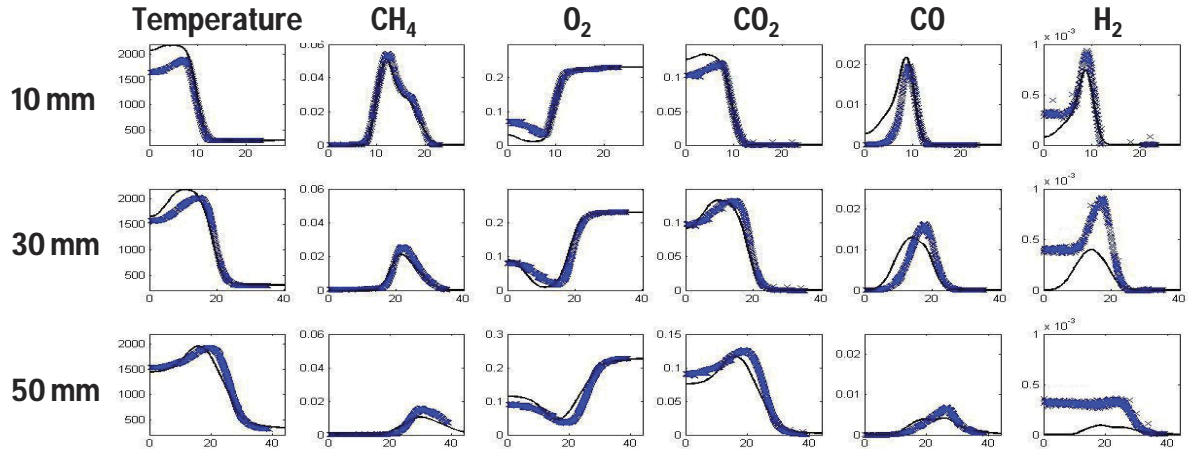
Mean Velocities



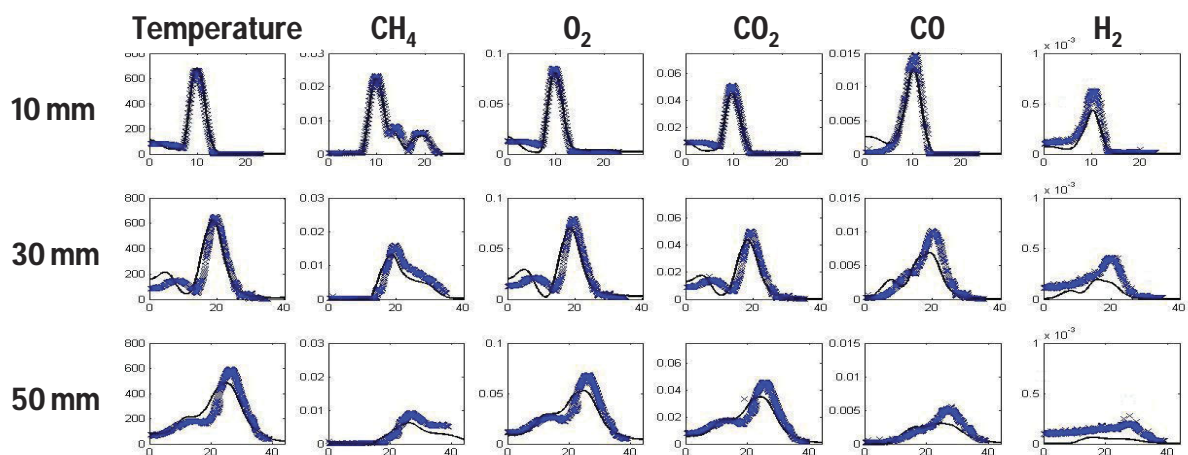
RMS Velocities



Results – SwB7 Scalars - Mean

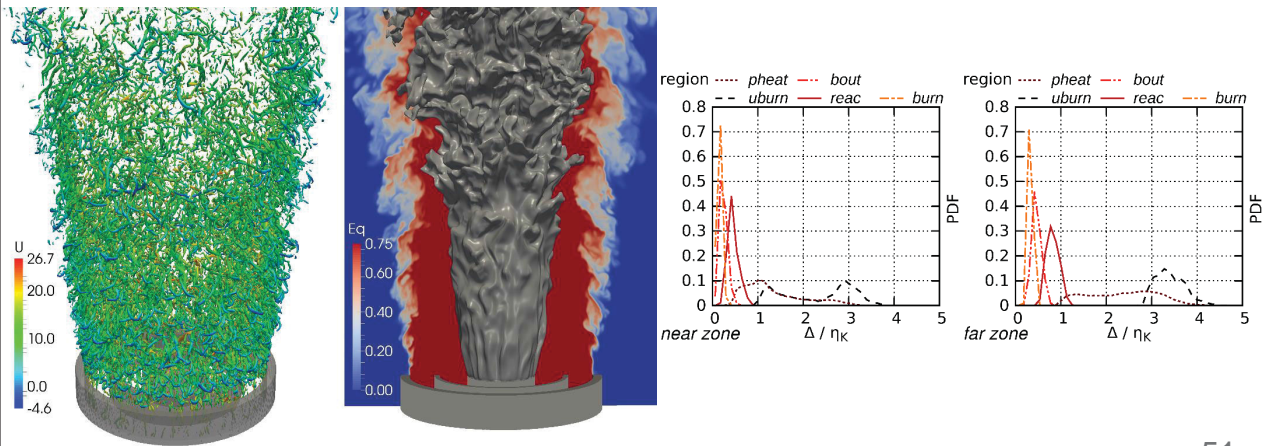


Results – SwB7 Scalars - RMS



Flame resolved simulation SwB1

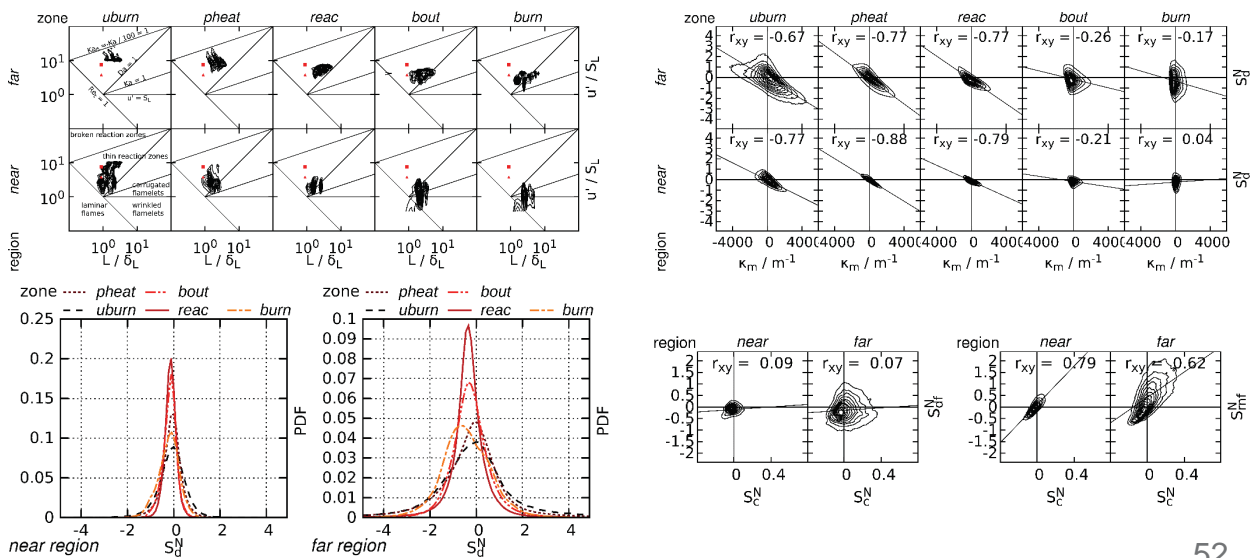
Resolution 100 μm , 1.6 billion cells
 10 M cores hours on 64,000 processors (JUQUEEN)
 Well sampled statistics (10 flow-tr. times inner stream)
 PFGM combustion model, progress variable resolved
 Submitted to CNF, database available to other groups



51

Flame resolved simulation SwB1

Analysis of the turbulent flame structure with
 conditioned PDFs and JPDFs and flamelet averages
 Conditioning on burner distance and reaction
 progress, as turbulence-flame interaction changes



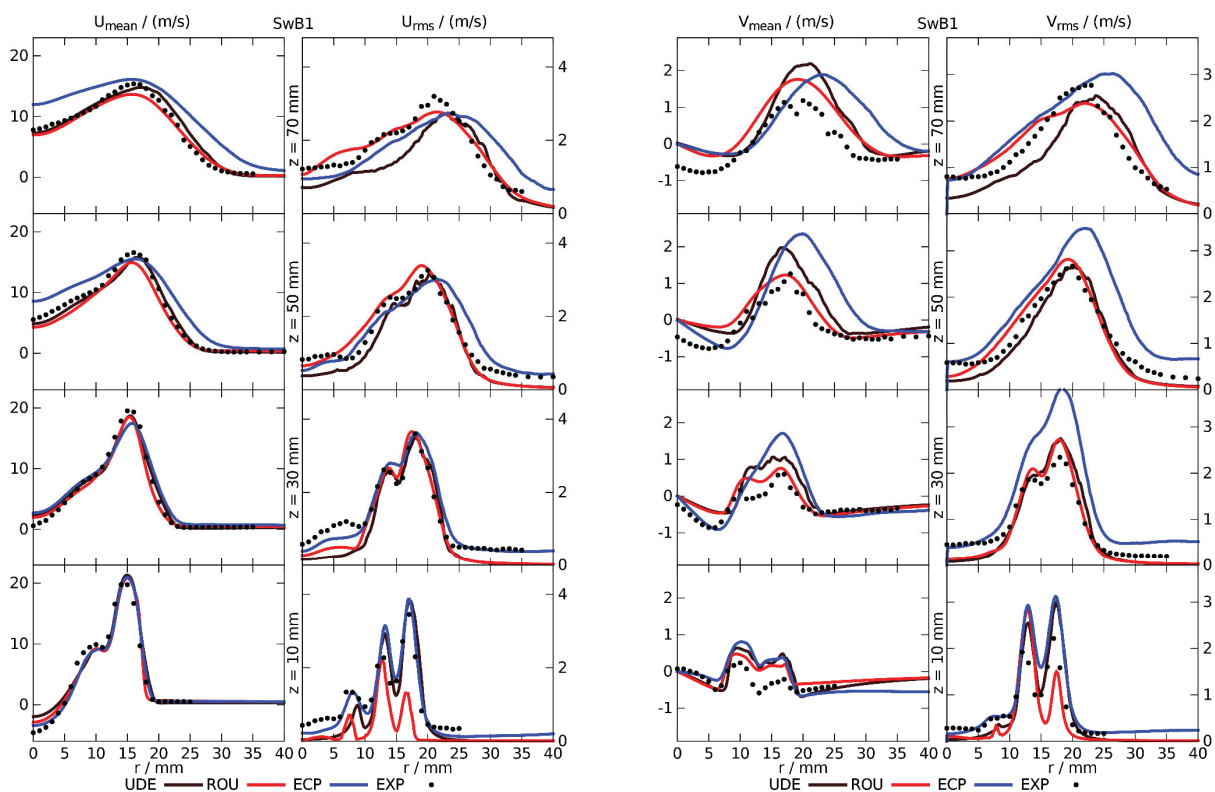
52

Simulation results - Contributions

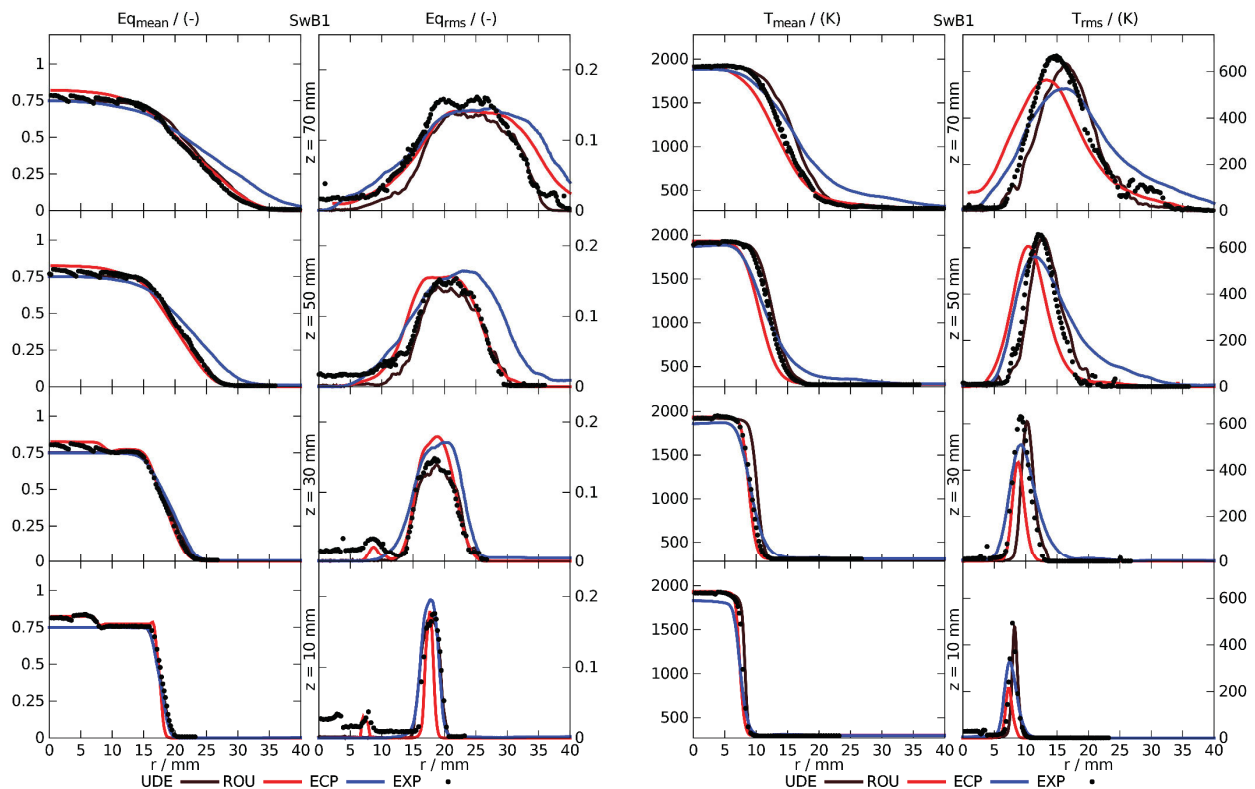
Contributor	EM2C, École Central, Paris R. Mercier, B. Fiorina	Universität Duisburg-Essen Proch, A. Kempf	INSA de Rouen, CORIA Nambully, Moureau, Domingo, Vervisch	Hanyang, Seoul, KR Jeon, Kim, Kim	Imperial College London Navarro Martinez
Cases	SwB1, SwB5	SwB1 , SwB5	SwB1, SwB5	SwB5, SwB9	SwB5
Turbulence model	Dynamic Germano	Sigma (Nicoud et al.)	Dynamic Germano	RANS k-ε	LES
Combustion model	F-TACLES	SwB1: FGM SwB5: ATF / FGM	Filtered Laminar Flame PDF FLF-PDF	Three-Environment PDF Model, IEM	Stochastic fields
Code	YALES2	PsiPhi	YALES2	MAST	BOFFIN
Schemes	O(4)	Cartesian, O(2)	O(4)	O(2)	O(2)
Domain/grid	unstructured SwB1: 13M SwB5: 30M	structured SwB1: 1600M SwB5: 103.2M	unstructured 50 M	unstructured, axisymmetric	wall-fitted Cartesian
Cost (Core _h)	SwB1: 5k SwB5: 15k (SGI-Altix)	SwB1: 10,000k (Blue Gene/Q) SwB5: 50K (CRAY XE6m)	1,300k (Blue Gene/P)	0.85k	-

53

Simulation results – SwB1 velocity



54



55

Publications

Experimental:

- M.S. Sweeney, S. Hochgreb, M.J. Dunn, R.S. Barlow, *Combust. Flame* 159 (2012) 2896–2911.
 M.S. Sweeney, S. Hochgreb, M.J. Dunn, R.S. Barlow, *Combust. Flame* 159 (2012) 2912–2929.
 R. Zhou, S. Balusamy, M. S. Sweeney, R. S. Barlow, S. Hochgreb, *Combust. Flame* 160 (2013) 2017–2028.
 M. Euler, R. Zhou, S. Hochgreb, A. Dreizler, *Combust. Flame* 161 (2014) 2842–2848.
 M.M. Kamal, R. Zhou, S. Balusamy, S. Hochgreb, *Proc. Combust. Inst.* 35 (2015) 3802–3811.
 M.M. Kamal, R.S. Barlow, S. Hochgreb, *Combust. Flame* 162 (2015) 3896–3913.
 M.M. Kamal, R.S. Barlow, S. Hochgreb, *Combust. Flame* 166 (2016) 76–79.

Numerical:

- S. Nambully, P. Domingo, V. Moureau, L. Vervisch, *Combust. Flame* 161 (2014) 1756–1774.
 S. Nambully, P. Domingo, V. Moureau, L. Vervisch, *Combust. Flame* 161 (2014) 1775–1791.
 F. Proch, A. M. Kempf, *Combust. Flame* 161 (2014) 2627–2646.
 R. Mercier, T. Schmitt, D. Veynante, B. Fiorina, *Proc. Combust. Inst.* 35 (2015) 1259–1267.
 T. Brauner, W. P. Jones, A. J. Marquis, *Flow Turbul. Combust.* (2016) 1–21.

56

Stratified flames: established + challenging test cases

Darmstadt flame fourth time TNF target

- Inclusion of heat loss is important for correct flame propagation
- Overview paper published in CNF, contributions from five groups
- New measurements and simulations on heat loss effect
- New measurements presented with hydrogen addition
- New simulations presented with new combustion models

Cambridge/Sandia flame third time TNF target

- No large effect of heat loss on flame propagation
- Temperature measurements for the bluff-body available
- New experimental analysis presented, focus on local flame structure and conditional analysis
- New approaches of comparing simulation and experiment
- New simulations presented, flame resolved results are available

57

Thank you for your attention!

Piloted jet flames with inhomogeneous inlets: model comparisons

Coordinator: Benoît Fiorina

The objective of the session was to compare recent simulations of the Sydney piloted burner. The burner geometry consists of two concentric tubes surrounded by a pilot annulus. It is centered in a wind tunnel supplying a co-flowing air stream at fixed velocity. A set of experimental data has been provided by Sydney university and Sandia Laboratory. In the configuration studied in the workshop, the central tube is fed with fuel whereas air is flowing through the outer tube. The air co-flow velocity is fixed at 15 m/s. The central pipe can be recessed upstream of the burner exit plane, varying therefore the mixing between fuel and air. For sufficiently large recession distance (L_r) of the inner tube respect to the burner exit plane, the mixture is nearly homogeneous at the burner exit, while intermediate recession distances lead to equivalence ratio inhomogeneities.

This experimental configuration, conducive to multiple flame structures, is extremely interesting for model validation. It is indeed representative of practical combustion chambers, which may exhibit strong equivalence ratio heterogeneities, promoting the development of mixed combustion regimes. The Sydney burner constitutes a challenging target for turbulent combustion models, which have in general their own flame affinity.

Three configurations have been selected: the first one (FJ200-5GP-Lr300-59) features a homogeneous composition in equivalence ratio at the burner exit plane ($L_r = 300$ mm), while the two others (FJ20-5GP-Lr75-80 and FJ20-5GP-Lr75-57) exhibit inhomogeneous mixture fraction profiles ($L_r = 75$ mm). Note that FJ200 refers to the condition where the fuel is fed from the inner tube and the air is fed through the outer tube, with a volumetric air to fuel ratio V_A/V_F equal to 2. The label 5GP corresponds to the five-gas pilot mixture, which is a stoichiometric mixture of acetylene, hydrogen, oxygen, nitrogen and carbon dioxide. The pilot mixture has been designed to have the same C/H ratio and adiabatic flame temperature as a stoichiometric methane/air mixture. 59, 57 and 80 are respectively the bulk jet velocities in m/s.

Fifteen teams were involved in the simulations: RWTH Aachen, Hangsu University & Karlsruhe Institute for Technology, Caltech, Purdue University, EM2C-CNRS at CentraleSupélec, Duisburg-Essen University, Princeton University, Zhejiang University, Stanford University, University of Munich, Technical University of Freiberg, The University of Sydney, Hanyang University, University of Michigan and KTH University.

The prescription of the Boundary Conditions is a critical issue in this configuration, especially for the inhomogenous case where mixture fraction gradients are expected to influence the turbulent flame structure. Non-reactive LES of the mixing process between fuel and air in the mixing tube have been performed by Princeton University. Two configurations have been investigated that correspond to $L_r = 300$ mm and $L_r = 75$ mm distances, respectively. Unsteady solutions of these simulations constitute a numerical database shared with the TNF workshop community. Six groups used this numerical database to prescribe the main inlet boundary conditions (in terms of mixing and velocity), whereas the others developed their own strategy.

The LES turbulent combustion modeling strategies followed by numerical teams differ by:

- the chemistry description, where both tabulated and reduced chemistry have been used. Tabulated chemistry methods are either based on premixed, non-premixed, or hybrid flamelets. Reduced chemistry employs mechanisms of different sizes (from 4 to 30 species).
- the turbulent combustion model, where modeling efforts may focus on different phenomena

such as the turbulent flame propagation or interactions between turbulent mixing and chemical reactions. Many different turbulent combustion models have been used such as presumed and transport PDF based models, thickened or filtered flame models, level set approaches, etc.

A model classification has been conducted, suggesting that eight models exhibit affinities for turbulent diffusion flames, three for turbulent premixed flames, and five for hybrid combustion regimes. An extensive comparison between numerical simulations has been performed on the three selected reactive configurations including i) mean and RMS radial profiles of axial velocity, temperature, mixture fraction, and CO mass fraction ii) scatter plots of temperature at different axial positions.

Except for the first radial profiles close to the burner exit, significant differences are observed between simulations and experiments. In particular, most of the computations do not capture the mixing between fuel and air, which makes the analysis of the combustion model difficult. A very large scattering is observed for CO, for which the production rate is very sensitive to the combustion regime.

Analysis and conclusions have to be conducted with great care as most of numerical data are preliminary. This exercise is however very promising, mainly for two reasons. First, the configuration is challenging and should break the models, especially regarding the prediction of CO formation. Second, as many groups are involved in the comparison, results can be conditioned by the type of model. For instance, it is possible to verify if several simulations conducted with turbulent combustion model dedicated to premixed flames will draw similar conclusions.

To go further into the analysis, most of the numerical results have to be consolidated. In particular, an improvement of the mixture fraction field is mandatory prior analyzing the turbulent combustion model impact. Ideally, mesh independency studies for mixing and velocity under non-reactive conditions should be conducted. To limit differences between computational set-up, groups should use the same prescription of boundary conditions. Complimentary velocity and mixture fraction measurements on cold configurations would be, in this context, very useful.

Piloted turbulent jet flame with inhomogeneous inlets

Model comparisons

Giampaolo Maio, Mélody Cailler, Benoît Fiorina

EM2C - CNRS
CentraleSupélec
University of Paris Saclay

Andreas Kempf
Duisburg Essen University

TNF 13, Seoul, Korea, 2016

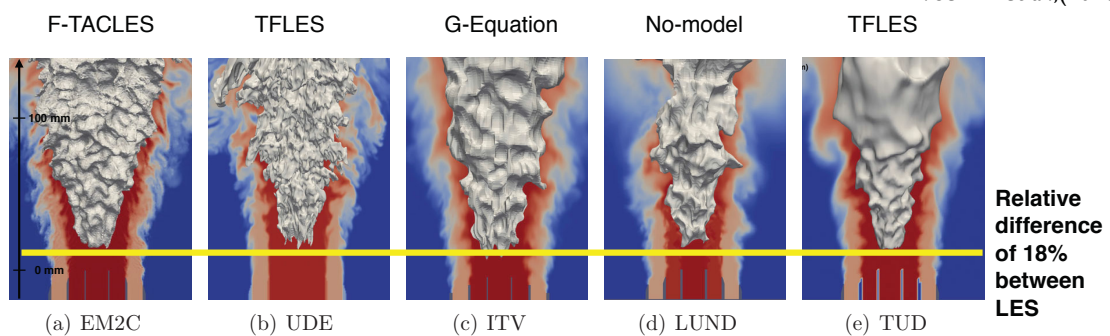
1

LES of premixed or weakly stratified flames

- Many LES combustion models have been designed to capture the flame propagation speed in homogenous or stratified fuel/air mixture:
 - Thickened Flame model for LES (Colin et al., 2000)
 - G-equation (Pitsch, 2005)
 - F-TACLES (Fiorina et al., 2010)
 - etc ...

Target flame for TNF 10-11-12: TSF-A (TU Darmstadt)

B. Böhm et al.,(2010)
F. Seffrin et al.,(2010)



Fiorina et al. Challenging modeling strategies for LES of non-adiabatic turbulent stratified combustion. Comb & Flame (2015)

2

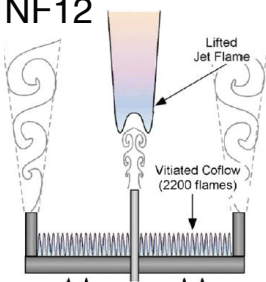
LES of non-premixed flames

- LES modeling objectives are to capture the competition between mixing and detailed chemistry that may cause ignition and extinctions events
- FPV model (Pierce and Moin, 2004; Ihme and Pitsch, 2005)
- MMC (Klimenko and Pope, 2003; Cleary and Klimenko, 2011)
- PDF Transport (Haworth 2010; Pope, 2015)
- etc.

Models challenged on non-premixed flames
TNF1 to TNF12



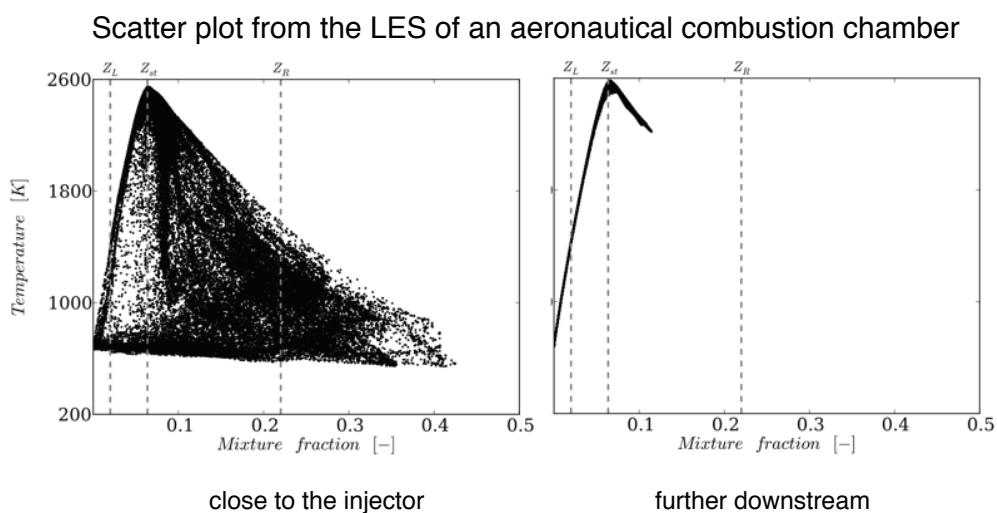
Sandia D - E flames
(Barlow et al. 1998)



Berkeley / Sydney JHC
(Cabra et al. 2002)

3

But life is not either premixed or non-premixed



4

Models have their own flame affinity:

- today all work on situation for which they have been designed to work
- how do they work on non-desirable situation?

Recent efforts in developing more general turbulent combustion model

- Reaction-diffusion manifolds, REDIM (Bykov and Maas, 2007)
- Multiple flamelet database (Nguyen et al. 2010; Franzelli et al. 2013)
- Flame index (Yamashita et al. 1996, Knudsen and Pitsch 2009)
- etc.

Need target flame configurations of practical applications:

Piloted Inhomogeneous Jet Flame Burner

5

Content

- Introduction and objectives
- Description of the experimental configuration
- Joined numerical study
 - Mixing tube computations for boundary conditions
 - Numerical set-up and models
 - Results analysis
 - Conclusions of the numerical study
- Influence of pilot flame parameters (T. Guiberti)
- Conclusions

6

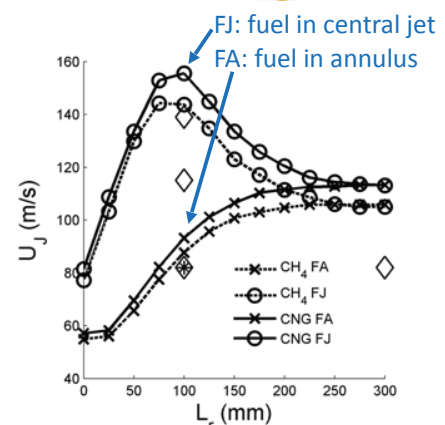
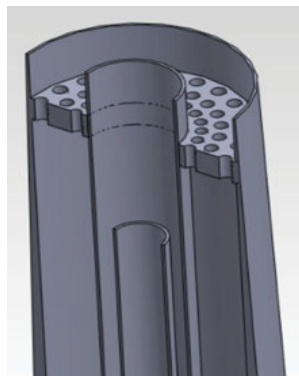
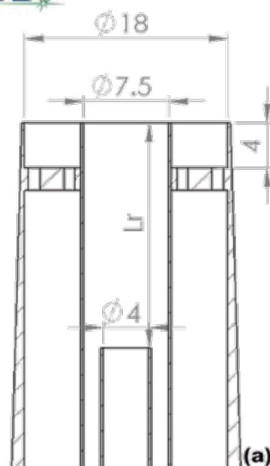
The Piloted Inhomogeneous Jet Flame Burner

S. Meares, A.R. Masri, *Combust. Flame* 161 (2014)

S. Meares, V.N. Prasad, G. Magnotti, R.S. Barlow, A.R. Masri, *Proc. Combust. Inst.* 35 (2015)

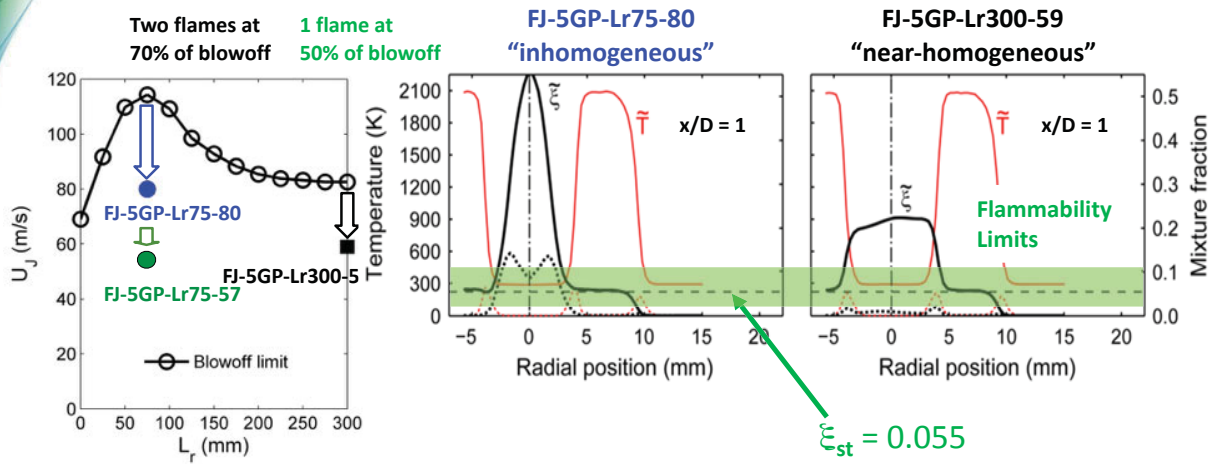
R.S. Barlow, S. Meares, G. Magnotti, H. Cutcher, A.R. Masri *Combust. Flame* 162 (2015)

Piloted Inhomogeneous Jet Flame Burner



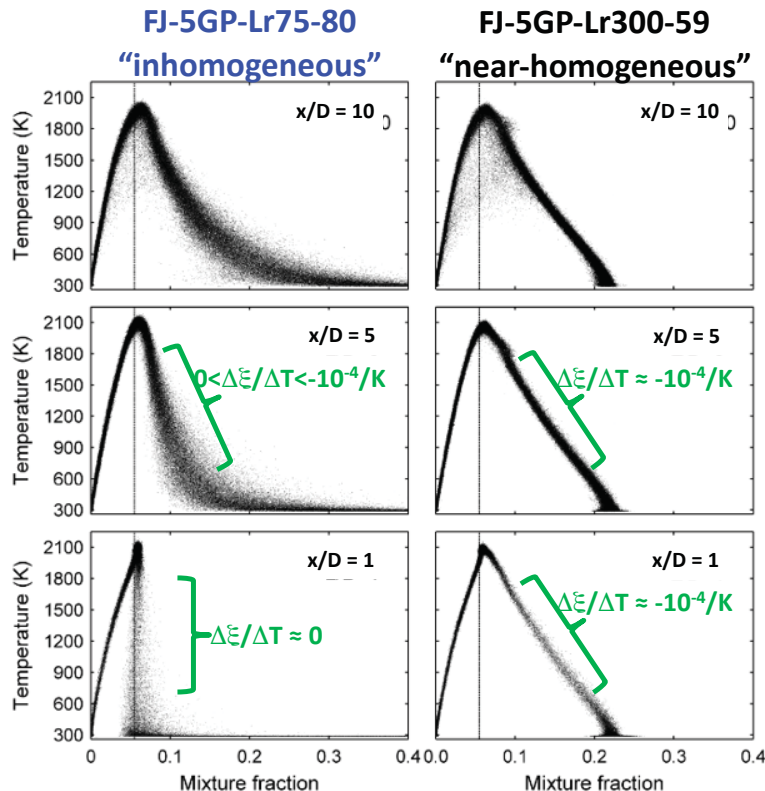
First flame series: air/fuel=2;
 $\phi=1$ pilot of C₂H₂/H₂/air, T_{ad}=2480 K

- Central 4-mm ID tube can be recessed by distance L_r
- Enhanced stability (~40% higher blowoff velocity for 75mm < L_r < 100mm)
- Multiple diagnostics: PIV, high-speed OH PLIF, Raman/Rayleigh/CO-LIF
 - S. Meares, A.R. Masri, *Combust. Flame* 161 (2014) 484-495
 - S. Meares, V.N. Prasad, G. Magnotti, R.S. Barlow, A.R. Masri, *Proc. Combust. Inst.* 35 (2015) 1477-1484



- Similar profiles of temperature and jet exit velocity (normalized)
- Very different profiles of mixture fraction near the burner exit ($x/D=1$)
- Mixture fraction, ξ , using Bilger's definition normalized to unity at 100% CH_4

T vs. Mixture Fraction



Joined numerical study: 5 groups for TNF12 and ...



Guido Kuenne, Anja Ketelheun, Amer Avdic, Johannes Janicka, Dirk Geyer, Andreas Dreizler



Philipp Trisjono, Konstantin Kleinheinz, Seongwon Kang and Heinz Pitsch



Emma Alenius, Christophe Duwig



Fabian Proch and Andreas Kempf



Renaud Mercier and Benoît Fiorina

11

... 15 groups for TNF13



Konstantin Kleinheinz and Heinz Pitsch



Qing wang, Han Wu and Matthias Ihme



Ping Wang and Ulrich Maas



Hagen Müller and Michael Pfitzner



Lukas Bischoff and Guillaume Blanquart



Pei Zhang and Haifeng Wang



Sebastian Popp and Christian Hasse



Bruce Perry, Michael Mueller



Matthew Cleary, Sebastian Galindo Lopez, Fatemeh Salehi and Assaad Masri



Yun Bai and Kun Luo



Namsu Kim and Yongmo Kim



Giampaolo Maio, Mélody Cailler, Renaud Mercier, Vincent Moureau and Benoît Fiorina



Malik Hassanaly and Venkat Raman



Martin Rieth, Fabian Proch and Andreas Kempf



Luis Cifuentes and Christophe Duwig

12

... 15 groups for TNF13



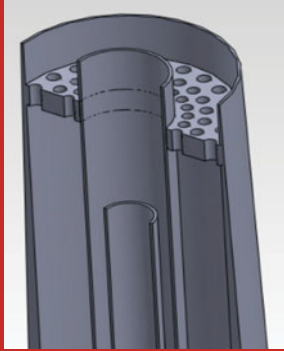
Konstantin Kleinheinz and Heinz Pitsch



Qing wang, Han Wu and Matthias Ihme



Boundary conditions for the main inlet ?



Michael
and
Sebastian
atemeh
d Masri
ongmo
and

Centra



Venkat Raman



Martin Rieth, Fabian Proch and Andreas Kemp



Luis Cifuentes and Christophe Duwig

13

Mixing Tube LES for the Sydney Inhomogeneous Inlet Burner

Bruce A. Perry, Michael E. Mueller



2016 TNF Workshop

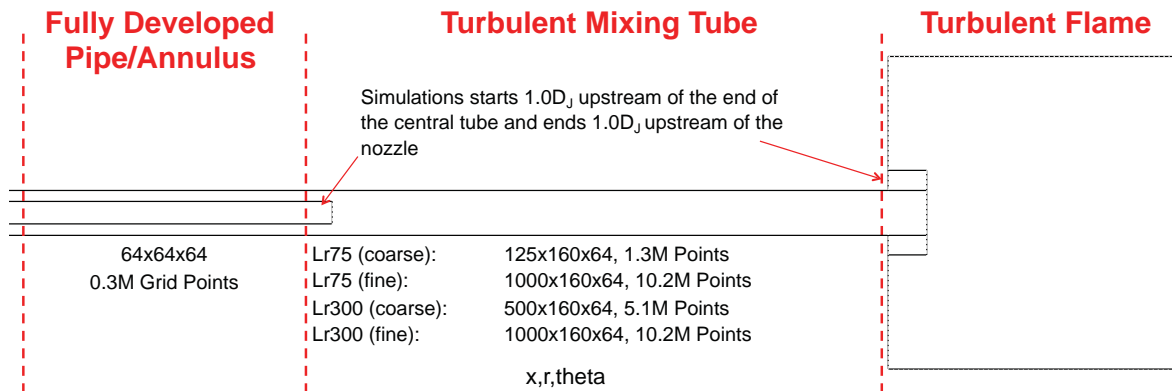


Computational Turbulent Reacting Flow Laboratory (CTRFL), Department of Mechanical and Aerospace Engineering, Princeton University

Numerical Setup



- LES solver: NGA¹ (low-Mach, structured, finite difference)
- Three domain approach: inflow boundary condition for the flame generated using two upstream simulations
- Grid: Uniform in x , stretched in r (Δr^+ @ wall = 0.6)



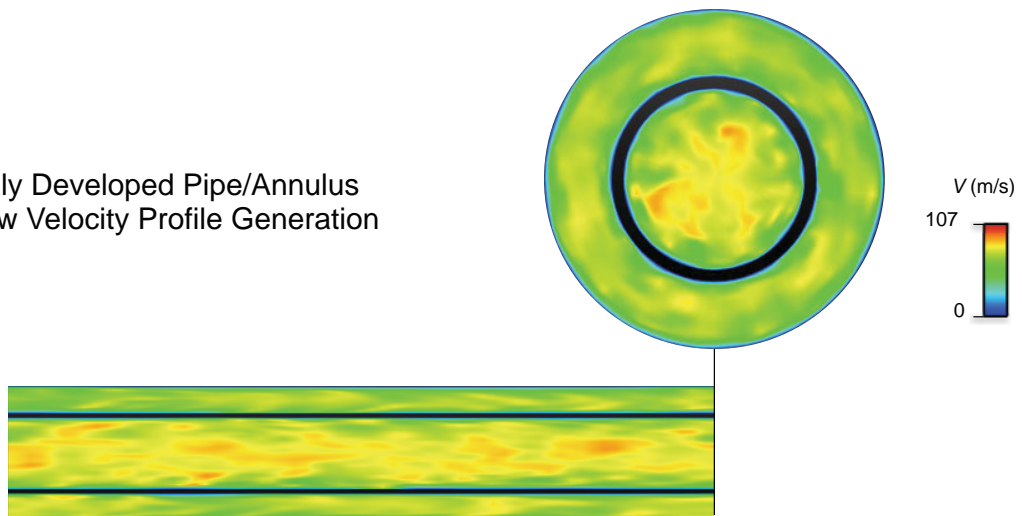
¹ O. Desjardins, G. Blanquart, G. Balarac, H. Pitsch. J. Comp. Phys., 227 (2008) 7125-7159

Three Domain Approach



Pipe/Annulus → Turbulent Mixing Tube → Turbulent Flame

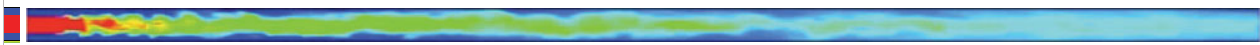
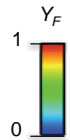
Fully Developed Pipe/Annulus
Inflow Velocity Profile Generation



Three Domain Approach



Pipe/Annulus → Turbulent Mixing Tube → Turbulent Flame

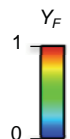
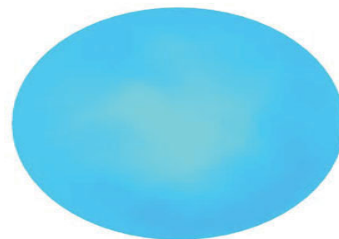
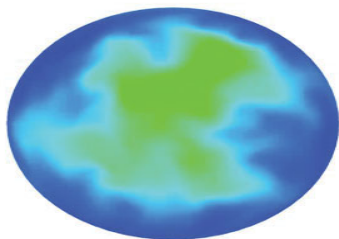


16

Three Domain Approach



Pipe/Annulus → Turbulent Mixing Tube → Turbulent Flame



Animation: 2.5 ms
Coarse Grid Simulation

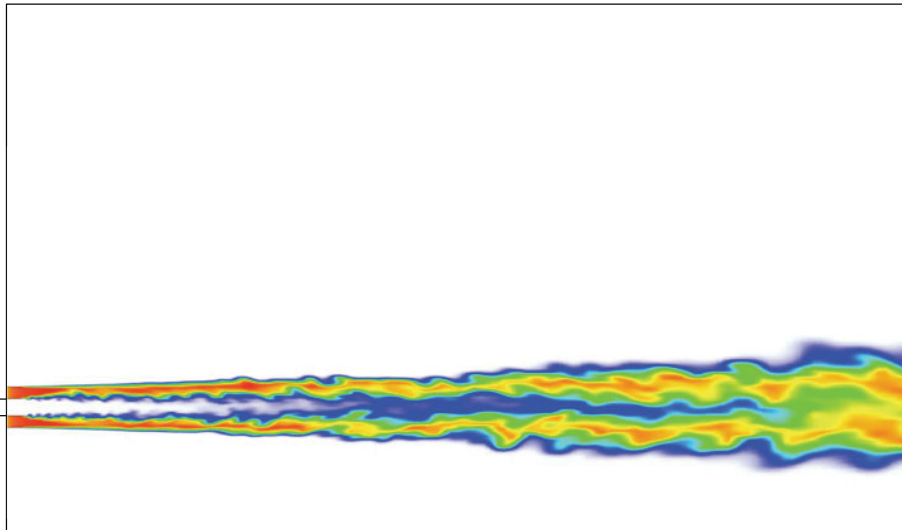


17

Three Domain Approach



Pipe/Annulus → Turbulent Mixing Tube → Turbulent Flame

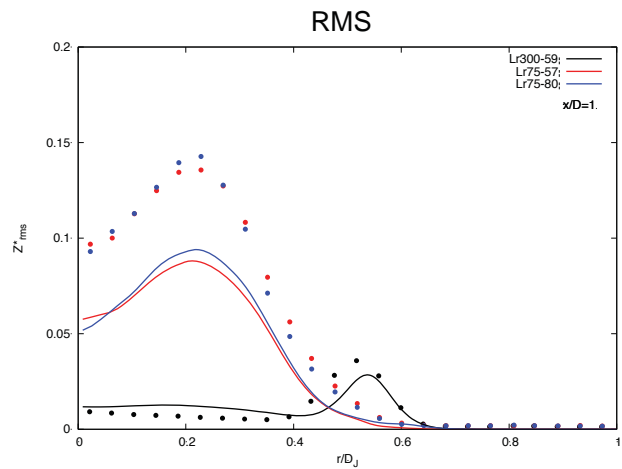
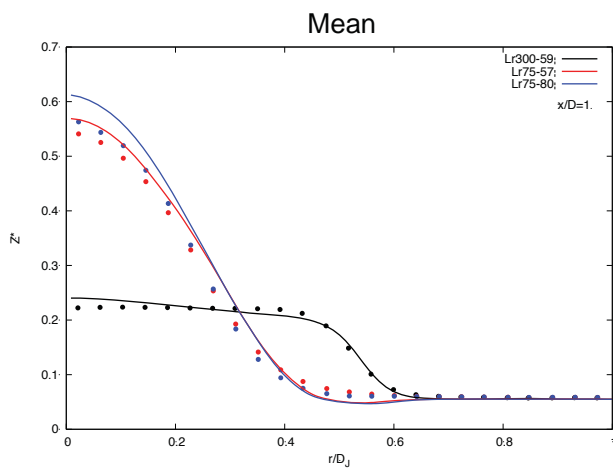


18

Comparison to Experiment



Mixture Fraction @ $x/D_J = 1$ from Flame Simulation



Note: only resolved contribution to RMS

THANKS FOR SHARING THE DATA TO OTHER GROUPS



19

Joined numerical study



ITV



UJS/KIT



CIT



PUR



PRI



ZJU



CentraleSupélec



EM2C



DUE



STA



UBM



TUF



SYD



HAN



MIC



KTH

20

Models

Group	Turbulent Combustion Model	Chemistry	Flamme affinity	Group	Turbulent Combustion Model	Chemistry	Flamme affinity
ITV	G-C Equation \mathcal{E} anal. model	Tab. Chem. (premixed & non-premixed)	PREM & DIFF	STA	FPV Pres. FDF	Tab. Chem. (non- premixed)	DIFF
UJS/KIT	REDIM Pres. FDF	Tab. Chem.	PREM & DIFF		FTACLES $\mathcal{E}=2$	Tab. Chem. (premixed)	PREM
CIT	FPV Pres. FDF	Tab. Chem. (non-premixed)	DIFF	UBM	laminar closure	Tab. Chem. (premixed & non-premixed)	PREM & DIFF
PUR	Transport FDF	Skeletal (19 species)	DIFF	TUF	FPV Pres. FDF	Tab. Chem. (non- premixed)	DIFF
PRI	FPV Pres. FDF	Tab. Chem. (non-premixed)	DIFF	SYD	MMC	Skeletal (22 species)	DIFF
ZJU	MCM	4-steps Chem.	PREM & DIFF	HAN	FPV Pres. FDF	Tab. Chem. (non- premixed)	DIFF
EM2C	TFLES \mathcal{E} anal. model	Tab. Chem. (premixed)	PREM	MIC	Transport FDF	Skeletal (19 species)	DIFF
DUE	TFLES \mathcal{E} anal. model	Tab. Chem. (premixed)	PREM	KTH	laminar closure	Skeletal (30 species)	PREM & DIFF

21

Models

Group	Turbulent Combustion Model	Chemistry	Flamme affinity	Group	Turbulent Combustion Model	Chemistry	Flamme affinity
ITV							DIFF
UJS							PREM
C							PREM & DIFF
P							DIFF
P							DIFF
Z							DIFF
EM2C	TFLES E anal. model	Tab. Chem. (premixed)	PREM	MIC	Transport FDF	Skeletal (19 species)	DIFF
DUE	TFLES E anal. model	Tab. Chem. (premixed)	PREM	KTH	laminar closure	Skeletal (30 species)	PREM & DIFF

Model flamme affinity:
 - Diffusion (8)
 - Premixed (3)
 - Both (5)

CODES

Group	Code	grid type	spatial scheme	temporal scheme	Turbulence SGS
DUE	PsiPhi	structured	2 nd ord. velocity 2 nd ord. TVD scalars	3rd order RK	Sigma
EM2C	YALES2	un-structured	4 th ord. velocity 4 th ord. scalar	4 th order TRK4	Dynamic Smag
ITV	CIAO	structured cylindrical	2 nd ord. velocity 3 rd ord. scalar	2 nd order Crank-Nicolson	Dynamic Smag.
KTH	OpenFOAM	un-structured	2 nd ord. linear velocity 2 nd ord. TVD scalars	2 nd order back. fin. diff.	Smag.
UBM	OpenFOAM	block-structured	2 nd ord. with high frequency filter		Vreman.
PRI	NGA	structured stretched in x and r	2 nd ord. velocity 3 rd ord. scalars		Dynamic. Smag
SYD	mmcFoam	structured	2 nd ord.	2 nd ord.	Smag.
STA	3DA	structured cylindrical	2 nd ord.	2 nd ord.	Dynamic. Smag
CIT	NGA	structured cylindrical	2 nd ord. velocity 3 rd ord. scalars		Dynamic. Smag
UJS	LESOCC2C	multi-block structured	2 nd ord.	2 nd ord.	Dynamic. Smag
PUR	LES-HPDF	structured cylindrical	2 nd ord.	Mix 1 st and 2 nd ord.	Dynamic. Smag
MIC	NGA	structured staggered	2 nd ord.	2 nd ord.	Dynamic. Smag
HAN	OpenFOAM	un-structured	2 nd ord.	2 nd ord.	Smag.
TUF	OpenFOAM	un-structured	2 nd ord.	2 nd ord.	Sigma.
ZJU	In-house code	structured cylindrical	2 nd ord.	2 nd ord.	Dynamic. Smag

CODES

Group	Code	grid type	spatial scheme	temporal scheme	Turbulence SGS
DUE	PsiPhi	structured	2 nd ord. velocity 2 nd ord. TVD scalars	3rd order RK	Sigma
EM2C	YALES2	un-structured	4 th ord. velocity 4 th ord. scalar	4 th order TRK4	Dynamic Smag
ITV	CIAO	structured cylindrical	2 nd ord. velocity 3 rd ord. scalar	2 nd order Crank-Nicolson	Dynamic Smag.
KTH	OpenFOAM	un-structured	2 nd ord. linear velocity 2 nd ord. TVD scalars	2 nd order back. fin. diff.	Smag.
UBM	OpenFOAM	block-structured	2 nd ord. with high frequency filter		Vreman.
PRI	NGA	structured stretched in x and r	2 nd ord. velocity 3 rd ord. scalars		Dynamic Smag
SYD	mmcFoam	structured	2 nd ord.	2 nd ord.	Smag.
STA	3DA	structured cylindrical	2 nd ord.	2 nd ord.	Dynamic Smag
CIT	NGA	structured cylindrical	2 nd ord. velocity 3 rd ord. scalars		Dynamic Smag
UJS	LESOCC2C	un-structured	2 nd ord.	2 nd ord.	Dynamic Smag
PUR	LES-HPDF	structured cylindrical	2 nd ord.	Mix 1 st and 2 nd ord.	Dynamic Smag
MIC	NGA	structured staggered	2 nd ord.	2 nd ord.	Dynamic Smag
HAN	OpenFOAM	un-structured	2 nd ord.	2 nd ord.	Smag.
TUF	OpenFOAM	un-structured	2 nd ord.	2 nd ord.	Sigma.
ZJU	In-house code	structured cylindrical	2 nd ord.	2 nd ord.	Dynamic Smag

OpenFoam: 4
 NGA: 3
 All are Low Mach

Main jet BC's

Group	Main jet	Group	Main jet
ITV	Own mixing tube simulation	STA	Own mixing tube simulation
UJS/KIT	Own mixing tube simulation	UBM	Princeton data
CIT	Own mixing tube simulation	TUF	Own mixing tube simulation
PUR	Own mixing tube simulation	SYD	Own mixing tube simulation
PRI	Princeton data !	HAN	Own mixing tube simulation
ZJU	Own mixing tube simulation	MIC	Princeton data
EM2C	Princeton data	KTH	Princeton data
DUE	Princeton data		

Main jet BC's

Group	Main jet	Group	Main jet
ITV	Own mixing tube simulation		Own mixing tube simulation
UJS/KIT			data
CIT			tube simulation
PUR			tube simulation
PRI		HAN	Own mixing tube simulation
ZJU	Own mixing tube simulation	MIC	Princeton data
EM2C	Princeton data	KTH	Princeton data
DUE	Princeton data		

Princeton data : 6
Own mixing tube simulations: 9

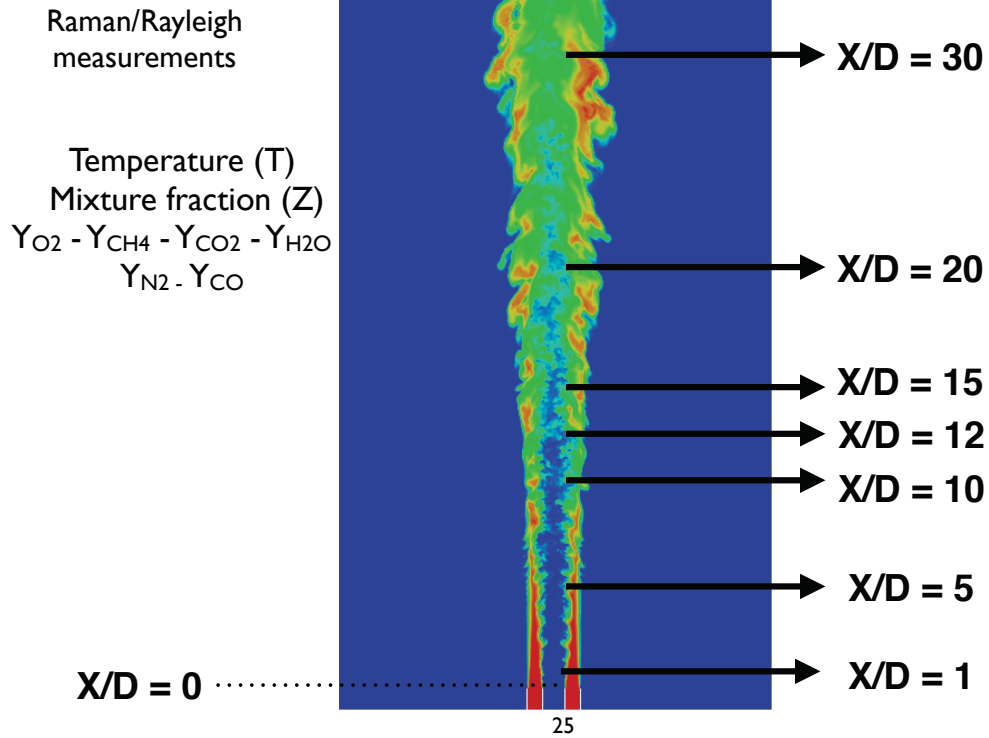
23

Flame configurations

Group	Lr300-U59	Lr75-80	Lr75-57	Group	Lr300-U59	Lr75-80	Lr75-57
ITV	x	x	x	STA			x
UJS/KIT			x	UBM	x	x	x
CIT	x		x	TUF			x
PUR	x	x	x	SYD	x		x
PRI	x	x	x	HAN			x
ZJU			x	MIC	x	x	x
EM2C	x	x		KTH	x		
DUE	x	x	x				

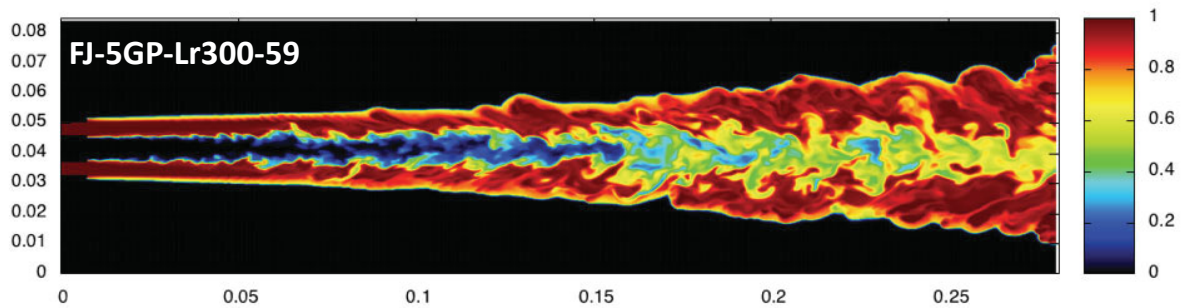
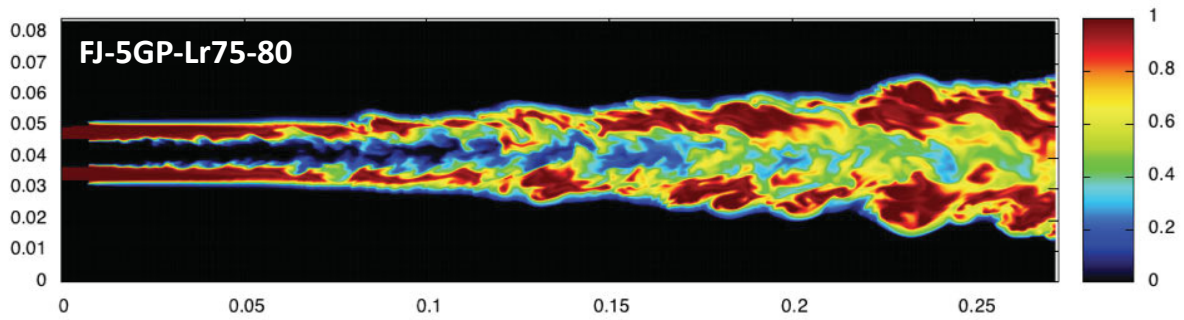
24

Experimental data Radial profiles



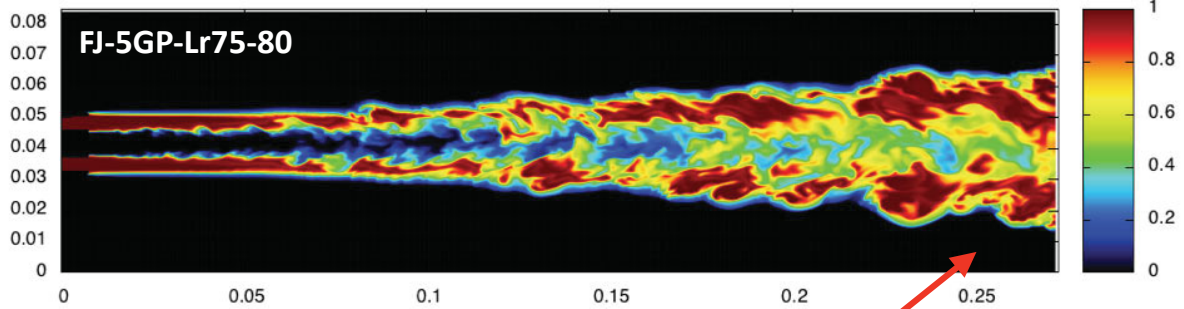
Normalized progress variable field (DUE)

$c = 0$: fresh gases
 $c = 1$: burnt gases

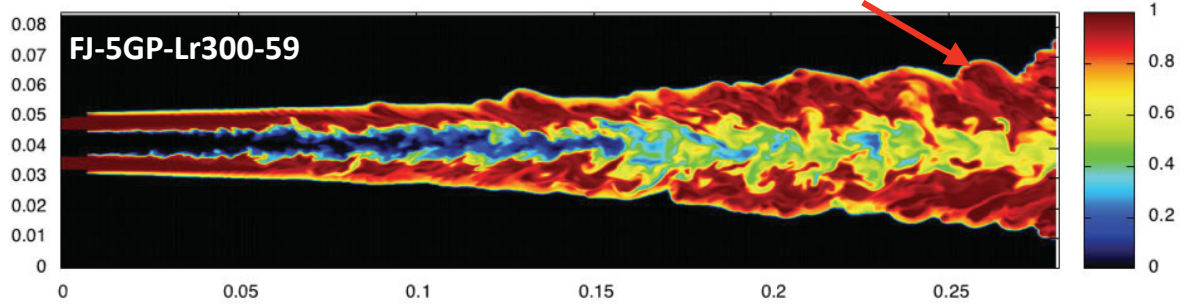


Normalized progress variable field (DUE)

$c = 0$: fresh gases
 $c = 1$: burnt gases



Equilibrium not reached at $X/D = 30$

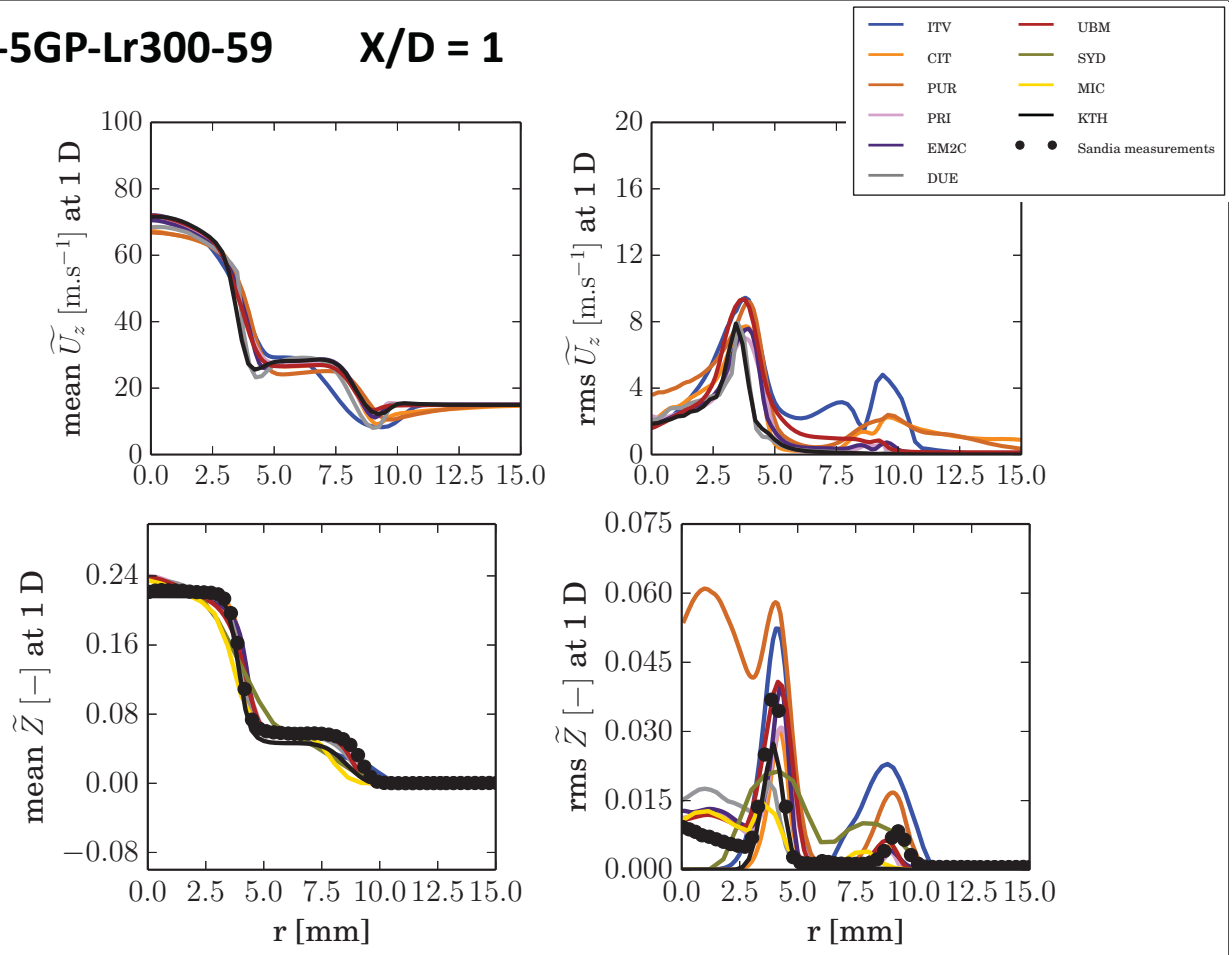


Mean and RMS radial profiles

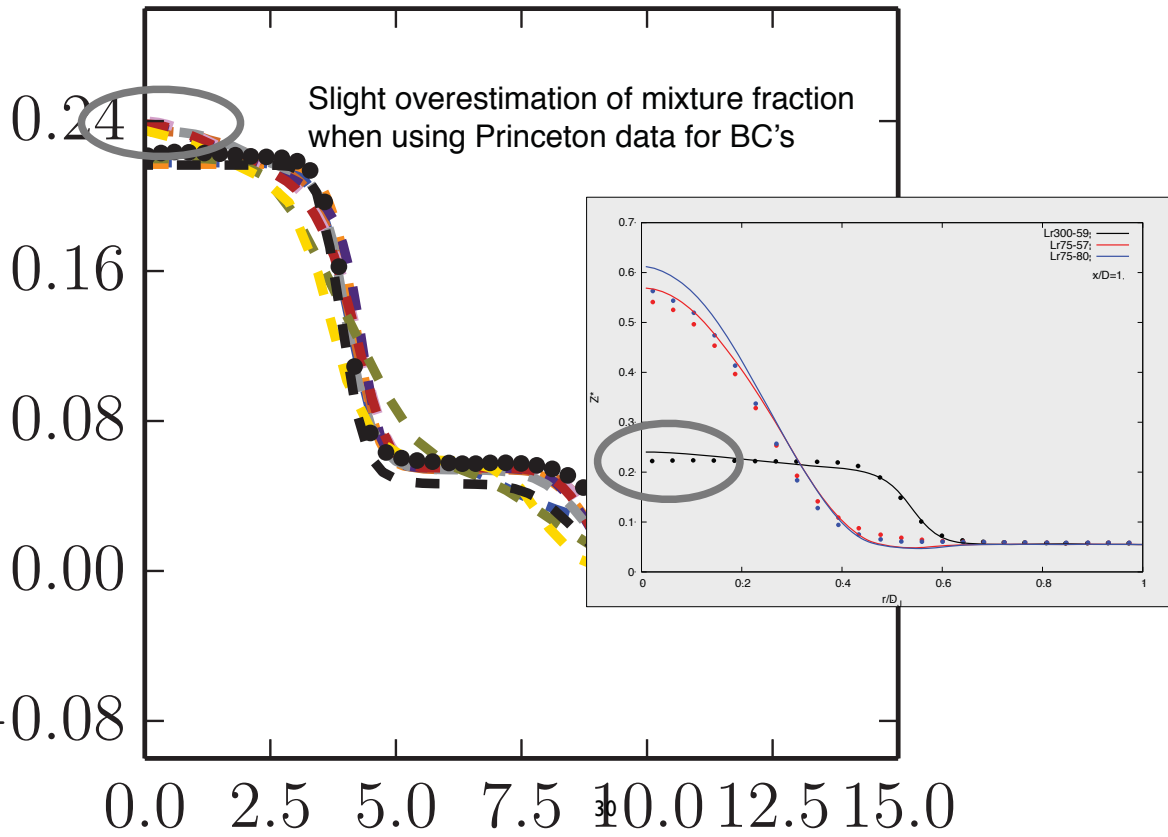
FJ-5GP-Lr300-59

28

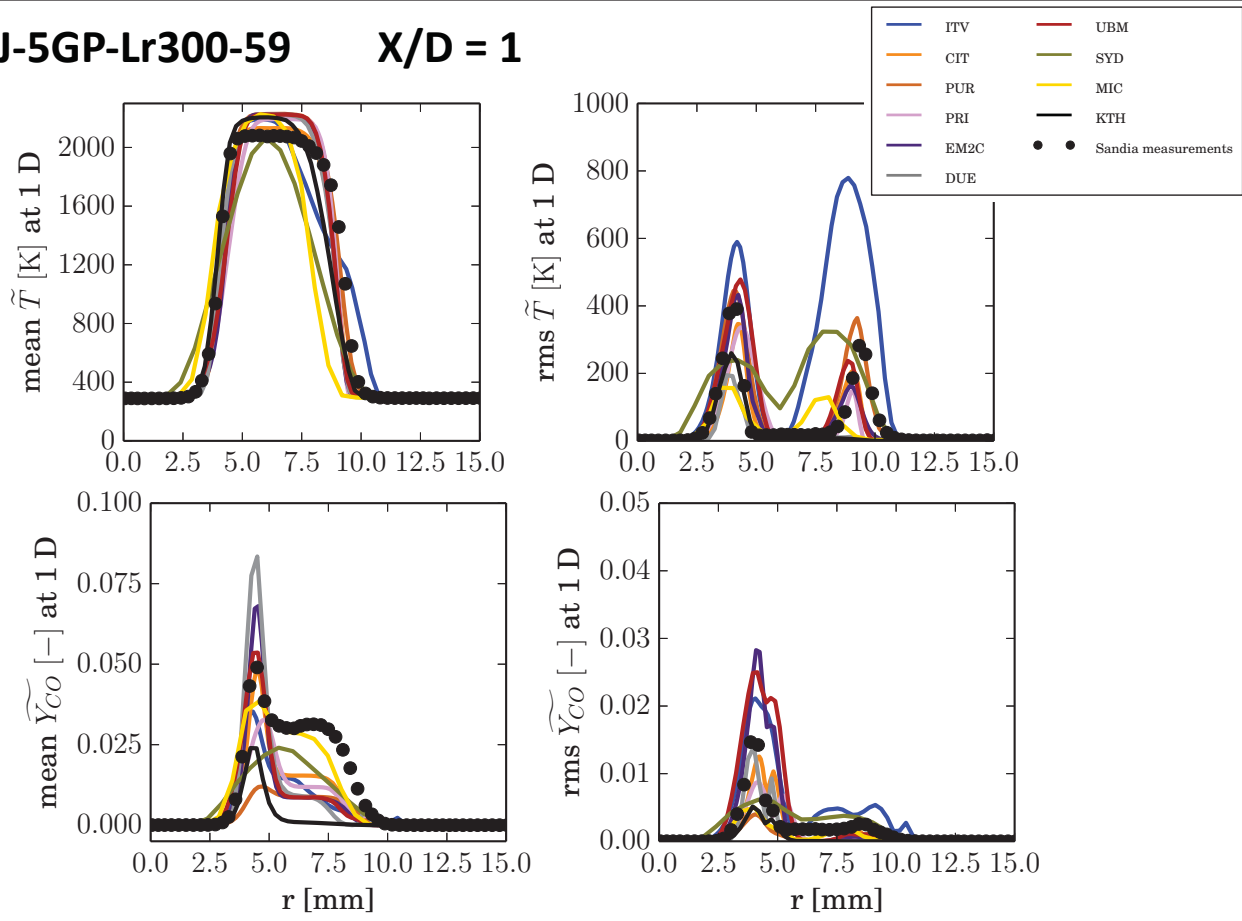
FJ-5GP-Lr300-59 X/D = 1



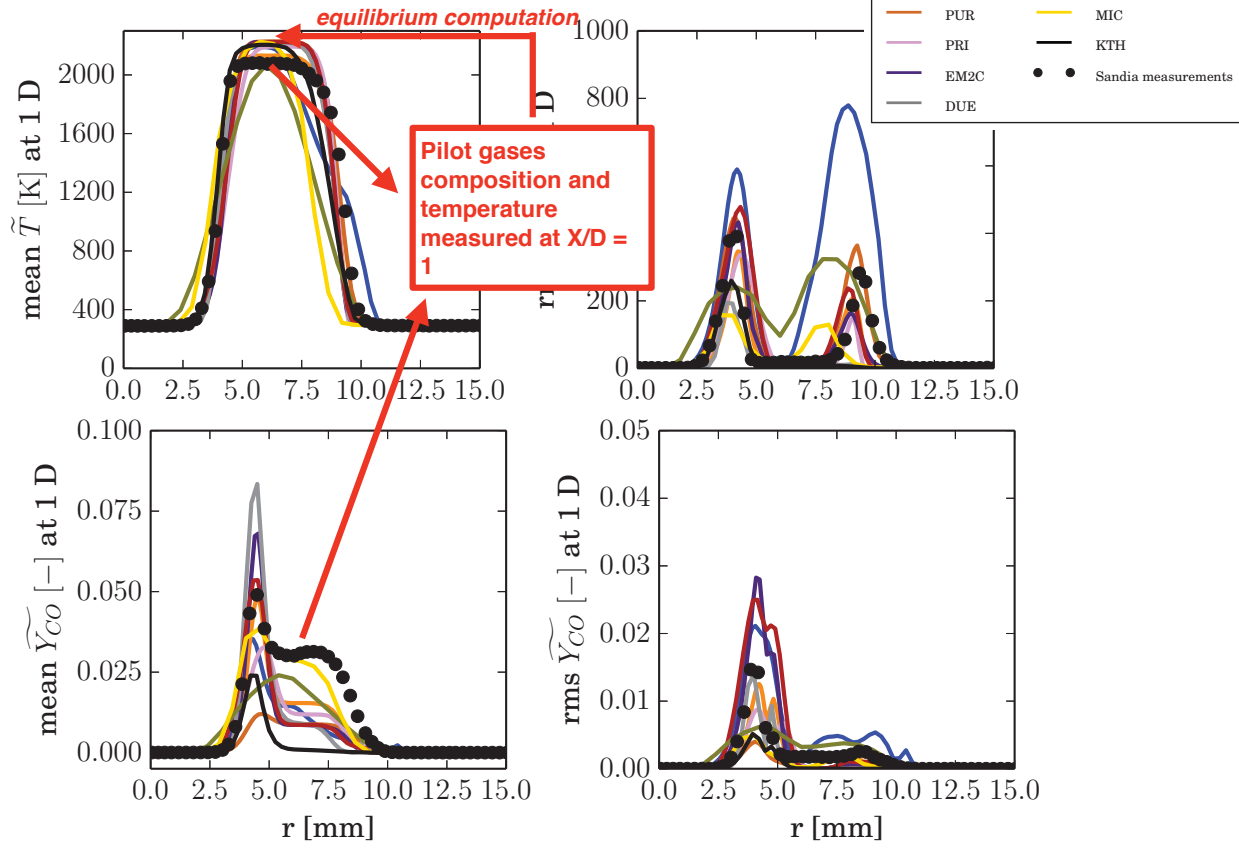
FJ-5GP-Lr300-59 X/D = 1



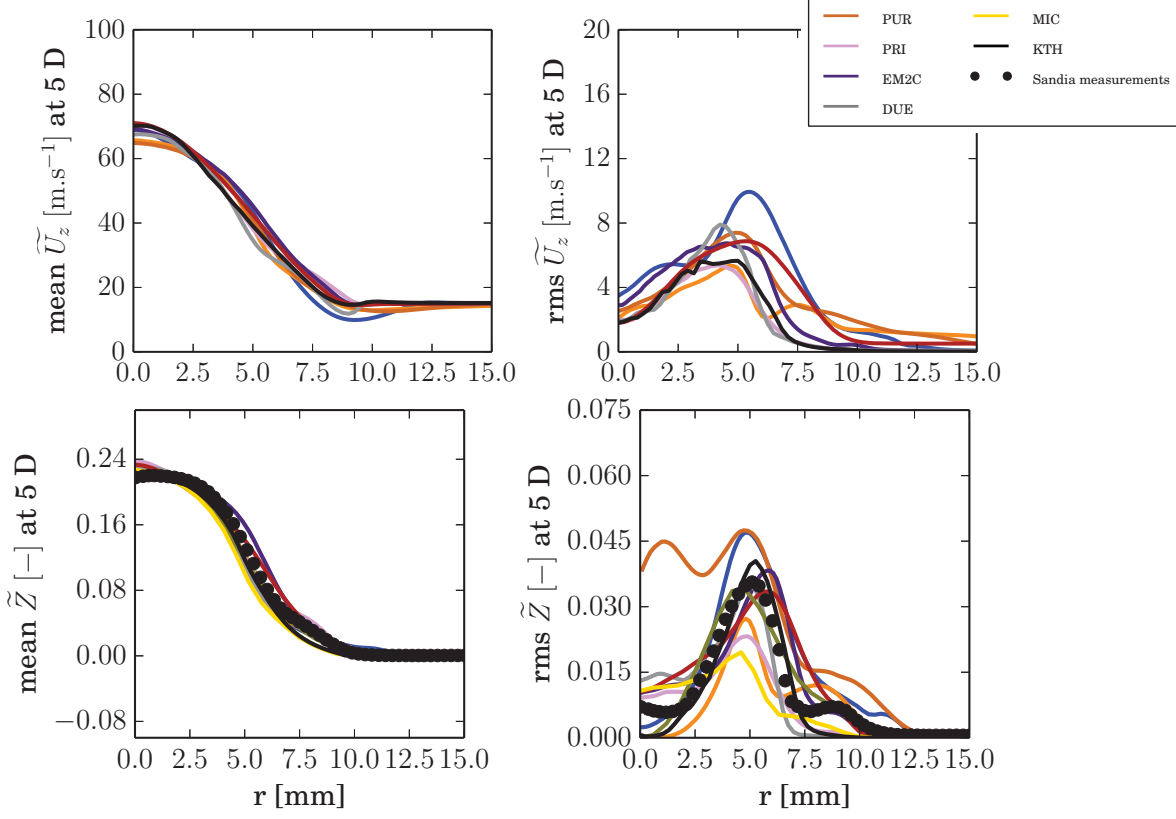
FJ-5GP-Lr300-59 X/D = 1



FJ-5GP-Lr300-59 X/D = 1



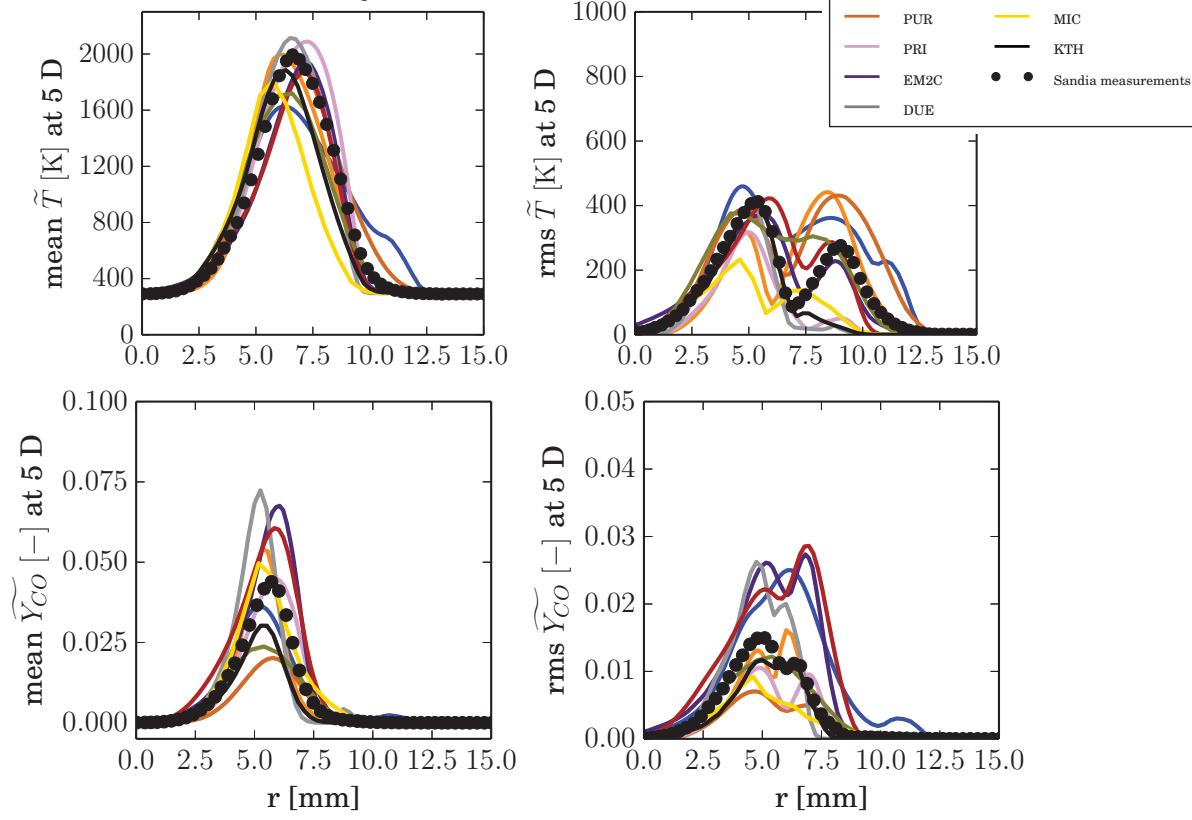
FJ-5GP-Lr300-59 X/D = 5



Still good agreement on mean quantities

but not on RMS

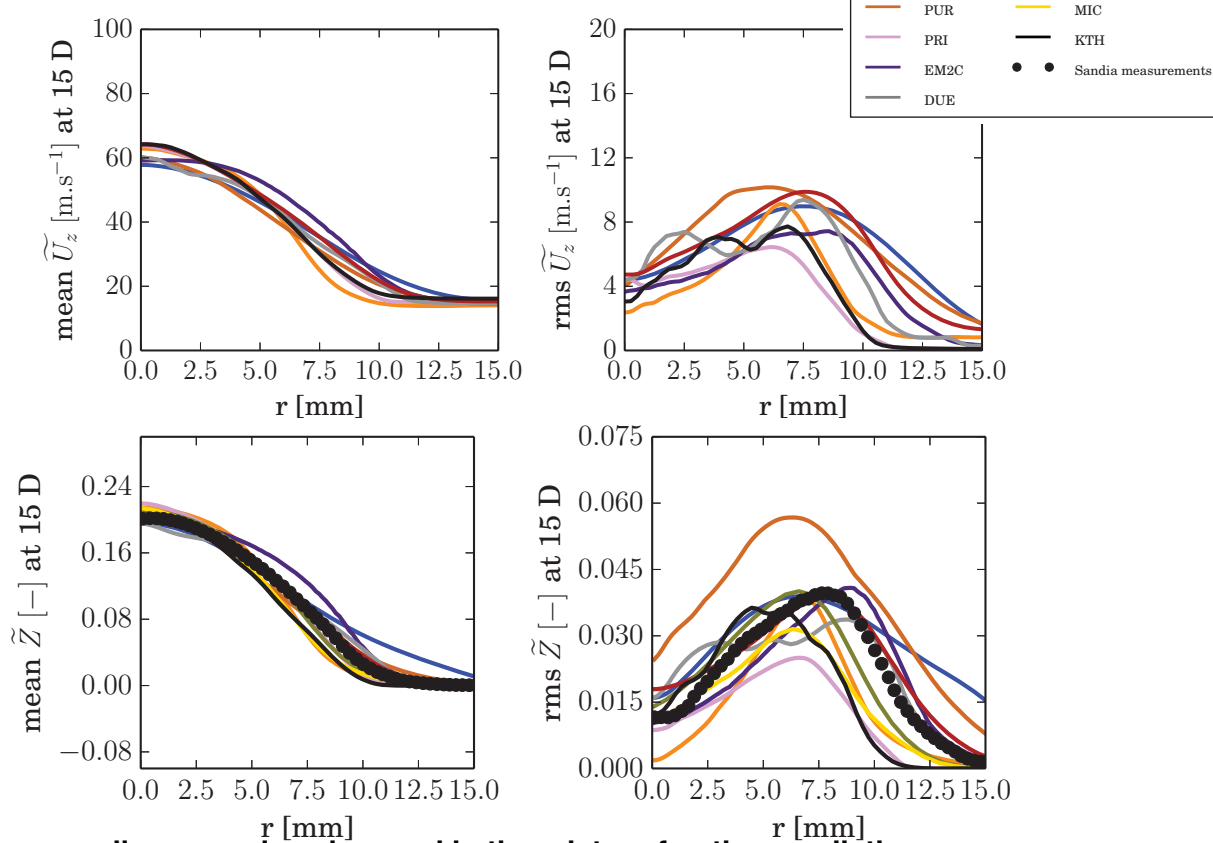
FJ-5GP-Lr300-59 X/D = 5



Very large differences (even is the mixing seems well predicted)

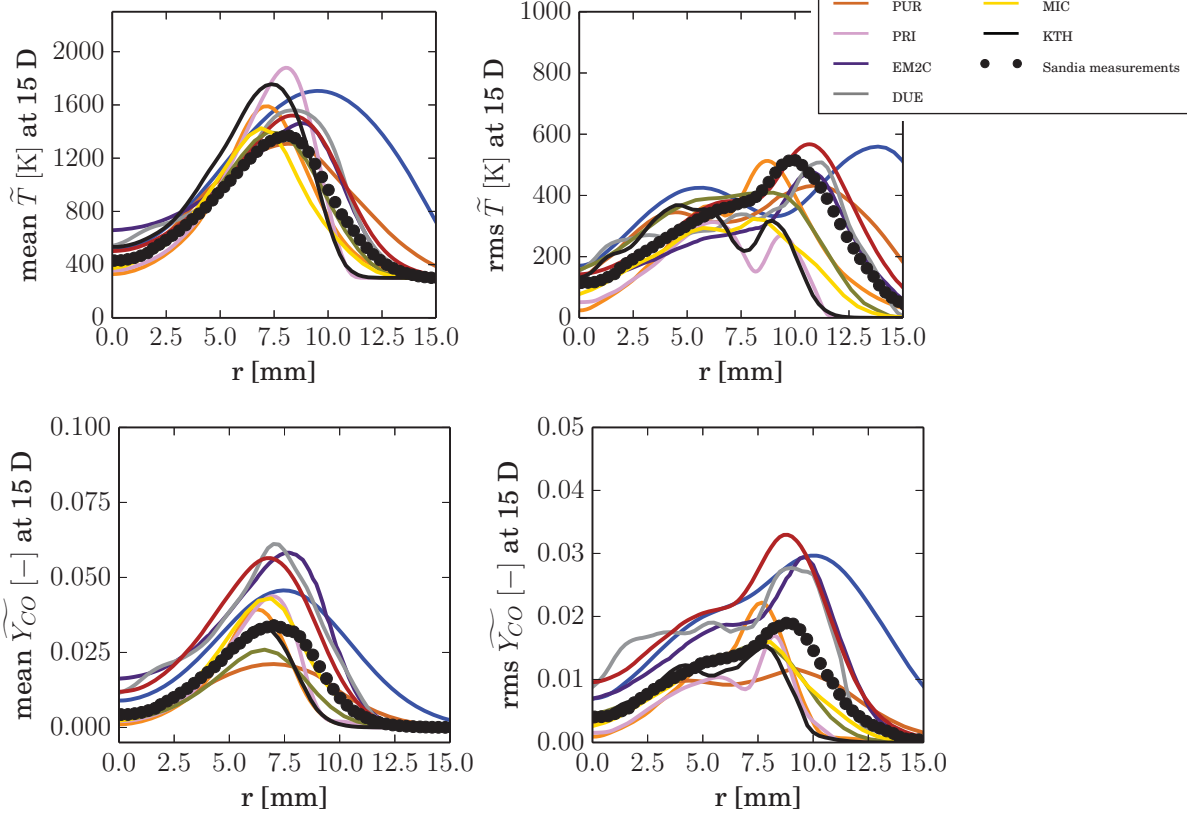
33

FJ-5GP-Lr300-59 X/D = 15



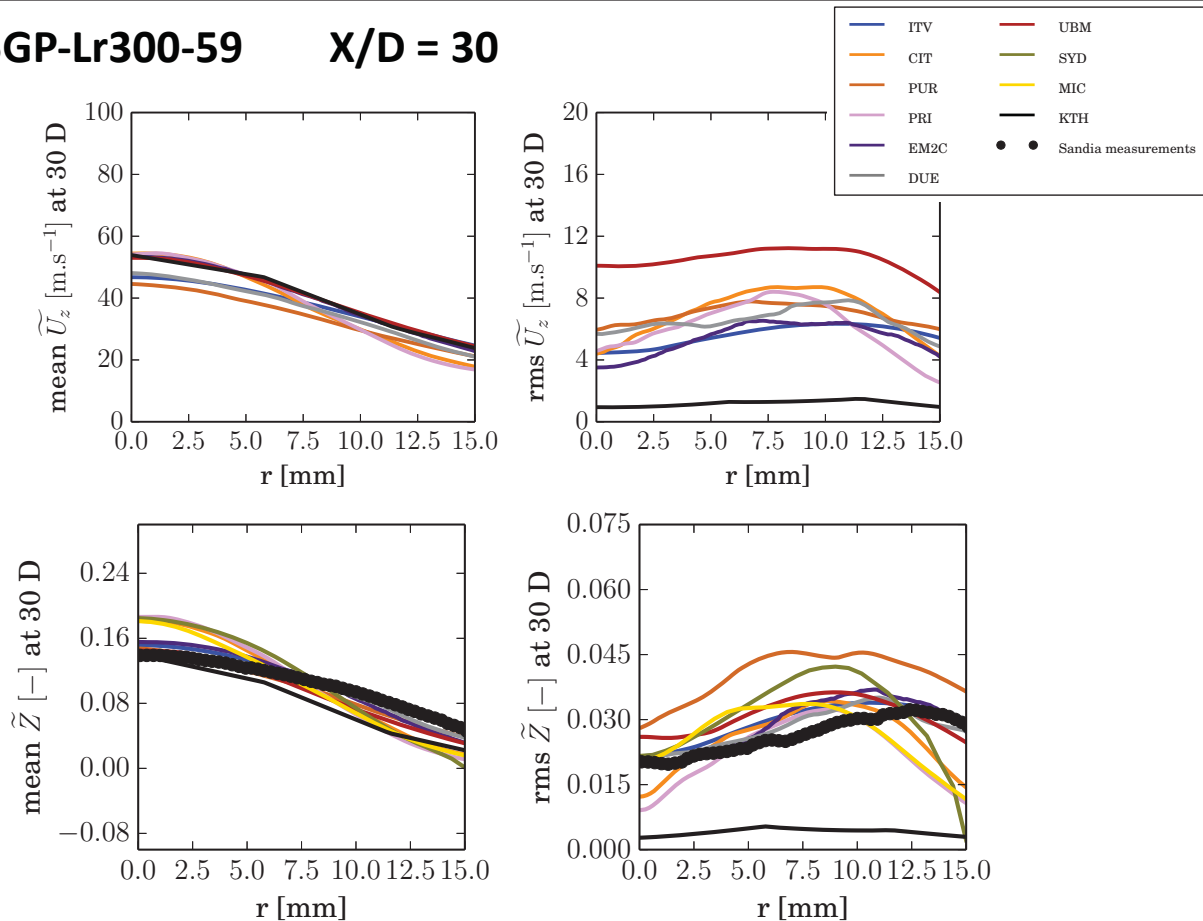
discrepancies observed in the mixture fraction prediction

FJ-5GP-Lr300-59 X/D = 15



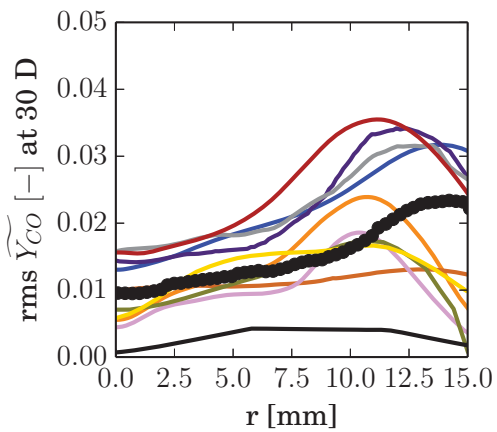
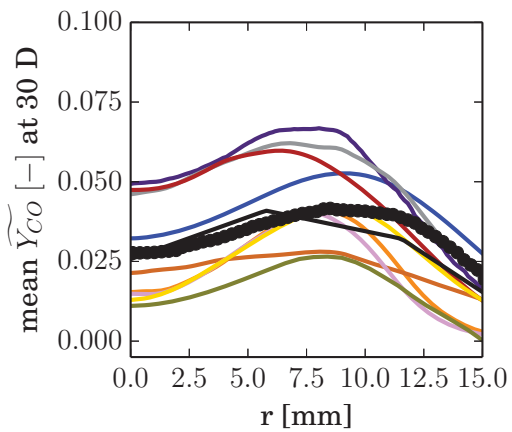
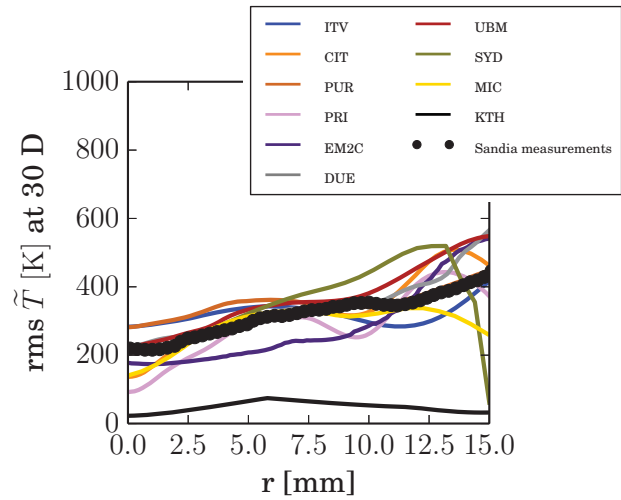
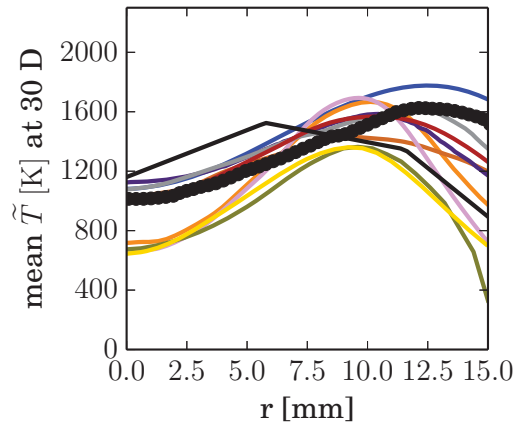
35

FJ-5GP-Lr300-59 X/D = 30

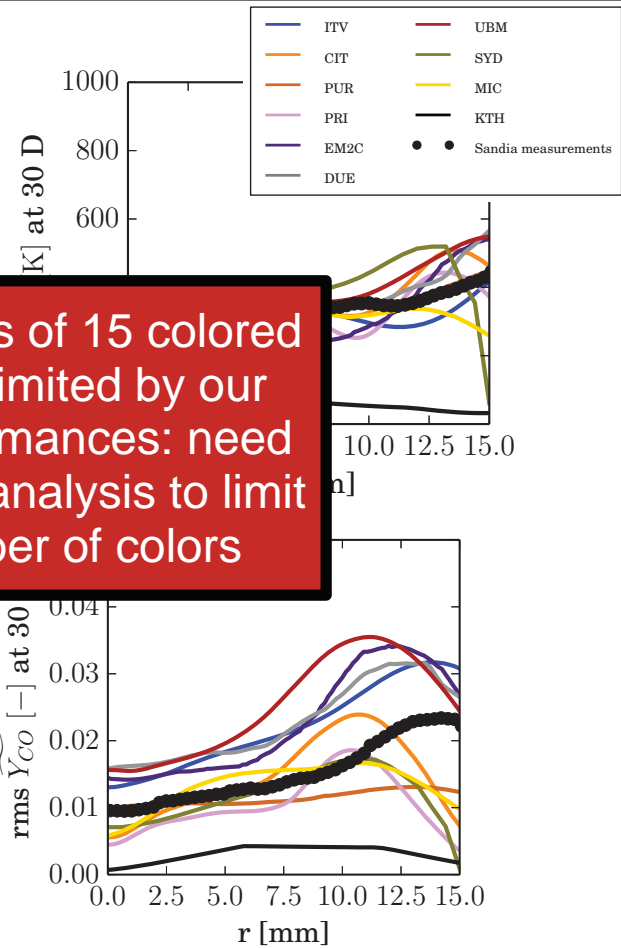
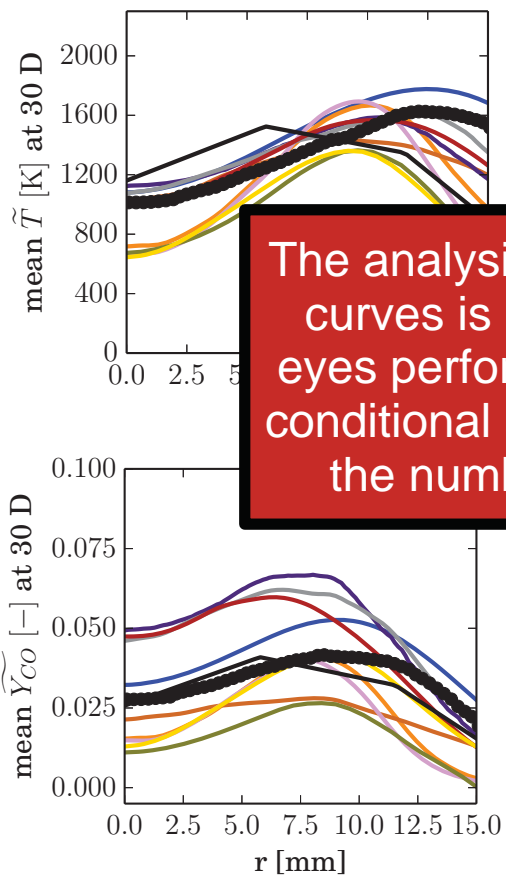


36

FJ-5GP-Lr300-59 X/D = 30



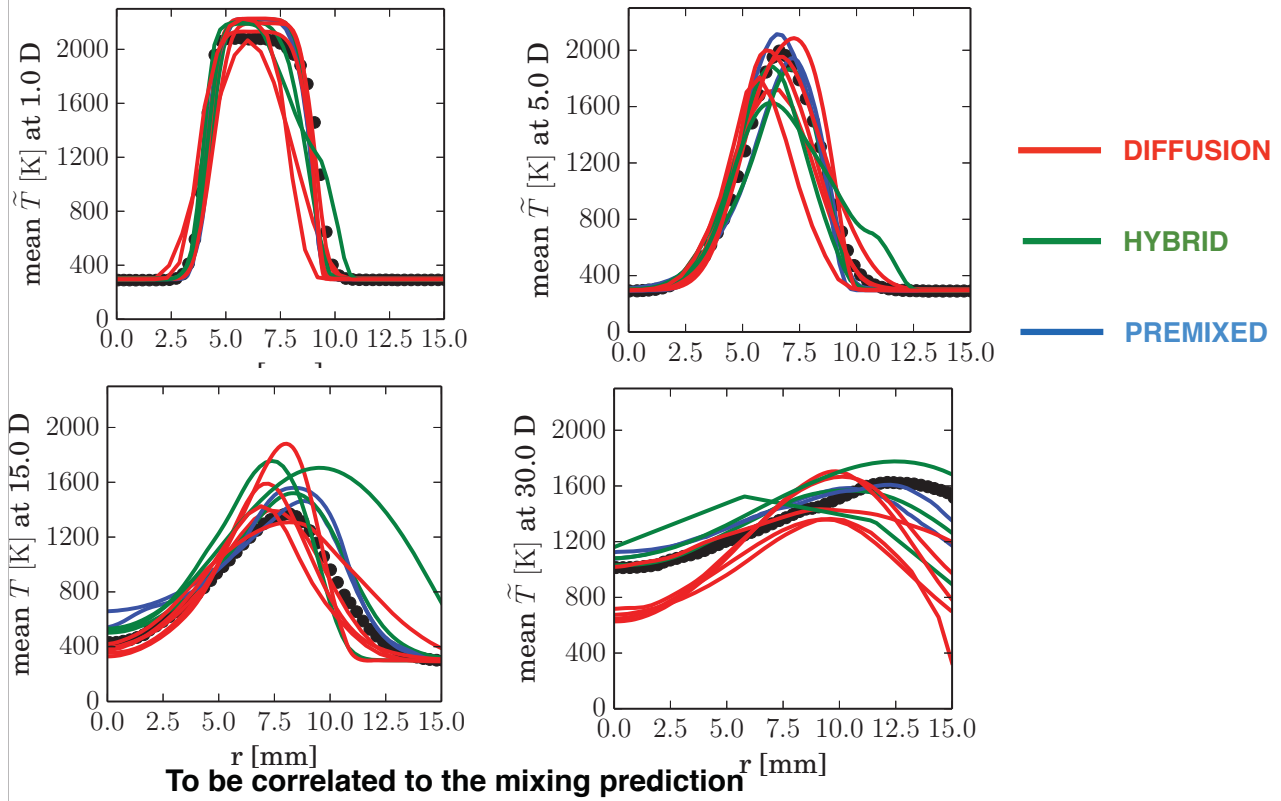
FJ-5GP-Lr300-59 X/D = 30



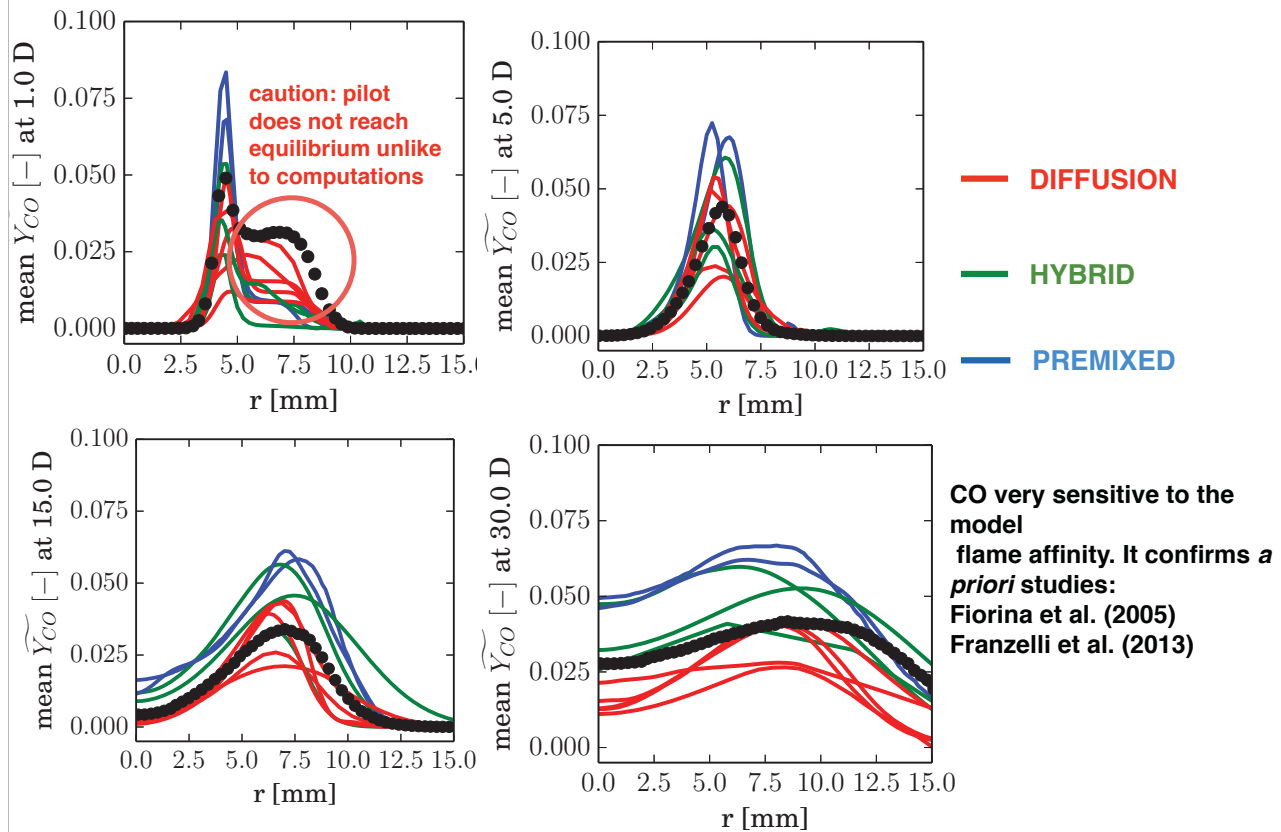
The analysis of 15 colored curves is limited by our eyes performances: need conditional analysis to limit the number of colors

FJ-5GP-Lr300-59

A conditional analysis based on the model affinity



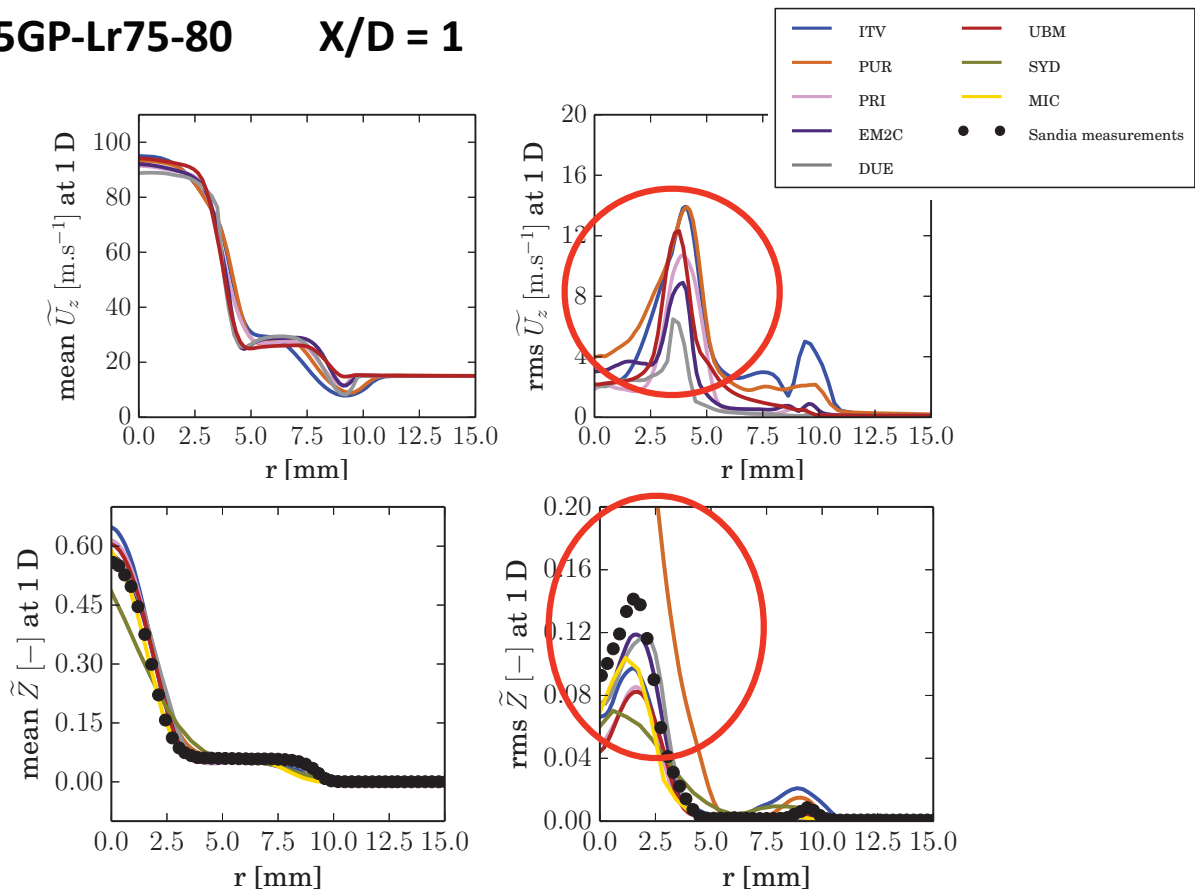
FJ-5GP-Lr300-59



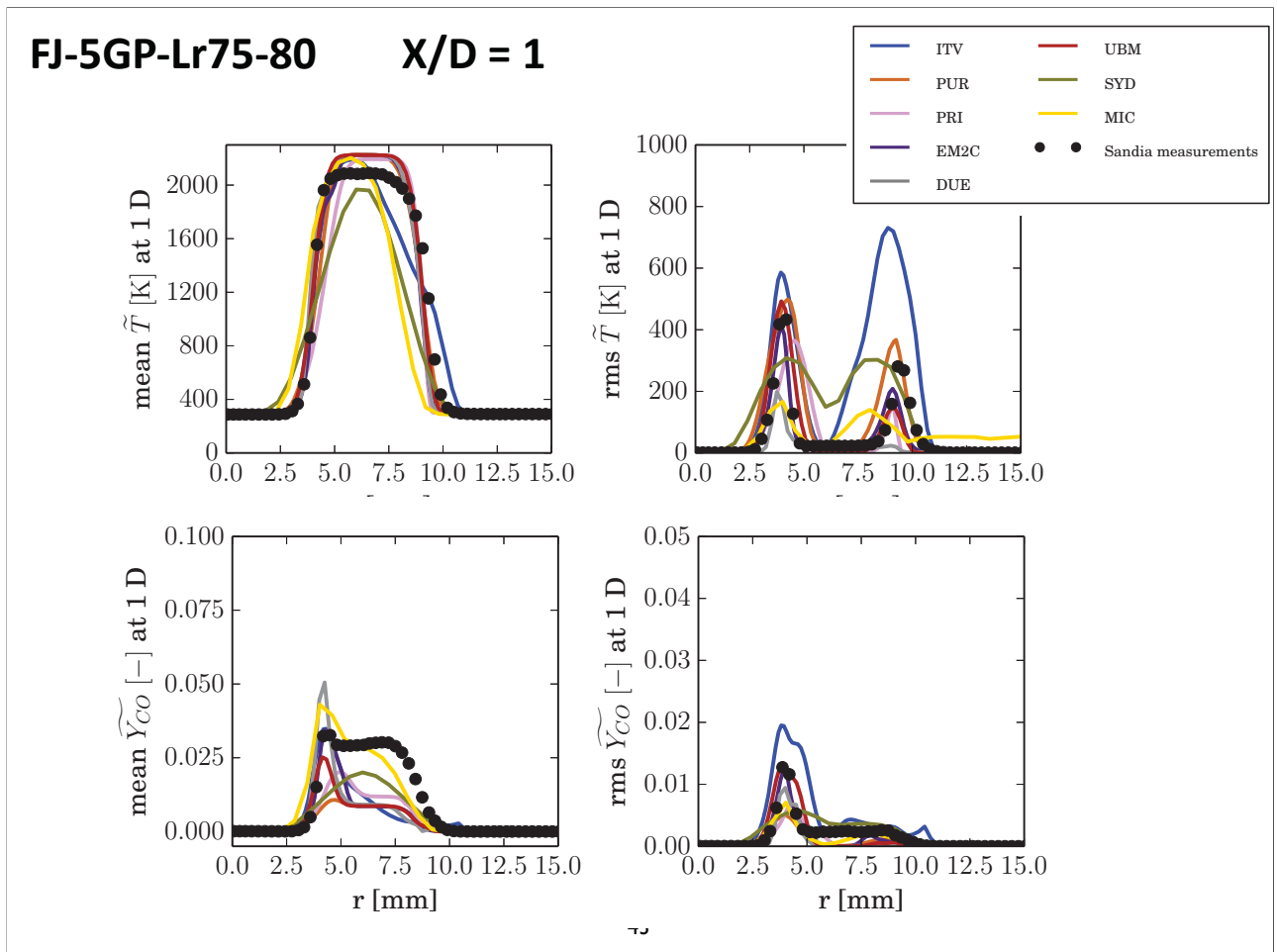
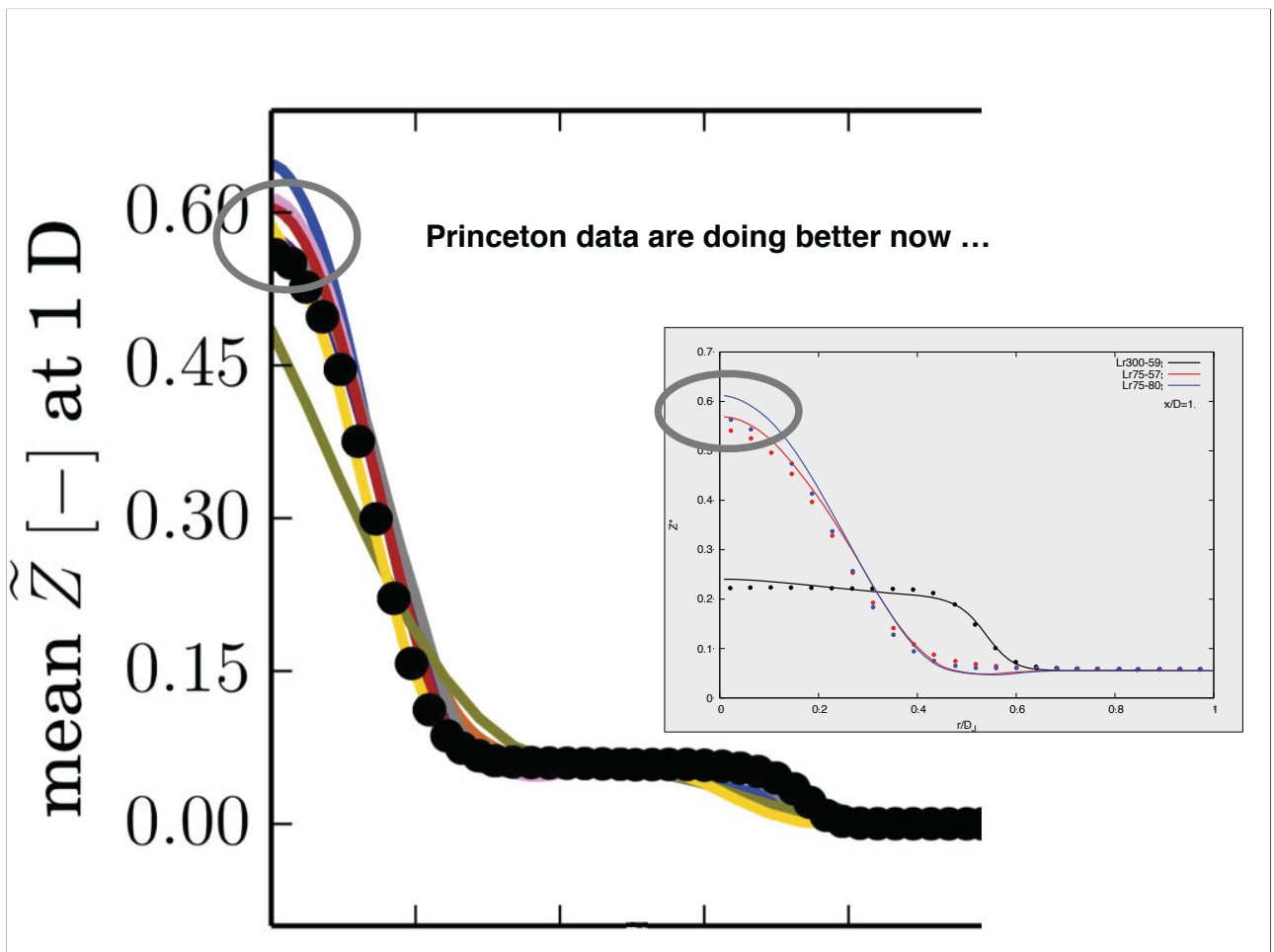
FJ-5GP-Lr75-80

40

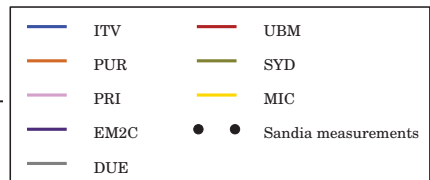
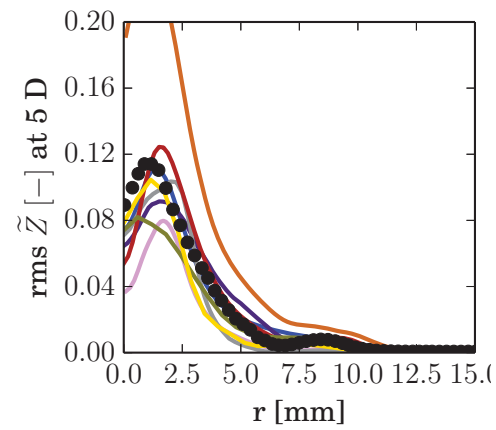
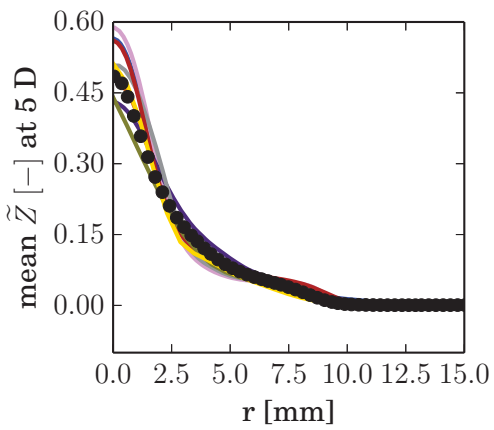
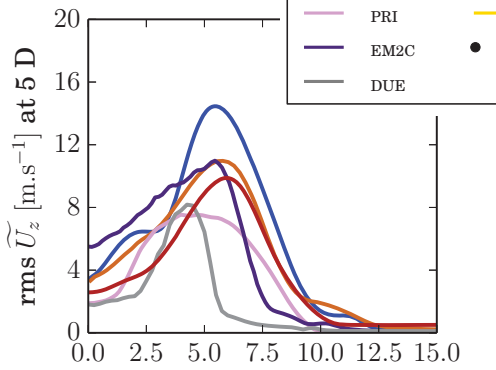
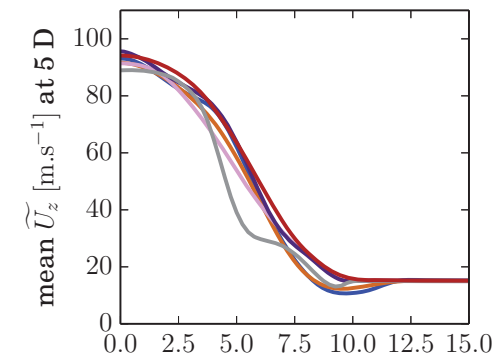
FJ-5GP-Lr75-80 X/D = 1



41

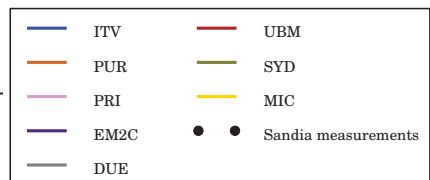
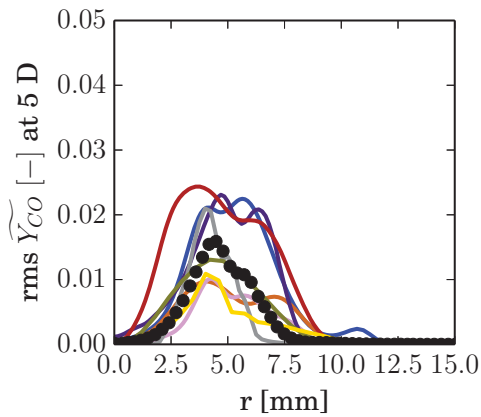
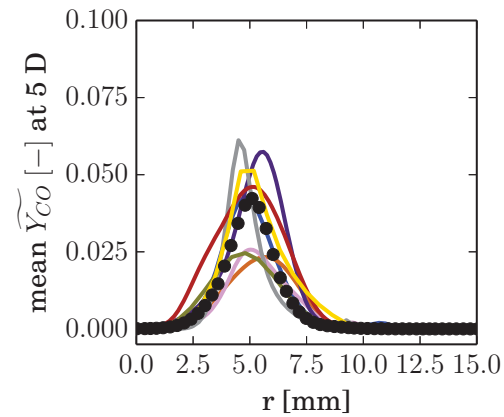
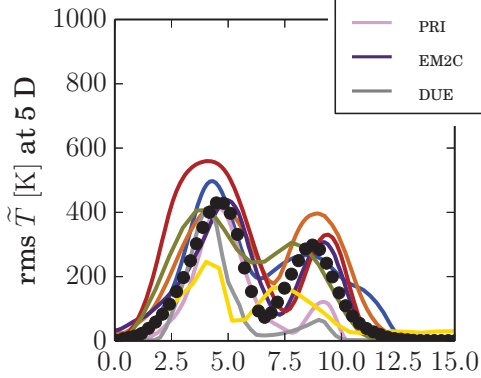
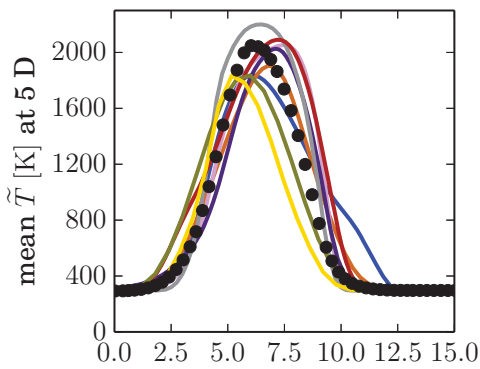


FJ-5GP-Lr75-80 X/D = 5



44

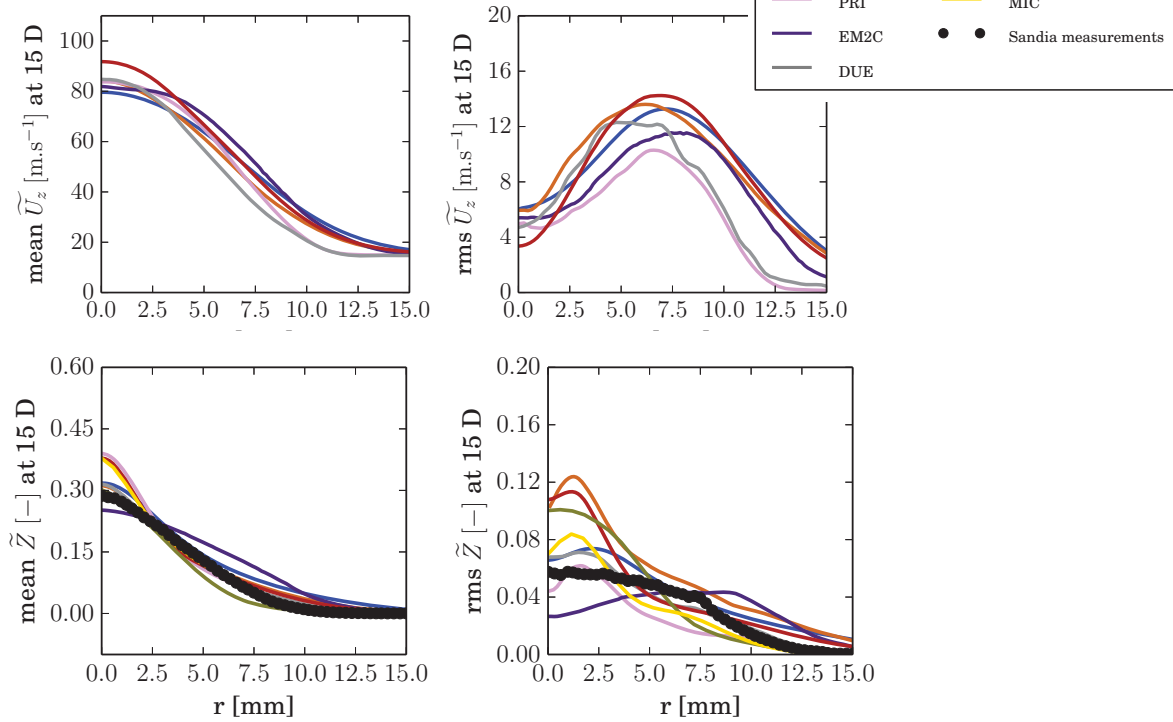
FJ-5GP-Lr75-80 X/D = 5



0 100

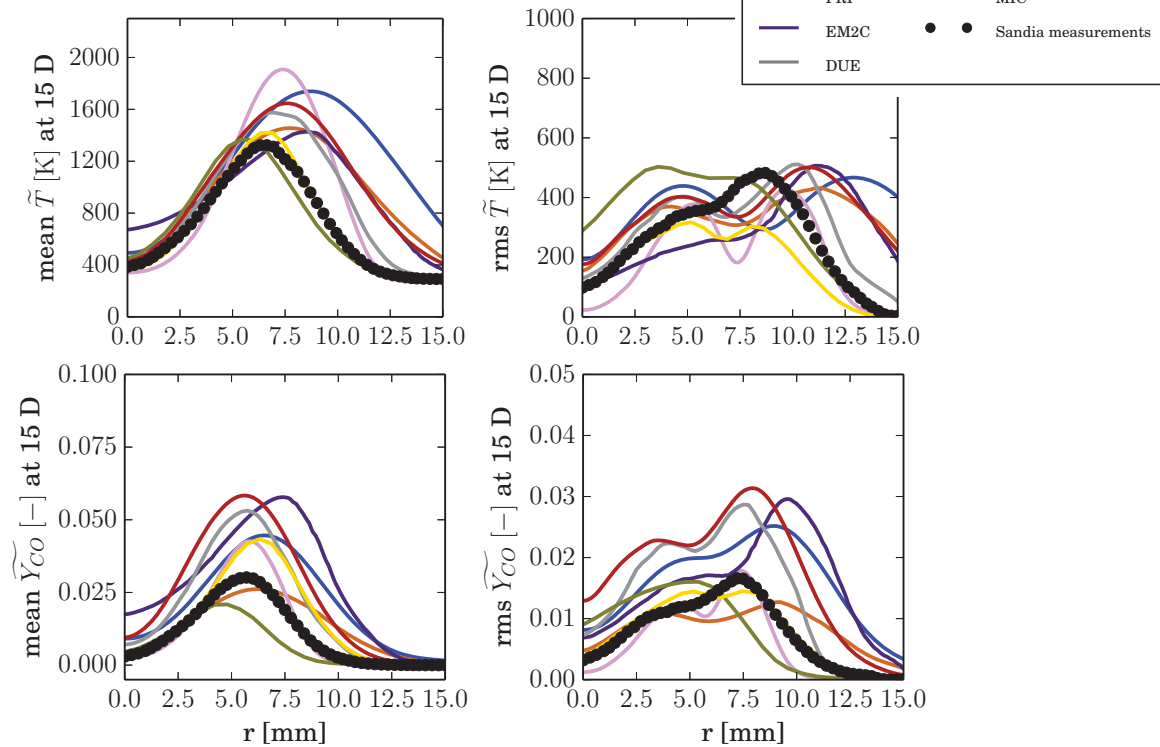
0 25

FJ-5GP-Lr75-80 X/D = 15



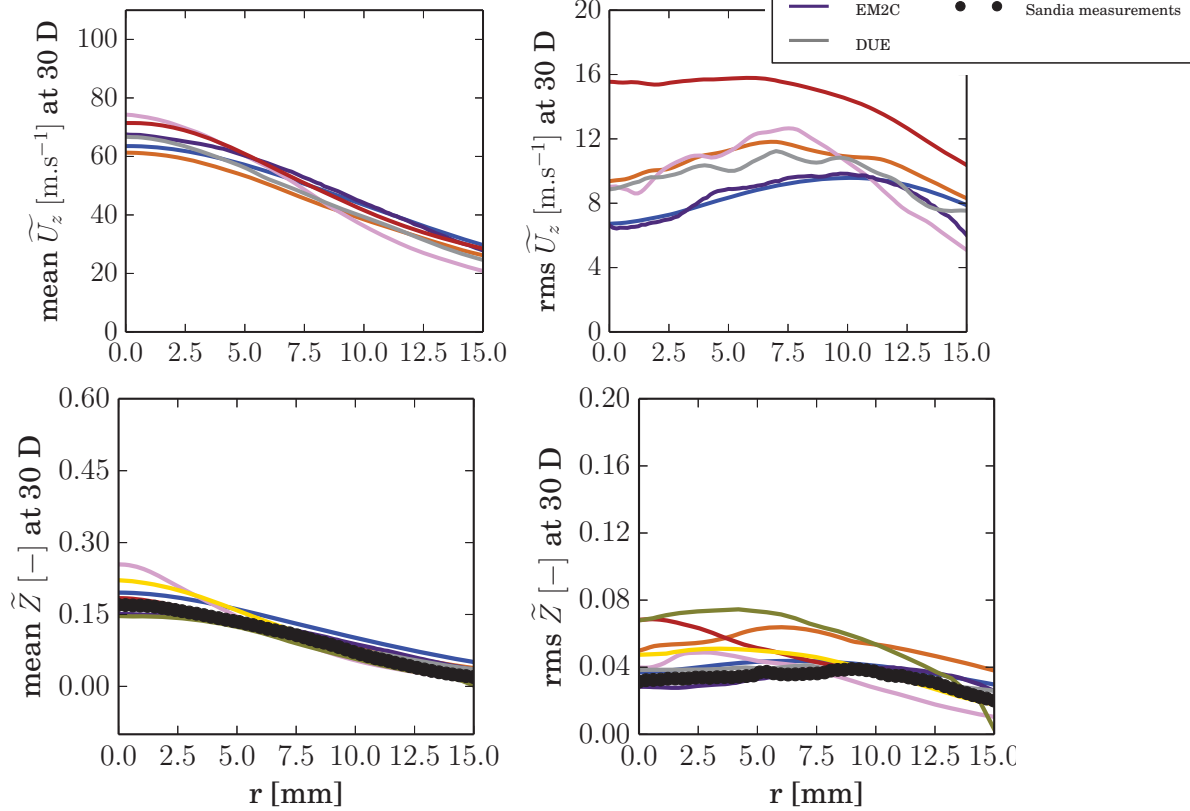
46

FJ-5GP-Lr75-80 X/D = 15

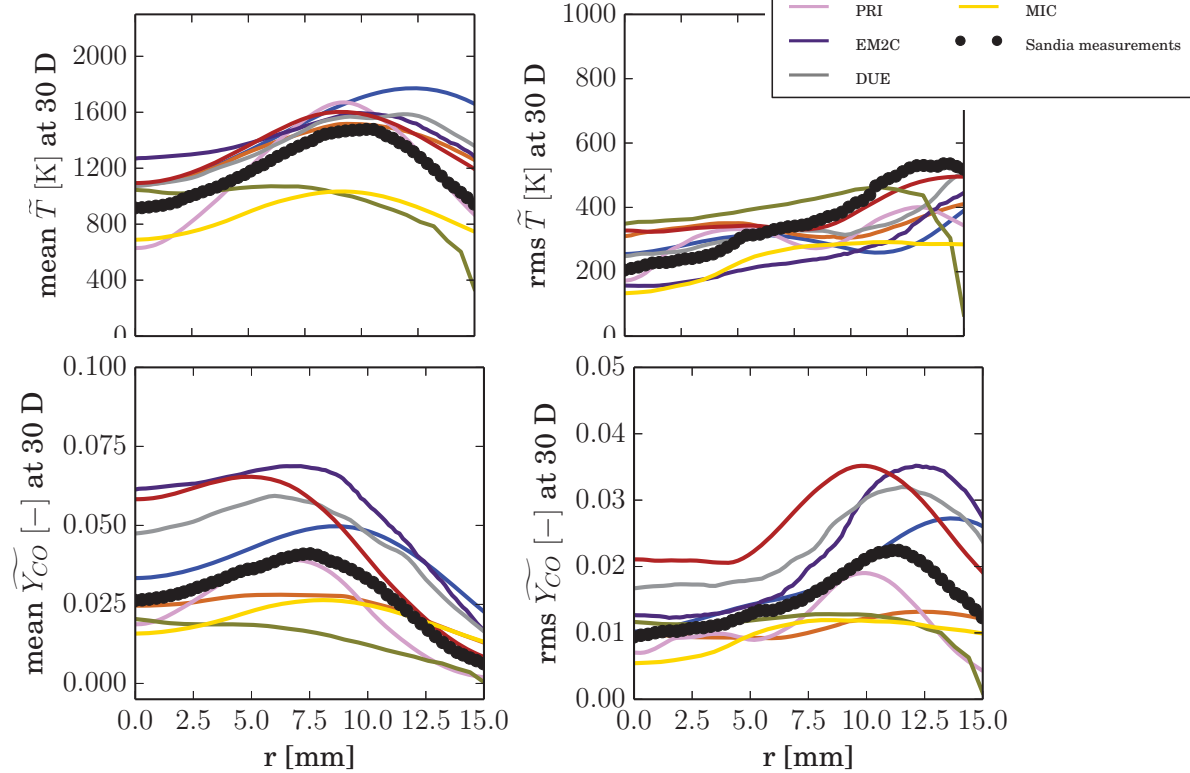


47

FJ-5GP-Lr75-80 X/D = 30

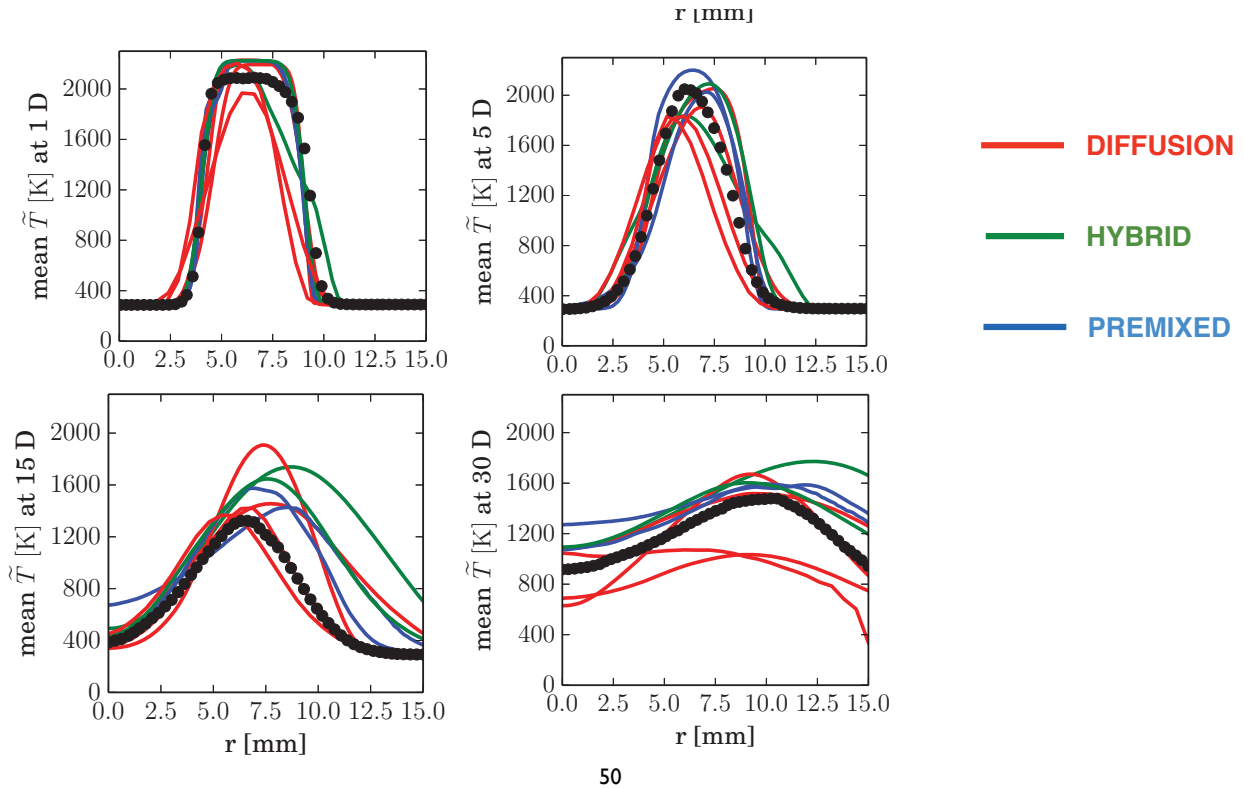


FJ-5GP-Lr75-80 X/D = 30



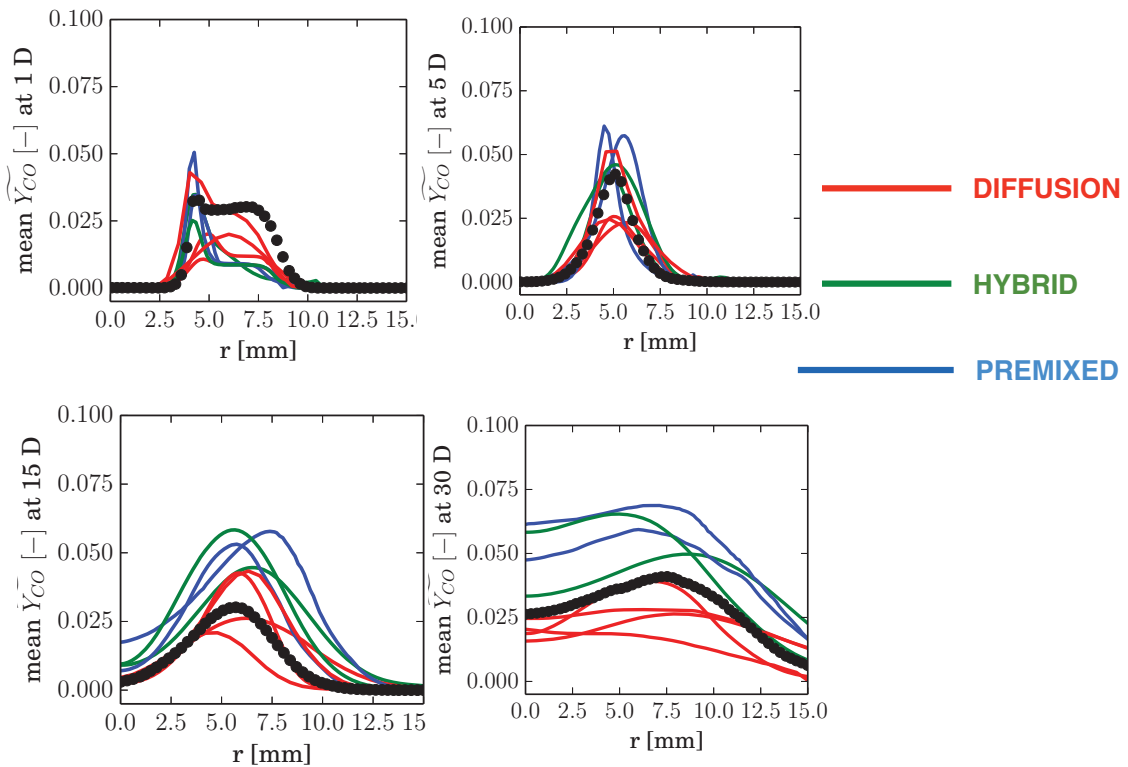
FJ-5GP-Lr75-80

A conditional analysis based on the model affinity



50

FJ-5GP-Lr75-80

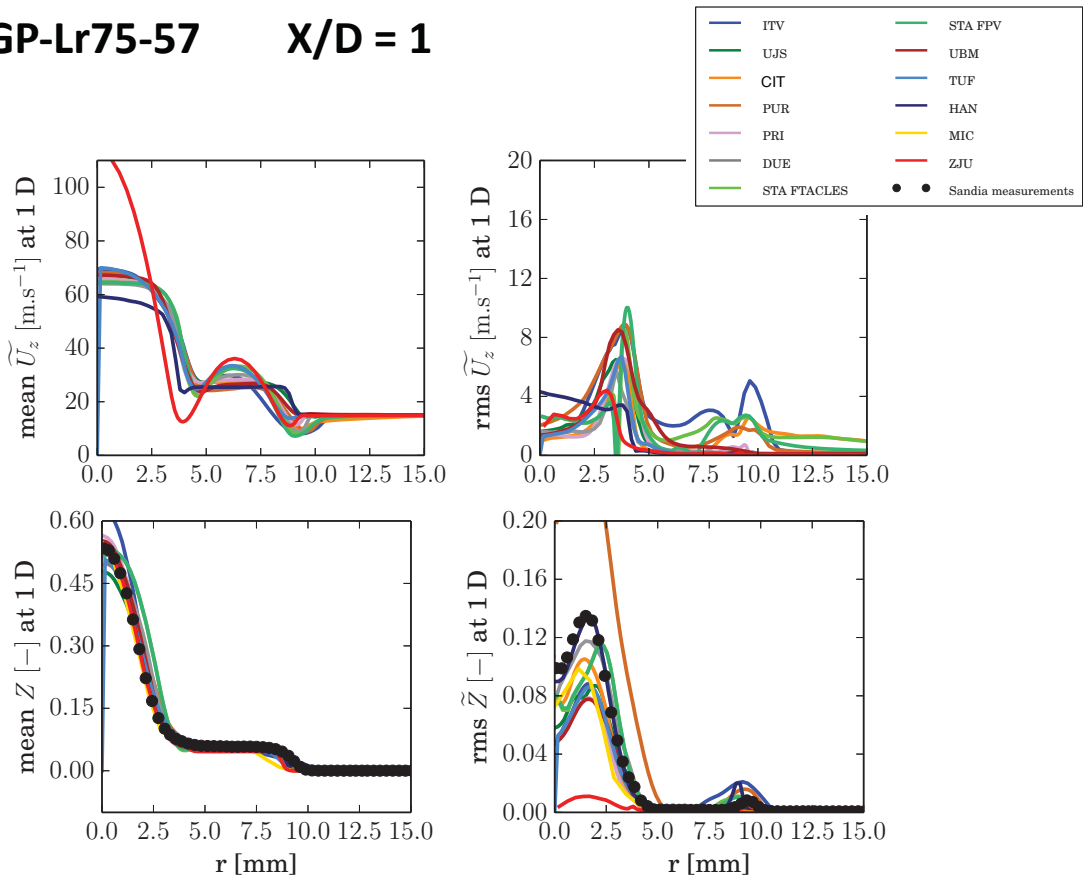


51

FJ-5GP-Lr75-57

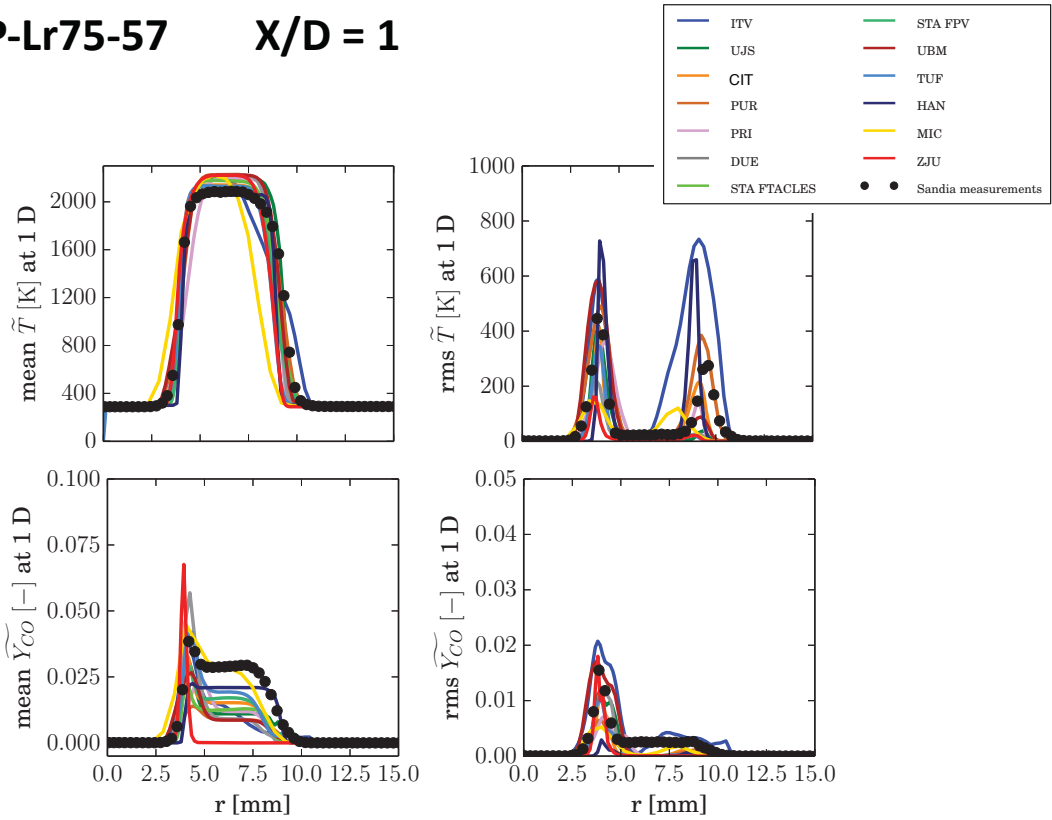
52

FJ-5GP-Lr75-57 X/D = 1



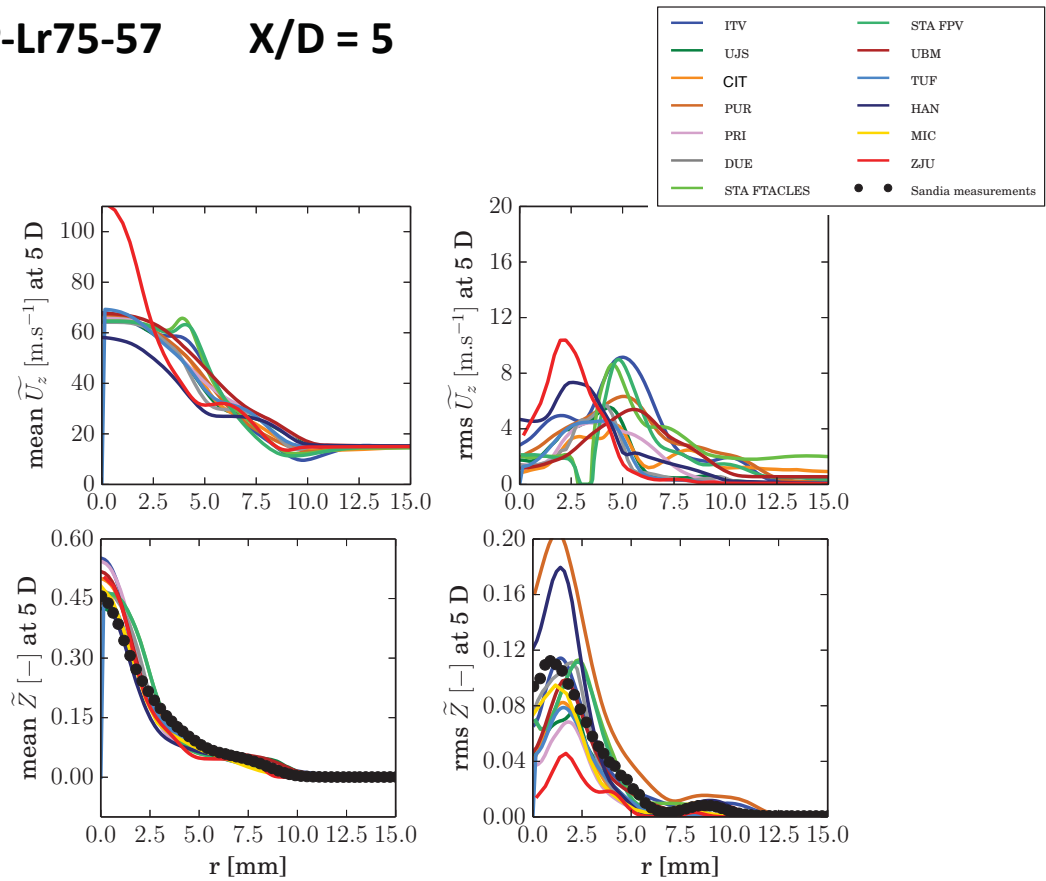
53

FJ-5GP-Lr75-57 X/D = 1



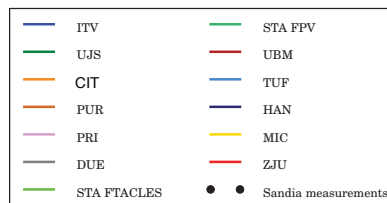
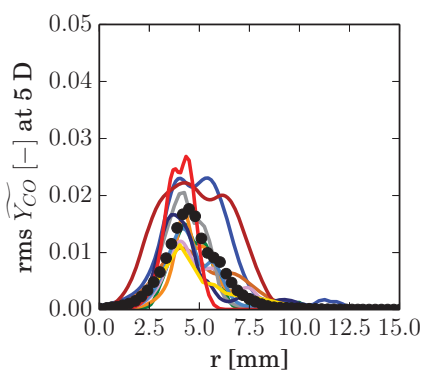
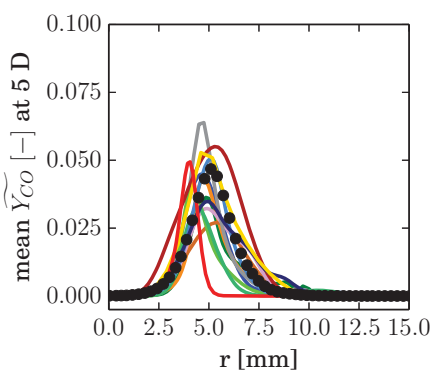
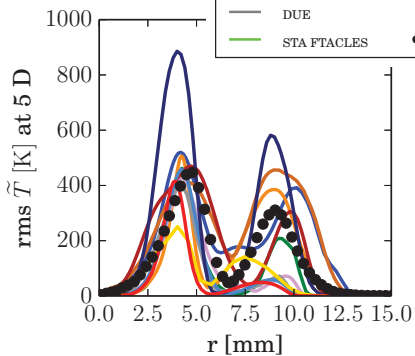
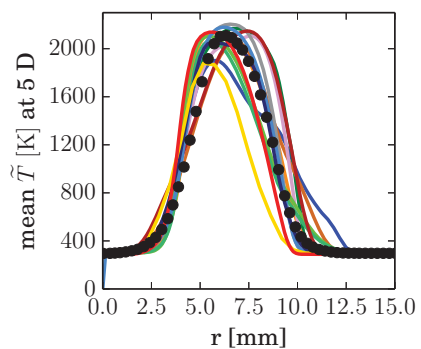
54

FJ-5GP-Lr75-57 X/D = 5

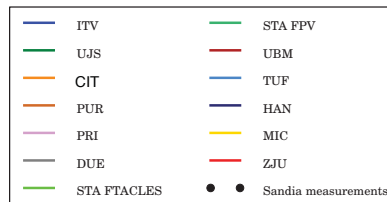
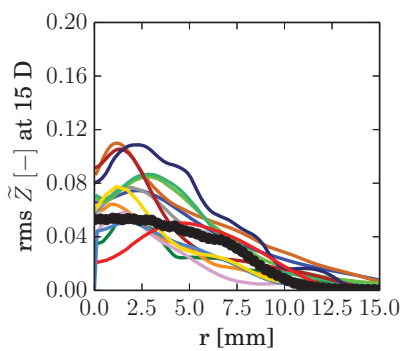
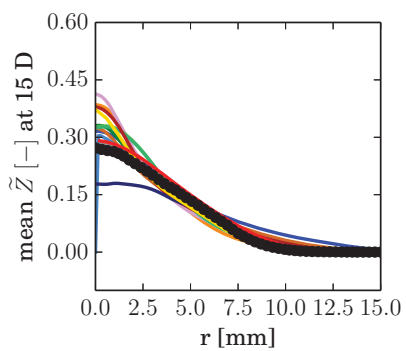
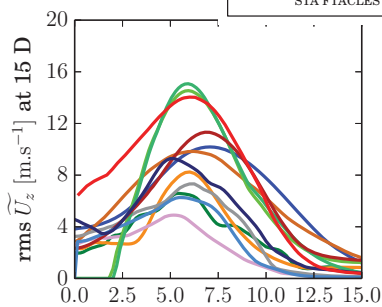
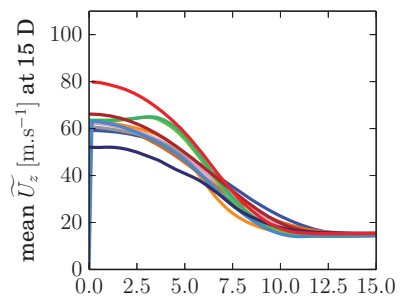


55

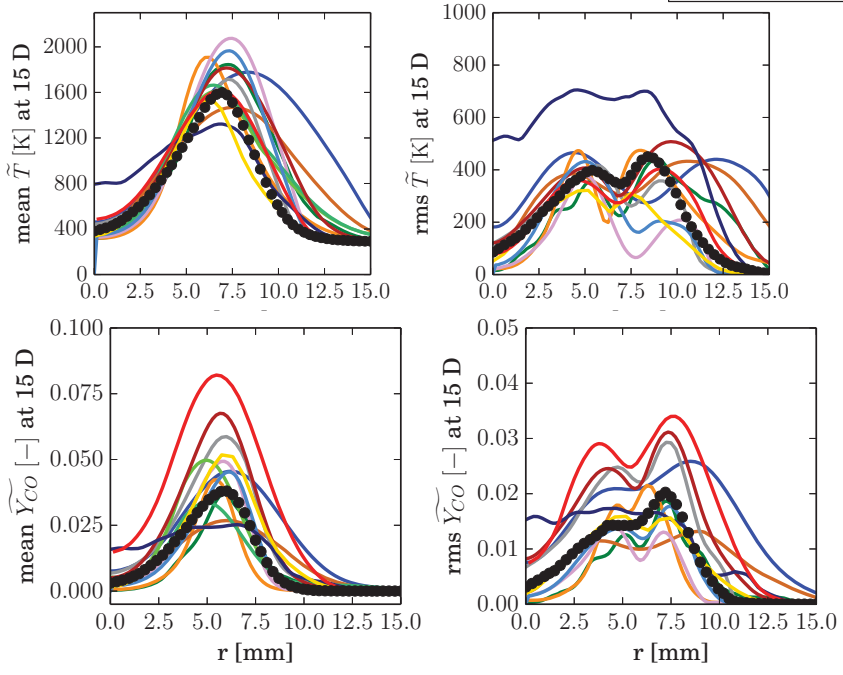
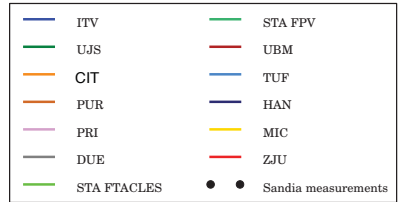
FJ-5GP-Lr75-57 X/D = 5



FJ-5GP-Lr75-57 X/D = 15

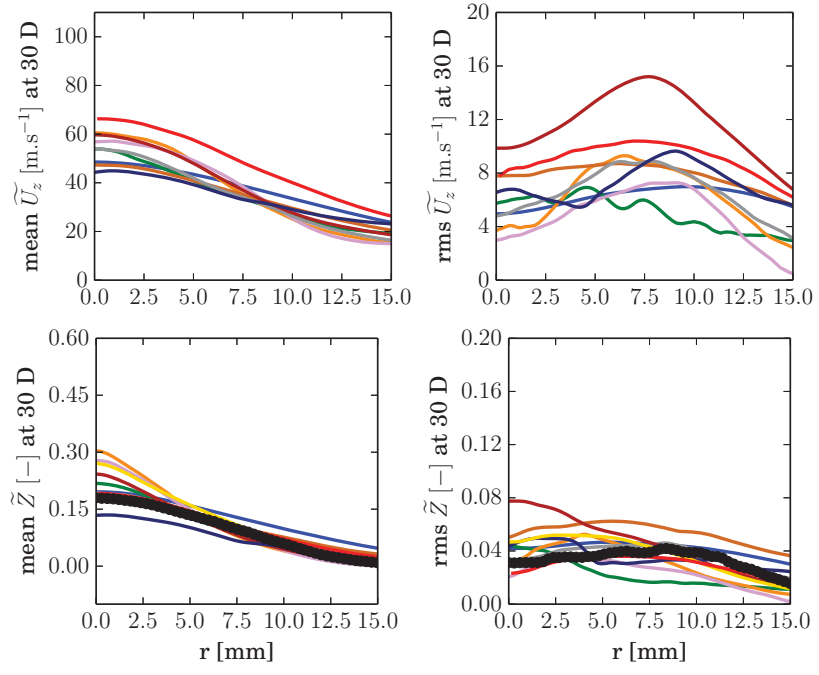
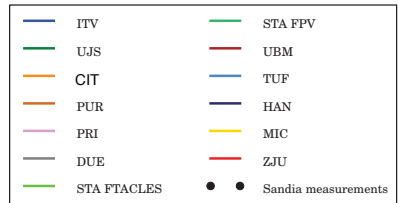


FJ-5GP-Lr75-57 X/D = 15



58

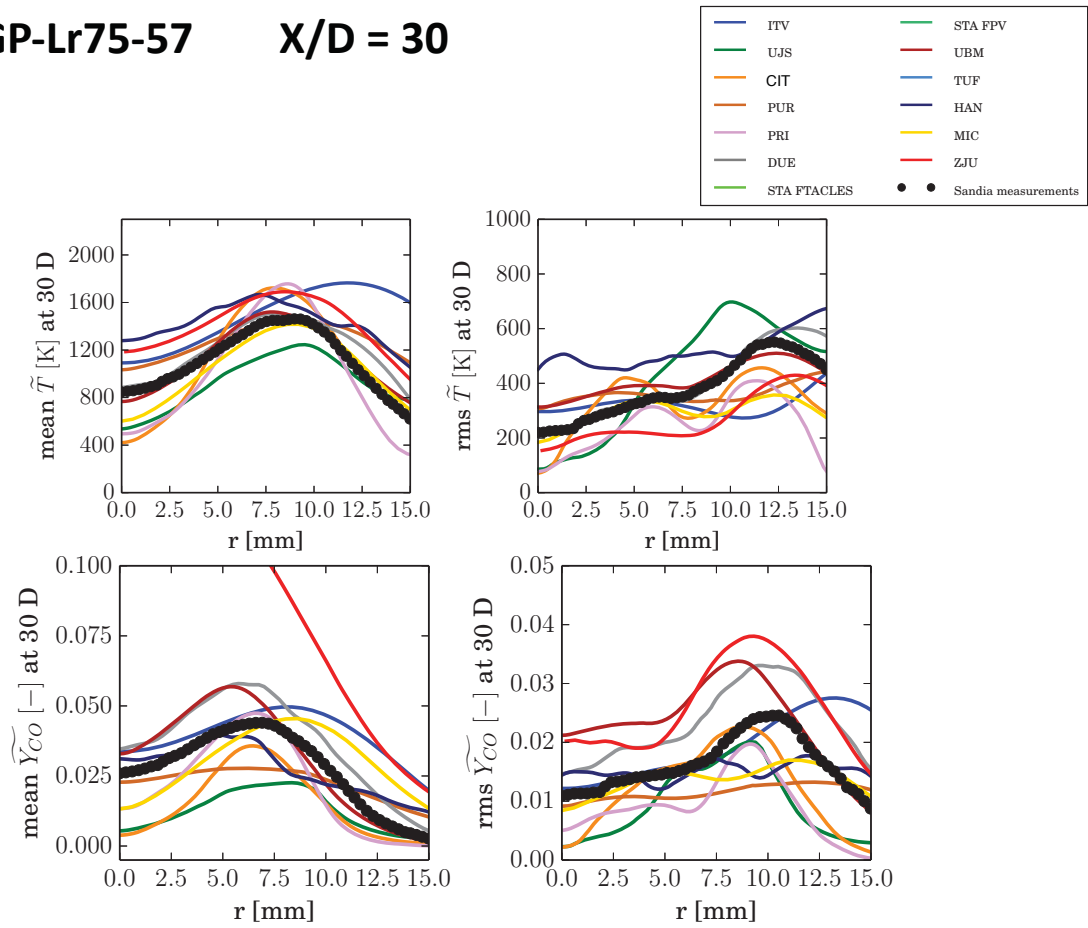
FJ-5GP-Lr75-57 X/D = 30



59

FJ-5GP-Lr75-57

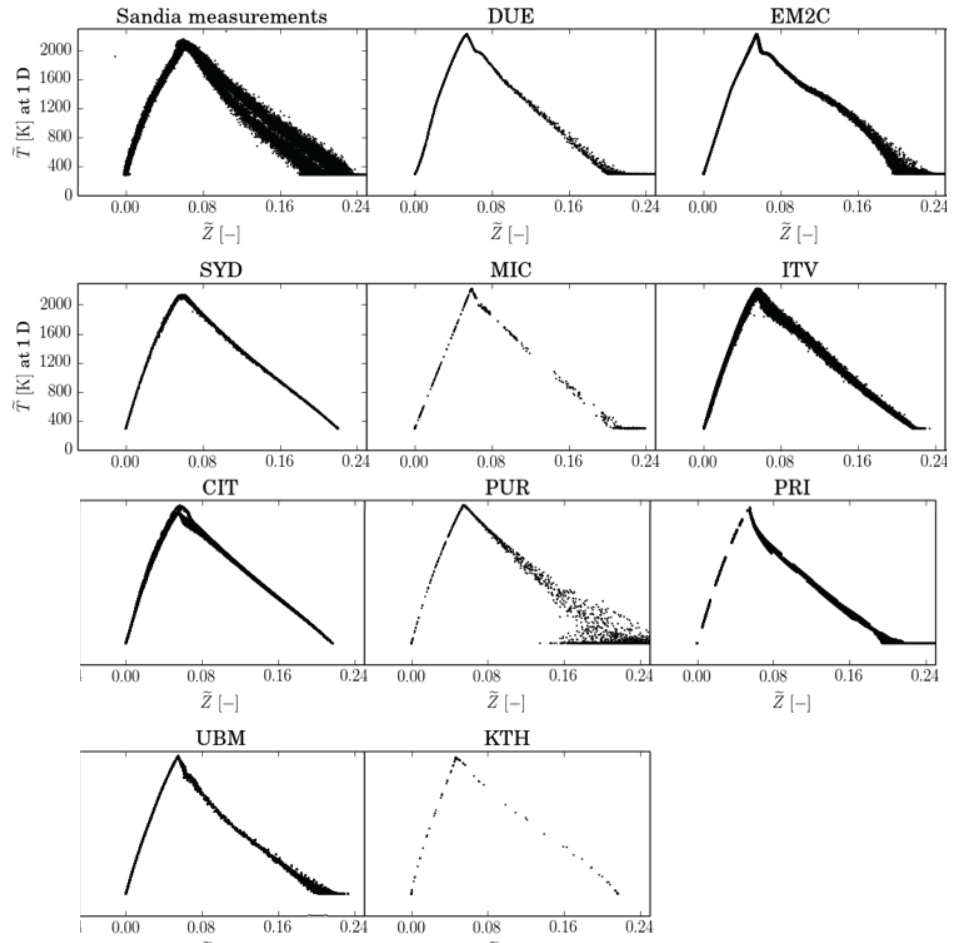
X/D = 30



Scatter plot

Temperature VS mixture fraction

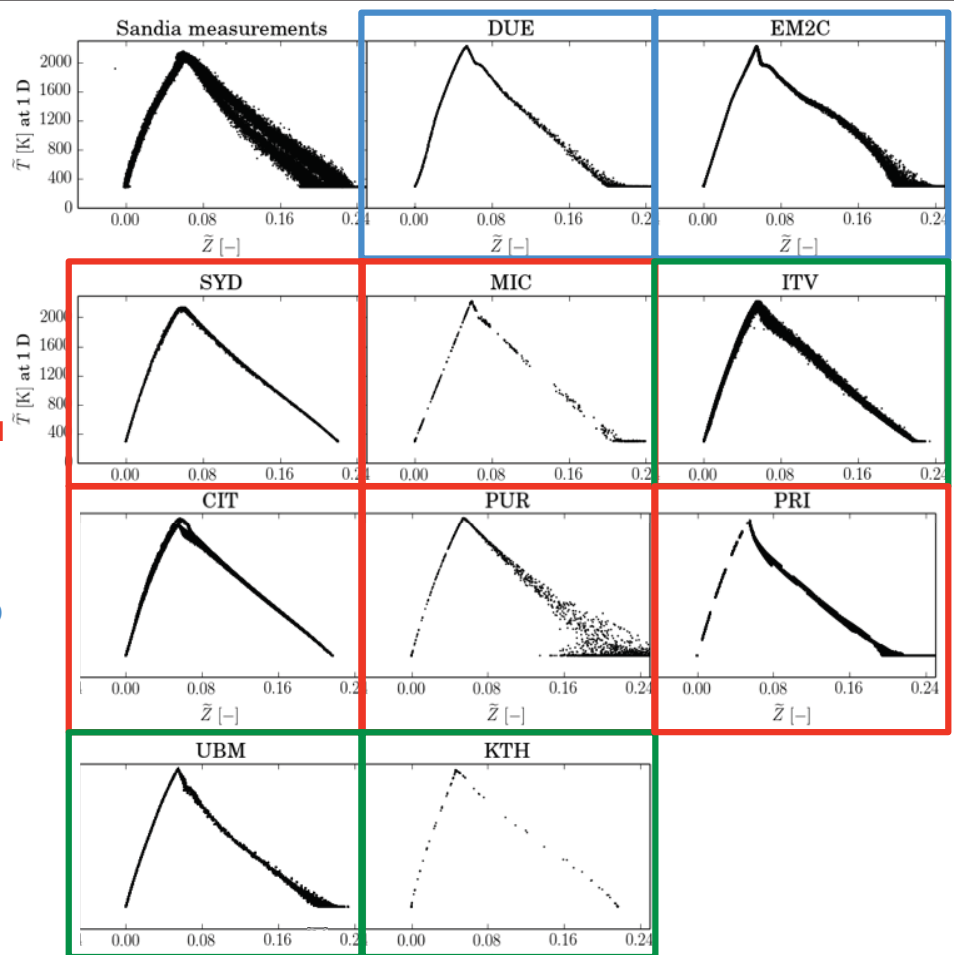
FJ-5GP-Lr300-59
X/D = 1



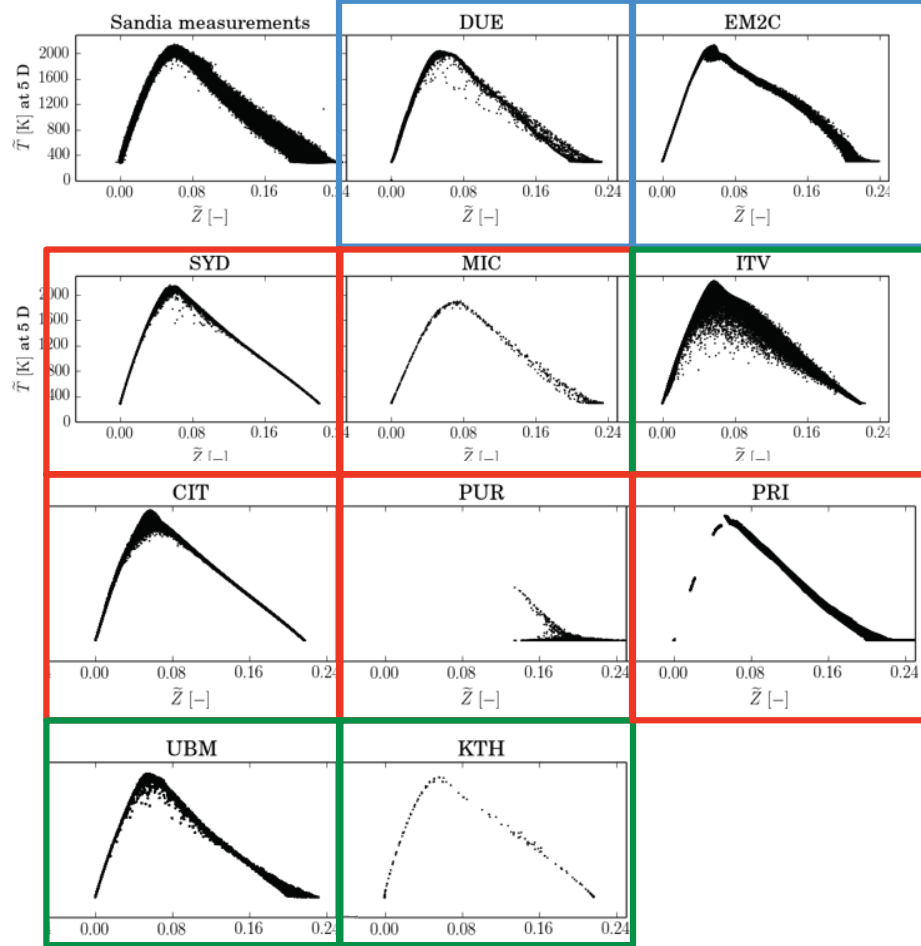
Temperature VS mixture fraction

FJ-5GP-Lr300-59
X/D = 1

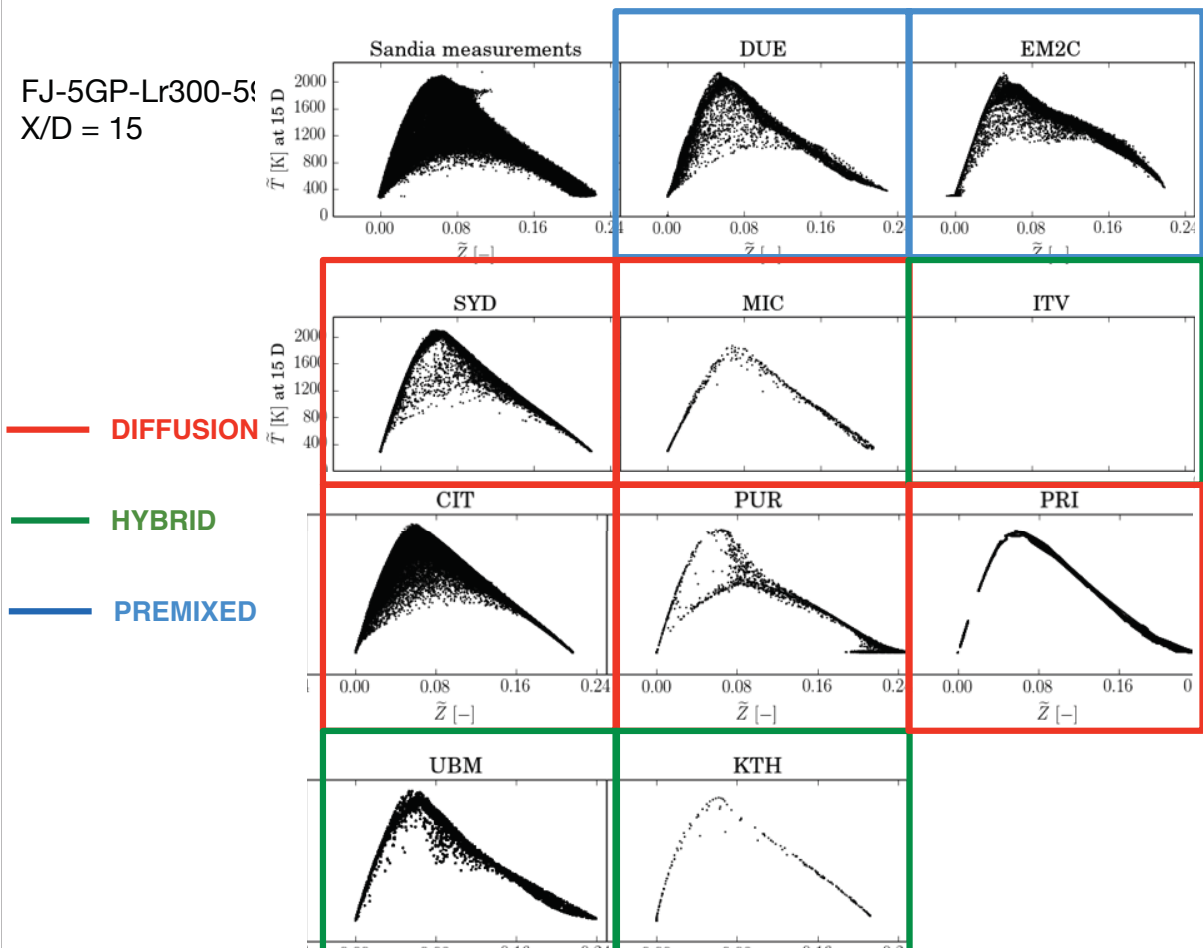
- DIFFUSION
- HYBRID
- PREMIXED



FJ-5GP-Lr300-59
X/D = 5

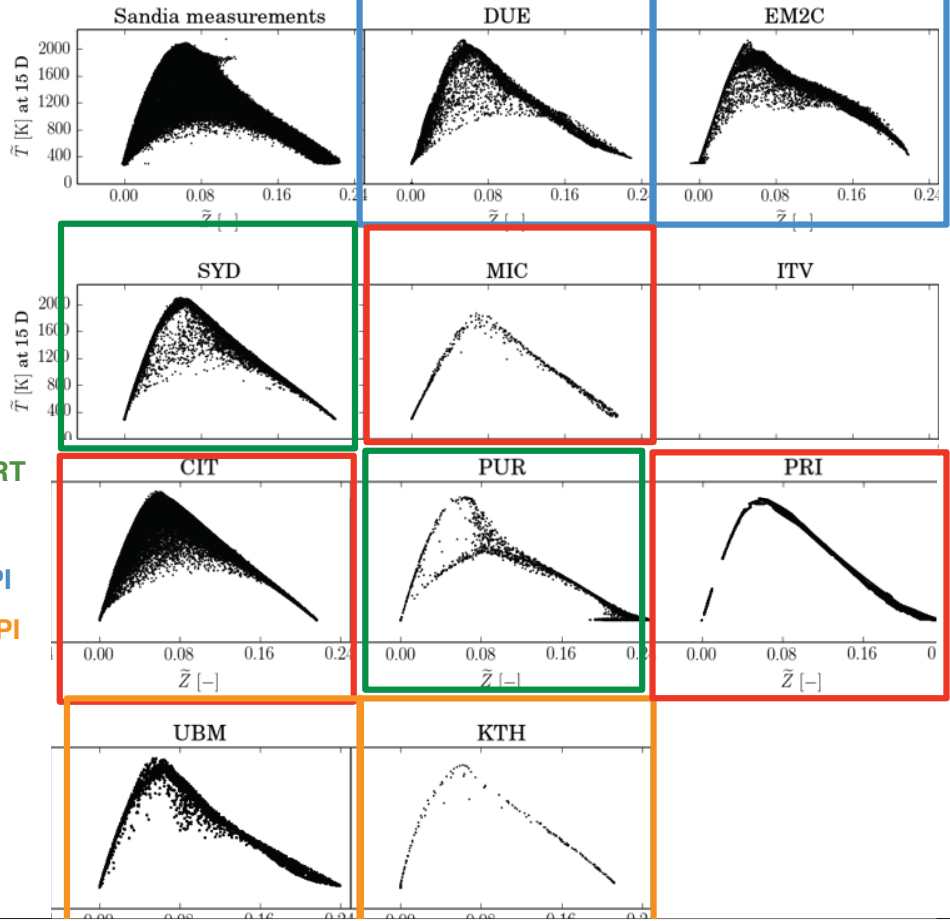


FJ-5GP-Lr300-59
X/D = 15



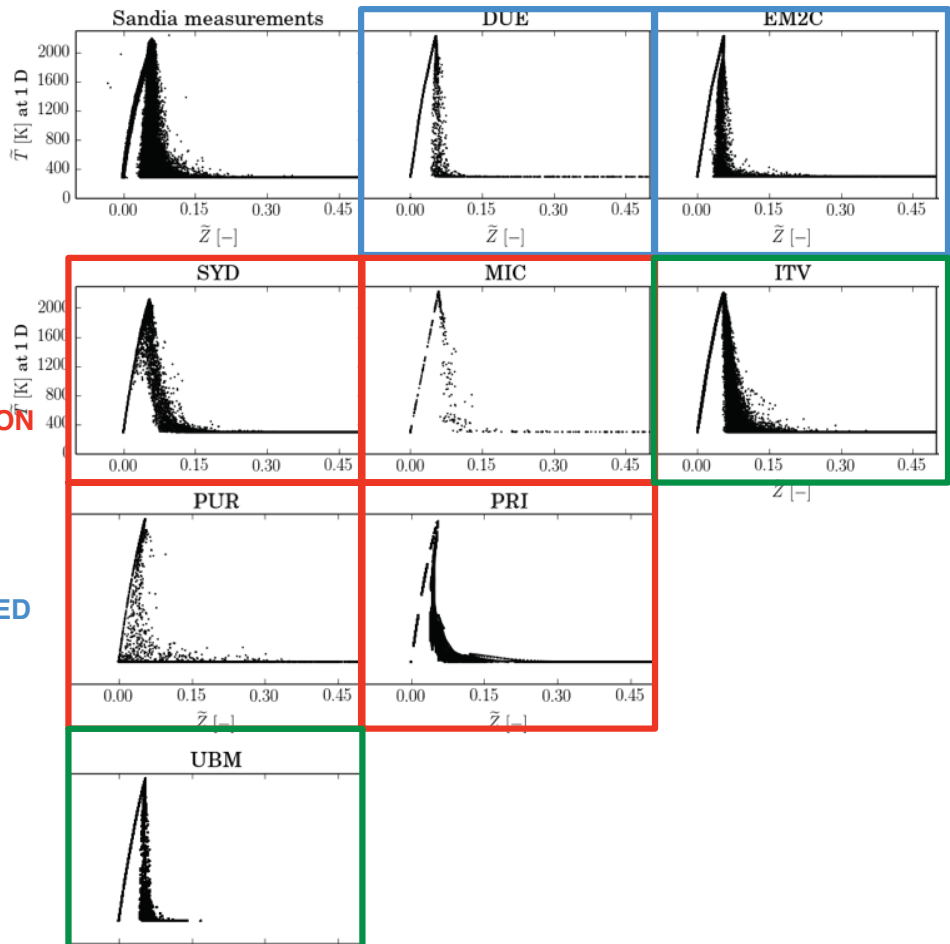
FJ-5GP-Lr300-59
X/D = 15

- FPV
- TRANSPORT PDF
- TFLES - FPI
- TFLES - FPI



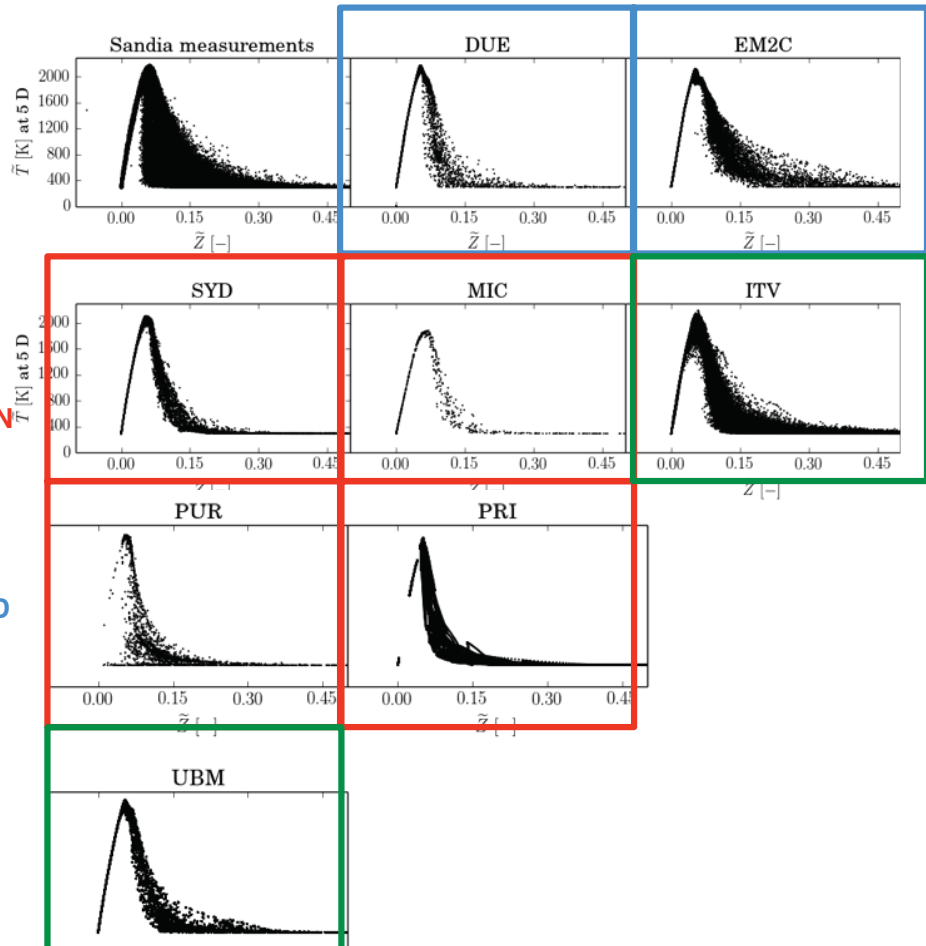
FJ-5GP-Lr75-80
X/D = 1

- DIFFUSION
- HYBRID
- PREMIXED



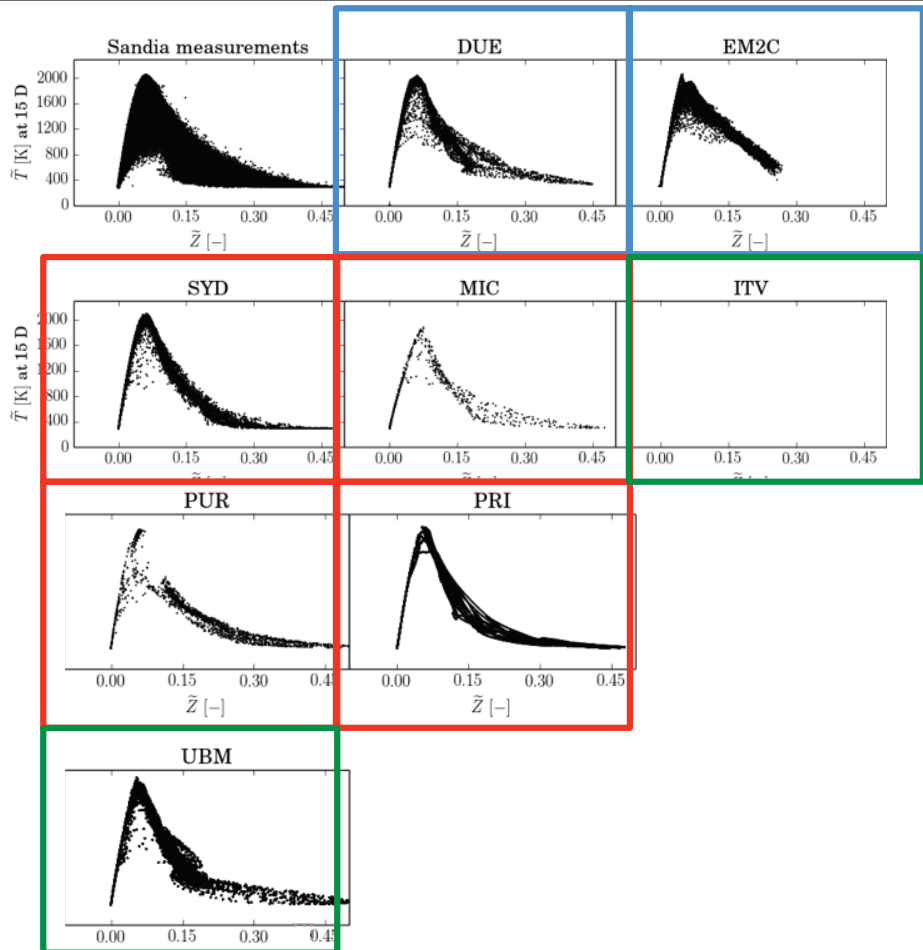
FJ-5GP-Lr75-80
X/D = 5

— DIFFUSION
— HYBRID
— PREMIXED

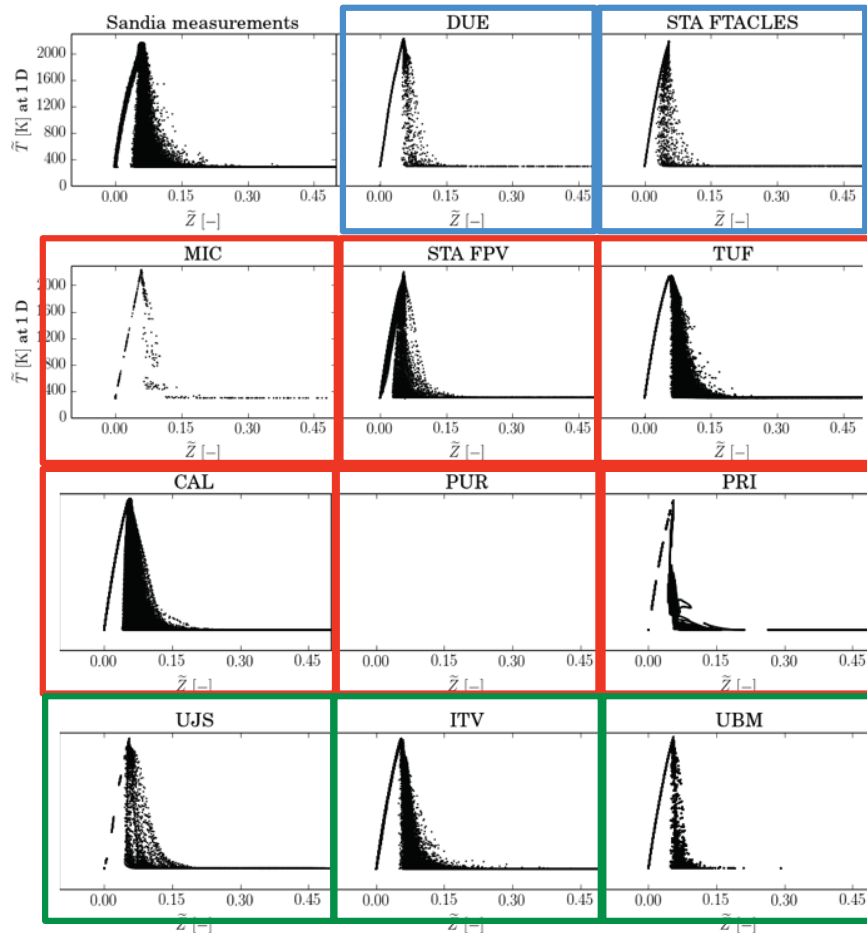


FJ-5GP-Lr75-80
X/D = 15

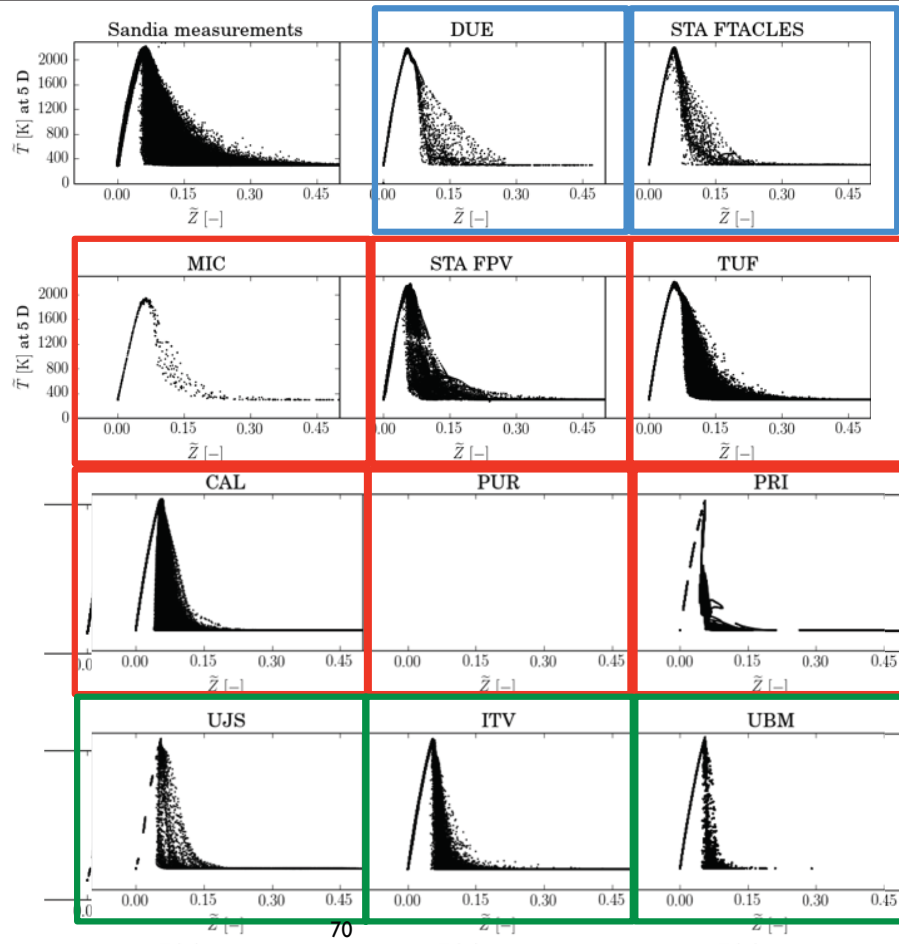
— DIFFUSION
— HYBRID
— PREMIXED



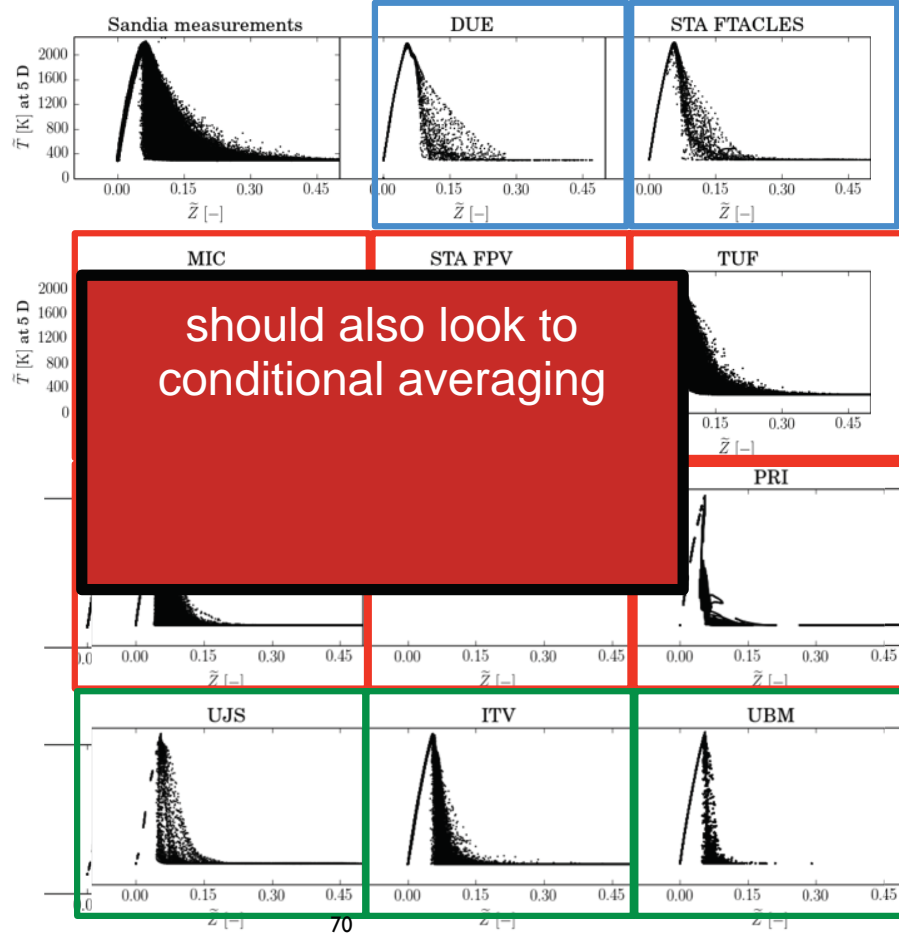
FJ-5GP-Lr75-57
X/D = 5



FJ-5GP-Lr75-57
X/D = 15



FJ-5GP-Lr75-57
X/D = 15



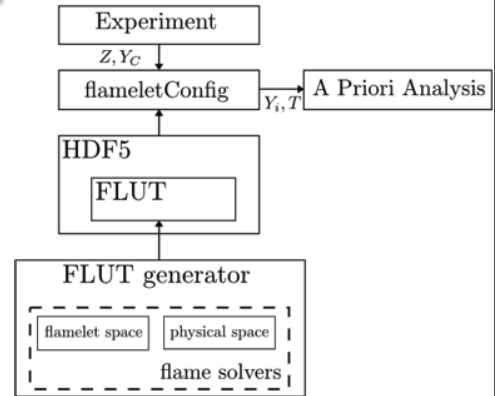
A priori analysis of the inhomogeneous configuration

Sebastian Popp and Christian Hasse

TU Freiberg

A priori analysis

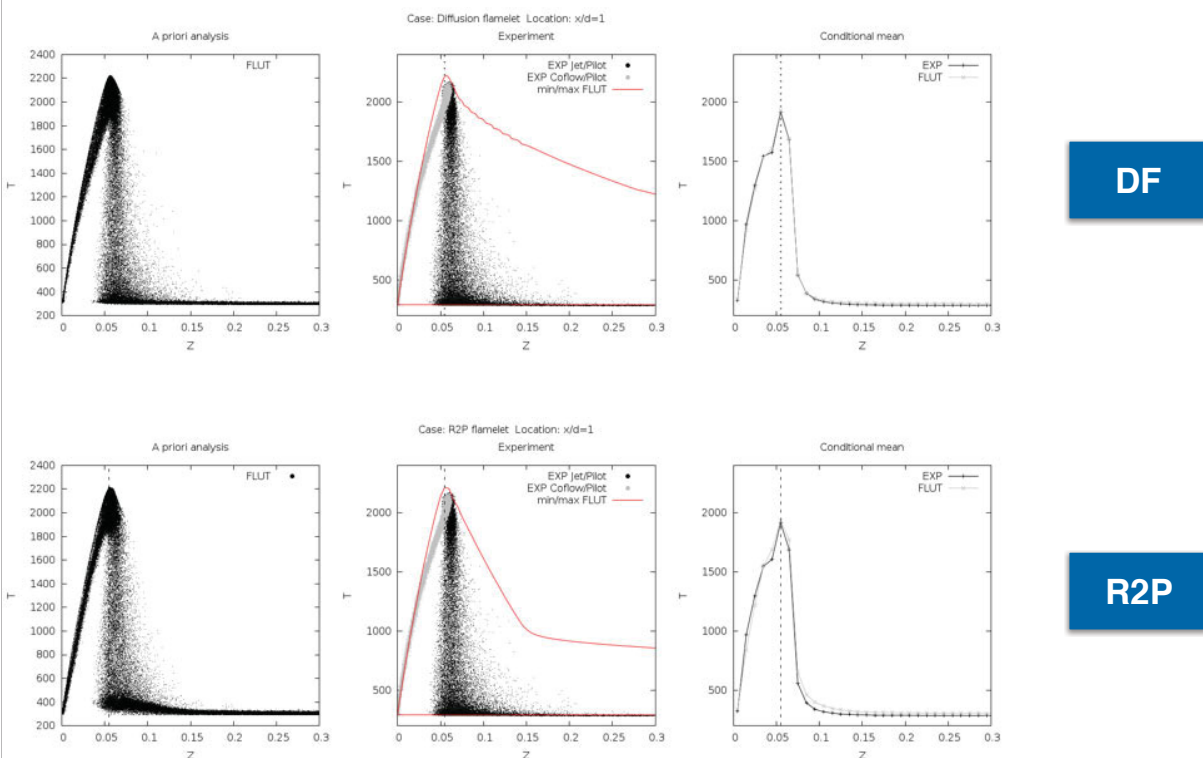
- Evaluation of the chemistry tabulation approach prior to LES-FPV computations
 1. Calculating Bilger mixture fraction and progress variable from Raman/Rayleigh measurements [1]
 2. Using these values to retrieve solution from flamelet lookup tables (FLUT)
 3. Comparing results with experimental data
 - Instantaneous scatter data
 - Conditional means



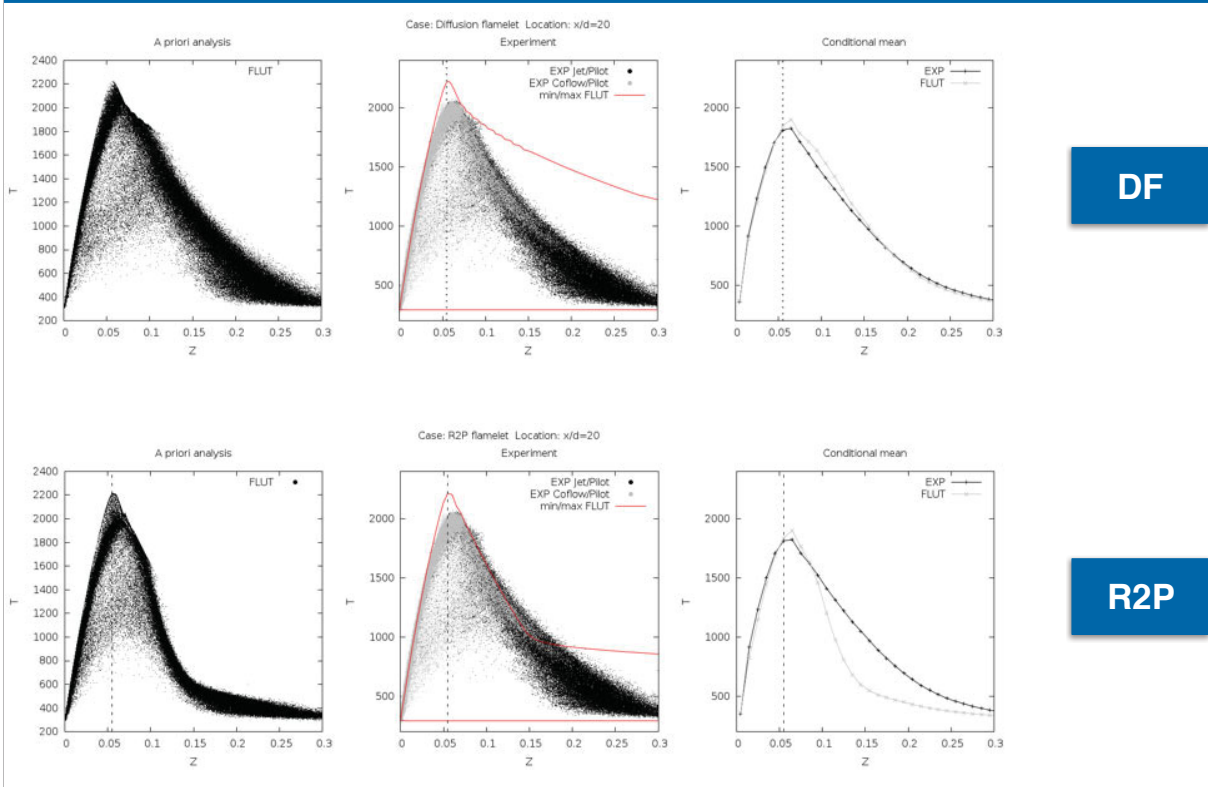
Flamelet lookup tables (FLUT)

- Diffusion flamelets (DF) / mixture fraction space
- Premixed reactants to products (R2P) calculations in physical space (strained premixed flames)
- other canonical flame, e.g. freely propagating flames, were tested but with unsatisfactory results

[1] R. Barlow *et al.*, Combustion and Flame 162 (2015)



[1] R. Barlow *et al.*, Combustion and Flame 162 (2015)



[1] R. Barlow *et al.*, Combustion and Flame 162 (2015)

Conclusions

- Preliminary data: results are in average 24h00 hours old. Too early to draw conclusions on the results.
- Required improvement of the prediction of mixture fraction (especially for the $L_r=75\text{mm}$ case) and probably the velocity field: mandatory before analyzing deeper the role of the combustion model
- Velocity and mixture fraction measurements on cold configurations would help a lot
- We post-process data from 15 groups ! having so many data enables to condition the results by many criteria:
 - the type of model
 - mesh size
 - type of code
 - student experience in TNF target flame simulations
- Further analysis should be done: conditional averaging in addition to the scatter plot: may evidence difference between models.

Perspective

- Continue the effort ! We have two years to:
 - improve consistency of the simulation (mesh independent solutions)
 - agree on a common set of BC's
 - the objective is to isolate the performance of the combustion model
- Then we could write a paper: who is next ?

blank

Influence of pilot flame parameters on the stability of turbulent jet flames

Thibault F. Guiberti, Hugh Cutcher, William L. Roberts, Assaad R. Masri

The objective of this part of the “Sydney Partially-Premixed Flame” session was to present a comprehensive study of the effects of pilot flame parameters on the stability of turbulent jet flames. The Sydney inhomogeneous-piloted burner was employed as the experimental platform with two different fuels: CNG and LPG. Various pilot flames were made from five gases: hydrogen, acetylene, oxygen, nitrogen, and argon, to enable sufficient range in exploring the influence of important pilot flame parameters such as its heat release, temperature, burnt gas velocity, equivalence ratio, and hydrogen to carbon ratio. Blow-off velocity measurements were conducted for non-premixed and partially premixed jet flames (both for homogeneous and inhomogeneous inlets), which led to the following conclusions:

- Increasing the pilot temperature benefits the jet flame stability and has an even greater influence than the pilot heat release, which was also shown to enhance flame stability.
- Increasing the pilot burnt gas velocity reduces the blow-off velocity, except for the limiting case of fully non-premixed jets.
- The pilot hydrogen to carbon ratio H/C was shown to have no significant influence on the jet flame stability in the examined range $3.0 \leq H/C \leq 5.0$.
- Resorting to lean pilots significantly enhances the stability of these globally rich jet flames. Modifying the pilot equivalence ratio also changes the optimal fuel tube recess distance that yields the largest blow-off velocity.
- One-dimensional laminar flame simulations showed that the experimental trends were similar to those obtained for rich mixtures counter-flowing against a hot stream of combustion products, which simulate the pilot/jet interface.

These results could be useful to modelers because they provide insight into the sensitivity of the jet flames stability to the implemented pilot boundary conditions. For example, the measured large influence of the pilot temperature implies that this parameter needs to be prescribed with great care in simulations. Neglecting heat losses near the pilot could lead to an overestimate of jet flame stability. Similarly, the pilot flame gas velocity, which is usually specified uniformly across the pilot stream, will need to be treated with more care. In studies regarding piloted turbulent flames, efforts are usually made to produce a pilot featuring the same hydrogen to carbon ratio as the main fuel because it facilitates post-processing of advanced laser diagnostics and modeling. It is evident from the results presented in this session that satisfying this criterion is not needed to capture the correct trends in jet flame stability. Trends reported here could also be extrapolated to other, more complex, modes of stabilization where the recirculation of heat plays a significant role in flame stabilization, such as bluff-body or swirl configurations.

Influence of Pilot Flame Parameters on the Stability of Turbulent Jet Flames

T.F. Guiberti^{1,2}, H. Cutcher¹, W.L. Roberts², A.R. Masri¹



¹School of Aerospace, Mechanical and Mechatronic Engineering, The University of Sydney, NSW 2006, Australia

²Clean Combustion Research Center, KAUST, Thuwal 23955, Saudi Arabia



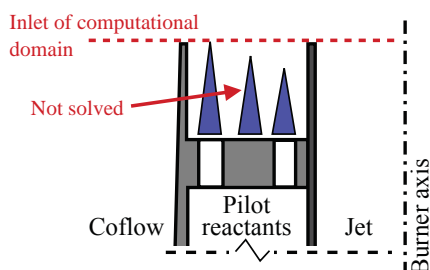
2016 International Workshop on Measurement and Computation of Turbulent Flames
Seoul, Korea, July 28–30, 2016



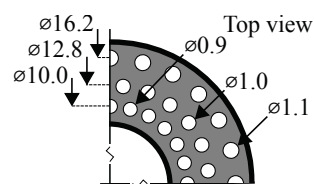
Context



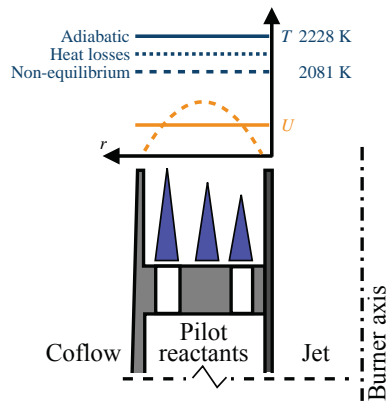
- Pilot boundary conditions (BC) for LES were the object of numerous discussions during the preparation of this session.



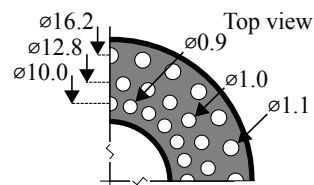
- The 72 laminar conical flames are not solved.
- The **temperature/velocity/species** radial profiles must be provided for the pilot stream, at the burner's exit plane.
- The pilot perforated plate was designed to yield flat profiles.



- Pilot boundary conditions (BC) for LES were the object of numerous discussions during the preparation of this session.



- The 72 laminar conical flames are not solved.
- The temperature/velocity/species radial profiles must be provided for the pilot stream, at the burner's exit plane.
- The pilot perforated plate was designed to yield flat profiles.

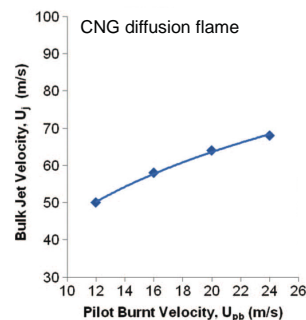


- The sensitivity of the turbulent flame to pilot conditions must be assessed.

- The sensitivity of the turbulent flame to the pilot temperature was evidenced numerically for flame F, which sits close to global extinction.
 - Q. Tang et al., Proc. Combust. Inst, 2000
 - R.R. Cao & S.B. Pope, Combust. Flame, 2005

Flame	Re_{jet}	U_j (m/s)	U_{pb} (m/s)	U_c (m/s)	T_p (K)	Result
F	44800	99.2	22.8	0.9	1860	Extinguished
F	44800	99.2	22.8	0.9	1880	Burning

- It is well known that increasing the pilot heat release improves stability.



(M. Juddoo et al., Combust. Theor. Model, 2011)

- Overall, the sensitivity of turbulent jet flames to pilot conditions is not well known.

- Both pilot velocity and heat release are modified at the same time.

- What are the main pilot parameters?

- Heat release Hr
- Temperature T_{ad}
- Burnt gas velocity U_{bp}
- Equivalence ratio ϕ_p
- Hydrogen to carbon ratio H/C

- Objective:

Analyze experimentally the influence of each of these parameters:

- independently,
- for non-premixed and partially-premixed (homogeneous and non-homogeneous inlets) flames.

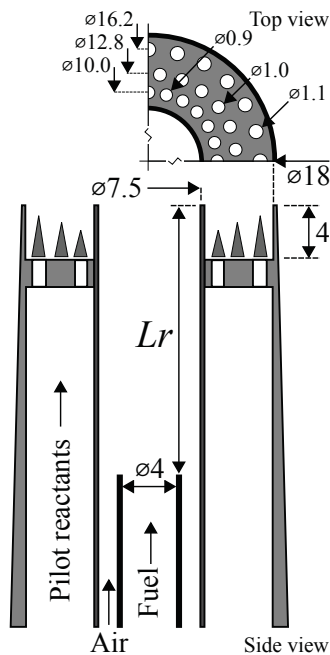
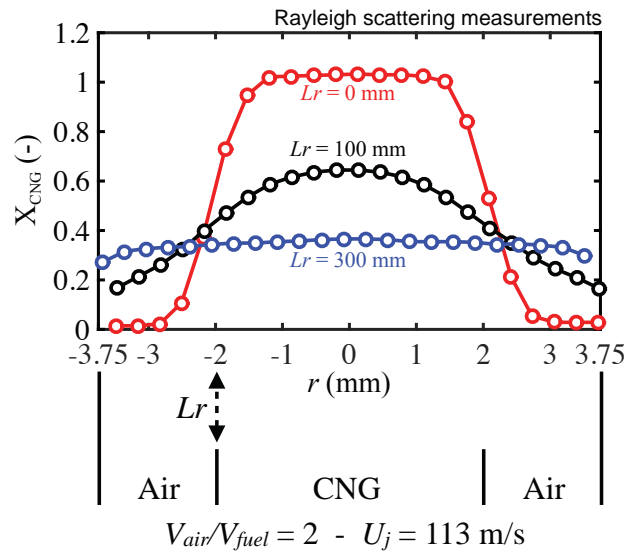
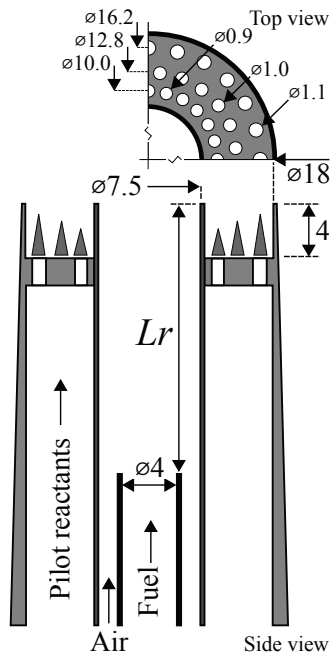
1. Sydney burner with inhomogeneous inlets

2. Influence of pilot characteristics on the stability of turbulent jet flames

- Heat release Hr
- Temperature T_{ad}
- Burnt gas velocity U_{bp}
- Equivalence ratio ϕ_p
- Hydrogen to carbon ratio H/C

3. Comparison with 1-D laminar simulations

4. Conclusions



- Two fuels are examined:
 - Compressed Natural Gas - CNG (=90% methane - CH₄)
 - Liquefied Petroleum Gas - LPG (=90% propane - C₃H₈)
- The global jet equivalence ratio is $\phi_p = 4.76$ ($V_A/V_F = 2$ for CNG and $V_A/V_F = 5$ for LPG).
- 24 pilot conditions are examined:
 - 5 gases pilot,
 - O₂ oxidizer,
 - C₂H₂ and H₂ fuels,
 - N₂ and Ar diluents.

Name	H_r (W)	T_{ad} (K)	U_{pb} (m.s ⁻¹)	ϕ_p	H/C	X _{N2} /X _{O2}	X _{Ar} /X _{O2}	
A1 (ref)	2220	2480		23.9	1.0	4.0	3.76	0.00
A2	2049	2480		23.9	1.0	4.0	3.00	1.20
A3	1879	2480		23.9	1.0	4.0	2.12	2.60
A4	1716	2480		23.9	1.0	4.0	1.12	4.20
A5	1559	2480		23.9	1.0	4.0	0.02	6.00
B1 (ref)	2220	2480		23.9	1.0	4.0	3.76	0.00
B2	2220	2552		23.9	1.0	4.0	2.97	0.60
B3	2220	2646		23.9	1.0	4.0	1.95	1.40
B4	2220	2739		23.9	1.0	4.0	0.92	2.20
B5	2220	2811		23.9	1.0	4.0	0.15	2.80
C1 (ref)	2220	2480	23.9	1.0	4.0	3.76	0.00	
C2	2220	2480	26.6	1.0	4.0	2.75	1.60	
C3	2220	2480	29	1.0	4.0	1.87	3.00	
C4	2220	2480	31.7	1.0	4.0	0.87	4.60	
C5	2220	2480	34.1	1.0	4.0	0.02	6.00	
D1	2220	2480	27.0	0.7	4.0	1.84	0.99	
D2	2220	2480	27.0	0.8	4.0	2.22	1.15	
D3	2220	2480	27.0	0.9	4.0	2.51	1.40	
D4	2220	2480	27.0	1	4.0	2.60	1.83	
D5	2220	2480	27.0	1.1	4.0	2.28	2.66	
D6	2220	2480	27.0	1.2	4.0	1.52	3.89	
D7	2220	2480	27.0	1.3	4.0	0.54	5.33	
E1	2220	2480	27.0	1.0	3	2.66	1.86	
E2	2220	2480	27.0	1.0	3.5	2.63	1.85	
E3	2220	2480	27.0	1.0	4	2.60	1.83	
E4	2220	2480	27.0	1.0	4.5	2.58	1.82	
E5	2220	2480	27.0	1.0	5	2.55	1.81	

-30 % variation

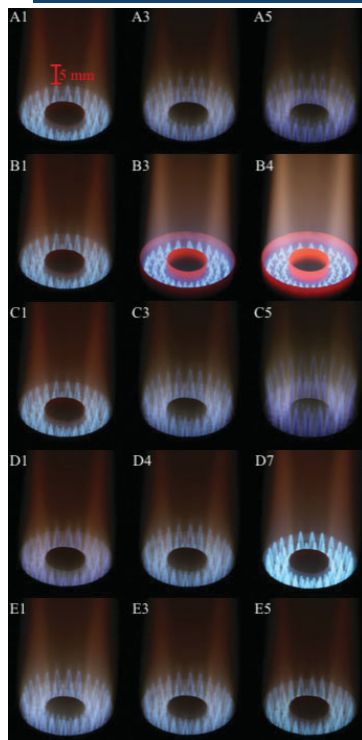
+14 % variation

+43 % variation

± 30% variation

± 25% variation

7



H_r

T_{ad}

U_{pb}

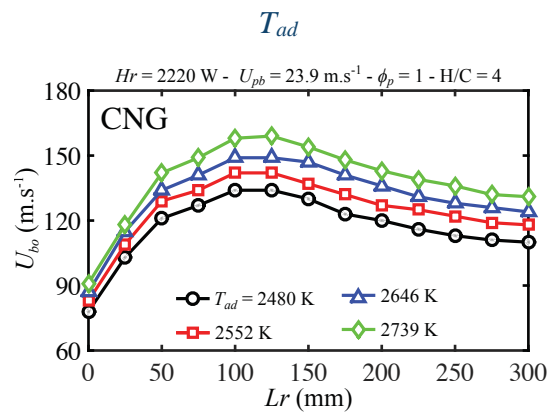
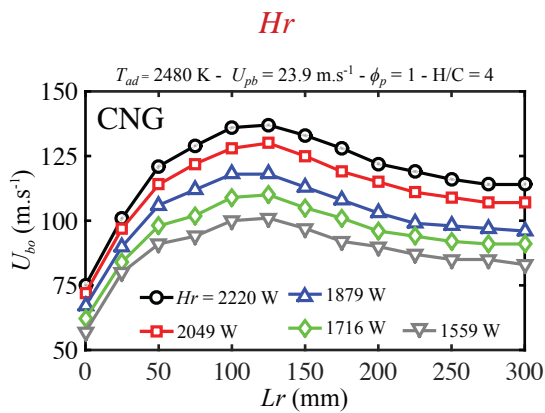
ϕ_p

H/C

- It is not possible here to change each parameter individually without also changing the pilot flames height.

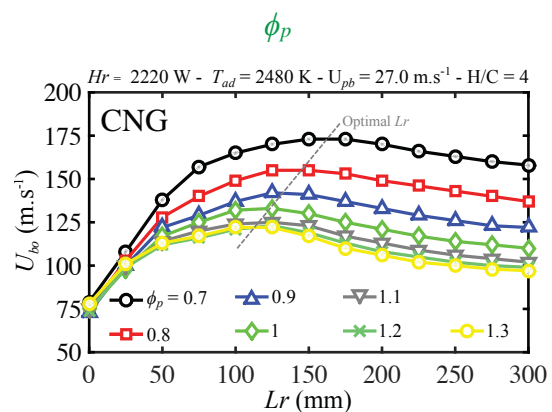
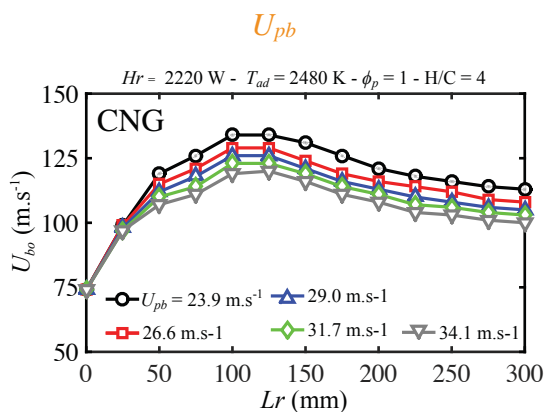
- It was verified that the pilot flames height does not have a significant influence on the turbulent flame stability limits.

8



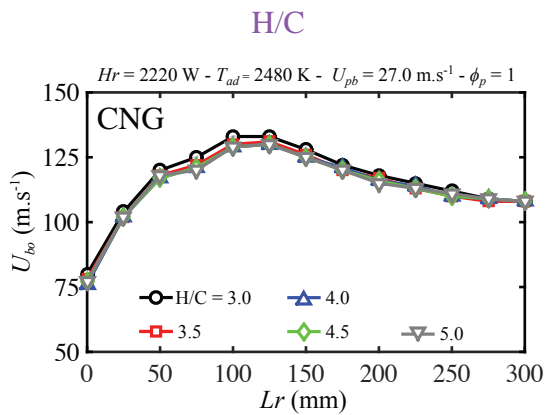
- The influence of the recess distance on the turbulent flame stability does not depend on the pilot heat release.
- Decreasing Hr decreases the turbulent flame stability.
- The influence of the recess distance on the turbulent flame stability does not depend on the pilot temperature.
- Increasing T_{ad} increases the turbulent flame stability.

9



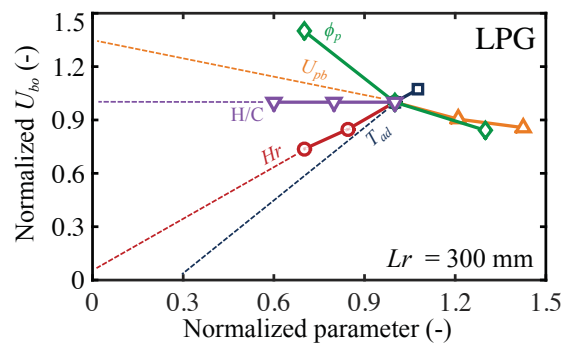
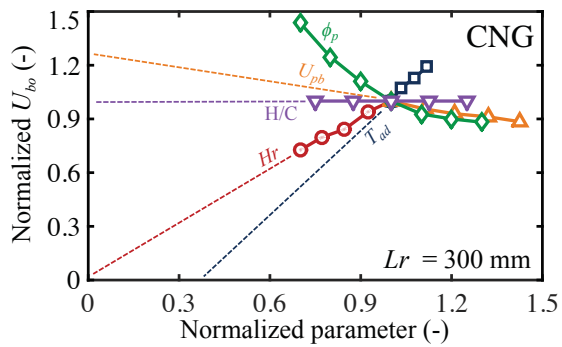
- The influence of the recess distance on the turbulent flame stability does not depend on the pilot velocity.
- Except for $Lr < 15 \text{ mm}$, increasing U_{pb} decreases the turbulent flame stability.
- Resorting to leaner pilot shifts the optimal Lr to larger values (*i.e.* richer mixtures in contact with the pilot).
- Decreasing ϕ_p below 1 increases the flame stability for $Lr > 0$.
- Increasing ϕ_p above 1 has a weak influence on the flame stability.

10



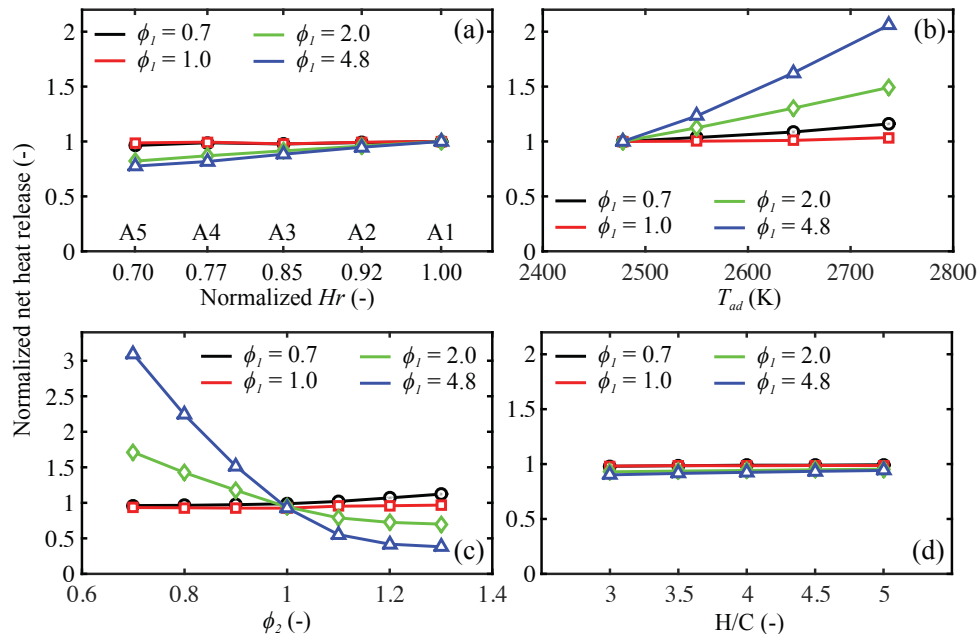
- The pilot hydrogen to carbon ratio has no or small influence on the blow-off velocity.

11



- Globally, T_{ad} and ϕ_p have the largest influence on the turbulent flame stability.
- Results are similar in trends and numbers for LPG.

12



- Trends are well captured by 1-D laminar counterflow simulations (except for U_{pb} , which needs to be analyzed with RANS).

13

- › **Pilot effects on the stability of turbulent flames were analyzed experimentally and numerically:**
 - The Sydney burner allows to examine non-premixed and partially-premixed (homogeneous and non-homogeneous inlets) flames
 - Increasing the pilot heat release or temperature increases flame stability. The pilot temperature was found to be a strong influential parameter.
 - Lean pilots significantly enhance the stability of globally rich jet flames. Modifying the pilot equivalence ratio also changes the optimal fuel tube recess distance.
 - Increasing the velocity of pilot burnt gases reduces flame stability for both homogeneous and inhomogeneous fuel/air mixtures.
 - The pilot hydrogen to carbon ratio has no significant influence on the flame stability in the examined range.
 - Simple laminar flame simulations for rich mixtures exhibit similar trends.

14

› Implications for advanced simulations:

- Temperature boundary conditions must be prescribed carefully.
- Prescribing either plug-flow or parabolic velocity profiles for the pilot will influence the results.
- While important for modeling strategies and post-processing of advanced diagnostics, conserving the same H/C for pilot and fuel is not important for stabilization.

› More generally:

- These findings are likely to be applicable to other types of flames where recirculation of heat plays a role in flame stabilization:
 - Swirling flames,
 - Bluff-body stabilized flames, *etc.*

15

Thank you for your attention !

Acknowledgments:

This work is supported by the Australian Research Council and CCRC-KAUST.

16

Progress variables and regime indicators in partially-premixed flames

Coordinators: Robert Barlow, Christian Hasse, Matthias Ihme

This session was presented in three parts to highlight recent work aimed at extending the basis for comparison of experimental and modeling results in partially premixed flames and to begin to explore methods for identifying the local combustion regime.

Progress variable for experiments in partially-premixed flames

Robert. Barlow, Gaetano Magnotti, Hugh Cutcher, Assaad Masri

Mixture fraction, Z , and progress variable, c , are central concepts in the turbulent combustion theory and in flamelet modeling of turbulent partially-premixed flames. It is common in both experimental and modeling studies to use Bilger's formulation for mixture fraction, which preserves the stoichiometric value in the presence of differential species diffusion. However, there is no such consensus on the definition of progress variable for partially-premixed flames. In flamelet modeling approaches with tabulated chemistry it is common to define progress variable as a sum of major product mass fractions, often without normalization. Examples for hydrocarbon flames include: Y_{CO_2} , $Y_{CO_2}+Y_{H_2O}$, $Y_{CO_2}+Y_{CO}$, $Y_{CO_2}+Y_{CO}+Y_{H_2O}$, and $Y_{CO_2}+Y_{CO}+Y_{H_2O}+Y_{H_2}$. Progress variable has also been defined on a molar basis as $Y_{CO_2}/w_{CO_2}+Y_{H_2O}/w_{H_2O}+Y_{H_2}/w_{H_2}$. More recently, various 'optimized' progress variables have been proposed that allow for improved efficiency and accuracy in storage and retrieval of thermochemical states from flamelet tables. These optimized progress variables can be linear combinations of many species, with weighting factors that can be positive or negative.

Experimental results on progress variable in partially premixed flames are rare the literature. Measurements of progress variable and its dissipation rate have been reported for premixed and stratified flames, based on Rayleigh scattering measurements of temperature, $c = (T - T_0)/(T_{eq}(Z) - T_0)$, where T_0 is the unburnt reactant temperature and $T_{eq}(Z)$ is the adiabatic equilibrium temperature for the local value of mixture fraction. Conditional mean values of the temperature burning index, which is similarly defined, have been reported for nonpremixed and partially premixed jet flames as an indicator of the probability of local extinction. However, a temperature-based progress variable is only appropriate for flames with negligible heat loss, and it is not favored in modeling.

Raman/Rayleigh experiments in methane-air flames yield temperature and the mass fractions of major species (N_2 , O_2 , CH_4 , CO_2 , H_2O , CO , and H_2). Therefore, an experimentally compatible progress variable should be calculated from mass fractions of a subset of these seven measured species. Three definition of progress variable were compared, and a definition based on the mass of oxygen bound in CO_2 , CO , and H_2O and normalized by the fully burnt state, rather than equilibrium, is argued to offer some advantages. This progress variable can be calculated easily in postprocessing of experimental or computational results, allowing for comparisons of such things as joint and conditional statistics of mixture fraction and progress variable, and well as gradients and dissipation rates of these quantities. Preliminary results of the joint statistics of mixture fraction and progress variable in two of the Sydney piloted flames are presented.

Flame identification and characterization based on 1D Raman/Rayleigh data

Sandra Hartl, Dirk Geyer, and Christian Hasse

Previously proposed methods such as the flame index or the combustion regime identifier require (at least) 3D scalar gradients. These approaches were designed for use in numerical computations, where such data is available. Current experimental techniques such as spontaneous Raman/Rayleigh

scattering cannot access this level of quantitative detail. Even correcting the 1D gradients derived from the Raman/Rayleigh experiment, using the crossed-sheet method, results in information normal to the reaction zone but not a general 3D gradient of major species. Therefore, the method proposed here solely relies on the spatial 1D Raman/Rayleigh line data, which is considered to be the footprint of the local combustion regime. Quantitative information on major species concentrations and temperature is only required in 1D to examine the spatial change in relevant regime markers, rather than full quantitative 3D information.

Based on the directly measured Raman species and the temperature, several flame markers namely the mixture fraction, the heat release rate and the chemical explosive mode (as introduced in the Chemical Explosive Mode Analysis – CEMA), respectively, can be derived. The calculation of the latter two quantities requires special attention since the necessary information about the minor species/radicals is not provided directly by the experiment but must be approximated. Further, experimental uncertainties and their effect on the analysis have to be accounted for.

The proposed method was briefly outlined and then applied for data from a fully resolved simulation of a complex triple flame, for which the full thermochemical state was available. This allowed quantifying the effect of the approximation procedure and the experimental uncertainties, which were superimposed on the fully resolved data. Based on the result, suitable combinations of flame markers to detect a local reaction zone (1) and to characterize it as either non-premixed or premixed (2) were proposed.

The approach was then applied for two TNF benchmark flames, namely the lean turbulent stratified flames from Darmstadt (case TSF-A) and the Sydney/Sandia burner with inhomogeneous inlets (case FJ200-5GP-Lr300-59). Selected experimental 1D lines (up to 6 mm in length) at different downstream locations were analyzed. The flame markers were computed based on the full thermochemical state approximated from the Raman/Rayleigh data. For the TSF-A case, lean premixed reaction zones with and without stratification could be identified clearly at all locations by a sign change of the chemical explosive mode and a local peak of the heat release rate. For the inhomogeneous inlets case, premixed reaction zones were detected in the mixing region between the pilot and the central jet. Further downstream, an additional non-premixed reaction zone could be identified with a local maximum in the heat release rate in the vicinity of stoichiometric mixture. These findings with respect to the combustion regime are consistent with the observed 1D profiles of the major species and the temperature as provided by the Raman/Rayleigh data.

In summary the proposed method allows to detect and characterize reaction zones based on the thermochemical state measured along a line by spontaneous Raman/Rayleigh scattering. It offers an alternative way to analyze experimental results focusing especially on the local combustion regime. Such an approach can also be used for comparing numerical and experimental data, which can be become especially useful for more complex combustion scenarios where the dominant mode of burning is unknown or varying locally in the turbulent flow field.

Progress variable and combustion regime: Relevance to modeling

Matthias Ihme, Hao Wu, Tianfeng Lu, Christian Hasse, and Rob Barlow

This presentation discussed recent progress on the development of reaction-progress variable formulations and combustion-regime indicators for combustion modeling.

Reaction Progress Variable: In relevance to the presentation on the development of a reaction progress variable for experiments (presentation by R. Barlow), computational aspects on requirements for a progress variable were reviewed. In regard to the utilization of progress variables for combustion simulations, the following observations were made:

- Since the progress variable is commonly defined from a linear combination of a set of species, it doesn't provide any new information that we wouldn't obtain by comparing species profiles.
- A main merit of considering a progress variable is that it is a natural parameterization of flamelet manifold models (FPI, FGM, FPV, ...), and becomes an intrinsic variable in any of these combustion models.
- Commonly, a progress variable is defined with respect to major species. As such, it becomes fairly insensitive in describing the inner flame-structure dynamics that is described by radicals and minor species.
- Another attractive property of the progress variable is its linkage to the combustion mode identification by considering alignments between mixture-fraction gradients and progress variable gradients. Since, however, a "combustion mode" is generic, this regime indicator should be insensitive to a particular definition of a progress variable. In other words, we should be able to identify the same "combustion mode" independent of a particular definition of a progress variable.
- To connect the definition of a progress variable between experiments and simulation, as useful extension is to take experimental errors into consideration, thereby increasing the signal-to-noise ratio and minimizing the propagation of experimental uncertainties.

A number of examples were discussed by considering different reactant mixtures and evaluating different progress-variable definitions. The merit of defining a progress variable by including constraints on maximizing the signal-to-noise ratio was illustrated, and the utility of this formulation relies on knowledge about the covariance of uncertainties among different species measurements.

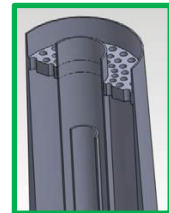
Combustion-regime Indicators: A summary on developments of regime indicators for combustion-mode analysis was provided, and limitations in regard to the (i) dependence on 1D-flame analysis, (ii) dependence on major species and (iii) lack of sensitivity to minor species and quantities of interest were reviewed. Merits and requirements for combustion-mode indicators with respect to combustion modeling were analyzed, suggesting that the definition of combustion-regime indicators in guiding the selection of combustion model requires detailed consideration of the flame-structure representation and consideration of user-specific quantities of interests. By addressing these aspects, a so-called *drift-term* was discussed as a compliance indicator between combustion models and CFD-solution. This compliance indicator doesn't rely on asymptotic limits of combustion-regimes (premixed, diffusion modes), and can find application for combustion-model adaptations.

References

- Barlow, R.S., et al. "Piloted methane/air jet flames: Transport effects and aspects of scalar structure." *Combustion and Flame*, 143.4 (2005): 433-449.
- Ihme, M., Shunn, L. and Zhang, J., "Regularization of reaction progress variable for application to flamelet-based combustion models." *Journal of Computational Physics*, 231, (2012): 7715-7721.
- Pruefer, U., Hartle, S., Hunger, F., Messig, D., Eiermann, M., Hasse, C., "A Constrained Control Approach for the Automated Choice of an Optimal Progress Variable for Chemistry Tabulation." *Flow, Turbulence and Combustion*, 94, (2015), 593-617.
- Wu, H. and Ihme, M. "Compliance of combustion models for turbulent reacting flow simulations." *Fuel*, 186, (2016): 853-863.

On defining progress variable for experiments in partially-premixed methane flames

Rob Barlow, Gaetano Magnotti
Sandia National Laboratories
Hugh Cutcher, Assaad Masri
The University of Sydney



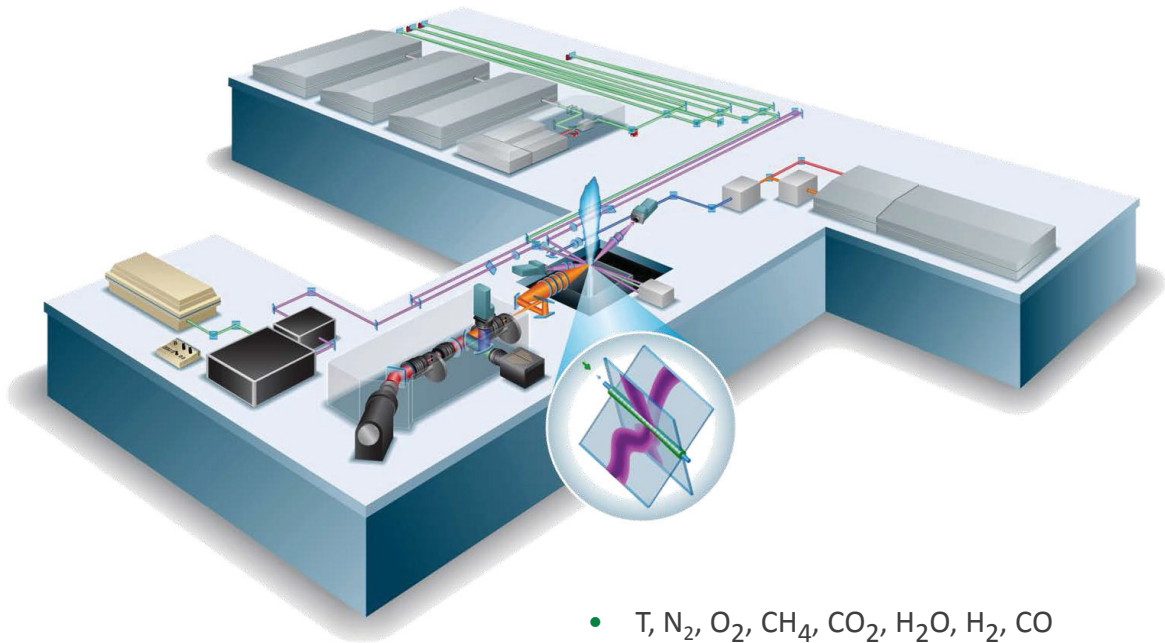
TNF Workshop, July 29, 2016



Objectives

- Define a progress variable that is:
 - appropriate for Raman/Rayleigh experiments
 - useful for comparison with simulations
- Preferences:
 - Use combination of measured species (not T)
 - Normalize (0-unburnt, 1-burnt)
 - Avoid assumptions regarding transport
 - Low measurement noise
- Investigate joint (Z,c) statistics and 1D dissipation terms in turbulent partially-premixed flames

Line-Imaged Raman/Rayleigh/CO-LIF



- T, N₂, O₂, CH₄, CO₂, H₂O, H₂, CO
- 6-mm segment, resolution ≤100μm,

Mixture Fraction & Equivalence Ratio

- Calculated from the 7 measured species
- Bilger mixture fraction (normalized to 1 for pure CH₄):

$$Z = \frac{2(Y_C - Y_{C,2})/w_C + (Y_H - Y_{H,2})/2w_H - (Y_O - Y_{O,2})/w_O}{2(Y_{C,1} - Y_{C,2})/w_C + (Y_{H,1} - Y_{H,2})/2w_H - (Y_{O,1} - Y_{O,2})/w_O}$$

- Equivalence ratio (oxygen needed/oxygen available):

$$\phi = \frac{X_{CO_2} + 2X_{CH_4} + X_{CO} + 0.5(X_{H_2O} + X_{H_2})}{X_{CO_2} + X_{O_2} + 0.5(X_{CO} + X_{H_2O})}$$

- Y—mass fractions; w—atomic wts; X—mole fractions



Progress Variables in Modeling Literature

- Y_{CO_2} (Kuenne 2011)
- $Y_{\text{CO}_2} + Y_{\text{CO}}$ [Fiorina 2003, 2005, Domingo 2008, Chen 2015],
- $Y_{\text{CO}_2} + Y_{\text{H}_2\text{O}}$ [Pierce&Moin 2004],
- $Y_{\text{CO}_2} + Y_{\text{CO}} + Y_{\text{H}_2\text{O}}$ [Proch 2014]
- $Y_{\text{CO}_2} + Y_{\text{CO}} + Y_{\text{H}_2\text{O}} + Y_{\text{H}_2}$ [Ihme 2008, 2010].
- $Y_{\text{CO}_2}/w_{\text{CO}_2} + Y_{\text{H}_2\text{O}}/w_{\text{H}_2\text{O}} + Y_{\text{H}_2}/w_{\text{H}_2}$ (normalized by equilibrium)
[van Oijen 2004, Vreman 2008,].
- ‘Optimized’ progress variables:
[Najafi-Yazdi 2012, Ihme 2012, Niu 2013, Prüfert 2015]



Progress Variables Considered Here

- c_C – based on sum of Y_{CO_2} , Y_{CO}
- c_Y – based on sum of Y_{CO_2} , Y_{CO} , $Y_{\text{H}_2\text{O}}$, Y_{H_2}
- c_O – based on mass of O bound to fuel (C or H)
- c_T – based on temperature (only to compare noise)

- Use ‘fully burnt’ rather than equilibrium as the reference state for normalization (deficient reactants fully converted to CO_2 , H_2O)
 - Avoids transport assumptions
 - Easily calculated from measured samples



Normalized Progress Variable based on Oxygen

- Mass of oxygen bound to fuel (C or H) divided by total that could be bound if the sample fully reacts to products (not equilibrium)
- Consistent with definitions of Z and ϕ (same 7 major species)
- Easy to calculate from experiments or simulations (post-process)

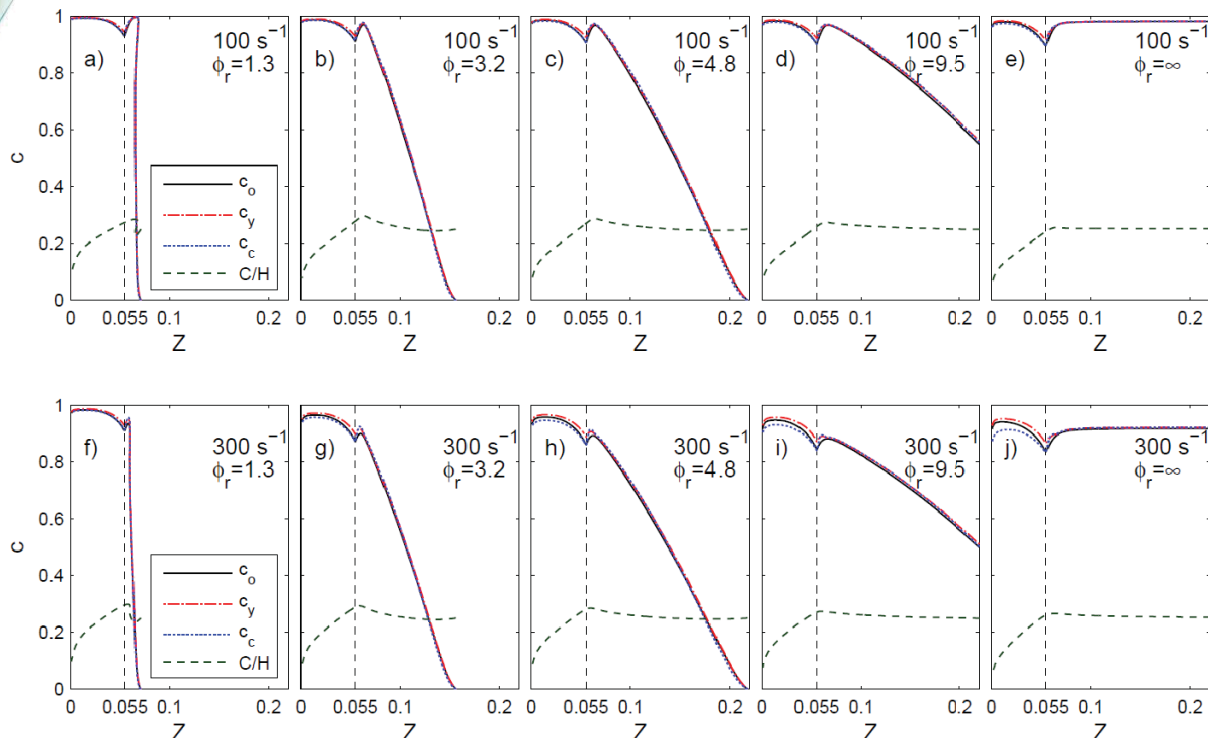
$$c_o = \frac{Y_{CO_2} \left(\frac{w_{O_2}}{w_{CO_2}} \right) + Y_{CO} \left(\frac{w_O}{w_{CO}} \right) + Y_{H_2O} \left(\frac{w_O}{w_{H_2O}} \right)}{\left(Y_{CO_2} \left(\frac{w_{O_2}}{w_{CO_2}} \right) + Y_{CO} \left(\frac{w_O}{w_{CO}} \right) + Y_{H_2O} \left(\frac{w_O}{w_{H_2O}} \right) + Y_{H_2} \left(\frac{w_O}{w_{H_2}} \right) + Y_{CH_4} \left(\frac{2w_{O_2}}{w_{CH_4}} \right) \right)} ; \phi < 1$$

$$c_o = \frac{Y_{CO_2} \left(\frac{w_{O_2}}{w_{CO_2}} \right) + Y_{CO} \left(\frac{w_O}{w_{CO}} \right) + Y_{H_2O} \left(\frac{w_O}{w_{H_2O}} \right)}{\left(Y_{CO_2} \left(\frac{w_{O_2}}{w_{CO_2}} \right) + Y_{CO} \left(\frac{w_O}{w_{CO}} \right) + Y_{H_2O} \left(\frac{w_O}{w_{H_2O}} \right) + Y_{O_2} \right)} ; \phi \geq 1$$

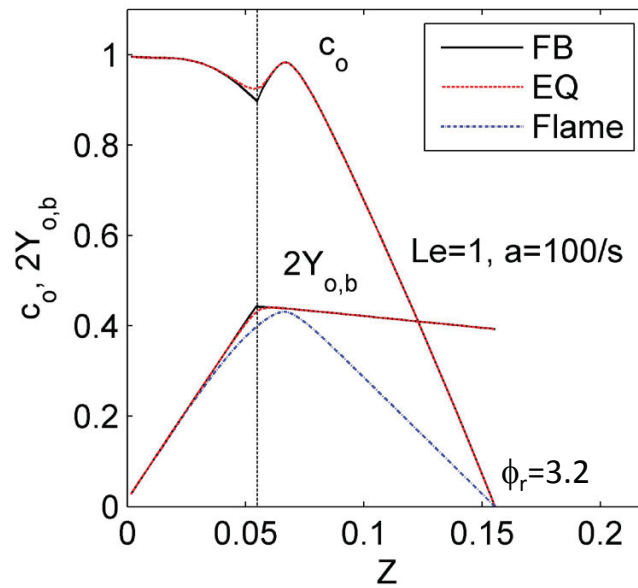


Progress Variables in Laminar Flame Calculations

flow against air (Chemkin, GRI 3.0, MCT, Soret)



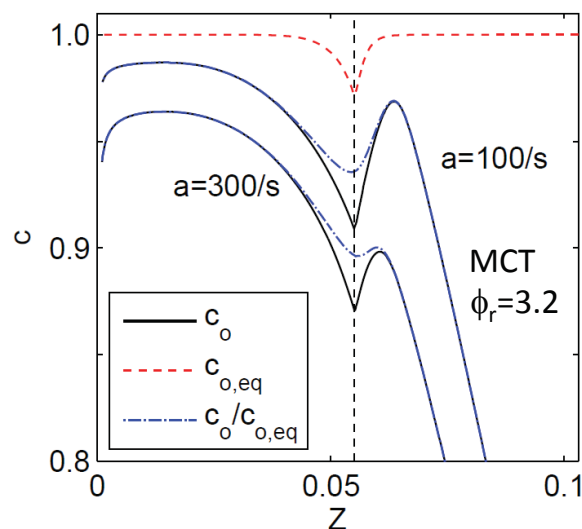
Equilibrium vs. Fully Burnt



- Blue curve looks familiar (not normalized)
- The 'dip' is due to finite rate chemistry (slow CO chemistry)
- Maximum difference in Y_{O_2} for EQ vs. FB is 3 percent, which occurs at Z_{st} .
- Slope discontinuity in c_o at Z_{st} is from FB normalization (this is a problem)

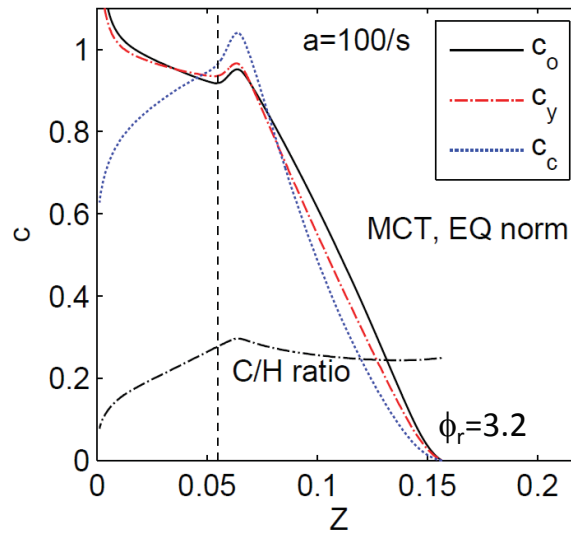
A simple correction to remove the cusp

- Calculate $c_{o,eq}$ for the equilibrium table (red curve, 0.97 at $\phi=1$)
- Renormalize flame results to generated the smooth blue curves



- Approximates normalization by the local equilibrium state

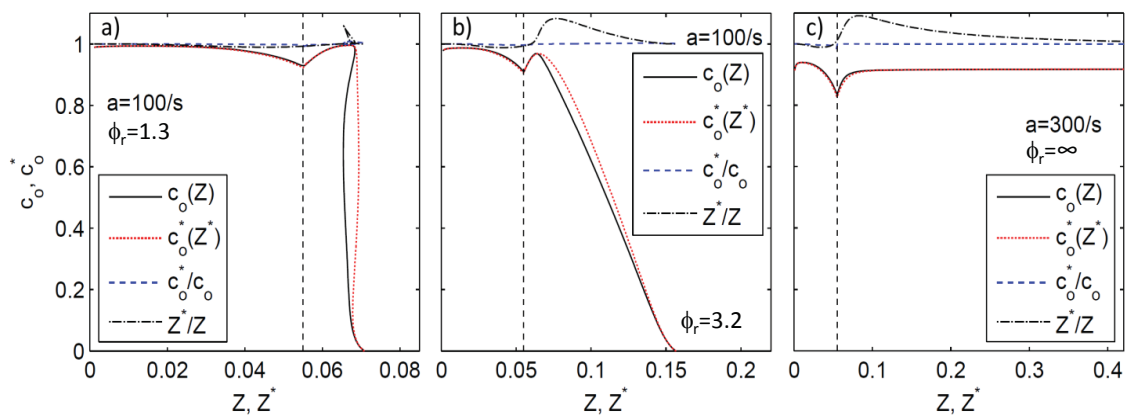
Equilibrium vs. Fully Burnt



- EQ normalization creates problems if diff-diff is important

Effect of including more species

- c_o, Z from 7 species ($N_2, O_2, CH_4, CO_2, H_2O, H_2, CO$)
- c_o^*, Z^* from 18 species (add $OH, H, O, CH_3, CH_2O, C_2H_2, C_2H_4, C_2H_6, CH_3OH, HCCO,$ and CH_2CO)

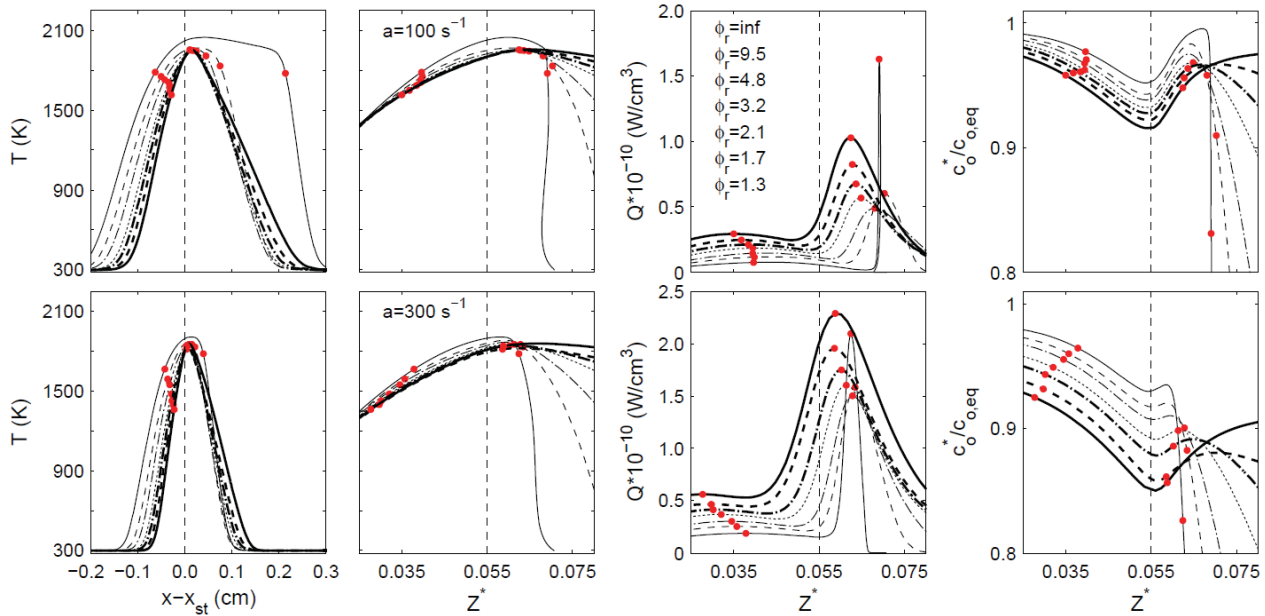


- Ratios plotted vs. Z for each point in the flame profile
- Only Z is significantly affected (effect should be smaller in experiments)



Heat Release and Progress Variable

- Counter flow flames: rich-side $\phi_r = 1.3, 1.7, 2.1, 3.2, 4.8, 9.5, \infty$
strain rate $a = 100 \text{ s}^{-1}, a = 300 \text{ s}^{-1}$
- Red dots at locations of lean and rich local maxima in heat release



COMBUSTION RESEARCH FACILITY

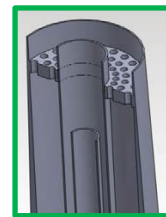
Sandia National Laboratories



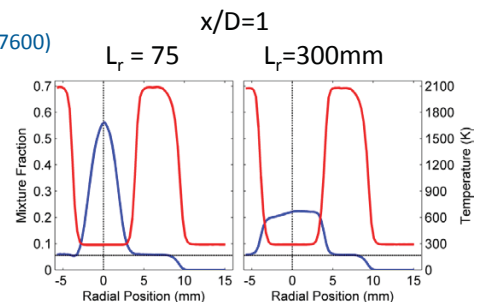
Turbulent Flame Results

- Sydney piloted flames, retractable center tube
- Near-field transition in mode of combustion
- New data set in 2015 (Hugh Cutcher, PCI 36)
- Better spatial resolution & lower noise
- More near-field profiles

CNF 161 (2014) 484–495
 PCI 35 (2015) 1477–1484
 CNF 162 (2015) 3516–3540



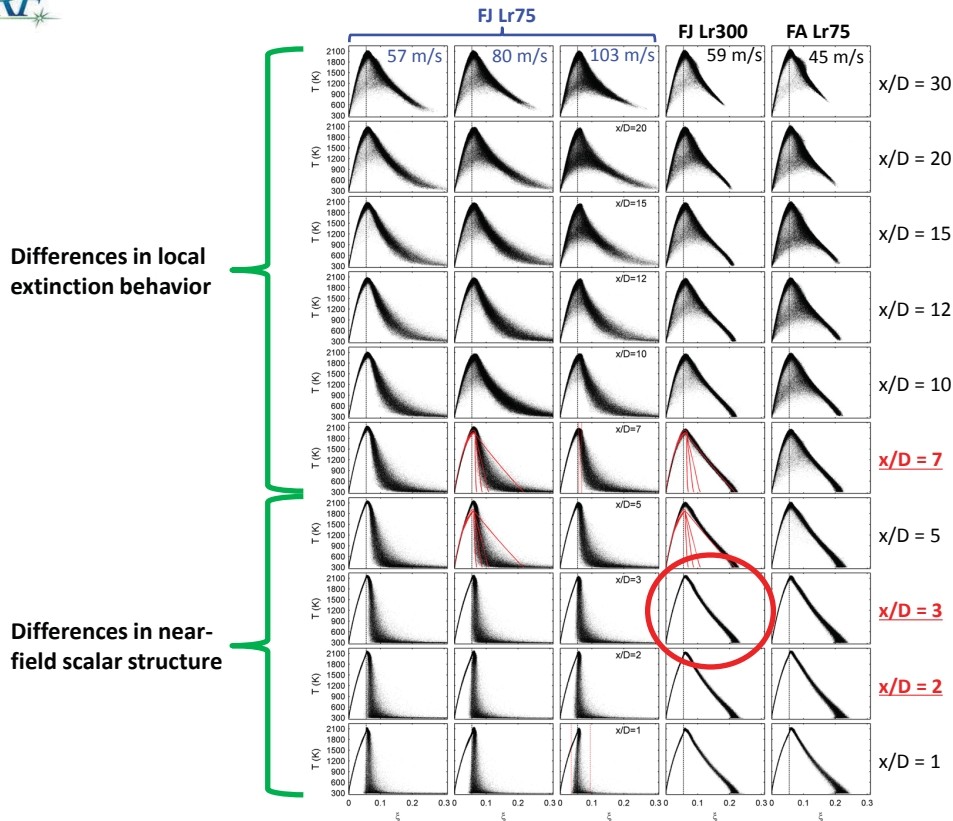
- Results from two flames (FJ-5GP)
 - Near-homogeneous inflow ($L_r = 300 \text{ mm}, U_b = 59 \text{ m/s}, Re_j = 27600$)
 - Inhomogeneous inflow ($L_r = 75 \text{ mm}, U_b = 80 \text{ m/s}, Re_j = 37500$)
- T-scatter plots and $P(Z,c)$
- Radial profiles of joint statistics
- ID dissipation terms



COMBUSTION RESEARCH FACILITY

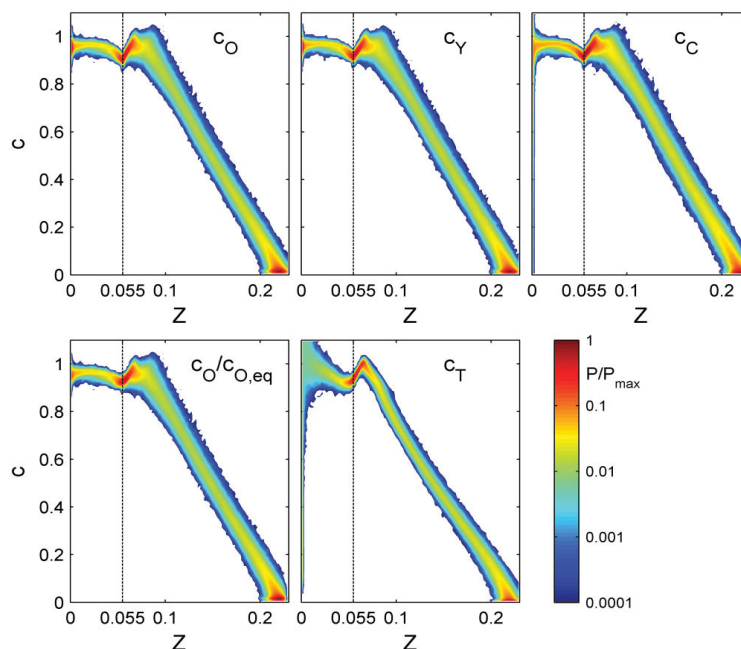
THE UNIVERSITY OF SYDNEY Sandia National Laboratories

Scatter Plots of T vs Z



Compare Measured Progress Variables

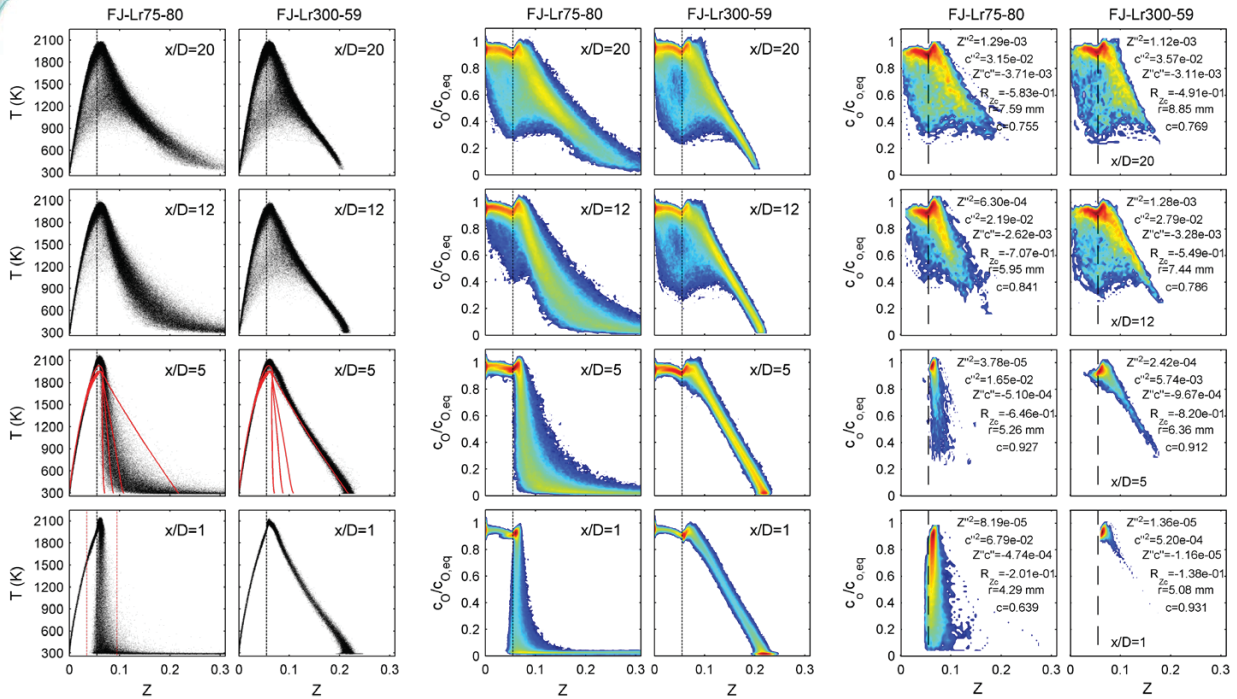
- Similar noise for c_O and c_Y . Slightly higher noise for c_C
- Lowest noise for c_T at high temperatures. High c_T noise at lean conditions.



Scatter Plots and Joint Histograms

All data from (+) side of each radial profile radial

0.3mm windows centered at $\tilde{Z}=0.065$



Density Weighted Point Statistics of Mixture Fraction and Progress Variable

Favre means:

$$\tilde{\xi} = \overline{\rho\xi}/\bar{\rho}, \quad \tilde{c}_0 = \overline{\rho c_0}/\bar{\rho}$$

Variances:

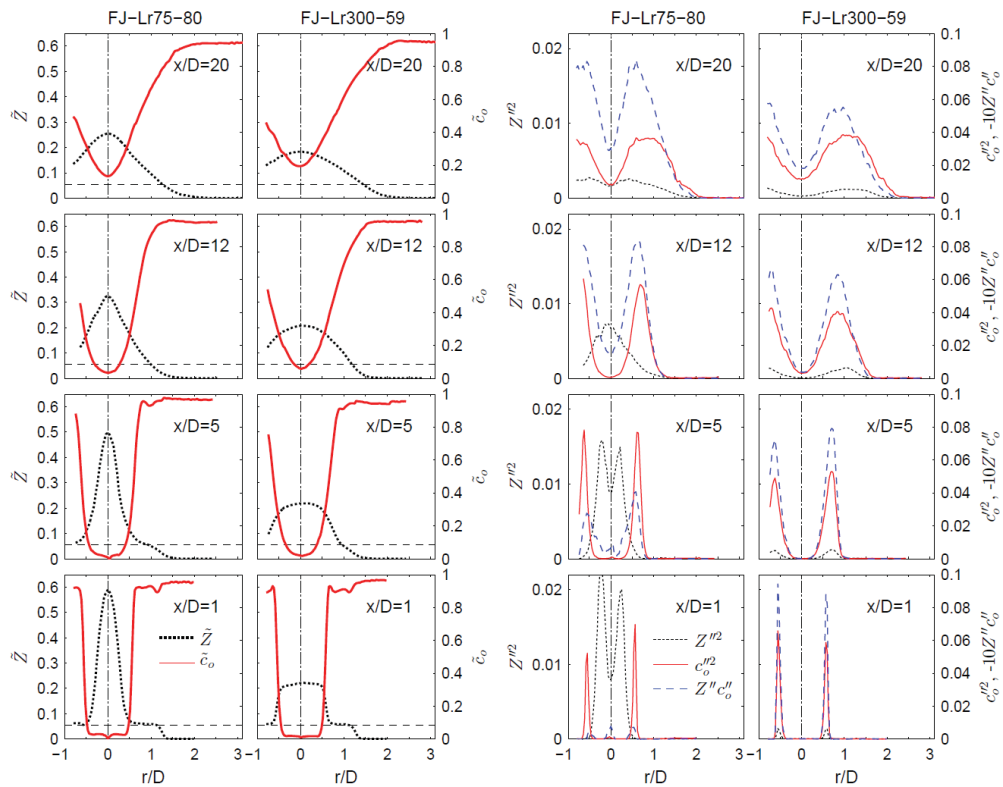
$$\tilde{\xi}''^2 = \overline{\rho(\xi - \tilde{\xi})^2}/\bar{\rho}, \quad \tilde{c}_0''^2 = \overline{\rho(c_0 - \tilde{c}_0)^2}/\bar{\rho}$$

Covariance:

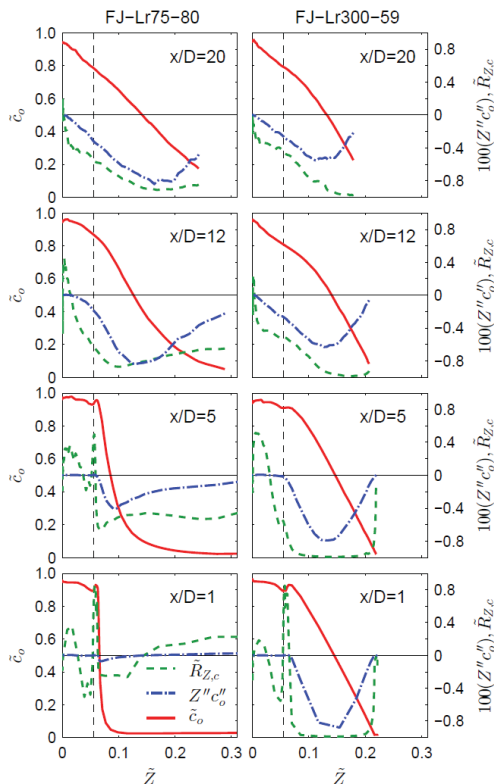
$$\tilde{\xi}''c_0'' = \overline{\rho(\xi - \tilde{\xi})(c_0 - \tilde{c}_0)}/\bar{\rho}$$

Correlation Coefficient: $R_{\xi c} = \tilde{\xi}''c_0'' / (\tilde{\xi}''^2 c_0''^2)^{1/2}$

Radial Profiles



Radial Profiles Plotted vs. \tilde{Z}



- $R_{Zc} \cong -1$ across rich side of the near-homogeneous flame
- $R_{Zc} \sim -0.2$ in the 'stratified-premixed' reaction zone.
- R_{Zc} dominated by correlated noise in the pilot
- $|R_{Zc}|$ decreases with increasing local extinction
- R_{Zc} has similar behavior in the two flames at $x/D=20$



Wavelet-Denoised, Single-Shot Example: FJ-Lr75-103, Re=48300, x/D=7

Z = mixture fraction

c = progress variable

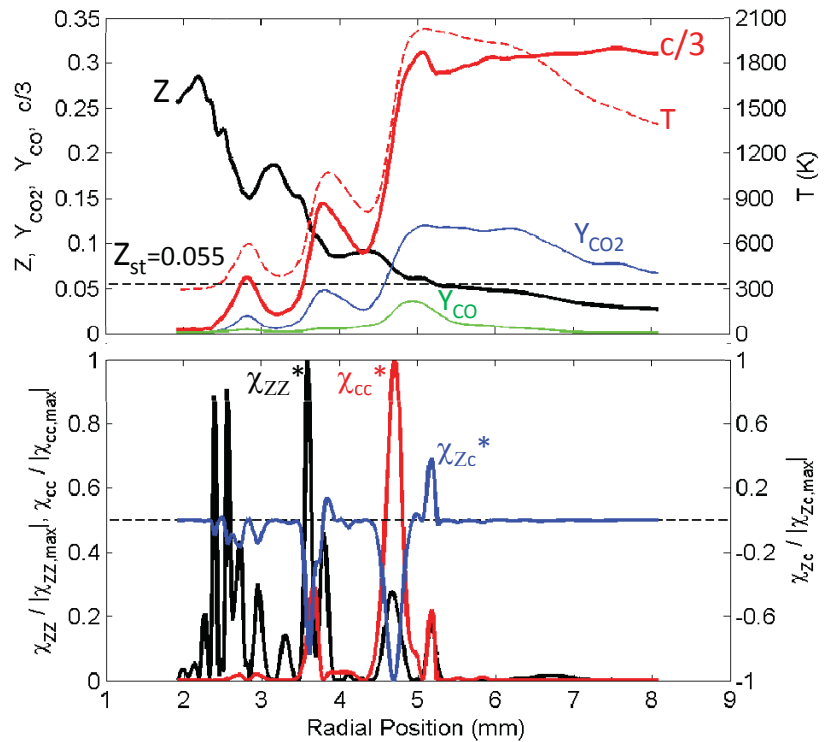
0.02 mm data spacing

1D (radial) dissipation

$$\chi_{ZZ} = 2D \left(\frac{dZ}{dr} \right)^2$$

$$\chi_{cc} = 2D \left(\frac{dc}{dr} \right)^2$$

$$\chi_{Zc} = 2D \left(\frac{dZ}{dr} \right) \left(\frac{dc}{dr} \right)$$



COMBUSTION RESEARCH FACILITY



Sandia National Laboratories



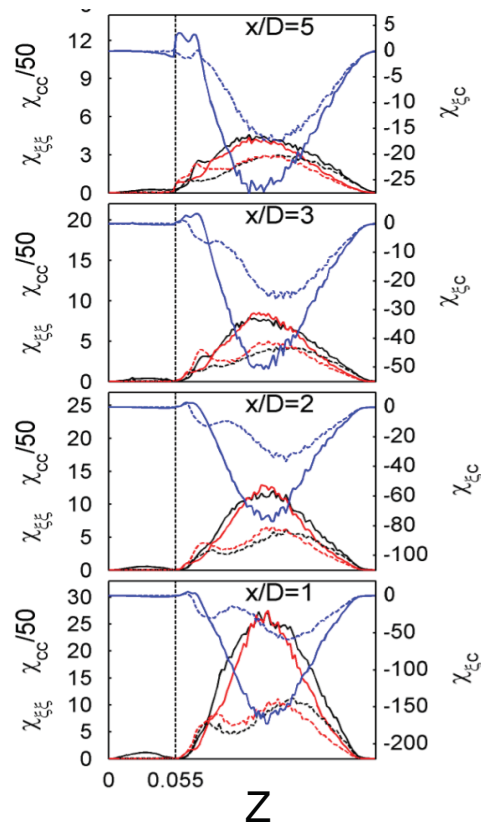
FJ-5GP-Lr300-59

- Conditional mean dissipation
- Solid: Instantaneous total gradient
- Dashed: Gradient of Favre fluctuation (Favre mean subtracted)
- Will report both

$$\chi_{ZZ} = 2D \left(\frac{dZ}{dr} \right)^2$$

$$\chi_{cc} = 2D \left(\frac{dc}{dr} \right)^2$$

$$\chi_{Zc} = 2D \left(\frac{dZ}{dr} \right) \left(\frac{dc}{dr} \right)$$



COMBUSTION RESEARCH FACILITY

Sandia National Laboratories



Summary and Discussion Issues

- Progress variable based on oxygen bound to fuel
 - Calculated from 7 measured major species in methane flames
 - Normalized by fully-burnt state of the sample (with the “simple fix”)
 - Useful for comparison with simulations???
- Observations
 - At $x/D=1$, $|\widetilde{Z''c''}|$ and $|R_{Zc}|$ are MUCH lower in the inhomogeneous case
 - Both increase as the combustion mode transitions
 - Assumption of statistical independence of Z,c not supported
 - Magnitude of R_{Zc} near stoichiometric is reduced by local extinction
- 1D dissipation terms ($\chi_{ZZ}, \chi_{Zc}, \chi_{cc}$)
 - Only 1D measured directly
 - Favre mean gradient can contribute more than half the total!
 - Regime indicators from gradients?

blank

Flame identification and characterization in partially premixed and stratified combustion based on 1D Raman/Rayleigh data

S. Hartl^a, D. Geyer^b and C. Hasse^a

(and many contributions through discussions with R. Barlow and A. Dreizler)

^a Technical University Freiberg
Numerical Thermo-Fluid Dynamics
Institute of Energy Process Engineering and Chemical Engineering Freiberg, Germany

^b Hochschule Darmstadt
University of Applied Sciences Thermodynamics and Alternative Propulsion Systems
Darmstadt, Germany

Flame Identification – SOTA

Some example for regime indicators

- Flame Index [1] / cross scalar dissipation of fuel and oxidizer
- normalized variants of the flame index [2,3]
- improved flame index for partially-premixed combustion [4]
- Combustion regime indicator [5,6]

They all rely on 3D scalar gradients. In addition, to tabulated gradients (for comparison) or local reaction rates are required. For LES, closure is required.

[1] H. Yamashita et al., Proc. Combust. Inst. 26 (1996)

[2] P. Domingo et al., Combust. Flame 140 (2005)

[3] P. Domingo et al., Combust. Theory and Modelling 6 (2002)

[4] B. Fiorina et al., Combust. Flame 140 (2005)

[5] E. Knudsen and H. Pitsch, Combust. Flame 156 (2009)

[6] E. Knudsen and H. Pitsch, Combust. Flame 159 (2012)

Flame Identification – SOTA



All regime indicator look at mixing or the balance of mixing and chemical reactions, i.e.

- if chemical reactions are mainly balanced by transport in the direction of the mixture fraction gradient \rightarrow non-premixed / partially premixed
- if chemical reaction are mostly balanced by transport along iso-mixture fractions contours \rightarrow stratified /premixed

“...current experimental techniques cannot access this level of quantitative detail” [1]

[1] R. S. Barlow et al., Combust. Flame 162 (2015)

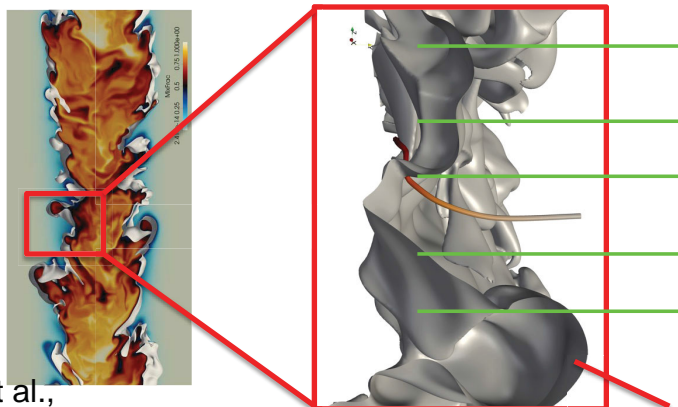
3

Flame Identification – SOTA



Challenges in regime analysis based on Raman/Rayleigh data

- instantaneous data along a line (1D)
- unknown orientation of flame and laser in single shot data
- crossed-sheet offers additional insight but relies on assumptions



A. Scholtissek et al.,
Combust. Flame, in press (2016)

Z_{st} iso-surface

4

Methods to determine the local mode of combustion

- for tabulation approaches (FPV, FGM, FPI,...), a priori / prior analysis can be carried to test the suitability of different tables
→ conclusions with respect to flame structure possible
- comparing LES and experimental data using conditional and unconditional averages and rms
- manifold drift terms (see next presentation by Matthias)

But: these methods do not directly analyze the experimentally obtained thermo-chemical state along the experimental 1D line for flame identification combustion mode determination

5

However:

- we have the local thermo-chemical state, which should be the “footprint” of the local mode of combustion
- there is 1D information (3-6 mm) available, which is usually larger than the reaction zone thickness → if the line passes through the reaction zone, significant changes should be observable



Can we use the thermo-chemical state and derived quantities along the line to identify the flame and potentially even characterize the mode of burning?

6

Raman/Rayleigh: What is available?



Directly measured quantities

- Raman species
- Temperature from combined Raman/Rayleigh measurements

Derived quantities (details see next slides):

- Bilger mixture fraction
- chemical explosive mode (CEM) from CEMA
- Heat release rate (HRR)

Potential issues to be considered:

- the complete thermo-chemical state is not known
- experimental uncertainty (accuracy + precision)
- spatial resolution

7

Flame Markers: Z and HRR



Bilger Mixture Fraction Z

$$Z = \frac{2(Y_C - Y_{C,\text{fuel}})/W_C + (Y_H - Y_{H,\text{fuel}})/(2W_H) - (Y_O - Y_{O,\text{fuel}})/W_O}{2(Y_{C,\text{ox}} - Y_{C,\text{fuel}})/W_C + (Y_{H,\text{ox}} - Y_{H,\text{fuel}})/(2W_H) - (Y_{O,\text{ox}} - Y_{O,\text{fuel}})/W_O}$$

Heat Release Rate (HRR)

$$\text{HRR} = \frac{1}{\rho} \sum_{i \in N_s} \dot{\omega}_i h_{f,i}$$

(source terms $\dot{\omega}_i$ and $h_{f,i}$ the enthalpies of formation of the species, $i \in N_s$)

8

- applied to identify premixed flame fronts in e.g. DNS [1,2] and for characterization of extinction and ignition processes [3,4]
 - analysis is local and does not depend on scalar gradients
1. balance equations of chemically reacting system:
$$\frac{D\Phi_j}{Dt} = \dot{\omega}_j(\Phi) + S_j(\Phi)$$
 2. chemical Jacobian: (contains chemistry-related information)
$$\mathbf{J}_{\dot{\omega}}^{ij} = d\dot{\omega}_i/d\Phi_j$$
 3. solve eigenvalue problem:
$$\lambda = \mathbf{bJ}_{\dot{\omega}}\mathbf{a}$$
 4. the (non-conservative) eigenvalue with max. real part is defined as λ_e (if $\text{Re}(\lambda_e) > 0$, it is called the chemical explosive mode – CEM)

Define **CM** based on eigenvalue: $\text{sign}(\text{Re}(\lambda_e)) \times \log_{10}(1 + |\text{Re}(\lambda_e)|)$

[1] R. Shan et al., Combust. Flame 159 (2012)

[4] S. Lyra et al., Combust. Flame 162 (2015)

[2] T. F. Lu et al., Journal of Fluid Mechanics 652 (2010)

[3] I. A. Dodoulas and S. Navarro-Martinez, Combust. Theory and Modelling 19 (2015)

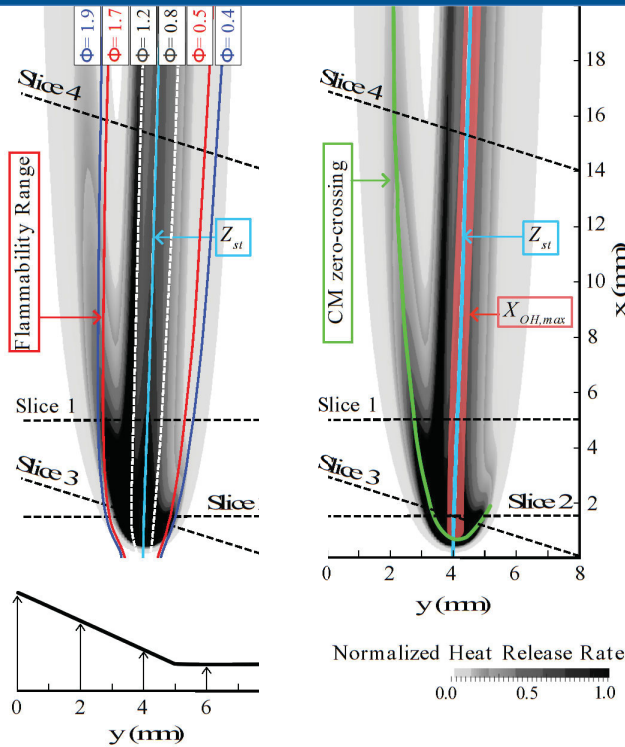
Approach

Coming back to the original question: Can the combinations of the flame markers be used to identify the flame and potentially even characterize the mode of burning?

Approach:

1. Evaluate the markers and their combinations in a complex fully resolved flame (triple flame → see next slides)
2. Evaluate the effects of
 1. approximation of full thermochemical state
 2. experimental uncertainty of Raman/Rayleigh measurement
 3. spatial filtering
3. Tests on experimental single shot line data from TNF benchmark flames (TSF-A and Sydney/Sandia)

Triple Flame Configuration

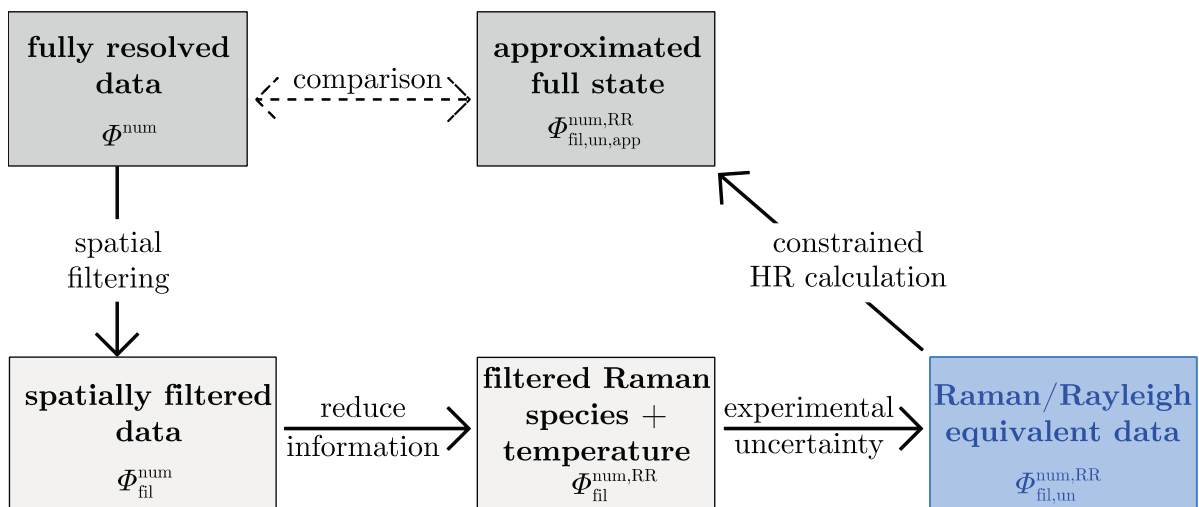


- fully resolved 2D computation with 400x300 grid points
- gradient of Z is defined along inlet ($dZ/dy=50$ 1/m)
- $T_{un}=300K$, $p=1bar$, $u_{in}=0.35m/s$
- GRI-Mech 3.0 mechanism
- CM zero-crossing in direct vicinity of maximum HRR
- lean premixed and rich premixed flame identified
- most significant HRR in non-premixed flame region

11

Aspects of Experimental Conditions

→ evaluate HRR and CM based on approximated full state ($\Phi_{fil,un,app}^{num,RR}$) and the fully resolved data (Φ^{num})



superscripts: num - numerical, exp - experimental, RR - Raman/Rayleigh
subscripts: fil - filtered, un - uncertainty, app - approximated

12

Experimental Uncertainty



filtered Raman
species +
temperature
 $\Phi_{fil}^{num,RR}$

experimental
uncertainty

Raman/Rayleigh
equivalent data
 $\Phi_{fil,un}^{num,RR}$

- add experimental uncertainties to $\Phi_{fil}^{num,RR}$
- use representative uncertainty values (accuracy [1] and precision [2]) of scalar measurements in CH₄/air flames → investigate **worst case scenario**
 - accuracy: constant positive/negative offset to Raman species and T, see table below
 - precision: additional normal scatter

Scalar	T	N ₂	CO ₂	H ₂ O	CO	H ₂
Accuracy (%)	2	2	4	3	10	10

[1] R. S. Barlow et al., Combust. Flame 162 (2015)

[2] R. S. Barlow et al., Combust. Flame 159 (2012)

13

Approximation of Full State



- (1) start from $\Phi_{fil,un}^{exp,RR} / \Phi_{fil,un}^{num,RR}$
- (2) constrained homogeneous reactor (HR) calculation to build up radical pool (for chemistry-based flame markers - CM and HRR)

Restrictions:

- sufficient number of radicals must build up
- limit discrepancy from adding radicals during the HR calculation
 - criterion based on derivation of initial mass fractions (derived from accuracy from scalar measurements [1])
 - integration time for the HR calculation bounded

→ approximated full state $\Phi_{fil,un,app}^{num,RR} / \Phi_{app}^{exp,RR}$ further used to calculate flame markers and evaluate flame structure

approximated
full state
 $\Phi_{fil,un,app}^{num,RR} / \Phi_{app}^{exp,RR}$

constrained
HR calculation

Raman/
Rayleigh data
 $\Phi_{exp,RR}$

constrained
HR calculation

Raman/Rayleigh
equivalent data
 $\Phi_{fil,un}^{num,RR}$

[1] R. S. Barlow et al., Combust. Flame 162 (2015)

14

Counterflow Flame Analysis

Premixed, non-premixed, stratified, partially-premixed counterflow flames tested (not shown here)

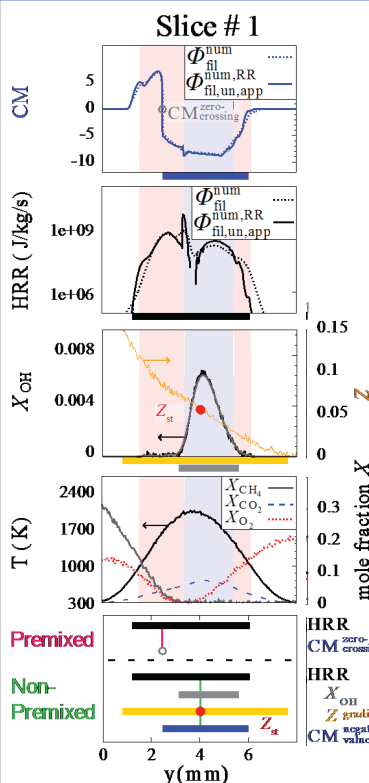
- CM zero-crossing combined with locally high HRR can identify premixed/stratified flame
- negative CM and significant HRR values in the vicinity of Z_{st} (and a Z gradient) non-premixed flame

→ Flame identification and characterization approach:

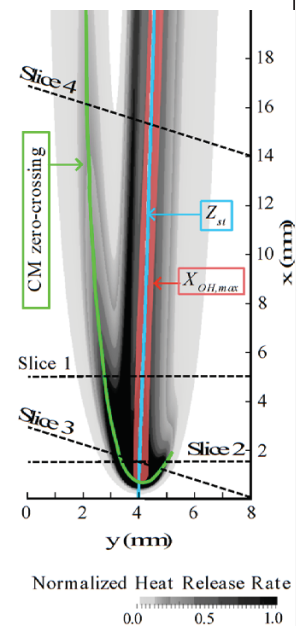
Premixed: CM zero-crossing, (locally) high HRR

Non-Premixed: negative CM, Z gradient in the vicinity of Z_{st} , significant HRR values, X_{OH} peak (if available)

Triple Flame Configuration

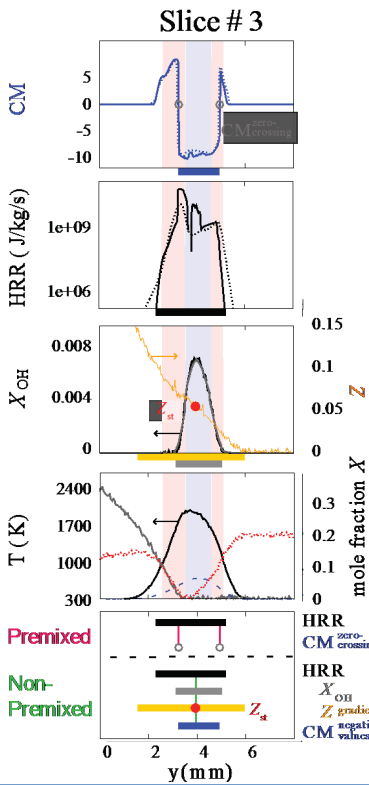


- filtered (Φ_{fil}^{num}) and approximated ($\Phi_{fil,un,app}^{num,RR}$) data show excellent agreement of CM profile and good agreement for HRR
- one CM zero-crossing appears
- high HRR values appear close to CM zero-crossings
- significant X_{OH} and HRR occur close to Z_{st} in the range of negative CM values
- Z gradient in proximity to Z_{st}

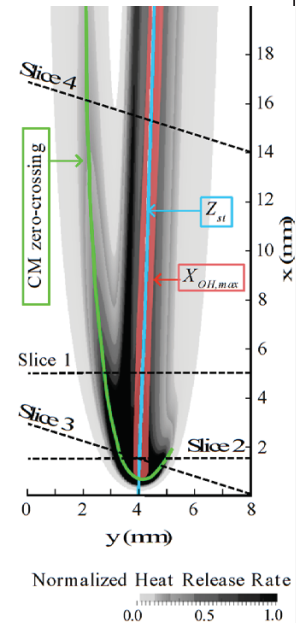


→ one non-premixed flame and one rich premixed stratified flame

Triple Flame Configuration (slice #3)



- filtered (Φ_{fil}^{num}) and approximated data ($\Phi_{fil,un,app}^{num,RR}$) show excellent agreement for CM profile and good agreement for HRR
 - two CM zero-crossings
 - high HRR values appear close to CM zero-crossings
 - significant HRR occur close to Z_{st} with negative CM values
 - Z gradient in proximity to Z_{st}
- two premixed flames (lean, rich) and a non-premixed flame between them



Lean premixed turbulent stratified flame (TSF-A)



- three-staged concentric tubes placed in air co-flow
- burnt gases, based on lean CH_4 /air composition, exit from central pilot tube to stabilize flame
- first and second tubes are defined by lean unburnt CH_4 /air mixture avoiding stoichiometric conditions over the whole flame
- detailed analysis of the TSF-A flame, see [1-4]

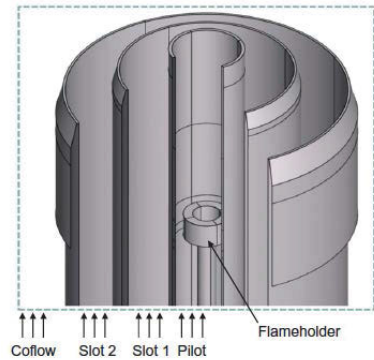
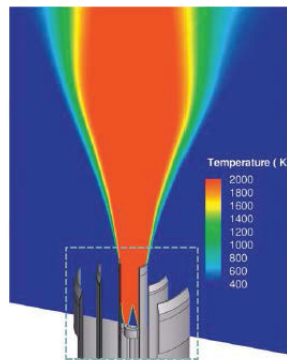


Illustration of the burner geometry and flame stabilization. Left: Time averaged temperature field taken from the simulation. Right: Cut out of the geometry at the pipe exit region. [2]

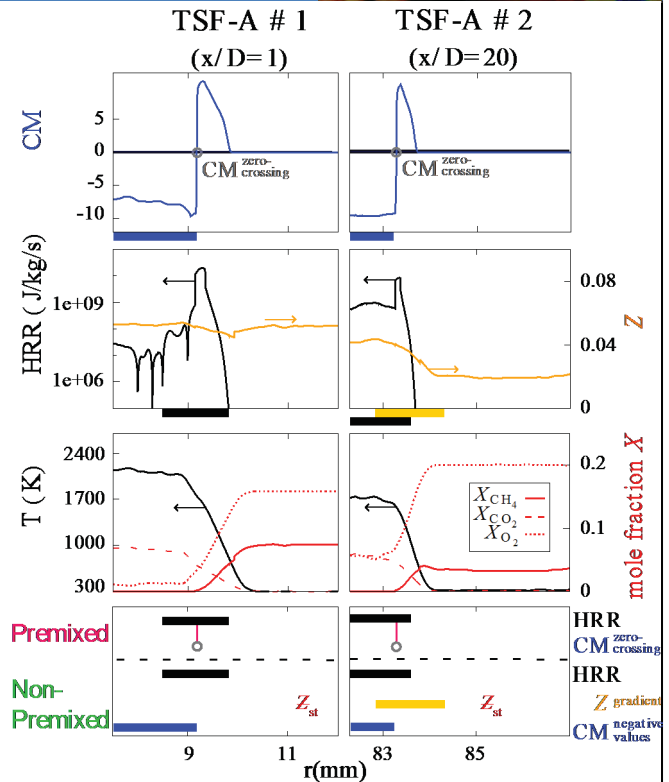
[1] F. Seffrin et al., Combust. Flame 157 (2010)
 [2] G. Kuenne et al., Combust. Flame 159 (2012)

[3] B. Fiorina, Combust. Flame, 162 (2015)
 [4] T. Stahler et al., Proc. Combust. Inst. (2016)

Lean premixed turbulent stratified flame (TSF-A)



- analysis of $\Phi_{app}^{exp,RR}$
- instantaneous T and Y_i data based on Raman/Rayleigh lines at different heights
- different levels of Z stratification
- CM profiles show initial increase (characteristic for the preheat zone) prior to a steep CM zero-crossing
- significant HRR values at CM zero-crossing
- no non-premixed /partially premixed flame can be identified

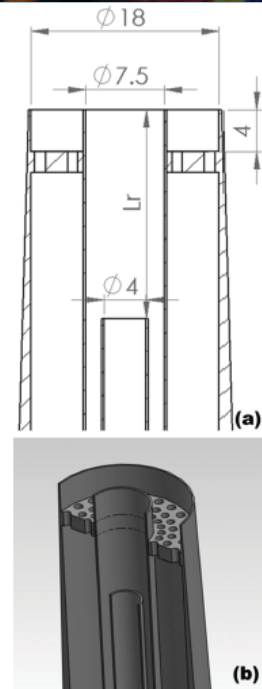


20

Sydney/Sandia burner with inhomogeneous inlets (FJ200-5GP-Lr300-59)



- two concentric tubes surrounded by a pilot
- operated with CH_4 through central tube and air from second tube
- FJ200-5GP-Lr300-59: near-homogeneous composition in mixing pipe
- 5-gas pilot burning a mixture to match the adiabatic equilibrium temperature and composition of stoichiometric CH_4/air
- flame structure is investigated in the following studies [1,2,3]



(a) Schematic of the burner with dimensions in mm (b) Isometric cutaway of the burner showing the pilot, mainjet, and recessed inner tube [1]

[1] S. Meares and A. R. Masri, Combust. Flame 161 (2014)
 [2] S. Meares et al., Proc. Combust. Inst. 35 (2015)
 [3] R. S. Barlow et al., Combust. Flame 162 (2015)

22

Sydney/Sandia burner with inhomogeneous inlets (FJ200-5GP-Lr300-59)



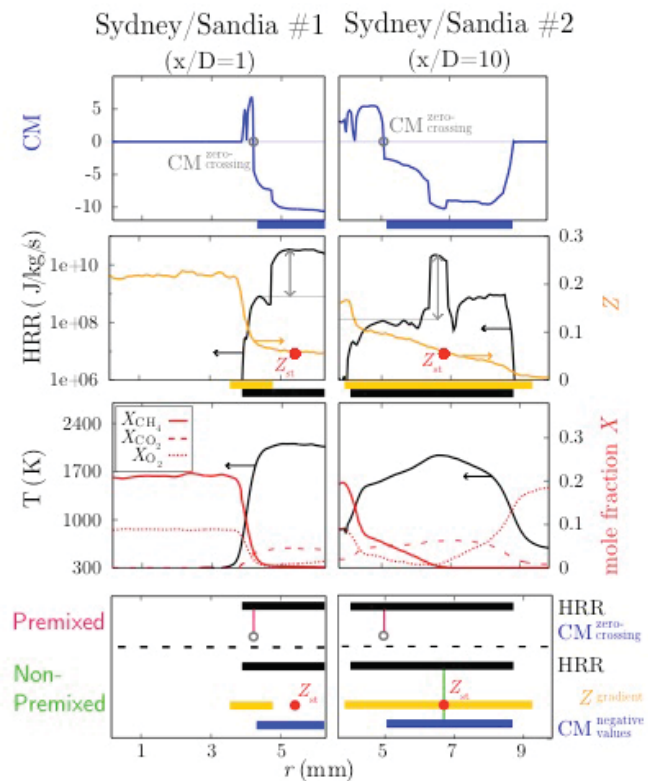
- analysis of $\Phi_{app}^{exp,RR}$
- differences in mixture fraction gradient at both positions
- Z crosses Z_{st} and coincides with negative CM and significant HRR

Sydney/Sandia #1:

- one CM zero-crossing and corresponding HRR
- significant HRRs for $r > 5\text{mm}$ (no notable mixture fraction gradient)

Sydney/Sandia #2:

- one CM zero-crossing with low HRR
- CM zero-crossing with smooth gradient to minimum CM value (merging of non-premixed and premixed reaction zone)



23

Summary



- Flame index/combustion regime index require at least 3D scalar gradients
- Such quantitative information is difficult to obtain experimentally
- Approach to use 1D Raman/Rayleigh line data to
 - detect reaction zones
 - identify mode of burning
- Tested successfully in fully resolved flames accounting for experimental uncertainty and available scalars from Raman/Rayleigh
- First promising tests on stratified (TSF-A) and partially-premixed/stratified (Sydney Sandia w. inh. inlets, DME-D) benchmark flames

26

blank

Progress Variable and Combustion Regime: Relevance to Modeling

MATTHIAS IHME, HAO WU
TIANFENG LU, CHRISTIAN HASSE, ROB BARLOW

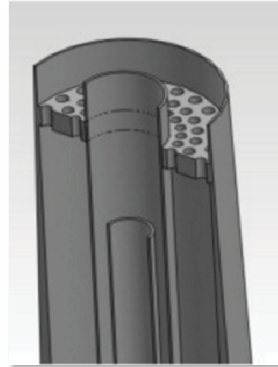
Stanford University

Overview

- 1) Reaction progress variable for combustion models
- 1) Characterization of combustion models: Implication of modeling

Stanford University

Reaction progress variable for combustion models



Stanford University

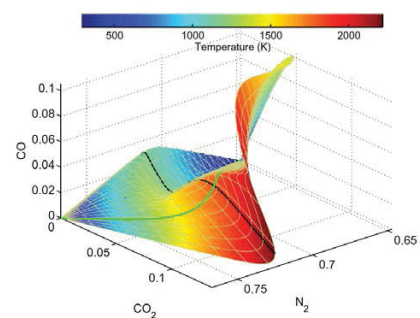
Reaction Progress Variable for Combustion Modeling

Parameterization of reaction-diffusion manifold models using reduced set of scalars $\phi = \phi(Z, C, \dots)$

- Mixture fraction, $Z \rightarrow$ scalar mixing
- Strain rate, a , or scalar dissipation rate, $\chi \rightarrow$ hydrodynamics/turbulence
- Reaction progress variable, $C \rightarrow$ chemistry

Reaction progress variable C commonly defined from combination of chemical species or temperature:

$$C = \sum_{i \in \mathcal{S}} w_i Y_i$$



Pope: PCI, 35, 2013

Stanford University

Reaction Progress Variable for Combustion Modeling

Requirements on progress variable

- Convenient transport equation for C in a combustion simulation.
- Comparable time scales for constituent reactive scalars
- Independent manifold-defining parameters
- Uniquely characterization in the thermochemical state-space.
- Smooth manifold (smaller curvature)
- Sparsity in the definition (fewer species involved)
- Consideration of experimental errors, maximize SNR

Algorithmic solution methods

- Linear optimization
- Genetic algorithm, ES
- bi-convex optimization problem with linear inequality constraints

Ihme et al. JCP, 231, 7715 (2012); Najafi-Yazdi et al. CF, 159, 1197 (2012); Niu et al. CF, 160, 776 (2013); Pruefer et al. FTC, 94 (2015)

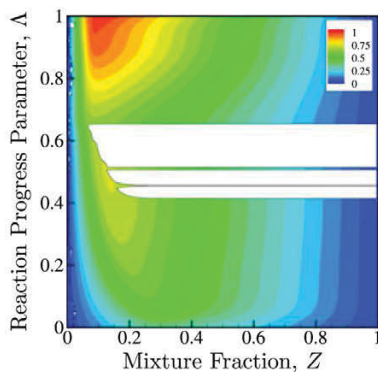
Stanford University

Reaction Progress Variable for Combustion Modeling Heptane/hydrogen-air mixture

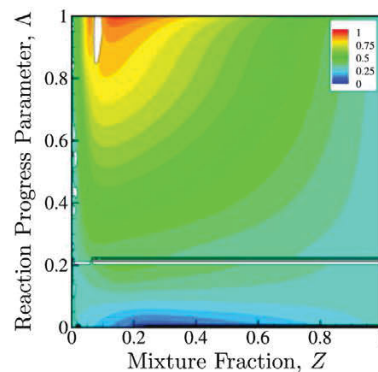
Species set

$$\mathcal{S}_1 = \{\text{H}_2\text{O}, \text{CO}_2, \text{CO}, \text{H}_2\}$$

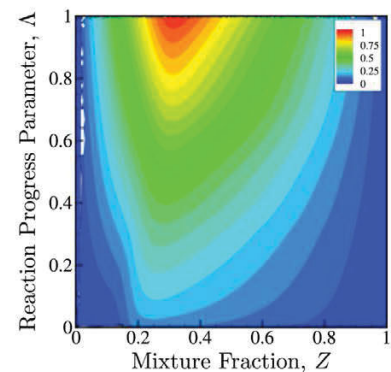
$$\mathcal{S}_2 = \{Y_i | \max(Y_i) \geq \epsilon\}$$



(a) \mathcal{S}_1 , equal w .



(b) \mathcal{S}_1 , optimal w .



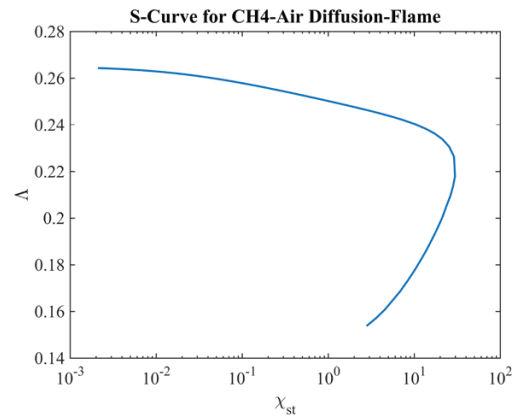
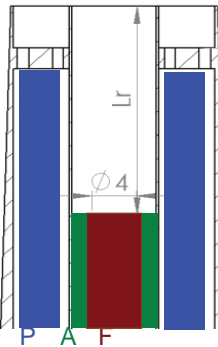
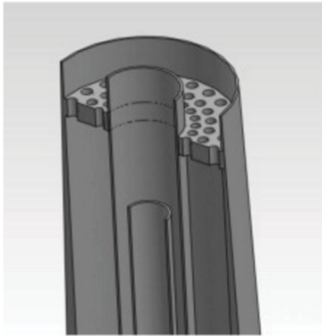
(c) \mathcal{S}_2 , optimal w .

Stanford University

Reaction Progress Variable for Combustion Modeling Methane/air – Sydney flame

Sydney burner

- Piloted turbulent flames with inhomogeneous inlets
- Partially premixed flame



S. Meares and A. R. Masri. A modified piloted burner for stabilizing turbulent flames of inhomogeneous mixtures. *Combust. Flame*, 161(2):484–495, 2014.

S. Meares, V. N. Prasad, G. Magnotti, R. S. Barlow, and A. R. Masri. Stabilization of piloted turbulent flames with inhomogeneous inlets. *Proc. Combust. Inst.*, 35(2):1477–1484, 2015.

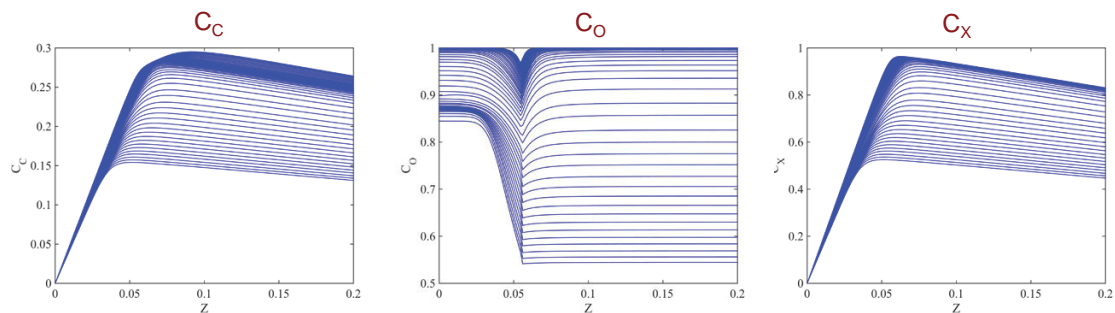
R. S. Barlow, S. Meares, G. Magnotti, H. Cutcher, and A. R. Masri. Local extinction and near-field structure in piloted turbulent CH₄/air jet flames with inhomogeneous inlets. *Combust. Flame*, 162(10):3516–3540, 2015.

Stanford University

Reaction Progress Variable for Combustion Modeling Methane/air – Sydney flame

Variable definitions of progress variables

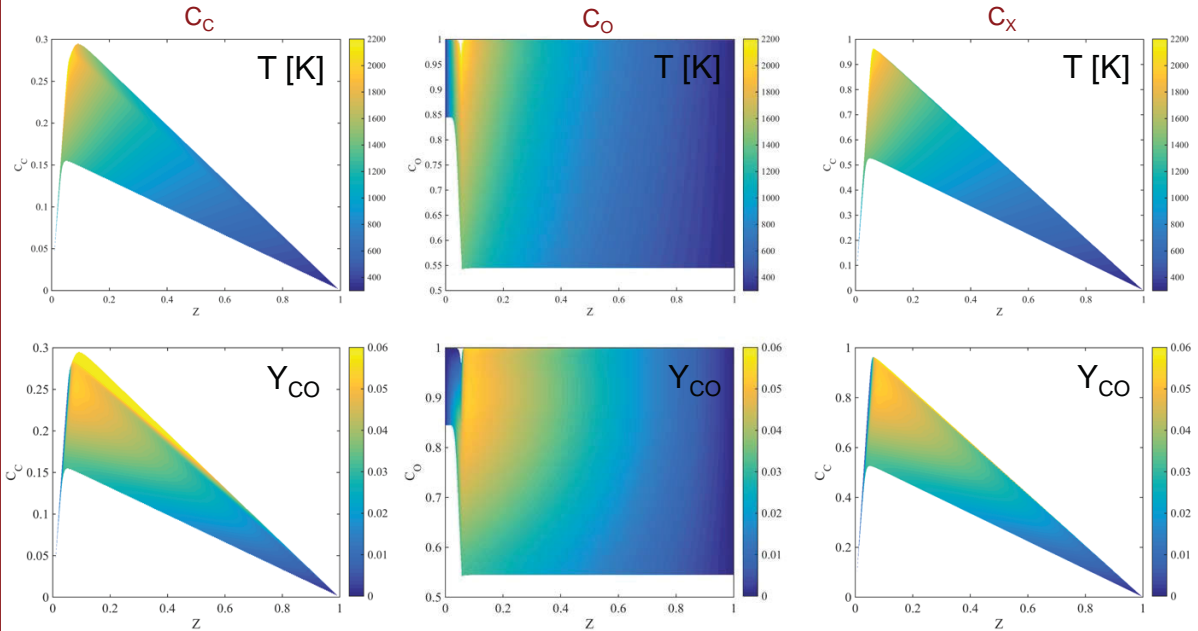
- Conventional (4-species progress variable): $C_C = Y_{H_2O} + Y_{CO_2} + Y_{H_2} + Y_{CO}$
- Rob's definition based on oxygen consumption based: C_O
- Optimized 6-species: C_X with $S = \{C_2H_2, CO_2, H_2, H_2O, NO\}$
- Experimentally optimal progress variable → maximize SNR



Stanford University

Reaction Progress Variable for Combustion Modeling Methane/air – Sydney flame

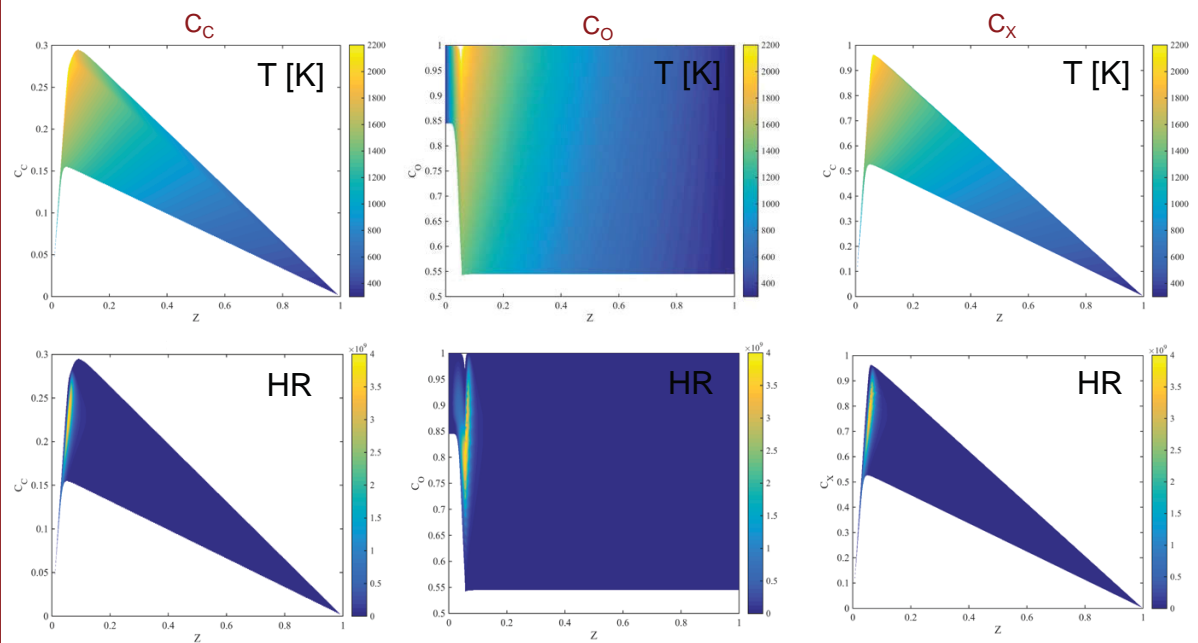
Representation of the thermochemical state-space



Stanford University

Reaction Progress Variable for Combustion Modeling Methane/air – Sydney flame

Representation of the thermochemical state-space



Stanford University

Reaction Progress Variable for Combustion Modeling Methane/air – Sydney flame

- Connect progress variable to measurements – formulation of progress variable to minimize experimental uncertainty
- Maximize signal-to-noise ratio (SNR)

$$\text{SNR}_C = \frac{\mu_C^2}{\sigma_C^2} = \frac{w^T \mu}{w^T \Sigma w}$$

μ ... mean of species mass fractions

Σ ... covariance matrix measuring uncertainty among species

- ➔ Solution through from two-stage optimization problem
 - standard quadratic programming problem with linear inequality constraints
 - 1D optimization problem to $\text{SNR} \rightarrow \max$

Stanford University

Reaction Progress Variable for Combustion Modeling Methane/air – Sydney flame

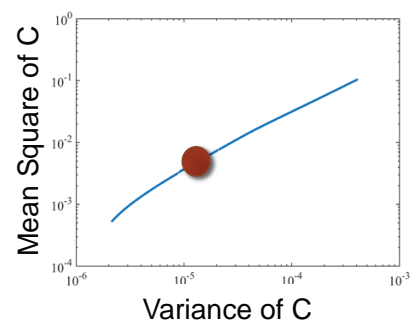
- Connect progress variable to measurements – formulation of progress variable that takes into account SNR
- Problem formulation: 4-species progress variable

Covariance Matrix Σ

	H2O	CO2	CO	H2
H2O	2e-5			6e-8
CO2		9e-5	7e-7	
CO			2e-6	2e-8
H2				1e-8

Diagonal elements estimated¹

Off-diagonal elements assumed



Flame Type	Temperature	H2O	CO2	CO	H2	SNR
CH4/Air	300K / 300K	1	1	1	1	180
CH4/Air	300K / 300K	0.75	0.13	0.16	2.95	365

¹ Barlow, R. S., et al. "Piloted methane/air jet flames: Transport effects and aspects of scalar structure." *Combustion and flame* 143.4 (2005): 433-449.

Stanford University

Reaction Progress Variable for Combustion Modeling Methane/air – Sydney flame

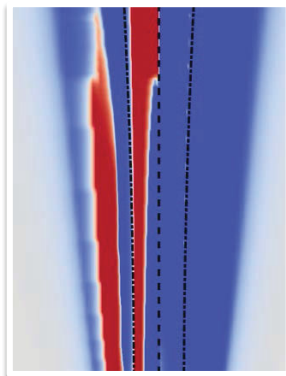
Conclusions

- Optimization methods overcomes *ad hoc* specification of progress variable
- Generalization to different fuels, and improvements in representation of combustion-manifold → improved model accuracy
- Application to measurements to maximize SNR

Stanford University

Characterization of combustion models

IMPLICATION OF MODELING



Stanford University

Combustion Regimes

Combustion regimes

- Asymptotic limits of premixed and non-premixed combustion

Purpose of combustion regime identification

- Model selection
- Theoretical analysis

Stanford University

Combustion Regimes

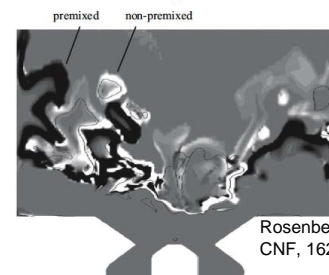
Regime identifications

- Yamashita-Takeno flame index: $\nabla Y_F \cdot \nabla Y_O$
- Alignment of mixture fraction and progress variable gradient: $\nabla Z \cdot \nabla C$
- FI/Oxi. diff. gradient: $D_O = |\nabla Y_{O,FPI}| / |\nabla Y_O|$
- Time-scale analysis
- CEMA
- Mode-analysis: curvature, Le-effects, flame-orthogonality, pressure effects

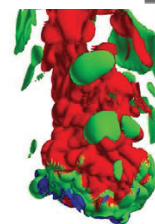
→ Useful for physical interpretation and combustion analysis

- Interpretation of preferential transport
- Ignition and scalar flux

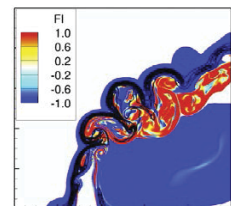
Fiorina et al., CNF, 140, 147, 2005
 Yamashita et al. PCI, 26, 27, 1996
 Lamouroux et al. CNF, 161, 2120, 2014
 Knudsen & Pitsch, CNF, 156, 678, 2009
 Lu et al., JFM, 652, 2010



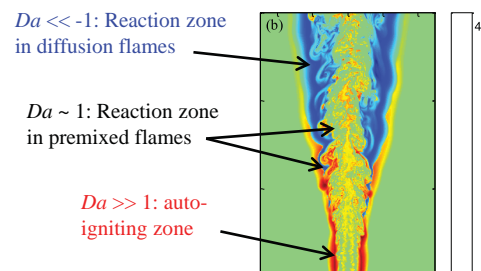
Rosenberg, et al. CNF, 162, 2015



Mizobuchi et al. PCI, 30, 2005



Lyra, et al. CNF, 162, 2015

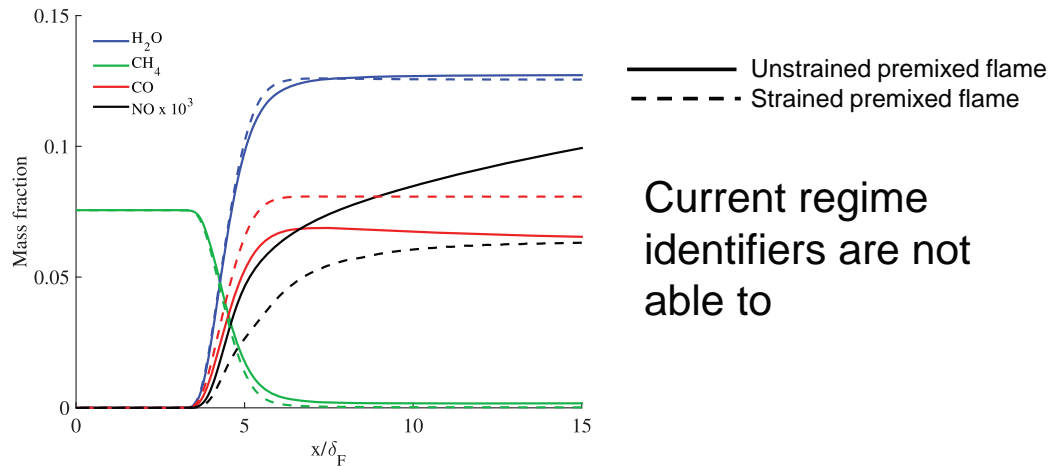


Stanford University

Combustion Regimes

Limitations of regime identifiers

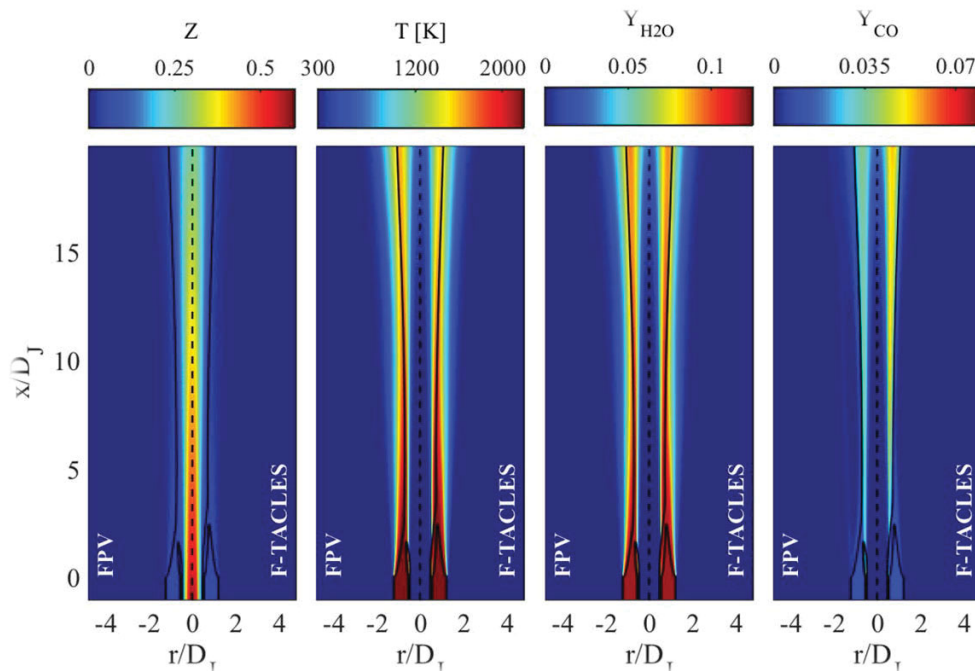
- Derived from 1D flame analysis, reduced chemistry
- Specific to particular mode
- Selective to major species
- Insensitive to minor species and flame topologies, or quantities of interest



Stanford University

Combustion Regimes Sydney flame (Lr75)

- FPV (non-premixed) Vs. F-TACLES (premixed)

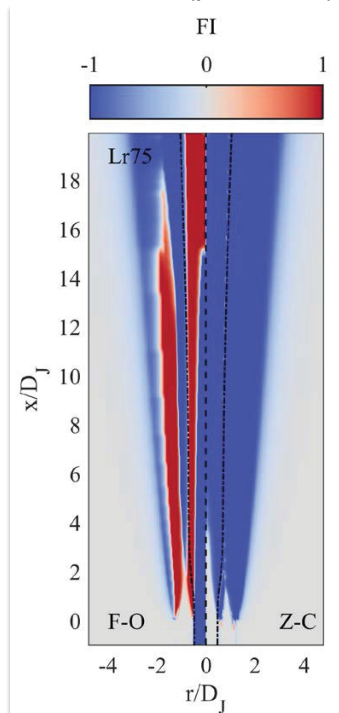


Stanford University

Combustion Regimes Sydney flame (Lr75)

- FPV (non-premixed) Vs. F-TACLES (premixed)

$$FI_{F-O} = \frac{\nabla \tilde{Y}_F \cdot \nabla \tilde{Y}_O}{|\nabla \tilde{Y}_F \cdot \nabla \tilde{Y}_O|}$$



$$FI_{Z-C} = \frac{\nabla \tilde{Z} \cdot \nabla \tilde{C}}{|\nabla \tilde{Z} \cdot \nabla \tilde{C}|}$$

Stanford University

Combustion Model Compliance Indicator

Model compliance indicator

- Indicator to identify compliance of combustion model and CFD solution
- Incorporate sensitivity to
 - quantities of interest (QoI): CO, NO, H2O
 - flame structure
- Guide selection of combustion models
- Bootstrapping

Wu, H., See, Y. C., Wang, Q., and Ihme, M., "A Pareto-efficient combustion framework with submodel assignment for predicting complex flame configurations." *Combustion and Flame*, 162, 4208-4230, 2016.

Stanford University

Combustion Model Compliance Indicator

Drift term

- Metric for assessing compliance between combustion manifold and local CFD-solution → departure from combustion manifold

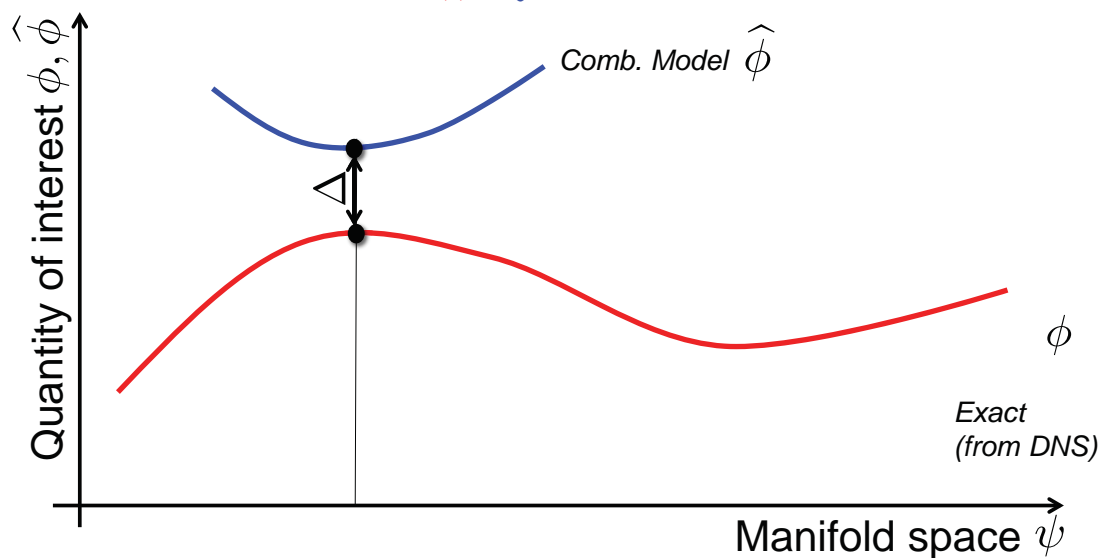
Wu, H., See, Y. C., Wang, Q., and Ihme, M., "A Pareto-efficient combustion framework with submodel assignment for predicting complex flame configurations." *Combustion and Flame*, 162, 4208-4230, 2016.

Stanford University

Combustion Model Compliance Indicator

Drift term

- Evaluate model error $\Delta = \hat{\phi} - \phi$



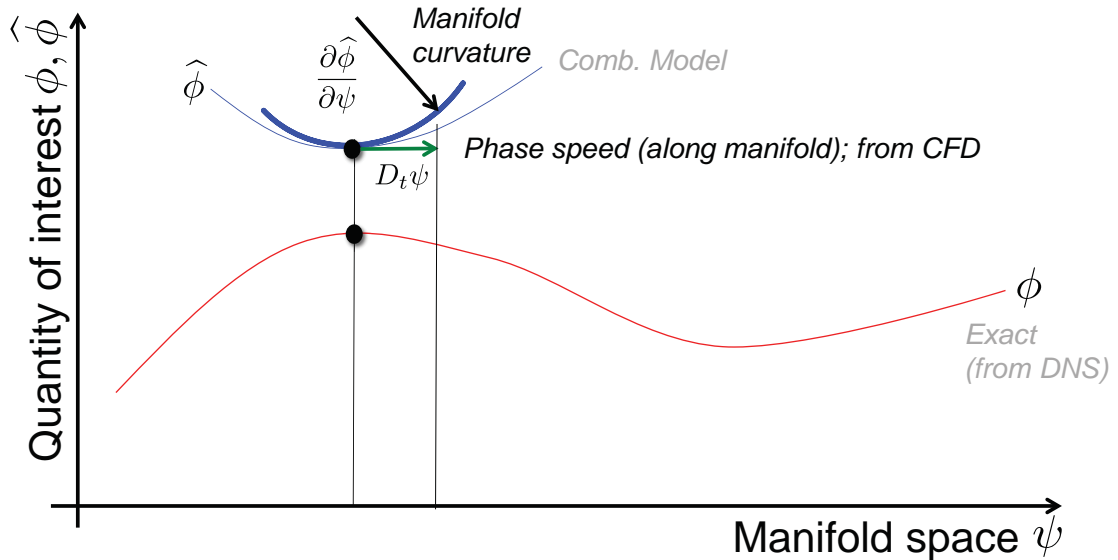
1 Pope, S. B. "Small scales, many species and the manifold challenges of turbulent combustion, *Proc. Combust. Inst.* 34, 2013

Stanford University

Combustion Model Compliance Indicator

Drift term

- Instead, evaluate **compatibility** between combustion model and CFD-solution



1 Pope, S. B. "Small scales, many species and the manifold challenges of turbulent combustion, Proc. Combust. Inst. 34, 2013

Stanford University

Combustion Model Compliance Indicator

Drift term

- Evaluate **compatibility** by expanding error: $\Delta = \hat{\phi} - \phi$
- Drift from manifold¹ for each quantity of interest, ϕ , and combustion model m

$$\mathcal{D}^m(\phi) = D_t \Delta|_{\Delta=0} \quad \text{Manifold slope}$$

$$\mathcal{D}^m(\phi) = D_t \phi|_{\phi=\hat{\phi}^m} - \frac{\partial \hat{\phi}^m}{\partial \psi^m} \cdot D_t \psi^m \quad \text{Phase speed}$$

$$\tilde{\mathcal{D}}^m(\tilde{\phi}) = \tilde{D}_t \tilde{\phi}|_{\tilde{\phi}=\hat{\phi}^m} - \frac{\partial \tilde{\phi}^m}{\partial \tilde{\psi}^m} \cdot \tilde{D}_t \tilde{\psi}^m$$

- Extension of drift term as model-compliance metric to LES quantities²

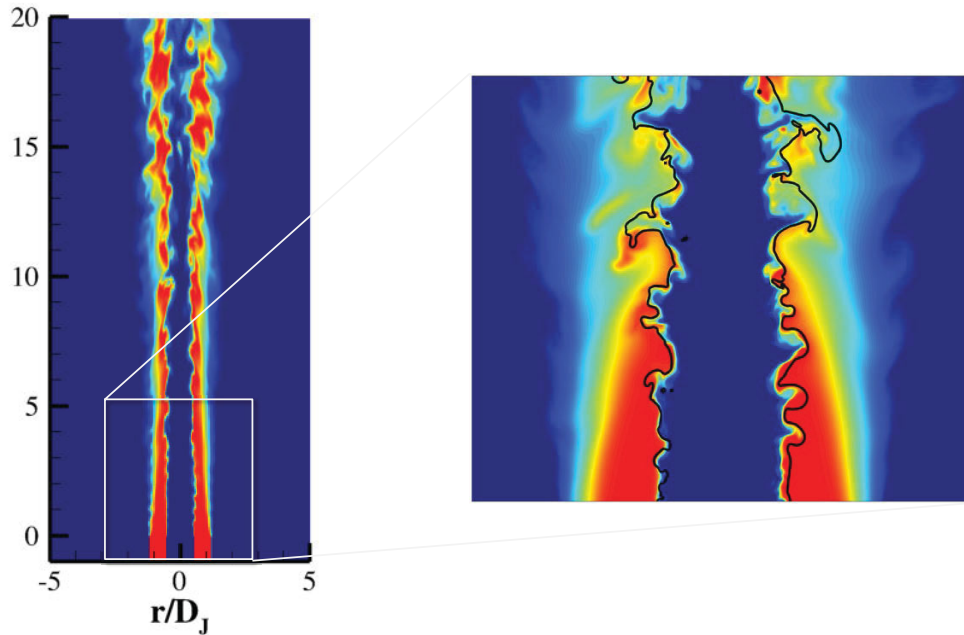
$$\mathcal{D}^m(\tilde{\phi}) = \underbrace{\tilde{\mathcal{D}}^m(\tilde{\phi})}_{\text{Combustion Model}} + \underbrace{\{D_t \tilde{\phi}|_{\tilde{\phi}=\hat{\phi}^m} - \tilde{D}_t \tilde{\phi}|_{\tilde{\phi}=\hat{\phi}^m}\}}_{\text{Closure Error}} - \{D_t \tilde{\phi}^m - \tilde{D}_t \tilde{\phi}^m\}$$

1 Pope, PCI, 34, 2013
2 Wu, Ihme, Fuel 2016

Stanford University

Combustion Model Compliance Indicator

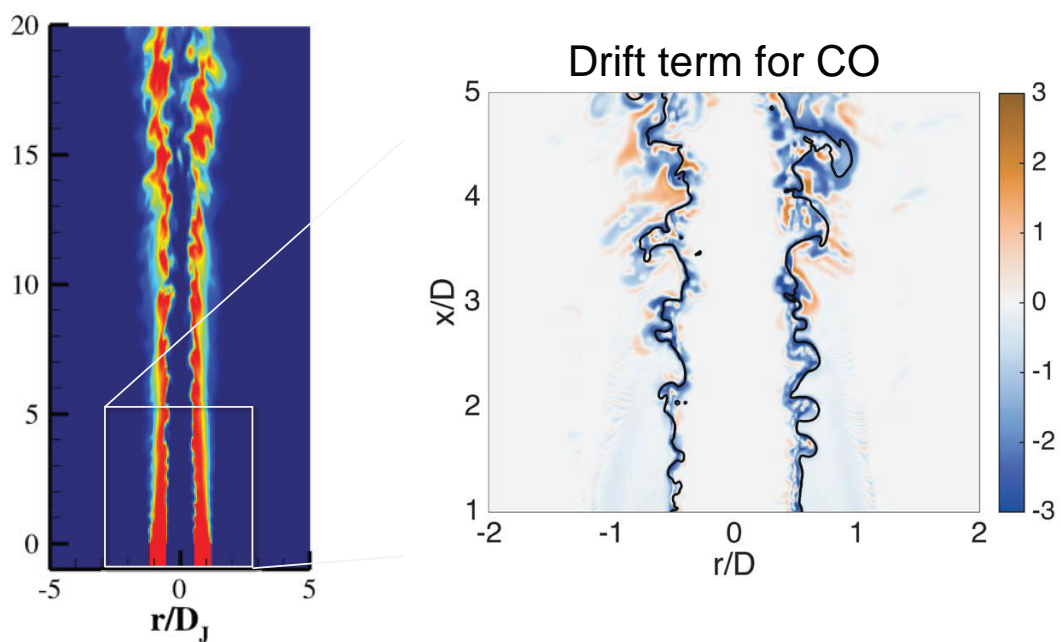
Application of drift term to LES of Sydney flame (Lr75)



Stanford University

Combustion Model Compliance Indicator

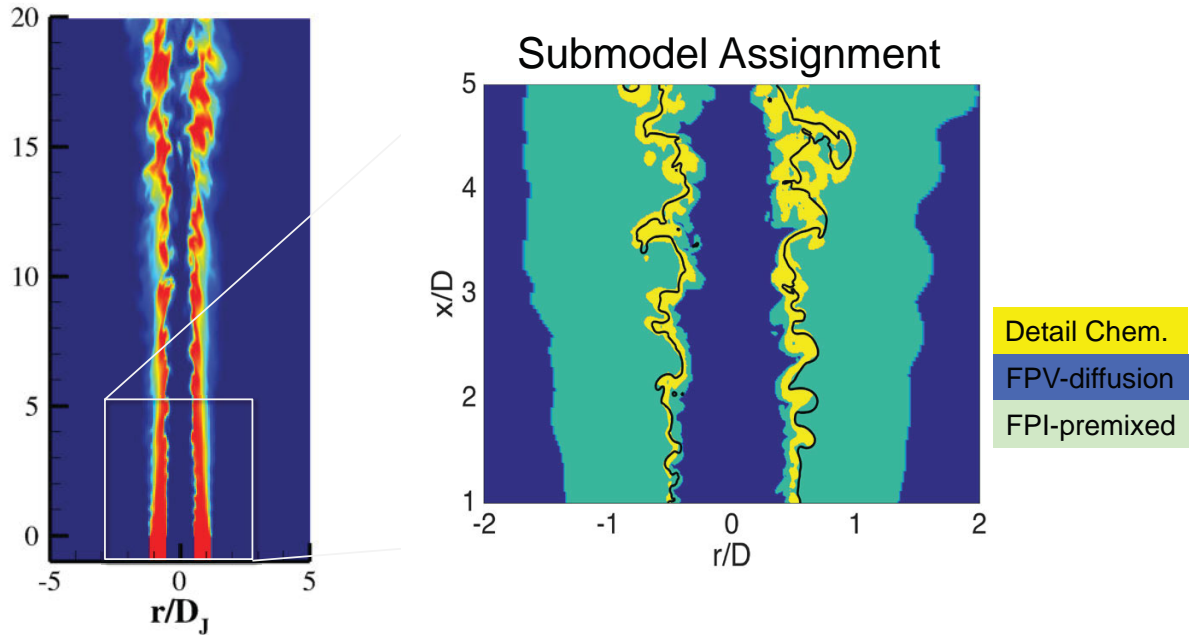
Application of drift term to LES of Sydney flame (Lr75)



Stanford University

Combustion Model Compliance Indicator

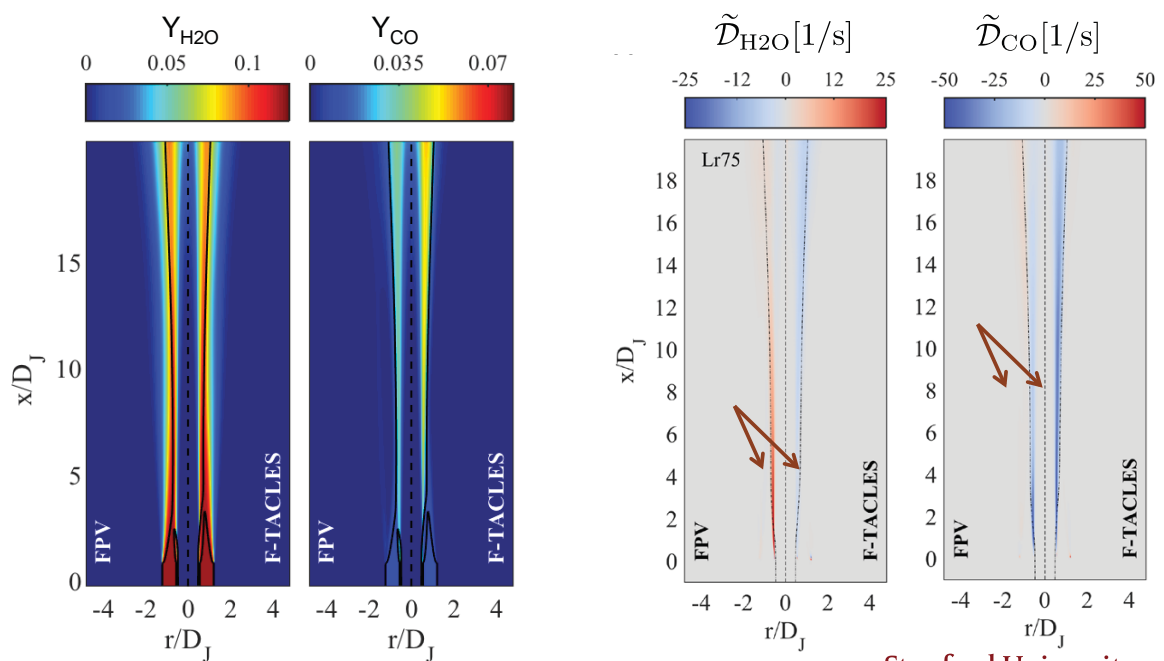
Application of drift term to LES of Sydney flame (Lr75)



Stanford University

Combustion Model Assessment

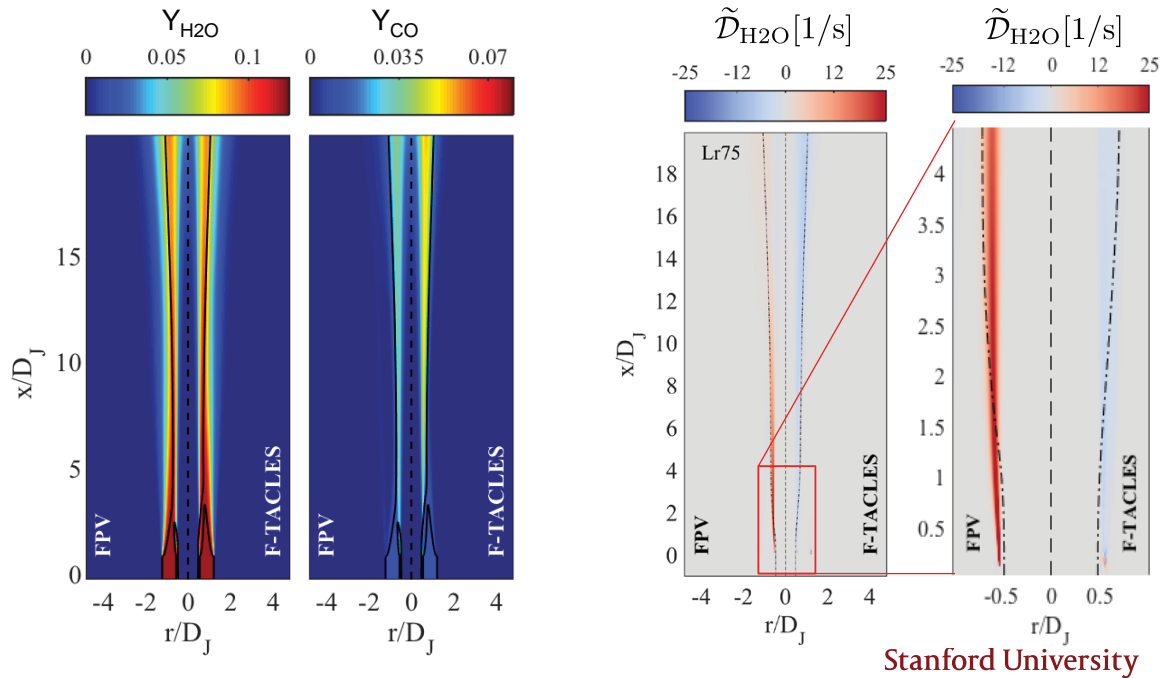
- Quantity of interest: H₂O, CO
- Combustion models: FPV (non-premixed) Vs. F-TACLES (premixed)



Stanford University

Combustion Model Assessment

- Quantity of interest: H₂O, CO
- Combustion models: FPV (non-premixed) Vs. F-TACLES (premixed)



Stanford University

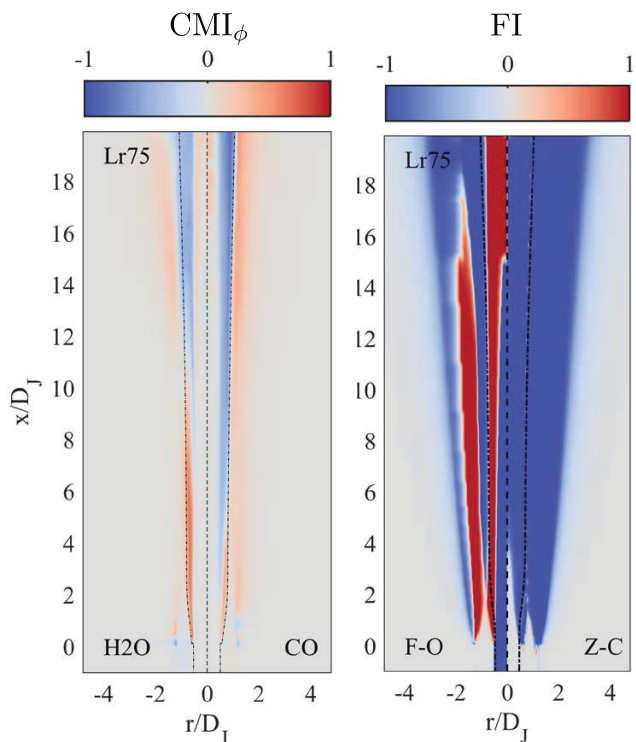
Combustion Model Indicator: CMI

- Combine species-specific drift-term to derive combustion model indicator

$$CMI_\phi = \frac{|\tilde{D}_\phi^{FPV}| - |\tilde{D}_\phi^{F-TACLES}|}{|\tilde{D}_\phi^{FPV}| + |\tilde{D}_\phi^{F-TACLES}|}$$

- Model assignment
 - CMI = 1 ... FPI (premixed)
 - CMI = -1 ... FPV (diffusion)

- field variable
- Sensitive to species



Stanford University

Summary and Conclusions

Optimal reaction progress variable

- Optimization methods overcomes *ad hoc* specification of progress variable
- Generalization to different fuels, and improvements in representation of combustion-manifold → improved model accuracy
- Application to measurements to maximize SNR

Combustion regime indicators and model compliance

- Regime indicators/flame indices are useful to guide physical interpretation; lack fine-grained description of species-sensitivities
- Guidance of combustion-model selection requires consideration of target species, flame structure
- Drift term provides potential use for combustion model selection

Stanford University

DME Jet Flames

Coordinator: Andreas Kronenburg

The session on dimethyl ether (DME) flames focused on the progress in measurements and computations of the turbulent piloted partially-premixed dimethyl ether (DME)/air jet flame series. The series was introduced in TNF11 and first results on simulations and their comparisons with experiments were reported at TNF12. The original flame series (flames D-G) comprised flames with jet exit Reynolds numbers between approximately 29,000 to 73,000 leading to varying degrees of local extinction. Experiments were performed at Sandia and included PIV, OH-LIF, and CH₂O-LIF imaging measurements, as well as joint Raman/Rayleigh/CO-LIF line measurements.

New measurements have now extended the parameter range of the original flame series: DME flame G' has a reduced pilot velocity to increase localized extinction and to reach extinction levels similar to the extensively studied Sandia Flame F of the methane air series. Line data and imaging data are now available for the entire flame series DME-D/E/F/G/G' including scalar dissipation measurements (1-D) for DME-D. Further experiments vary the amount of premixing for flame F with air. In addition to the original experiments with fuel consisting of air and DME mixed in a ratio of 4:1, the new experiments include fuel streams with air:DME ratios of 6:1 and 8:1. This variation promotes the transition from non-premixed combustion towards premixed combustion and shifts the stoichiometric mixture fraction contour relative to the shear layer reducing the separation distance between the CH₂O and OH LIF fields and potentially posing additional challenges to the modellers.

As for TNF12, the computations included contributions by four different groups: RANS-MEPDF (Hanyang), LES-PDF (Beijing/Cornell), LES-CMC (Stuttgart), and LES-FPV (Freiberg). Additional results using LES-MMC have been provided by Stuttgart. Notable is the good prediction of flame DME-D by all models. The LES-CMC computations show a very low sensitivity of the results towards the chemical mechanism (with the exception of CH₂O). This is owed to the flame conditions and the quality of computations is likely be more dependent on the mechanism during low temperature ignition and in cases of significant premixed flame propagation. The MEPDF, PDF and MMC models have also been applied to flame F with some success. In particular, the LES-PDF computations agree well with the experimental data and highlight the dependence of the results on the implementation of the molecular transport term. Differential diffusion effects can be captured well, however, they have minor effects and do not markedly affect the conditionally averaged moments. This aspect of the PDF computations is now in agreement with the LES-FPV results presented at TNF12, and we can conclude that non-unity Lewis number effects do not play a major role.

New auto-ignition DME experiments of the Sydney group are now available. The fuel jet consists of DME and air with ratios varying from pure DME to ratios of DME to air equalling 1:7. The jet is surrounded by a hot co-flow with temperatures ranging from 1200K to 1500K. The experimental campaign includes lift-off height graphs, simultaneous OH and CH₂O PLIF, temporal evolution and statistics of the flame base and ignition kernels and simultaneous acoustic and chemiluminescence data. First RANS-PDF computations show strong dependencies on the chemical mechanism during ignition events.

Goals for TNF14 should comprise computations of the entire piloted jet flame series (Sandia DME D-G') with focus on the accurate prediction of the degree of localized extinction, in particular in flames G and potentially G'. We should also seek clarification of the predictions' dependencies on the chemical mechanisms. This may include the need for a quantitative comparison of formaldehyde as this is the measured species with the most pronounced differences for all flame and flow conditions. The new Sydney flame series provides a testing environment for all models and includes flame conditions where sensitivities on mechanisms can be expected. As such, the experiments constitute an attractive alternative (and/or addition) for model development and validation, but care should be taken to avoid potential undesired sensitivities that were observed for the Berkeley hydrogen and methane flames in vitiated co-flow (Cabra flames).

Piloted DME Jet Flames

Coordinator:
Andreas Kronenburg

13th International Workshop on
Measurement and Computation of Turbulent Flames

28th July – 30th July 2016
Incheon, Korea



University of Stuttgart



Piloted DME Jet Flames

Contributors

Contribution	Affiliations	Researchers
Exp: Velocity, CH ₂ O, OH	Sandia	J. Frank, B. Coriton, S.-K. Im, M. Gamba
Exp: Temperature, Species	Sandia, Ohio State	F. Fuest, G. Magnotti, R. Barlow, J. Sutton
Exp: Temperature, Species	Sydney	A. MacFarlane, M. Dunn, M. Judoo, A.R. Masri
LES - flamelet	Freiberg	C. Hasse
LES - CMC	Stuttgart	A. Kronenburg, O. Stein
RANS - PDF	Hanyang	S. Jeon, Y. Kim
LES - PDF	Peking, Cornell	Y. Yang, J. You, S. Pope
LES - MMC	Stuttgart	G. Neuber, A. Kronenburg, O. Stein



University of Stuttgart



Outline

Overview of activities

- Reminder: Overview of Sandia DME Target Jet Flames
- Status of Species/Temperature Measurements
- Simulations
 - Follow-up from 2014
 - LES-CMC, LES-flamelet
 - RANS-PDF
 - LES-PDF
- New Flame (Sydney)
- Summary

Some discussion on DME in next session



Flow Conditions

- Standard Flame Series (D-G) Air:DME = 4:1
 - Progression of Re_D with same stoichiometric mixture fraction ($\zeta_{st} = 0.35$) as Air:CH₄ = 3:1
- **New: Vary amount of premixing for Flame F with Air:DME = 4:1, 6:1, and 8:1**
 - Transition towards premixed combustion
 - Shift location of ζ_{st} contour relative to shear layer
 - New modeling challenge?

Flame	D_{41}	E_{41}	F_{41}	F_{61}	F_{81}	G_{41}
φ_{jet}	3.6	3.6	3.6	2.4	1.8	3.6
ξ_{st}	0.35	0.35	0.35	0.48	0.60	0.35
Re_D	29,300	43,900	58,600	54,500	52,500	73,300
Q_{jet} (LPM)	120	180	240	240	240	300
V_{jet} (m/s)	45.9	68.8	91.8	91.8	91.8	115
V_{coflow} (m/s)	0.9	0.9	0.9	0.9	0.9	0.9





Current Experimental Data Sets

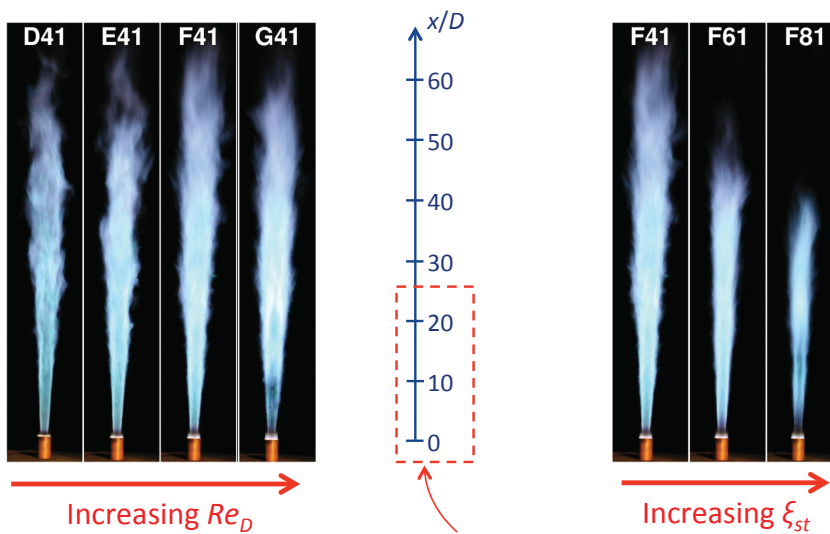
Flame	ϕ_{jet}	ξ_{st}	Re_D	Stereo PIV	OH/CH ₂ O LIF	Tomo PIV	Raman/Rayleigh/CO LIF
D_{41}	3.6	0.35	29,300	✓	✓	✓	✓
E_{41}	3.6	0.35	43,900	✓	✓	✓	✓
F_{41}	3.6	0.35	58,600	✓	✓	✓	✓
F_{61}	2.4	0.48	54,500	✓	✓		
F_{81}	1.8	0.60	52,500	✓	✓		
G'_{41}	3.6	0.35	73,400	✓	✓	✓	✓
	3.6	0.35	73,400				✓

Flame G'_{41} has reduced pilot velocity with increased localized extinction

- Line Data: F. Fuest, G. Magnotti, J.A. Sutton, R.S. Barlow
- Imaging Data: B. Coriton, S-K Im, M. Gamba, J.H. Frank



Flame Series Photographs



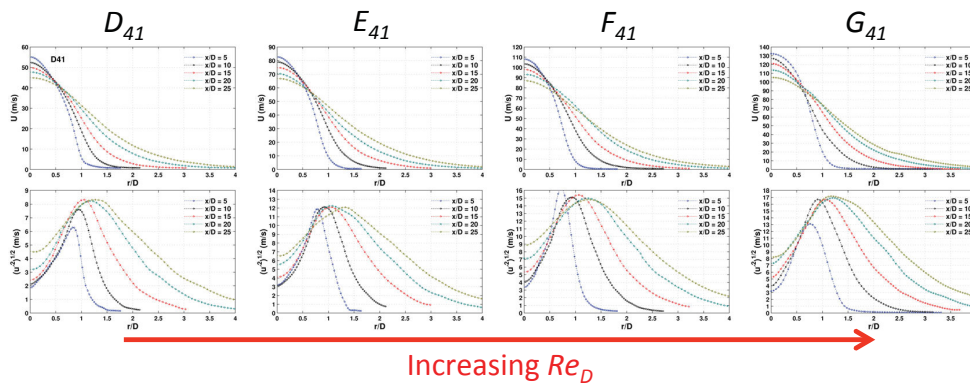
Measurements in Near-Field
up to $x/D = 25$



Velocity Field Statistics

- Jet Exit Velocity (Hot Wire Anemometry)
- Mean and RMS velocity profiles at $x/D = 5, 10, 15, 20$ and 25 (Stereo PIV)

Axial Velocity Component:



COMBUSTION RESEARCH FACILITY

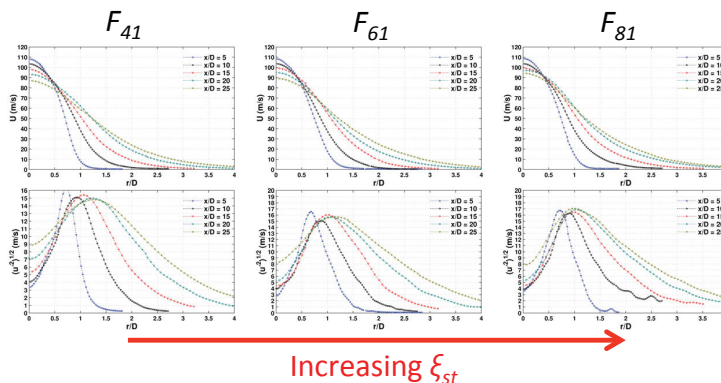
Sandia National Laboratories



Velocity Field Statistics

- Jet Exit Velocity (Hot Wire Anemometry)
- Mean and RMS velocity profiles at $x/D = 5, 10, 15, 20$ and 25 (Stereo PIV)

Axial Velocity Component:

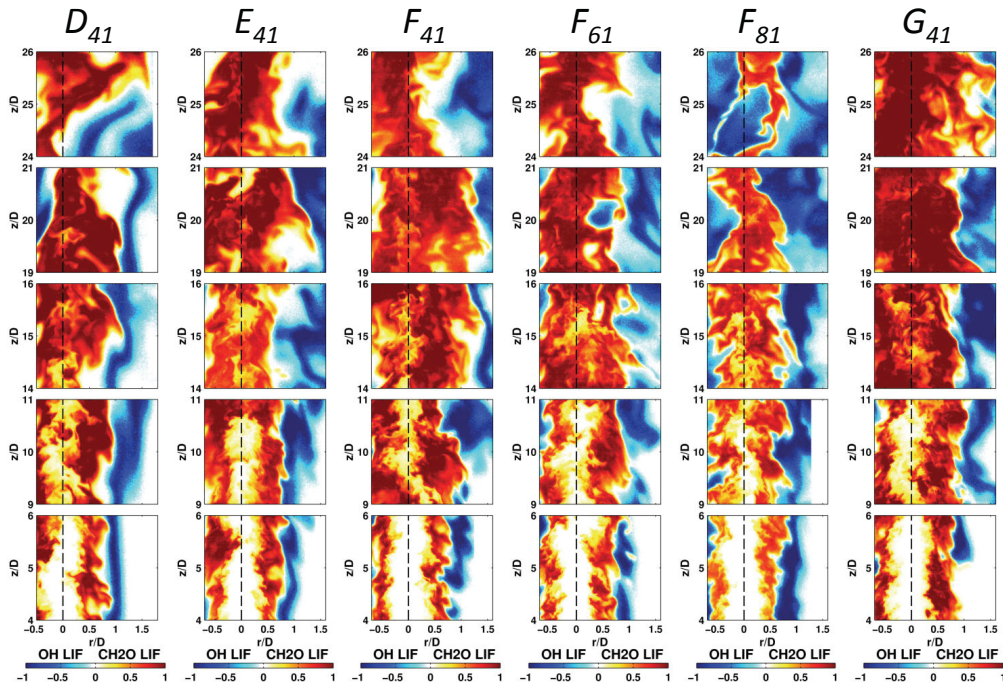


COMBUSTION RESEARCH FACILITY

Sandia National Laboratories



CH₂O/OH LIF Imaging for x/D = 5-to-25



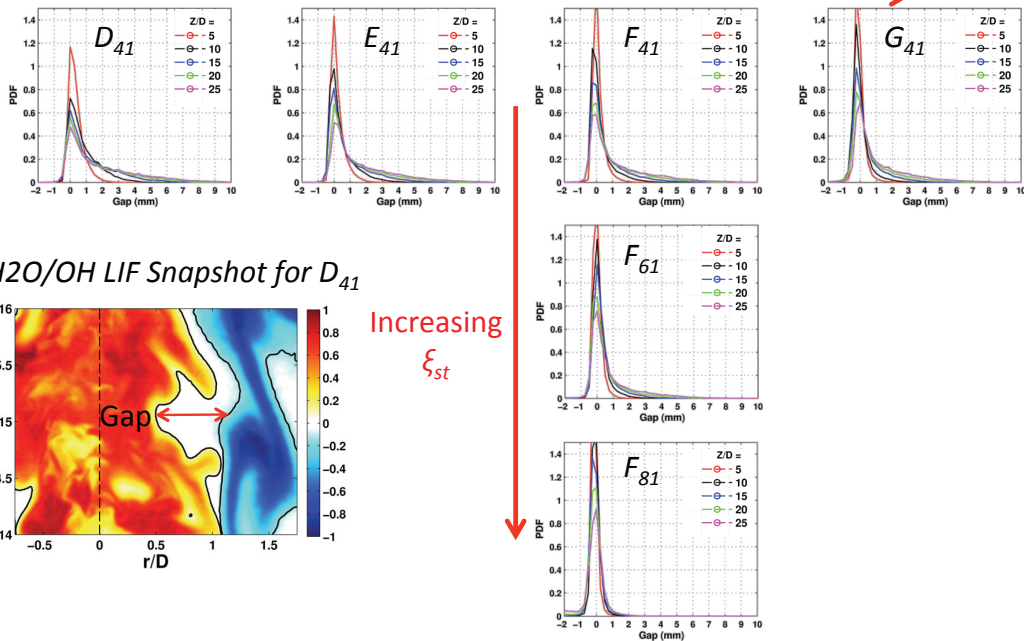
COMBUSTION RESEARCH FACILITY

Sandia National Laboratories



Separation Distance between CH₂O LIF and OH LIF fields

Increasing Re_D

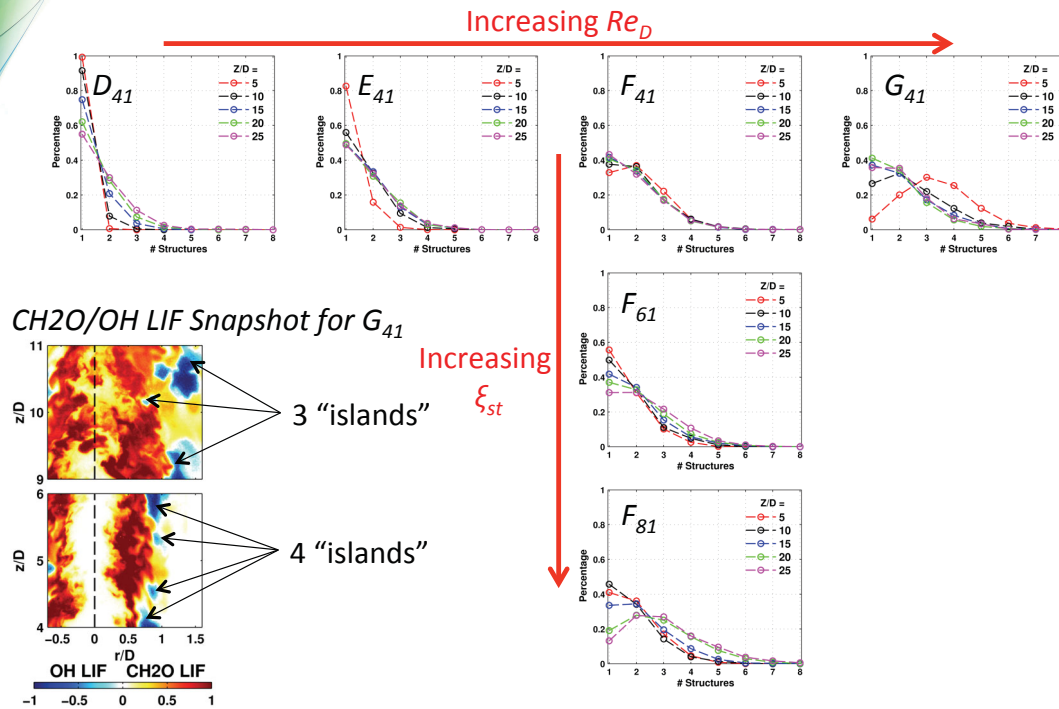


COMBUSTION RESEARCH FACILITY

Sandia National Laboratories



Number of "Islands" per OH LIF snapshot

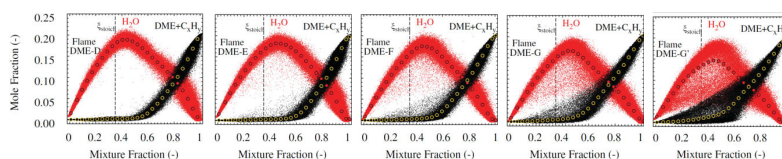


COMBUSTION RESEARCH FACILITY

Sandia National Laboratories

Raman/Rayleigh/CO-LIF scalar measurements of turbulent piloted DME flame series

- Scalar data for flame DME-D and DME-F published 2015 PROCI
- Ascii data available
- Preliminary results for entire series as poster presentation at this TNF
- Conditional scatter plots of mole fractions of H₂O and DME+C_xH_y for flames DME-D/E/F/G/G'
- G' as additional case with reduced pilot velocity (80% of DME-G) to further increase local extinction



$x/d = 7.5$

Sandia National Laboratories THE OHIO STATE UNIVERSITY

LAVISION

Scalar dissipation rate measurements in turbulent flame DME-D

- Shown previously that a number of experimental issues make accurate scalar dissipation rate measurements very challenging, e.g. TNF6,7,8 and for example:

D. Geyer, A. Kempf, A. Dreizler, J. Janicka, Scalar dissipation rates in isothermal and reactive turbulent opposed-jets: 1D-Raman/Rayleigh experiments supported by LES, Proc. Combust. Inst. 30 (2005) 681–689

G.-H.Wang, N.T.Clemens, R.S.Barlow, P.L.Varghese, A system model for assessing scalar dissipation measurement accuracy in turbulent flows, Meas. Sci. Technol. 18 (2007) 1287–1303

J. H. Frank, S. A. Kaiser, High-resolution imaging of dissipative structures in a turbulent jet flame with laser Rayleigh scattering, Exp. Fluids 44 (2008) 221–233



Scalar dissipation rate measurements in turbulent flame DME-D

- For quantitative comparison to turbulent combustion simulations following issues need to be addressed:
 - Three-dimensionality
 - Spatial resolution/averaging
 - Measurement noise
 - Mixture diffusivity function of temperature and mixture composition
 - Transported/flamelet vs. derived scalar dissipation rate (from local species concentrations and temperature)
 - DME flames: Undetected intermediate hydrocarbons
 - Turbulent transport vs. differential diffusion
- Some issues discussed on poster, a couple examples here
- Paper in preparation, data can be made available



Scalar dissipation rate measurements in turbulent flame DME-D

Three-dimensionality and spatial orientation of the flame

- Raman/Rayleigh → 1D measurement, reduced values (see Figure)
 - OH-PLIF or Planar Rayleigh for 3D angle correction
 - mass diffusivity from simultaneous temperature/species measurement
- 3D or pseudo 3D-techniques usually mass diffusivity not accessible

→ Proposed practice for comparison:
Extract angle/radial component from simulations?

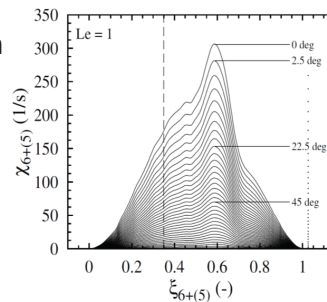


Figure: Effect of flame orientation on radial component of scalar dissipation rate.



Scalar dissipation rate measurements in turbulent flame DME-D

Spatial averaging, necessary spatial resolution, and noise

Common practice:

- Determination of spatial resolution limit and noise impact by 1D dissipation spectra and cutoff wavelength λ_C
- Estimation of smallest scales from scaling law,

x/d	r_{st}/d	$\pi\lambda_B^{\bar{T}_{max}}$ (μm)	$\pi\lambda_B^{T_{PDF}}$ (μm)	$\pi\lambda_B^{k_{Ray}}$ (μm)	$\lambda_B = 2.3\delta Re_\delta^{-3/4} Sc^{-1/2}$
1	0.67	310	215	124	
5	0.89	398	234	319	
7.5	0.9	405	246	290	
10	0.91	411	279	268	
20	1.61	432	246	293	
40	2.35	627	297	397	

Comparing Batchelor scales of DME-D at radial location of mean stoichiometric mixture fraction from dissipation spectra and scaling law using mean T_{max} and temperature distribution from measurement.



Computations

Follow-up of 2014

- Freiberg (LES-flamelet)
- Stuttgart (LES-CMC)

New computations of further flames

- Hanyang (RANS - multi-environment PDF)
- Beijing/Cornell (LES-PDF)
- Stuttgart (LES-MMC)

⇒ second attempt at comparisons of the DME flames

⇒ evolution rather than revolution



University of Stuttgart



Numerical Setup



LES-Flamelet/Progress Variable

- LES flamelet-progress variable approach
- OpenFOAM based solver

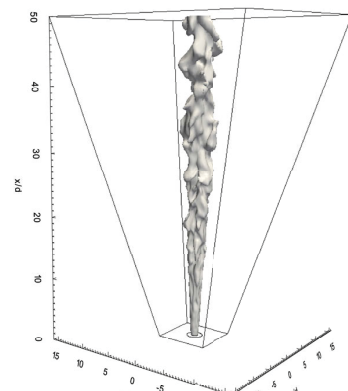
Tabulated chemistry

- Flamelet look-up tables (FLUT)
- Beta filtered density function (FDF)
- Diffusion flamelet with unity Lewis number
- Zhao mechanism [1]

LES

- Spatial and temporal discretization: 2nd order
- Sub-grid turbulence: sigma model
- Stretched rectilinear grid with ~10 mio cells
- Turbulent velocity inlet boundary condition from pipe flow LES

Computational domain (bounding box 50d x 30d x 30d) with iso-surface of the stoichiometric mixture fraction



LES flamelet-progress variable modeling and measurements of a turbulent partially-premixed dimethyl ether jet flame
 Sebastian Peppé¹, Franziska Hunger², Sandra Hartl¹, Danny Messig³, Bruno Cortese⁴, Jonathan H. Frank⁵, Frederik Faust⁶, Christian Hasse⁷
¹Chair of Mechanical Engineering, TU Braunschweig, Leibniz Universität Hannover, Germany
²Combustion Research Facility, Sandia National Laboratories, Livermore, CA, USA
³Department of Mechanical and Aerospace Engineering, The Ohio State University, Columbus, OH, USA

[1] Z. Zhao *et al.*, International Journal of Chemical Kinetics (2008)

Experiment

- Temperature from Rayleigh signals based on effective Rayleigh cross sections

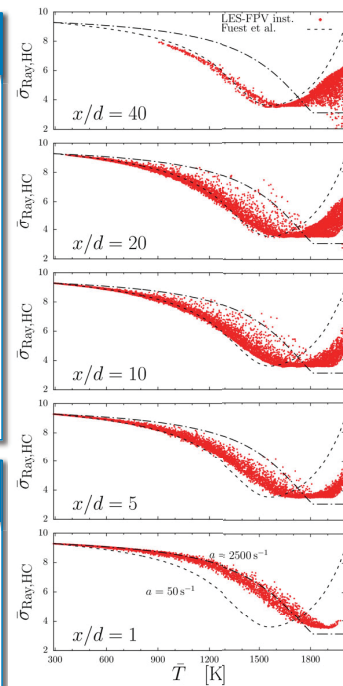
$$\sigma_{\text{Ray,eff}} = \sum_i X_i \sigma_{\text{Ray},i}$$

- Intermediate species not accessible by measurements
 → model for $\sigma_{\text{Ray,HC}}$ based on 1D flame calculation [1]

$$\sigma_{\text{Ray,eff,exp}} = \frac{\sum_{i=1}^6 X_i \sigma_{\text{Ray},i} + X_{\text{HC}} \sigma_{\text{Ray,HC}}}{\sum_{i=1}^6 X_i + X_{\text{HC}}}$$

Simulation

- $\sigma_{\text{Ray,HC}}$ computation with intermediate species from LES-FPV shows strain dependence compared to single flamelet solutions



[1] F. Fuest *et al.* Combustion and Flame 159 (2012)

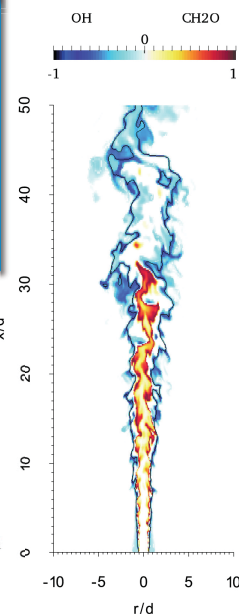
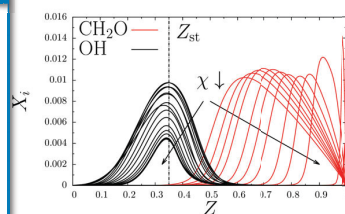
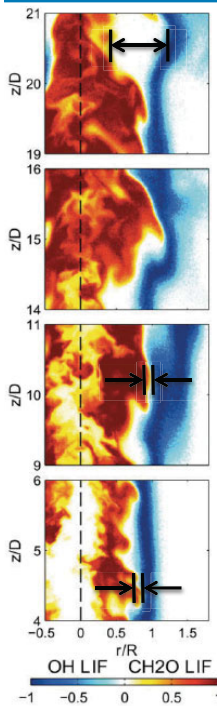
17

Separation of CH₂O- and OH-layers

- DME- increased amount of intermediate C_xH_y
- Single-shot LIF measurements (*Coriton et al.* [3])
- Characteristic separation features (downstream evolution of gap formation between CH₂O- and OH-layers)

Flamelet structure

- Identical separation features
- Dependent on scalar dissipation rate
- $\chi \propto (\nabla Z)^2$



TNF 12 Proceedings (2014)

18

LES-CMC - Stuttgart (Kronenburg & Stein)

- CMC

$$\gamma \frac{\partial Q_\alpha}{\partial t} + \gamma \nabla (\gamma \bar{u}_\eta Q_\alpha) = \gamma \tilde{\omega}_{\eta,\alpha} + \gamma \tilde{N}_\eta \frac{\partial^2 Q_\alpha}{\partial \eta^2} + Q_\alpha \nabla (\gamma \bar{u}_\eta) + \nabla (\gamma [\langle \bar{u} Y_\alpha | \eta \rangle - \bar{u}_\eta Q_\alpha])$$

- Issues of last workshop: grid resolution and chemistry

- Domain: 10Dx10Dx60D and 10Dx10Dx40D (fine)
- LES resolution: 72x72x240 and 144x144x512
- CMC resolution: 2x2x60 and 16x16x60

- Chemistry

- Z. Zhao, M. Chaos, A. Kazakov, F.L. Dryer, Int. J. Chem. Kin., 40 (2008) 1-18 (53 species, 291 reactions)
- E.W. Kaiser, T.J. Wallington, M.D. Hurley, J. Platz, H.J. Curran, W.J. Pitz, C.K. Westbrook, J. Phys. Chem. A, 104 (2000) 8194-8206 (79 species, 351 reactions)
- W.K. Metcalfe, S.M. Burke, S.S. Ahmed, H.J. Curran, "A Hierarchical and Comparative Kinetic Modeling Study of C1–C2 Hydrocarbon and Oxygenated Fuels", Int. J. Chem. Kinet. (2013) 45(10) 638–675. (Aramco 1.3: 124 species, 766 reactions)

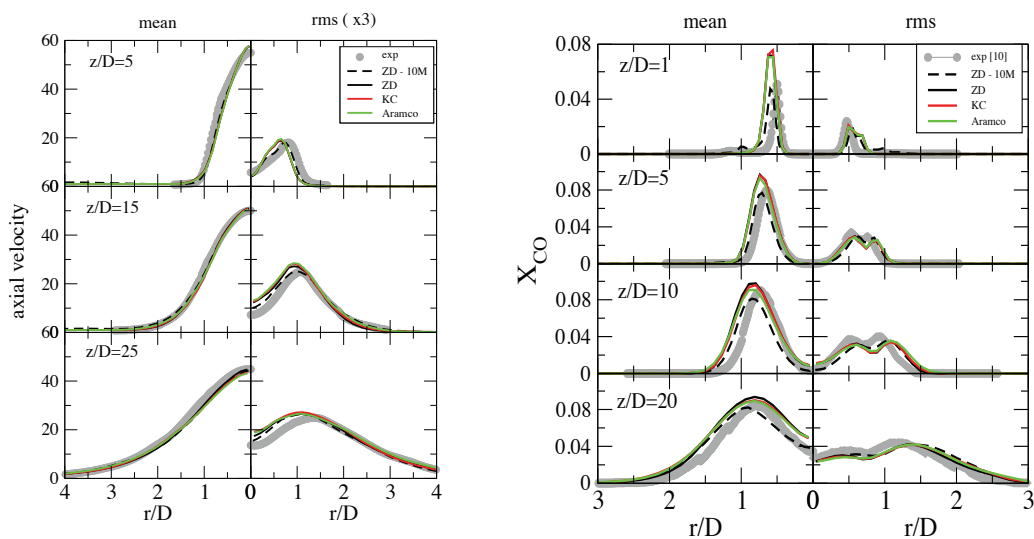


University of Stuttgart



LES-CMC

- Axial velocity (left) and CO (right)

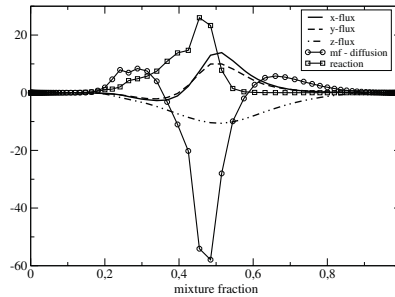


University of Stuttgart

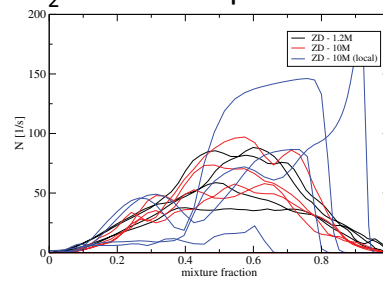
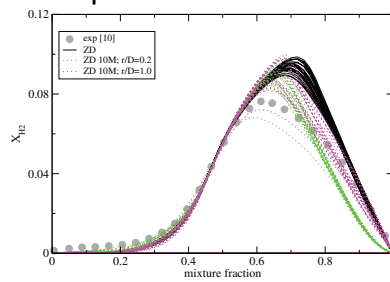


LES-CMC

- Transport budgets at $z/D=1$, $r/D=0.2$



- Temporal variation of conditional H_2 and of dissipation rate



University of Stuttgart



CMC Summary

- independence of results on mechanism
- differences in CH_2O , but direct comparison with measurements not possible (normalization required)
- around 1M LES cells provide sufficient resolution
- differences due to spatial resolution of CMC cells
- conditional fluxes and variation in conditional dissipation



University of Stuttgart



Multi-Environment PDF Modeling by Hanyang

- Closed joint composition PDF transport equation with IEM mixing model

$$\frac{\partial f_\phi}{\partial t} + \langle U_i \rangle \frac{\partial f_\phi}{\partial x_i} - \frac{\partial}{\partial x_i} \left(\Gamma_t \frac{\partial f_\phi}{\partial x_i} \right) = - \frac{\partial}{\partial \Psi_i} \left[\left(C_\phi \frac{\varepsilon}{k} (\langle \phi_i \rangle - \Psi_i) + S_i(\Psi) \right) f_\phi \right]$$

- Formulation of MEPDF approach

$$f_\phi(\Psi; x, t) = \sum_{n=1}^{N_e} P_n(x, t) \prod_{\alpha=1}^{N_s} \delta(\Psi_\alpha - \langle \phi_\alpha \rangle_n(x, t))$$

where N_s : # of composition vector

N_e : # of environment

m-th moments

$$\langle \phi_1^{m_1} \dots \phi_{N_s}^{m_{N_s}} \rangle = \sum_{n=1}^{N_e} P_n(x, t) \prod_{\alpha=1}^{N_s} \langle \phi_\alpha \rangle_n^{m_\alpha}$$

where m_α are the typical chosen to be non-negative integers

Multi-Environment PDF Modeling

- Transport equations of weights and weighted abscissas

$$\frac{\partial p_n}{\partial t} + \langle U_i \rangle \frac{\partial p_n}{\partial x_i} - \frac{\partial}{\partial x_i} \left(\Gamma_t \frac{\partial p_n}{\partial x_i} \right) = a_n$$

$$\frac{\partial \langle s \rangle_n}{\partial t} + \langle U_i \rangle \frac{\partial \langle s \rangle_n}{\partial x_i} - \frac{\partial}{\partial x_i} \left(\Gamma_t \frac{\partial \langle s \rangle_n}{\partial x_i} \right) = b_n$$

- a_n and b_n

let $a_1 = a_2 = 0$, select $m=1, 2$

$$b_1 = \frac{1}{\langle \phi \rangle_1 - \langle \phi \rangle_2} \sum_{n=1}^2 p_n \Gamma_t (\nabla \langle \phi_n \rangle)^2 + C_\phi \frac{\varepsilon}{k} (p_1 \langle s \rangle_2 - p_2 \langle s \rangle_1) + p_1 S(\langle \phi \rangle_1)$$

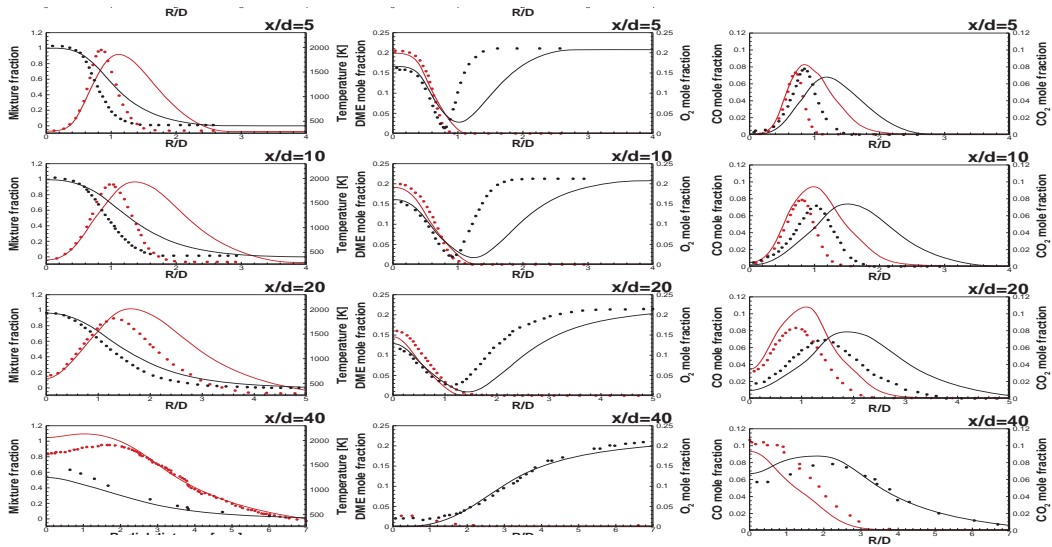
$$b_2 = \frac{-1}{\langle \phi \rangle_1 - \langle \phi \rangle_2} \sum_{n=1}^2 p_n \Gamma_t (\nabla \langle \phi_n \rangle)^2 + C_\phi \frac{\varepsilon}{k} (p_1 \langle s \rangle_2 - p_2 \langle s \rangle_1) + p_2 S(\langle \phi \rangle_2)$$

- Setup

Standard $k - \varepsilon$ model
 2-ENV PDF approach
 with IEM mixing model
 Model constant for IEM : $C_\phi = 2.0$
 Time step : $1.e-5 \text{ s}^{-1}$

2-ENV PDF
 Fuel : 1.0 / 0.0
 Pilot : 0.6/0.4
 Oxid : 0.0 / 1.0

2014: Validation II: Piloted DME/Air Jet Flame (3-ENV)

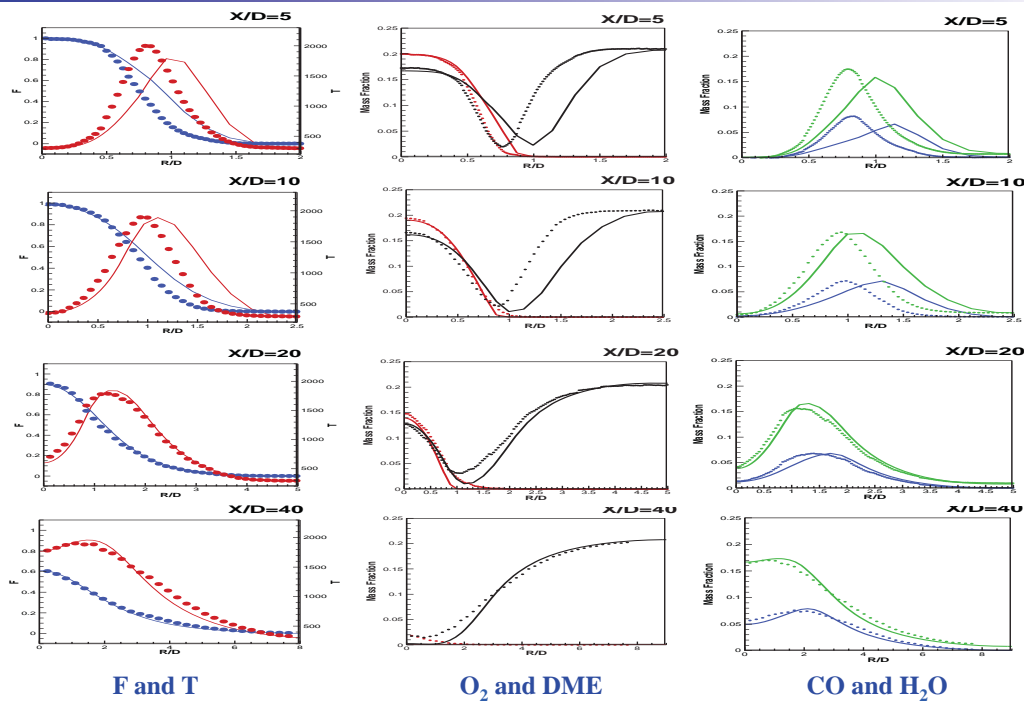


Predicted and measured radial profiles for unconditional mean of temperature, mixture fraction, mole fraction of DME, O_2 , Co and CO_2 .



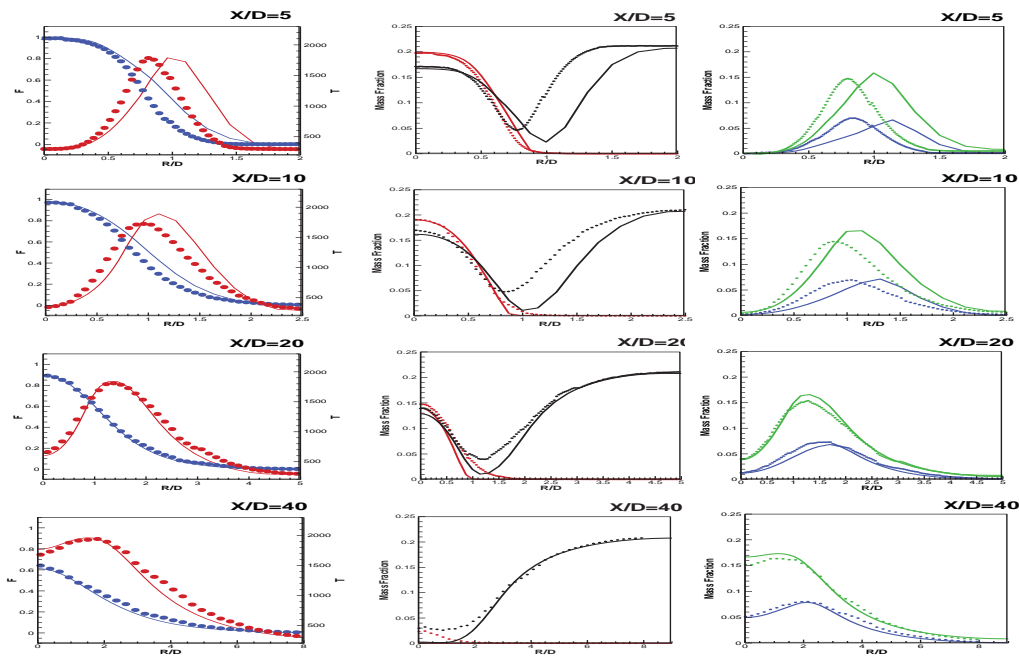
Combustion Analysis and Virtual Engine Lab

2016: Piloted DME/Air Jet Flame D ($U_{jet}=45.9m/s$)



Predicted and measured radial profiles for unconditional mean of temperature and species

2016: Piloted DME/Air Jet Flame F ($U_{jet}=91.8\text{m/s}$)



Predicted and measured radial profiles for unconditional mean of temperature and species

MEPDF Summary

- The Multi-Environment PDF approach has been applied to numerically investigate the piloted DME/air turbulent non-premixed jet flames.
- The present MEPDF model yields the overall agreement with experimental data. These discrepancies are mainly attributed to uncertainties of **inflow boundary conditions** as well as shortcomings in the **RANS-based turbulence model** and **MEPDF approach using IEM mixing model**.

Future:

- Extension to the 3-ENV PDF approach to capture the realistic conditional profiles for three feeding systems with local extinction and re-ignition.
- Improvement of the micro-mixing model in conjunction with the MEPDF approach.
- Extension to the LES-based MEPDF with the improved physical models and numerical procedures.

PDF Methods by Peking/Cornell

- Large-eddy simulation/PDF modeling
 - Computational domain: $60D \times 30D \times 2\pi$
 - 39-species skeletal mechanism [Lu *et al.*, 2013]
 - $128 \times 72 \times 32 = 0.3$ million grid points
 - 20 particles/cell
 - IEM model with molecular transport with $C_M = 15$
 - Flames D and F
 - Approx 18000 CPUh on the TH-2A for 15 flow through times, ~15% for LES



J. You, Y. Yang, and S. B. Pope, *Combust. Flame*, 2016 (submitted)

T contours from
LES/PDF of DME-D

29

Mixing models

- Classical IEM model (**IEM-RW**)

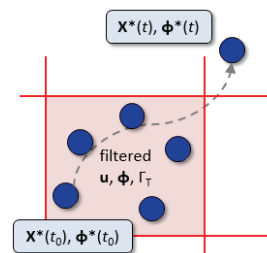
$$d\mathbf{X}^*(t) = \left(\tilde{\mathbf{u}} + \frac{\nabla \bar{\rho}(\Gamma + \Gamma_T)}{\bar{\rho}} \right)^* dt + (2\Gamma^* + 2\Gamma_T^*)^{1/2} d\mathbf{W}$$

$$\frac{d\phi_\alpha^*(t)}{dt} = -\Omega_m^*(\phi_\alpha^* - \tilde{\phi}_\alpha^*) + S(\phi^*)$$

- IEM model with molecular transport (**IEM-MD**)

$$d\mathbf{X}^*(t) = \left(\tilde{\mathbf{u}} + \frac{\nabla \bar{\rho} \Gamma_T}{\bar{\rho}} \right)^* dt + (2\Gamma_T^*)^{1/2} d\mathbf{W}$$

$$\frac{d\phi_\alpha^*(t)}{dt} = -\Omega_m^*(\phi_\alpha^* - \tilde{\phi}_\alpha^*) + \left[\frac{1}{\bar{\rho}} \frac{\partial}{\partial x_j} \left(\bar{\rho} \Gamma \frac{\partial \tilde{\phi}_\alpha}{\partial x_j} \right) \right]^* + S(\phi^*)$$



- IEM model with molecular transport and differential diffusion (**IEM-DD**)

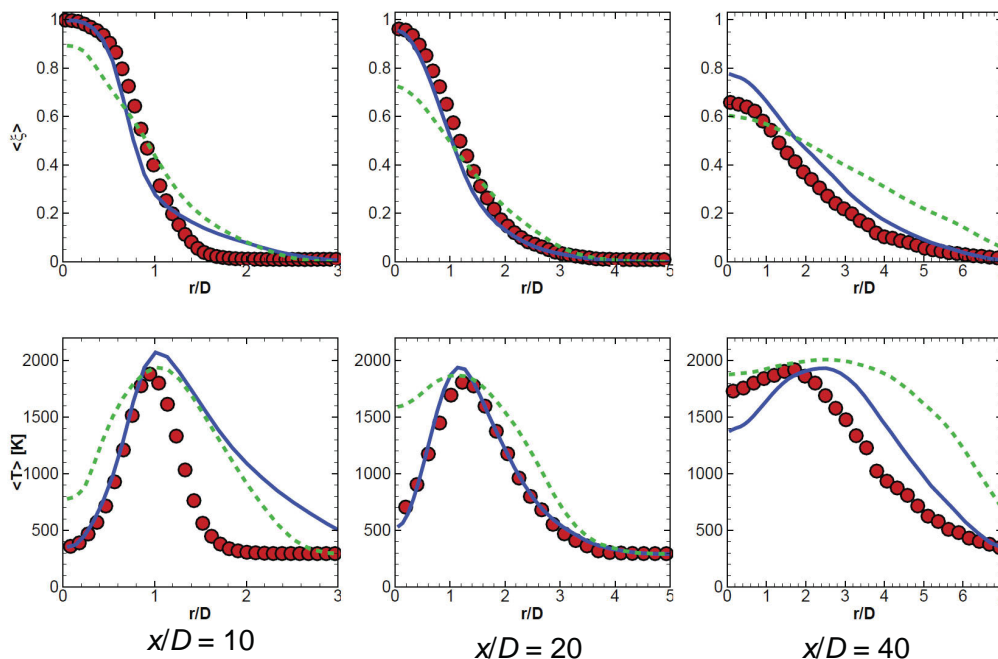
$$\frac{d\phi_\alpha^*(t)}{dt} = -\Omega_m^*(\phi_\alpha^* - \tilde{\phi}_\alpha^*) + \left[\frac{1}{\bar{\rho}} \frac{\partial}{\partial x_j} \left(\bar{\rho} \Gamma_{(\alpha)} \frac{\partial \tilde{\phi}_\alpha}{\partial x_j} \right) \right]^* - \left[\frac{1}{\bar{\rho}} \frac{\partial \bar{\rho} \tilde{\phi}_\alpha V_{c,j}}{\partial x_j} \right] + S(\phi^*)$$

$$V_{c,j} = -\sum_{\alpha=1}^{n_s} \Gamma_\alpha \frac{\partial \phi_\alpha}{\partial x_j}$$

30

2014: Mean profiles

●: Experiment —: LES/PDF with DD ---: LES/PDF without DD



31

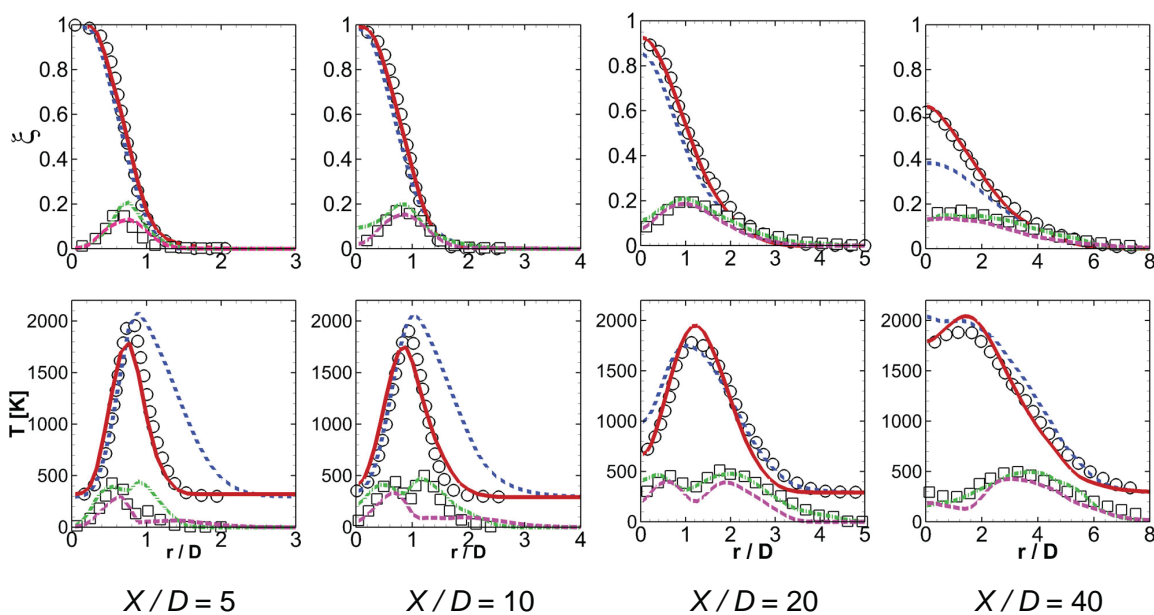


University of Stuttgart



2016: Mean and rms profiles (DME-D)

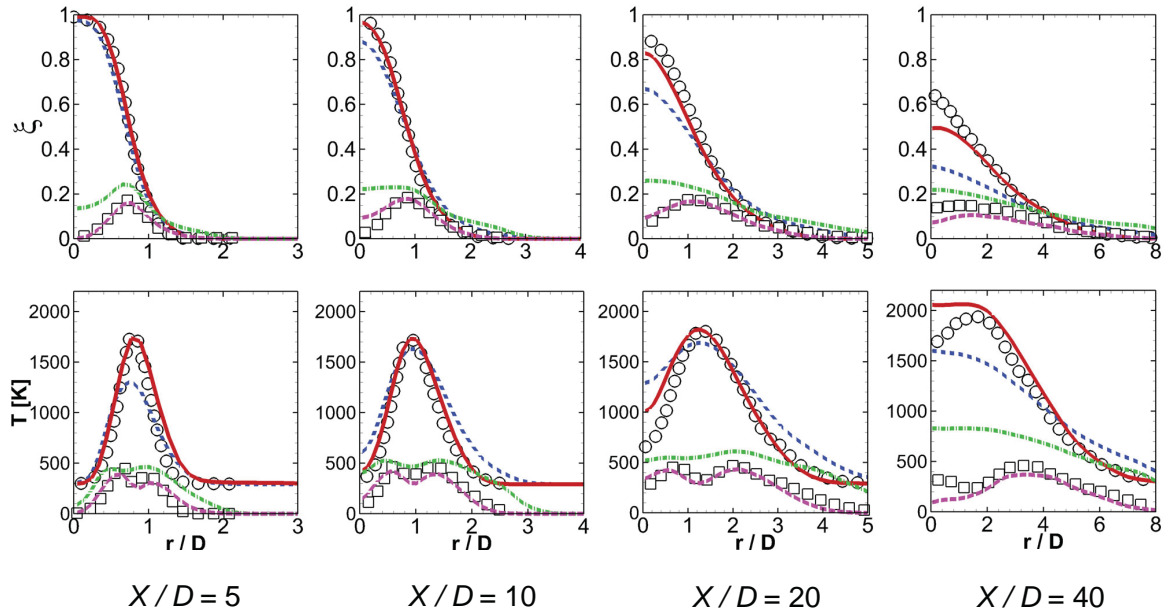
○: Experiment ---: mean, LES/PDF with IEM-RW —: mean, LES/PDF with IEM-MD
 ---: rms, LES/PDF with IEM-RW ---: rms, LES/PDF with IEM-MD



32

2016: Mean and rms profiles (DME-F)

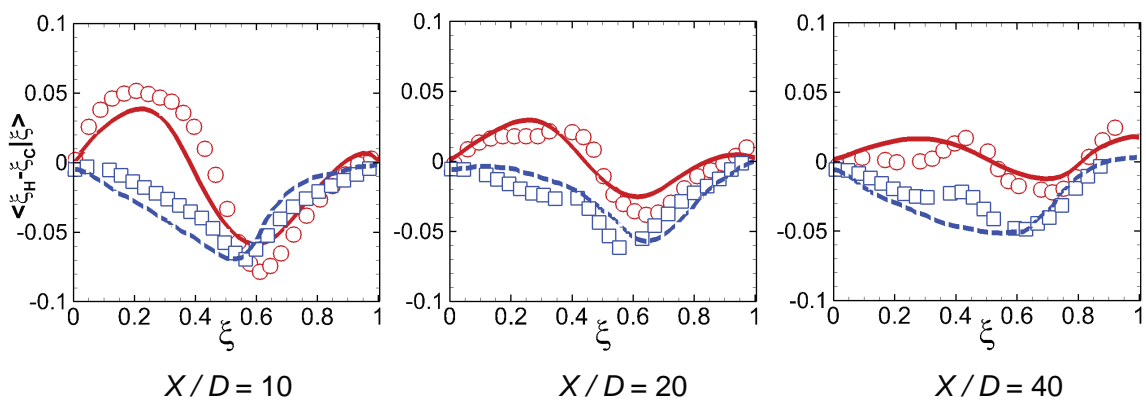
O: Experiment
 ---: mean, LES/PDF with IEM-RW
 —: mean, LES/PDF with IEM-MD
---: rms, LES/PDF with IEM-RW
 ---: rms, LES/PDF with IEM-MD



33

Effects of differential diffusion

Experiment (**O**: DME-D, **□**: DME-F), LES/PDF with IEM-DD (—: DME-D, ---: DME-F)



- Differential diffusion is incorporated into the PDF modeling
- Differential diffusion only has minor effects on predictions

34

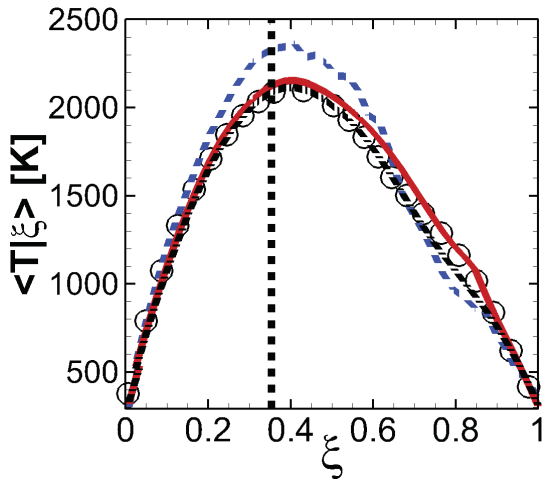
Mean profiles conditioned on ξ -space

○ : Experiment

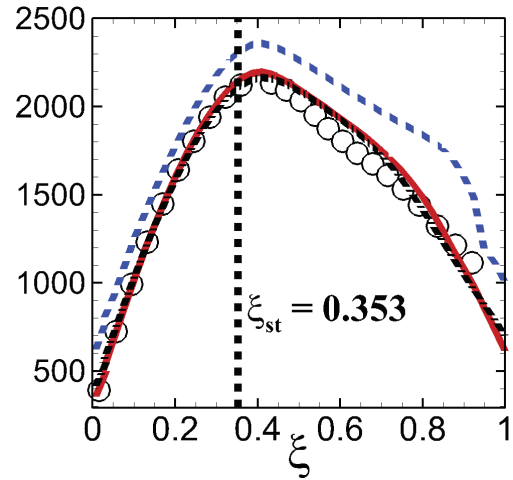
---: LES/PDF with IEM-RW

—: LES/PDF with IEM-MD

---: LES/PDF with IEM-DD



$X/D = 10$



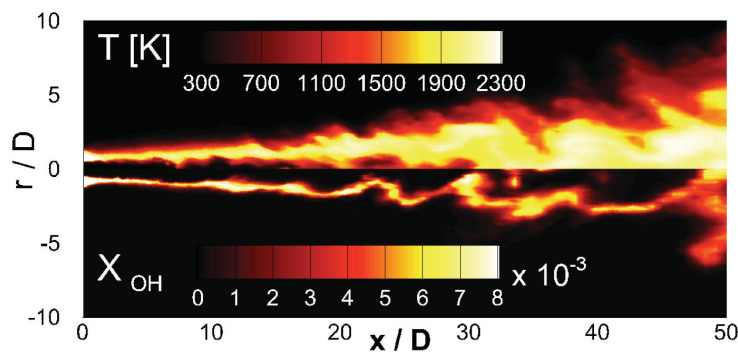
$X/D = 40$

DME-D

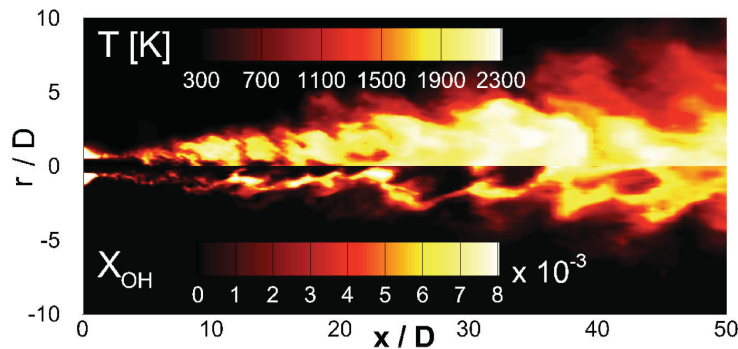
35

Temperature contour plots

IEM-MD



DME-D

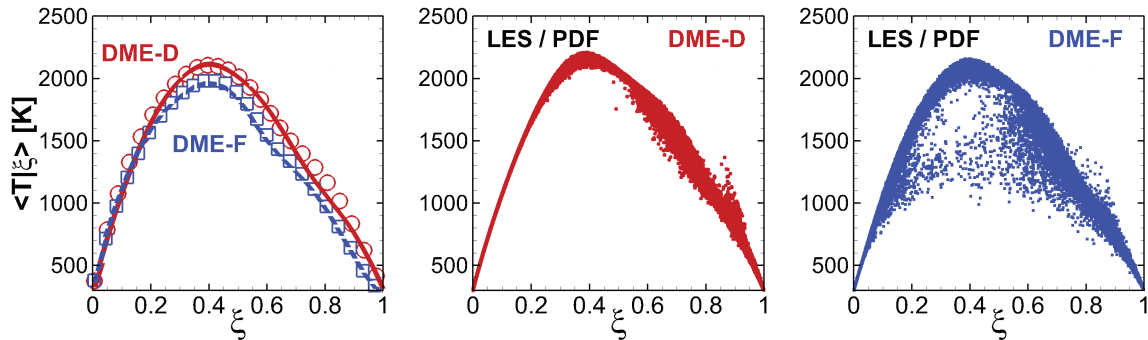


DME-F

36

Local extinction

More local extinctions in DME-F



$X/D = 10$

37

Conclusions and Future work

- *A priori* assessment of LES/PDF with three mixing models (IEM-RW, IEM-MD, IEM-DD) for DME-D and DME-F flames
 - Better quantitative agreement for mixture fraction, temperature and major species mole fractions obtained by IEM-MD than IEM-RW
 - Molecular transport has significant effects on PDF model predictions
 - Differential diffusion only has minor effects in these target flames
 - NOW AGREEMENT BETWEEN DIFFERENT GROUPS!
- Future work
 - Molecular transport in LES/PDF of premixed turbulent combustion

38

Multiple Mapping Condition by Stuttgart

- stochastic particle method
- sparse particle method (approx. 1 particle per 10 LES cells)
- particle evolution

$$dx_i^p = A_i^p dt + b_{ij}^p d\omega_j$$

$$d\phi_\alpha^p = (W_\alpha^p + S_\alpha^p) dt$$

- Mixing model – modified Curl's

$$\phi_\alpha^p(t + \Delta t) = \phi_\alpha^p(t) + \gamma \left(\bar{\phi}_\alpha^{p,q}(t) - \phi_\alpha^p(t) \right)$$

$$\phi_\alpha^q(t + \Delta t) = \phi_\alpha^q(t) + \gamma \left(\bar{\phi}_\alpha^{p,q}(t) - \phi_\alpha^q(t) \right)$$

$$\gamma = 1 - \exp(-\Delta t / \tau_L^{p,q})$$

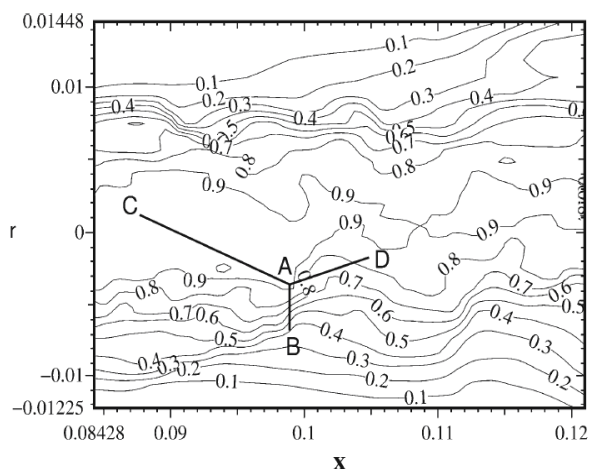


University of Stuttgart



Particle Selection

- Compensate low particle number
- Particle pair selection based on physical and composition space



© M.J. Cleary, A.Y. Klimenko, *Flow Turbulence Combust* (2009) 82:477 - 491.

$$\hat{d}_{p,q}^2 = \sum_{i=1}^3 \left(\frac{d_{x_i}^{p,q}}{r_i} \right)^2 + \left(\frac{d_{\bar{f}}^{p,q}}{f_m} \right)^2$$

A-B: small d_x , big d_f

A-C: big d_x , small d_f

A-D: medium d_x , medium d_f

→ A will mix with D



University of Stuttgart



Numerical Setup

- 1.5M cells
- 150,000 particles – 1 particle/10 LES cells
- Approx. 8000 CPUh on Intel® Xeon® CPU E5-2680 processor for 14 flow through times
- Chemical mechanism by Zhang (53 species, 291 reactions)
- The solver mmcFoam is based on reactingFoam in OpenFOAM 2.4.x
- Computed entire series → paper 3A01

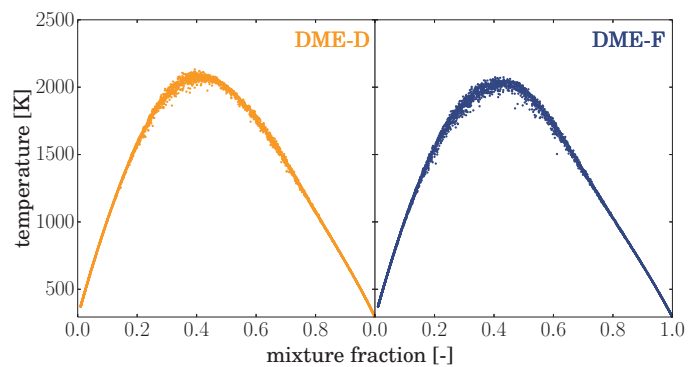
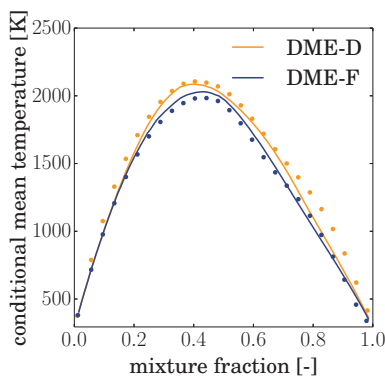


University of Stuttgart



Conditional means

$z/D=10$

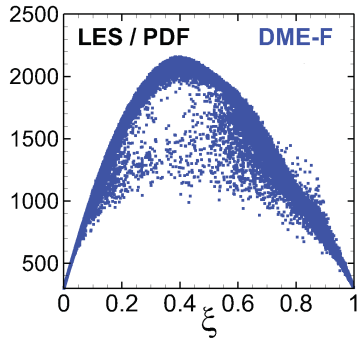


University of Stuttgart

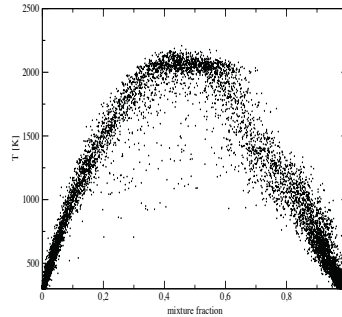


Comparison

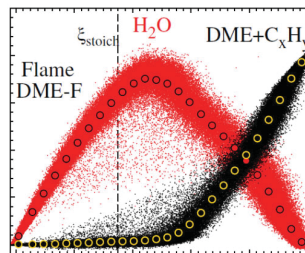
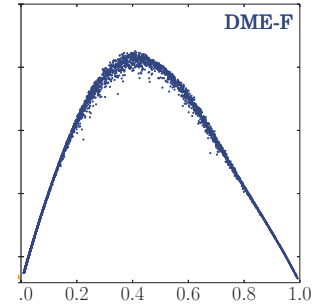
PDF – $z/D=10$



Exp – $z/D=7.5$



MMC – $z/D=10$



University of Stuttgart

University of Sydney Hot Coflow Turbulent Autoignition DME Experiment



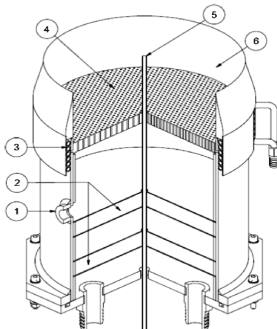
Andrew MacFarlane
Mathew Dunn
Mrinal Juddoo
Assaad Masri



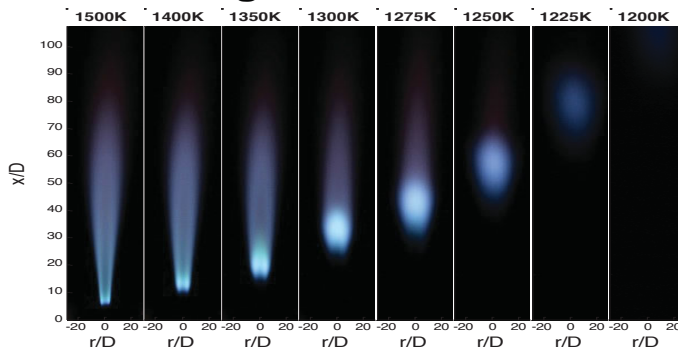
Configuration and geometry has generated significant interest (numerical and experimental) for investigating turbulent autoignition of hydrogen and methane

Dimensions

- Co-flow diameter of 197 mm
- Jet diameter is 4.45mm
- ~1800x1.6 mm stabilize lean H_2 /air flames

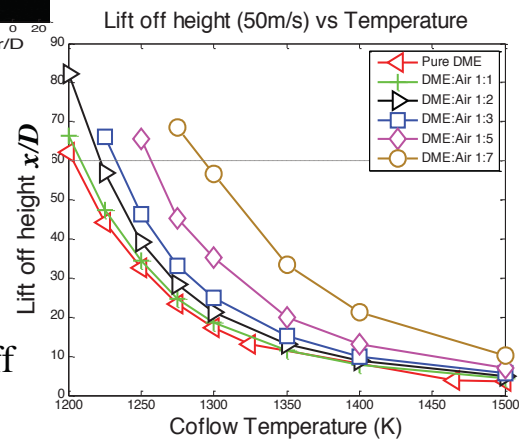


Flames feature a strong sensitivity of lift off height to hot coflow temperature



$U_{jet}=50\text{m/s}$, 3:1 air:DME jet
 H_2 +air hot coflow

Influence of jet dilution on mean liftoff height vs. hot coflow temperature



Large parameter matrix examined, looking at T_{coflow} , U_{jet} and jet dilution

Paper being presented at the symposia, flame base dynamics and high speed OH + CH₂O PLIF/ heat release data not reported here (see TNF poster...)

-Experimental data available:

- Liftoff height graphs: flame base and flame kernel

(mean, rms, min, max)

- Simultaneous high speed OH + CH₂O PLIF

- Temporal evolution and statistics of the flame base and ignition kernels

- Simultaneous acoustic and chemiluminescence data

Four DME mechanisms have been evaluated in 0D, 1D and 2D RANS TPDF CFD calculations

Piloted turbulent flames test DME mechanisms for particular quantities extinction, re-ignition, flame speed etc

The hot coflow burner tests DME mechanisms under conditions perhaps more relevant to applications: where turbulent ignition occurs...

Do we have consistency between different mechanisms for DME?

- **Burke et al. (113sp)**

Burke, Ultan, Kieran P. Somers, Peter O'Toole, Chis M. Zinner, Nicolas Marquet, Gilles Bourque, Eric L. Petersen, Wayne K. Metcalfe, Zeynep Serinyel, and Henry J. Curran. "An Ignition Delay and Kinetic Modeling Study of Methane, Dimethyl Ether, and Their Mixtures at High Pressures." *Combustion and Flame* 162, no. 2 (February 2015): 315–30. doi:10.1016/j.combustflame.2014.08.014.

- **Pan et al.(27sp)**

Pan, Lun, Sage Kokjohn, and Zuohua Huang. "Development and Validation of a Reduced Chemical Kinetic Model for Dimethyl Ether Combustion." *Fuel* 160 (November 15, 2015): 165–77. doi:10.1016/j.fuel.2015.07.066.

- **Zhao et al. (53sp)**

Zhao, Zhenwei, Marcos Chaos, Andrei Kazakov, and Frederick L. Dryer. "Thermal Decomposition Reaction and a Comprehensive Kinetic Model of Dimethyl Ether." *International Journal of Chemical Kinetics* 40, no. 1 (January 2008): 1–18. doi:10.1002/kin.20285.

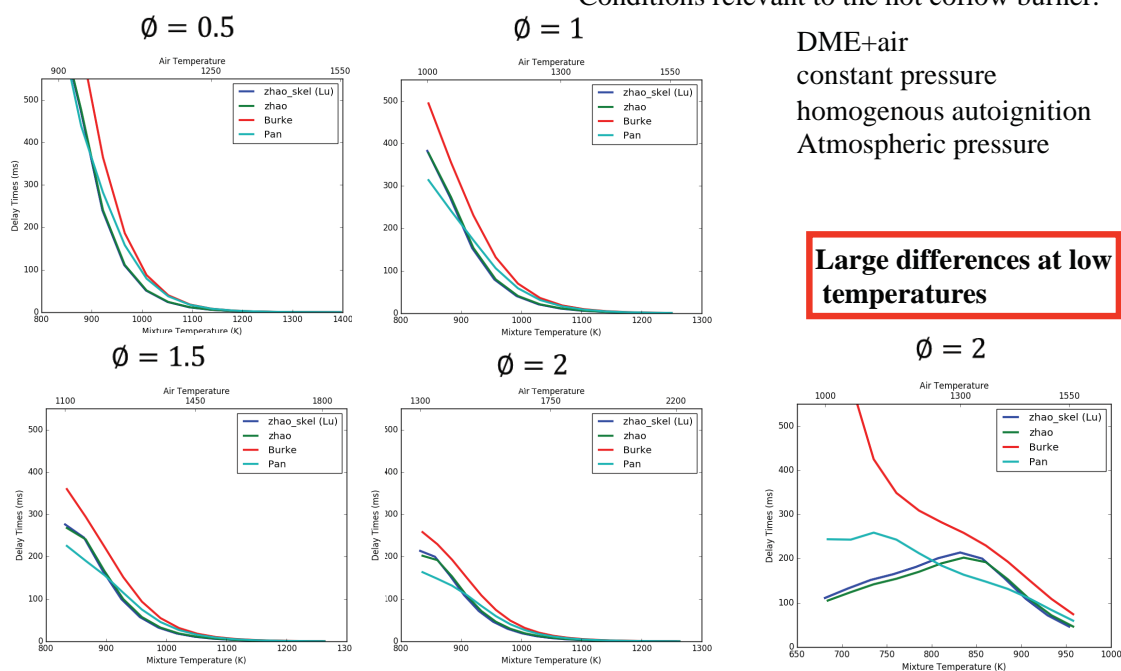
- **Lu et al. (39sp skeletal)**

Bhagarwala, Ankit, Zhaoyu Luo, Han Shen, Jeffrey A. Sutton, Tianfeng Lu, and Jacqueline H. Chen. "Numerical and Experimental Investigation of Turbulent DME Jet Flames." *Proceedings of the Combustion Institute* 35, no. 2 (2015): 1157–66. doi:10.1016/j.proci.2014.05.147.

Autoignition simulations (0D) indicate significant differences between DME mechanisms

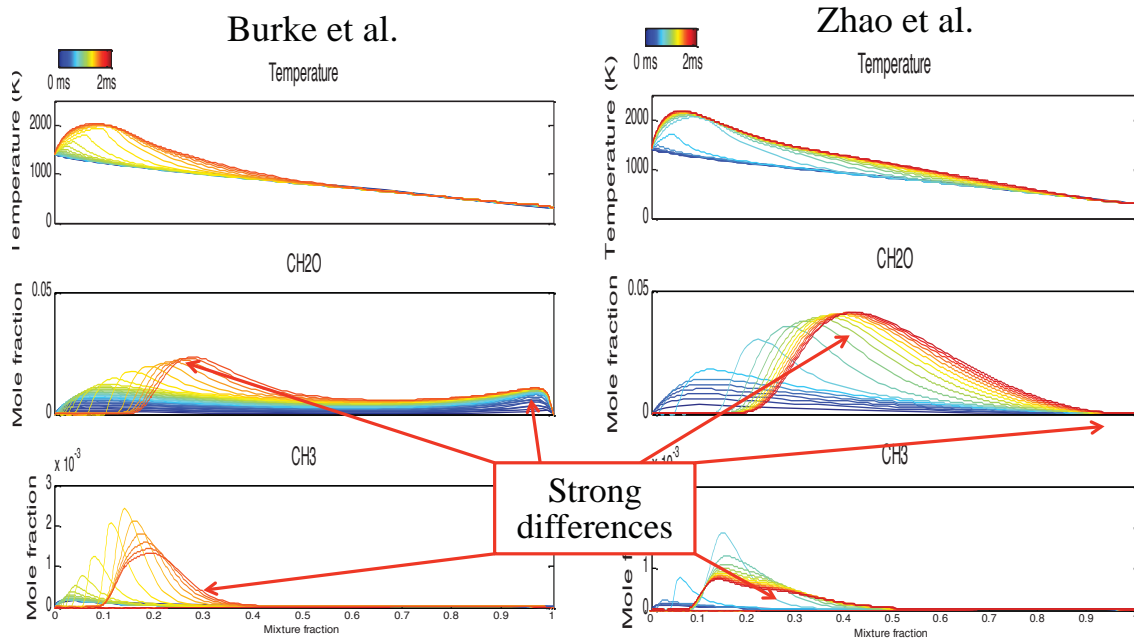
Conditions relevant to the hot coflow burner:

DME+air
constant pressure
homogenous autoignition
Atmospheric pressure

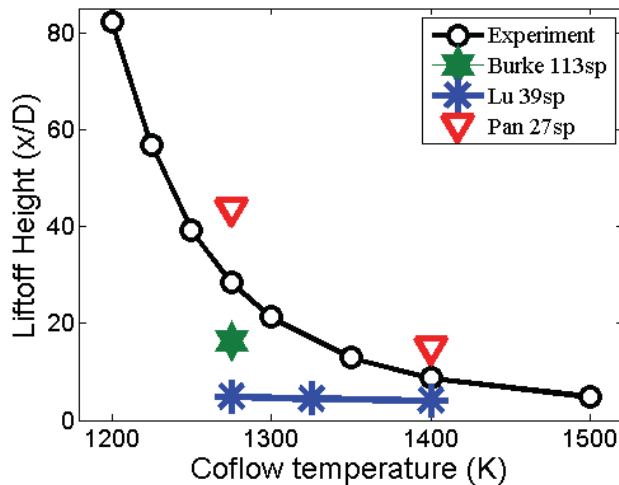


Transient opposed flow simulations using different mechanisms indicate qualitative differences for key radicals

3 (air):1(DME), $T_{\text{coflow}}=1400$ K, $S=200$ s⁻¹



2D RANS transported PDF results indicate significant differences between mechanisms



Mean liftoff height for
3(air):1(DME) jet
 $U_{\text{jet}}=50$ m/s

Lu mechanism not great results...
Burke and Pan mechanism give encouraging results –
but no perfect!

*Same code/setup as used in: Dunn, Matthew J., Assaad R. Masri, Robert W. Bilger, and Robert S. Barlow. "Finite Rate Chemistry Effects in Highly Sheared Turbulent Premixed Flames." *Flow, Turbulence and Combustion* 85, no. 3-4 (December 1, 2010): 621-48. doi:10.1007/s10494-010-9280-5.

Conclusions

- Progress in modelling -> first computations of flames with higher Re
- Ok, but not perfect
- Differential diffusion not important
- Simulate flames with more extinction (Flames E-G)

- New challenges for the modellers
 - New data
 - New flames



Turbulent counterflow flames

Coordinator: Jonathan Frank
Presenters: J.H. Frank, S.B. Pope, R.P. Lindstedt

Contributors

Experiments

B. Coriton, J.H. Frank (Sandia), A. Gomez (Yale)
K.H.H. Goh, F. Hampf, P. Geipel (Imperial College)

Simulations/Modeling

A. Ruiz, G. Lacaze, J. Oefelein (Sandia)
R.R. Tirunagari, S.B. Pope (Cornell)
M. Rieth, F. Proch, A. Kempf (Duisberg-Essen)
L. Tian, R.P. Lindstedt (Imperial College)

The session on turbulent counterflow flames extended experimental and computational studies from TNF12 using the two burner designs from Yale University and Darmstadt/Imperial College. The counterflow configuration enables flexibility of studying premixed, non-premixed, and partially premixed flames in a compact geometry with optical access, flame stabilization away from solid boundaries, short residence times, and high fuel flexibility. For premixed flames, the burner can be operated in reactant-vs-product or reactant-vs-reactant configurations. Challenges include complex inflow conditions due to turbulence generation processes inside nozzles and intrinsic bulk motions. Presentations included the following topics:

LES study of internal flow dynamics and boundary conditions (Sandia/Yale): LES calculations of the internal flow dynamics and boundary conditions for the Yale burner were performed at Sandia National Laboratories. Results demonstrated the importance of calculating the turbulence generation and evolution within the converging nozzles starting upstream of the turbulence generator plates. Calculations agreed well with measured velocity statistics at the nozzle exit for two different turbulence generator plate positions. Requirements for grid resolution and run times for convergence of temporal statistics were investigated. Simulations showed the anisotropy in TKE spectra at the nozzle exits. This work will ultimately provide a validated strategy for imposing time dependent turbulent boundary conditions at the nozzle exits that account for inherent anisotropy to reduce computational cost and thereby facilitate high-fidelity simulations of turbulence-chemistry interactions in the inter-nozzle region.

LES/PDF parametric studies in premixed CH₄ flames (Cornell): LES/PDF calculations were performed for lean-to-stoichiometric turbulent premixed CH₄/N₂/O₂ flames in the Yale burner. Conditional statistics were used to compare simulations with data from parametric experimental studies performed at Sandia. The critical parameters included bulk strain rate (1400-2240s⁻¹), equivalence ratio of the upper nozzle (0.5-1.0), turbulent Reynolds number (470-1050), and product stream temperature (1700-1950 K). For this range of conditions, good agreement was achieved for PDFs of the product layer thickness as well as the probability of localized extinction. This agreement may have been facilitated by using a sufficiently small ratio of the resolved turbulent and molecular diffusivities and a sufficiently large normalized mixing rate to approach the DNS limit. However, the ratio of the grid spacing to the laminar flame thickness was too large for the LES/PDF to be considered in the DNS limit. Despite the coarse spatial resolution, the particle-mesh method yielded a flame speed close to the laminar flame speed. This extension of PDF methods to premixed combustion contributes to the development of modeling approaches that are applicable to different modes of combustion.

Measurements and analysis of new flame conditions and fuels (Imperial College) Influence of chemistry on combustion regime transitions were investigated by varying the fuel (CH₄, DME, ETOH) and upper nozzle equivalence ratio (0.2-1.0). Combustion regime transition trends were quantified

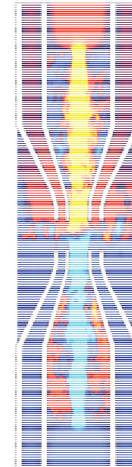
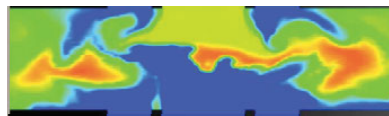
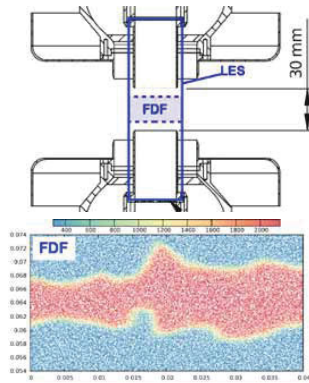
using combined OH LIF and Mie scattering imaging to identify different states of mixing and chemical reaction along with conditional velocities from PIV measurements. Fuel chemistry effects influenced the conditional velocity statistics, and the impact of fuel chemistry on fluid state probabilities indicated an approximate scaling with Da number.

Modeling lean premixed CH₄ flames with LES/FDF and moment methods (Duisburg-Essen, Imperial College): Simulations of lean premixed CH₄ counterflow flames ($\Phi=0.8, 0.9$) in the reactant-vs-reactant configuration of the Darmstadt/Imperial College burner were extended from TNF12 using both LES/FDF calculations and moment methods. LES/FDF results showed good agreement with mean profiles of velocity and progress variable with differences in the fluctuations, particularly near the burner stagnation plane. Moment method calculations included SMC and extended SMC, which used recent dilation and scrambling models. Improved agreement with experiments for extended SMC was most significant for progress variable statistics. Discrepancies in turbulent velocity statistics may result from redistribution of TKE by rotation of the stagnation plane.

Goals for TNF14: Goals for TNF14 should include more contributors with different modeling approaches, testing models across different modes of combustion using the counterflow geometry, and using simulations of internal flow to specify boundary conditions at the nozzle exits. A comparison of the two existing internal flow simulations of the Yale burner geometry would be useful. Goals should also include more detailed analysis of conditional statistics using experiments and high-fidelity simulations that focus on the inter-nozzle region. This effort could include additional fuels and flame conditions and sufficiently long simulation times to study the temporal evolution of localized extinction and re-ignition.

Experiments and Simulations in Turbulent Counterflow Flames

Coordinator: Jonathan Frank



13th International Workshop on Measurement and Computation of Turbulent Flames

July 28-30, 2016

Seoul, Korea



Contributors

• Experiments

- K.H.H. Goh, F. Hampp, P. Geipel, R.P. Lindstedt (Imperial College)
- B. Coriton and J.H. Frank (Sandia), A. Gomez (Yale)

• Simulations

- A. Ruiz, G. Lacaze, J. Oefelein (Sandia)
- R.R. Tirunagari, S.B. Pope (Cornell)
- M. Rieth, F. Proch, A. Kempf (Duisberg-Essen)

TNF 12 also included simulations from:

- L. Sgouria, H. Kolla, J. Chen (Sandia)
- Z. Jozefik, H. Schmidt (Brandenburg) and A.R. Kerstein (Consultant)
- K. Kemenov and W. Calhoon (CRAFT Tech.)



Issues Raised at TNF 12

- Detailed treatment of boundary conditions
- Parametric comparisons of simulations and experiments using conditional statistics
- Expand range of conditions/fuels
- Test models across different combustion modes
- Explore need to expand conventional regime diagram
- More contributors with different simulation approaches



Outline

- Brief introduction of counterflow configurations
- LES study of internal flow dynamics and boundary conditions (Sandia/Yale)
- LES/PDF parametric studies in premixed CH₄ flames (Cornell Univ.)
- LES/FDF extended and improved calculations of lean CH₄ flames (Univ. Duisburg-Essen)
- Measurements and analysis of new conditions/fuels (CH₄, DME, ETOH) (Imperial College)



Turbulent Counterflow Flames

Advantages:

- The configuration is suitable for non-premixed, partially-premixed and premixed flames
- Geometry is compact and has good optical access
- Flames stabilize away from solid boundaries
- Short residence time, high fuel flexibility
- 1D Statistics along burner centerline

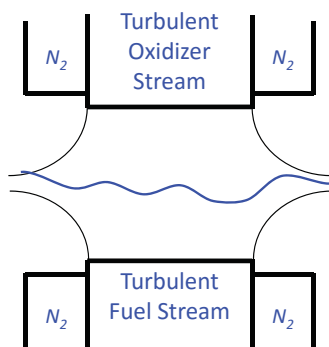
Challenges:

- Limitation has been small turbulent Reynolds numbers $O(50-100)$, which have more recently increased
- Developing turbulence
- Complex inflow conditions (turbulence generated inside nozzles)
- Intrinsic bulk motions



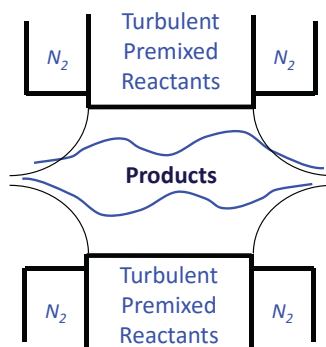
Flow Configurations

Non-Premixed & Partially-premixed Flame



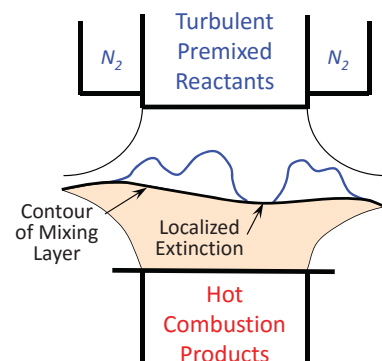
- Adiabatic
- Low amount of localized extinctions

“Twin”-Premixed Flames



- Flame/Flame interactions
- Adiabatic
- Low Karlovitz number

Premixed Flame vs. Burnt Products



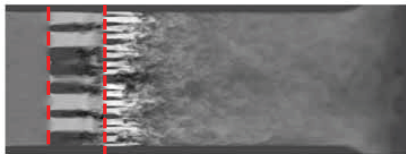
- “back support” / heat losses, stratification
- Localized extinctions
- High Karlovitz number



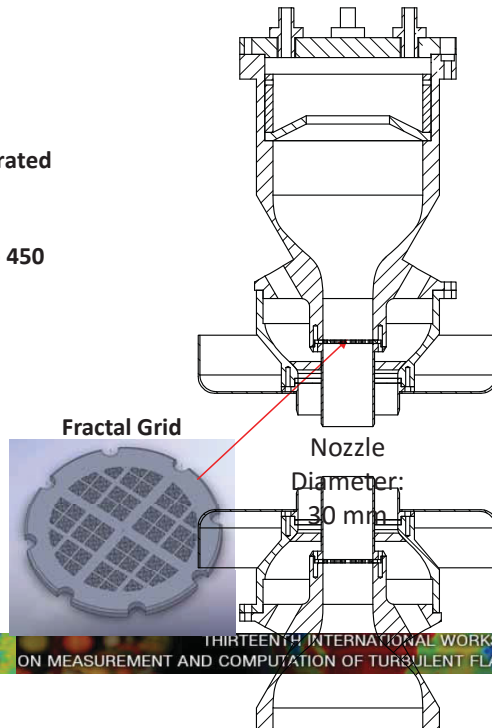
Darmstadt / Imperial College Nozzle

- Same geometry, different turbulence generation schemes:
 - DA: perforated plate (4.0 mm hole)
 - IC: Fractal grid
- Turbulence levels were enhanced using fractal grids located 10 mm downstream of the perforated plates.
- Fractal Grid: Reynolds number increased up to 450

Flow Visualization inside nozzle
(LES – Stein *et al.*, 2011)



IC current Nozzle Design

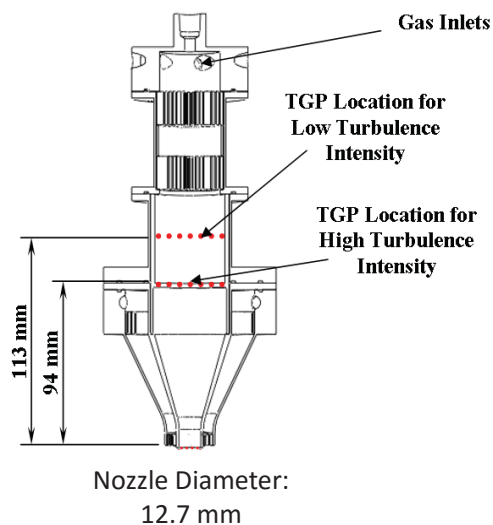
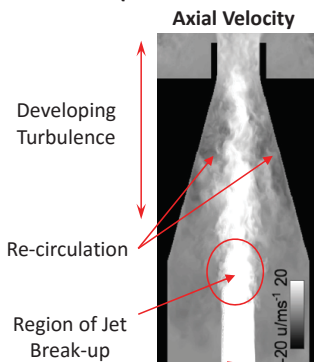


Yale Turbulent Nozzle

To achieve a tenfold increase in Re_t to $O(1000)$ (Coppola *et al.*, 2009):

- Operate at high flow rates with oxygen enrichment to prevent flame extinction at large strain rates.
- Force flow through a strategically positioned high-blockage turbulence generator plate.
- Let turbulence develop inside contraction nozzle.

Flow visualization inside nozzle
(LES - Pettit *et al.* 2010)



Burner References

- **Darmstadt**

- D. Geyer, A.M. Kempf, A. Dreizler, J. Janicka, Combust. Flame 143 (2005) 524-548
- D. Geyer, A. Dreizler, J. Janicka, et al., Proc. Combust. Inst. 30 (2005) 71-718
- D. Geyer, A.M. Kempf, A. Dreizler, J. Janicka, Proc. Combust. Inst. 30 (2005) 681-689
- B. Bohm, O. Stein, A.M. Kempf, A. Dreizler, Flow Turb. Combust. 85 (2010)73-93
- O. Stein, B. Bohm, A. Dreizler, A.M. Kempf, Flow Turb. Combust. 87 (2011) 425-447

- **Imperial College**

- P. Geipel, K.H.H. Goh, R.P. Lindstedt, Flow Turb. Combust. 85 (2010) 397-419
- K.H.H. Goh, P. Geipel, F. Hampp, R.P. Lindstedt, Fluid Dyn. Res. (Special Issue) 45 (6) (2013) 061403.
- K.H.H. Goh, P. Geipel, F. Hampp, R.P. Lindstedt, Proc. Combust. Inst. 34 (2013) 3311–3318
- K.H.H. Goh, P. Geipel, R.P. Lindstedt, Combust. Flame (2014)

- **Yale University**

- G. Coppola, A. Gomez, Exp. Therm. Fluid Sci. 33 (2009) 1037-1048
- G. Coppola, B. Coriton and A. Gomez, Combust. Flame 156 (2009) 1834-1843
- M.W.A. Pettit, B. Coriton, A. Gomez, A.M. Kempf, Proc. Combust. Inst. 33 (2010) 1391-1399



Large Eddy Simulation of Turbulent Counterflow Configuration

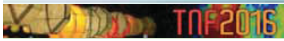
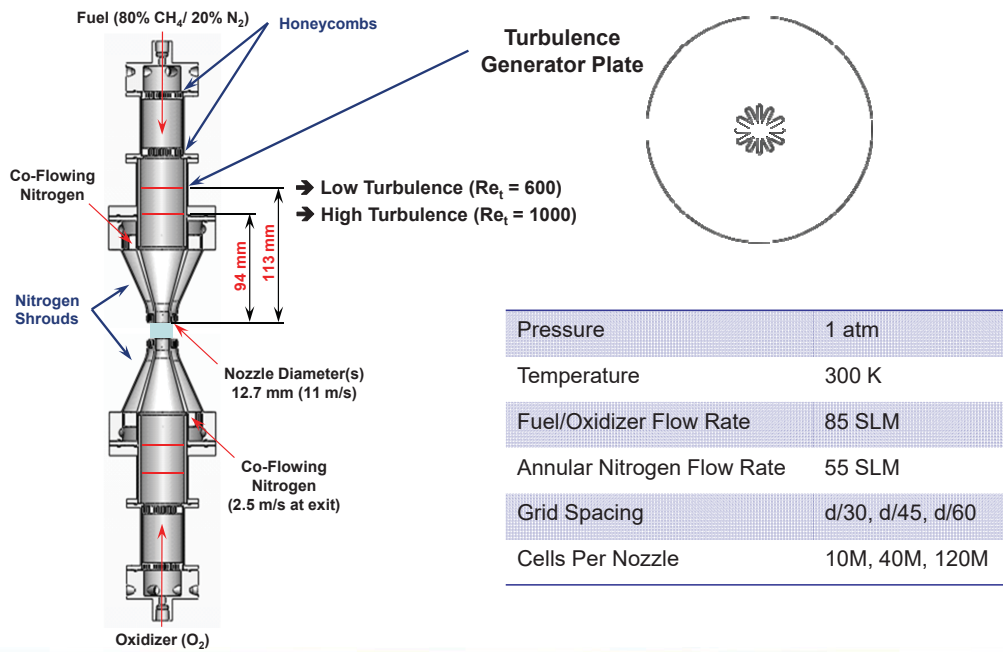
Sensitivity of Internal Flow Dynamics and Boundary Conditions

A. M. Ruiz, B. Coriton, G. Lacaze, J. H. Frank, J. C. Oefelein

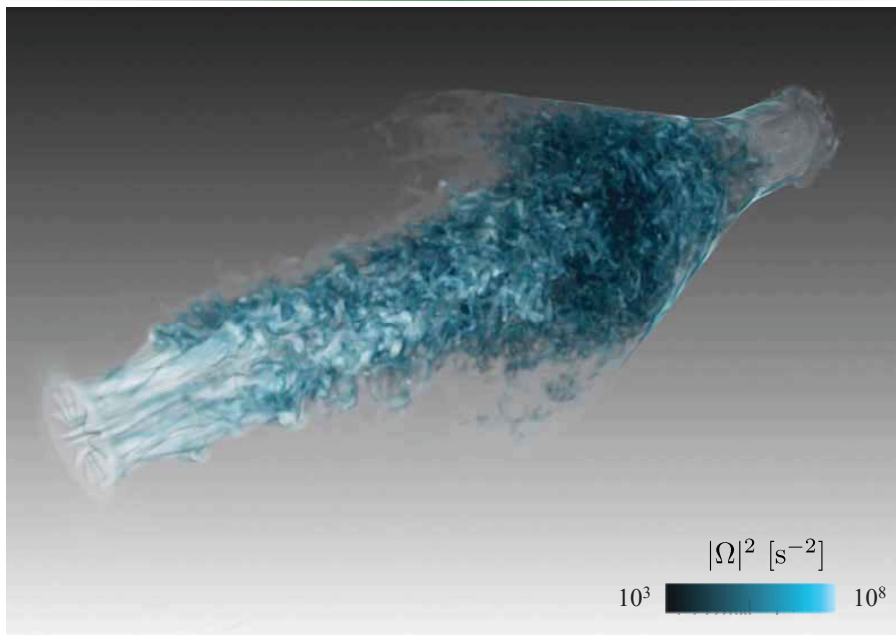
**Combustion Research Facility
Sandia National Laboratories, Livermore, CA 94551**



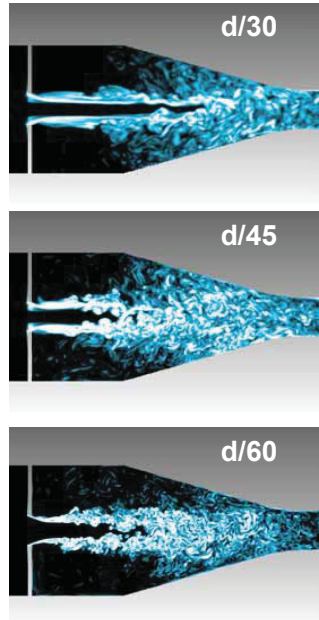
Yale/Sandia configuration



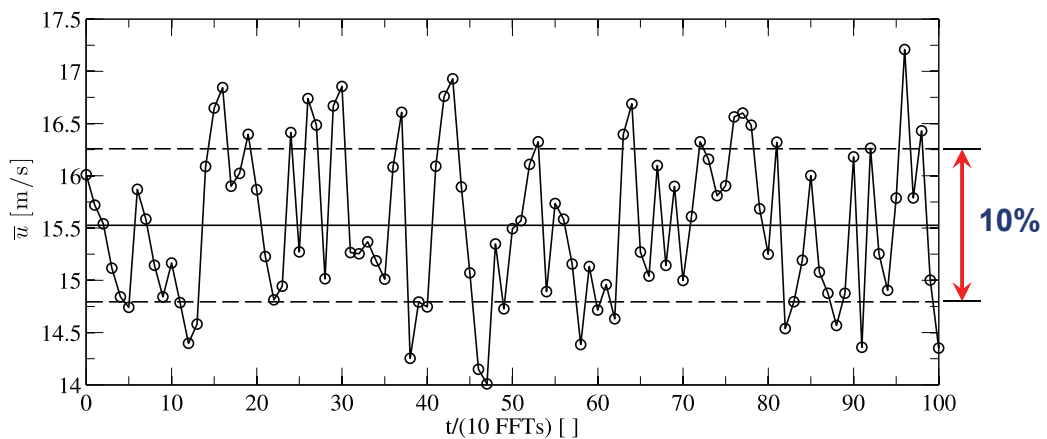
Simulation of internal flow through turbulence generator plate



Effects of grid resolution



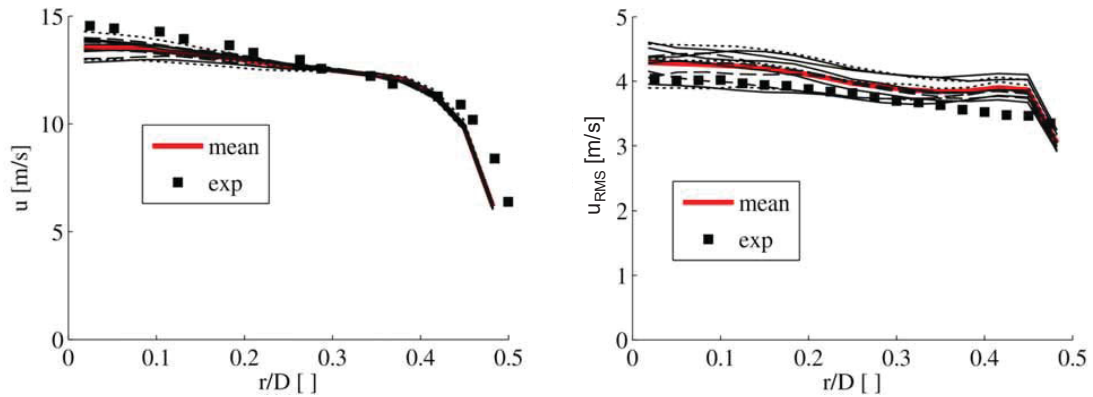
Analysis of hot-wire measurements on jet centerline at nozzle exit



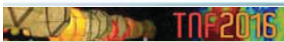
Sliding mean of 10 FFT has RMS of 5% variability
(1 FFT = 9 ms for $Q = 85$ SLM)



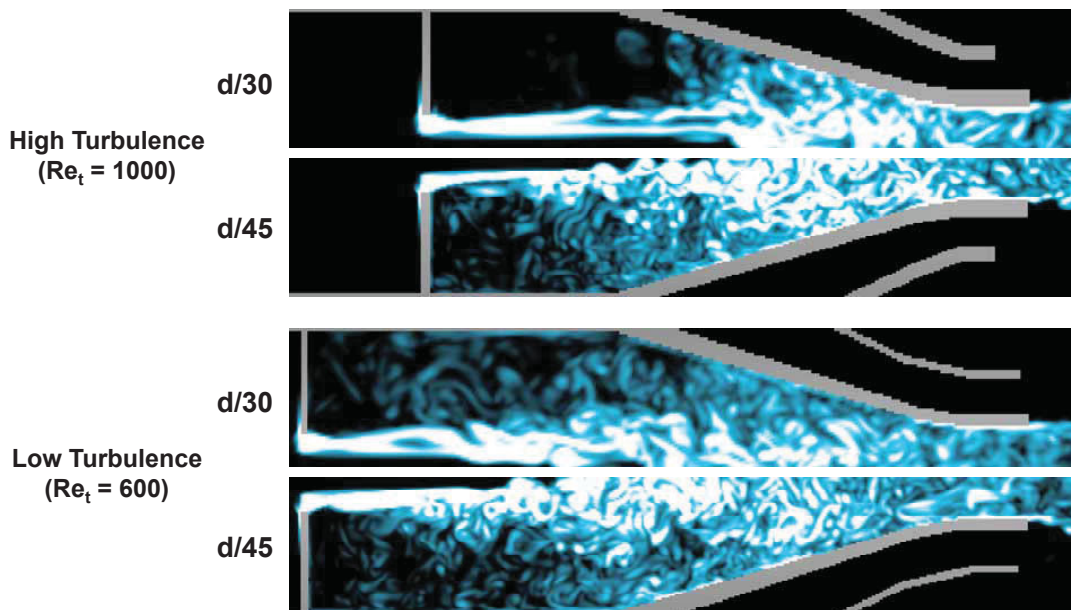
Radial profiles at nozzle exit (HT, $Re_t = 1000$, $d/30$, 10M cells)



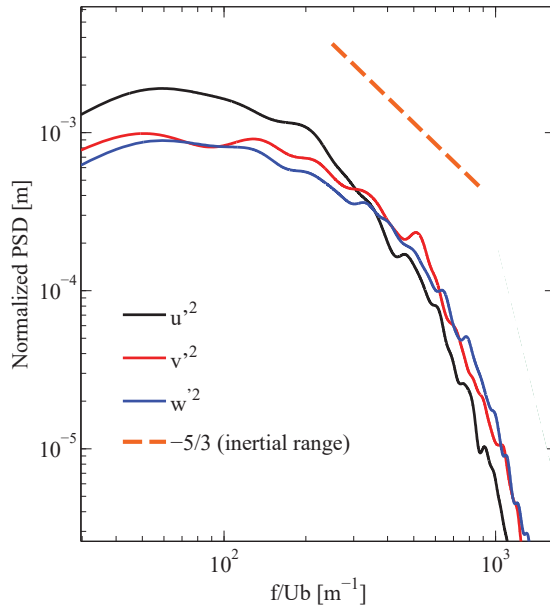
$\leq 10\%$ variability in both mean and RMS velocity
(black lines represent 10 FFT averages from LES)



Interplay between TGP, transition length, recirculation zone is complex



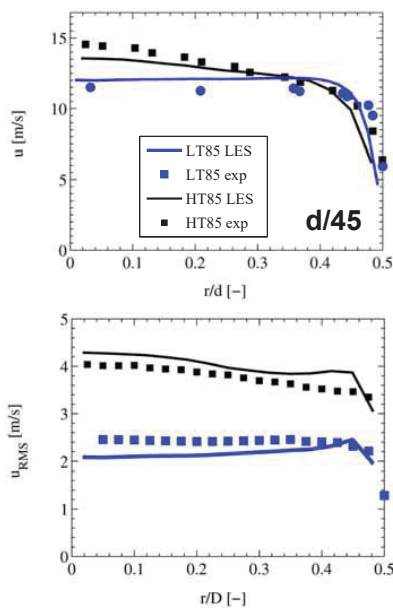
Anisotropic characteristics of centerline flow at nozzle exit



- Spectrum of turbulent kinetic energy in axial and transverse directions ($d/60$, 10 FTT)
- More energy observed in the axial velocity fluctuations than transverse fluctuations
- Transverse fluctuations follow a more classical energy cascade (slope is closer to $-5/3$)
- Uppermost wavenumber is cutoff for $d/60$ (i.e., entire spectrum resolved at nozzle outlet)



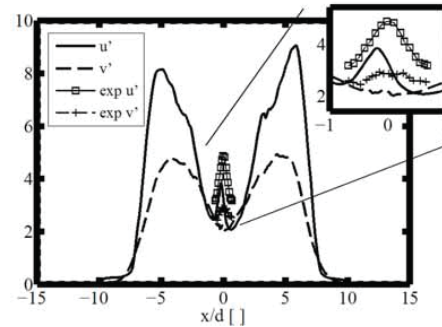
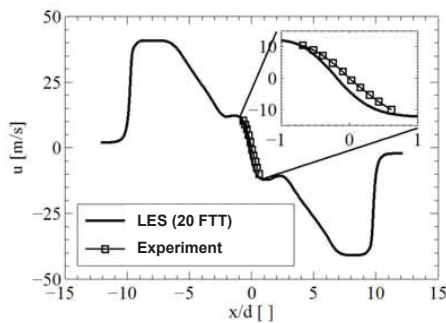
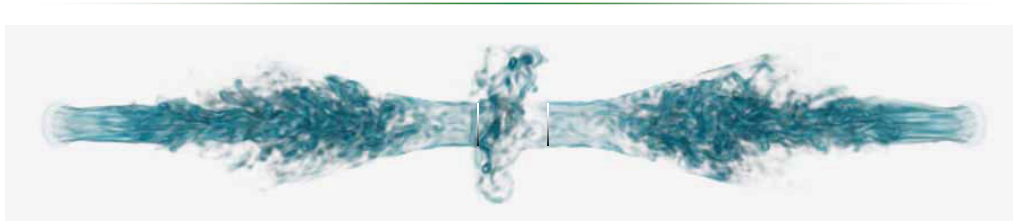
Transient exit conditions reproduced with reasonable fidelity



Good agreement with experimental data at nozzle exit obtained by simply changing turbulence generator plate position just as in experiment



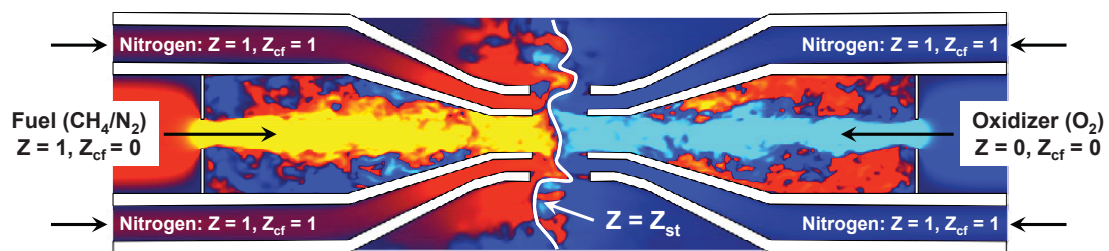
Apply same methodology to opposed jet configuration



Comparisons of axial mean and RMS profiles across stagnation plane produce reasonable agreement with measured profiles



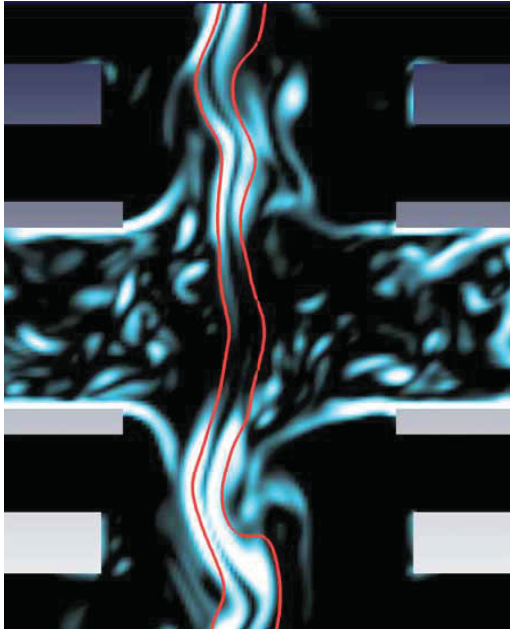
Now let's add combustion using 3-stream flamelet approximation



- **Steady flamelet with two conserved scalars transported**
 - Mixture fraction
 - Co-flow mixture fraction
- **Tabulation at the bulk strain rate only ($a = 1000 \text{ s}^{-1}$) using GRI-Mech 3.0**
 - Instantaneous response of the flame structure to turbulent stretch
 - Unity Lewis number (no preferential diffusion)



How do unsteady flame dynamics and heat-release affect turbulence?

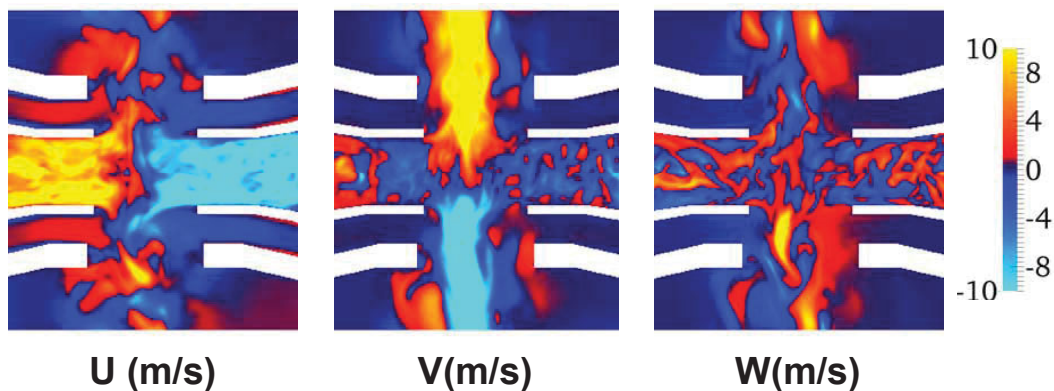


- Animation shows vorticity field in blue, temperature isocontour in red ($T = 2000\text{ K}$)
- Heat release damps turbulent fluctuations since hot products are more viscous
- Vorticity layers created in flame zone due to baroclinic torque and dilation
- Turbulence makes flame thinner (strain rate effects), induces curvature

TNF2016

Sandia National Laboratories

How do unsteady flame dynamics and heat-release affect turbulence?



TNF2016

Sandia National Laboratories

Summary

- **Imposing “standardized conditions” at the nozzle exits can significantly reduce computational cost**
 - Coupled effects of heat release on turbulent inflow conditions, and anisotropic turbulence on flame dynamics must be quantified
- **Current goal is to minimize challenges related to complex internal nozzle flow**
 - Geometrically complex cavity, developing turbulence, recirculating flow
- **Nozzle exit conditions require minimum of 10 FTT for initialization/statistics (10% variability in velocity)**
 - Provides transient exit conditions that agree well with measured data by simply changing turbulence generator plate position just as in experiment
- **Observations**
 - Turbulence is anisotropic, degree of anisotropy changes as function of plate position
 - Heat release has little impact on mean velocity statistics at nozzle exits
 - Heat release impact on RMS velocity statistics at nozzle exits?



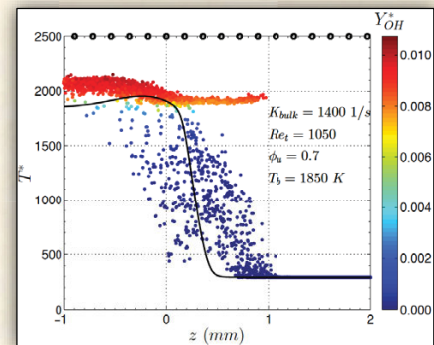
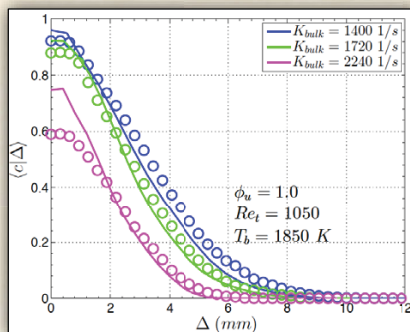
LES/PDF Calculations of Partially-Premixed Counterflow Flames

Ranjith R. Tirunagari & Stephen B. Pope

Sibley School of Mechanical & Aerospace Engineering

Cornell University

Ithaca, NY, USA



TNF Workshop
Seoul, Korea
July 28-30, 2016

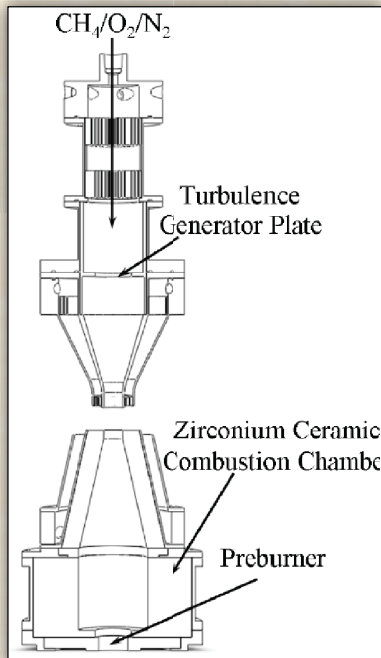
Publications on Counterflow Flames

- **Inflow BCs Methodology:** R. R. Tirunagari, M. W. A. Pettit, A. M. Kempf and S. B. Pope, A simple approach for specifying velocity inflow boundary conditions in simulations of turbulent opposed-jet flows, *Flow Turbul. and Combust.*, 2016, in press, DOI: 10.1007/s10494-016-9743-4
- **Parametric Study of the Premixed Mode:** R. R. Tirunagari and S. B. Pope, An investigation of turbulent premixed counterflow flames using large-eddy simulation/probability density function methods, *Combust. Flame* 166 (2016) 229-242
- **LES/PDF in the DNS Limit:** R. R. Tirunagari and S. B. Pope, LES/PDF for premixed combustion in the DNS limit, *Combust. Theor. and Model.*, 2016, in press, DOI: 10.1080/13647830.2016.1188991
- **Extinction/Re-ignition Characterization:** R. R. Tirunagari and S. B. Pope, Characterization of extinction/reignition events in turbulent premixed counterflow flames using strain-rate analysis, *Proc. Combust. Inst.*, 2016, in press, DOI: 10.1016/j.proci.2016.07.019

Partially Premixed Counterflow Flames

Experiments: Coriton, Frank & Gomez (2013)

Cold premixed



Range of critical parameters

Parameter	Range	Quantity varied
K_{bulk}	$1400 \text{ s}^{-1} - 2240 \text{ s}^{-1}$	Distance between the two nozzles
ϕ_u	0.5 - 1.0	CH_4 concentration in the top nozzle
Re_t	470 - 1050	Distance between the TGP & top nozzle exit
T_b	1700 K - 1950 K	Molar ratio of N_2/O_2 in the bottom nozzle
ϕ_b	1.0	-

3 Hot products

Large-Eddy Simulation/Probability Density Function (LES/PDF) Approach

- Large-Eddy Simulation (LES):
 - Resolved velocity field
 - NGA finite difference code for resolved velocity
 - Lagrangian dynamic Smagorinsky model

- Probability Density Function (PDF):

- Joint PDF of composition
- HPDF particle/mesh code
- IEM mixing model

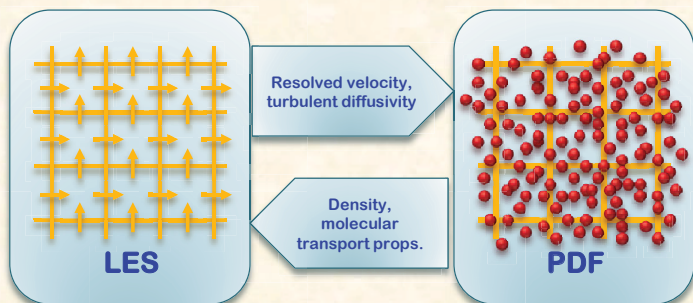
- Chemistry

- 16-species ARM1 mechanism for methane

- Molecular transport:

- Random-walk implementation
- Unity Lewis number

4 ■ Thermal diffusivity obtained from CHEMKIN's TRANLIB



Differential Equations (PDF)

- Each particle carries information on its position $\mathbf{X}^*(t)$ and composition $\phi^*(t)$
 - Composition vector: $\phi = \{z, h_s\}$
 - z is a vector of species specific mole numbers, h_s is the sensible enthalpy of the mixture
- Particle position, $\mathbf{X}^*(t)$, SDE:

$$d\mathbf{X}^* = \left[\bar{\mathbf{U}} + \frac{\nabla \bar{\rho} (\bar{D}_T + \bar{D})}{\bar{\rho}} \right]^* dt + [2(\bar{D}_T^* + \bar{D}^*)]^{1/2} d\mathbf{W}$$

- D_T - turbulent diffusivity; D - molecular diffusivity; W - Wiener process
- Particle composition, $\phi^*(t)$, ODE:

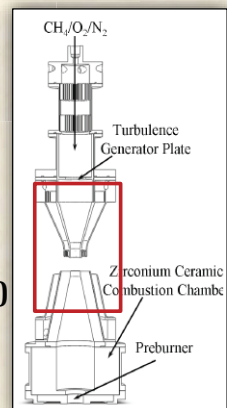
$$\frac{d\phi^*}{dt} = -\Omega^*(\phi^* - \bar{\phi}^*) + \mathbf{S}(\phi^*) \quad \Omega = C_m \frac{\bar{D}_T + \bar{D}}{\Delta^2}, C_m = 4.0$$

5

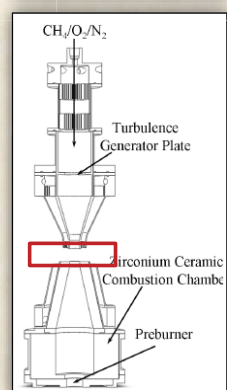
Inflow Methodology – Choice of Domain

- A single large-domain high fidelity LES
 - “PsiPhi” code, M. W. A. Pettit, Imperial College
- Use velocities at nozzle exits as inflow boundary conditions on the small domain
- Experimental data close to nozzle exit planes
- Transform velocities from large-domain LES on small-domain inlet planes to match:
 - Mean radial profiles
 - R.M.S. radial profiles
 - Longitudinal integral length scale on the CL

Large-domain LES
(including the nozzles)



Small-domain LES/PDF
(excluding the nozzles)

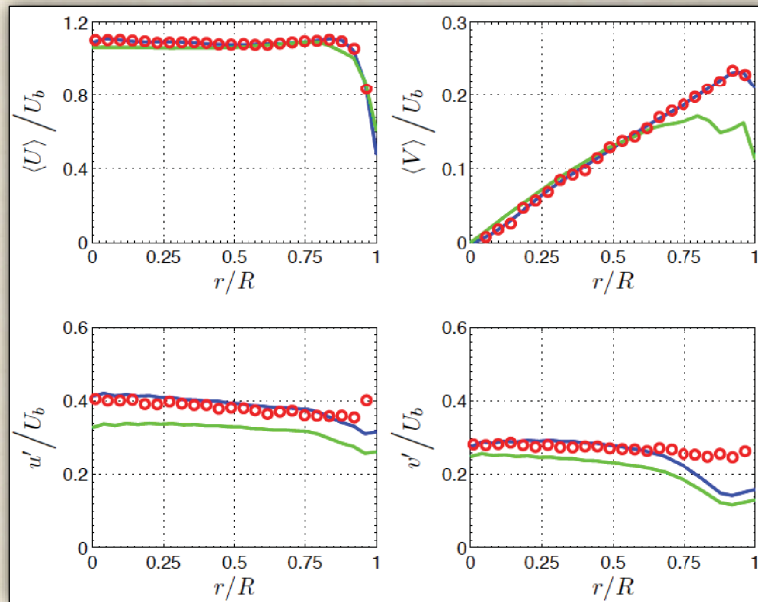


6

Inflow Methodology

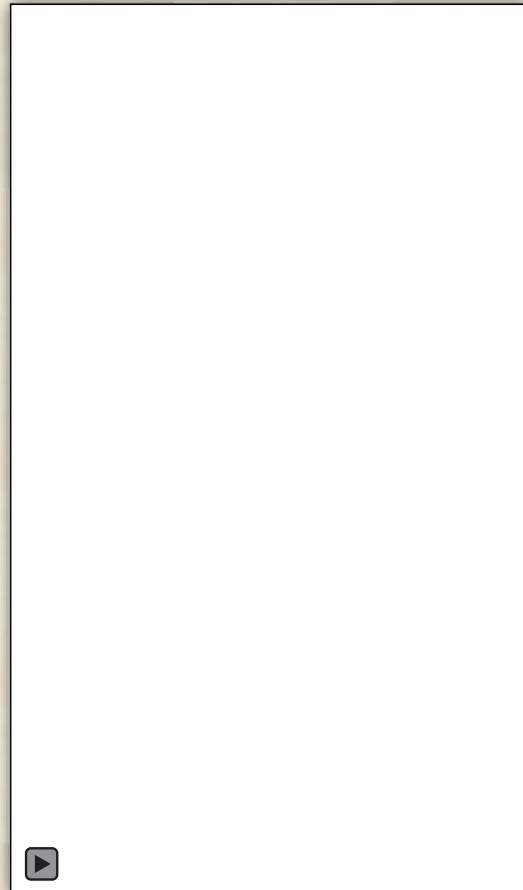
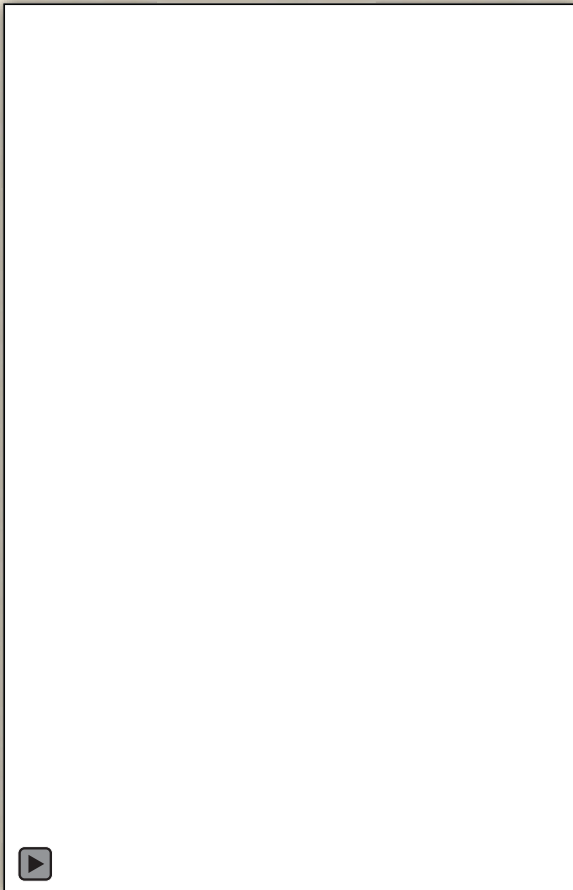
- o Experiments
- Scaled data
- Large-domain LES

Mean & R.M.S.



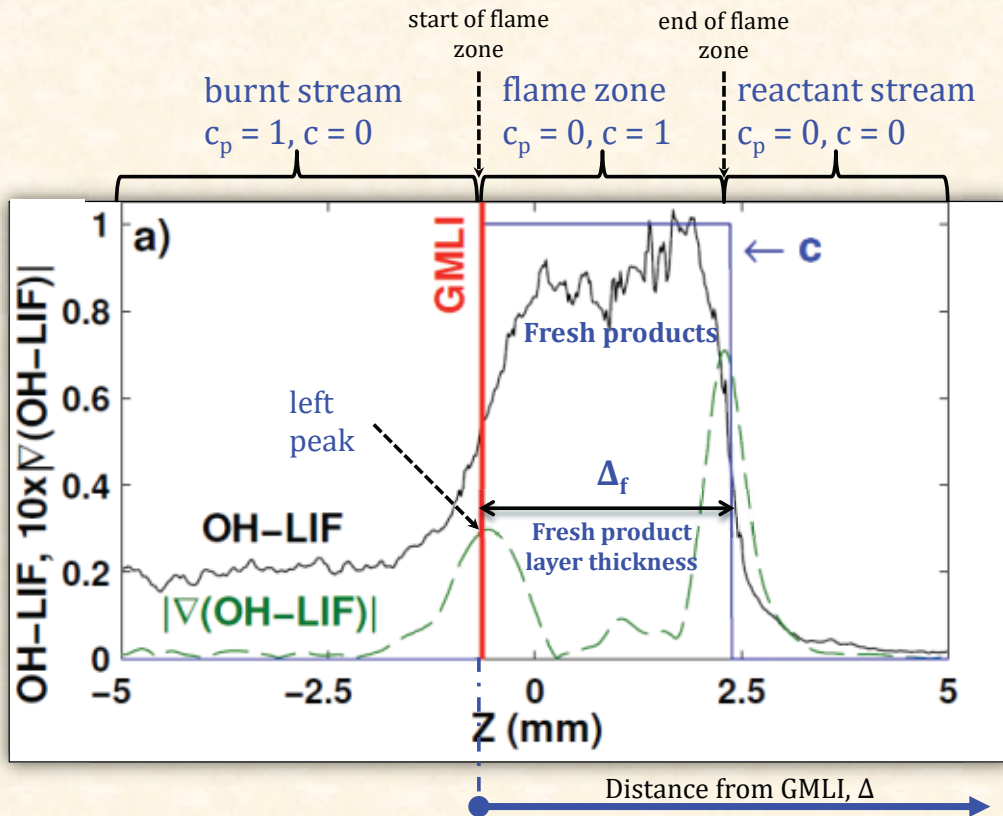
- Reference: R. R. Tirunagari, M. W. A. Pettit, A. M. Kempf and S. B. Pope, A simple approach for specifying velocity inflow boundary conditions in simulations of turbulent opposed-jet flows, *Flow Turbul. and Combust.*, 2016, in press, DOI: 10.1007/s10494-016-9743-4

7



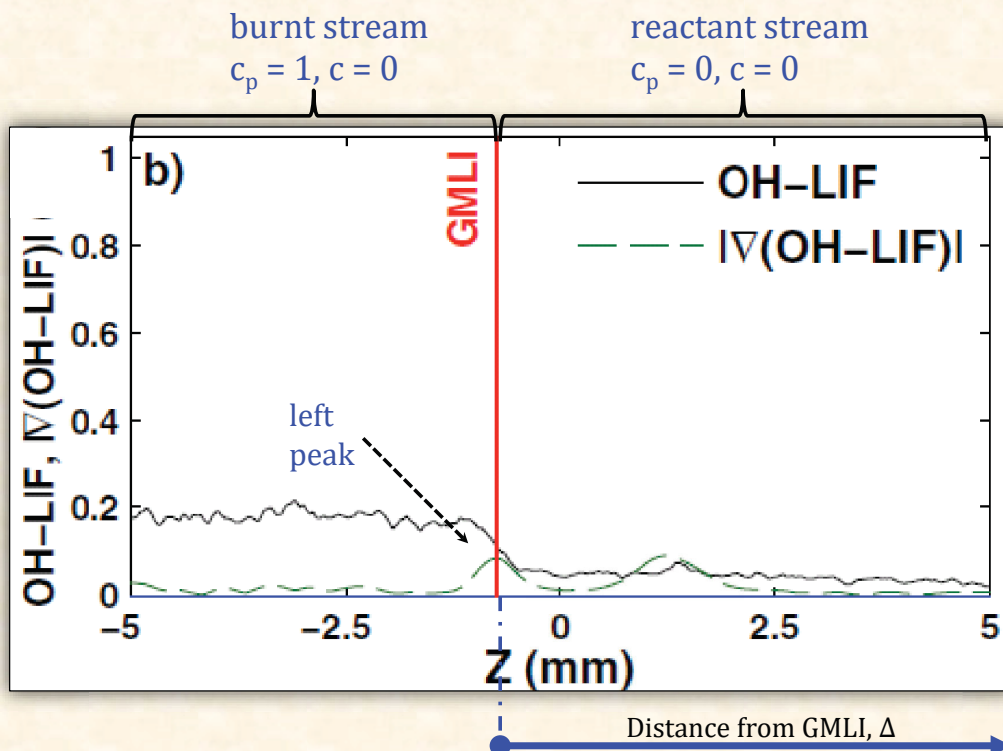
8

Centerline Profile: Definitions (Burning Case)



9

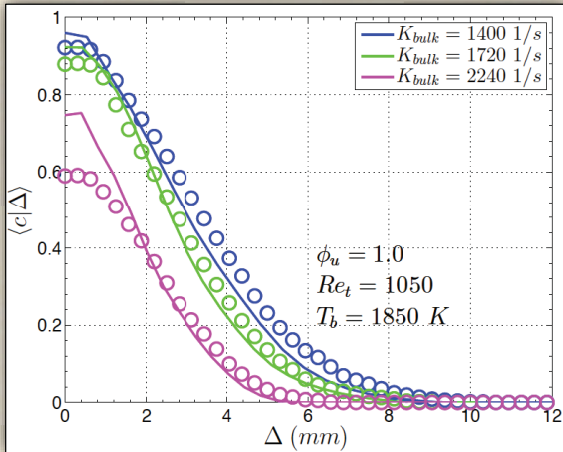
Centerline Profile: Definitions (Extinguished Case)



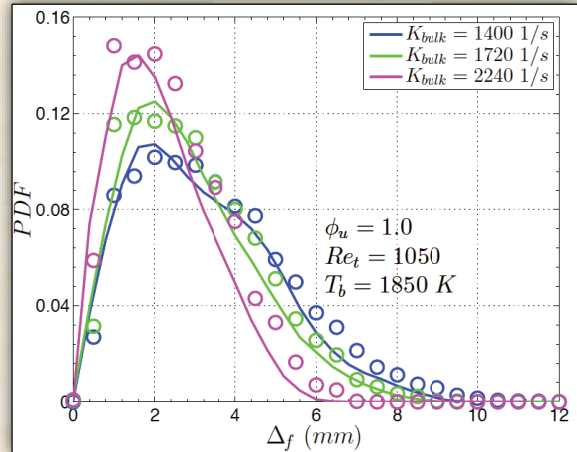
10

Effect of Bulk Strain Rate

Mean of fresh product, conditional on distance from the GMLI



PDF of fresh product layer thickness (burning samples only)



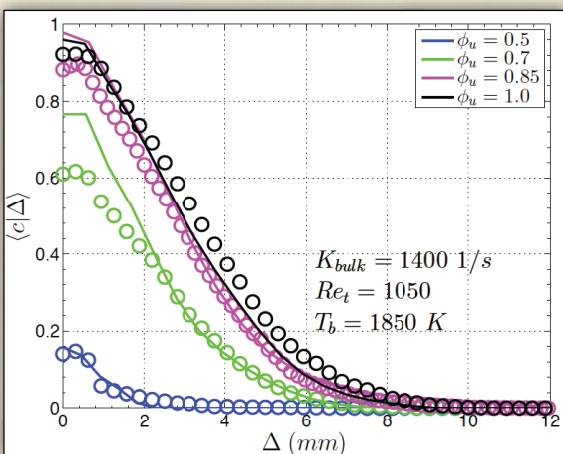
- Increase in bulk strain rate:
 - Probability of localized extinction increases
 - Thickness of fresh product layer decreases

Lines: Simulations
Dots: Experiments

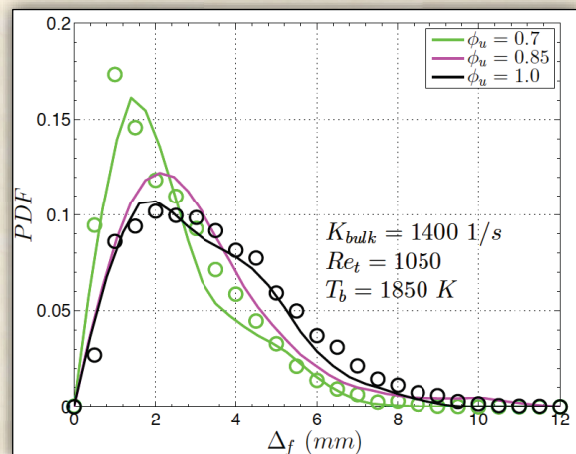
11

Effect of Reactants Equivalence Ratio

Mean of fresh product, conditional on distance from the GMLI



PDF of fresh product layer thickness (burning samples only)



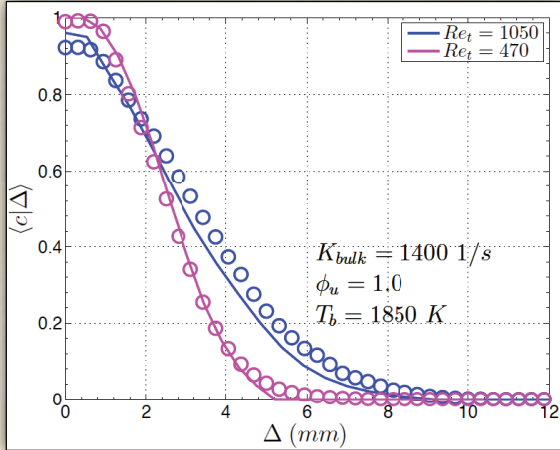
- With decreasing equivalence ratio:
 - Increased local extinction
 - The fresh product layer becomes thinner

Lines: Simulations
Dots: Experiments

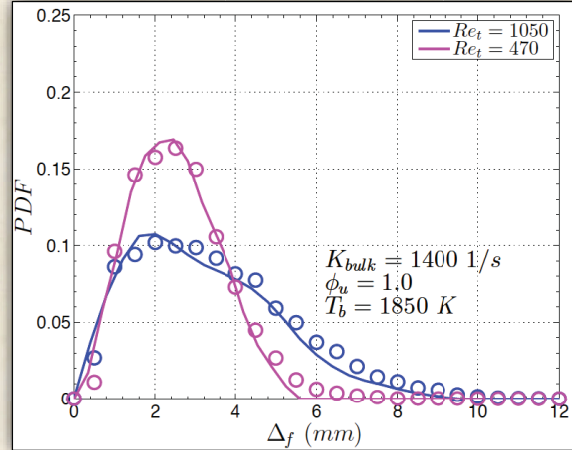
12

Effect of Turbulent Reynolds Number: Stoichiometric Flame

Mean of fresh product, conditional on distance from the GMLI



PDF of fresh product layer thickness (burning samples only)



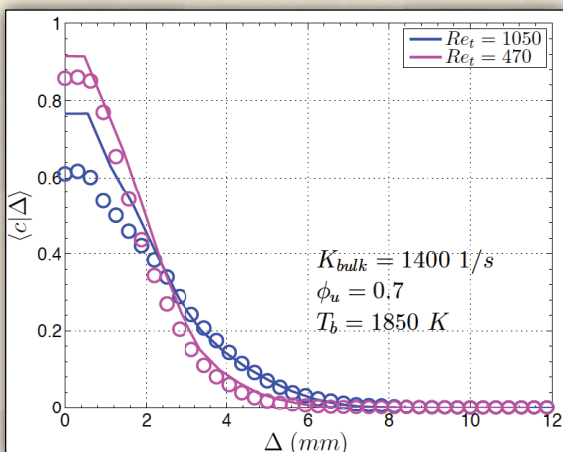
- Increase in the turbulent Reynolds number leads to:
 - an increased local extinction
 - broader distribution of product layer thickness

Lines: Simulations
Dots: Experiments

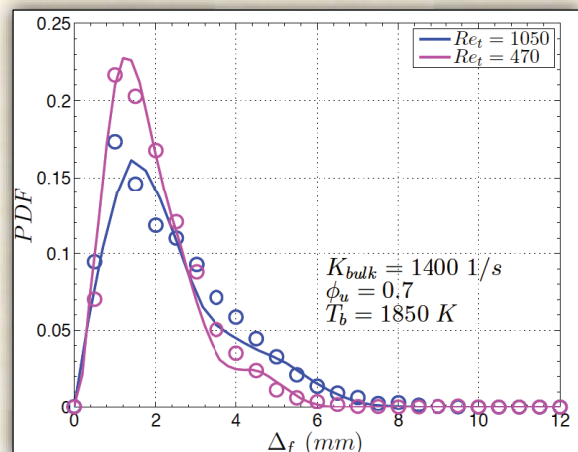
13

Effect of Turbulent Reynolds Number: Lean Flame

Mean of fresh product, conditional on distance from the GMLI



PDF of fresh product layer thickness (burning samples only)



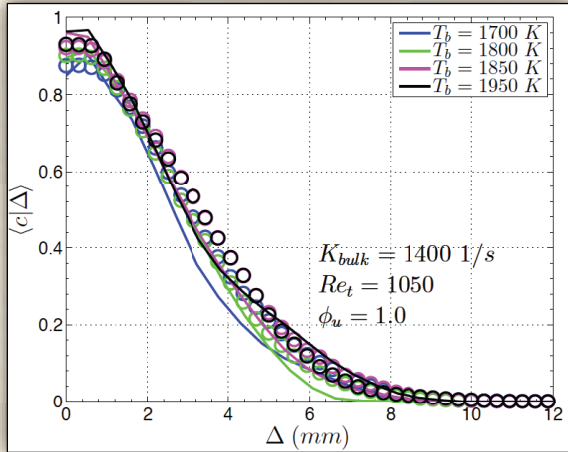
- Similar affect of Re_t for both lean and stoichiometric flames
- Lean flame has more probability of localized extinction

Lines: Simulations
Dots: Experiments

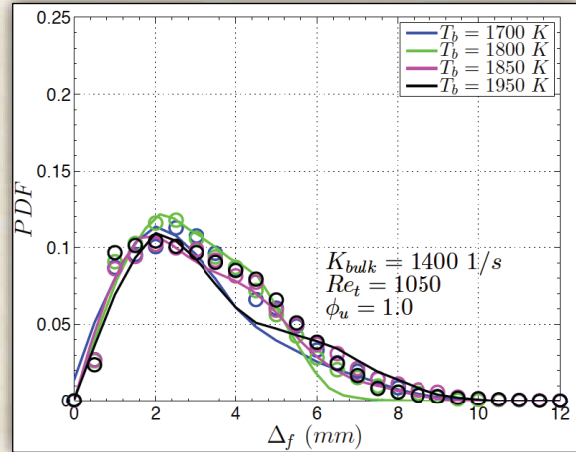
14

Effect of Product Stream Temperature: Stoichiometric Flame

Mean of fresh product, conditional on distance from the GMLI



PDF of fresh product layer thickness (burning samples only)



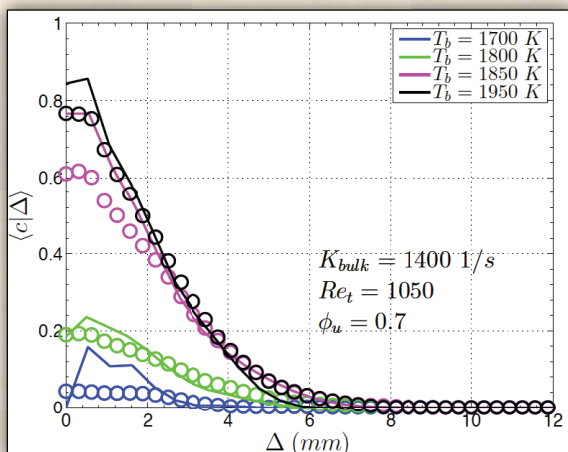
- Product stream temperature has **negligible effect** on the stoichiometric flame

Lines: Simulations
Dots: Experiments

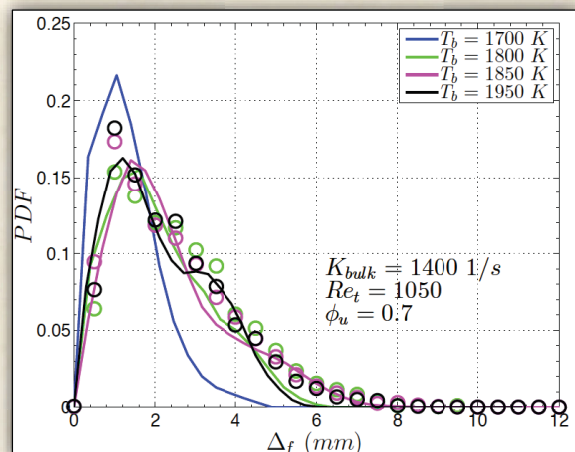
15

Effect of Product Stream Temperature: Lean Flame

Mean of fresh product, conditional on distance from the GMLI



PDF of fresh product layer thickness (burning samples only)

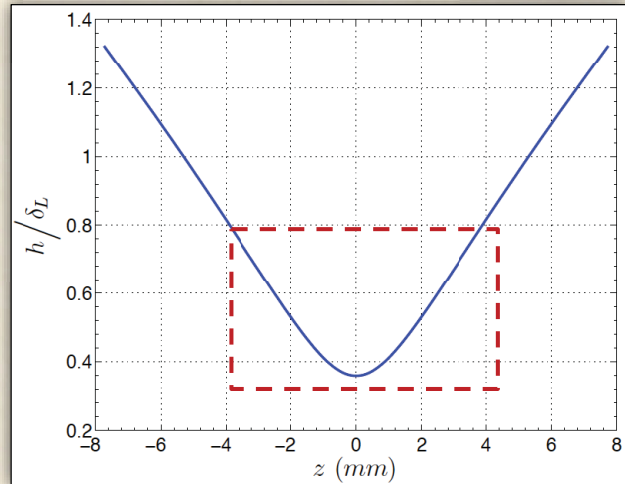
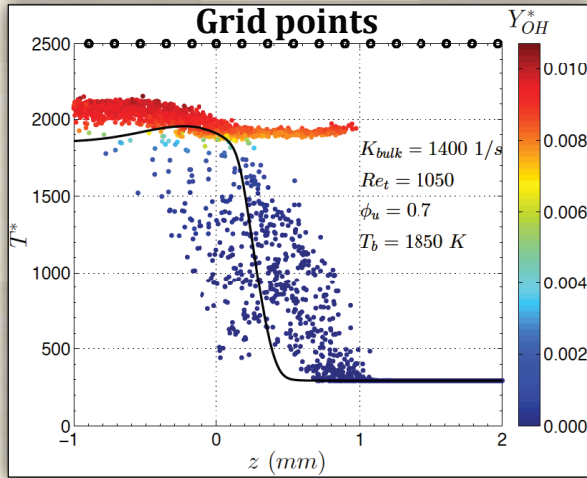


- Product stream temperature has **significant effect** on the lean flame
- Probability of localized extinction increases as we decrease the stream temperature

Lines: Simulations
Dots: Experiments

16

Why Successful? DNS?



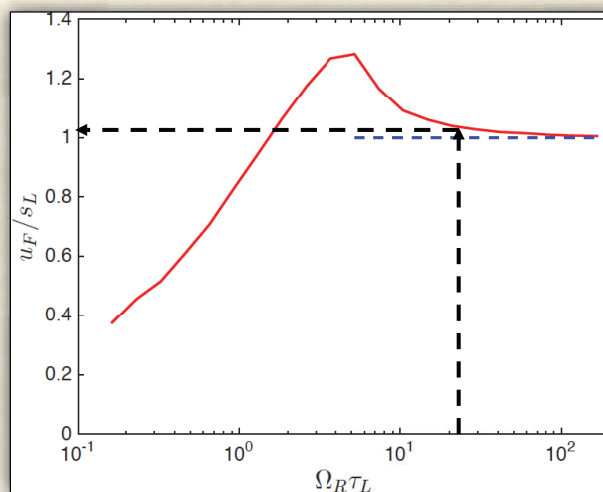
Dots: Particle data
Line: Laminar Profile

- For $z = [-4, 4]$, $h/\delta_L = [0.36-0.8]$
- Grid is too coarse for DNS by at least a factor of 4

17

Approaching the DNS Limit

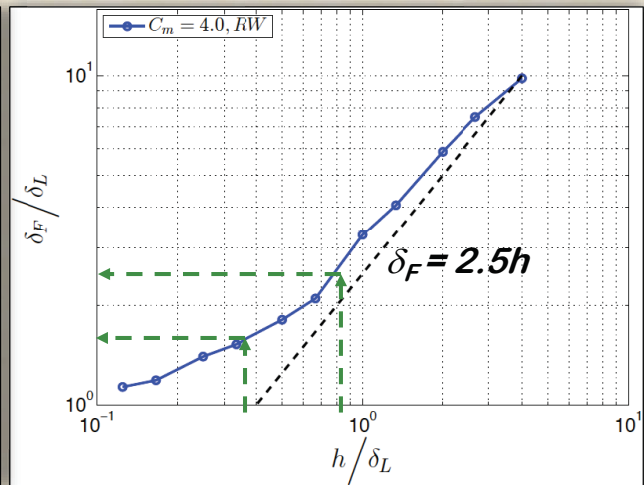
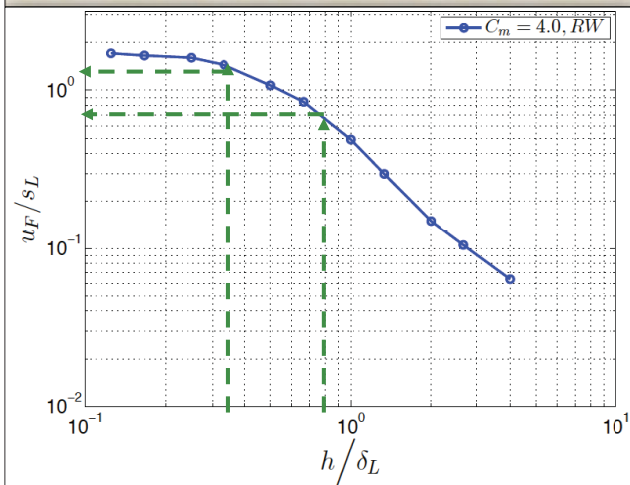
- In the DNS limit:
 - Turbulent to molecular diffusivity, $D_T/D \rightarrow 0$
 - Normalized mixing rate, $\Omega_R \tau_L \rightarrow \infty$
 - Normalized mesh spacing, $h/\delta_L \rightarrow 0$



For $\Omega_R \tau_L > 1$, u_F is within 30% of s_L

18

Strained, Counterflow Flame: Flame Speed & Thickness

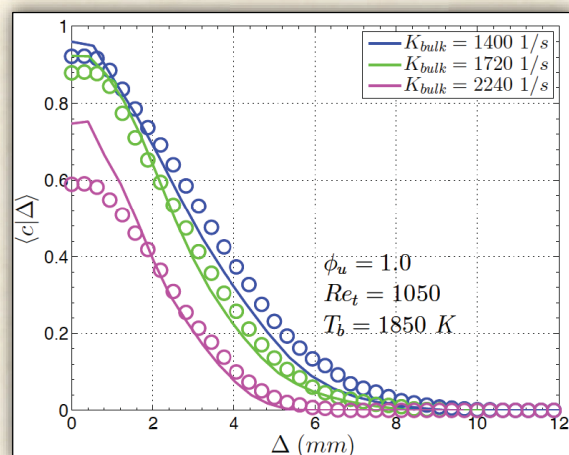


- For $h/\delta_L = [0.36-0.8]$:
 - $u_F/s_L = [0.7-1.2]$ → relatively **narrow** range
 - $\delta_F/\delta_L = [1.5-2.5]$ → grid spacing is too **coarse** to resolve laminar thickness

19

Conclusions

- LES/PDF applied to partially-premixed counterflow flames
- Simple sub-models: the same as in numerous studies of non-premixed flames
- Excellent agreement with experimental data of Coriton, Frank & Gomez (2013):
 - Degree of local extinction
 - Product layer thickness
- Effects of:
 - Bulk strain rate
 - Equivalence ratio
 - Turbulence Reynolds number
 - Product-stream temperature



20

TNF2016: Session on Counterflow Flames

Coordinator **Jonathan Frank**

13th International Workshop on Measurement and Computation of Turbulent Flames

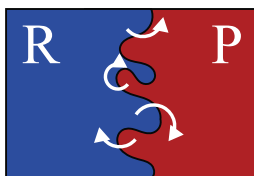
Martin Rieth and Andreas Kempf, Universität Duisburg Essen.
Fabian Hampf, Lu Tian, Peter Lindstedt, Imperial College London,

The ICL contributors would like to acknowledge the support of the AFOSR and EOARD under Grant FA8655-13-1-3024. We also thank Dr Chiping Li, Dr Gregg Abate and Dr Russ Cummings for encouraging the work as well as Dr Robert Barlow for his support.

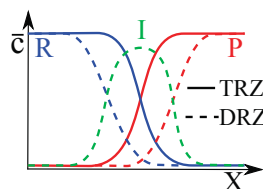
Fuel effects and combustion regime transitions

- ❑ Evolution of Combustion Processes with Da number.
- ❑ Multi-Fluid Post-Processing Methodology.
- ❑ Fluid States and Conditional Velocities.
- ❑ Computational Studies.
- ❑ The Impact of Pressure Gradients.
- ❑ Summary.

Thin Reaction Zones (TRZ)

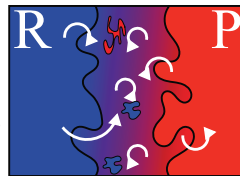


- ❑ Thin flame fronts.
- ❑ Fast chemistry inside laminar-like flame fronts.

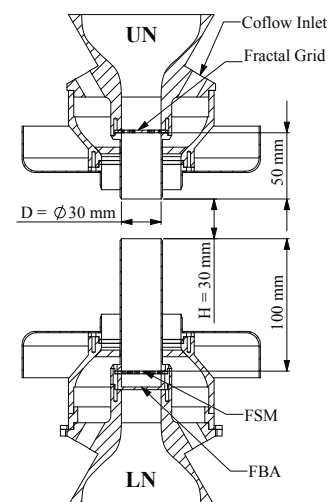


R – Reactants;
P – Products;
I – Intermediates.

Distributed Reactions (DRZ)



- ❑ No clear flame fronts.
- ❑ Stronger interactions of turbulence and chemistry.



Revised opposed
jet configuration

- ❑ Combustion regime transitions not well understood.
- ❑ An extended framework to move beyond the two-fluid (reactants/products) BML [1] theory of premixed turbulent combustion.
- ❑ Trends in statistics obtained via a multiple fluid approach [2] are explored.
- ❑ Conventional extinction criteria removed by supporting the combustion process with hot combustion products [3,4].
- ❑ Significant thickening of the CH layer observed with increasing Karlovitz number [5-7].

Parameter	Condition
UN Exit Velocity	11 m/s @ 320 K
Fuel	DME, EtOH, CH ₄
Φ_{UN}	0.0 - 1.0
Turbulence	Cross Fractal Grid
Re_t	~ 390
LN Exit Velocity	~ 4.3 m/s @ STP
Fuel	H ₂ - $\Phi_{LN} = 1.0$
Diluent	CO ₂
T_{NE}	1700 K

[1] Swaminathan, Cambridge University Press (2011).
 [3] Mastorakos et al., Combust. Flame 102 (1995)
 [5] Zhou et al., Proc. Combust. Inst. 35 (2015).
 [7] Zhou et al., Combust. Flame (2015).

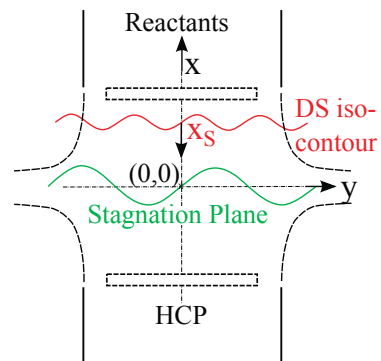
[2] Spalding, Comp. Tech. App., CTAC95 (1996).
 [4] Hampp and Lindstedt, Proc. Combust. Inst. (2016).
 [6] Zhou et al., Combust. Flame (2015).

The influence of chemistry on combustion regime transitions investigated by means of:

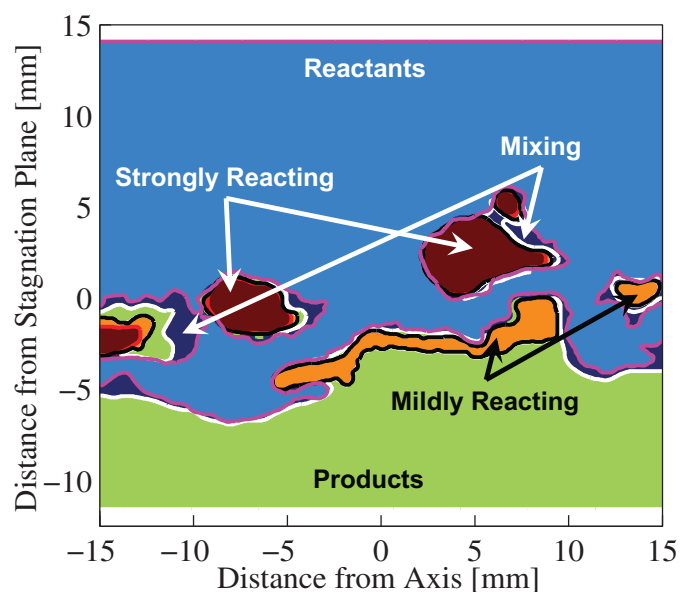
- ❑ Fuel variation: Dimethyl Ether (DME), Ethanol (EtOH), Methane (CH₄).
- ❑ Equivalence ratio (Φ): The upper nozzle (UN) Φ is varied from 0.0 – 1.0.

Property	Unit	DME	EtOH	CH ₄
Formula	-	CH ₃ OCH ₃	C ₂ H ₅ OH	CH ₄
MW	kg/kmol	46.1	46.1	16.0
Evaporation Temperature	K	248	352	~110
Autoignition Temperature	K	508	642	~850
Lower Heating Value	MJ/kg	27.6	28.9	55.5
Ignition Limit	vol %	3.4 / 18.6	3.3 / 19.0	4.5 / 16.0
Cetane; RON/MON	-	55 – 60	110 / 90	~120

- ❑ Reactants: Fresh reactants from the UN that have not undergone any thermal alteration (i.e. no oxidation or mixing processes) provide the first reference state.
- ❑ Hot Combustion Products (HCP): The hot combustion products that emerge from the LN provide a well defined second reference state.
- ❑ Mixing Fluid: A fluid state without detectable OH signal that has been exposed to a thermal change (i.e. via mixing with HCP) – density segregation.
- ❑ Strongly Reacting Fluid: Strong OH signal intensity regions caused by self-sustained (e.g. flamelet) burning. Conventional extinction criteria apply.
- ❑ Mildly (or Weakly) Reacting Fluid: A fluid state with modest levels of OH, e.g. ultra lean flames sustained by thermal support from an external enthalpy source or combustion products approaching equilibrium.
- ❑ All data shown is aligned on the density segregation (DS) iso-contour (x_s).



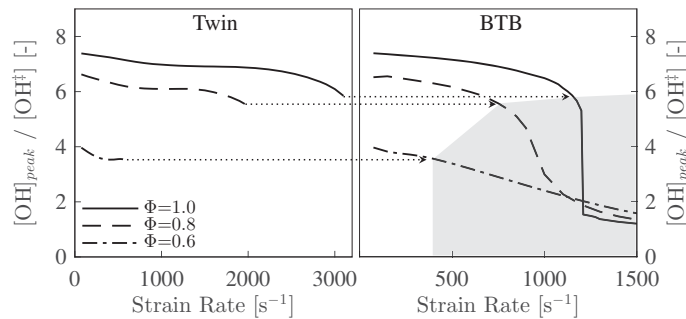
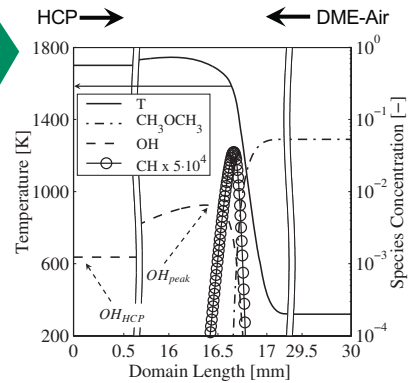
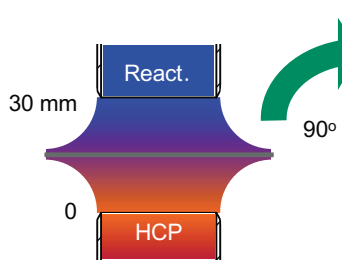
- ❑ Simultaneous Mie scatter / PIV / OH – PLIF diagnostic setup.
- ❑ 3000 instantaneous image pairs per condition.
- ❑ Quantification of chemistry impact on burning modes via multi-fluid post-processing.
- ❑ The spatial resolution of the multi-fluid algorithm was determined to be 0.25 mm (around three Kolmogorov length scales in reactants).
- ❑ The additional OH above the HCP concentration is from combustion of the fuel.



The peak OH concentrations normalised with the HCP value vs rate of strain for twin and back-to-burnt opposed jet flames shown below.

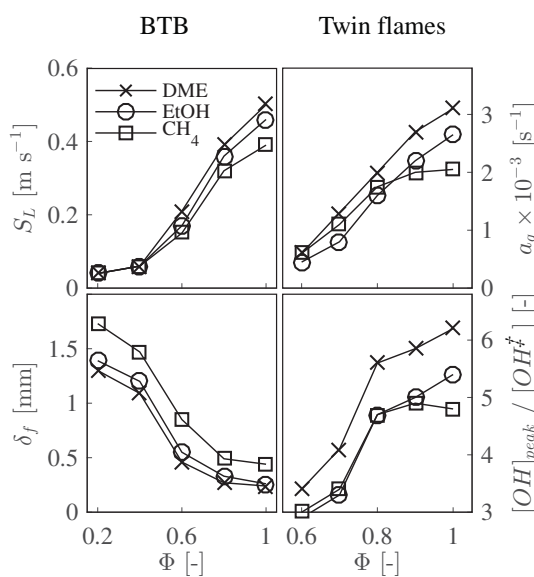
The OH peak concentrations between the two geometries correlate up to the twin flame extinction point.

Beyond the extinction point the impact of the HCP dominates (grey shaded area below).



Sample calculation with $a = 825 \text{ s}^{-1}$ and $\phi = 0.80$ (above).

Hampp, F., PhD Thesis, Imperial College, (2016).



- S_L Laminar burning velocity.
- δ_f Laminar flame thickness.
- a_q Extinction strain rate.
- $[OH]_{peak}$ Peak OH concentration.
- $[OH\#]$ HCP OH concentration.

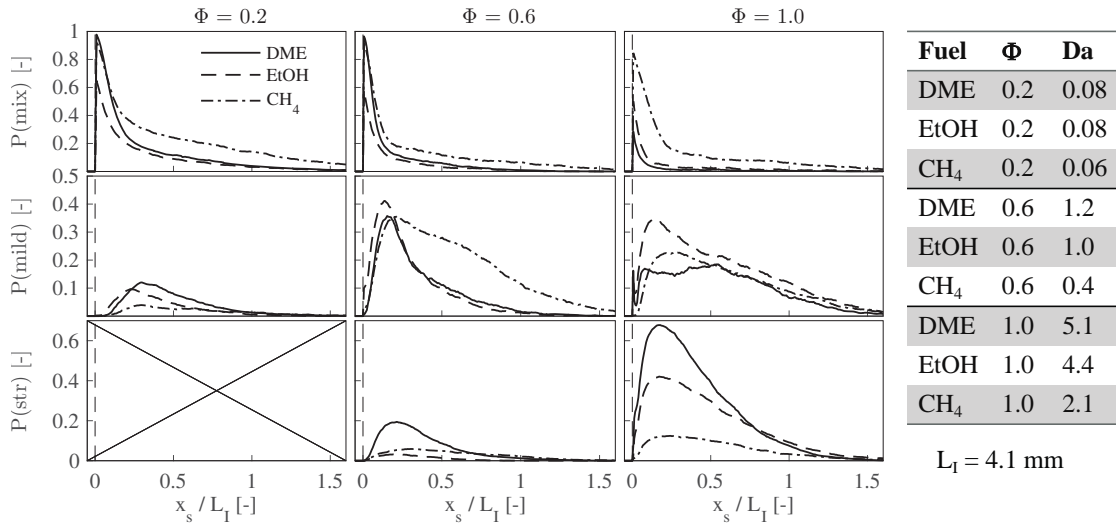
Total strain:

$$a_T = a_b + a_t = 2 \cdot \frac{U_b}{H} + \left(\frac{\varepsilon_r}{\nu_r} \right)^{1/2}$$

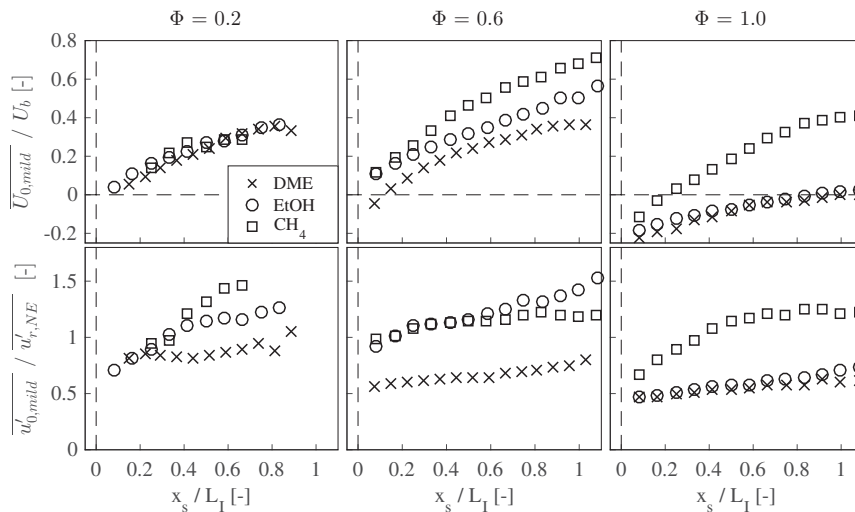
$$a_T \approx 4000 \text{ s}^{-1}$$

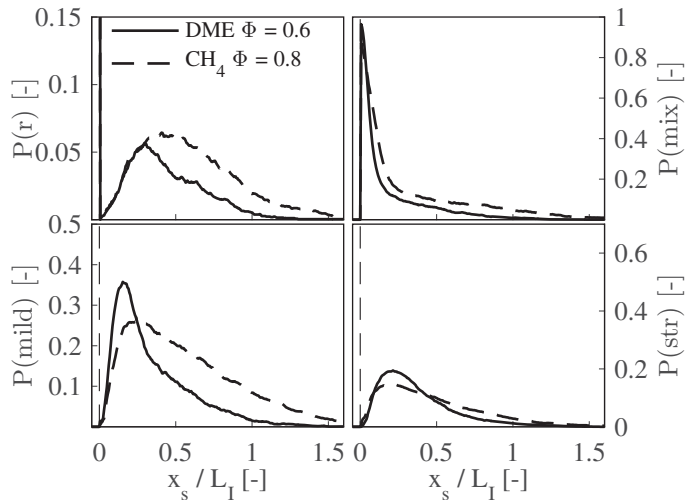
Hampp, F., PhD Thesis, Imperial College, (2016).

- The DME/EtOH mixing fluid probability is more strongly reduced than for CH₄ with Φ .
- The mildly (weakly) reacting peak probability similar for $Da \leq 1$, reduced for DME $\Phi = 1$.
- The strongly reacting peak probability increasing with Da with up to 70% for DME $\Phi = 1$.



- $\Phi = 0.2$: The mildly (weakly) reacting fluid velocity are similar.
- $\Phi = 0.6$: DME/EtOH separate from CH₄ (auto-ignition properties).
- $\Phi = 1.0$: DME/EtOH coincide while CH₄ remains affected by HCP.

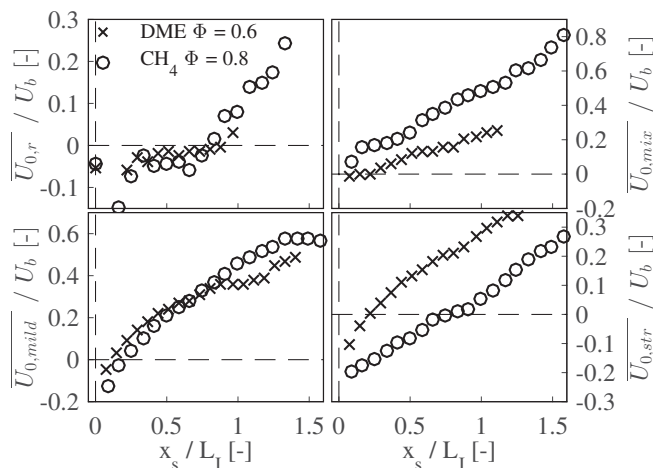




Fuel	Φ	Da
DME	0.6	1.2
CH ₄	0.8	1.5

The Da number appears to provide an approximate scaling. (r = reactants; mix = mixing fluid; mild = mildly (weakly) reacting fluid; str = strongly reacting fluid).

Hampp, F., PhD Thesis, Imperial College, (2016).



- The mildly reacting (mild) and reactant (r) fluid velocities coincide at similar Da.
- The drop in mixing (mix) fluid velocity for DME can be expected from the earlier transition to a chemically active state.
- The more negative strongly reacting fluid (str) velocity for CH₄ is consistent with the higher heat release.

Hampp, F., PhD Thesis, Imperial College, (2016).

Experimental cases studied

Imperial College Turbulent Opposed Jet Burner, back-to-back (twin flame) configuration by Goh *et al.* [8]. Here, methane with equivalence ratios of 0.9 and 0.8.

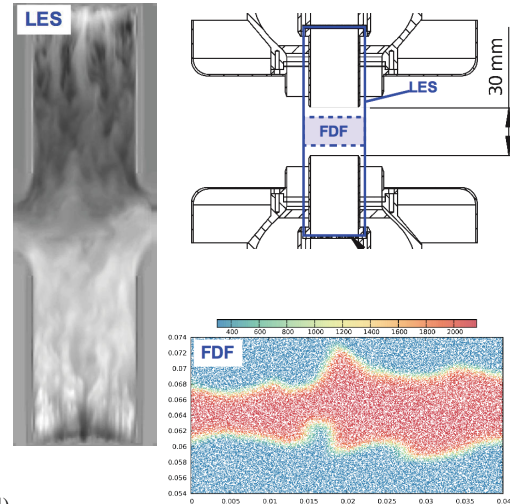
Simulation method

Large eddy simulation with transported filtered density function

- PsiPhi code.
- Domain includes nozzles and starts at fractal grids.
- 1.7 million cells (0.5 mm resolution).
- 8 million particles (between nozzles - 20 per cell).

Modeling details:

- Low-Mach variable density solver.
- Sigma SGS model.
- Modified Curl's mixing model.
- 4-step reaction mechanism.

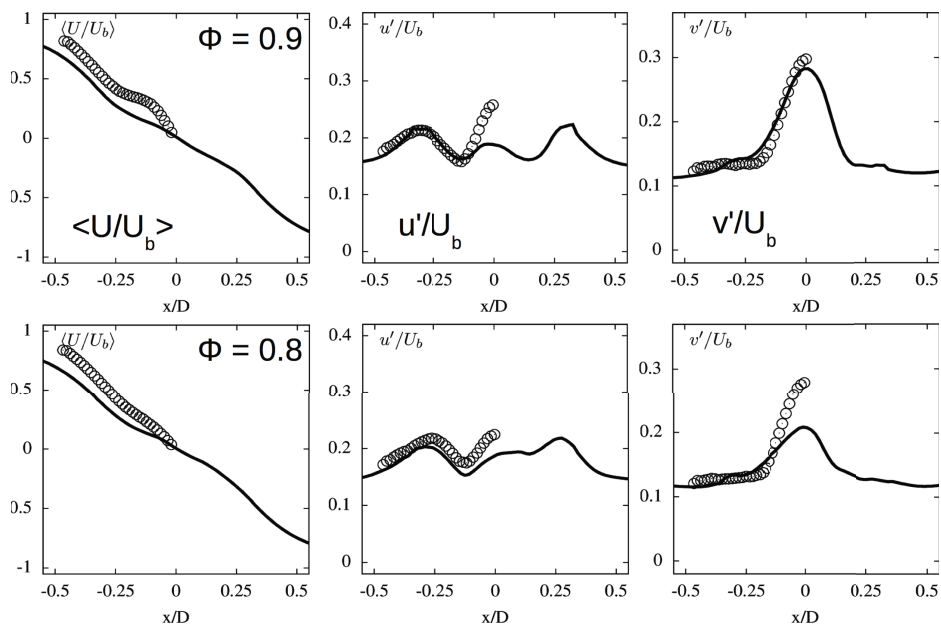


[8] K.H.H. Goh, P. Geipel and R.P. Lindstedt, Combust. Flame 161 (2014).

LES/FDF results

Flow field statistics (along centerline)

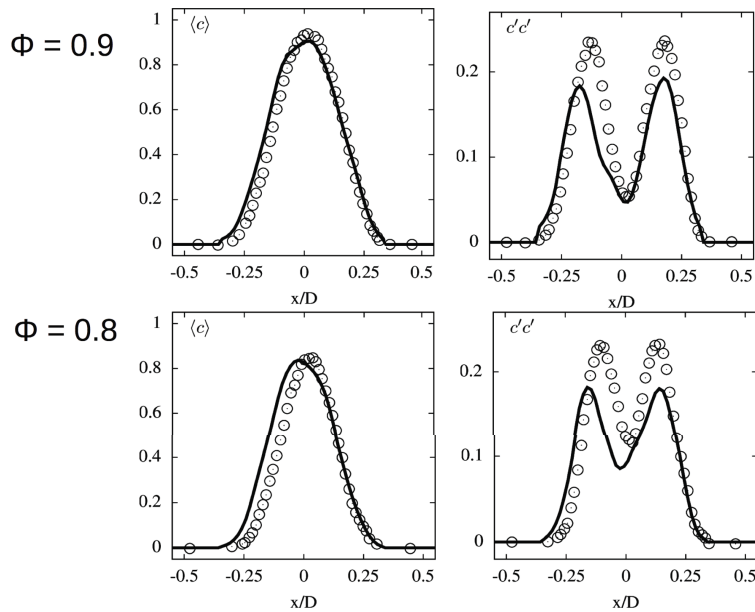
From left to right: mean axial velocity, axial velocity fluctuations, radial velocity fluctuations. Top: equivalence ratio of 0.9, bottom: equivalence ratio of 0.8.



LES/FDF results

Progress variable (along centerline)

Left: mean progress variable, right: progress variable variance. Top: equivalence ratio of 0.9, bottom: equivalence ratio of 0.8.

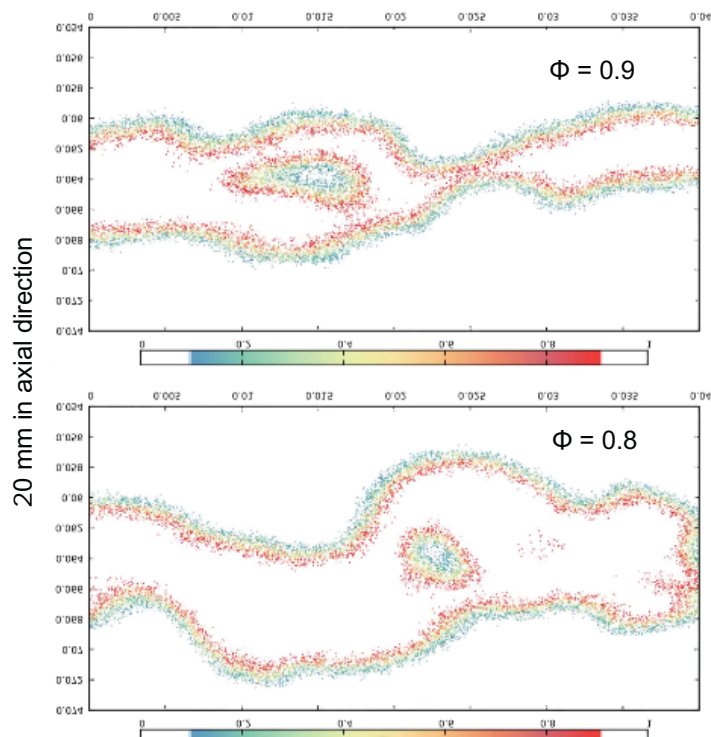


LES/FDF results

40 mm in radial direction

Flame Behavior

Only particles with reaction progress variables between 0.1 and 0.9 are shown.



- The models for pressure strain terms have long been a key task for the closure of the transport equations of Reynolds stresses and scalar fluxes.
- Dilatation and flamelet scrambling effects need to be considered [9]. Models based on constant-density flows are insufficient [10].

$$\phi_{ij} = - \left[\overline{u_i'' \frac{\partial p'}{\partial x_j}} + \overline{u_j'' \frac{\partial p'}{\partial x_i}} \right] = \phi_{ij}^R + \phi_{ij}^D + \phi_{ij}^T$$

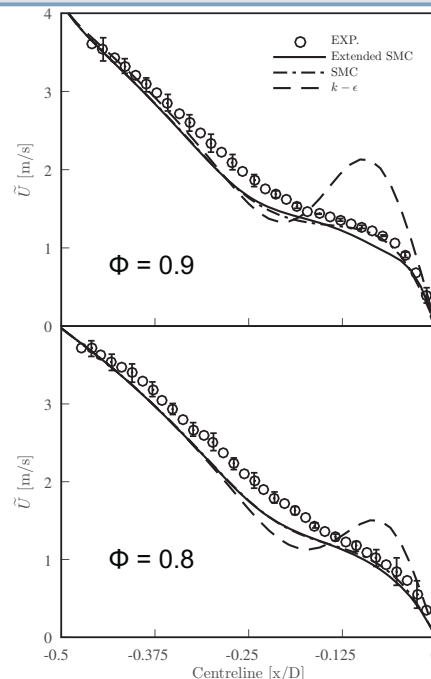
Redistribution $\phi_{ij}^R = - \left[\overline{u_i'' \frac{\partial p'}{\partial x_j}} + \overline{u_j'' \frac{\partial p'}{\partial x_i}} - \frac{2}{3} \delta_{ij} \overline{u_l'' \frac{\partial p'}{\partial x_l}} \right] = \phi_{ij}^{CD} + \phi_{ij}^A \leftarrow$ Preferential acceleration model [10]

Dilatation $\phi_{ij}^D = \frac{2}{3} \delta_{ij} p' \frac{\partial \overline{u_l''}}{\partial x_l} = \frac{2}{3} \delta_{ij} \left\{ p' \frac{\partial}{\partial x_i} \left[\rho D_c \frac{\partial c''}{\partial x_i} \right] \frac{\partial \rho^{-1}}{\partial c} + p' S_c \frac{\partial \rho^{-1}}{\partial c} \right\}$ 1st term is normally neglected [11]

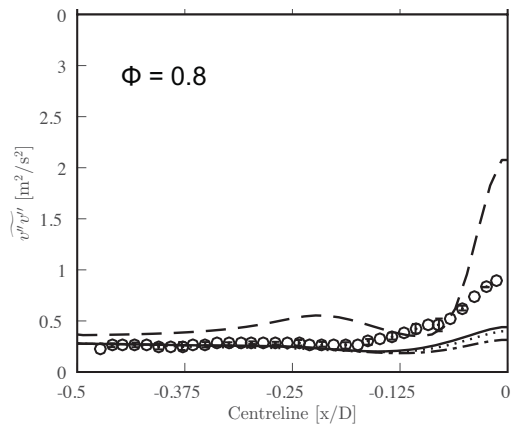
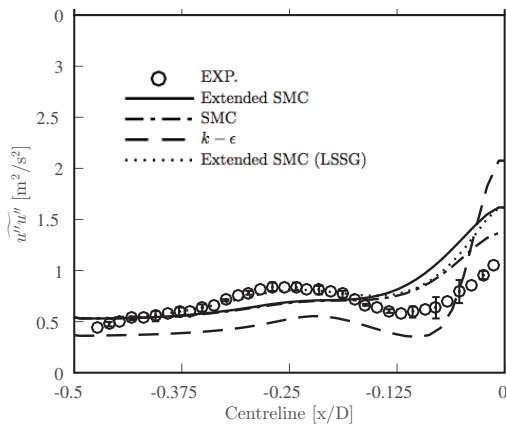
Transport $\phi_{ij}^T = - \frac{2}{3} \delta_{ij} \overline{\frac{\partial p' u_l''}{\partial x_l}}$ Neglected? Together with Triple-moment? Or?

[9] Lu Tian, Lu, R.P. Lindstedt, Combust. Theory Model. (submitted); [10] R.P. Lindstedt, E.M. Váos, Combust. Flame 116 (1999); [11] W.P. Jones, Ch.6 in Turbulent Reacting Flows (1993).

- Modelling results obtained from transient simulations by using the governing equations integrated in conservation form.
- Variable predictor–corrector variant (with splitting error control) of the PISO algorithm with a TVD scheme [10].
- The computational domain was from nozzle to stagnation plane with symmetry conditions applied.
- Grid resolution similar to the experimentally estimated Kolmogorov scale in the cold flow.
- The SMC closure is that of Haworth and Pope [12] and the extended SMC adds recently derived dilatation and scrambling models [9]. Experimental data from Goh et al. [8].

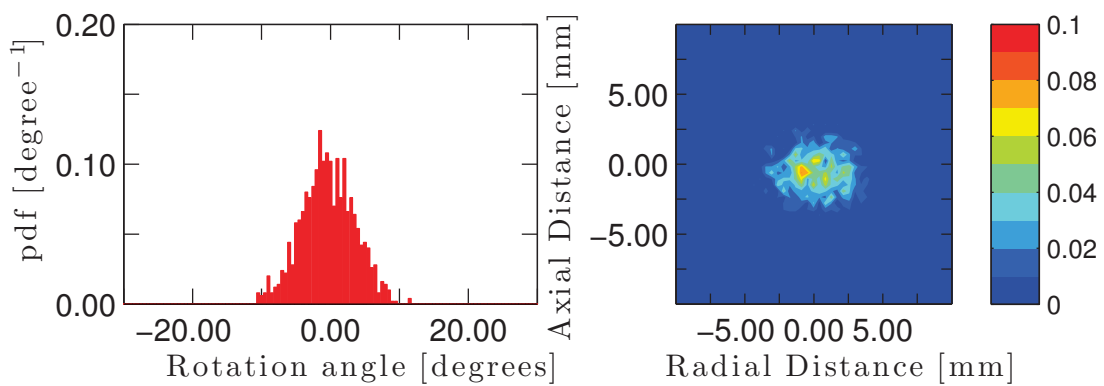


[12] D. Haworth, S.B. Pope, Phys. Fluids 30 (1987).

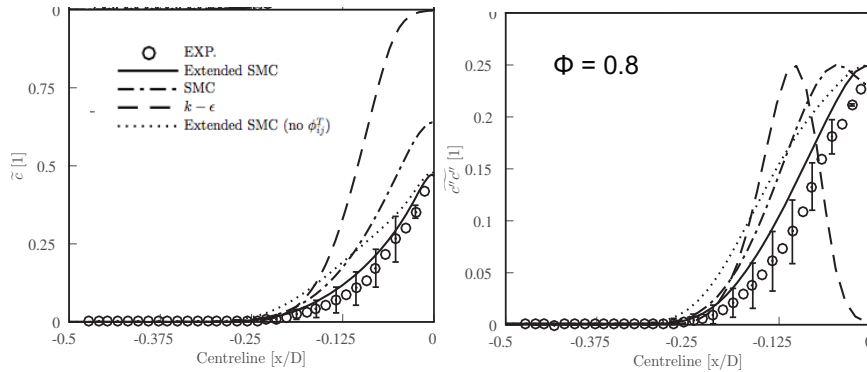


- The SMC closure is that of Haworth and Pope [12] and the extended SMC adds recently derived dilation and scrambling models [9]. Experimental data from Goh et al. [8]. The LSSG model is the Lagrangian form derived by Pope [13] of the SSG model of Speziale et al. [14].

[13] S.B. Pope, Phys. Fluids 6 (1994); [14] C.G. Speziale, S. Sarkar, T.B. Gatski, J. Fluid Mech 227 (1991).



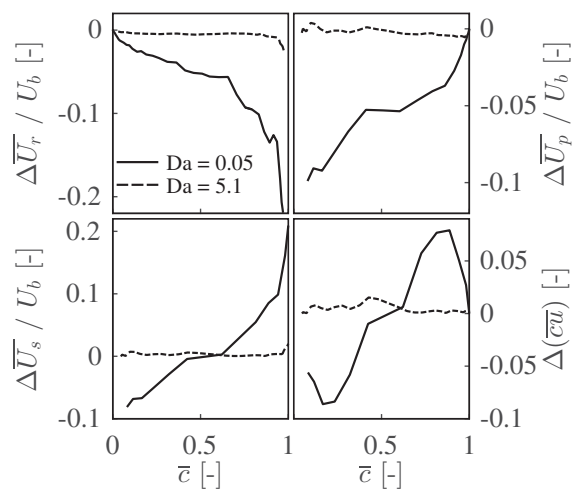
- Rotation of the stagnation plane may contribute to the redistribution of turbulent kinetic energy [8].



- The SMC closure is that of Haworth and Pope [12] and the extended SMC includes recently derived dilation and scrambling models [9]. Experimental data from Goh et al. [8].

Hampp, F., PhD Thesis, Imperial College (2016).

- Bimodal statistics can be evaluated by computing the differences for conditional velocities ($\Delta \bar{U}_r$, $\Delta \bar{U}_p$, $\Delta \bar{U}_s$) and the scalar flux $\Delta(\bar{c}u)$ via:
- (i) Particle density segregation [15].
- (ii) OH-PLIF based methods [16].
- Good agreement at high Da as at most thin interfaces separate reactants from OH rich products.
- Significant deviations arise as the Da number is reduced.



[15] I. G. Shepherd, R. K. Cheng, P. J. Goix, Proc. Combust. Inst. 23 (1991); [16] P. Petersson, J. Olofsson, C. Brackman, H. Seyfried, J. Zetterberg, M. Richter, M. Aldén, M. A. Linne, R. K. Cheng, A. Nauert, D. Geyer, A. Dreizler, Appl. Optics 46 (2007).

Experiments

- ❑ Combustion regime transition trends can be quantified using a novel multi-fluid approach – fuel chemistry effects do influence conditional velocity statistics.
- ❑ A distinct impact of fuel chemistries has been observed on fluid state probabilities (CH_4 , EtOH, DME and JP-10) – approximate scaling with the Da number.
- ❑ Need to account for multiple chemical time scales – more data on different fuels desirable.

Modelling

- ❑ Pressure dilatation/flamelet scrambling models important for turbulent kinetic energy and scalar flux. Overall good agreement with comprehensive SMC,
- ❑ Rotation of the stagnation plane might contribute to the redistribution of turbulent kinetic energy – reproduced by LES/FDF.
- ❑ More comparative modelling studies using different approaches are required.

Flame-Wall Interaction

Coordinators: Andreas Dreizler and Johannes Janicka

The general importance of Flame-Interaction (FWI) was discussed already in TNF12 where a number of challenging and open issues with regard to modelling were addressed. In addition, the need for suitable benchmark configurations was identified. Based on these findings the objective of the FWI-session at TNF13 was twofold:

1. Introduce a new benchmark configuration that is available as a TNF target flame. The configuration is detailed below together with the experimental data already available and a summary of the first numerical steps.
2. Show the progress made in simulating the physical processes associated with near-wall reactive flows and identify important shortcomings of modeling flame-wall interactions to steer future efforts.

Sidewall Quenching: A new TNF target flame

A target flame must fulfill a number of requirements. In addition to well-defined and reproducible inflow and boundary conditions a statistically resilient database including information on flow and scalar fields must be obtained. For the latter, statistically stationary flames interacting with walls are preferable compared to transient flames propagating (in mean perpendicularly) against walls. FWI-geometries based on sidewall quenching (SWQ) are therefore preferable to head-on quenching (HOQ) [1].

The new SWQ-geometry [2] consists of a converging Morel nozzle with quadratic cross-section to provide a top-hat velocity exit profile (edge length 40 mm). Premixed fuel (so far methane) and dry air are fed to the burner plenum at room temperature. Honeycombs and fine meshes homogenize the flow before it enters the converging part of the nozzle. Sharp edges at the nozzle exit minimize recirculation zones. Turbulence intensities can be enhanced by an optional turbulence grid (blockage 45%). A dry air co-flow surrounds the central flow. A circular ceramic rod (\varnothing 1 mm) is placed above the nozzle stabilizing a V-shaped flame. One branch of this V-flame approaches a water-cooled steel wall (\sim 300 K). Since the mean axial flow is parallel to the wall side-wall quenching (SWQ) occurs. In contrast to a previously used head-on quenching burner [3] this SWQ-burner leads to quasi-stationary flame-wall interaction.

Experiments are performed with a Reynolds number of 5000 (based on the hydraulic diameter of the nozzle exit) corresponding to a bulk flow velocity of 1.9 m/s. Two equivalence ratios ($\phi=0.83$ and 1) with and without inserted turbulence grid (TG) are analyzed. The burner geometry tends to create Helmholtz resonances at 104 Hz that are observable only for the laminar case (w/o turbulence grid). In turn minor vertical fluctuations of the flame tip at the wall appear (\pm 200 μ m). For turbulent cases these resonances are insignificant.

The special feature is that direct numerical simulations (DNS) of this target configuration will be possible. In the context of model development this enables a coherent interaction between DNS and experiments.

Experimental data and discussion

At present the following parameters have been investigated:

1. Two components of the flow field have been recorded simultaneously with the flame front position (2C-PIV & OH-PLIF) at low (10 Hz) and high (10 kHz) sampling rates. Based on these experiments for the turbulent case the flame surface density as well as the laminar flame speed as function of wall distance has been extracted. These parameters were used to determine the mean reaction rate. In addition, the flame brush was determined. Results are summarized in [2]. Data are available upon request.

2. The boundary layer of the velocity has been deduced for non-reacting and combusting cases using 2C-PIV. Using the quadrant splitting scheme it becomes evident that the flame-flow interactions in the close vicinity of the heat release zone dominate magnitude and sign of the turbulent stresses. In contrast to non-reacting conditions, during flame approach and FWI turbulence destruction dominates. This corresponds to a regime change from quadrants 2 and 4 (turbulence production) to quadrants 1 and 3 (turbulence dissipation). These experimental findings are consistent with results from DNS. The data is available once the paper has been accepted for publication.
3. Gas temperature and CO mole fractions have been measured quantitatively by conventional rotational-vibrational CARS probing the Boltzmann distribution of molecular nitrogen and laser-induced fluorescence of the CO molecule following two-photon excitation of the electronic B-state. Additionally, planar OH-LIF was used to identify the relative distance between the instantaneous CARS/CO-LIF probe volume and the instantaneous flame front location. Despite the remaining oscillations due to Helmholtz resonances observed in the laminar cases, conditional averaging allowed to evaluate thermochemical states in zones upstream and downstream the FWI-zones as well as in the close vicinity of flame-wall interactions. The presence of the wall causes significant differences compared to an unbounded premixed flame. Joining these results with findings from DNS that are discussed below, the observed changes in the thermochemical state due to FWI are dominated by diffusion processes rather than low temperature chemical kinetics. For more complex fuels this situation might change. The data are available once these results have been published (paper in preparation).

Simulation results

A laminar 3D simulation of the above mentioned SWQ-Burner was performed using a tabulated chemistry approach (FGM) [4] for the $Re = 5000$ case without turbulence grid. The Reynolds number was based on the nozzle diameter and the bulk inlet velocity at ambient conditions (1 bar, 300 K). The inflow gas was a stoichiometric methane-air mixture that was surrounded by co-flow of pure air. The wall at which the flame quenching took place had a temperature of 350 K. The combustion was modeled with a FGM approach using the mixture-fraction, the CO_2 mass fraction, and the enthalpy as control variables. The wall was resolved resulting in a y^+ of less than one. The simulation could capture the major species and temperature distribution as well as the velocity profiles that were obtained experimentally. The flame geometry could be captured as well. Hence the main structure of the Flame-Wall-Interaction was predicted correctly which qualifies the simulation models for technical designing regarding the wall heat load and flame stability. Furthermore, the simulation revealed an expansion of the flow field in the third dimension of the SWQ-Burner that complicates a 2D simulation. While the experimental result showed high CO concentrations at low temperatures within the quenching region only low concentration of CO could be predicted by the FGM simulation.

In order to investigate the phenomena underlying these discrepancies a 2D laminar simulation of a generic SWQ configuration was performed using detailed chemistry. The wall was resolved with $y^+ = 0.5$. The inlet velocities were adapted such that the flame geometry matched the measured flame front, in particular the angle between the flame and the wall. Detailed chemistry was applied using the Smooke [5] mechanism and the GRI 3.0 [6] mechanism. For each mechanism the diffusion model was varied using the unity Lewis number assumption as well as the mixture averaged diffusion modeling. Simulation results were evaluated using a Lagrangian analysis method. This method enables to distinguish between CO due to chemical formation and CO that accumulated due to diffusion from the surrounding. The simulations revealed a moderate influence of the reaction mechanism and the diffusion model. All detailed chemistry simulations could predict the temperature and in contrast to the FGM also the CO concentration within the scattering of the experimental data. The Lagrangian analysis revealed a diffusive flux of CO from the quenching flame towards the wall which results in high CO concentrations at low temperatures. Furthermore, the method showed a negative accumulated chemical source of CO at the wall. As a consequence of the dominating diffusive origin of CO near the wall the poor prediction of the FGM regarding the CO

concentration became explainable. In this regard it became apparent that the physical processes evolving within the SWQ-Burner are partially in conflict with the pre-tabulation assumptions.

Proceedings of numerical simulations

Several groups contributed to the TNF's progress regarding the numerical simulation of FWI. Specifically, the works of SINTEF (Trondheim, A. Gruber), UMich (Michigan, V. Raman), EM2C (Paris, O. Gicquel), UniBW (Munich, M. Pfitzner) and TUD (Darmstadt, J. Janicka) were presented and are summarized in the following:

At SINTEF they considered the near-wall hydrogen-air combustion by means of direct numerical simulations using a detailed reaction mechanism. Besides the anchored rich V-flame initiated in 2010, freely propagating flames, being homogeneous premixed as well as stratified were considered more recently. Besides the physical insights and a new theoretical model for flame flashback, A. Gruber suggested validation metrics that can be derived from the extensive results database. Specifically, those comprise the global flame shape, the wall heat flux and flame propagation speed which shall be well suited to assess RANS and LES models.

The University of Michigan considered the boundary layer flashback with regard to hydrogen enriched gas turbine applications. To reduce the computational effort V. Raman investigated the suitability of flamelet models for the chemistry reduction. The difficulty of this latter is the modified flame structure near walls interacting with the fluid and thermal boundary layer. The flamelet simulations performed lead to a reasonable prediction of the flashback velocity. However, a certain discrepancy to the reference remained being possibly related to chemical processes induced by the wall presence that are not included in the flamelet.

As a step towards the simulation of FWI in complex applications, the group at UniBW performed LES of a premixed swirl burner where the thermal influence of the central bluff body and outer walls has a significant impact onto the flame shape. To predict those, they applied the flame surface density model with near-wall modifications according to Wichmann and Bruneaux as well as Al-Shalan and Rutland. Judged on measured OH* chemiluminescence, both of these modifications qualitatively yielded a significant improvement when compared to the standard formulation. A more detailed assessment as well as the modeling of non-premixed FWI remained to be done.

Radiation and conjugate heat transfer represent two further processes involved in FWI as addressed by the group of EM2C. O. Gicquel outlined the difficulties in modeling these physics which they addressed by the coupling of different numerical codes and schemes being optimized for LES-combustion, radiation, and wall heat conduction, respectively. It was demonstrated that radiation causes deviations from the classical log-law flow near the wall. For a hot channel flow, they showed the capability of their OERM-radiation model leading to a close agreement of the LES with DNS reference data for the wall heat flux and temperature profile. The more complex configurations considered are the Darmstadt impinging jet burner and the Valogaz burner. For the impinging jet burner, the reactive LES with conjugate heat transfer showed very good agreement with the temperature profile measured along the wall surface. For the Valogaz burner, it was demonstrated, that the inclusion of heat losses is required such that the simulated flame is of V-shape as measured in contrast to the M-shape as predicted by an adiabatic approach.

The group at TUD performed first numerical simulations of the above mentioned SWQ experiments which are accordingly detailed above. In summary, the three dimensional simulation performed using tabulated chemistry provided a good prediction of the global behavior and insight into the flowfield as an important step for further simulations. However, the tabulated chemistry failed to predict the near-wall CO concentration which was confirmed by subsequently performed detailed chemistry simulations using a reduced, two-dimensional domain.

References

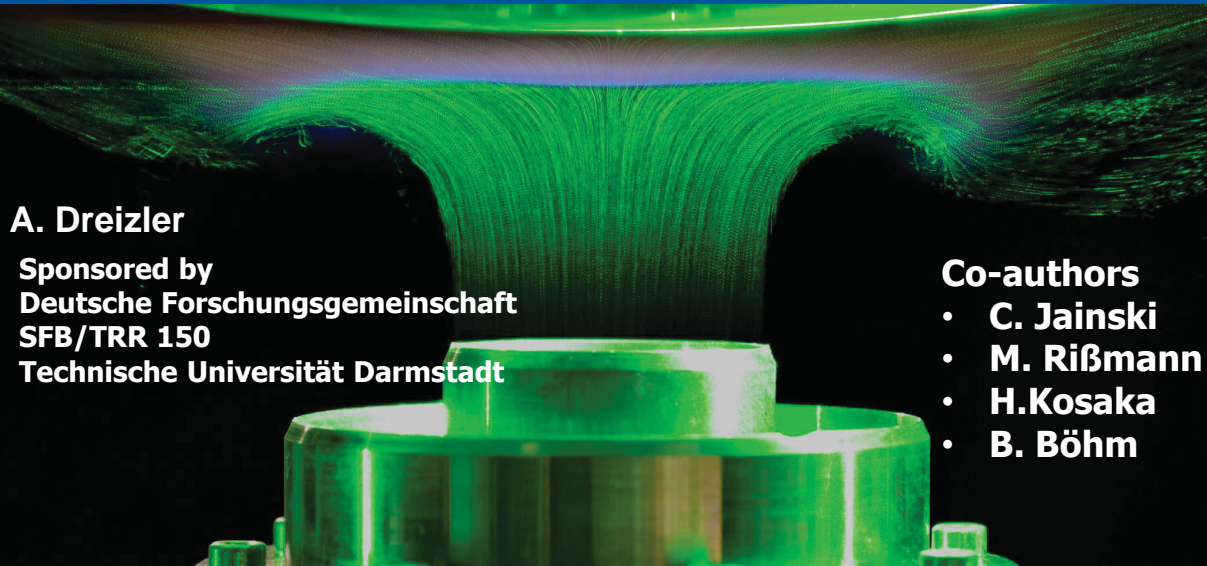
1. Dreizler, A., Böhm, B., Proc. Combust. Inst. 35 (2015) 37-64.

2. Jainski, C., Rissmann, M., Böhm, B., Dreizler, A., Proc. Combust. Inst. <http://dx.doi.org/10.1016/j.proci.2016.07.113>.
3. Mann, M., Jainski, C., Euler, M., Böhm, B., Dreizler, A., Comb. Flame 161 (2014) 2371-2386.
4. Oijen, J. van, Goey, L. de, Combustion Science and Technology 161 (1) (2000) 113–137
5. Smooke, M. D., Giovangigli, V., Lecture Notes in Physics, vol. 384, pp. 1–28, Springer-Verlag, 1991.
6. Smith, G. P., Golden, D. M., Frenklach, M., Moriarty, N. W., Eiteneer, B., Goldenberg, M., Bowman, C. T., Hanson, R. K., Song, S., Gardiner, W. C., Lissianski, V. V., Qin, Z., GRI-MECH 3.0, URL http://www.me.berkeley.edu/gri_mech/, 1999.

Flame wall interactions New Target Configuration for TNF?



Institute Reactive Flows and Diagnostics RSM,
TU Darmstadt



A. Dreizler

Sponsored by
Deutsche Forschungsgemeinschaft
SFB/TRR 150
Technische Universität Darmstadt

Co-authors

- **C. Jainski**
- **M. Reißmann**
- **H. Kosaka**
- **B. Böhm**

28.07.2016 | TNF 13 | FWI-Session | Andreas Dreizler | 1

Outline



- Motivation - why Flame-Wall Interaction (FWI) suits the TNF
- Experimental Approach at TU Darmstadt
- Side Wall Quenching
 - Flow field and flame brush
 - Flame dynamics of turbulent flames
 - Flame surface density
 - Mean reaction rate modelling
 - Boundary layers: non-reactive versus reactive cases
 - Thermo-chemical states: CO versus T
 - Laminar flames
 - Turbulent flames
 - Conclusions

} Paper 1A10

28.07.2016 | TNF 13 | FWI-Session | Andreas Dreizler | 2



Flame-wall interaction (FWI)

- Topical subject with relevance for
 - Safety technology: flame arresters
 - Catalytically assisted combustion
 - Micro-combustion
 - Gas turbine combustion (lean, low NO_x)
 - Internal combustion engines (cold start, downsizing)



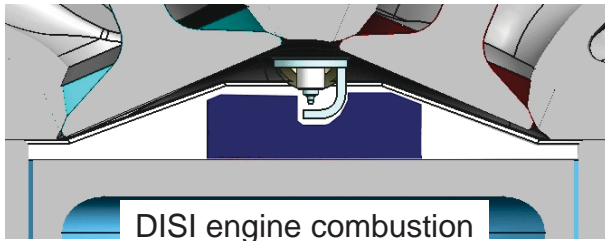
Davy's mine lamp
British Museum (1817)

General properties of FWI

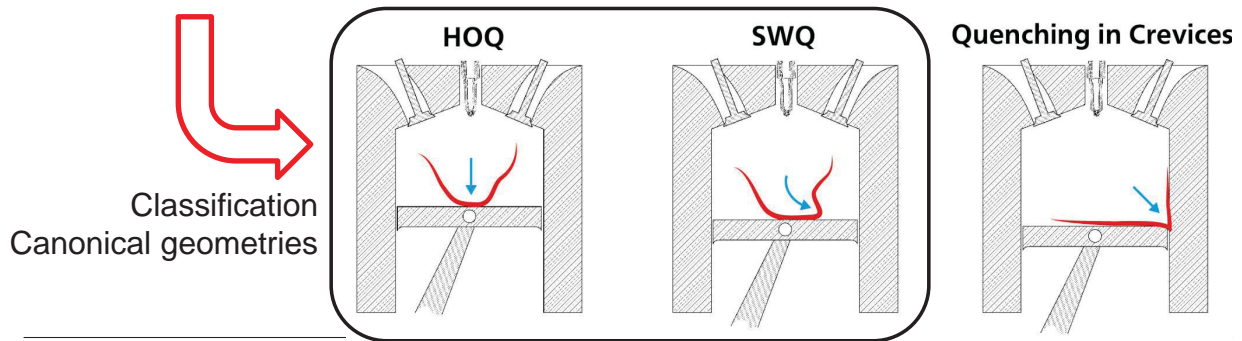
- When flame approaches closer than a few flame thicknesses to the wall (for premixed combustion)
 - Intense coupling between flame and wall
 - Large heat fluxes (exceeding 1 MW/m² for HC-fuels at 1 bar)
 - Flame quenching causing incomplete combustion
 - Emission of unburned hydrocarbons and CO
 - Relevant especially for engine combustion
 - Contribution to heat loss ~30%
 - Contribution to unburned hydrocarbons ~40%

Flame-Wall Interaction in IC engines

- Focus here: **premixed** flames

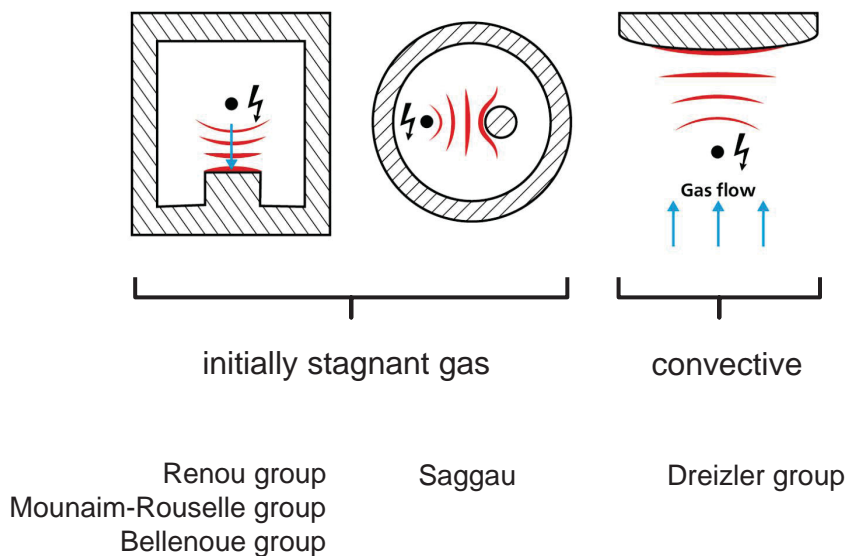


Cinematographic Mie scattering of evaporating droplets



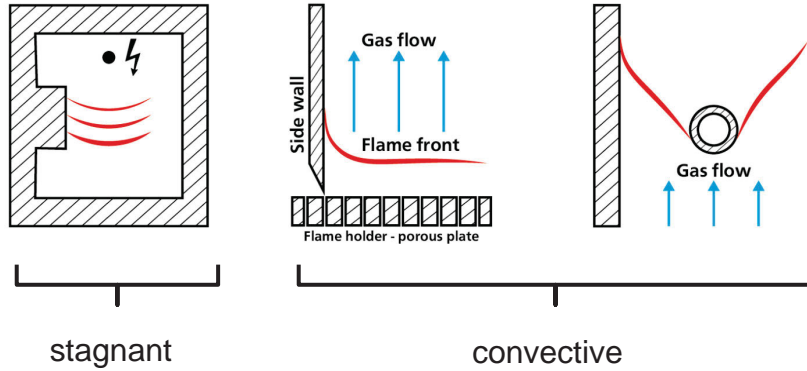
28.07.2016 | TNF 13 | FWI-Session | Andreas Dreizler | 5

Head-on quenching – canonical geometries



28.07.2016 | TNF 13 | FWI-Session | Andreas Dreizler | 6

Sidewall quenching – canonical geometries



Bellenoue group.

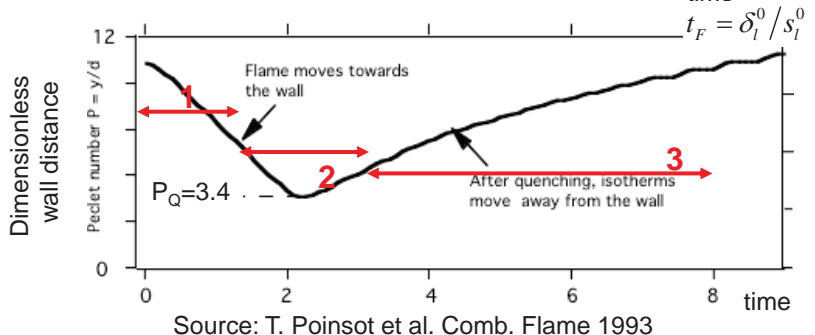
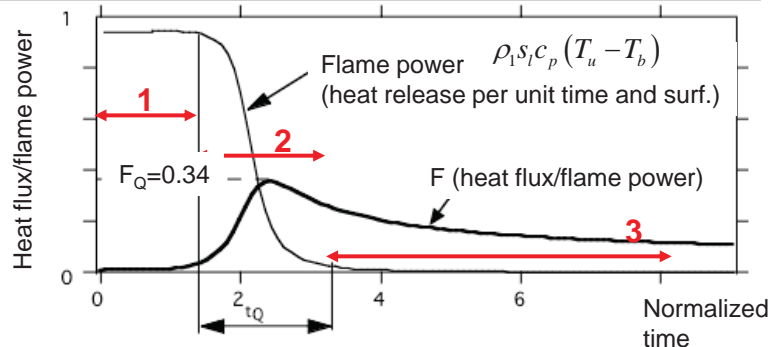
Clendening group
Saffmann
Schulz, Dreier group

Escudie group
Dreizler group

Laminar head-on quenching: results of 1D-DNS

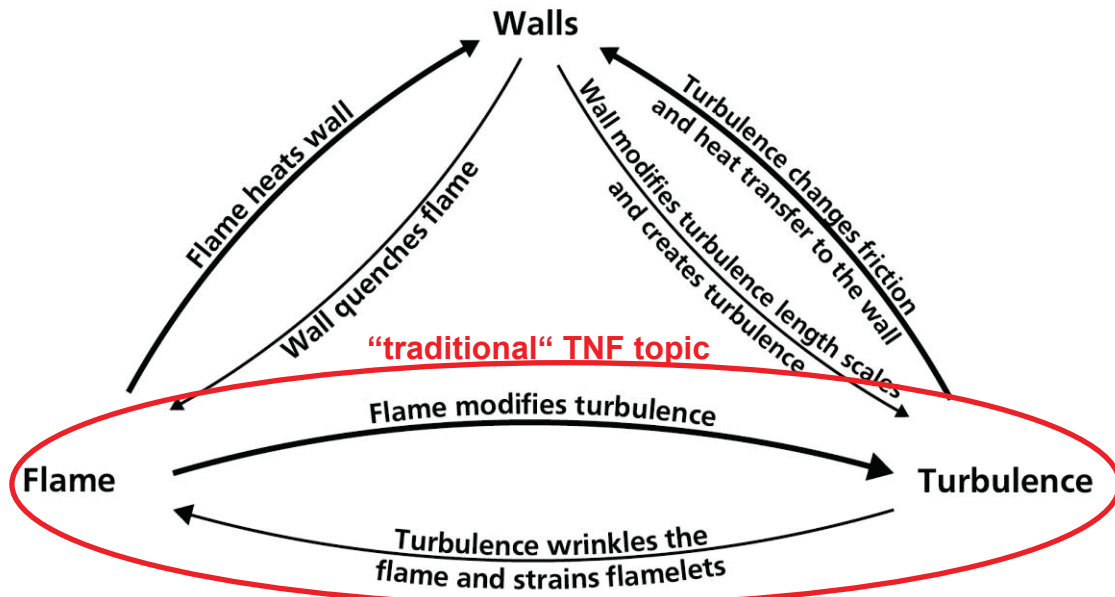
Three stages

- Flame approach (1)
- Flame quenching (2)
- Post-quench period (3)



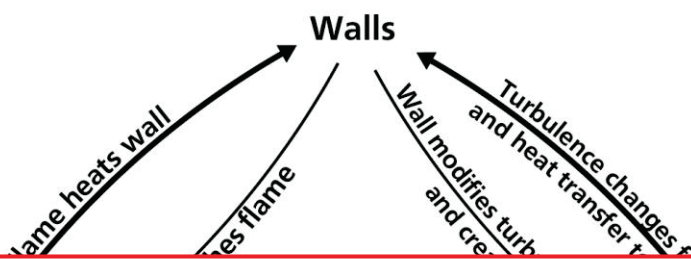
Source: T. Poinset et al. Comb. Flame 1993

Impact of turbulence in FWI



Source: T. Poinso and D. Veynante, Theoretical and Numerical Combustion 2005

Impact of turbulence in FWI



Studied by DNS (Poinso, Haworth, Bruneaux, Rutland, Chen, Gruber, ...)

Still very limited number of comprehensive experimental studies going beyond quenching distances and heat transfer

See review article A. Dreizler, B. Böhm, PCI 35, 2015

→ DNS and experiemntal data available for model developing and testing

Great topic for TNF: extension of turbulence-chemistry interaction

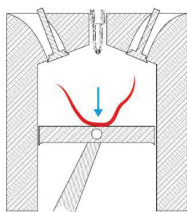
Source: T. Poinso and D. Veynante, Theoretical and Numerical Combustion 2005

Outline

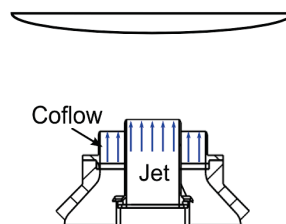
- Motivation - why Flame-Wall Interaction (FWI) suits the TNF
- **Experimental Approach at TU Darmstadt**
- Side Wall Quenching
 - Flow field and flame brush
 - Flame dynamics of turbulent flames
 - Flame surface density
 - Mean reaction rate modelling
 - Boundary layers: non-reactive versus reactive cases
 - Thermo-chemical states: CO versus T
 - Laminar flames
 - Turbulent flames
 - Conclusions

Fundamental Flame-Wall Interaction

Head-on quenching

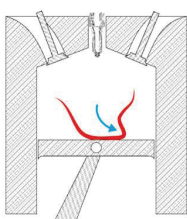


HOQ Burner

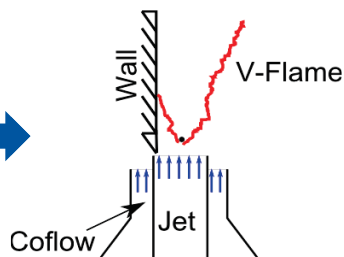


- transient
- 1D when laminar
- flame ignited by laser spark
- low sample number

Side-wall Quenching

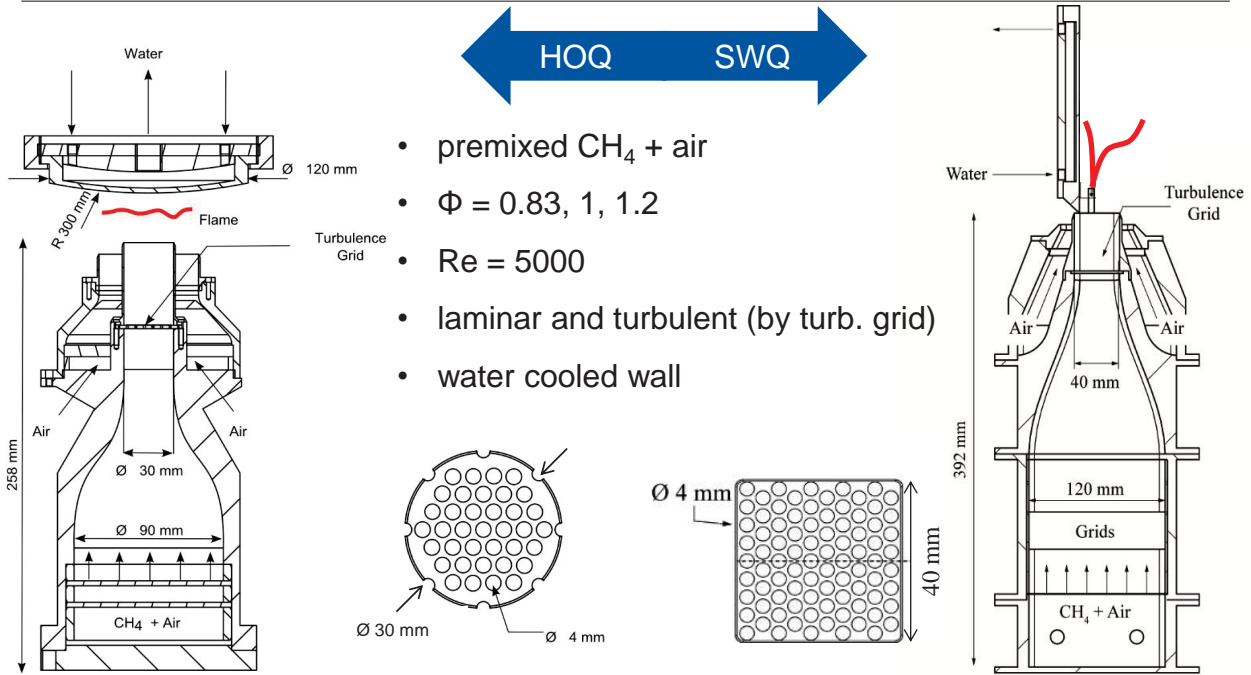


SWQ Burner



- Statistically stationary
- 3D
- high sample number

Experimental conditions

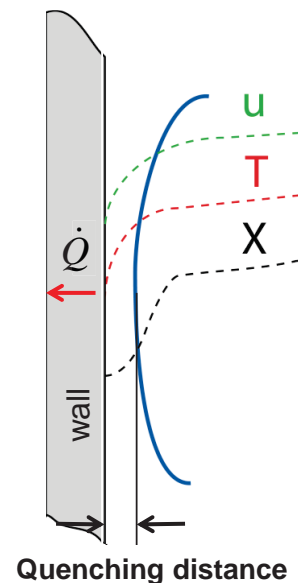


28.07.2016 | TNF 13 | FWI-Session | Andreas Dreizler | 14

Experiments in FWI: parameters of interest

- Quenching distances, visualization of flames near walls
- Wall temperature and heat flux \dot{Q}
- Flow field studies near walls
 - Velocity boundary layers **u**
- Reaction rates near walls → see paper 1A10; 1B05
- Thermo-chemical states during FWI
 - Thermal boundary layers **T**
 - Concentration boundary layers **X**

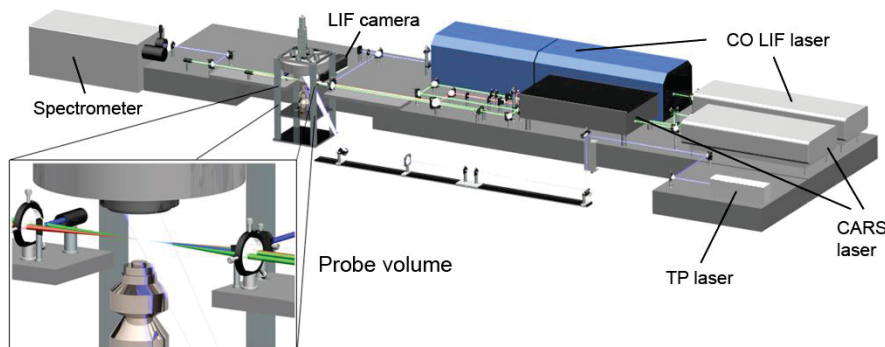
Focus today



28.07.2016 | TNF 13 | FWI-Session | Andreas Dreizler | 15

Measurement techniques

Gas Velocity	Flame Front Position	Gas Temperature	CO Concentration
(Stereo) Particle Image Velocimetry (PIV)	Planar LIF of OH radical Flame front from OH gradient	ro-vibrational ns-CARS	Two Photon LIF of CO molecule
2 D/3 Components Rep. Rate: 10 kHz	2 D Rep. Rate: 10 kHz/10 Hz	0 D Rep. Rate: 10 Hz	0 D Rep. Rate: 10 Hz



28.07.2016 | TNF 13 | FWI-Session | Andreas Dreizler | 16

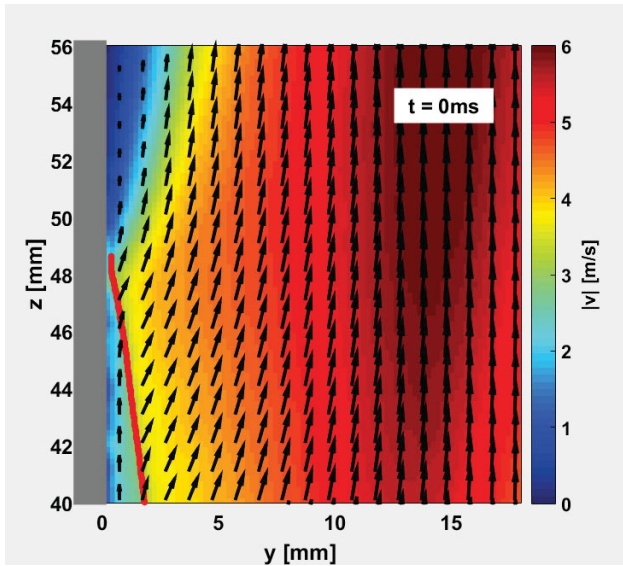
Outline

- Motivation - why Flame-Wall Interaction (FWI) suits the TNF
- Experimental Approach at TU Darmstadt
- **Side Wall Quenching**
 - **Flow field and flame brush**
 - Flame dynamics of turbulent flames
 - Flame surface density
 - Mean reaction rate modelling
 - Boundary layers: non-reactive versus reactive cases
 - Thermo-chemical states: CO versus T
 - Laminar flames
 - Turbulent flames
 - Conclusions

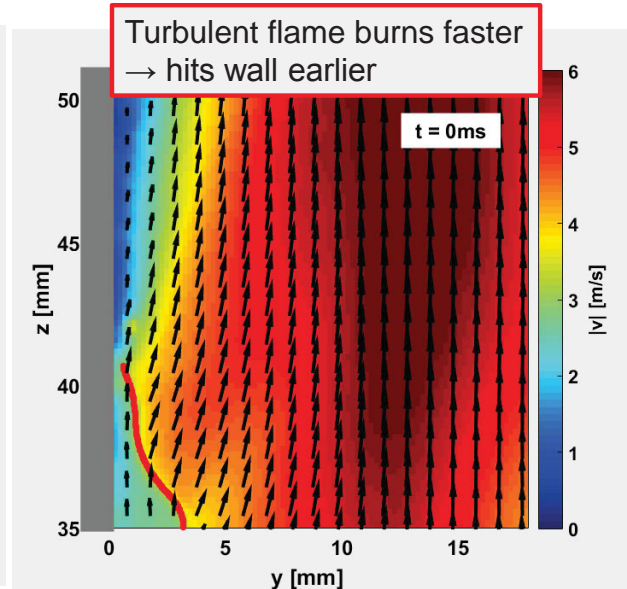
28.07.2016 | TNF 13 | FWI-Session | Andreas Dreizler | 17

Laminar vs. turbulent flame – instantaneous flame front and flow field

laminar, $\phi = 1.0$

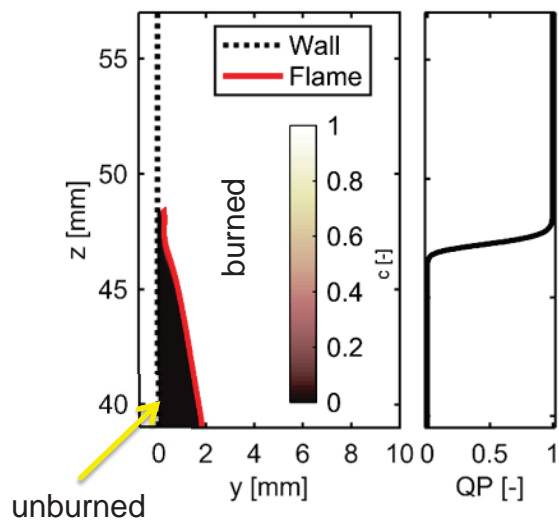


turbulent, $\phi = 1.0$

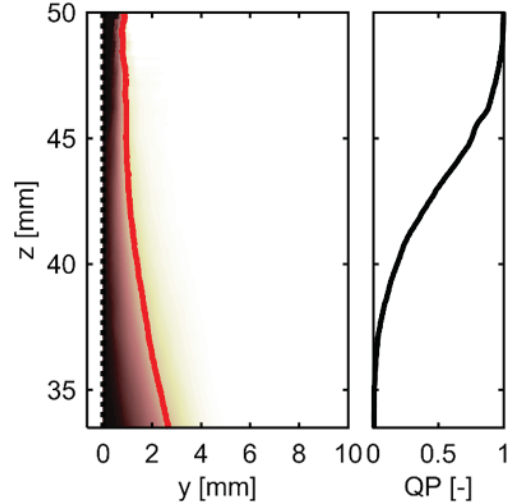


Flame brush and quench probability

laminar



turbulent

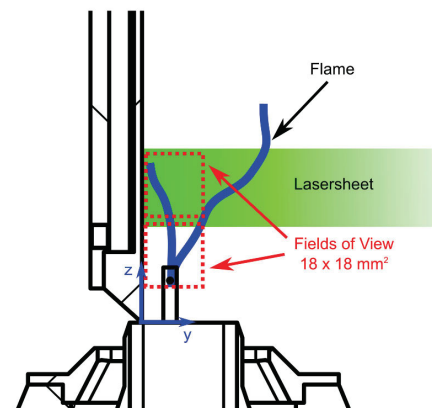


Outline

- Motivation - why Flame-Wall Interaction (FWI) suits the TNF
- Experimental Approach at TU Darmstadt
- Side Wall Quenching
 - Flow field and flame brush
 - Flame dynamics of turbulent flames
 - Flame surface density
 - Mean reaction rate modelling
 - **Boundary layers: non-reactive versus reactive cases**
 - Thermo-chemical states: CO versus T
 - Laminar flames
 - Turbulent flames
- Conclusions

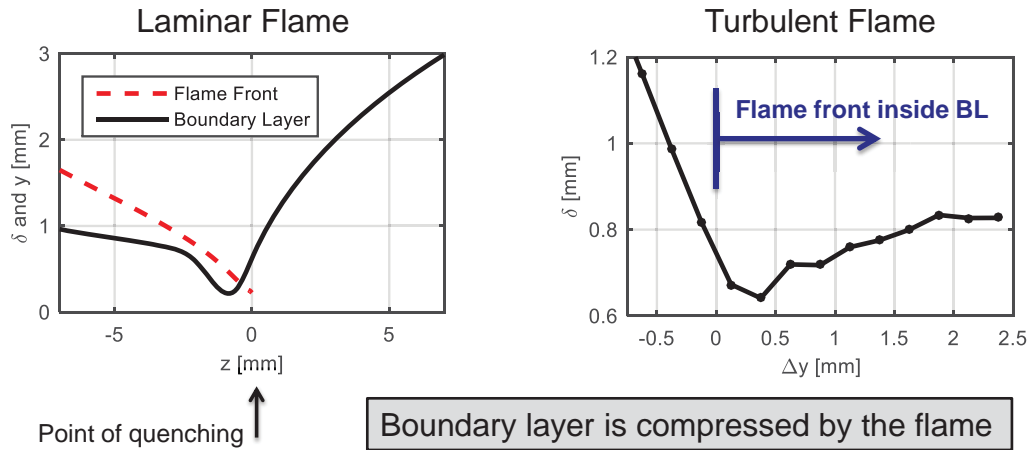
PIV/OH-PLIF: Experimental Setup

- Simultaneously PIV and OH-PLIF at 10 kHz and 20 Hz
- Two fields of view ($18 \times 18 \text{ mm}^2$)
- PIV
 - Al_2O_3 particles
 - 2D/2C
 - 32x32 pixel interrogation windows
 - 75% overlap
- OH
 - High speed dye laser system ($35 \mu\text{J}/\text{pulse}$)
 - $\text{Q}_1(6)$ -line
 - Canny-edge filter for flame front detection



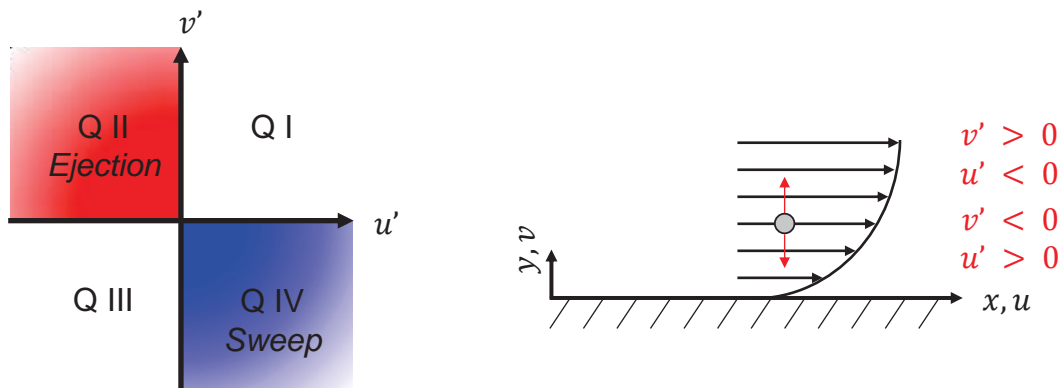
Boundary Layer Thickness δ

- Difficult to define δ in a reacting boundary layer
- Here: $\delta = 0.95 \cdot U_\infty$ with U_∞ = free stream velocity in unburned regions



Quadrant-Splitting Scheme

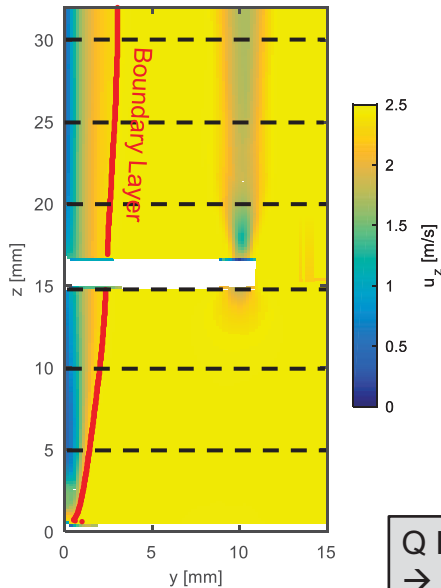
- Turbulent motions in the boundary layer classified in a $u'v'$ quadrant-splitting scheme (Wallace et al. (1972) and Willmarth & Lu (1972))
- Responsible for turbulence production and destruction (Reynolds stress $-\overline{\rho u'v'}$)



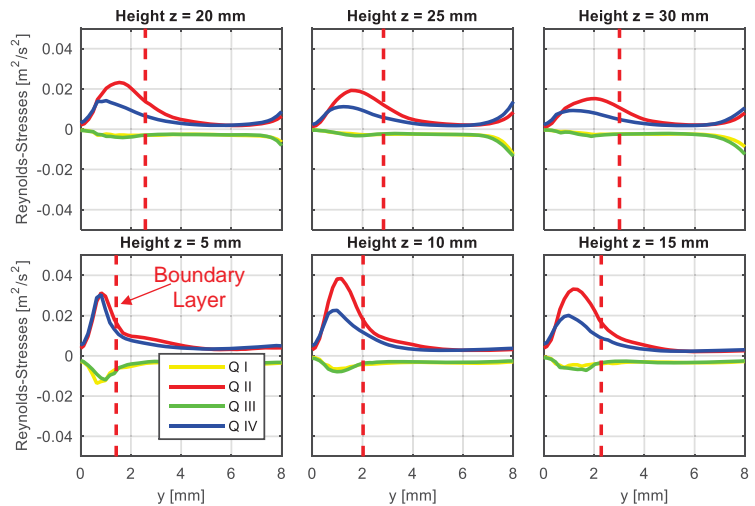
S.K. Robinson, Annu. Rev. Fluid Mech. 1991: Quadrants II and IV are dominant in a turbulent boundary layer → turbulence production

Cold Turbulent Boundary Layer

Mean Axial Velocity



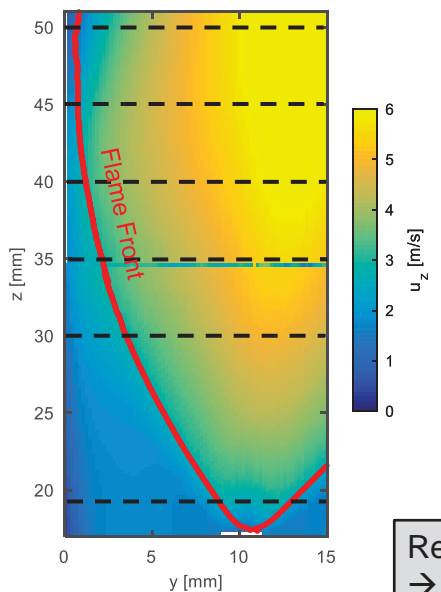
Quadrant Contribution



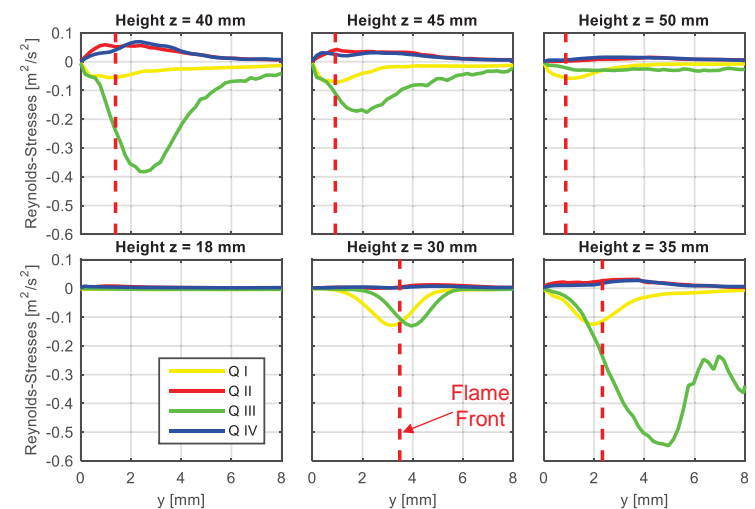
Q II and IV are also dominant in the experimental data
→ turbulence production, in accordance to literature

Hot Turbulent Boundary Layer

Mean Axial Velocity



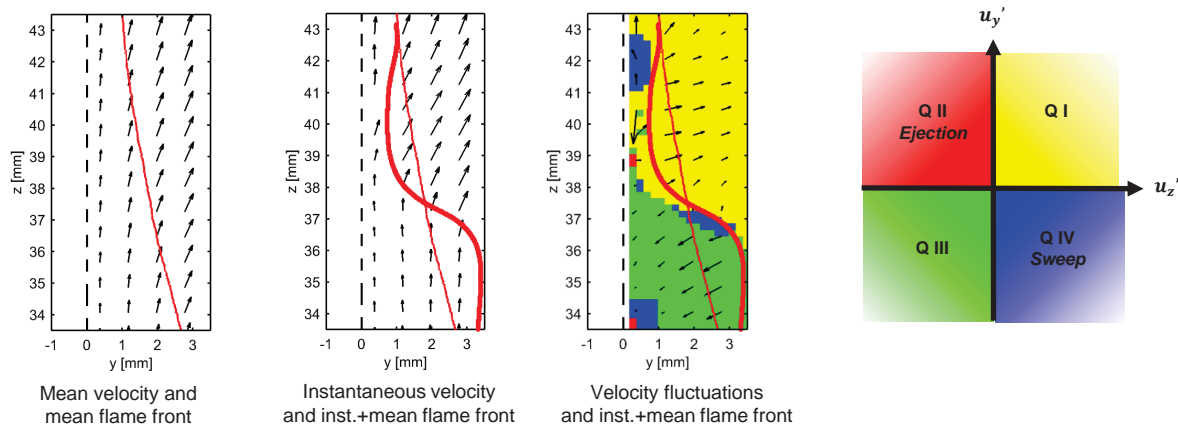
Quadrant Contribution



Regime change from Q II and IV to Q I and III
→ turbulence destruction, consistent with DNS by
Alashaalan & Rutland, Combust. Sci. Technol. 2002

Flame/Turbulence Interaction

- Velocity **boundary layer thickness** compressed by flame
- Quadrant analysis shows that Reynold stresses **switch** from turbulence production (ejection and sweeps) **to turbulence damping**
- Turbulent flame dominates boundary layer properties at FWI-zone



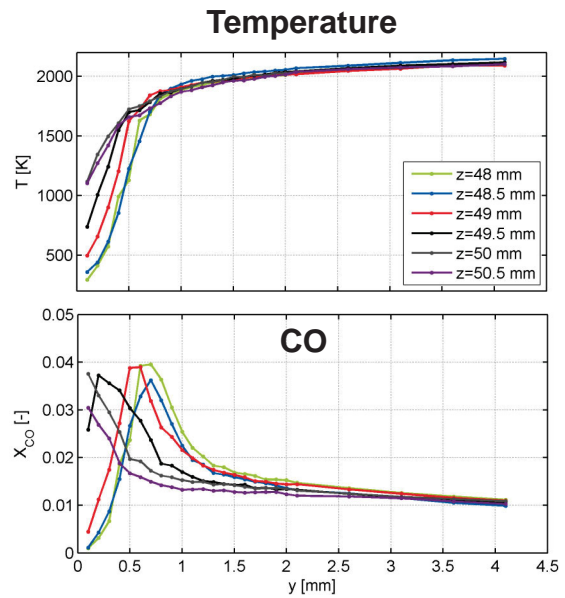
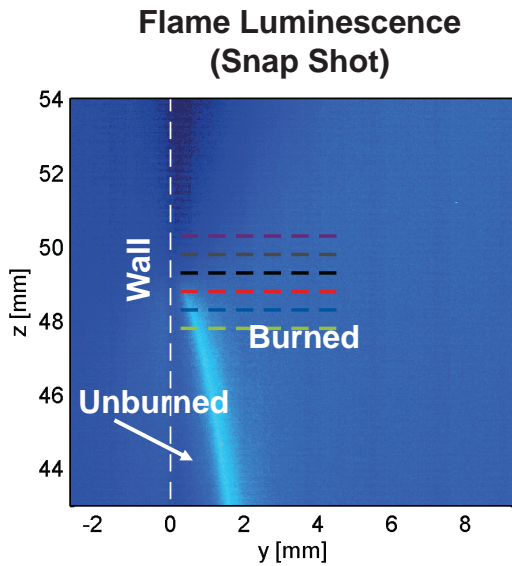
28.07.2016 | TNF 13 | FWI-Session | Andreas Dreizler | 26

Outline

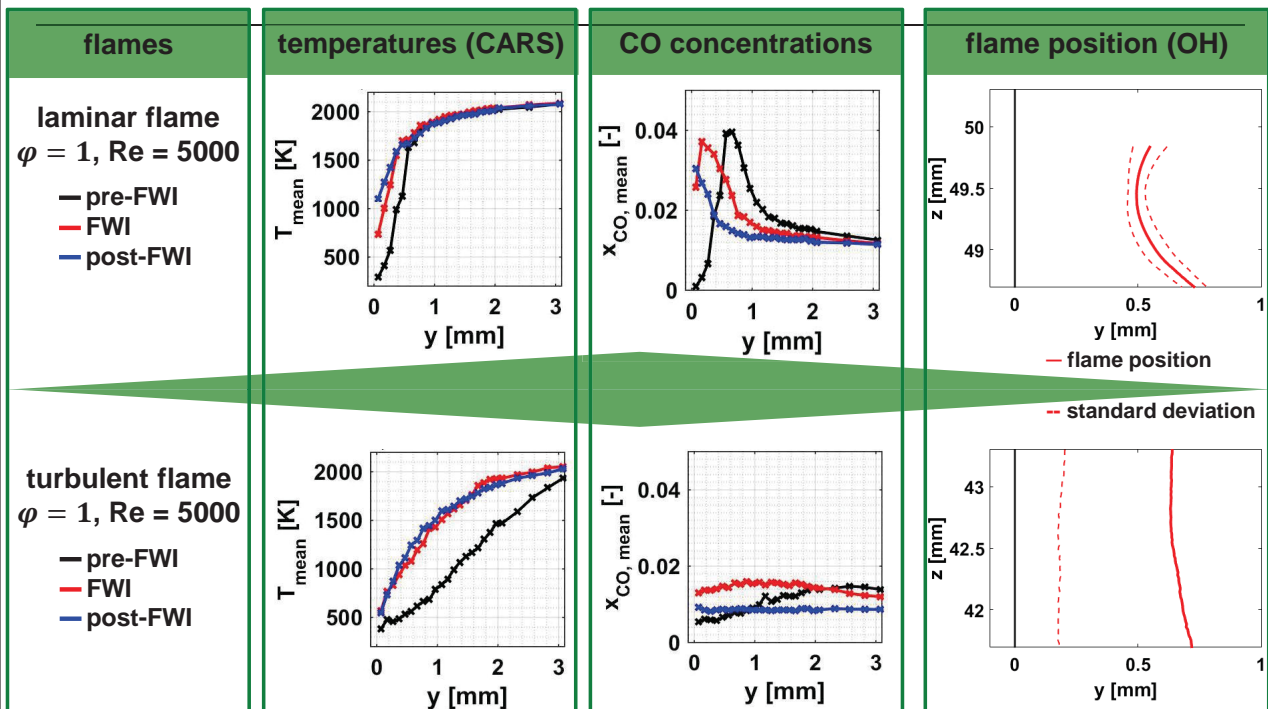
- Motivation - why Flame-Wall Interaction (FWI) suits the TNF
- Experimental Approach at TU Darmstadt
- Side Wall Quenching
 - Flow field and flame brush
 - Flame dynamics of turbulent flames
 - Flame surface density
 - Mean reaction rate modelling
 - Boundary layers: non-reactive versus reactive cases
 - **Thermo-chemical states: CO versus T**
 - **Laminar flames**
 - **Turbulent flames**
 - Conclusions

28.07.2016 | TNF 13 | FWI-Session | Andreas Dreizler | 27

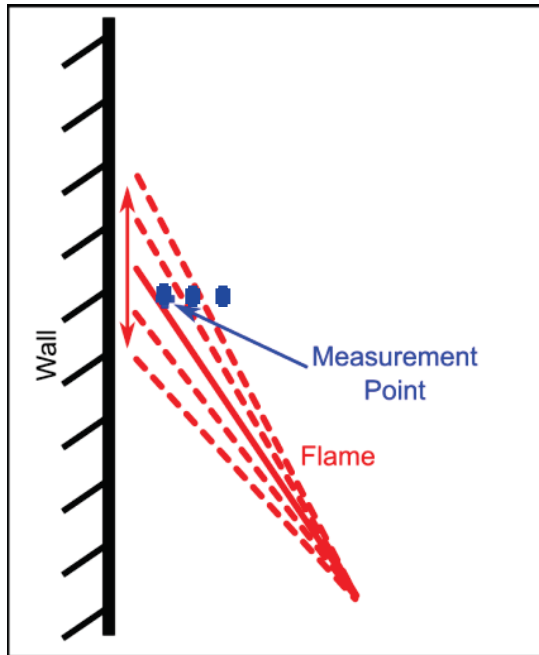
Laminar side wall quenching ($Re = 5000$, $\Phi = 1.0$, w/o TG)



Mean quantities reveal significant differences between laminar and turbulent flames



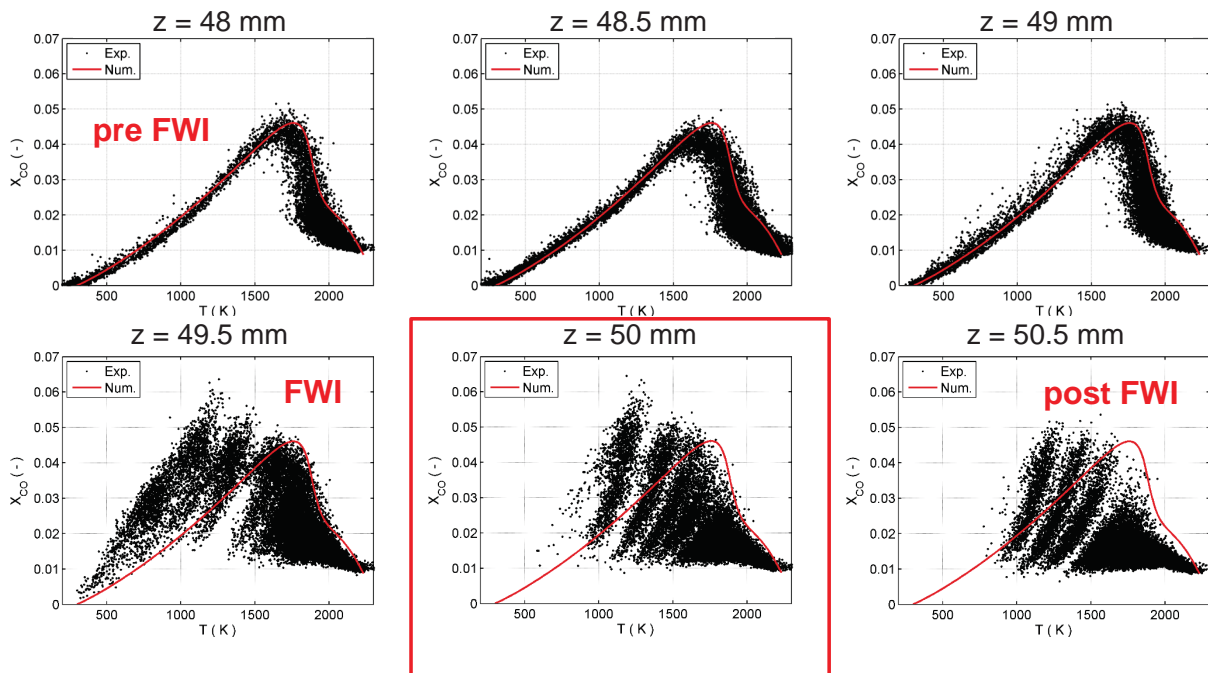
Space-fixed measurement of thermo-chemical states



28.07.2016 | TNF 13 | FWI-Session | Andreas Dreizler | 30



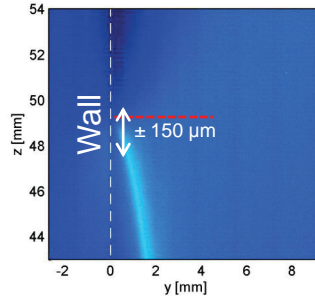
Thermo-chemical states – laminar (Re = 5000, $\Phi = 1.0$, w/o TG)



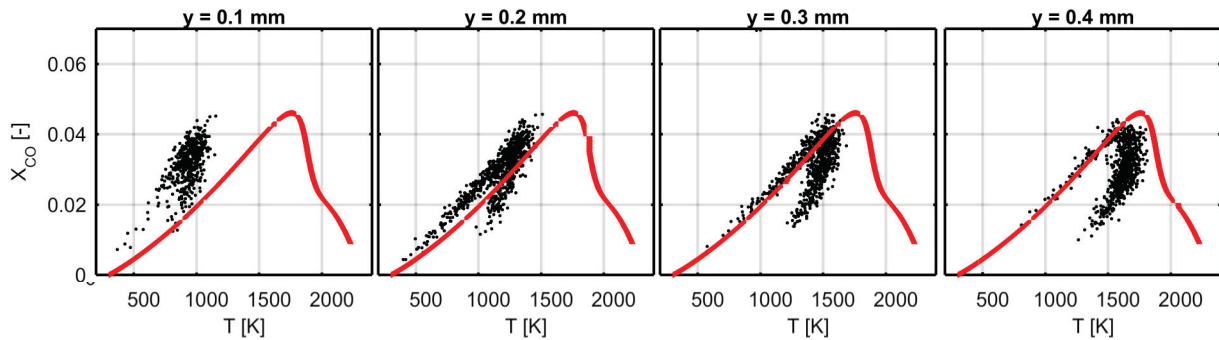
28.07.2016 | TNF 13 | FWI-Session | Andreas Dreizler | 31



Thermo-chemical states for $z = 50.0$ mm ($Re = 5000$, $\Phi = 1.0$, w/o TG)

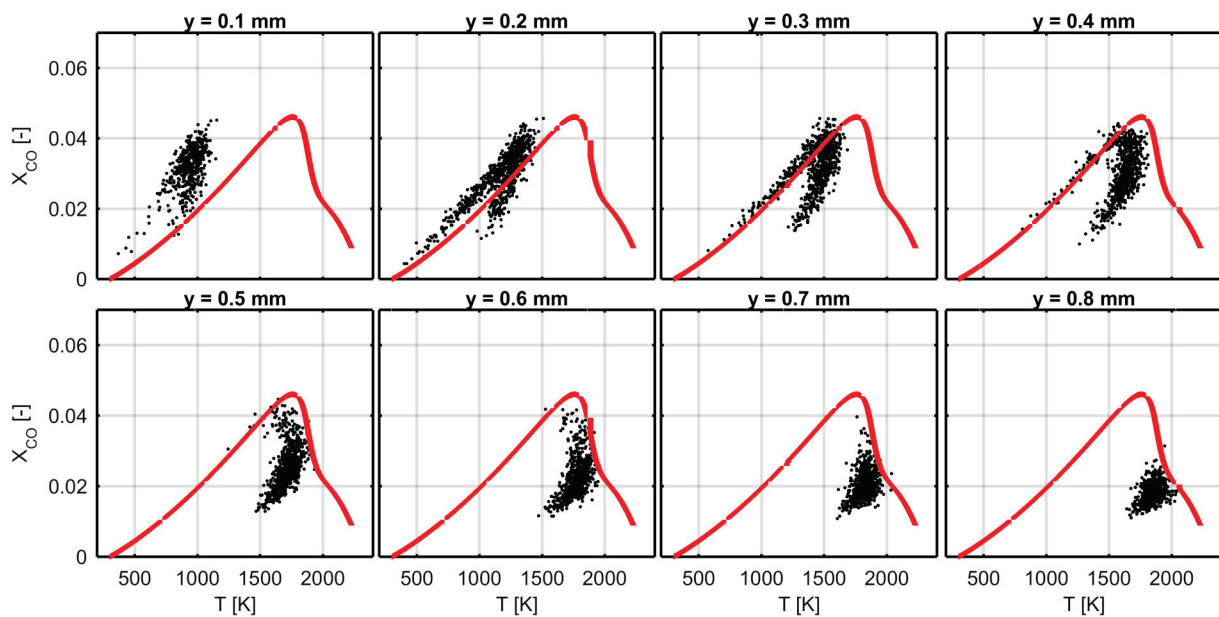


- Spatial conditioning (axial & wall-normal)
- Flame tip fluctuates up and down ($\pm 150 \mu\text{m}$)
- Different thermo-kinetic states in one measurement point



28.07.2016 | TNF 13 | FWI-Session | Andreas Dreizler | 32

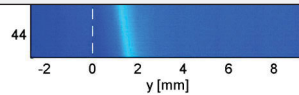
Thermo-chemical states for $z = 50.0$ mm ($Re = 5000$, $\Phi = 1.0$, w/o TG)



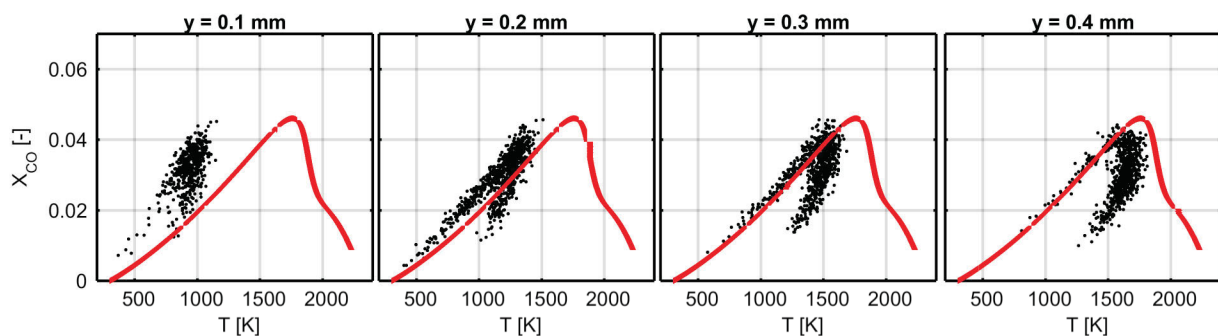
28.07.2016 | TNF 13 | FWI-Session | Andreas Dreizler | 33

Thermo-chemical states for $z = 50.0$ mm ($Re = 5000$, $\Phi = 1.0$, w/o TG)

- **CO-consumption branch:** strongly influenced for wall distances $y < 0.8$ mm
 - **CO-production branch:** influence starts for $y \leq 0.2$ mm
 - **Time-scales** of CO-consumption a factor of 100 larger than for CO-production
- **Heat losses more pronounced for CO-consumption branch**

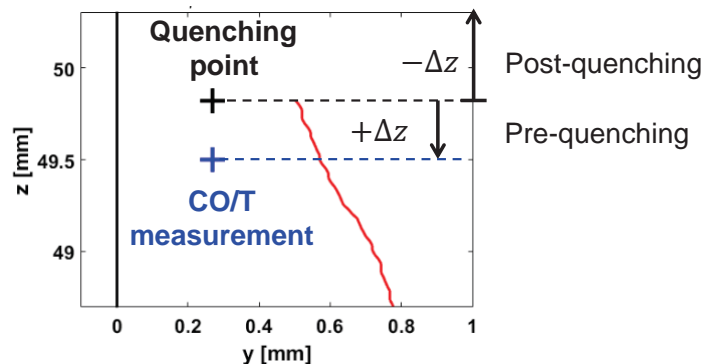
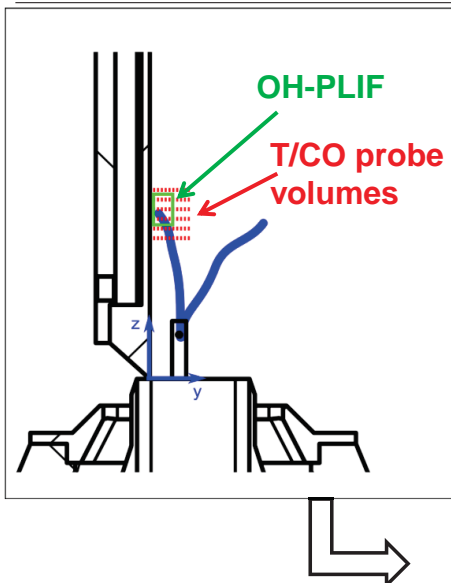


→ Different thermo-kinetic states in one measurement point



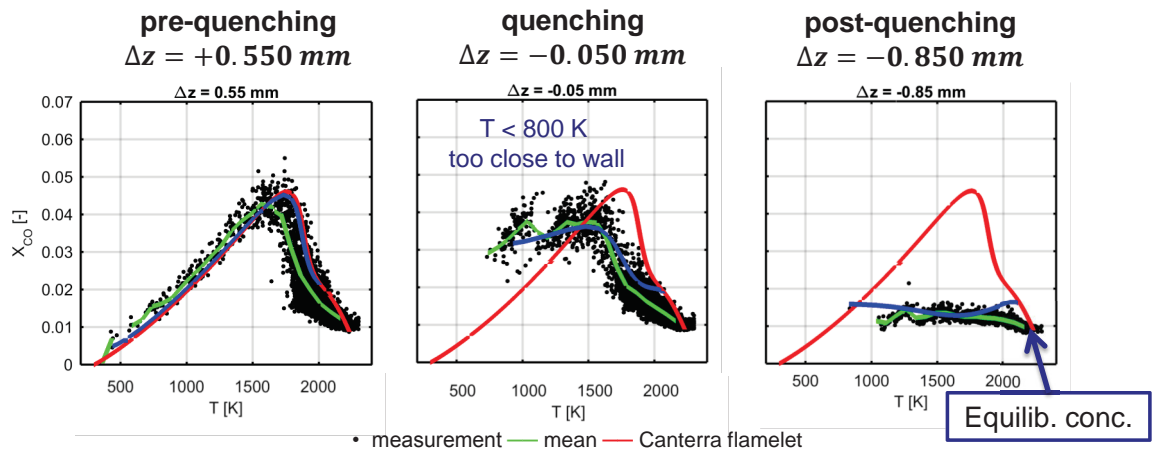
28.07.2016 | TNF 13 | FWI-Session | Andreas Dreizler | 34

Analysis of thermo-chemical states relative to quenching point – flame fixed



28.07.2016 | TNF 13 | FWI-Session | Andreas Dreizler | 35

Conditioning on quenching – flame fixed analysis

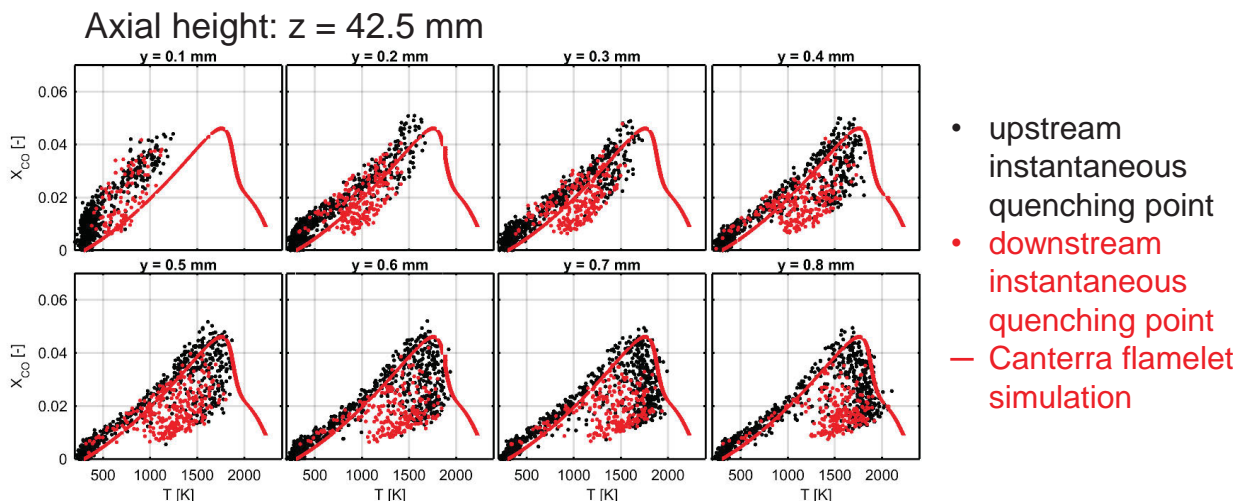


Pre-quenching: undisturbed flame

Quenching and post-quenching: strong deviation from undisturbed flame

J. Janicka: Comparison to 2D-DNS reveals **dominance of diffusion** over kinetic effects that cause this observation

Turbulent flame – space fixed analysis ($\phi = 1$, $Re = 5000$, with TG)



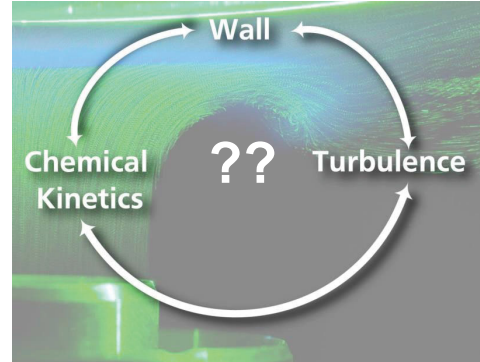
→ Similar to laminar case but with more intermediate states

→ **CO-consumption more influenced than CO-production**

CO-consumption takes place at time-scales significantly longer than time-scales typical for heat transfer

Conclusions – thermo-chemical states

- Significant differences of CO-T-scatter plots compared to adiabatic flames
 - Comparison to 2D DNS (not shown) reveals for CH₄-flames that **diffusion** rather than low temperature chemistry is **dominant**
 - Quenching of flames near walls is observed at **small spatial scales**
- Implication for combustion modeling:
- High resolution required
 - Appropriate turbulence-chemistry-interaction models needed to account for presence of wall



Thank you for your kind attention

Open issues for flame-wall interaction (1)

- For steady and unsteady flame-wall interaction a more detailed understanding is required with regard to...
 - ...Structure of velocity boundary layers
 - ...Structure of thermal boundary layers
 - ...Structure of concentration boundary layers
 - Unsteady heat transfer and impact of turbulent heat flux
 - ...
- **Valid models for near-wall turbulent combustion to be developed**
- Understanding the influence of
 - Wetted surfaces (fuel or oil films)
 - Deposits

Experiments
Theory
Modeling
Simulation

FWI research at RSM/TUD – people and paper



A. Dreizler



B. Böhm



M. Mann
2009 - 13



C. Jainski
2011 -



M. Reißmann
2014 -



H. Kosaka
2015 -

- **Mann, M., et al.:** *Transient flame-wall interactions: Experimental analysis using spectroscopic temperature and CO concentration measurements.* Combust. Flame (2014).
- **Dreizler, A., et al.:** *Advanced laser diagnostics for an improved understanding of premixed flame-wall interactions.* Proceedings of the Combustion Institute (2015)
- **Jainski, C., et al.:** *Experimental Investigation of Flame Surface Density and mean Reaction Rate during Flame-Wall Interaction.* Proceedings of the Combustion Institute (2016)
- **Bohlin et al.:** *Ultrabroadband coherent Raman imaging for near-wall probing of flame-wall interactions: simultaneous thermometry and multispecies measurements,* Proceedings of the Combustion Institute (2016)

Measurement techniques

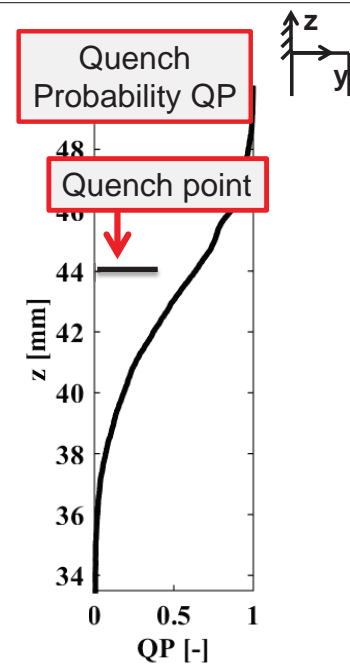
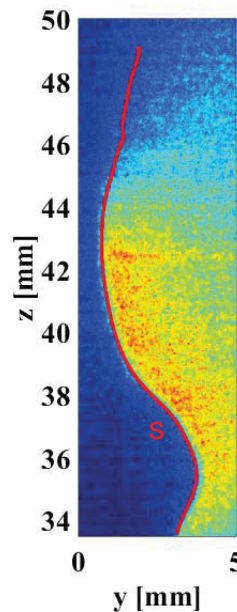
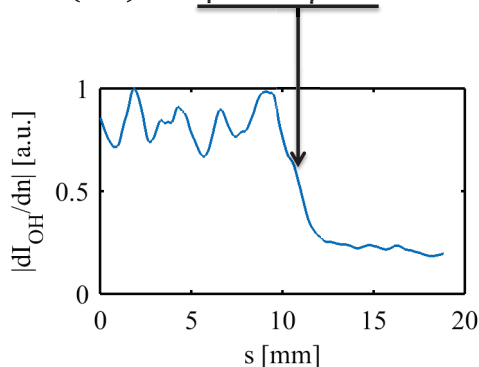
Fluid Velocity	Flame Front Position	Fluid Temperature	CO Concentration
Resolution: Wall-nearest loc.: ~0.4 mm	Resolution: Wall-nearest loc.: ~0.1 mm	Resolution: Wall-nearest loc.: ~0.05 mm	Resolution: Wall-nearest loc.: ~0.1 mm
Precision and Accuracy: similar to PIV far from walls	Uncertainty: ±0.05 mm	Precision: 2.5 – 8%	Precision: 8 – 11 % Accuracy: ≤20% in most regions
Challenge: Too few particles very close to wall, beam steering	Challenge: Noisy signal, IRO blurring	Challenge extension to 1D See paper 1B05	Challenge: Spatial resolution, calibration, 0D extension to 1D?

simultaneously

simultaneously

Post-processing of OH PLIF

- Flame front detection:
 - I. Canny-Edge-Filter
 - II. Threshold of flame-normal $\nabla(OH)$ for quench point



Modelling of turbulent premixed flames

- Flame surface density (FSD) model requires mean reaction rate $\overline{\dot{\omega}_R}$:
 1. turbulent flame \rightarrow ensemble of laminar flamelets
 2. flame-flow interaction \rightarrow local consumption speed s_l * flame surface density Σ

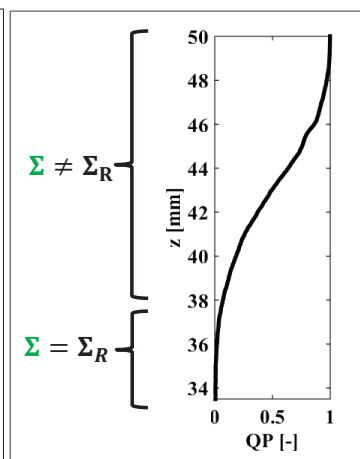
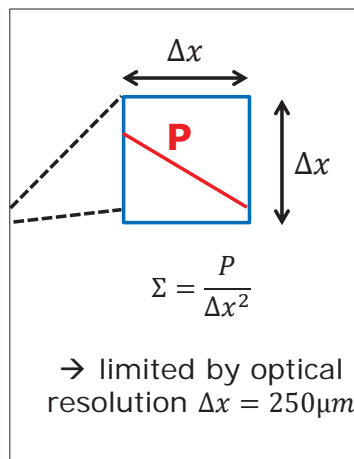
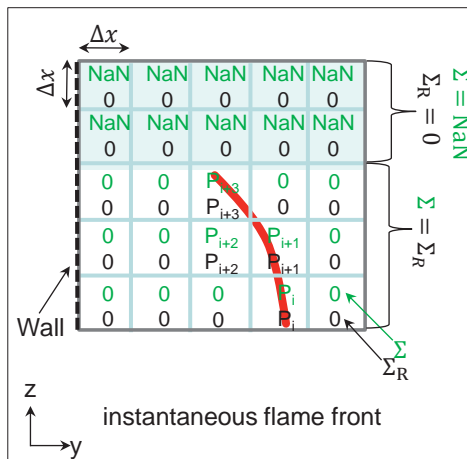
Density and fuel mass fraction of unburned mixture – **known**

$$\overline{\dot{\omega}_R} = \rho_1^0 Y_1^0 s_l \Sigma$$

↙
↘

OH PLIF + PIV **OH**

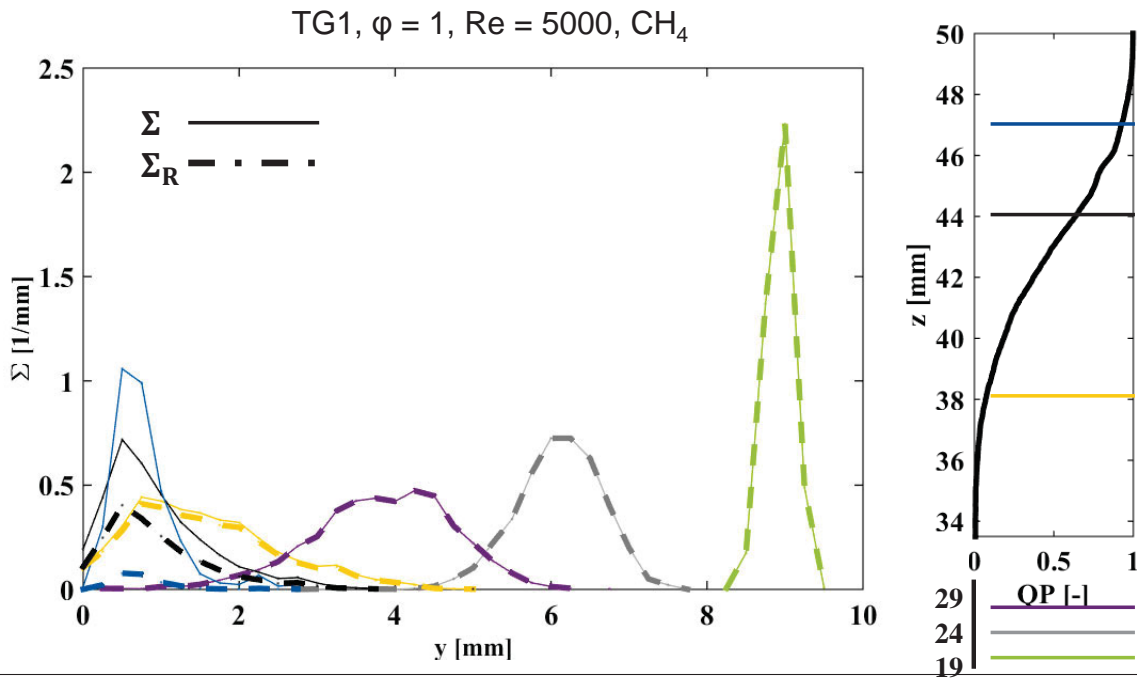
Flame surface density – definition



Σ **ignores** quenching
 Σ_R **considers** quenching

Probability of quenching as function of height z over nozzle exit

Flame surface density – results



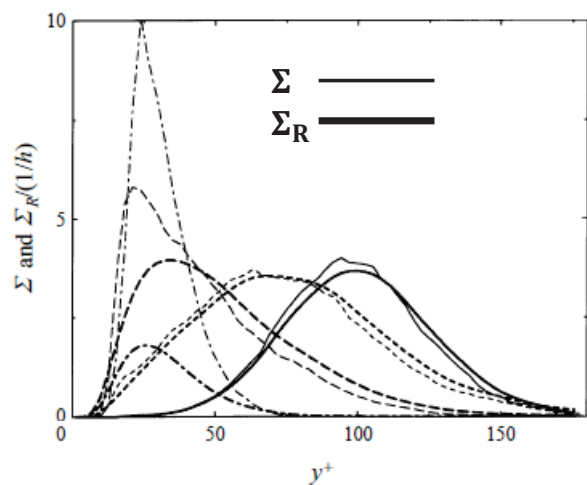
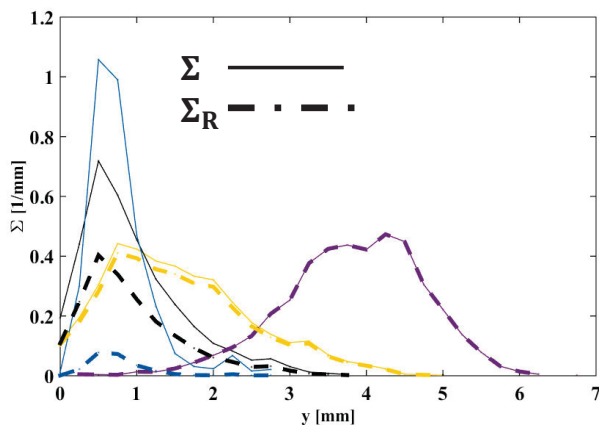
28.07.2016 | TNF 13 | FWI-Session | Andreas Dreizler | 46



Flame surface density – comparison to DNS

RSM 2015: **EXP**
SWQ configuration

Bruneaux et al. 1997: **SIM**
HOQ configuration

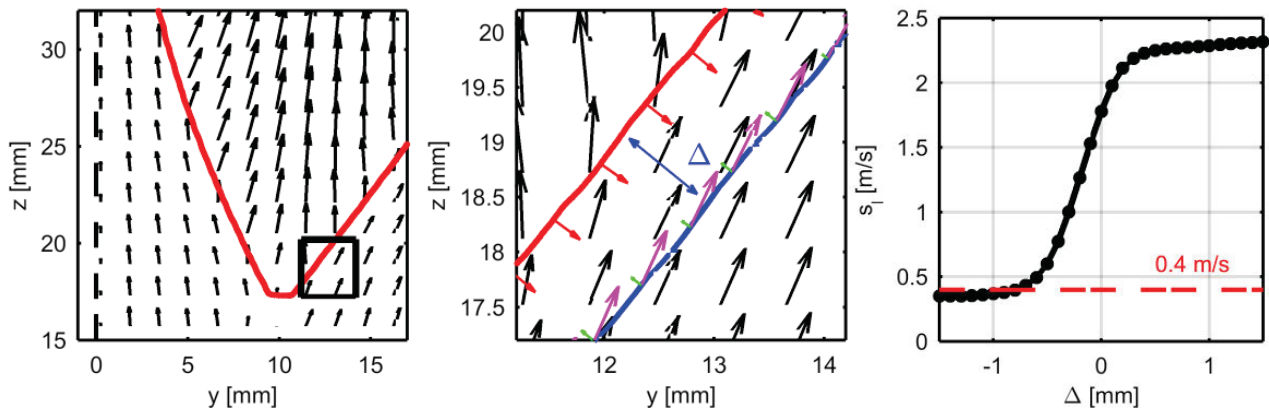


28.07.2016 | TNF 13 | FWI-Session | Andreas Dreizler | 47



Flame consumption speed s_l

- s_l determined from **laminar configuration**
- Use of undisturbed flame branch

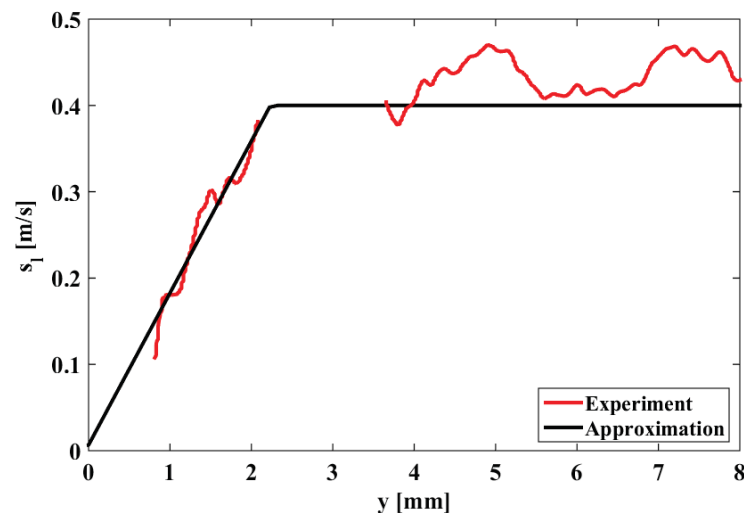


Green arrows: flame normal velocity components

1 mm ahead of flame front flame normal velocity matches laminar burning velocity

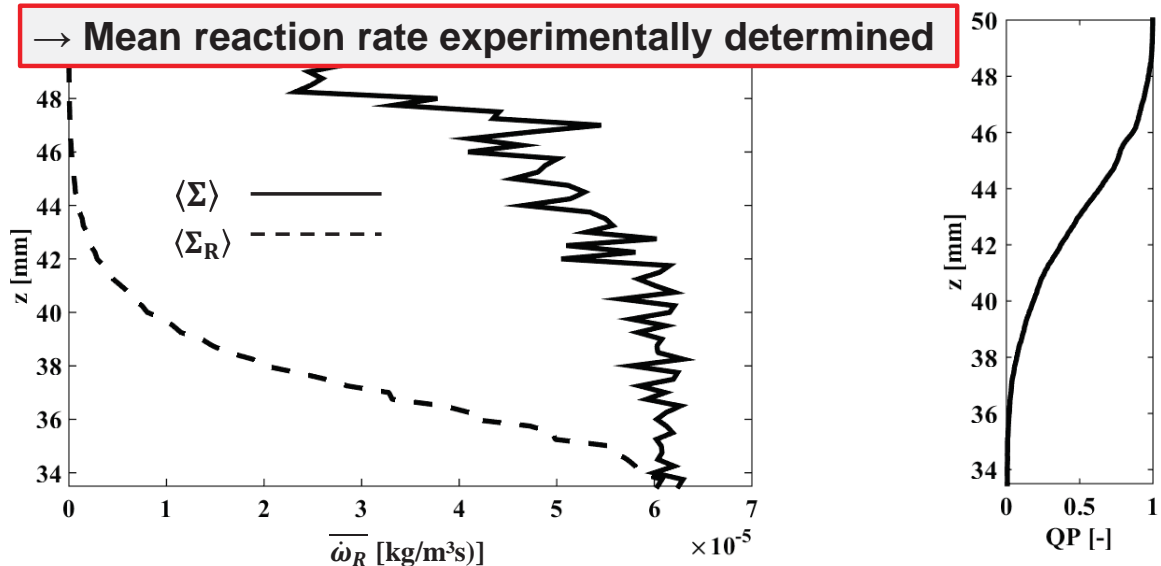
Flame consumption speed s_l

- wall closest point @ $y = 1$ mm,
because of s_l refers to unburnt
mixture



Mean reaction rate $\overline{\dot{\omega}_R}$

$$\overline{\dot{\omega}_R}(z) = \rho_1^0 Y_1^0 \langle s_l(y) \Sigma(y, z) \rangle$$



Conclusions from PIV-OH PLIF measurements

- **Impact of turbulence on FWI in SWQ-configuration:**
 1. Analysis of FSD Σ reveals:
 - Relaminarization of the flame near the wall
 - “Reacting“ FSD Σ_R necessary for correct SWQ description and modelling
 2. Mean reaction rate $\overline{\dot{\omega}_R}$:
 - Deduced from flame surface density
 - Important quantity for modelling
- **Comparison to literature:**
 - Good agreement with HOQ DNS from Bruneaux (1997)
 - FSD Σ_R agrees qualitatively well with model based on velocity fluctuations from Watkins (1996) – see Jainiski et al., PCI 2017

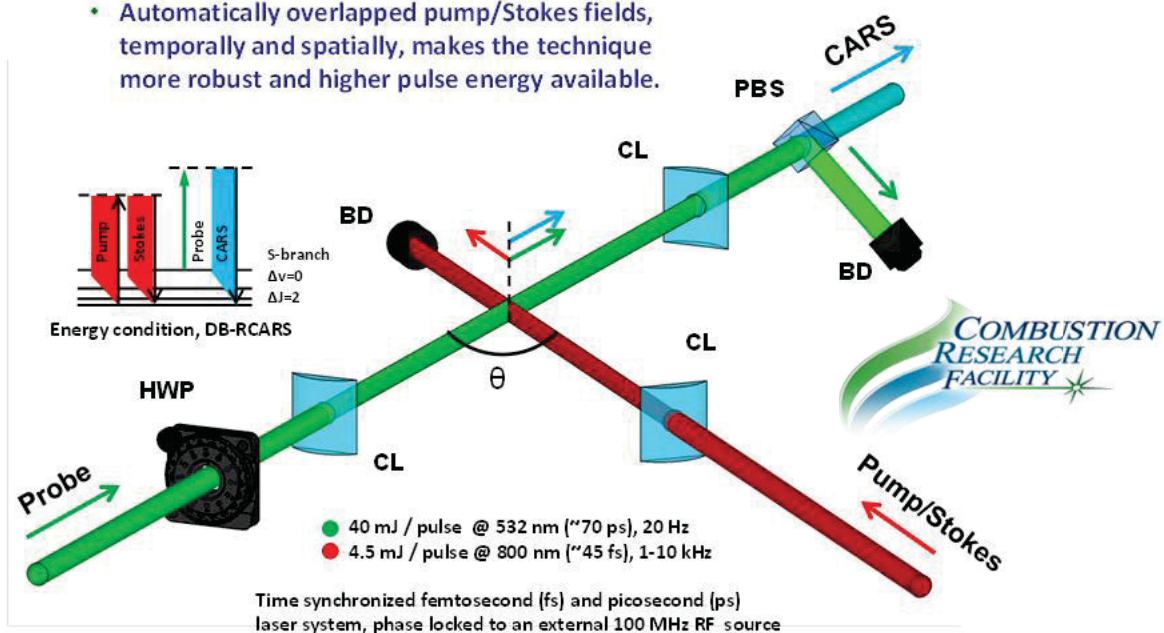
Open issues for diagnostics needs (2)

- Information lacking for:
 - Instantaneous structure of thermal boundary layers
 - Need for measurement of 1D-temperature profiles → **1D fs/ps CARS**
 - Unsteady heat transfer and impact of turbulent heat flux
 - Simultaneous temperature and velocity measurements near walls

Two-beam fs/ps hybrid 1D-CARS

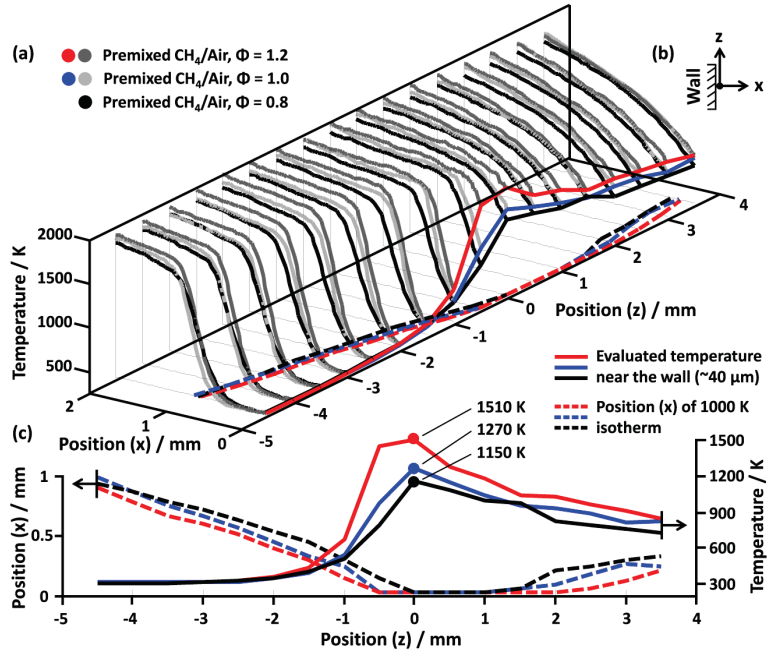
(A. Bohlin, C. Klierer – CRF Sandia Livermore, USA)

- Improved spatial resolution ($< 50 \mu\text{m}$).
- Automatically overlapped pump/Stokes fields, temporally and spatially, makes the technique more robust and higher pulse energy available.



Open issues for diagnostics needs (3)

- 1D-CARS-thermometry
- Cooperation with CRF-Sandia
- C. Kliewer, A. Bohlin, C. Jainski, A. Dreizler
- PCI 36, 2017

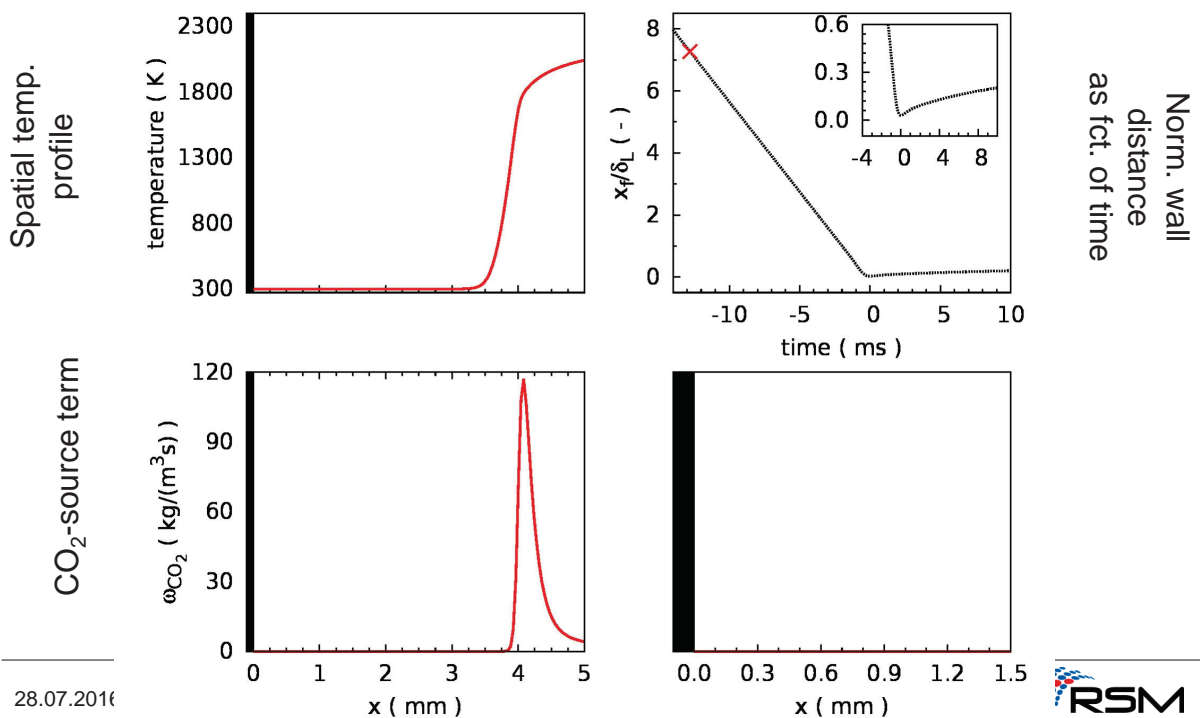


28.07.2016 | TNF 13 | FWI-Session | Andreas Dreizler | 54



Dynamics of HOQ: 1D-simulation

Source: T. Meier, G. Künne; A. Keteheun, J. Janicka (Darmstadt)



28.07.2016



blank

TNF 2016



Seoul, July 2014

Near wall reactive flows

J. Janicka



Institute for Energy and Powerplant Technology



Outline

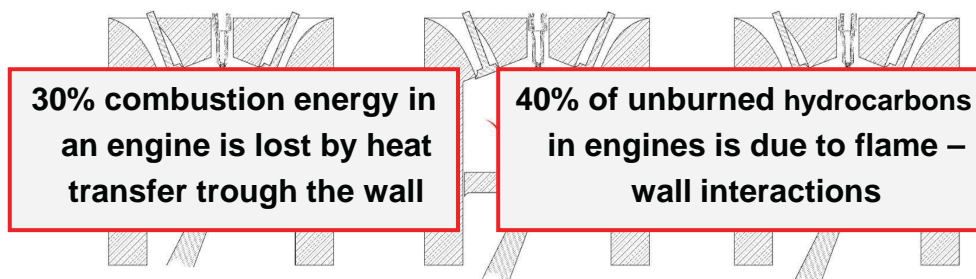
- **Motivation and challenges**
- **Contributions**
 - Andrea Gruber
 - Venkat Raman
 - Olivier Gicquel
 - Michael Pfitzner
 - Johannes Janicka
- **TNF strategy**

Outline

- **Motivation and challenges**
- **Contributions**
 - Andrea Gruber
 - Venkat Raman
 - Olivier Gicquel
 - Michael Pfitzner
 - Johannes Janicka
- **TNF strategy**

Technological and scientific significance

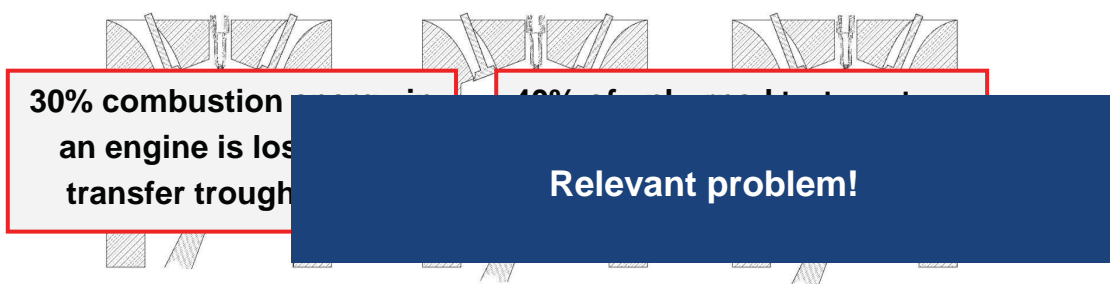
- e. g. in IC-Engines:
 - ▶ 90% of the charge burns in proximity of *cold* walls
 - ▶ Local quenching leads to UHC and CO formation
 - ▶ Geometrical complexity of the combustion chamber (cylinder) has a special influence



Courtesy of A. Dreizler

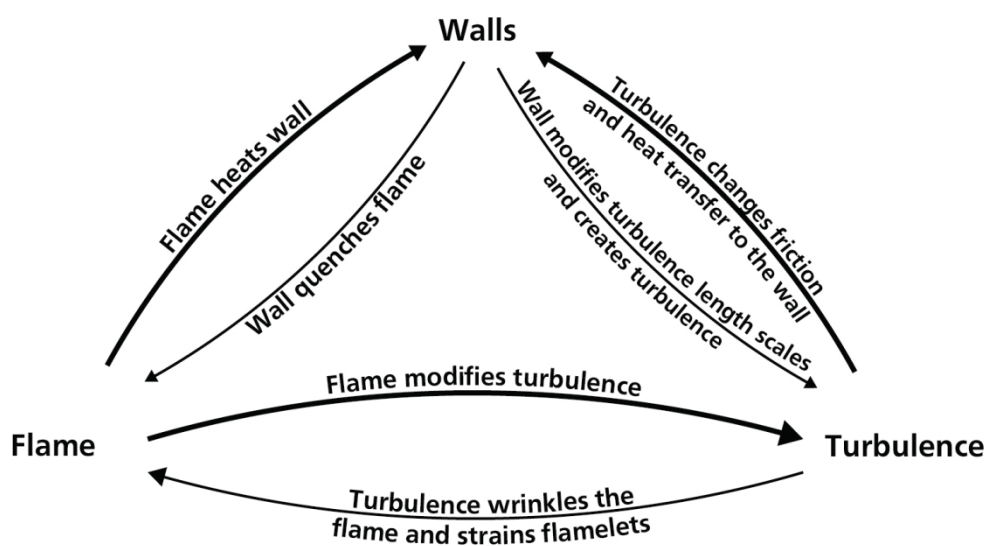
Technological and scientific significance

- e. g. in IC-Engines:
 - ▶ 90% of the charge burns in proximity of *cold* walls
 - ▶ Local quenching leads to UHC and CO formation
 - ▶ Geometrical complexity of the combustion chamber (cylinder) has a special influence



Courtesy of A. Dreizler

Scientific challenge



Source: Poinso and Veynante, Theoretical and Numerical Combustion 2005

Scientific challenge

- ▶ **Appropriate chemistry reduction strategy in presence of heat losses**
- ▶ **Appropriate low-temperature chemistry**
- ▶ **Appropriate turbulence-chemistry interaction (TCI)**
- ▶ **Two-way coupling for heat transfer**

Taken from Francesca's talk of 2014 TNF

Outline

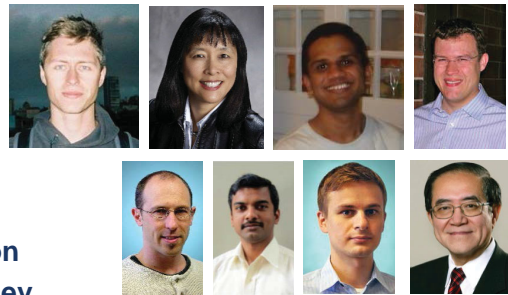
- **Motivation and challenges**
- **Contributions**
 - **Andrea Gruber**
 - **Venkat Raman**
 - **Olivier Gicquel**
 - **Michael Pfitzner**
 - **Johannes Janicka**
- **TNF strategy**

Acknowledgements

■ The work at SINTEF, DLR Stuttgart and TU Munich has been conducted with support from the BIGCCS Centre, performed under the Norwegian research program Centres for Environmental friendly Energy Research (FME). The authors acknowledge the following partners for their contributions: ConocoPhillips, Gassco, Shell, Statoil, TOTAL, GDF SUEZ and the Research Council of Norway (193816/S60).

■ The work at Sandia National Laboratories (SNL) was supported by the Division of Chemical Sciences, Geosciences, and Biosciences, Office of Basic Energy Sciences of the US Department of Energy (DOE). SNL is a multiprogramme laboratory operated by Sandia Corporation, a Lockheed Martin Company for the US DOE under Contract DE-AC04-94AL85000. Part of the work was supported by the Combustion Energy Frontier Research Center (CEFRC), an Energy Frontier Research Center funded by the US DOE, Office of Science, Office of Basic Energy Sciences (BES) under Award No. DESC0001198. This research used resources of the Oak Ridge Leadership Computing Facility at the Oak Ridge National Laboratory, which is supported by the Office of Science of the US DOE under Contract No. DE-AC05-00OR22725.

- Sandia NL: Dr. Jacqueline H. Chen and Hemanth Kolla
- NREL: Dr. Ray W. Grout
- University of New South Wales: Prof. Evatt R. Hawkes
- Oak Ridge NL: Dr. Ramanan Sankaran
- University of Southampton: Prof. Edward S. Richardson
- Princeton University: Prof. C.K. Law and Dr. Damir Valiev



DNS FWIs cases (1)

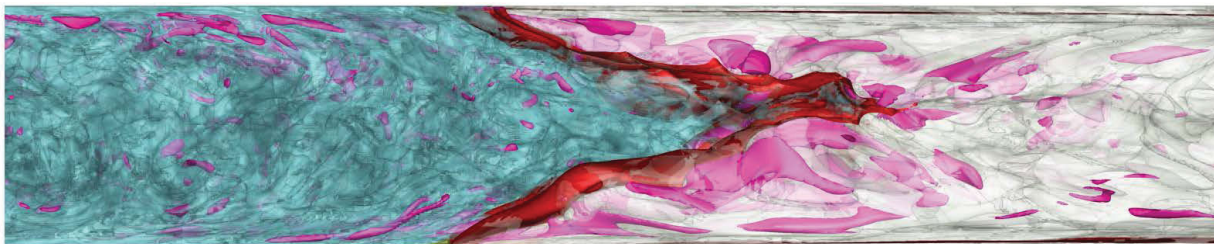
Shared parameter space: $Re_\tau \sim 180$ ($Re_c \sim 3200$), hydrogen-air mix, $T_u = 750K$, $T_w = 750K$



Anchored v-flames (2010), premixed $\phi=1.5$



Freely-propagating flames (2012-2016), premixed $\phi=0.55$ and stratified $0.2 < \phi < 1.2$



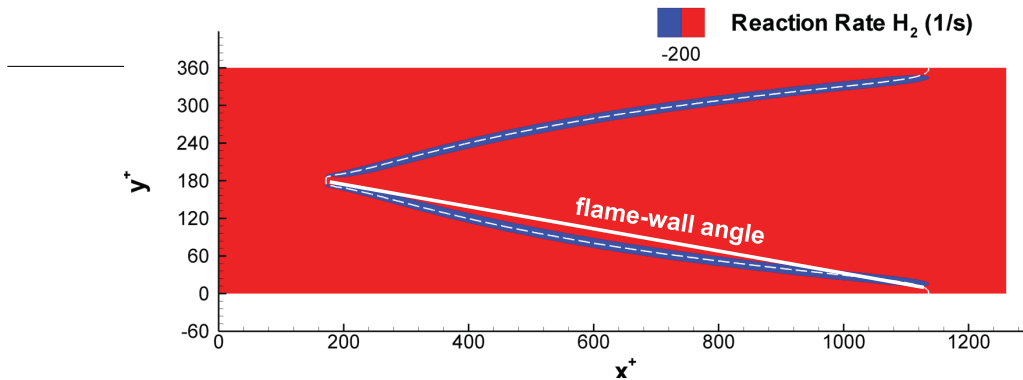
DNS FWIs cases (2)

Proposed validation metrics for RANS/LES

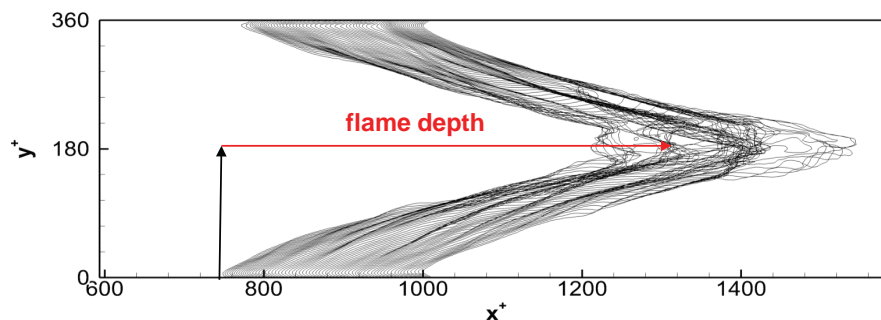
1. Global flame shape
 - Mean flame-wall angle in anchored case
 - Mean flame depth in freely propagating case
2. Mean wall heat flux value and downstream location in anchored case
3. Size and strength of reverse flow pockets in freely propagating case
4. Laboratory reference global flame front speed in freely propagating case
5. ...

Metrics 1 & 2 constitute a first model approximation, while 3 & 4 pose more severe requirements on the model's accuracy!

Global Flame Shape

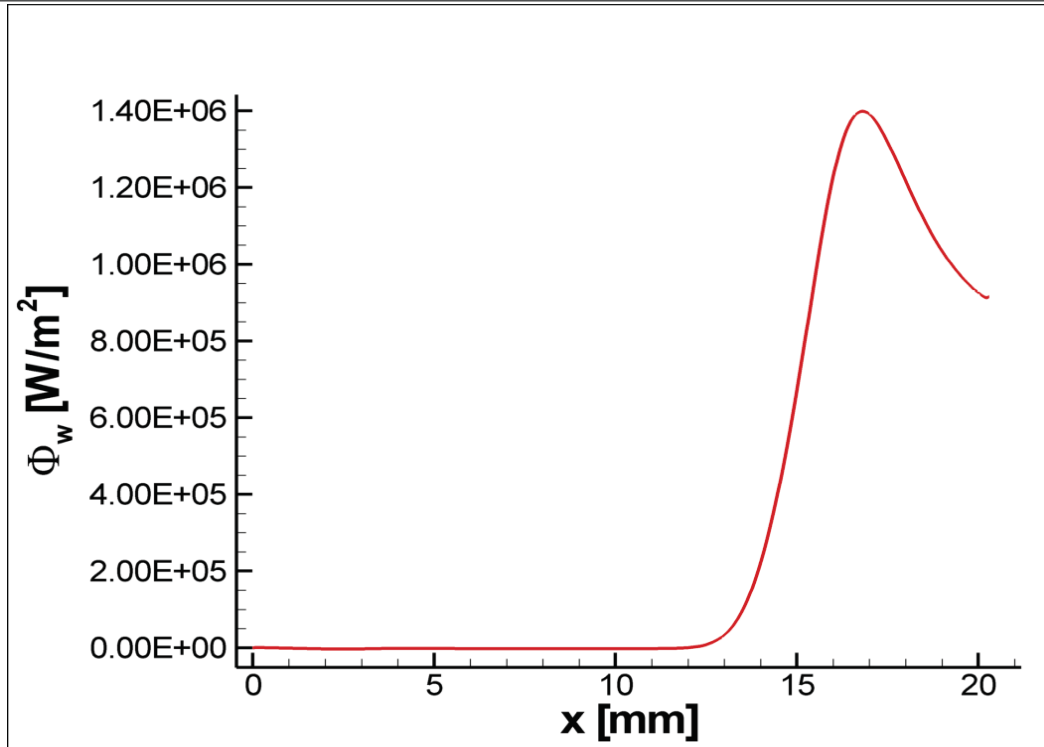


➤ **Anchored case: the model has to reproduce the mean flame-wall angle and wall impingement location**



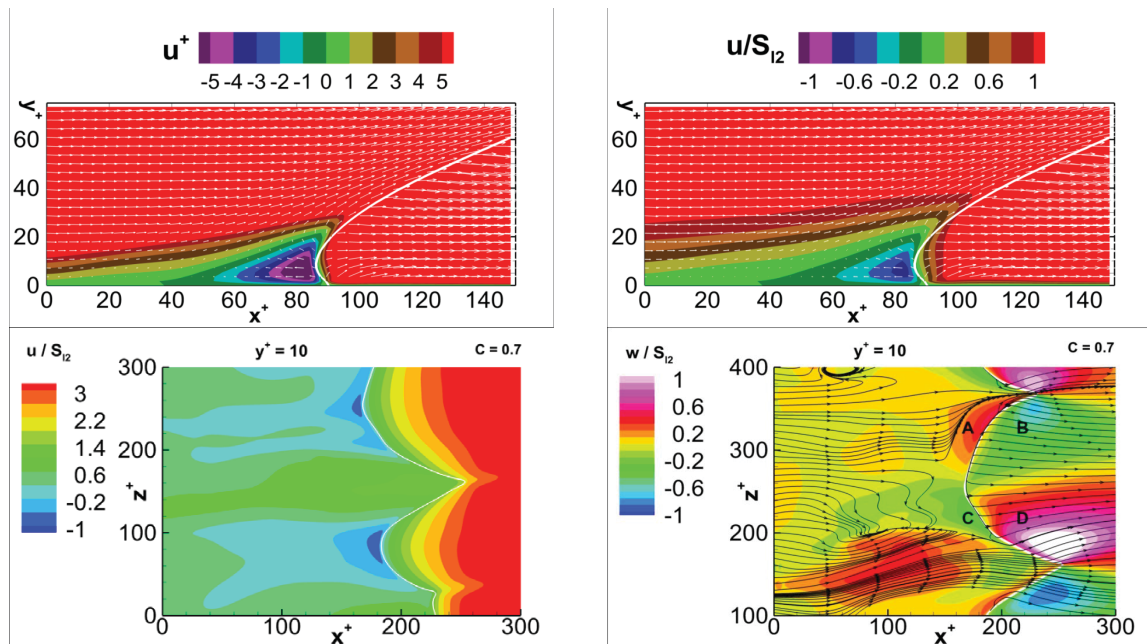
➤ **Freely propagating case: the model has to reproduce the mean flame depth and global flame front speed**

Mean Wall Heat Flux



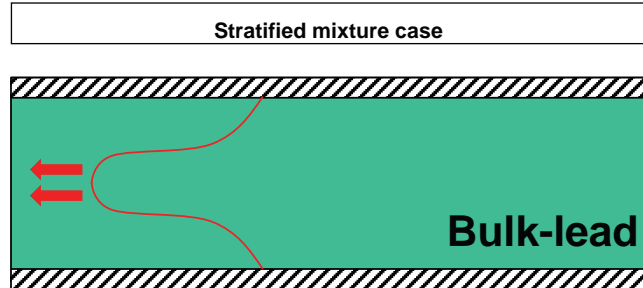
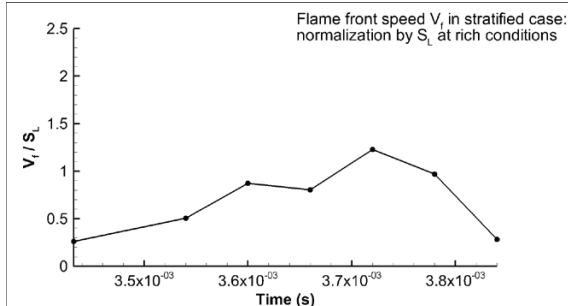
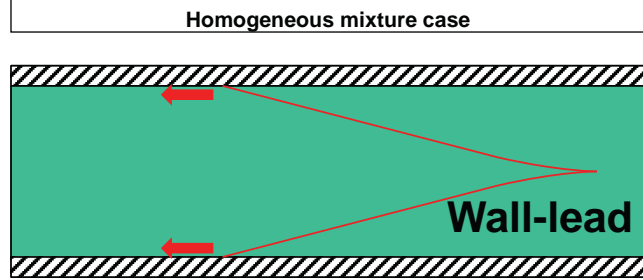
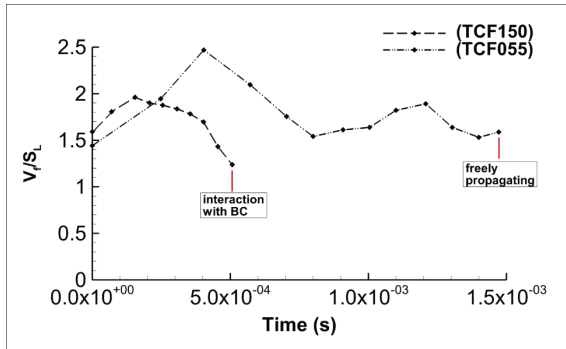
Mean wall heat flux peaks at $x^+ \sim 1043$ or 883 wall units downstream of anchor

Reverse Flow Pockets



- Reverse flow pocket size is $\sim 40 \times 20$ wall units (x - and y -plane)
- Reverse flow pocket spacing is ~ 100 wall units in spanwise z -direction (mimic streaks' spacing)
- Reverse flow pocket backflow maximum strength is $\sim 4/5$ of S_L

Global Flame Front Speed in Laboratory Reference



Time histories of the flame front (global) velocity V_f

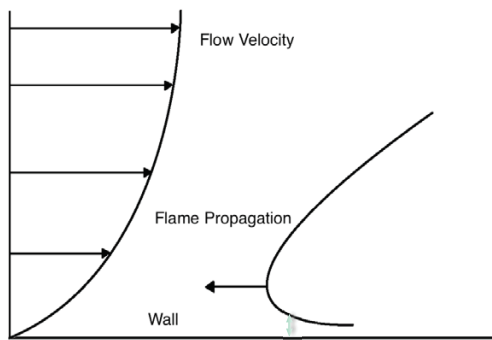
DNS data indicates a flame front speed $V_f \sim 1.5-2.0$ times the laminar flame speed S_L in the homogeneous mixture case and $V_f \sim 0.5-1.0$ in the stratified case (S_L at rich conditions)

Outline

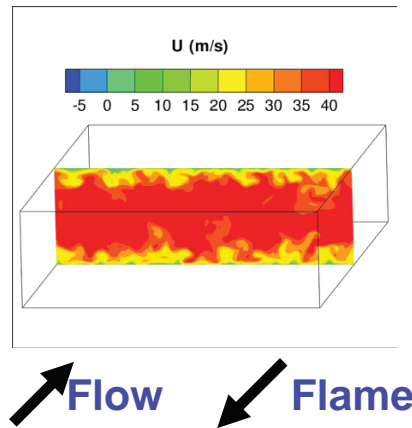
- Motivation and challenges
- Contributions
 - Andrea Gruber
 - Venkat Raman
 - Olivier Gicquel
 - Michael Pfitzner
 - Johannes Janicka
- TNF strategy

Boundary layer flashback (BLF)

- Focus on hydrogen-enriched gas turbines
 - Increased flammability and laminar flame speed
- BLF is triggered by the low near-wall velocity.
- The flame creeps upstream at the wall and drives the entire front.



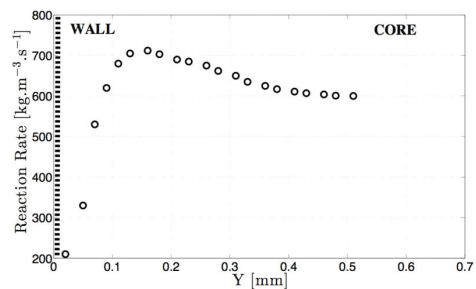
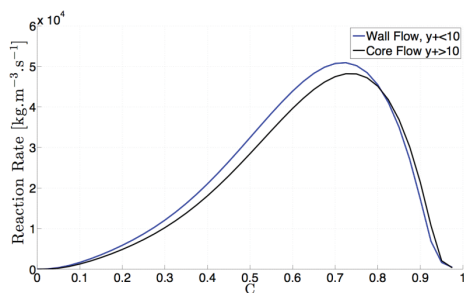
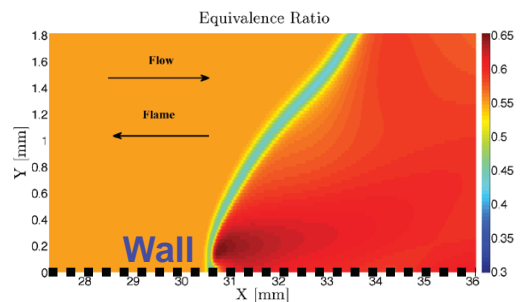
Quenching distance



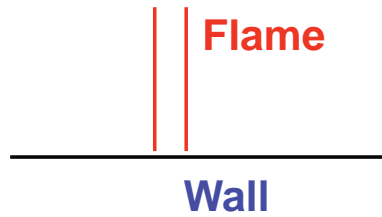
Predicting the flame propagation near the wall is crucial

Near-wall flame structure

- Near-wall modifications
 - Increasing heat loss makes the flame thicker
 - Radical recombination makes the flame thinner
 - Affects turbulent flow structure in the boundary layer

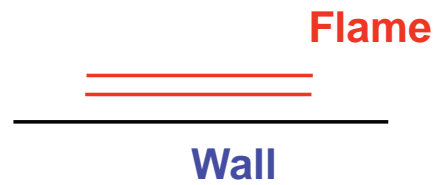


Various heat loss modes



The wall affects the combustion process

The heat sink varies throughout the reaction zone

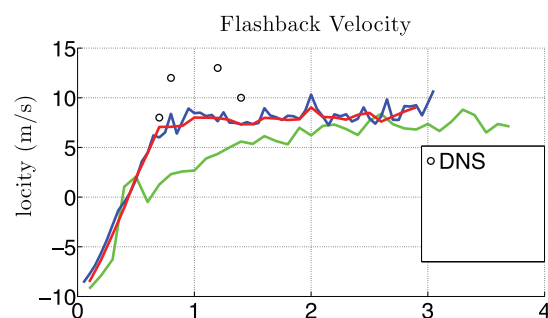
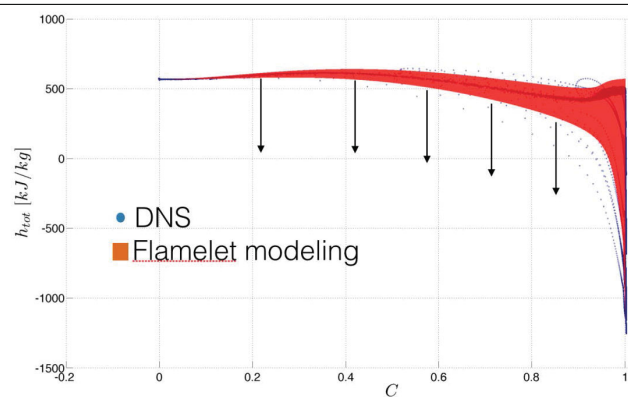


The wall affects the reactants state

The heat sink is uniform for the reactants

LES modeling of boundary layer flashback

- Capture heat loss with flamelet modeling : extrapolation needed for non burning solutions
- Leads to reasonable predictions of flashback velocity



Outline

- **Motivation and challenges**
- **Contributions**
 - Andrea Gruber
 - Venkat Raman
 - **Olivier Gicquel**
 - Michael Pfitzner
 - Johannes Janicka
- **TNF strategy**

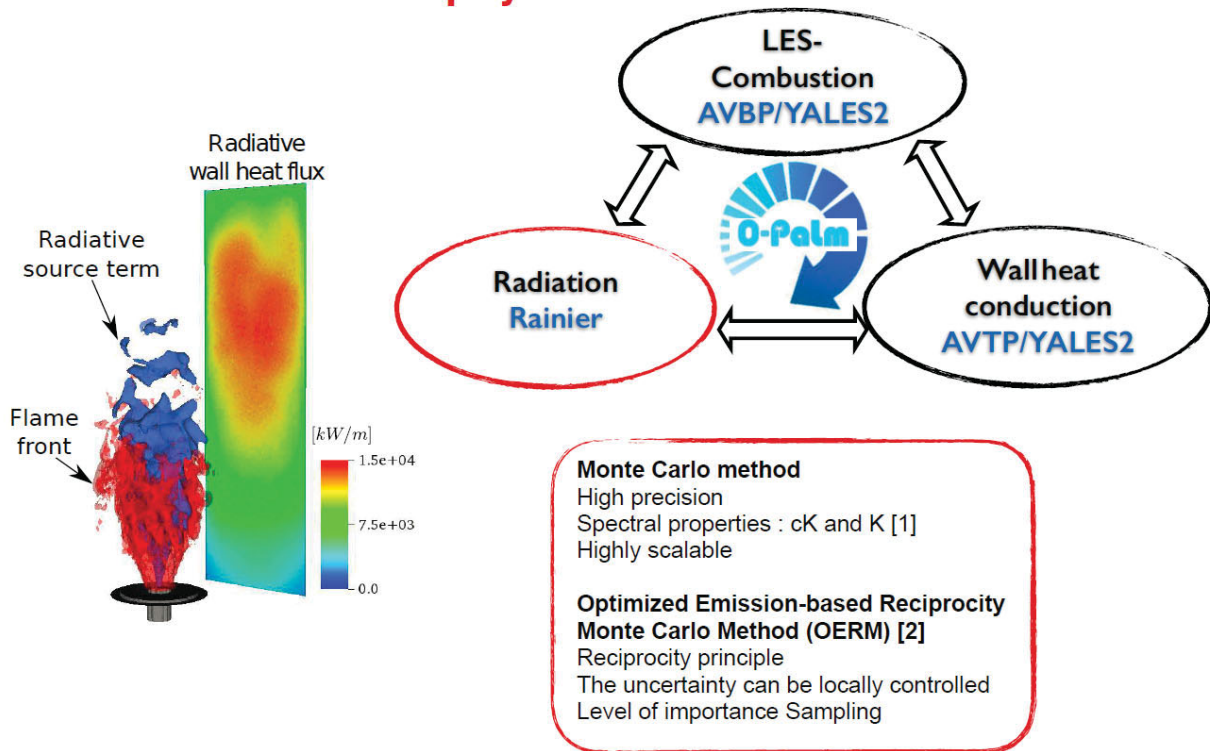


Combustion-Radiation- Conjugate Heat Transfer

TNF 2016 - EM2C Contribution
*Ronan Vicquelin, Jean Taine, Olivier
Gicquel*



Framework for multiphysics heat transfer

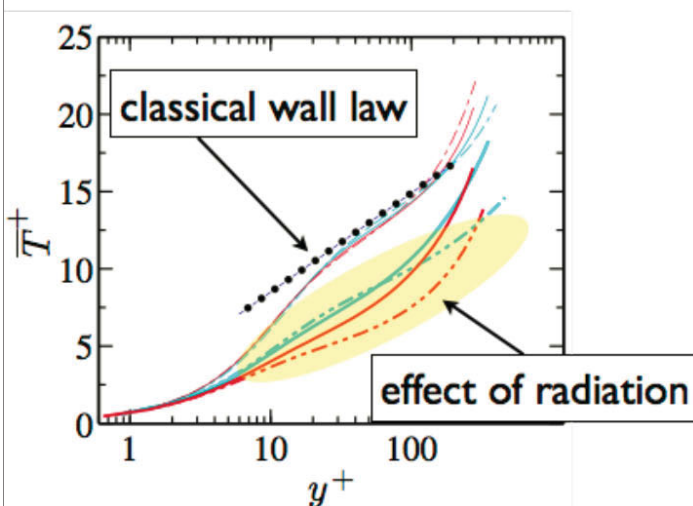


[1] A. Soufiani, J. Taine, Int J. Heat Mass Transfer 40 (1997) 987–991.

[2] Zhang, Y. F., Gicquel, O., and Taine, J. (2012). International Journal of Heat and Mass Transfer, 55(25–26):8172–8177.

Radiation in Turbulent boundary Layers

Coupled DNS of channel flow for different Re, p, ...



Effects of Radiation

- Addition of a wall radiative flux
- Wall conductive flux **modified** up to 100%
- Non-universal structure of the turbulent boundary layers

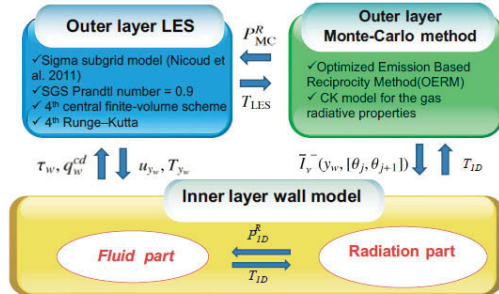
Zhang, Y. F., Vicquelin, R., Gicquel, O., and Taine, J. (2013). Physical study of radiation effects on the boundary layer structure in a turbulent channel flow. International Journal of Heat and Mass Transfer, 61(0):654–666.

Vicquelin, R., Zhang, Y. F., Gicquel, O., and Taine, J. (2014). Effects of radiation in turbulent channel flow: analysis of coupled direct numerical simulations. Journal of Fluid Mechanics, 753:360–401.

Zhang, Y. F. and Vicquelin, R. (2016). Controlling bulk reynolds number and bulk temperature in channel flow simulations. Journal of Computational Physics, 305:208–216.

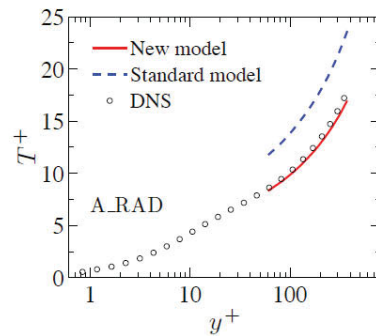
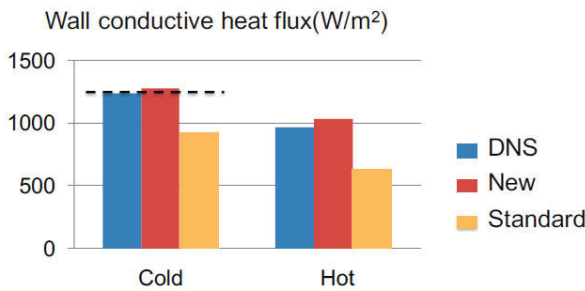
A new model to account for radiative effects

Coupled Wall-modeled LES of channel flows



A new wall model to account for radiation

- 1D TBLE
- Turbulent Prandtl number formula
- Semi-local mixing length model
- Position of the LES feed-back point
- Analytical radiation model



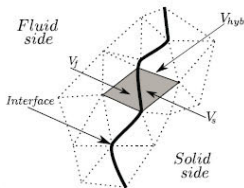
Zhang, Y. F., Vicquelin, R., Gicquel, O., and Taine, J. (2013). A wall model for les accounting for radiation effects. *International Journal of Heat and Mass Transfer*, 67(0):712-723.

Reactive LES and conjugate heat transfer

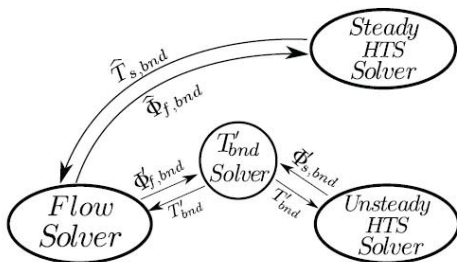
C. Koren PhD Thesis

Automatic determination of LES/CHT coupling time step using an interface model + PID controllers

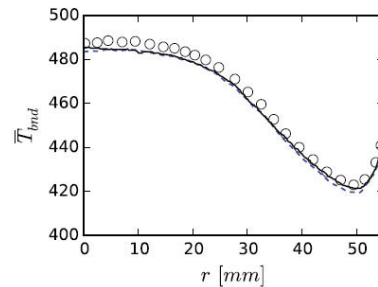
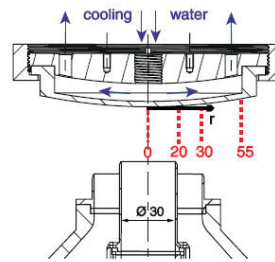
Hybrid-Cell Neumann Dirichlet



$$\frac{dT_{bnd}}{dt} = -\frac{\bar{\Phi}_f + \bar{\Phi}_s}{\rho_f c_{pf} V_f + \rho_s c_{ps} V_s}$$



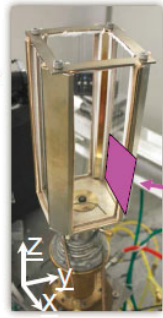
[1] Singh et al. *Flow Turbulence and combustion*, 2013



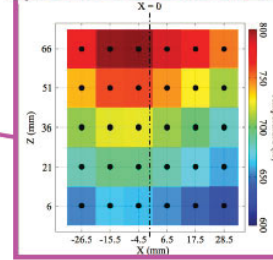
Radial mean temperature profiles.
Circles: Experiment
Black line: Numerical result

Valogaz burner:
confined swirled flame with
non-adiabatic walls

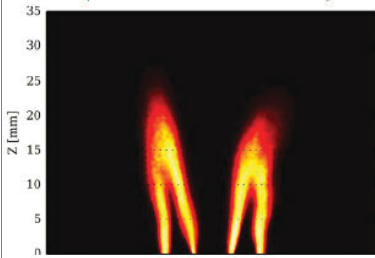
T.F. Guiberti, D. Durox, P. Scoufflaire, T. Schuller. PROCI 2015.



Laser Induced
Phosphorescence (LIP)

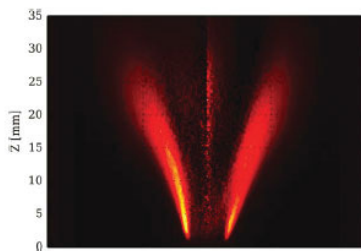


*Adiabatic
LES with F-TACLES
(Fiorina et al. 2010)*



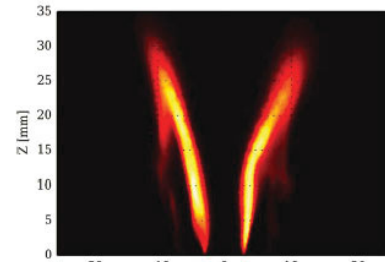
Normalized mean
volumetric heat release

Experiments



Normalized Abel
deconvoluted mean
OH chemiluminescence

*Non-Adiabatic
LES with F-TACLES
(Mercier et al. 2014)*



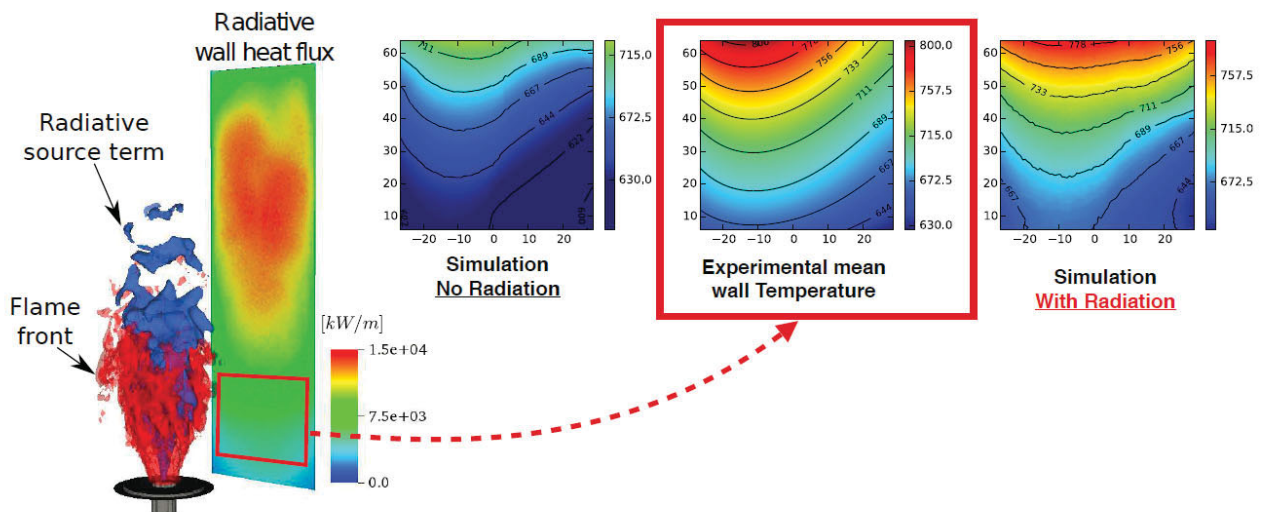
Normalized mean
volumetric heat release

R. Mercier, T. F. Guiberti, A. Chatelier, D. Durox, O. Gicquel, N. Darabiha, T. Schuller, B. Fiorina.
Experimental and numerical investigation of the influence of thermal boundary conditions on premixed swirling flame stabilization. *Combustion and Flame*, Vol.171, pp 42-58 (2016)

Reactive LES - Radiation - Conjugate heat transfer

C. Koren PhD Thesis

Multiphysics LES framework enables a
prediction of wall temperature with less than 10 Kelvin error



Guiberti, T., Durox, D., Scoufflaire, P. and Schuller, T. (2015) Impact of heat loss and hydrogen enrichment on the shape of confined swirling flames. *Proceedings of the Combustion Institute*, 35:1356-1392.

Guiberti, T., Durox, D., Zimmer, L., and Schuller, T. (2015) Analysis of topology transitions of swirl flames with the combustor side wall. *Combustion and Flame*, 162:4342-4357.

Mercier, R., Guiberti, T. F., Chatelier, A., Durox, D., Gicquel, O., Darabiha, N., Schuller, T., and Fiorina, B. (2016). Experimental and numerical investigation of the influence of thermal boundary conditions on premixed swirling flame stabilization. *Combustion and Flame*, 171:42-58.

Outline

- **Motivation and challenges**
- **Contributions**
 - Andrea Gruber
 - Venkat Raman
 - Olivier Gicquel
 - **Michael Pfitzner**
 - Johannes Janicka
- **TNF strategy**

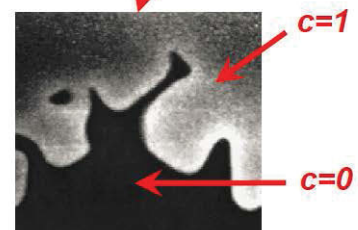
1) Transport equation:

$$\frac{\partial \bar{\rho} \tilde{c}}{\partial t} + \frac{\partial \bar{\rho} \tilde{u}_i \tilde{c}}{\partial x_i} + \frac{\partial}{\partial x_i} (\bar{\rho} \tilde{u}_i \tilde{c} - \bar{\rho} \tilde{u}_i \tilde{c}) = \frac{\partial}{\partial x_i} \left(\overline{\rho D \frac{\partial c}{\partial x_i}} \right) + \bar{\omega}_c$$

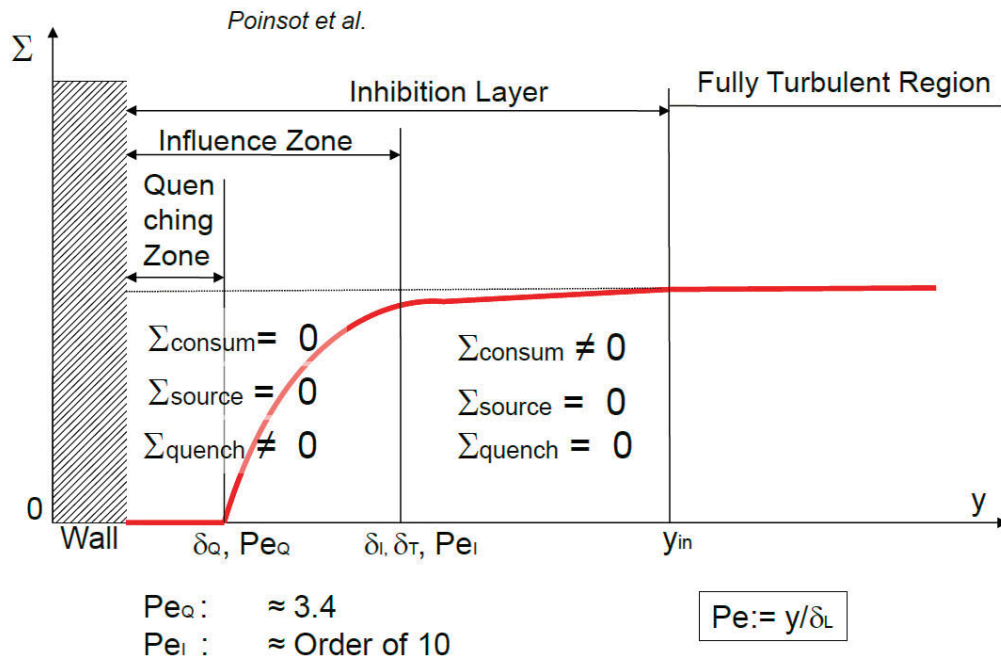
2) Modelling the r.h.s via **Flame Surface Density** formulation:

$$\frac{\partial}{\partial x_i} \left(\overline{\rho D \frac{\partial c}{\partial x_i}} \right) + \bar{\omega}_c \approx \rho_u s_L \Sigma$$

$$\tilde{c} = 1 - \frac{\tilde{Y}_{Fuel}}{Y_{Fuel,0}} \quad \tilde{T} = \frac{\tilde{T} - T_u}{T_b - T_u}$$



Modeling Heat Loss effects (premixed flames)



Modeling Heat Loss effects (based on analytical calculations)

Progress variable based on Y : $\tilde{c}_Y = 1 - \frac{Y_F}{Y_{F,u}}$

Progress variable based on T : $\tilde{c}_T = \frac{T - T_u}{T_b - T_u}$

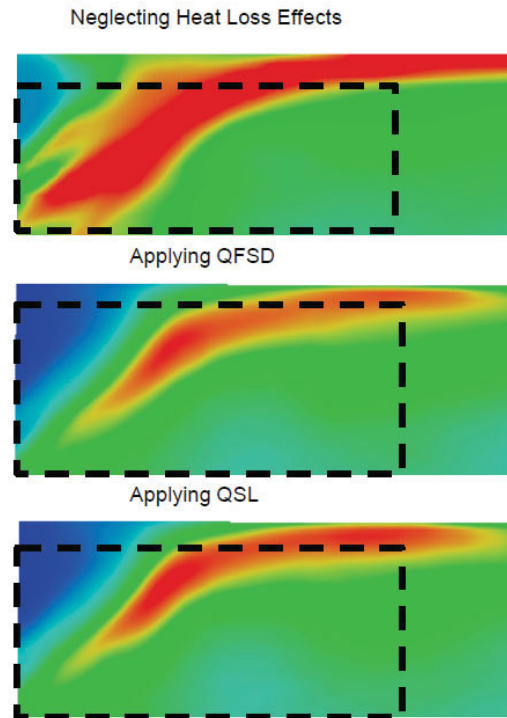
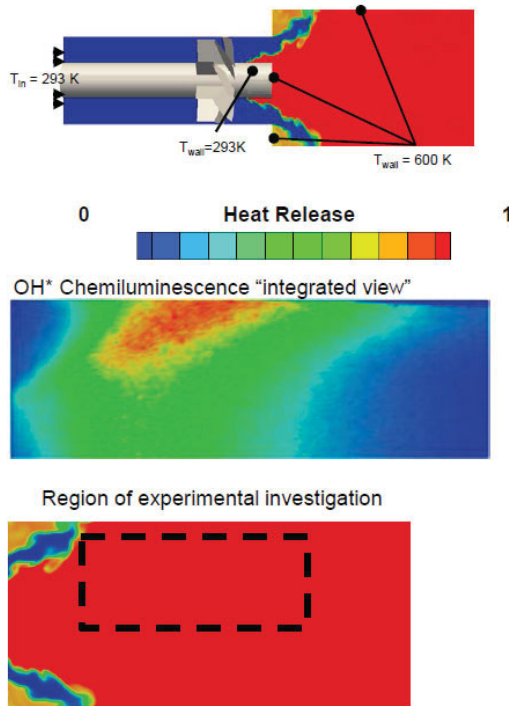
Heat loss parameter: $\tilde{A} = \tilde{c}_Y - \tilde{c}_T$

1st model: $s_{L,Q} = s_L^0 Q_{SL}$ $Q_{SL} = e^{-c_Q \beta \tilde{A}}$ Wichman and Bruneaux

2nd model: $\Sigma_Q = \Sigma \tilde{Q}_{FSD}$ $\tilde{Q}_{FSD} = (1 + c_y \tilde{A}_w) \exp \left[-\beta \left(\frac{\tau \tilde{A}}{(1 + \tau \tilde{c}_T)(1 + \tau \tilde{c}_Y)} \right)^{c_x} \right]$ Al-Shalan, Rutland

Keppeler R., Pfitzner M., Chong L.T.W., Komarek Th., Polifke W.: Including heat loss and quenching effects in algebraic models for Large Eddy Simulation of premixed combustion, ASME paper GT2012-68689, ASME Turbo Expo, June 11-15, 2012, Copenhagen, Denmark (2012)

Simulation Results (Polifke swirl combustor)



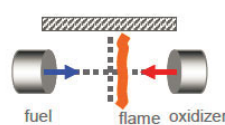
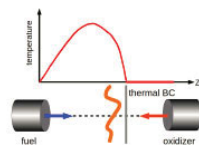
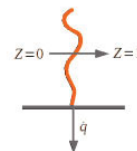
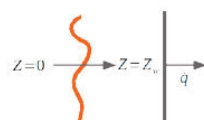
Enthalpy defect models – non-premixed flames

- Several different options to model enthalpy loss
- Specification of Z , h , c alone not sufficient to define chemical state
- Different options result in different mappings

→ Chose model corresponding to physical situation!

frozen

equilibrium

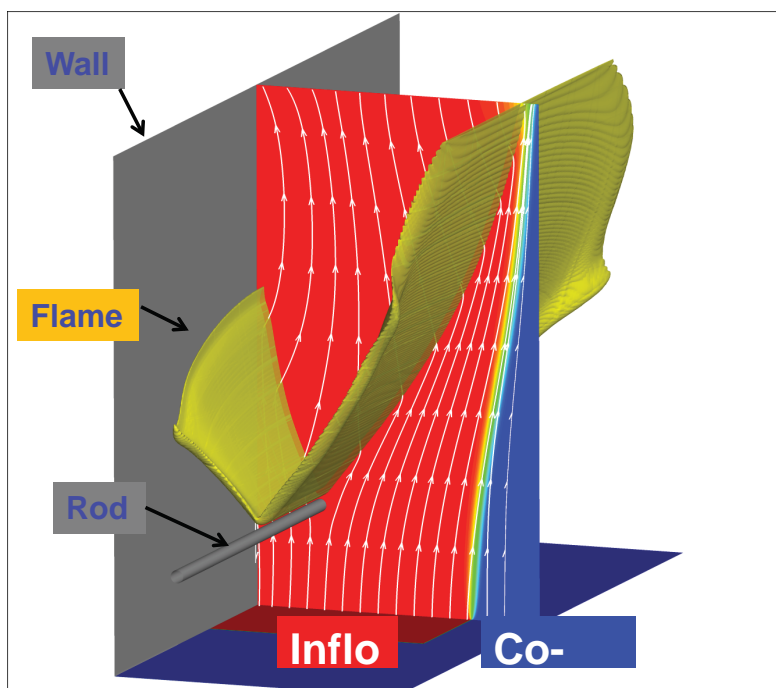


convective htc

Outline

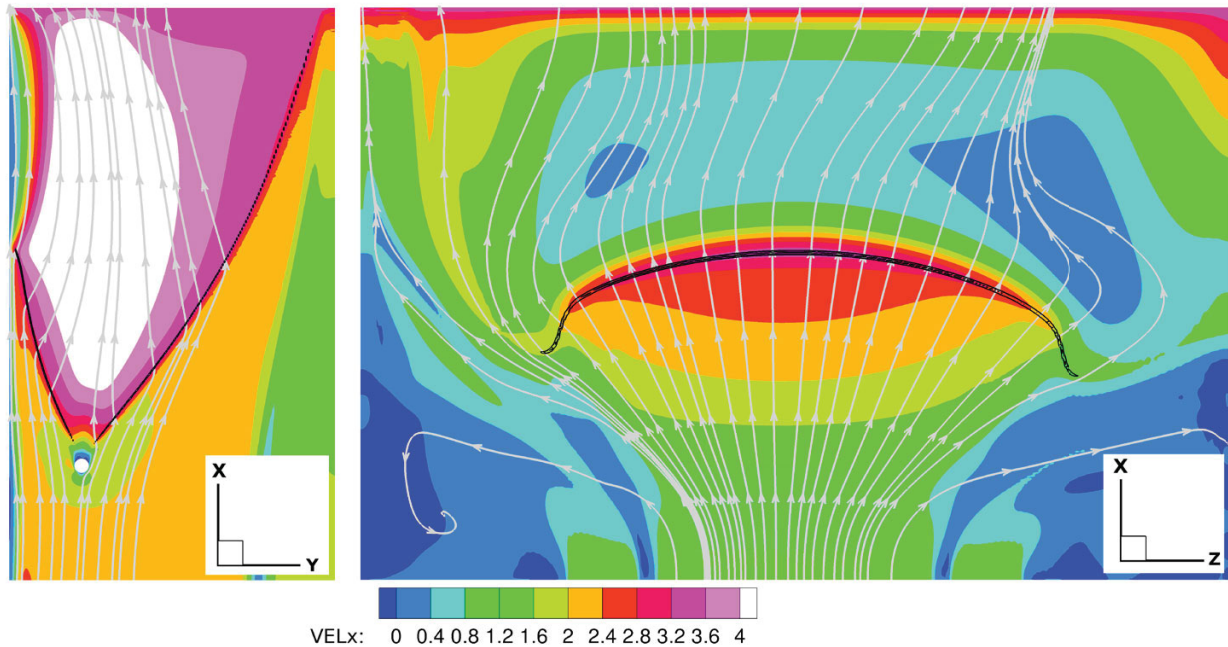
- **Motivation and challenges**
- **Contributions**
 - Andrea Gruber
 - Venkat Raman
 - Olivier Gicquel
 - Michael Pfitzner
 - **Johannes Janicka**
- **TNF strategy**

Side-Wall-Quenching configuration

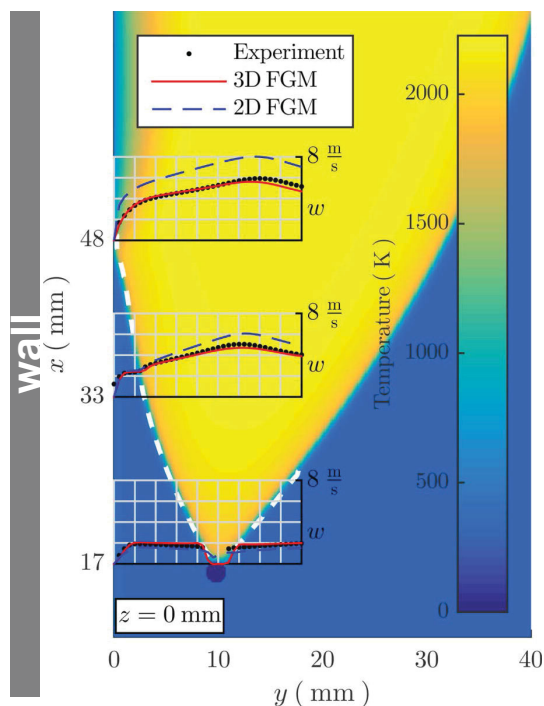


- 3D laminar FGM
- 24.5 Mio cells
- Wall Temp = 350 K
- Stoichiometric Inflow
- Air co-flow
- Fluid Temp = 300 K
- Re = 5300

Blocking effect of flame leading to 3D flow characteristic



Velocity profiles and flame position



Legend:

White dashed line : experimental flame front
Color map : numerical temperature field

3D FGM captures

- Flame position
- Velocity profiles

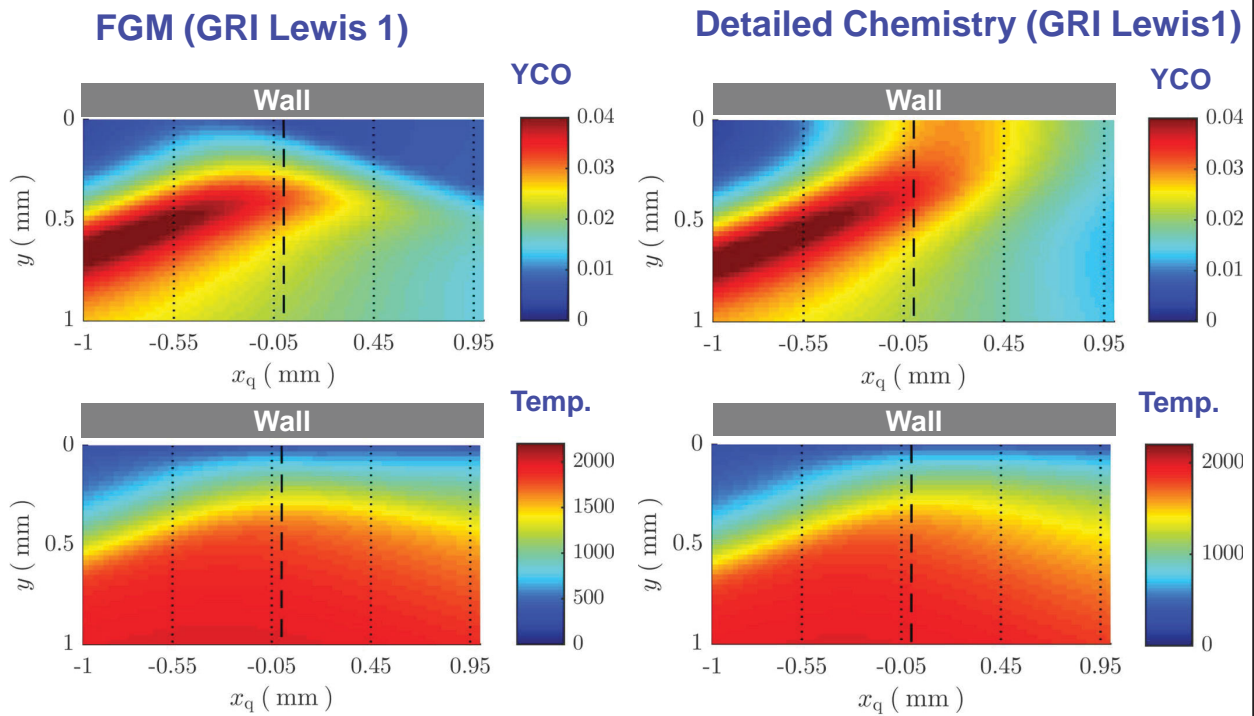
2D FGM captures

- Flame position if inflow is adjusted

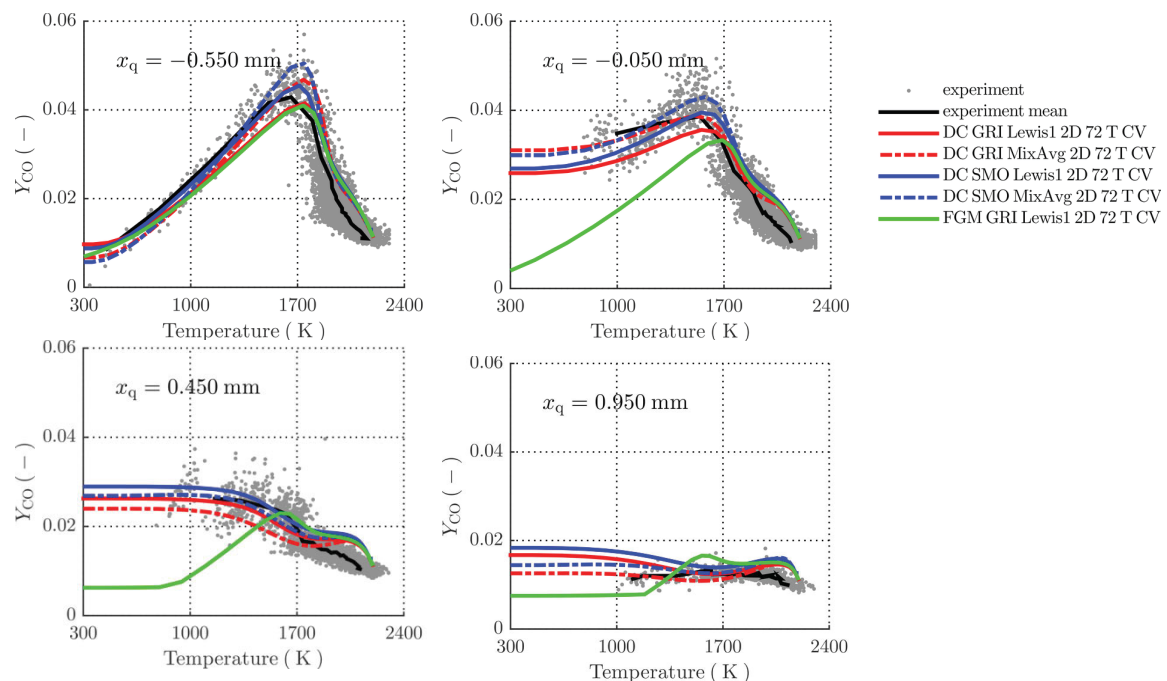
But:

- Velocity can not be captured due to 3D character of the Flow.

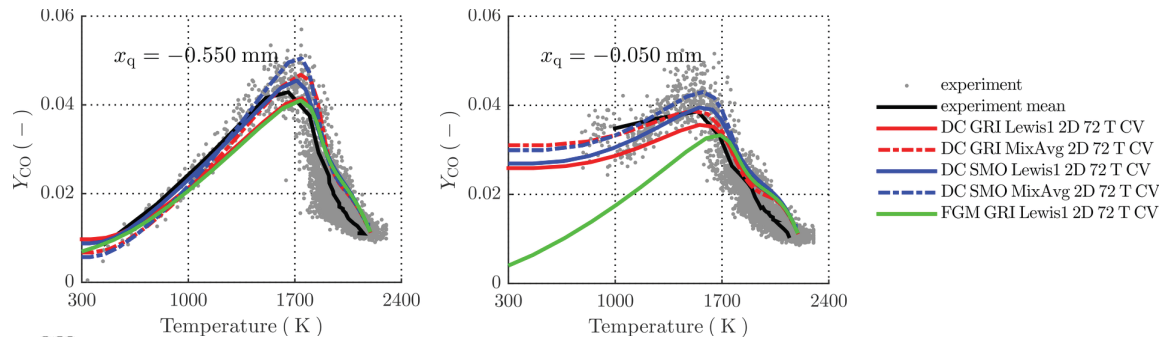
Detailed Chemistry vs. FGM Temperature and CO



Effects of chemical mechanism and diffusion model

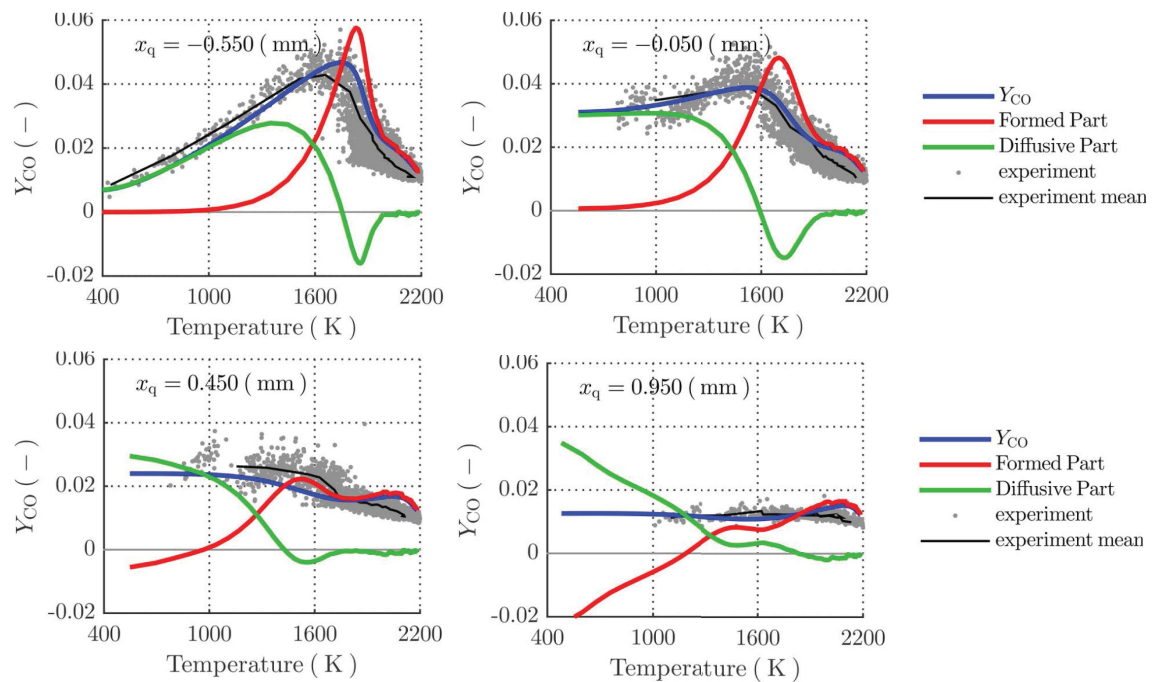


Effects of chemical mechanism and diffusion model

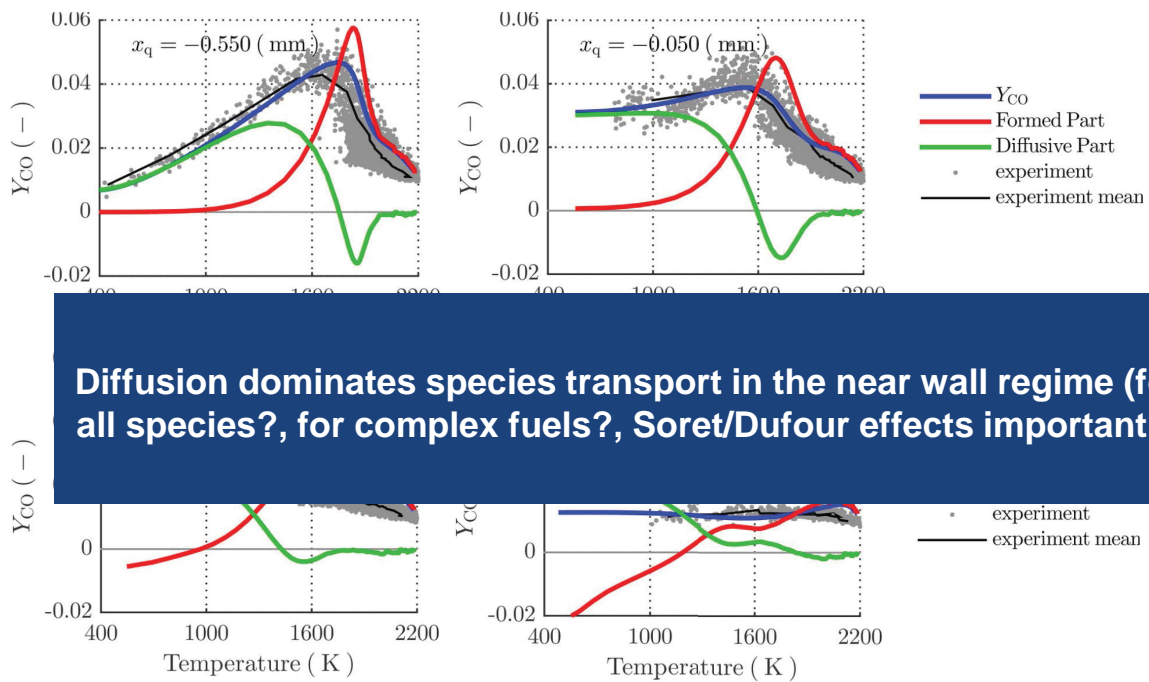


Classical reduction strategy applicable for mean flame structure but not for minor species (for complex fuels?)

Origin of CO near Wall



Origin of CO near Wall



Outline

- **Motivation and challenges**
- **Contributions**
 - Andrea Gruber
 - Venkat Raman
 - Olivier Gicquel
 - Michael Pfitzner
 - Johannes Janicka
- **TNF strategy**

A good TNF candidate??

- Global philosophy of TNF workshop
 - Generic configuration with well defined boundary conditions
 - Fluid mechanics and turbulence structure as simple as possible
 - Take fuels with well know detailed kinetic
 - Carry out reliable measurements
 - Concentrate on turbulence-chemistry interaction
- Near wall reactive flows
 - true
 - Not true →complex structure due to wide range of Re-number
 - Always difficult due to low-T kinetics
 - Experimental challenges at walls however DNS possible
 - true

A good TNF candidate??

- Global philosophy of TNF workshop
 - Generic configuration with well defined boundary conditions
 - Fluid mechanics and turbulence structure as simple as possible
 - Take fuels with well know detailed kinetic
 - Near wall reactive flows
 - true
 - Not true →complex structure due to wide range of Re-number
 - Always difficult due to low-T kinetics
 - Experimental challenges at walls however **DNS possible**
 - true
- 1st time in TNF history**
chemistry interaction

Scientific challenge(detailed)

- ▶ **Appropriate chemistry reduction strategy in presence of heat losses**
 - Reduction based on 3 variable (f,c,h) are not sufficient?
 - Additional dimensions?
 - Diffusion flame modelling even more difficult?
- ▶ **Appropriate low-temperature chemistry**
 - Reliable low-T kinetics for more complex fuels are not established
 - Which questions must be posed and which degree of complexity is required to provide the right answer (main structure, minor species, flame extinction)?

Scientific challenge(detailed)

- ▶ **Appropriate chemistry reduction strategy in presence of heat losses**
 - Reduction based on 3 variable (f,c,h) are not sufficient?
 - Additional dimensions?
 - Diffusion flame modelling even more difficult?
- ▶ **Appropriate low-temperature chemistry**
 - Reliable low-T kinetics for more complex fuels are not established
 - Which questions must be posed and which degree of complexity is required to provide the right answer (main structure, minor species, flame extinction)?

Combination of high resolution requirement and complex chemistry might support a revival of RANS or hybrid modelling

Scientific challenge(detailed)

- ▶ **Appropriate turbulence-chemistry interaction (TCI)**
(Answer depend on modelling context) e.g.
 - **PDF/FDF: Modelling of mixing term (I) in near wall regime (II) for scaler with different boundary condition**
 - **Same problem for reduced models with large(er) no. of control variable**
 - **Kinematic models (e.g. FSD, ATF, BML): adequate model for turbulent/filtered flame speed**

- ▶ **Two-way coupling for heat transfer**
 - **Not our urgent problem**

Scientific challenge(detailed)

- ▶ **Appropriate turbulence-chemistry interaction (TCI)**
(Answer depend on modelling context) e.g.
 - **PDF/FDF: Modelling of mixing term (I) in near wall regime (II) for scaler with different boundary condition**
 - **Same problem for reduced models with large(er) no. of control variable**
 - **K**

- ▶ **Two-way coupling for heat transfer**
 - **Not our urgent problem**

Challenge for the next 10 TNF years

Possible target configuration

- ▶ **Andreas' SWQ-burner (laminar and turbulent configuration)**
 - **Available**
 - **Measurements: T, CO, velocity, flame front,.. (Andreas talk)**
 - **Laminar kinetics in 2-D geometry**
 - **Detailed simulation of turbulence generator (we could provide boundary conditions, e.g. time dependent inlet profiles)**

Possible target configuration

- ▶ **Andrea's near wall DNS (anchored V-flame, freely-propagating flame)**
 - **Available**
 - **Everything including boundary conditions**

New burners

Coordinators: Wolfgang Meier and Bill Jones

Two burners were presented in this session: The first one was a dual swirl gas turbine model combustor for partially premixed flames that was developed by KIT and DLR within the collaborative research center SFB606. The second was the industrial gas turbine swirl burner G30 DLE from the Siemens SGT-100 turbine that was investigated in a high-pressure test rig.

The SFB dual swirl burner was operated with methane and air at thermal powers of typically 25 kW. Raman multispecies and temperature measurements as well as PIV velocity measurements have been performed for two cases: (1) A stable flame with $P_{th} = 22.5$ kW, $\phi = 0.63$ and air split ratio between outer and inner swirler of 1.6; (2) an oscillating flame with $P_{th} = 25.0$ kW, $\phi = 0.70$ and air split ratio of 1.6. The frequency of the thermo-acoustic oscillation was 392 Hz. The burner and the experimental results have been published in Arndt et al., *Exp. Fluids* 56:69 (2015). So far, only one numerical simulation was performed for a case with $P_{th} = 30$ kW, $\phi = 0.85$. Further experimental and numerical simulations are currently performed.

The industrial gas turbine swirl burner was operated with natural gas and preheated air ($T = 670$ K) in a pressure range up to 6 bar and thermal powers up to 1.08 MW. Experimental data sets have been established from measurements with laser Raman scattering, particle image velocimetry, laser induced fluorescence and exhaust gas analysis. A description of the experiments has been published in Stopper et al., *Combust. Flame* 160, 2103-2118 (2013) and also in German in Stopper's Ph.D. dissertation (<http://elib.uni-stuttgart.de/handle/11682/3966>). However, details of the combustor geometry are subject to confidentiality and have been supplied to only a small number of special cooperation partners of Siemens. There are a few publications about numerical simulations of the flames, for example from G. Bulat in cooperation with B. Jones (*Proc. Combust. Inst.* 34, 3155), C. Fureby (*Proc. Combust. Inst.* 35, 3175) and N. Swaminathan (*Proc. ASME Turbo Expo GT2012-68483*) or by Abou-Taouk et al., *Combust. Sci. Technol.* 188, 21-39 (2016), and Filosa et al., AIAA-2014-3916.

New Burners and Flames

Wolfgang Meier

DLR Institute of Combustion Technology, Stuttgart

TNF2016 Workshop, Seoul, Korea, 28-30 July 2016

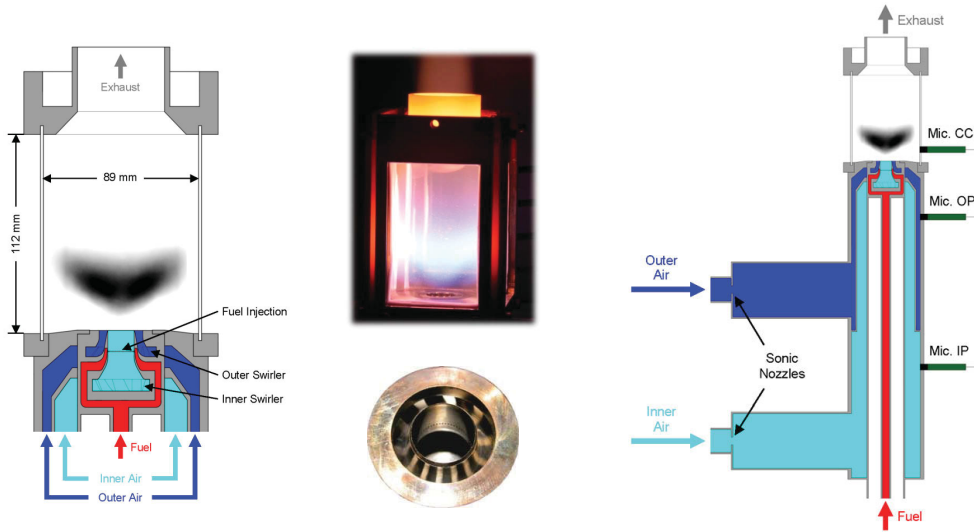


Outline

- Dual swirl gas turbine model combustor for partially premixed flames, developed by KIT and DLR within the collaborative research center SFB606.
- Industrial gas turbine burner Siemens G30 (elevated pressure).



SFB Dual Swirl Burner for Partially Premixed Flames

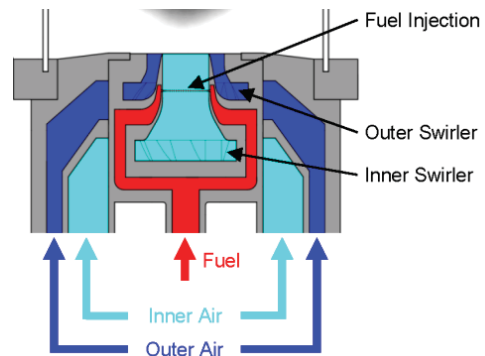


- Atmospheric pressure, thermal powers ≈ 25 kW
- 2 separate feed lines and plenums for air supply, 2 swirlers
- Fuel (CH_4) supplied through 60 holes arranged on a circle in inner nozzle



Nozzle Configuration

- Configuration of fuel supply (through 60 holes) allows operation with liquid or gaseous fuel.
- Liquid fuel is atomized at the lip of the inner nozzle.
- Operation with perfectly premixed gaseous fuel and air possible.
- Air split ratio between inner and annular nozzle is additional selectable parameter.

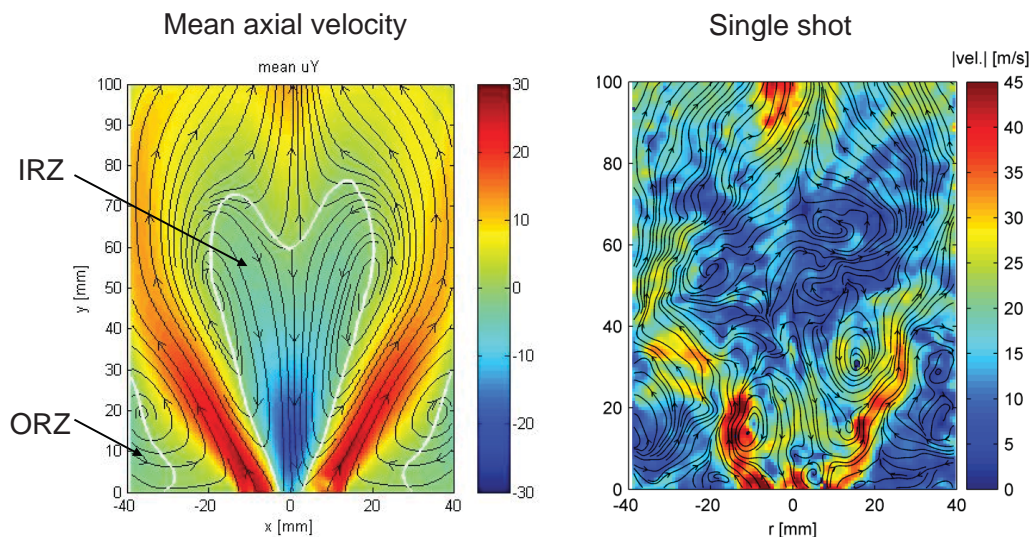


CH₄/Air Partially Premixed Flames

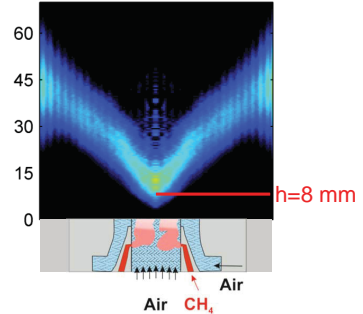
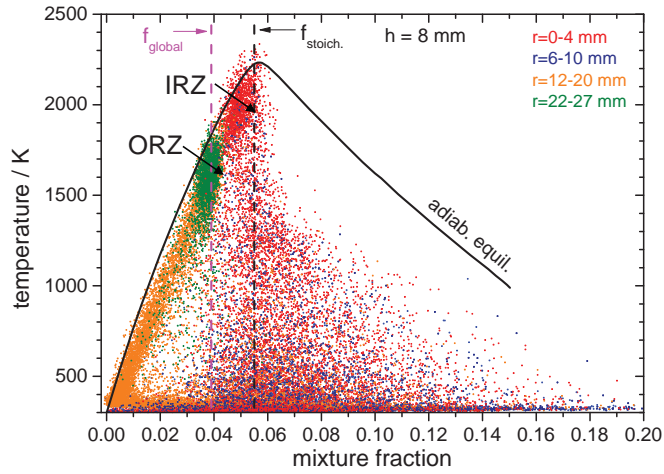
- Depending on operating conditions, flames burn stably or exhibit thermoacoustic oscillations.
- Raman multispecies and temperature measurements as well as PIV velocity measurements have been performed for 2 cases:
 - Stable flame: $P_{th} = 22.5 \text{ kW}$, $\phi = 0.63$, air split ratio 1.6.
 - Oscillating flame: $P_{th} = 25.0 \text{ kW}$, $\phi = 0.70$, air split ratio 1.6, $f_{osc.} = 392 \text{ Hz}$



Flowfield



Thermochemical State: Scatterplots T-f at h=8 mm



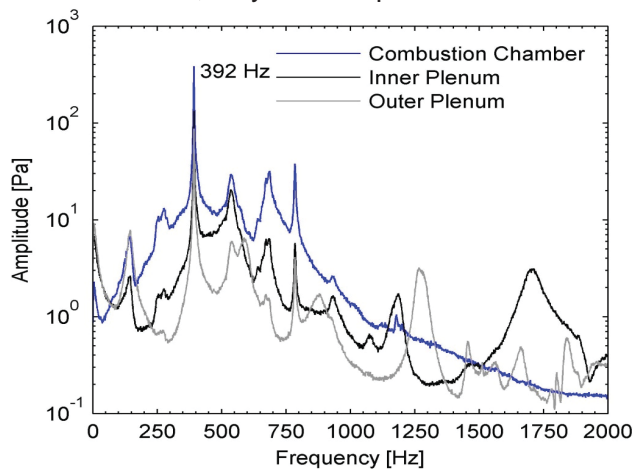
Hardly any reaction below h=8 mm, state mainly determined by mixing.

Large variation of thermochemical state



Thermo-acoustic Oscillations

- Oscillating test case: 25 kW, $\phi = 0.7$, air-split (outer/inner nozzle) = 1.6
- Several acoustic modes, only one coupled with heat release



Measured spectra

- Thermo-acoustic oscillation at $f \approx 390$ Hz
- Corresponds to resonance: $\lambda/2 =$ length of inner plenum



LES Simulation

For an oscillating flame with 30 kW, $\phi = 0.85$

- C. Kraus, L. Selle, T. Poinso, C.M. Arndt, H. Bockhorn:
“Influence of heat transfer and material temperature on combustion instabilities in a swirl burner”
Proc. ASME Turbo Expo 2016, GT2016-56368

Use of AVBP code developed at CERFACS and IFPEN.

References for Experiments

- C. Arndt, M. Severin, C. Dem, M. Stöhr, A.M. Steinberg, W. Meier ““Experimental analysis of thermo-acoustic instabilities in a generic gas turbine combustor by phase-correlated PIV, chemiluminescence, and laser Raman scattering measurements”, Exp. Fluids 56:69 (2015).
- W. Meier, C. Dem, C.M. Arndt, “Mixing and reaction progress in a confined swirl flame undergoing thermo-acoustic oscillations studied with laser Raman scattering”, Experimental Thermal and Fluid Science 73, 71-78 (2016).



Quick Glance at High-pressure Experiments at DLR



Siemens Industrial Gas Turbine Burner

Experiments performed at high-pressure test rig at DLR Stuttgart.



Diameter of burner nozzle 86 mm.

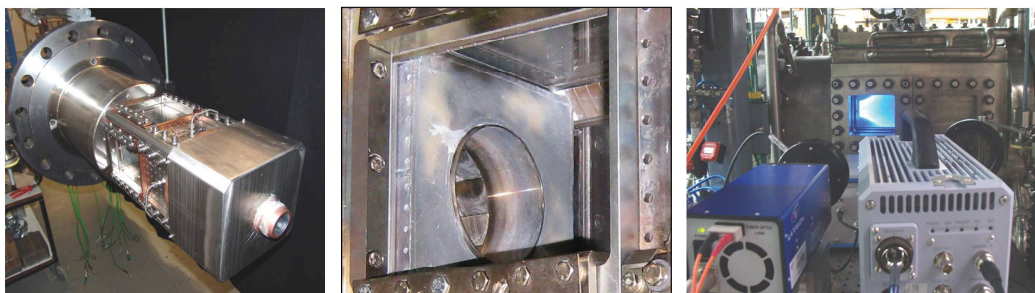
From U. Stopper, Ph.D. Dissertation, 2014

Siemens G30 DLE swirl burner from SGT-100 turbine

- Details of geometry are subject to confidentiality.



Siemens G30 DLE in Optical Combustion Chamber



Cross section of squared combustion chamber 165 x 165 mm².

Operating conditions

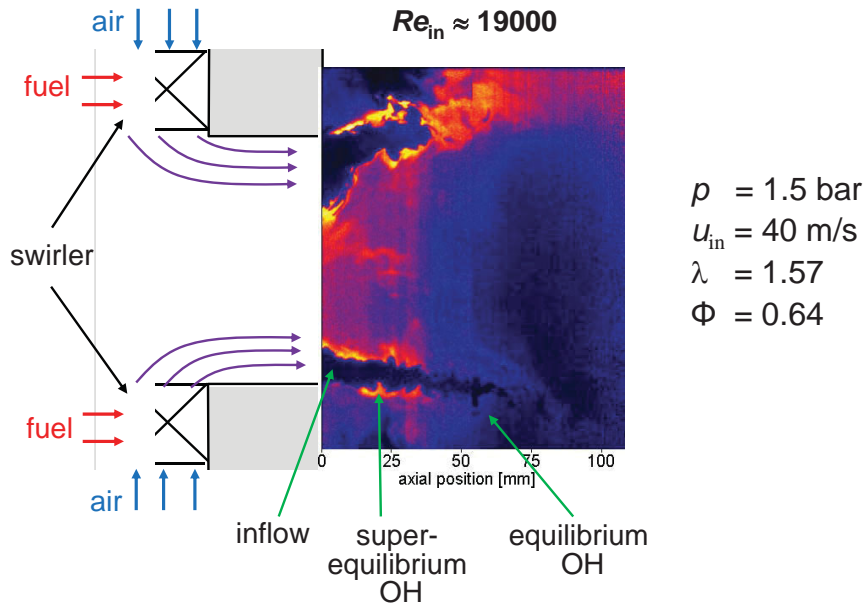
- Natural gas / air
- $p = \text{up to } 6 \text{ bar}$, $P_{\text{th}} = 0.335 - 1.08 \text{ MW}$, $T_{\text{air}} = 670 \text{ K}$

Measurement techniques:

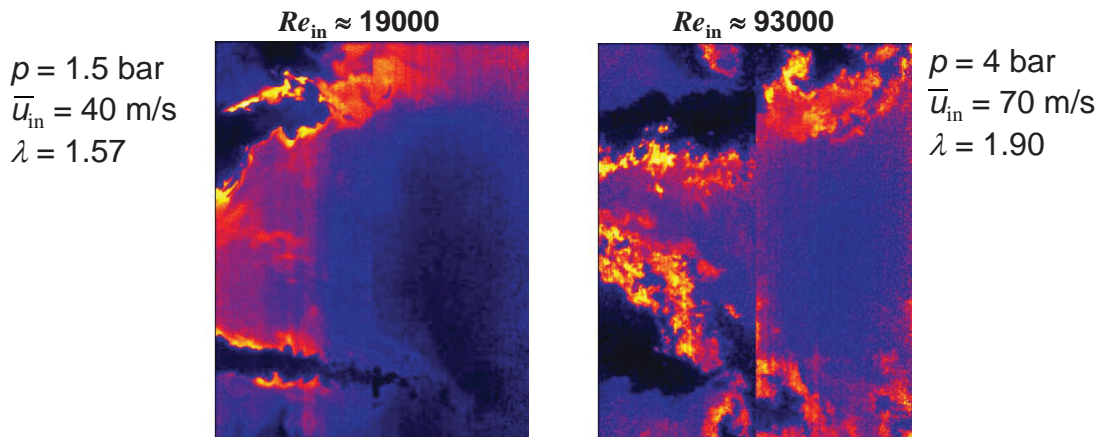
Raman scattering, particle image velocimetry, laser induced fluorescence, exhaust gas emissions



Flame Structures from OH-PLIF Measurements



Effect of Turbulence on OH Structures

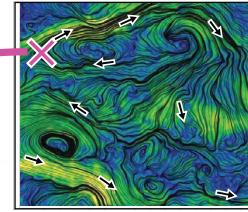
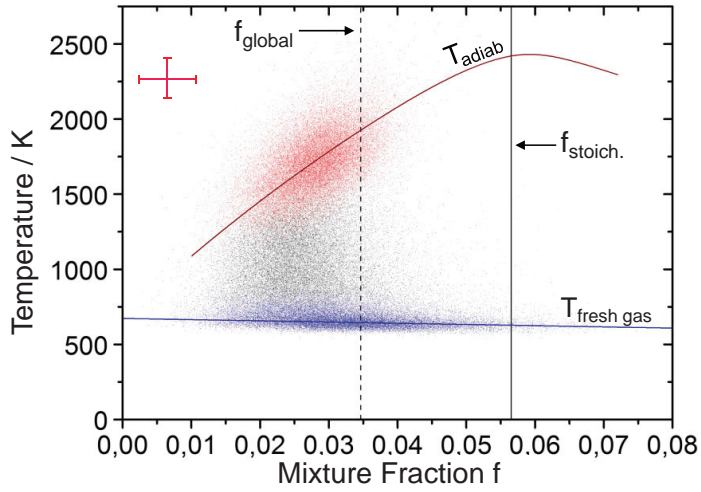


Flame at higher Re more corrugated and fragmented



Scatterplot of Temperature vs. Mixture Fraction

Single shot results from inner shear layer



single shot results:

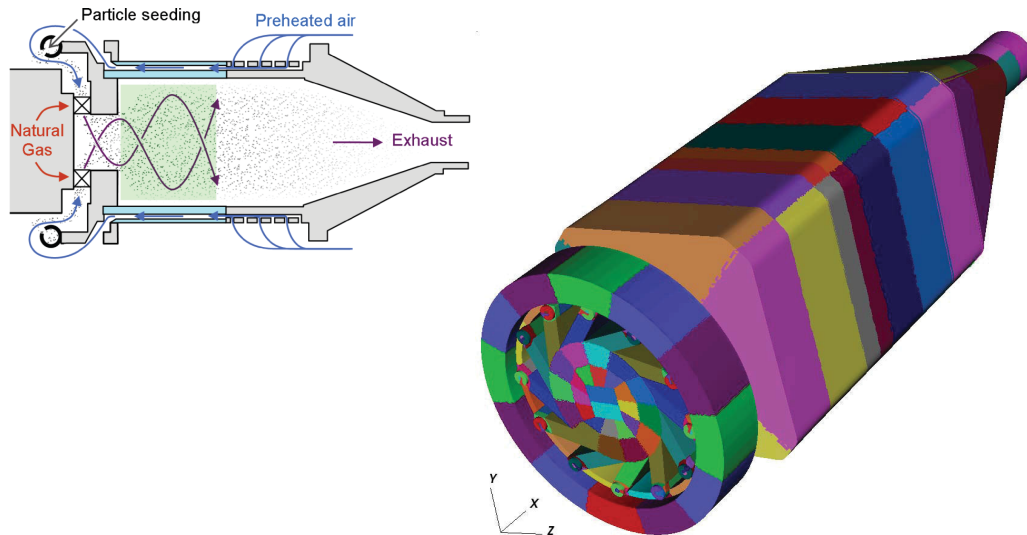
- exhaust gas
- intermediate states
- fresh gas



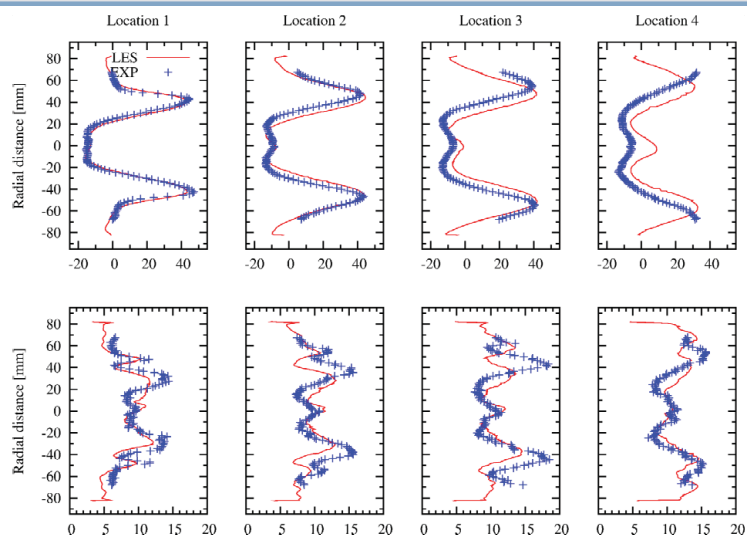
Imperial College
London

Bill Jones: Numerical Simulation of Siemens Combustor

Industrial Gas Turbine Combustor: Siemens SGT-100

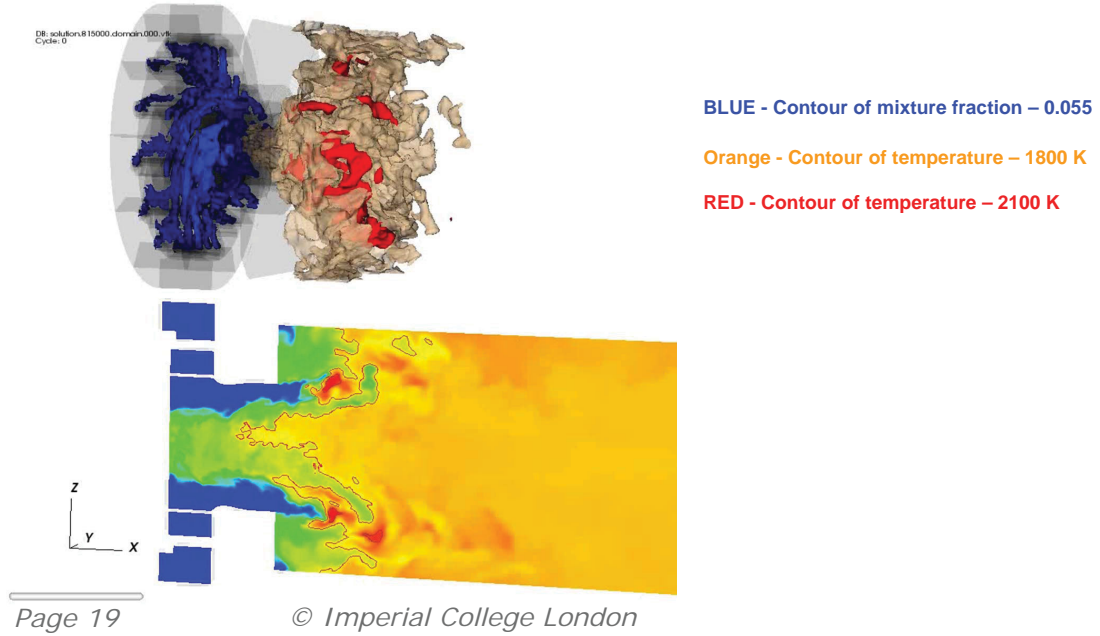


Mean and RMS Velocity Profiles

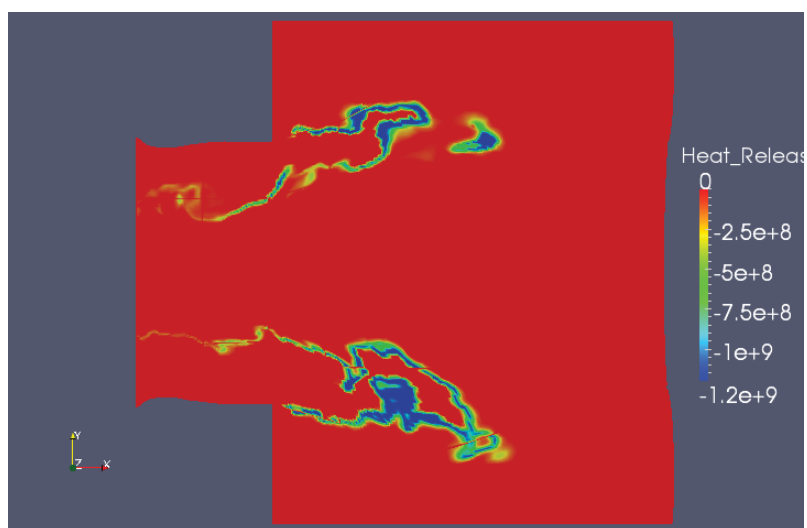


Comparison of mean (top) and RMS (bottom) Axial Velocity (m/s) profiles.

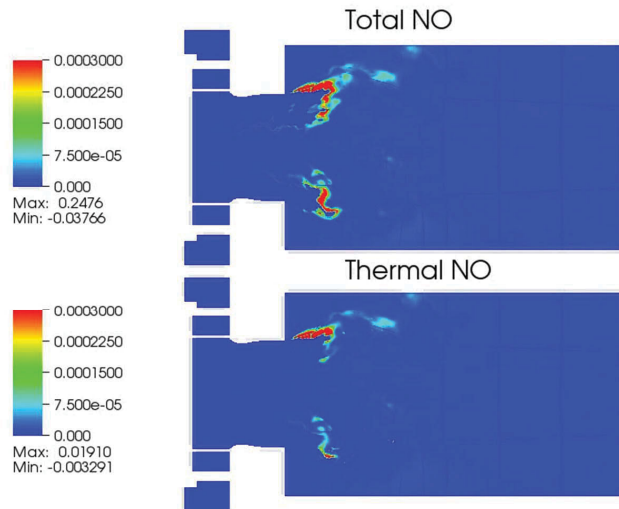
LES of the SGT-100: Animation



Snapshot of Heat Release Rate



LES of SGT-100: NO Formation Rate



References

- Stopper et al., "Experimental Study of Industrial Gas Turbine Flames Including Quantification of Pressure Influence on Flow Field, Fuel/Air Premixing and Flame Shape", *Combust. Flame* 160, 2103-2118 (2013).
- Stopper et al., "PIV, 2D-LIF and 1D-Raman measurements of flow field, composition and temperature in premixed gas turbine flames", *Experimental Thermal and Fluid Science* 34, 396-403 (2010).
- Sadasivuni et al., "Application of scalar dissipation rate model to Siemens DLE combustors", *Proc. ASME Turbo Expo 2012, GT2012-68483*.
- G. Bulat, W.P. Jones, A.J. Marquis, "Large Eddy Simulation of an industrial gas-turbine combustion chamber using the sub-grid PDF method", *Proc. Combust. Inst.* 34, 3155-3164 (2013).
- Bulat et al., "Reacting flow in an industrial gas turbine combustor: LES and experimental analysis", *Proc. Combust. Inst.* 35, 3175-3181 (2015).
- G. Bulat, W.P. Jones, S. Navarro-Martinez, "Large eddy simulations of isothermal confined swirling flow in an industrial gas-turbine", *Int. J. Heat and Fluid Flow* 51, 50-64 (2015).
- Filosa et al., "Numerical Investigations of a Low Emission Gas Turbine Combustor using Detailed Chemistry", *AIAA-2014-3916, AIAA Propulsion and Energy Forum and Exposition 2014: 50th AIAA/ASME/SAE/ASEE Joint Propulsion Conference*.
- A. Abou-Taouk, B. Farcy, P. Domingo, L. Vervisch, S. Sadasivuni & L.-E. Eriksson, "Optimized Reduced Chemistry and Molecular Transport for Large Eddy Simulation of Partially Premixed Combustion in a Gas Turbine", *Combust. Sci. Technol.* 188, 21-39 (2016).



Progress in modeling and measuring turbulent combustion processes at high pressures

William Roberts, Hong G. Im, Gaetano Magnotti, Joe Oefelein, Jonathan Frank

The session started with an overview of a few existing high pressure facilities designed for studying canonical flames, followed by the description of the new KAUST facilities that will be available for international collaboration. The KAUST high pressure combustion facility currently includes the primary duct, which is oriented horizontally to preserve axisymmetry (especially as buoyancy to inertia forces scales as pressure squared) and designed to optimize optical access. The facility can handle up to 45 bar pressure, with the capability to provide 0.5 kg/s continuous air flow and a wide range of gaseous fuels. There are a number of flame geometries in the queue including a TNF flame D, an inverse diffusion flame, the Sydney partially premixed flame, and the premixed flame of the University of Michigan. There are some high speed diagnostics available including 10 kHz OH PLIF and stereo PIV. A 10 Hz ns CARS system is currently available, and fs CARS capabilities will be developed by G. Magnotti and R. Lucht. Also discussed was how these flames should be scaled at elevated pressures. For example, if the jet exit Reynolds number is fixed, the exit velocity decreases linearly with increasing pressure, resulting in the Damkohler number variation in a non-linear fashion with pressure. Based on scaling, increasing Re with pressure while maintaining Da approximately constant is proposed as a first set of parametric studies for the TNF community.

To guide the experimental effort, large eddy simulations (LES) capabilities have been developed by the KAUST group in collaboration with University of Rome and initial simulations at various pressure conditions have been conducted. Syngas flames at $Re = 16700$ for different pressure conditions up to 5 atm were simulated and the results were compared. For the fixed inflow velocity, the effect of elevated pressure most notably resulted in the reduced level of the scalar dissipation rate. The characteristic time scale analysis based on the computational singular perturbation (CSP) technique yielded that the increased pressure leads to the fastest chemical time scales following a power law with exponent smaller than one, implying a reduction in the regions where the system dynamics is driven by chemistry.

The Sandia group focused on their investigations of the structure and dynamics of multiphase flows at high pressures. There are two extremes considered. At subcritical, or certain supercritical operating pressures relative to the injected liquid component, the classical situation exists where a well-defined molecular interface separates the injected liquid from ambient gases due to the presence of surface tension. Interactions between dynamic shear forces and surface tension promote primary atomization and secondary breakup processes that evolve from a dense state, where the liquid exists as sheets filaments or lattices intermixed with sparse pockets of gas, to a dilute state, where drop-drop interactions are negligible and dilute spray theory can be used. At pressures above critical conditions of the injected liquid, however, internal thermal gradients can form within the gas-liquid interface due to a combination of thickening within the interface and reduced molecular mean free path. The interfacial structure enters the continuum length scale regime and disappears as interfacial fluid temperatures rise above the critical temperature of the local mixture. Lack of inter-molecular forces, coupled with broadening interfaces, promote diffusion dominated mixing prior to atomization. As a consequence, injected jets evolve in the presence of exceedingly large but continuous thermo-physical gradients in a manner markedly different from classical assumptions.

The results from the modeling of high pressure flows highlighted research challenges. For multiphase flows, imaging has shown that diffusion-dominated mixing is pronounced over atomization and spray processes. The kinematic viscosity decreases with increasing pressure, which induces a significant increase in Reynolds number at conditions of interest (e.g., 1 order of magnitude relative to typical TNF atmospheric jet flames). Thermodynamic nonidealities and transport anomalies can significantly affect scalar mixing, especially in colder regions of the flow. Further, significant variability in chemical mechanisms designed to handle the same species needs to be better quantified. Skeletal mechanisms derived from the same detailed mechanism exhibit significant differences in key quantities at conditions of interest, and mechanisms designed for pressures above approximately 20 bar do not exist. Target cases aimed at model validation for high pressure systems will become increasingly important in the coming years (e.g., design of diagnostically accessible pressure vessels and adaptation of laser diagnostics to more complex fuels, in high-pressure environments).

Should TNF add Experiments and Simulations at Elevated Pressure?

Joe Oefelein, Hong Im, and Bill Roberts
Wolfgang Meier, Jonathan Frank, and Gaetano Magnotti
13th TNF Workshop
30 July 2016

outline

- Proposed experimental facility and flame for high pressure studies – Roberts
- Diagnostics for high pressure – Magnotti
- Status of current simulations – Im and Frank

Effects of pressure on laminar flame

Highly diluted ethylene-air



1 atm

16 atm

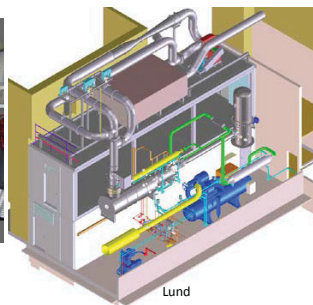
Dramatic changes in chemistry, gradients, and buoyancy

HP TNF

- Need to extend TNF flames to more realistic conditions (e.g., Re , Ka) and elevated pressure
- TNF has been extraordinarily successful because it has allowed many labs globally to apply their expertise to the exact same flame
 - modeling and/or measurement technique
- However, operating these TNF flames at pressure is very expensive (i.e., infrastructure, diagnostics, operating costs) and this model will not work as well
- Want to preserve the modeling tractability
 - Well-defined boundary conditions
 - Axisymmetry
- Propose we choose a few facilities with flexible capabilities and operate these as 'user facilities' where researchers can bring their own capabilities and techniques
 - Rather than a distributed network, adopt the CRF model, applied to high pressure flames
 - Propose the CCRC at KAUST as one of these facilities

Current High Pressure Facilities

- DLR-Stuttgart: 2 MW, 40 bar
- NASA Glenn RC: 4.5 kg/s air, 20 bar
- NETL: 1.4 kg/s, 22 bar, 700 K
- AFRL: 15 kg/s, 40 bar, 900 K
- Paul Scherrer Institute: 0.3 kg/s, 30 bar, 823 K



- TU-Darmstadt: 0.15 kg/s, 10 bar, 773 K
- Penn State: 0.27 kg/s, 24 bar, 870 K
- Lund: 1.3 kg/s, 16 bar, 1000 K
- UC-Irvine: 1.0 kg/s, 15 bar, 920 K
- Purdue: 0.45 kg/s, 150 bar, heating also

HP-TNF Objectives

- Build an experimental apparatus to study canonical turbulent non-premixed flames at high pressures
 - Want to preserve axisymmetry, so must be vertical
- Able to measure soot, temperature, major & minor species, velocity
 - Requires multiple optical ports
- Pressures as high as 45 bar
- Able to use various fuels
 - Pure H_2 & H_2/N_2
 - Pure C_2H_4 & C_2H_4/N_2
 - Syngas (CO/H_2)
 - Pure CH_4 & CH_4/H_2 and CH_4/air
- Ability to vary O_2/N_2 ratio as desired
- Design in flexibility to include a wide variety of burners



High Pressure Combustion Duct

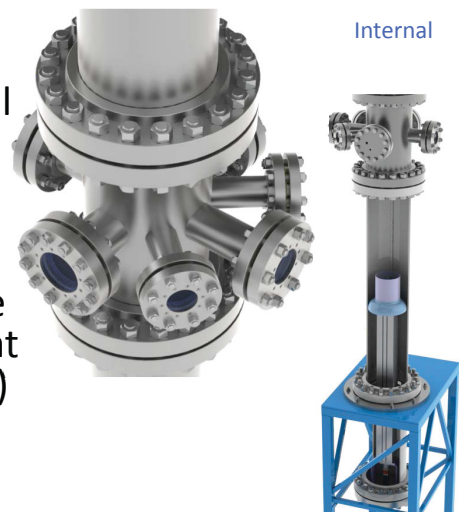


- Designed to be a 'user facility'
 - Simple interface between burner and facility (PLC control)
 - Interested in collaborations in both burners and diagnostics
- 45 bar peak pressure, 0.5 kg/s air flow rate, high capacity of fuels
- Very good optical access



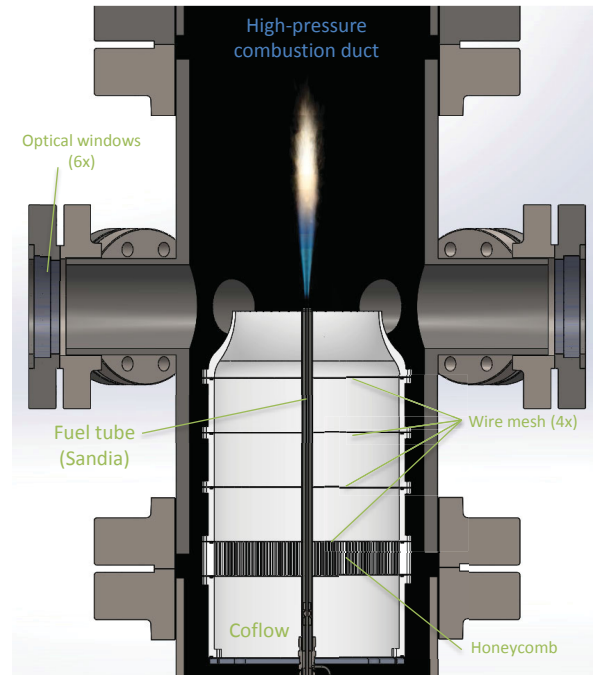
HPCD

- Up to 1.5 m of burner translation
 - Currently only z-axis
 - Depending upon burner geometry, may accommodate x- and y- as well
- 6 UV fused silica windows
 - Two orthogonal and two at 45° for stereo PIV
 - Windows are off-set some distance from centerline; may wish to mount lenses internally (design underway)
- Self-contained PLC safety controls
 - Experiments should be self-contained and operate on labview

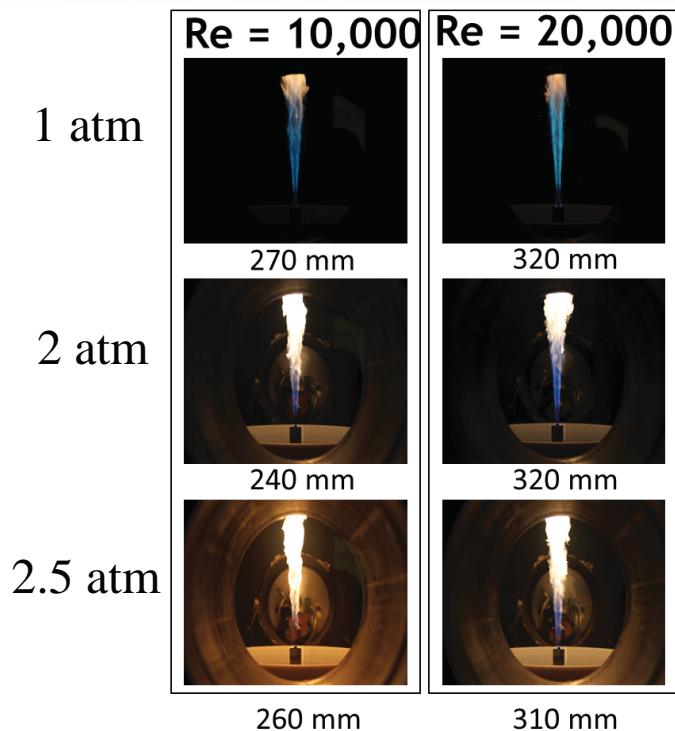


KAUST C₂H₄/N₂ Flame

- 65% nitrogen dilution variant of ISF-3 Target Flame 2 (Sandia) at KAUST
 - Same geometry as Sandia
 - Much shorter and less luminous
 - Main jet: 35% C₂H₄, 65% N₂
 - $D = 3.3$ mm
 - Re 10,000 & 20,000
 - Pilot: lean premixed C₂H₄/Air
 - 6% total heat release
 - Coflow: 250-mm OD, 1.0 m/s
 - Housed in high-pressure (40 atm) combustion duct
 - Inner diameter ~410 mm



Effect of Pressure



HP Lab Diagnostic Capabilities

- 10-kHz stereoscopic PIV (now)
- 10-kHz OH-PLIF (now)
- 10-Hz time resolved LII (laser and camera for HP)
- 50-Hz Raman (TBD)
- 10-Hz FRS (TBD)
- 10-Hz ns-CARS (in another building)
- TGS for thermometry (TBD)
- Working with Lucht on CPP fs-CARS for single shot, high rep rate (e.g., 50 kHz) N₂ thermometry
- Gaetano Magnotti to develop HP diagnostics

How to scale up TNF?

- As we increase pressure, how do we assure some tractability to atmospheric pressure flames?
- How do we intelligently change physical parameters?
- For example, consider Sandia D flame:
 - if we keep exit velocity constant, Re and mass flux scale linearly with pressure. May lead to facility limitations.
 - if we keep mass flux constant, Re is constant but Richardson number increases as P^2 ; how important are buoyancy effects?
 - what happens to Ka or Da in these two cases?
- Propose new high pressure flame, allowing very high Re , but still tractable with Sandia series.

Superflame Scaling Arguments

- Sandia Flame D as baseline
 - 25% CH₄ / 75% Air, $Re = 22,400$, $D = 7.2$ mm, piloted
- Want to explore increasing Re while keeping other parameters constant
- Flamelet calculations indicate that increasing pressure by a factor of 10 reduces chemical time scale by 1.9 (F. Bisetti)
- Define ratios: $\frac{Da}{Da_0} = \frac{D U_0 \tau_0}{D_0 U \tau}$ $\frac{Re}{Re_0} = \frac{D U v_0}{D_0 U_0 v}$
- Scaling arguments:



$$\text{Velocity: } \frac{U}{U_0} = \left(\frac{Re}{Re_0}\right)^{1/2} \left(\frac{Da}{Da_0}\right)^{-1/2} \left(\frac{v}{v_0}\right)^{1/2} \left(\frac{\tau}{\tau_0}\right)^{-1/2} \quad \text{Diameter: } \frac{D}{D_0} = \left(\frac{Re}{Re_0}\right)^{1/2} \left(\frac{Da}{Da_0}\right)^{1/2} \left(\frac{v}{v_0}\right)^{1/2} \left(\frac{\tau}{\tau_0}\right)^{1/2}$$

$$\text{Power: } \frac{P}{P_0} = \left(\frac{U}{U_0}\right) \left(\frac{D}{D_0}\right)^2 \left(\frac{\rho}{\rho_0}\right) = \left(\frac{Re}{Re_0}\right)^{3/2} \left(\frac{Da}{Da_0}\right)^{1/2} \left(\frac{v}{v_0}\right)^{3/2} \left(\frac{\rho}{\rho_0}\right) \left(\frac{\tau}{\tau_0}\right)^{1/2}$$

Superflame Scaling Ratios

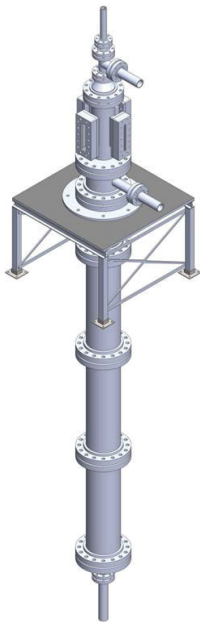
- Want to increase pressure and Re by factor of 10, while keeping Da constant by clever choice of burner diameter and exit velocity

	Baseline	High Pres	Ratio
Reynold's number	22,400	224,000	10
Damköhler number	-	-	1
Pressure (atm)	1	10	10
Temperature (K)	300	300	1
Diameter (mm)	7.20	5.22	0.73
Velocity (m/s)	50	69	1.38
Chemical time scale	-	-	0.53
Viscosity (St)	0.162	0.016	0.10
Power (LHV) (kW)	18	129	7.25

Planned Flames and Burners

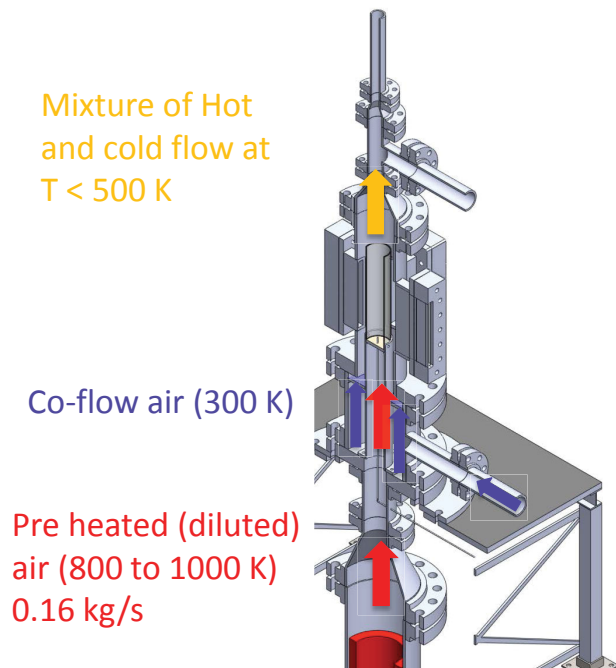
- Currently working on Shaddix sooting flame
 - Based on Sandia D piloted flame (slightly different pilot geometry)
 - CEM and flame height
 - PIV and OH-PLIF
 - TiRe LII
- chnB CO/H₂/N₂ flame
 - PIV and OH-PLIF in fall
- Sydney/Sandia partially premixed flame
 - Blowoff studies initially (late fall)
- Turbulent Inverse Diffusion Flame
 - Stability limits, OH-PLIF (winter)
- Coanda Burner
 - Stability limits (spring)
- Driscoll's premixed turbulent flame (summer 2017)

HP Rig for autoign and spray flames



Should be operational by 1 Oct

Flow and operating conditions



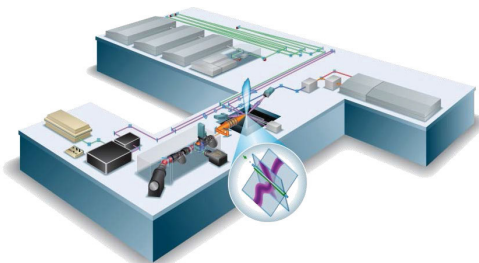
- Operating pressure to 40 bar
- Pre-heater temperature: 300 to 1000 K
- Central fuel jet, gaseous or liquid
- Multiple air co-flows
- Able to preheat air to 1000 K at 0.16 kg/s (300scfm)
- 4 quartz windows are arranged for laser diagnostics
- Large N_2 storage for MILD combustion studies

Challenges and Opportunities in Temperature and Major Species Measurements in High Pressure Combustion Environment

Gaetano Magnotti

Motivation

- Newly developed high pressure combustion rigs (KAUST) offer the possibility to study classical and novel TNF canonical flame at pressures up to 40 bar
- 1D Temperature and major species measurements in atmospheric pressure canonical flames have played a key role in developing and validating turbulence-chemistry interaction models within the framework of the TNF workshop
 - 4 out of 6 talks yesterday included results from Sandia's 1D Raman/Rayleigh/CO-LIF instrument
 - 1D Raman/Rayleigh/CO-LIF instrument not adequate at higher pressure
- Diagnostics development is needed to provide accurate and precise multi-scalar measurements in these more challenging environments





Diagnostics Challenges in High Pressure Combustion

- Enclosed combustors
 - Limits on the laser irradiance, focusing etc...
- Limited optical access
 - Large optical windows become more problematic at higher pressures
- Increased molecular collisions (pressure broadening, quenching)
- High spatial resolution
- High speed acquisition (> kHz) very desirable
 - Large datasets, converged conditional statistics, probability distribution functions, time-series, auto-correlation and integral time scales
 - Helpful to contain cost in high pressure facilities
 - Temporally resolve combustion dynamics
- Interest in very luminous flames with higher levels of soot and soot precursors

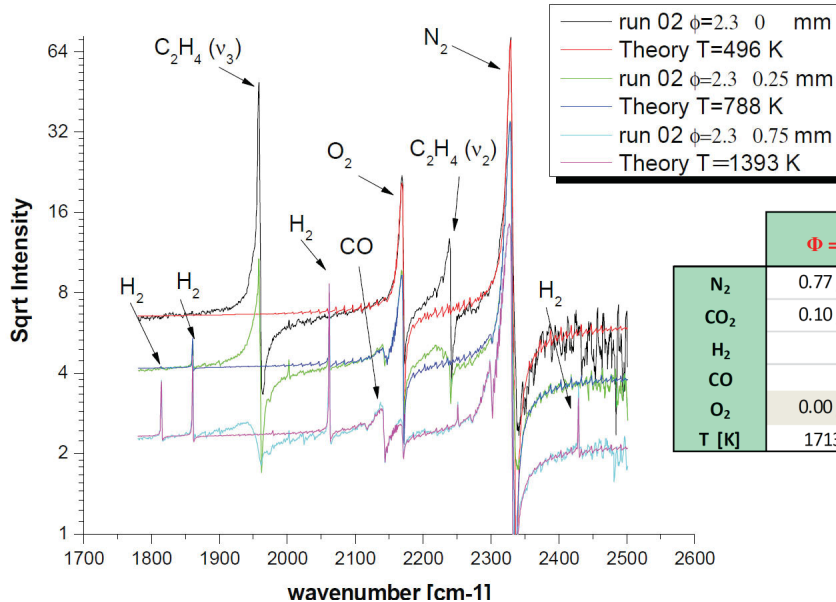


Ns-Laser Diagnostics for Temperature and major specie

- **Limited to 5-100 Hz.**
- Incoherent approaches: 1D Raman/Rayleigh scattering and CO-LIF
 - Requires long-pulse ns lasers to avoid windows damage
 - Filtered Rayleigh scattering
 - Requires large optical access.
 - High levels of fluorescence interference expected. Polarization separation spectroscopy helps
 - LIF not quantitative at high pressure because of collisional quenching
- Coherent Anti-Stokes Raman Spectroscopy
 - Limited optical access required
 - Complex set-up and data analysis
 - Point measurement with poor spatial resolution
 - Pressure broadening cause accuracy degradation at high pressure
 - WIDECARS for T, and 6 species (N₂, O₂, CO₂, CO, H₂ and C₂H₄) in C₂H₄-air flames (Cutler et al. Journal of Raman Spectroscopy, April 2016)
- Transient Grating Spectrography
 - Single-point temperature measurements at high pressure.
 - Promising but further development needed



Ns-Laser Diagnostics for Temperature and major specie



	$\Phi = 0.85$	$\Phi = 1$	$\Phi = 1.7$
N ₂	0.77 ± 0.03	0.78 ± 0.03	0.66 ± 0.03
CO ₂	0.10 ± 0.02	0.11 ± 0.02	0.04 ± 0.01
H ₂		0.00 ± 0.003	0.06 ± 0.01
CO		0.00 ± 0.004	0.12 ± 0.02
O ₂	0.00 ± 0.01		
T [K]	1713 ± 77	1809 ± 67	1843 ± 76



kHz ns-Laser Diagnostics for Temperature and Species

- 10 kHz PIV and PLIF are increasingly popular and are already providing great insight in turbulent combustion (TNF flames and beyond)
 - Sandia, DLR, Sydney and many others.
 - 10 kHz stereoscopic PIV and OH PLIF currently available at KAUST
 - Energy insufficient for Temperature and species measurements
- Pulse burst laser
 - 1J @ 532 nm @ 10 kHz up to 25 ms (Sutton, Ohio State)
 - Commercial pulse burst laser available (Spectral Energies Quasimodo, 600 mJ @ 532 nm @ 10 kHz up to 1 ms)
- 1D Raman/Rayleigh @ 10 kHz applied to turbulent flames (Sutton)
- Same fundamental limitations of ns-laser diagnostics at high pressure
 - Collisional broadening and quenching
 - Large optical access



Ultrafast CARS

- Commercial lasers operating up to **10 kHz** with mj/pulse and pulse duration <100 fs
- Benefits of short pulse duration
 - Low total energy: reduce breakdown, and window damage
 - Time-gated elimination of non-resonant signal
 - Large spectral bandwidth
 - All major species and Temperature can be probed simultaneously
 - High-stability, strongly reducing shot-to-shot noise due to dye lasers
 - **Collision free measurements**
 - High irradiance enabling **1D and 2D measurements**
- Fs-CARS has the potential to extend the capability of Sandia's 1D Raman/Rayleigh instrument to high pressure environment at kHz rate
 - Chirped probe pulse: probe beam has spectral bandwidth comparable to the pump and Stokes (Bob Lucht at Purdue, Grisch @ CORIA, Stefan Nolte at Friedrich-Schiller-Universität Jena)
 - Hybrid ps-fs CARS: the probe is a spectrally narrow ps beam (Kliever, Kearney, Meyer, Roy, Attal-Tretout)

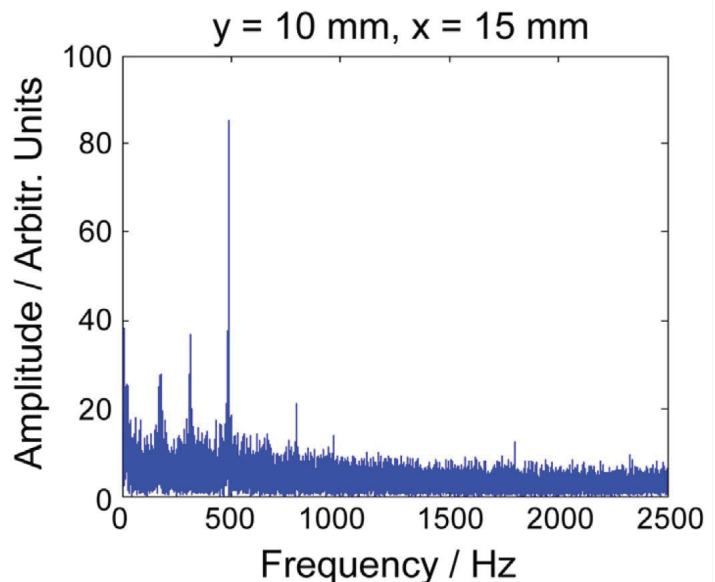
COMBUSTION RESEARCH FACILITY

Sandia National Laboratories



CPP-CARS Temperature measurements at 5 kHz

- Simpler setup: a glass rod introduces the needed chirp
- More complex model
 - Genetic algorithms used to fit the numerous parameters needed
- Temperature measurements at 5 kHz in the DLR Gas Turbine Model Combustor Flame V (Dennis PROCI 2015)



Peak frequencies attributed to the dominant longitudinal thermoacoustic pulsation, the precessing vortex core and combination of the two

COMBUSTION RESEARCH FACILITY

Sandia National Laboratories

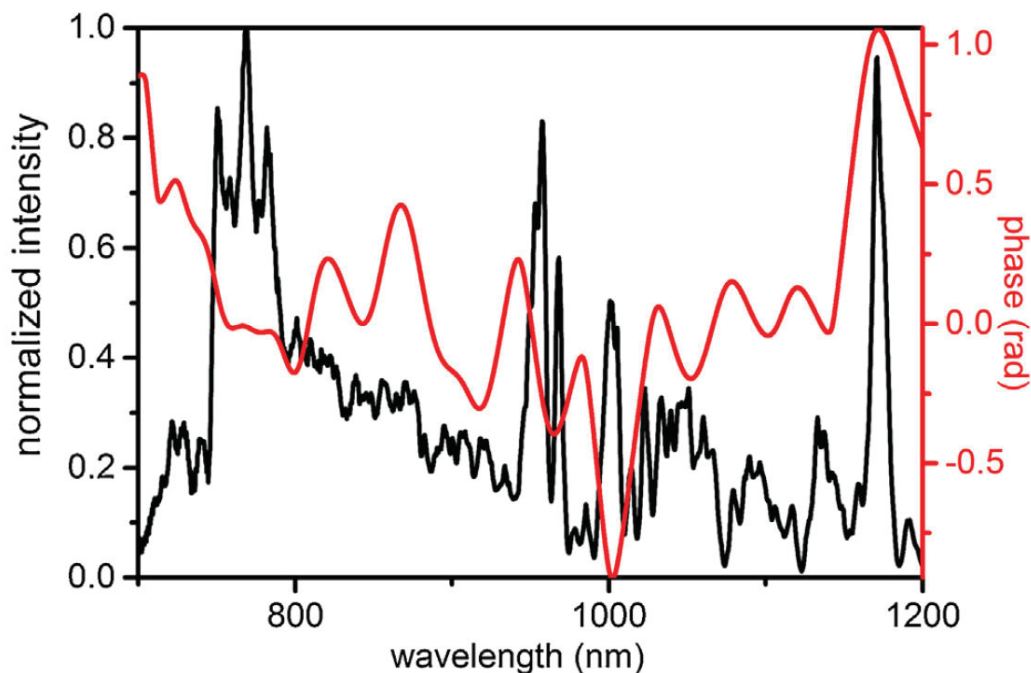


CPP-CARS species measurements

- Selected species mole fraction ratioed to N₂
 - Limited by bandwidth of fs laser
- Shorter pulses
 - Sub 7 fs pulses provide sufficient spectral bandwidth to probe all species at once
- Matthaus (Vibrational Spectroscopy 85 2016)
 - OPCPA, <7 fs, 30 kHz
 - 2 beam approach introduced by Kliwer
 - No OPA needed
 - Temperature in gas cell up to 5 bar
 - CO₂, O₂ and N₂ detected, but quantitative analysis requires improved modelling



CPP-CARS species measurements





Hybrid fs-ps CARS

- Probe beam is spectrally narrow
 - Spectra similar to ns CARS
 - Simple models
 - Compromise between spectral resolution and pulse duration
 - <3 ps and collisions are negligible up to 50 bars in N₂
 - Above collisional linewidth must be measured
 - Species measurements may have more restrictive criteria
 - 2 approaches to produce the probe beam
 - External ps laser (Kliewer 90 ps laser)
 - High spectral resolution
 - 1D and 2D imaging at 10 Hz
 - Major species detection when coupled with sub 7fs pulses
 - Spatial resolution <100 microns
 - Collaboration between Sandia and TU Darmstadt to study flame-wall interaction (Bohlin 1B05)



Hybrid fs-ps CARS

- Ps beam obtained from fs laser (Keaney, Meyer, Attal-Tretout)
 - Automatic synchronization of pump-pulse and probe
 - Inefficient conversion process
 - 1 kHz Temperature measurements in particle laden flames (Hoffmeister 2016)
 - O₂ and T measurements in flat flames
 - Pressure measurements
 - Limited to 0D and ~ 500 microns measurement volumes
- Minor species detection
 - Fs Electronic Enhanced Resonance CARS
 - It has some potential but significant development needed
 - Possible alternative to LIF for minor species detection
In high pressure environment





Conclusions

- High pressure combustion environments are very challenging for the application of 1D Raman/Rayleigh/CO-LIF spectroscopy
- Development of ultrafast CARS will enable temperature and species measurements
 - Some encouraging results, but significant development needed, especially for species measurements
 - Fs-CARS developed for these more challenging environment will also benefit atmospheric TNF flames
 - High speed
 - High spatial resolution and proximity to a wall
 - Fuel flexibility
 - Minor species measurements remain a greater challenge
 - Fs ERE CARS?

blank



Simulations of Turbulent Flames at Elevated Pressure

Hong G. Im, Bok Jik Lee, Francisco Hernandez Perez
Clean Combustion Research Center, KAUST

Mauro Valorani, Pietro Ciottoli, University of Rome, La Sapienza



Simulation of Turbulent Flames at High Pressure



- Simulation campaign aligned with the experimental effort in the Clean Combustion Research Center (CCRC) at KAUST
- The CCRC is setting up a high pressure combustion test facility operating at up to 45 atm
- The simulations will guide the experimental operation conditions and cross-validate with the laser diagnostic measurements of various flame observables



Sandia/ETH-Zurich Flame A (CO/H₂/N₂)



- Nonpremixed turbulent flame at $p=1$ atm
- Fuel composition: 40% CO, 30% H₂, 30% N₂
- Fuel jet velocity $U_{\text{jet}} = 76$ m/s, $Re = 16700$
- Nozzle:
 - inner diameter 4.58 mm
 - outer diameter 6.34 mm
- Oxidizer: air at 0.75 m/s
- Characterization of similar flames at higher pressures is to be conducted at CCRC in 2016

Large Eddy Simulations I



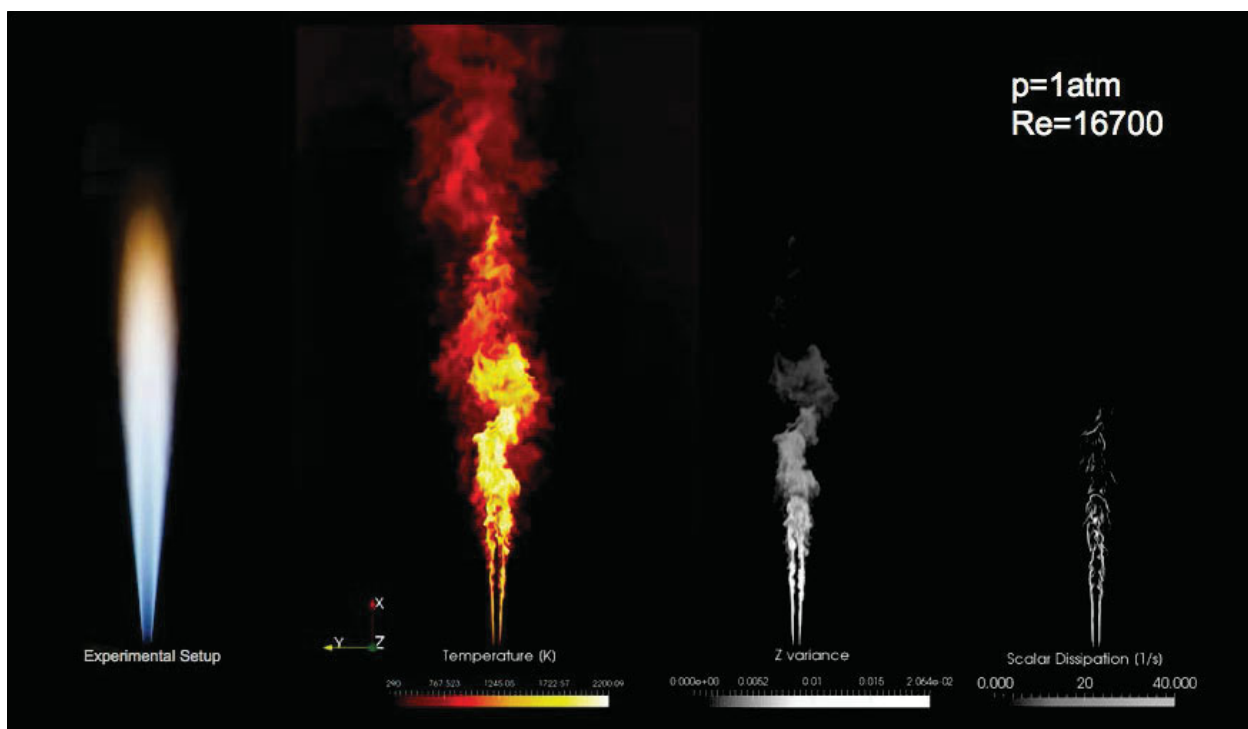
- Simulations were conducted at
 - $p = 1$ atm for validation
 - $p = 2, 5$ atm to investigate flame characteristics at higher pressures
- Approximately 7M points were used for a 3D cylindrical domain with
 - $R=169$ mm and $L = 960$ mm
- The steady laminar flamelet model (SLFM) was adopted for modeling combustion
- Flamelets were constructed based on H₂/CO mechanism consisting of 12 species and 33 reactions (Li et al. 2007)

Large Eddy Simulations II



- A presumed filtered density function (FDF) approach was employed to represent the subgrid-scale turbulence-chemistry interaction:
 - assumed beta-shape FDFs
 - characterized by the resolved mixture fraction and its subgrid variance
- The resolved mixture fraction and its subgrid variance were obtained by solving transport equations
- Smagorinsky model was used for subgrid stresses
- Filtered governing equations were solved using OpenFOAM 2.4
- In particular, a modified version of the flameletFoam solver (Muller et al. 2013) was utilized

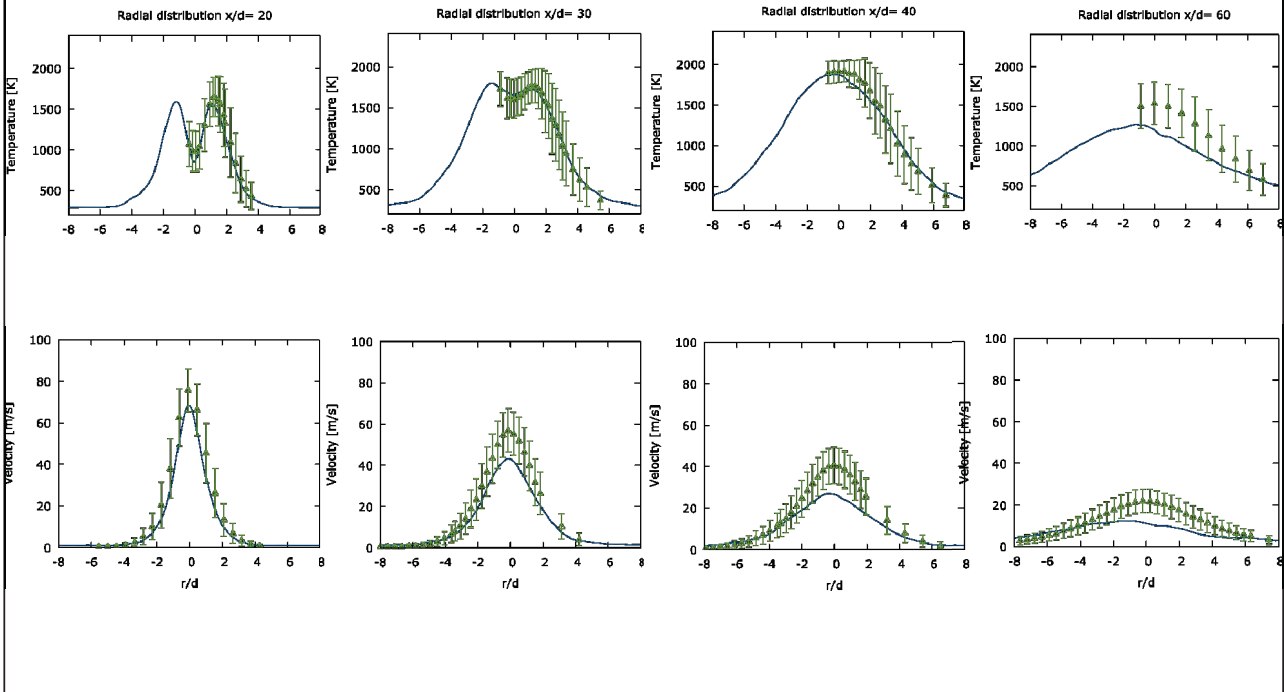
Validation for Flame A



Validation for Flame A: Predictions vs Measurements I



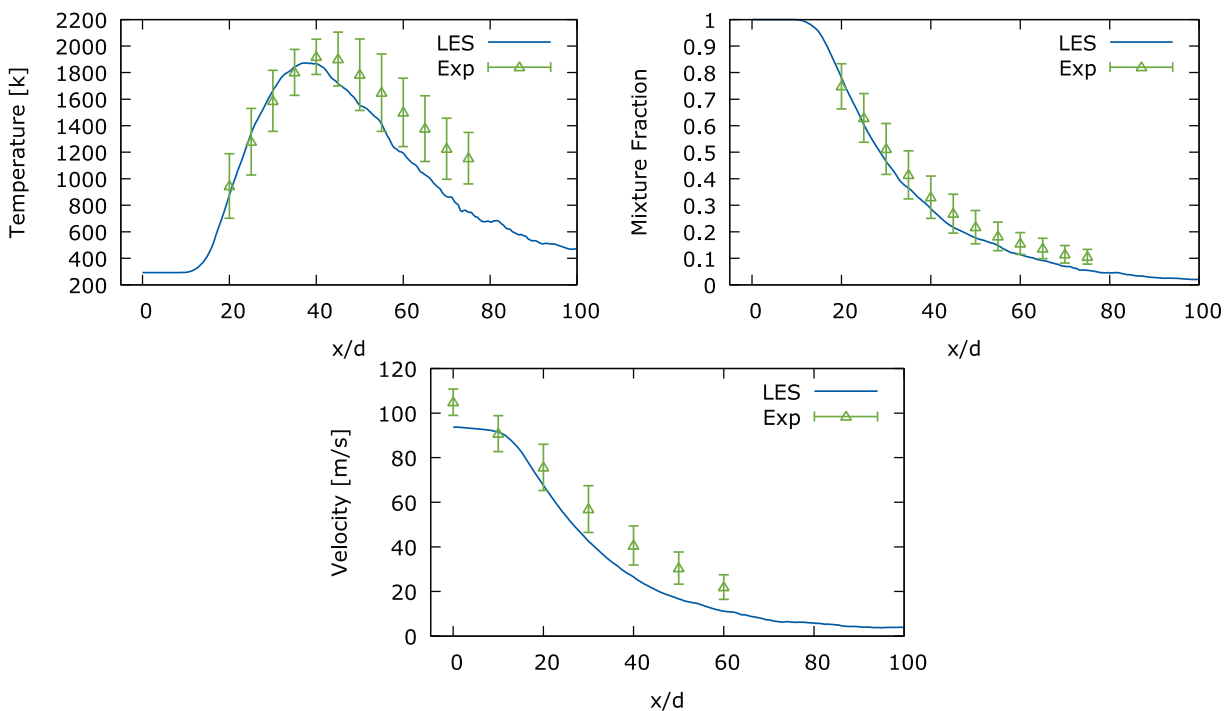
- Radial distribution of mean T and U at x stations



Validation for Flame A: Predictions vs Measurements II



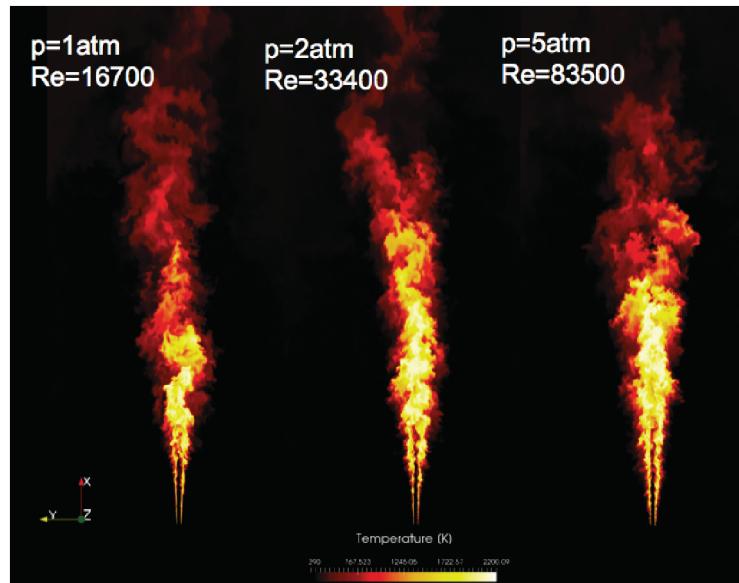
- Axial distribution of mean T, Z, and U



Flame A at Higher Pressures



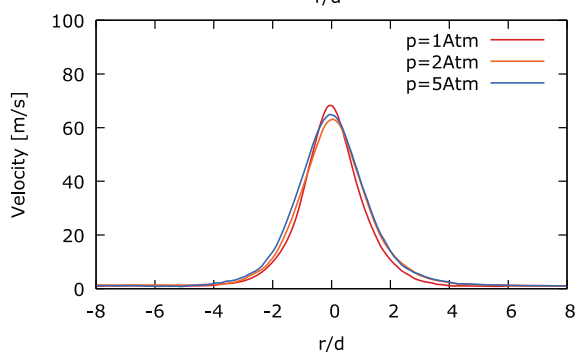
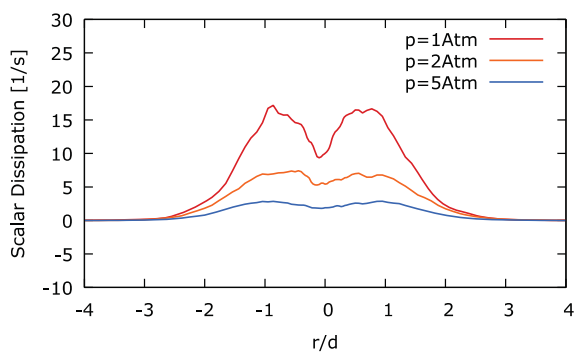
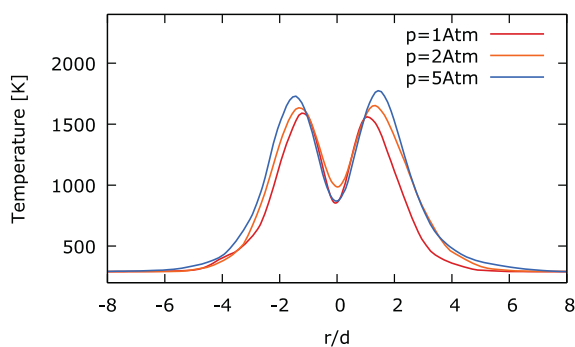
- The mean velocity of jet (76 m/s) was kept constant, hence Re was increased at higher pressures
- Modified the fully-developed turbulent pipe flow profile according to the increased Re
- Adopted the same mesh
- Flamelet libraries were updated to span the required range of pressures



Effects of Pressure I



- Radial distribution of mean T, Scalar Dissipation Rate (SDR), and U at x/d=20



$$\chi = 2D|\nabla Z|^2$$

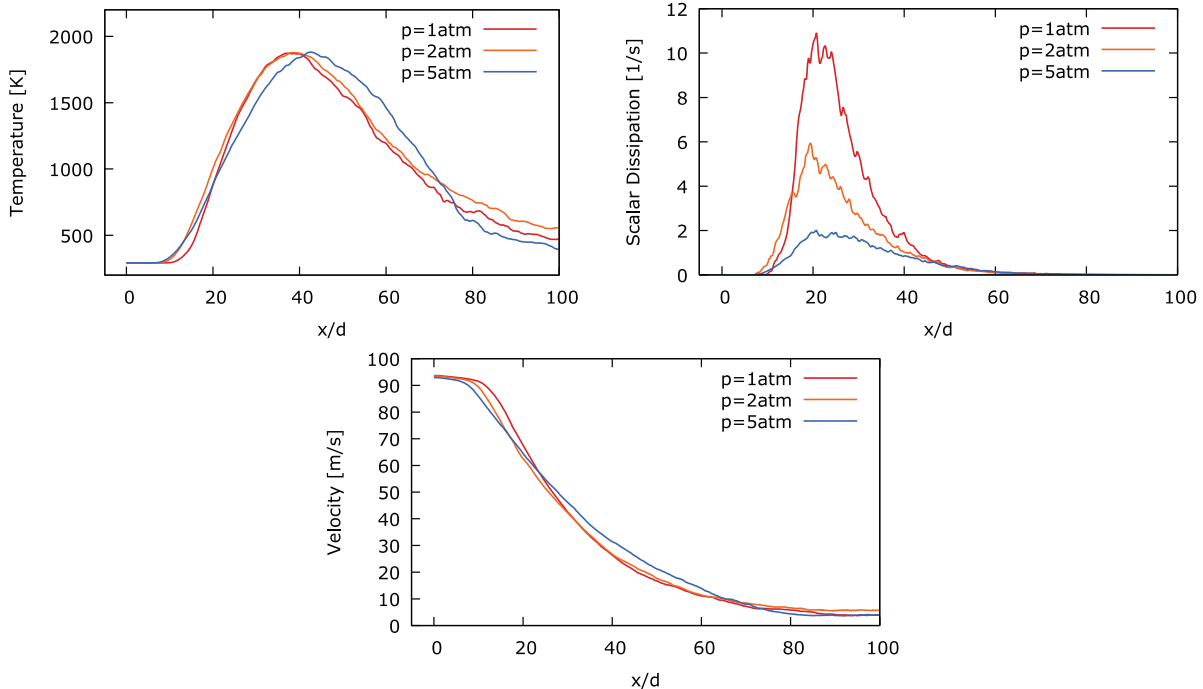
$$D \propto \rho^{-1}$$

$$\chi p \approx const$$

Effects of Pressure II



- Axial distribution of mean T, Scalar Dissipation Rate (SDR), and U



CSP Analysis of Flamelet Solutions I



$$\frac{\partial Y_\alpha}{\partial t} = \frac{1}{2} \chi \frac{\partial^2 Y_\alpha}{\partial \xi^2} + \frac{\dot{\omega}_\alpha}{\rho}, \quad \alpha = 1, \dots, N_s$$

$$\frac{\partial T}{\partial t} = \frac{1}{2} \chi \left(\frac{\partial^2 T}{\partial \xi^2} + \frac{1}{c_p} \frac{\partial c_p}{\partial \xi} \frac{\partial T}{\partial \xi} \right) + \frac{\dot{\omega}_T}{c_p \rho}$$

- $\mathbf{x} = \{Y_\alpha, T\}$ state vector
- $\mathbf{g}(\mathbf{x})$ chemical source term
- \mathbf{J}_g Jacobian of $\mathbf{g}(\mathbf{x})$
- $\mathbf{J}_g = \mathbf{A} \mathbf{\Lambda} \mathbf{B}$
- \mathbf{A}, \mathbf{B} right and left eigenvector matrix of \mathbf{J}_g
- $\mathbf{\Lambda}$ eigenvalue matrix of \mathbf{J}_g
- $\mathbf{L}(\mathbf{x})$ diffusive term

Tangential Stretching Rate (TSR) extension to reaction-diffusion systems

- Weighted average of the chemical source term Jacobian eigenvalues
- **TSR**: reciprocal of the most energetic time scale associated with the **chemical source term**
- **Extended TSR** reciprocal of the most energetic time scale of the **reaction-diffusion system**

$$\frac{\partial \mathbf{x}}{\partial t} = \mathbf{L}(\mathbf{x}) + \mathbf{g}(\mathbf{x}), \quad \text{BCs on } \mathbf{x}, \quad \mathbf{x}(0) = \mathbf{x}_0$$

$$\frac{\partial \mathbf{x}}{\partial t} = \sum_{i=1, N} \mathbf{a}_i(\mathbf{x}) h^i(\mathbf{x}) \quad h^i = \mathbf{b}^i \cdot (\mathbf{L}(\mathbf{x}) + \mathbf{g}(\mathbf{x}))$$

$$\tilde{\tau}_{ext} =: \frac{\mathbf{L}(\mathbf{x}) + \mathbf{g}(\mathbf{x})}{|\mathbf{L}(\mathbf{x}) + \mathbf{g}(\mathbf{x})|}$$

$$W_{i,ext} := \frac{h^i}{L + g} (\tilde{\tau}_{ext} \cdot \mathbf{a}_i) = \frac{h^i}{L + g} \sum_{k=1}^N \frac{h^k}{L + g} (\mathbf{a}_k \cdot \mathbf{a}_i)$$

$$\omega_{\tilde{\tau}_{ext}} := \tilde{\tau}_{ext} \cdot \mathbf{J}_g \cdot \tilde{\tau}_{ext} = \sum_{i=1}^N W_{i,ext} \lambda_i$$

CSP Analysis of Flamelet Solutions II



Test cases:

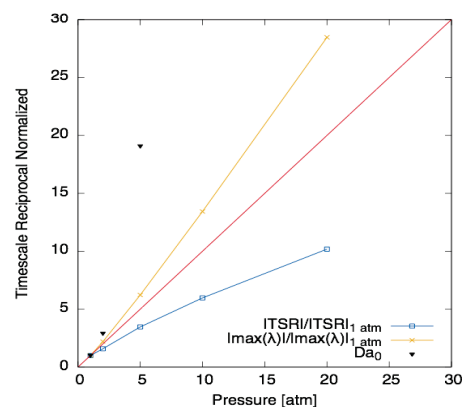
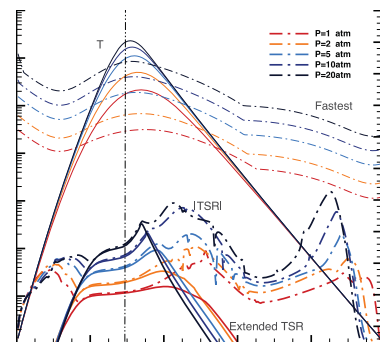
- flamelets adopted for Sandia/ETH-Zurich Flame A LES computations
- Fu:** 40% CO, 30% H₂, 30% N₂, **Ox:** Air
- Scalar Dissipation = 100s⁻¹**
- P = 1, 2, 5, 10, 20 atm**

Pressure increase leads to:

- higher temperatures
- smaller timescales**
- shrinking of the region** where the system dynamics is governed by chemical kinetics (where the TSR and the extended TSR coincide)

At stoichiometric mixture fraction (Z=0.295):

- inverse of fastest time scale follows a power law with exponent larger than one
- TSR (most energetic chemical timescale), follows a power law with exponent smaller than one**



CSP Analysis of Flamelet Solutions III

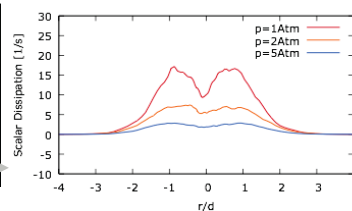
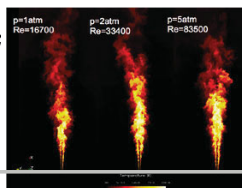


LES results for p=1,2,5 atm:

$$\chi = 2D|\nabla Z|^2$$

$$D \propto \rho^{-1}$$

$$\chi p \approx const$$



- scalar dissipation decreases almost linearly with pressure increase

Test cases:

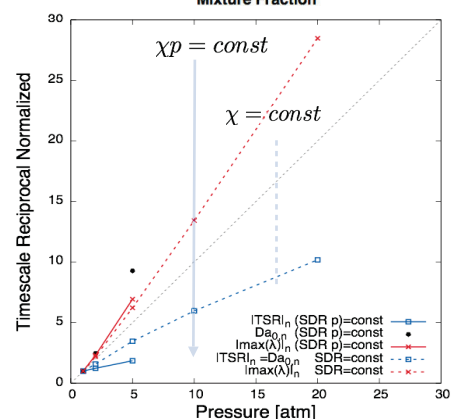
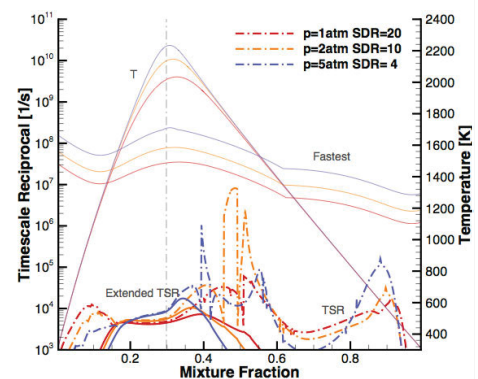
- p=1atm SDR=20s⁻¹
- p=2atm SDR=10s⁻¹
- p=5atm SDR= 4s⁻¹

Pressure increase leads to:

- higher temperatures
- smaller fastest timescales**

At the stoichiometric mixture fraction (Z=0.295):

- reciprocal of fastest time scale follows a power law with exponent larger than one
- TSR (most energetic chemical timescale), is almost constant**



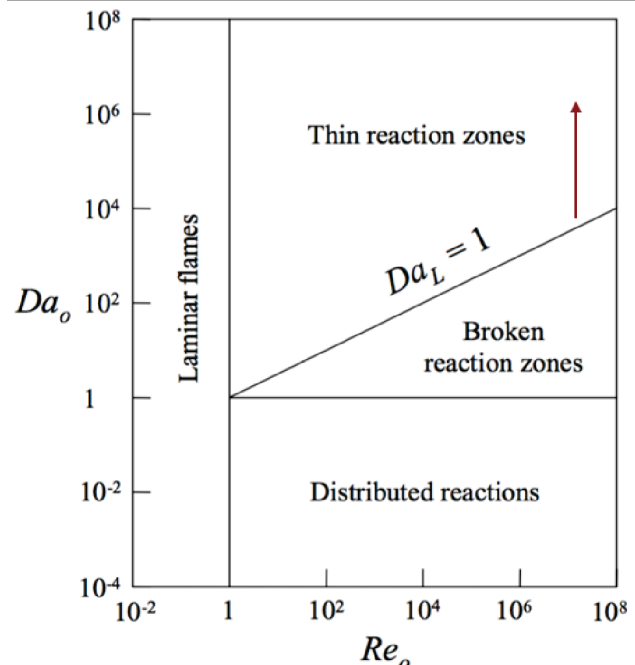
Pressure and Local Flamelet Assumption



$$Re_0 = \frac{\rho U_{jet} D}{\mu} = p \frac{U_{jet} D}{RT\mu} \propto p$$

$$Da_0 \propto \frac{1}{\chi_{st}} p^{1+\frac{\alpha}{2}}$$

- An increase in pressure leads to higher Da_0
- The combustion regime remains in the thin reaction zone
- The validity of the local laminar flamelet assumption is ensured



Summary



- LES predictions show that
 - increasing pressure results in higher temperatures and a reduction in the scalar dissipation rate (SDR)
 - the velocity field is not strongly affected by the pressure increase
- CSP analysis of flamelets reveals that an increase in pressure leads to
 - higher temperatures
 - shorter time scales
 - a shrinkage of the region where the system dynamics is governed by chemical kinetics
- Experimental characterizations and model validation are needed

Challenges and Progress in Modeling Turbulent Combustion Processes at Elevated Pressures

Joseph C. Oefelein

with contributions from

Rainer Dahms, Guilhem Lacaze, Layal Hakim

Combustion Research Facility

Sandia National Laboratories, Livermore, CA 94551

Support Provided by the U.S. DOE

Office of Science – Basic Energy Science Program

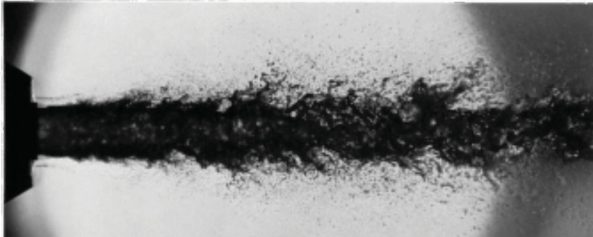
Office of Energy Efficiency and Renewable Energy – Vehicle Technologies Program

Oak Ridge National Laboratory – Oak Ridge Leadership Computing Facility

is Gratefully Acknowledged

Effects of pressure on liquid injection are not well understood

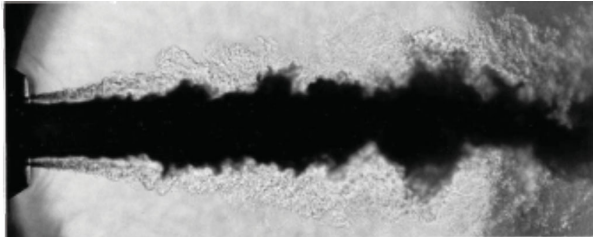
10 bar



At “Low” Pressures ...

- Molecular interface separates injected liquid from ambient gases
- Interactions between dynamic shear forces and surface tension promote primary atomization and breakup
- Spray evolves from dense to dilute state in classical manner

60 bar



At “High” Pressures ...

- Interfacial diffusion layers develop presumably due to lower surface tension
- Lack of inter-molecular forces promotes diffusion dominated turbulent mixing prior to atomization
- Interfacial region between jets interact in presence of exceedingly large gradients

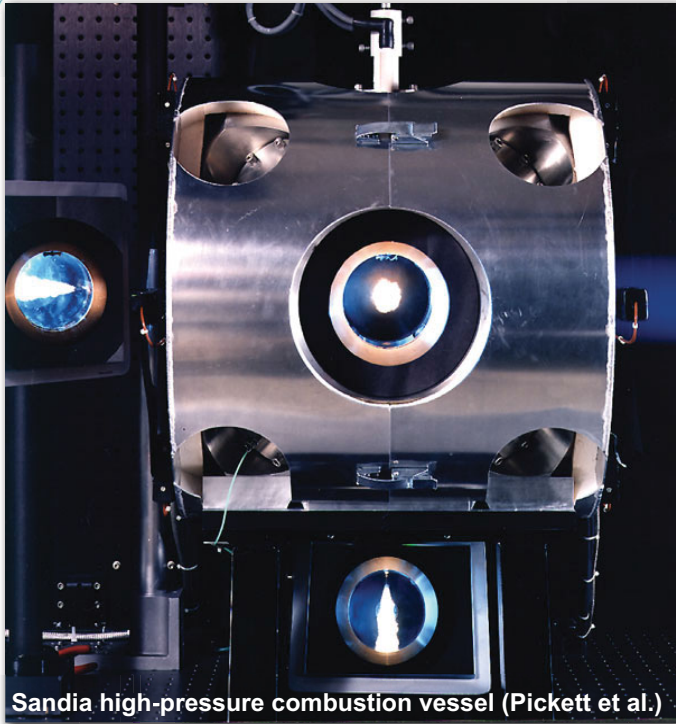
Shear-coaxial injection of liquid-N₂ and He
(N₂: $p_c = 34$ bar, $T_c = 126$ K)

W. Mayer, *et al.* (1998). Atomization and breakup of cryogenic propellants under high-pressure subcritical and supercritical conditions. *Journal of Propulsion and Power*, **14**(5): 835-842.

Why?



Consider the Sandia "Spray-A" experiment (n-Dodecane – Air) ...



Injection and Initial Conditions

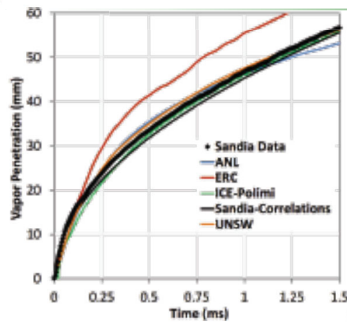
Fuel Temperature:	363 K
Chamber Temperature:	450, 900 K
Chamber Pressure:	30, 60 bar
Peak Velocity:	600 m/s
Jet Reynolds Number:	O(100,000)
Nozzle Diameter:	0.09 mm
Chamber Volume:	(1000d) ³

Available Data

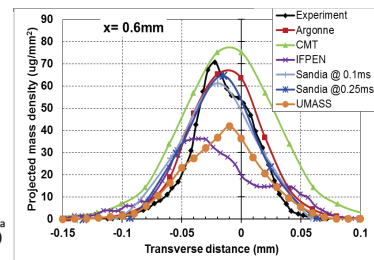
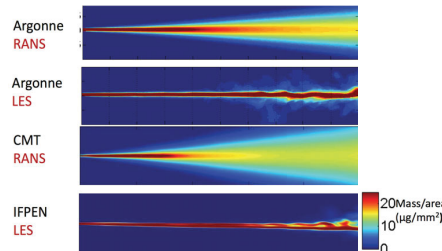
- Rate of injection
- Rayleigh scattering images
- Schlieren movies
- Liquid length versus time
- Vapor length versus time



Deficiencies in model development have been demonstrated for years

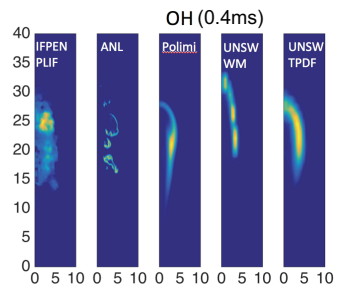
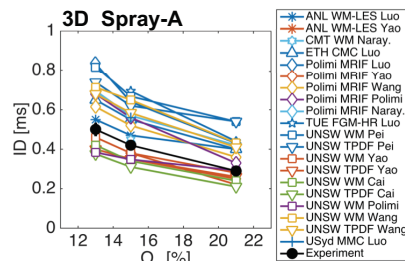
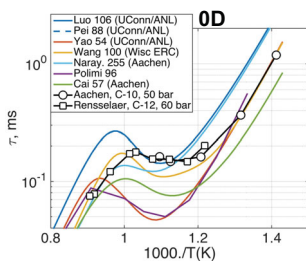


Projected Mass Distribution



Inconsistencies in non-reacting calculations observed in all ECN workshops (here ECN4)

- Correct vapor penetration but large scatter in other quantities

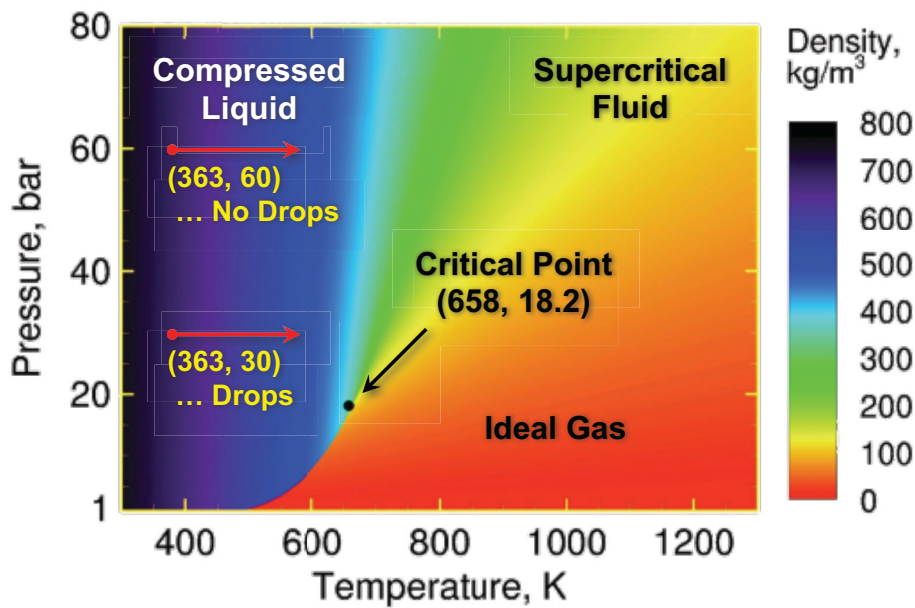


Similarly, large scatter is observed in reacting calculations

- Large variability between chemical mechanisms and shock tube data, and scatter in ignition delay (ID) in Spray-A simulations

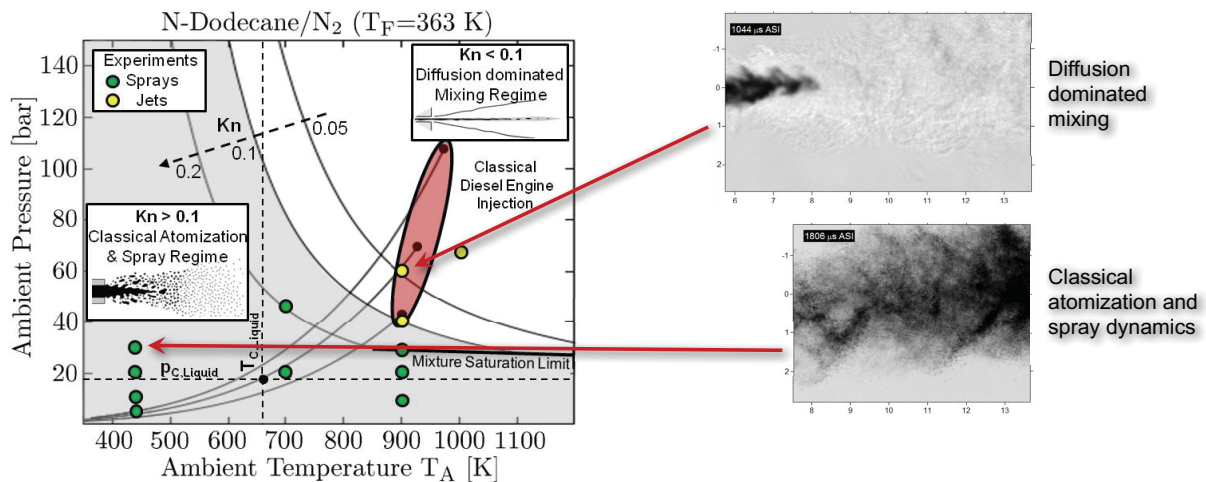
There is a distinct lack of discriminating data due to many competing effects in both models and numerical methods ... 4

Direct injection processes in this experiment exhibit similar behavior



We see drops when n-Dodecane is injected at 363 K, 30 bar, but not at 363 K, 60 bar

Theory suggests what causes the transitional physics

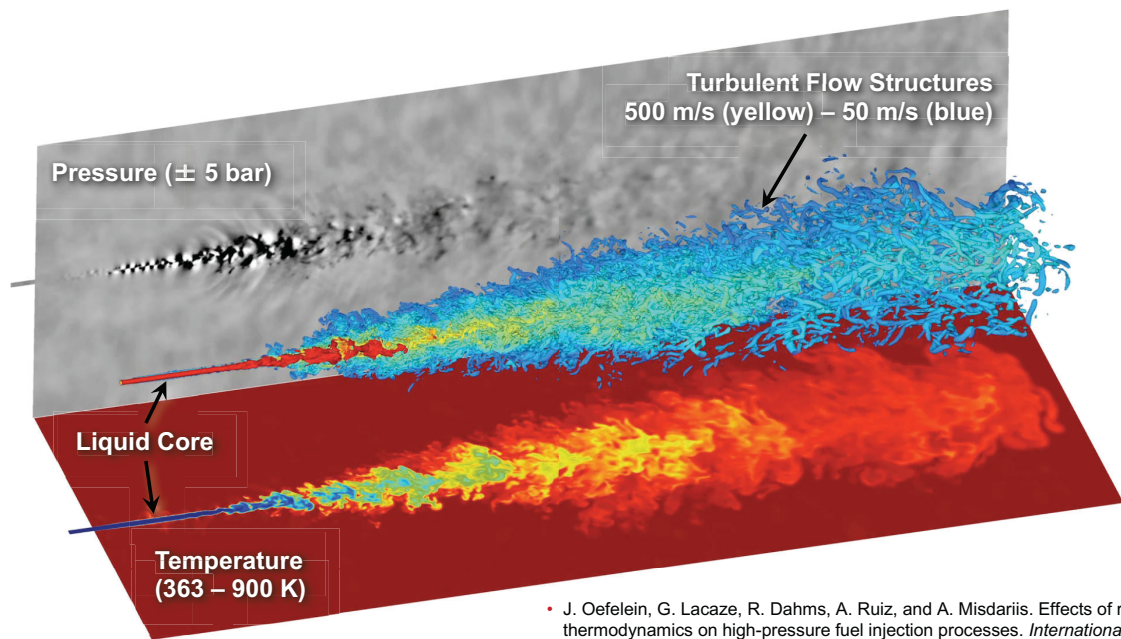


Transition from spray to diffusive mixing occurs through combination of broadening interfaces, reduced mean free path, vanishing surface tension

- R. N. Dahms and J. C. Oefelein. On the transition between two-phase and single-phase interface dynamics in multicomponent fluids at supercritical pressures. *Physics of Fluids*, **25**: 092103, 2013.
- R. N. Dahms and J. C. Oefelein. Non-equilibrium gas-liquid interface dynamics in high-pressure liquid injection systems. *Proceedings of the Combustion Institute*, **35**:1587–1594, 2015.



LES using real-fluid thermodynamics, transport provides additional insights



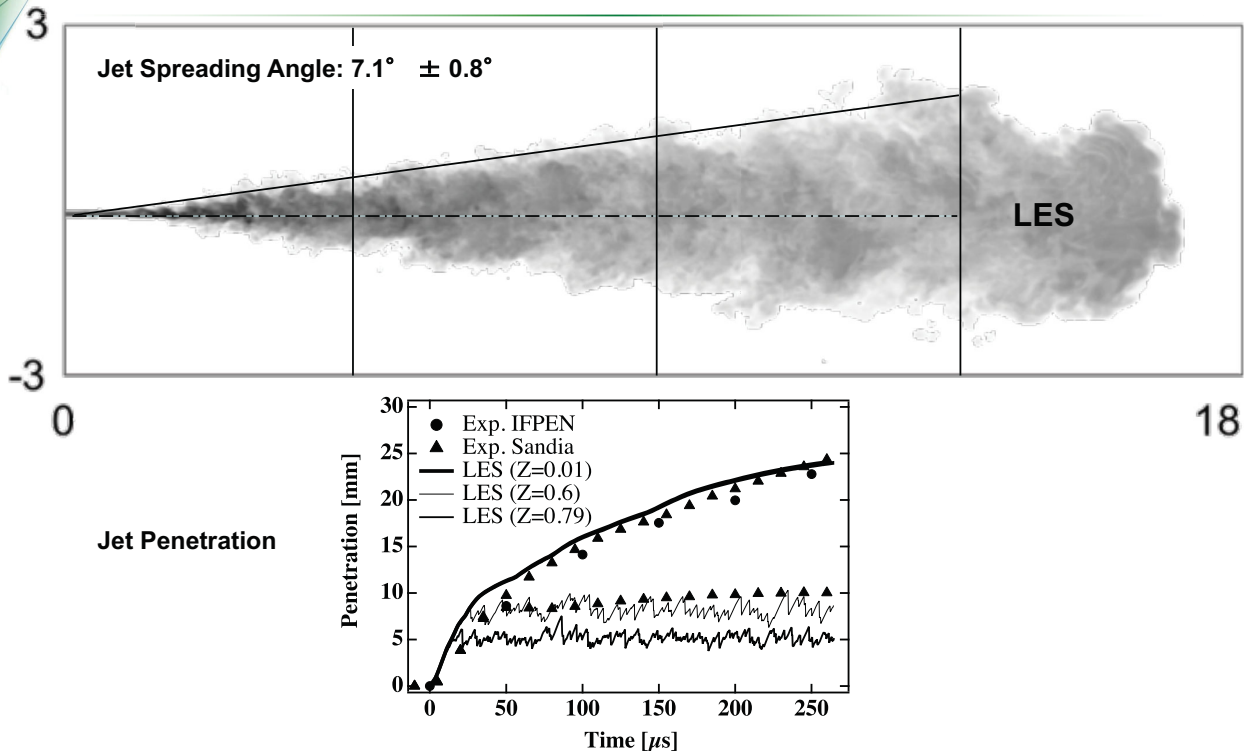
- J. Oefelein, G. Lacaze, R. Dahms, A. Ruiz, and A. Misdariis. Effects of real-fluid thermodynamics on high-pressure fuel injection processes. *International Journal of Engines*, 7(3):1–12, 2014.
- G. Lacaze, A. Misdariis, A. Ruiz, and J. C. Oefelein. Analysis of high-pressure diesel fuel injection processes using LES with real-fluid thermodynamics and transport. *Proceedings of the Combustion Institute*, 35:1603–1611, 2015.

COMBUSTION RESEARCH FACILITY

Sandia National Laboratories



Good agreement with available experimental data

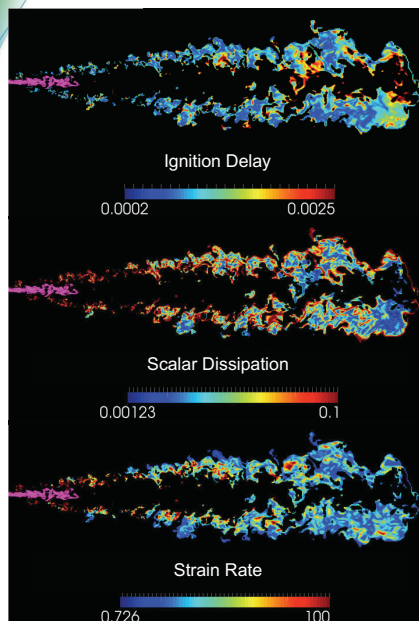


COMBUSTION RESEARCH FACILITY

Sandia National Laboratories

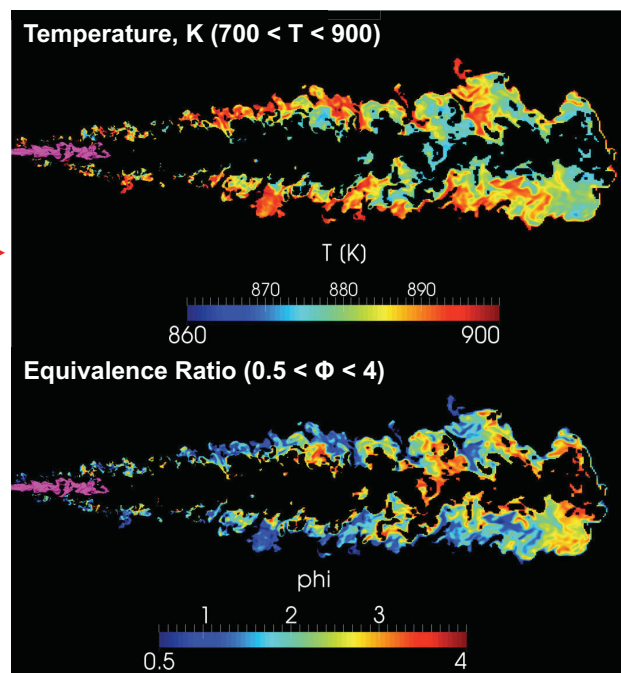


Results not available from experiment highlight flammable regions ...



Autoignition most likely to occur where ignition delay time, scalar dissipation rate, and strain rate are simultaneously minimized

Identification of flammable regions used to identify conditions where the chemical model must perform accurately



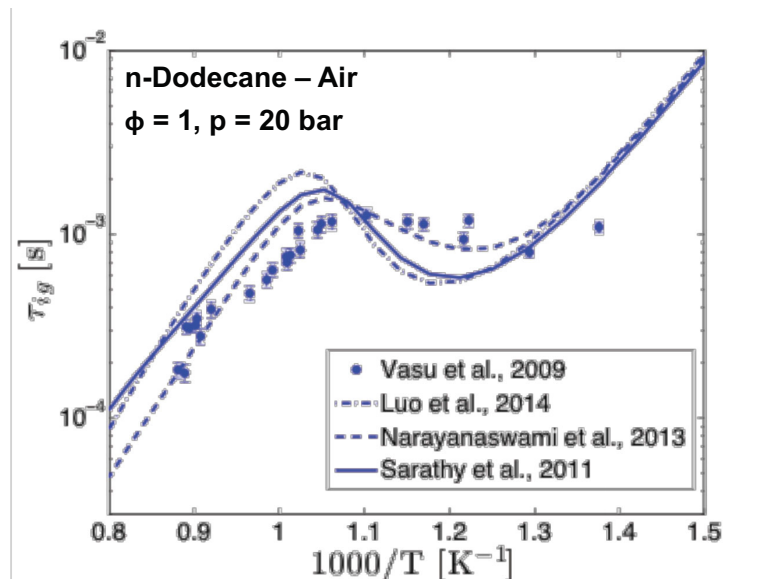
Pressure: 60 ± 5 bar



Selection of candidate mechanisms presents interesting questions

- Sarathy et al., 2011
 - 2-methyl-alkanes and n-alkanes up to C12 (2755 species and 11173 reactions)
 - Validated for n-dodecane – air auto-ignition delay times ...
 - Against experimental data
 - Up to 20 bar from low to high temperatures (600 – 1500 K)
- Narayanaswami et al., 2013
 - Skeletal mechanism (255 species and 2289 reactions)
 - Reduced from Sarathy et al., 2011
 - Directed relation graph with error propagation (DRGEP) and isomer lumping
 - Modification of some reaction rates based on recent theoretical and experimental analysis
 - Validated for n-dodecane – air auto-ignition delay times
 - Against experimental data and detailed mechanism
 - Up to 20 bar from low to high temperatures (600 – 1500 K)
- Luo et al., 2014
 - Skeletal mechanism (105 species and 420 reactions)
 - Reduced from Sarathy et al., 2011
 - DRG with expert knowledge (DRGX) and DRG-aided sensitivity analysis (DRGASA)
 - Validated for n-dodecane – air auto-ignition delay times
 - Against experimental data and detailed mechanism
 - Up to 20 bar and from low to high temperatures (600 – 1500 K)

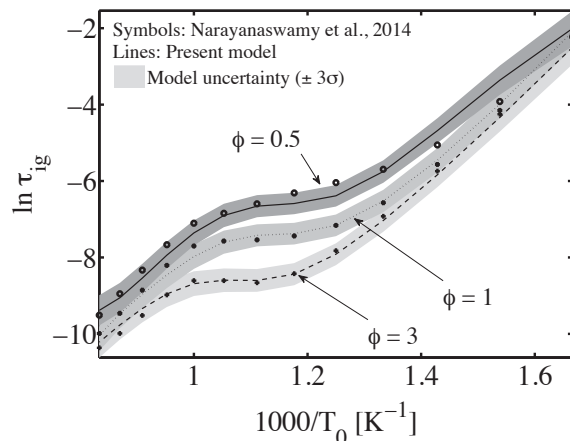
There is a wide range of variability between mechanisms (true in general)



e.g., Predicted ignition delay time (even within designed ranges) exhibit notable differences, particularly in NTC region and at high temperatures

Given variability, UQ used to optimize chemical models for simulations

- **Objective**
 - Design model around specified range of operating conditions (p , T , ϕ) using detailed reference mechanism
 - Optimize model to capture specific chemical characteristics (e.g., ignition delay, flame propagation, selected emissions)
 - Minimize implementation cost for CFD
- **Approach**
 - Start with simplest model form such as models that follow Arrhenius laws for reaction rates (Westbrook et al. 1981, Misdariis et al. 2014)
 - Functionalize pre-exponential factors and activation energies w.r.t. operating conditions
 - Use Bayesian inference to fit the most probable surfaces over specified range of conditions
 - Calculate uncertainties relative to reference and add model complexity as needed



Approach provides “simplest” least expensive model optimized to provide selected characteristics with error bars on predictions

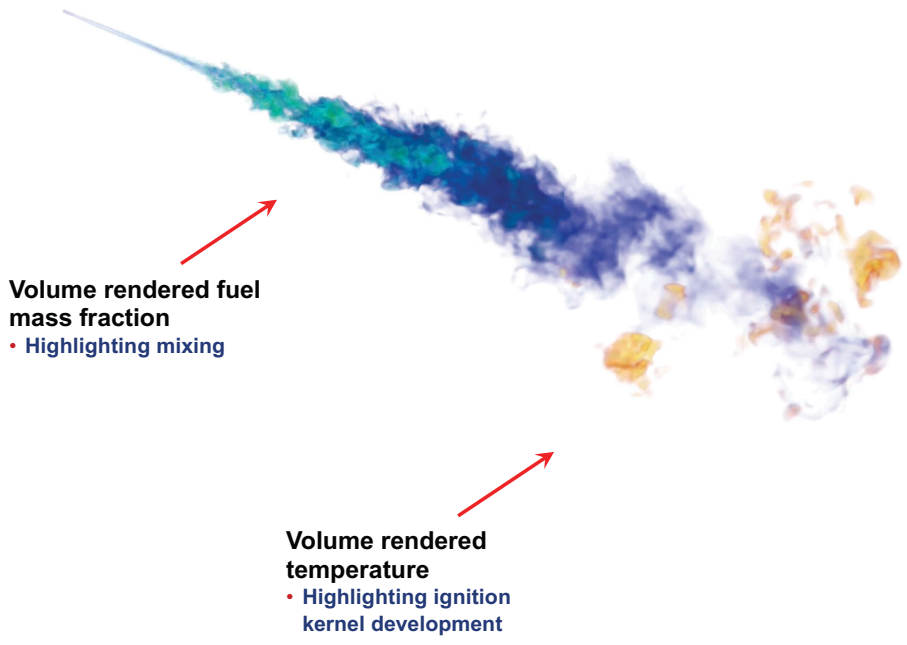
Here 12 species, 5 step model optimized for ignition delay using Narayanaswami et al. as reference

L. Hakim, G. Lacaze, M. Khalil, H. N. Najm, and J. C. Oefelein. Modeling auto-ignition transients in reacting Diesel jets. *ASME 2015 Internal Combustion Engine Division Fall Technical Conference*, Paper 2015-1120, November 8-11 2015. Accepted for publication in the *Journal of Engineering for Gas Turbines and Power*.



Modeled instantaneous fluctuations facilitate formation of ignition kernels

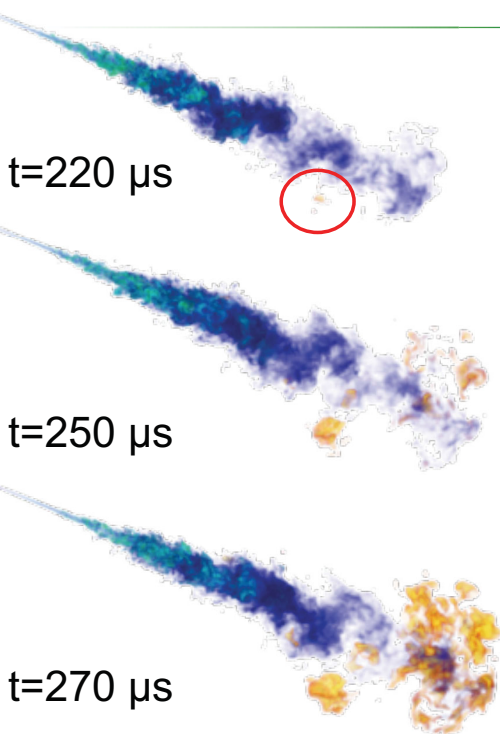
L. Hakim, G. Lacaze, and J. C. Oefelein. Large eddy simulation of autoignition transients in a model Diesel injector configuration. SAE World Congress, Paper 2016-01-0872, April 12-14, 2016.



COMBUSTION RESEARCH FACILITY



Ignition sequence



First kernel, diameter $\approx 500 \mu$ m (too small to be optically detected in experiment)
Location: tip of the jet, off-axis

Independent kernels appear, diameter $\approx 500 \mu$ m to 2mm (still very small for optical detection)
Location: tip of the jet, off-axis

Many small kernels present in the "jet tip" region ... impact on schlieren?



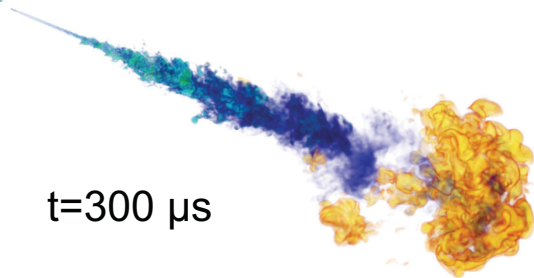
Schlieren images by Skeen *et al.*, PCI, 2015

COMBUSTION RESEARCH FACILITY



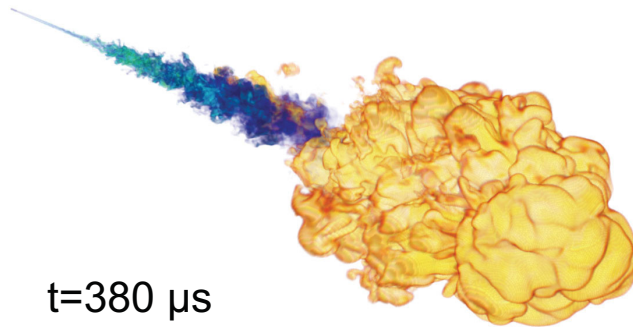


Ignition sequence



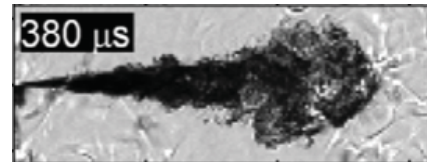
t=300 μs

Single flame structure with upstream independent kernels, flame expands through dilatation and autoignition



t=380 μs

Main flame region at the jet extremity, autoignition locations observed ahead of main front



Schlieren images by Skeen *et al.*, PCI, 2015

COMBUSTION RESEARCH FACILITY

Sandia National Laboratories



Toward Quantitative Imaging of Turbulent Mixing Dynamics in High-Pressure Fuel Injection Systems

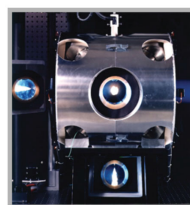
Jonathan Frank (PI), Adam Ruggles, Erxiong Huang – Reacting Flows (8351)

Scott Bisson – Remote Sensing & Energetic Materials (8353)

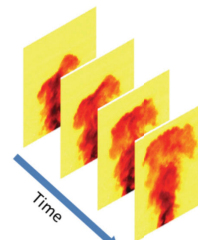
Brian Patterson – Combustion Chemistry (8353)

Lyle Pickett, Julien Manin, Scott Skeen, Panos Sphicas, Dave Cicone – Engine Combustion (8362)

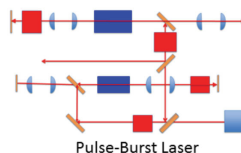
Funded via Sandia LDRD



High-Pressure Fuel Injection



High-speed Imaging



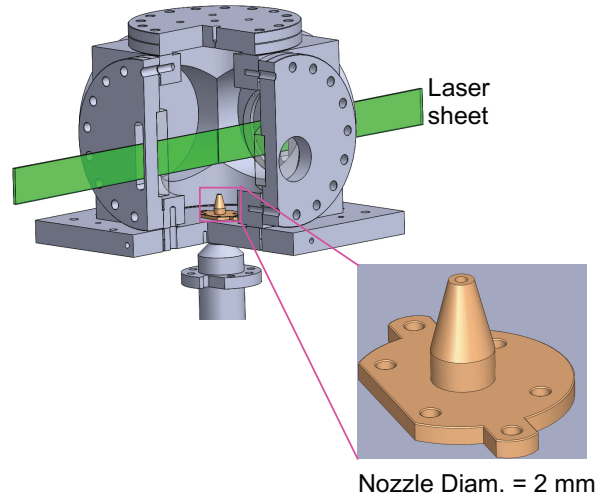
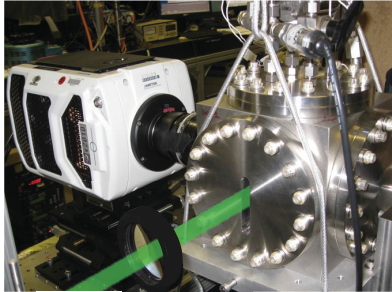
Pulse-Burst Laser

COMBUSTION RESEARCH FACILITY

Sandia National Laboratories



New Pressure Vessel For Imaging of Canonical High-Pressure Flow in Well-Controlled Environment

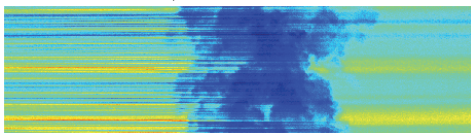


- Pressure vessel rated to 30 atm.
- Measured range of $P_{\text{injector}}/P_{\text{ambient}}$
- Helium injected into methane
- Cold trap to remove condensates



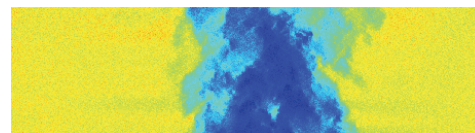
Development of Beam Steering Correction for High-Pressure Imaging

Laser Propagation Direction



$P_{\text{inj}} = 15 \text{ atm.}$

$P_{\text{amb}} = 8 \text{ atm.}$



After wavelet filtering

Developed new method to correct for stripes while minimizing impact on physical structures



100 kHz Rayleigh Scattering Measurements of High-Pressure Gas Jets

$P_{inj} = 15 \text{ atm.}$

$P_{amb} = 8 \text{ atm.}$

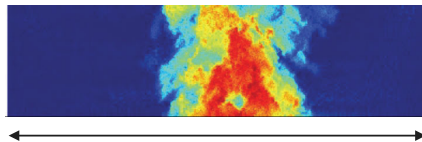
$P_{inj} = 42 \text{ atm.}$

$P_{amb} = 8 \text{ atm.}$

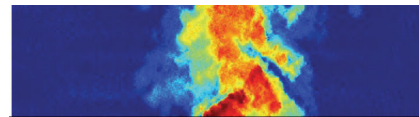
x/D

25

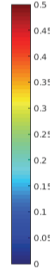
18



42 mm



Mole Fraction of Jet Gas



Time resolved measurements of helium mole fraction

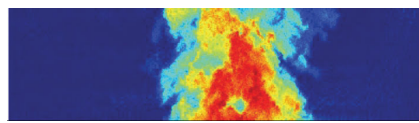
$\Delta t = 10 \text{ us, } t_{burst} = 5 \text{ ms}$

COMBUSTION RESEARCH FACILITY

Sandia National Laboratories

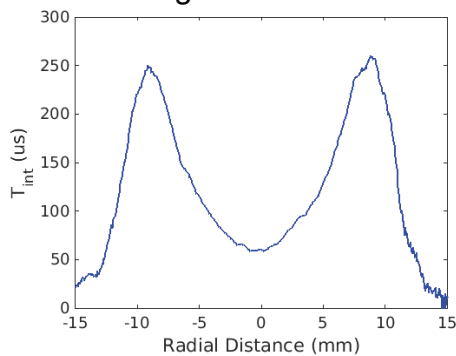


100 kHz Rayleigh Scattering Imaging of High-Pressure Gas Jet

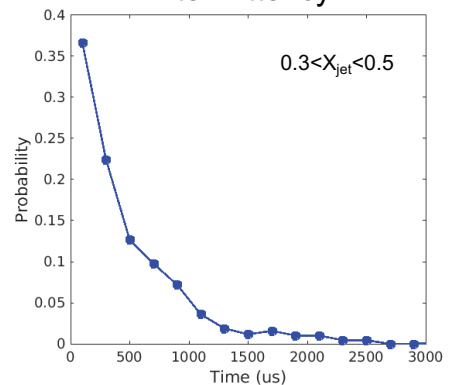


42 mm

Integral Time Scales



Jet Centerline Intermittency



COMBUSTION RESEARCH FACILITY

Sandia National Laboratories



Diesel Ignition/Combustion Linked to Transient Mixing

Diesel "Spray A" conditions

Ambient Gas	Fuel
900 K	373 K
60 bar	1500 bar
15% O ₂	n-dodecane

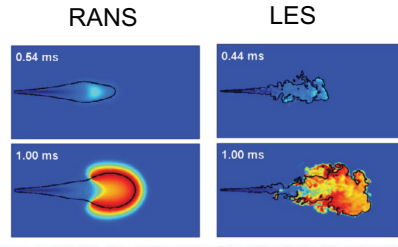
150 kHz schlieren imaging



- Cool flame in...
 - Schlieren "tr... scale organi...
 - Cool flame t...
- High-tempera...
 - Low-density (2000 K) zones appear again
 - Flame "lift-off" stabilizes at approx. 17 mm
- Accurate CFD modeling of ignition is needed

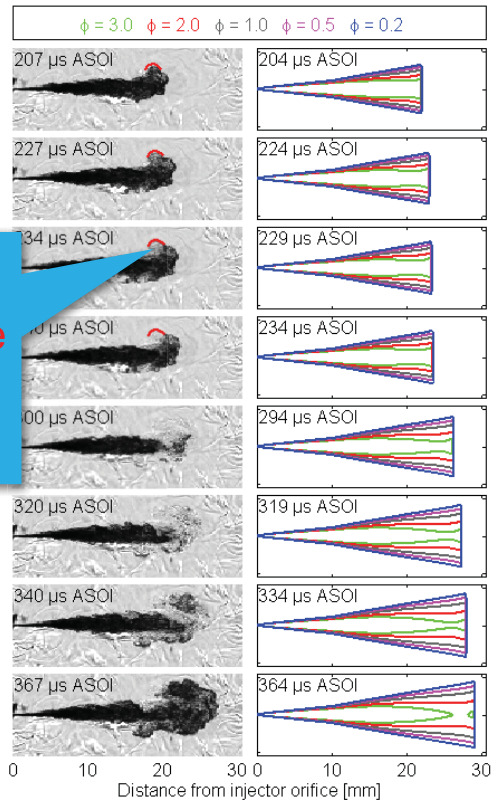
How does local mixture state evolve prior to autoignition?

Pei et al.
Combust. Flame
in press



Schlieren

Jet Model Predictions of Equivalence Ratio



COMBUSTION RESEARCH FACILITY

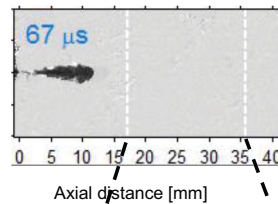
Sandia National Laboratories



Transient spray mixture fraction measured in vaporized region of non-reacting injection

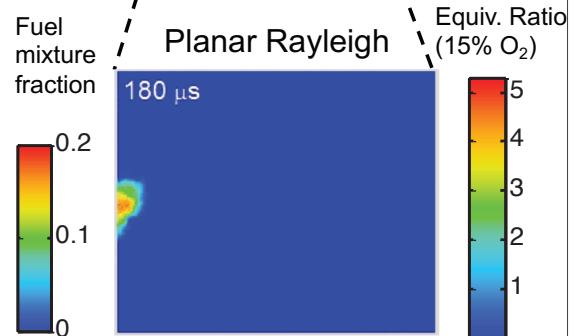
- Rayleigh imaging quantifies transient mixture fraction / equivalence ratio for the first time
 - Target condition Spray A has massive research effort to understand engine spray combustion
- Jet mixing - large structures shed to side and re-entrained
 - Larger residence time in hot mixtures
- Obvious target for high-fidelity LES studies
 - Verify accurate mixing field as preliminary step towards predicting ignition/combustion
 - Quantify variance, needed input for CFD

150 kHz schlieren imaging



Ambient Gas
900 K
60 bar
15% O₂

Region of interest for ignition and lift-off stabilization



Ambient Gas
900 K
60 bar
0% O₂

COMBUSTION RESEARCH FACILITY

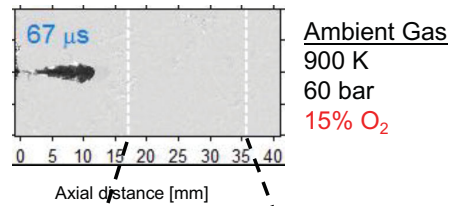
Sandia National Laboratories



Transient Temperature History Important to Ignition

- Rayleigh imaging quantifies transient mixture fraction / equivalence ratio for the first time
 - Target condition Spray A has massive research effort to understand engine spray combustion
- Jet mixing - large structures shed to side and re-entrained
 - Larger residence time in hot mixtures
- Obvious target for high-fidelity LES studies
 - Verify accurate mixing field as preliminary step towards predicting ignition/combustion
 - Quantify variance, needed input for CFD

150 kHz schlieren imaging



Region of interest for ignition and lift-off stabilization

Ambient Gas
900 K
60 bar
0% O₂



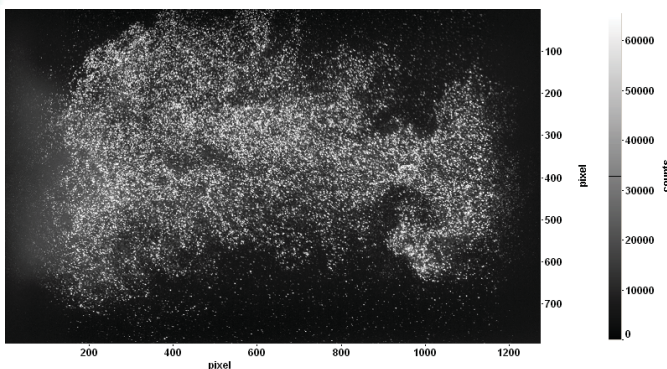
COMBUSTION RESEARCH FACILITY

Sandia National Laboratories

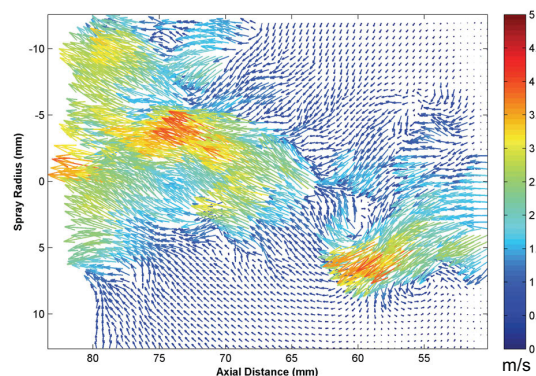


Single-Shot PIV in Non-reacting Fuel Injection

Particle/Drop Scattering



Single Shot



Chamber: T= 460K, P = 30 bar
Spray A: dodecane

Vectors determined from combination of seed particles and spray droplets.
Images captured at end of injection ($\Delta t_{inj, delay} = 10$ ms).

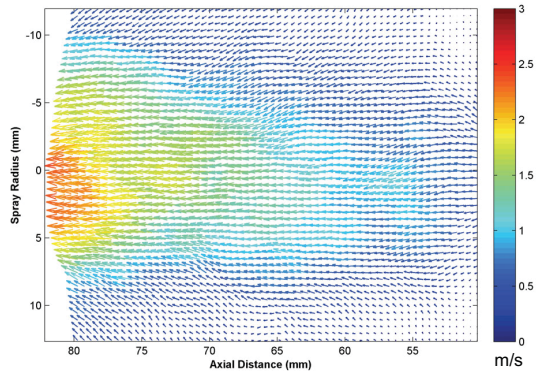
COMBUSTION RESEARCH FACILITY

Sandia National Laboratories

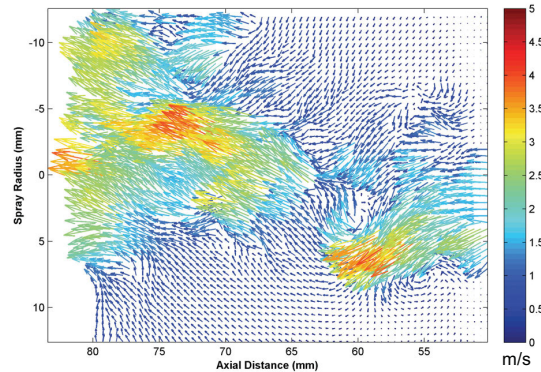


Demonstrated Single-Shot PIV in Non-reacting Fuel Injection

Average of 25 Shots



Single Shot



Chamber: T= 460K, P = 30 bar
Spray A: dodecane

Vectors determined from combination of seed particles and spray droplets.
Images captured at end of injection ($\Delta t_{inj.delay} = 10$ ms).



Summary

- Theory suggests that the transition from atomization to diffusion dominated mixing at high pressures occurs through broadening interfaces, reduced mean free path, vanishing surface tension
- Using this theory as basis, real-fluid model was applied using LES to focus on the effects of high-pressure thermodynamics and transport in the “Spray-A” case
- Analysis of transient mixing processes revealed the nature of flammable regions just prior to autoignition and related ranges in pressure, temperature, and equivalence ratio
- Highlighted the wide variability that exists between leading detailed and skeletal chemical mechanisms, applied UQ methods to derive “optimal” chemical model
- Demonstrated progressive use and development of LES that combines theory, experiments, and detailed analysis aimed at both discovery and predictive models

blank

Key Challenges and Priorities



1. Stratified flames, flames with inhomogeneous inlets, new TNF gaseous flames
2. Regime identification, regime independent models, progress variables
3. DME-/complex fuel flames, counter flow flames
4. New horizons: Flame-wall interaction, high pressure flames

30.07.2016 | TNF 13 | 1



Stratified TUD/CAM



- Higher stratification cases
- Improve CO-prediction
- H₂-addition
- Higher u'/s_1

30.07.2016 | TNF 13 | 2



Inhomogeneous inlet flame from Sydney



EXP:

- measure flow velocity and mixture fraction for non-reactive configuration for recession distance of 300 mm and 75 mm
- Why use a global jet-equivalence-ratio so rich (5.0)?

SIM

- Agree on B.C., including pilot (non-equilibrium)
- Investigate influence of heat transfer of pilot
- Prove mesh independency (and comparison of mesh size in flame region?)
- Improve CO-prediction
- Perform conditional averaging for better physical understanding

30.07.2016 | TNF 13 | 3



New TNF gas flames



- Flames with much higher u'/s_f ?
- Flames with steeper mixture fraction gradients?
- Flames with regime crossing that are less sensitive to BC, more close to an industrial-type design?
- Combining these features (u'/s_f -gradZ-regime crossing)?

30.07.2016 | TNF 13 | 4



Regime identification and regime independent models



- Important and seems to be a hot topic for TNF14
- Different indicators available, but how to validate?
- Develop regime-independent combustion models
- What is the best validation case for regime-independent combustion models?
- Is there any additional experimental data necessary?

30.07.2016 | TNF 13 | 5



Progress variable definitions



- Interesting because cross-dissipation seems to become accessible → can be used to identify the local regime in which the flame is burning
- Consider to use the new PV definition for comparison to simulation (replacing T vs. Z)
- Should it be normalized?
- Subtract mean before calculating scalar dissipation (PV, Z, cross dissipation)?

30.07.2016 | TNF 13 | 6



DME-flames/complex fuels

- Raman needs intermediate species measurements (ongoing)
- Simulation progressed from last TNF such that flames up to case F are fairly well predicted, flames with more extinction (flame G and G`) remain open
- New Sydney DME flame emerged where chemistry matters more and impacts turbulence-(low temperature) chemistry interaction, this could be a new target case

Counter-flow flames

- Agree on standardized inflow conditions → shorter domain, focus on zone relevant for studying turbulent flames
- Compare inflows generated by Sandia and Univ. Duisburg-Essen
- Include cases with higher turbulence levels
- More experimental parameters to be measured (CH_2O , OH , T_{ray}) → analyse low temperature kinetics, conditional statistics
- Investigate influence of complex-fuel chemistry on turbulence-chemistry interaction (as obvious from comparing DME to CH_4 flames)
- More contributors!

Exp

- Measure more scalars
- Measure wall temperature and heat transfer
- Parametric variation (wall temperature, fuel variation, surface coatings, effusion cooling, ...)

Sim

- Reduction strategy? How many parameters?
- How to handle diffusion flames?
- Complex fuels, influence of low-temperature kinetics?
- Pollutant formation?
- Turbulence-chemistry interaction models influenced by presence of wall?

SWQ-flame proposed as future TNF-target configuration

High pressure flames

- Interesting topic
- Challenging for various reasons
 - Diagnostics: accuracy, precision, spatial resolution, beam steering, ...
 - Boundary conditions: Are they known sufficiently well? Reproducibility? ...
 - Chemical reaction mechanisms: validity at high pressures?
 - Include sprays and spray combustion?
 - Avoid soot in the TNF context
- How to proceed?

blank

1. **Quantitative high repetition rate laser diagnostics for the study of auto-ignition in a jet-in-hot-coflow and for the validation of numerical simulations**
C. Arndt, J. Prause, M. Papageorge, F. Fuest, W. Meier, J. Sutton, M. Aigner
2. **DNS of turbulent premixed flames at high Reynolds and Karlovitz numbers**
A. Attili, S. Luca, F. Bisetti
3. **Comparative study of RANS-EDC, LES-CSE and LES-FGM simulations of Delft jet-in-hot-coflow (DJHC) natural gas flames**
H. Bao, X. Huang, J. Labahn, A. Vasavan, D.J.E.M. Roekaerts, C. Devaud, J.A. van Oijen
4. **On defining progress variable for experiments in partially-premixed methane flames**
R.S. Barlow, G. Magnotti, H.C. Cutcher, A.R. Masri
5. **Joint statistics of mixture fraction and progress variable in piloted methane jet flames with inhomogeneous inlet flows**
R.S. Barlow, G. Magnotti, H.C. Cutcher, A.R. Masri
6. **Pressure effects on flame length in turbulent non-premixed flames**
W.R. Boyette, W.L. Roberts
7. **Effects of pressure on syngas/air turbulent nonpremixed flames**
P.P. Ciottoli, B.J. Lee, H.G. Im, M. Valorani
8. **Effects of heat release and localized extinction on vorticity-strain-rate alignment in piloted partially-premixed CH₄/air jet flames using tomographic particle image velocimetry**
B. Coriton, J.H. Frank
9. **Unsteady flamelet analysis utilizing in-situ tracked mixture fraction trajectories in DNS of turbulent non-premixed combustion**
F. Dietzsch, A. Scholtissek, C. Hasse
10. **Applications of LES-PDF method to premixed, non-premixed and stratified flames**
I. Dodoulas, S. Navarro-Martinez
11. **Local extinction in a turbulent partially-premixed DME/air jet flame series**
F. Fuest, R.S. Barlow, G. Magnotti, J.A. Sutton
12. **Scalar dissipation rate measurements in a turbulent partially-premixed dimethyl ether/air jet flame**
F. Fuest, R.S. Barlow, G. Magnotti, J.A. Sutton
13. **mmcFoam - A new object-oriented multiple mapping conditioning turbulent combustion code**
S. Galindo-Lopez, L.F. Zhao, M.N. Khan, A. Majbouri, F. Salehi, M.J. Cleary, A.R. Masri, G. Neuber, S. Vo, C. Straub, J. Kirchmann, O.T. Stein, A. Kronenburg, Y. Ge, B. Sundaram, L. Dialameh, A.Y. Klimenko, A. Varna, E.R. Hawkes
14. **Critical assessment of differential diffusion flamelet modeling in turbulent oxy-fuel flames**
S. Gierth, F. Hunger, S. Popp, C. Hasse, M. Ihme
15. **Impact of exhaust gas enthalpy on fluid state probabilities**
F. Hampf, R.P. Lindstedt

16. **Flamelet modeling of differential molecular diffusion in oxy-fuel turbulent jet flames**
C. Han, R.S. Barlow, H. Wang
17. **Multi-Environment PDF Modeling for Turbulent DME/AIR Pilot Jet Flames**
S.T. Jeon, Y. Kim
18. **Investigation of thermoacoustic sources and their dynamics from experiments and LES**
S. Kheirkhah, P. Saini, J. M. Cirtwill, K. Venkatesan, S. Yellapantula, A. M. Steinberg
19. **Multi-environment PDF modeling for piloted turbulent flame with inhomogeneous inlets**
N.S. Kim, S.W. Park, Y. Kim
20. **A mixing timescale model for TPDF simulations of turbulent premixed flames**
M. Kuron, Z. Ren, E. R. Hawkes, H. Zhou, H. Kolla, J. H. Chen, T. Lu
21. **Large eddy Simulation of Sydney piloted jet flame with inhomogeneous inlets using a dynamic second-order moment closure model**
K. Luo, Y. Bai, W. Bi, J. Fan
22. **High speed 10KHz imaging of OH/CH₂O for DME issuing into a hot coflow burner with preliminary laminar calculations**
A.R.W. Macfarlane, M.J. Dunn, M. Juddoo, A.R. Masr
23. **LES modeling of piloted jet flames with inhomogeneous inlets using tabulated chemistry methods**
G. Maio, M. Cailler, R. Mercier, V. Moureau, B. Fiorina
24. **Response of a laminar premixed flame to equivalence ratio oscillations**
W. Meier, H. Ax
25. **Comparisons of uncertainties from turbulence and chemical kinetics models in turbulent combustion simulations**
M.E. Mueller, V. Raman
26. **Large eddy simulations of a piloted jet flame with inhomogeneous inlets using a flamelet/progress variable approach and the Eulerian stochastic fields method**
H. Müller, M. Pfitzner
27. **A new mode-switching approach for modeling turbulent flames with inhomogeneous partially premixed inlets**
B.A. Perry, M.E. Mueller, A.R. Masri
28. **Differential diffusion effects and flamelet analysis in a hydrogen jet in cross flow configuration**
S. Popp, F. Dietzsch, A. Abdelsamie, D. Thevenin, C. Hasse
29. **Large eddy simulation of auto-ignition in a turbulent jet in hot coflow**
J. Prause, C. M. Arndt, B. Noll, M. Aigner
30. **Analysis of the reaction zone dynamics in a turbulent premixed bluff-body burner based on a flame resolved simulation with tabulated chemistry**
F. Proch, P. Domingo, L. Vervisch, A.M. Kempf

31. **Mixture fraction-progress variable dependence in partially-premixed flames**
E.S. Richardson, T.B. Matheson, N.H. Meah, D.O. Lignell, C.S. Yoo, J.H. Chen
32. **LES/FDF of a lean premixed methane counterflow flame**
M. Rieth, F. Proch, A.M. Kempf
33. **Raman/Rayleigh spectroscopy in premixed methane flames including hydrogen addition**
S. Schneider, N. Luciano, D. Geyer, A. Zschuttschke, A. Scholtissek, C. Hasse, A. Dreizler
34. **ns-CARS temperature measurements of flame quenching close to a wall**
K. Sesha-Giri, D. Lacoste, J. Damazo, E. Kwon, W. Roberts
35. **Simulation of Sandia flames D, E and F with a novel MMC mixing model**
A. Varna, M.J. Cleary, E.R. Hawkes
36. **Use of data mining to determine whether spray flames will extinguish**
A.P. Wandel
37. **Petascale direct numerical simulation of a high Ka laboratory premixed jet flame**
H. Wang, E.R. Hawkes, J.H. Chen
38. **Large eddy simulations of the Darmstadt turbulent stratified flames with REDIM reduced kinetics**
P. Wang, C. Wang, G. Steinhilber, Z. He, U. Maas
39. **Compliance of flamelet models for turbulent reacting flow simulations with applications to Sydney piloted flames with inhomogeneous inlets**
H. Wu, M. Ihme
40. **Effects of molecular transport in LES/PDF of piloted turbulent DME/air jet flames**
J. You, Y. Yang, S.B. Pope
41. **Sensitivity and Lagrangian analysis for RANS-PDF simulations of turbulent premixed jet flames**
H. Zhou, S. Li, Z. Ren

blank

Quantitative High Repetition Rate Laser Diagnostics for the Study of Auto-Ignition in a Jet-in-Hot-Coflow and for the Validation of Numerical Simulations

Christoph Arndt¹, Juliane Prause¹, Michael Papageorge², Frederik Fuest², Wolfgang Meier¹,
Jeffrey Sutton¹, Manfred Aigner²

¹ German Aerospace Center (DLR), Institute of Combustion Technology, Stuttgart, Germany

² Ohio State University, Department of Mechanical and Aerospace Engineering, Columbus, OH, USA
email: christoph.arndt@dlr.de

Laser based imaging techniques for combustion processes with frame rates in the kHz range have developed rapidly in recent years. Their use for the study of transient combustion processes and unpredictable phenomena, such as thermo-acoustic combustion instabilities, flashback, transitional states, local extinction or auto-ignition has broadened the understanding of flame dynamics. Further, these techniques can provide validation data for numerical simulations which are not attainable by low-repetition rate systems.

Large Eddy Simulations (LES) provide time-resolved information of the flow-field and flame dynamics, and hence it makes sense to validate those using time-resolved measurements. However, finding useful quantities for comparison is not self-evident, and numerical studies that use results from time-resolved laser diagnostics as validation data are rare in the literature.

In the current study, quantitative high repetition rate planar laser measurement techniques have been developed to study flame-stabilization and auto-ignition in the DLR Jet-in-Hot-Coflow (DLR JHC) burner [1,2,3,4]. A schematic overview of the DLR JHC is shown in Fig. 1.

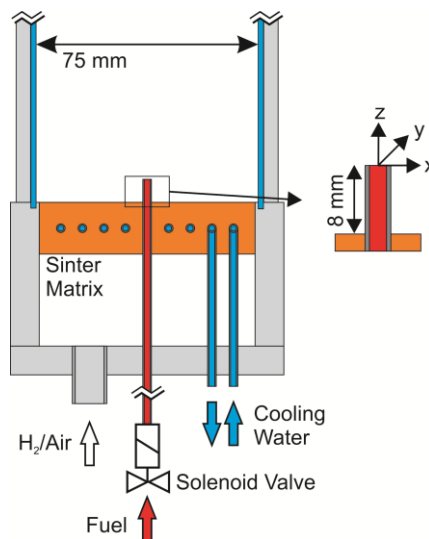
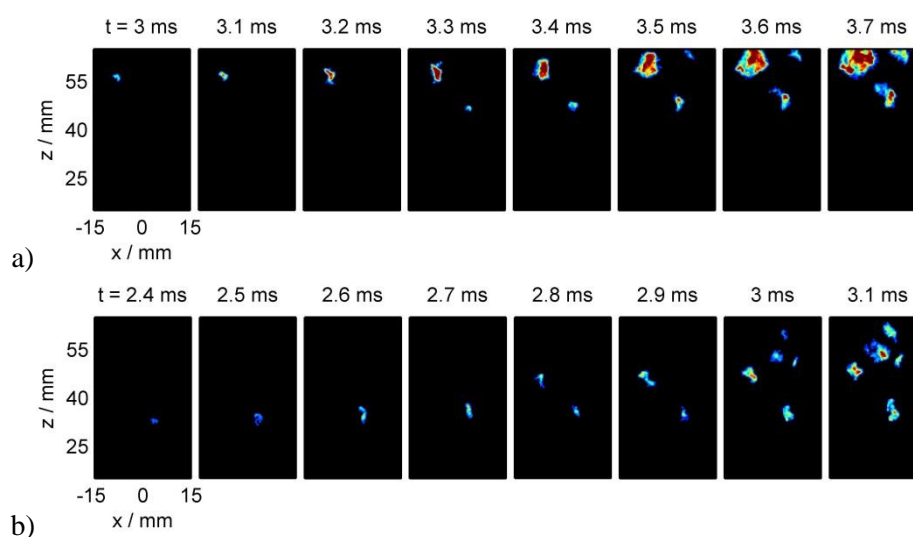


Fig. 1.: Schematic overview of the DLR Jet-in-Hot-Coflow burner.

Here, a turbulent methane jet was injected either continuously or in a pulsed manner via a solenoid valve into a hot, vitiated coflow generated by the exhaust gas of a lean premixed hydrogen/air flame. Rayleigh scattering was applied to measure the temperature, mixture fraction, and scalar dissipation rate field. Planar laser-induced fluorescence of OH was applied to study the development of ignition kernels with high spatial resolution. In order to quantify the OH concentration, a novel strategy for shot-to-shot calibration of the OH PLIF images has been developed based on the known OH concentration (from equilibrium calculations) in the vitiated coflow.

The boundary conditions of the experiment were carefully measured, since temperature fluctuations of a few Kelvin can influence auto-ignition delay quite severely and hence have to be covered by

numerical simulations. Comparison of the LES simulations to profiles of OH and mixture fraction showed good agreement. As a challenging test case, fuel was injected in a transient manner into the hot coflow. The behavior of the impulsively started jet was studied with high speed planar Rayleigh imaging to characterize the mixture fraction and scalar dissipation rate field during transient fuel injection and the onset of auto-ignition. It was found that auto-ignition occurred on the windward side of bulges of the fuel jet, where the scalar dissipation rate was low and where long residence times of the igniting fluid parcel are expected. With temporally resolved measurements, it is also possible to study the of ignition kernel growth in dependence of the ignition height. Figure 2 shows two exemplary ignition events measured with time-resolved OH* chemiluminescence. The ignition kernel shown in Fig. 2a) forms at a comparably high axial location, the kernel shown in Fig. 2b) forms at a low axial location.



*Fig. 2: a) Ignition kernel growth at high axial locations
b) Ignition kernel growth at low axial locations*

It was found that ignition kernels at lower axial locations grow significantly slower than those at higher axial locations. This was attributed to the higher local strain and scalar dissipation rates at lower axial locations, which do not only hinder the formation of ignition kernels, but also their growth.

References

- [1] C. M. Arndt, J. D. Gounder, W. Meier, M. Aigner, Auto-ignition and flame stabilization of pulsed methane jets in a hot vitiated coflow studied with high-speed laser and imaging techniques, *Appl. Phys. B* 108 (2012) 407-417.
- [2] C. M. Arndt, R. Schießl, J. D. Gounder, W. Meier, M. Aigner, Flame stabilization and auto-ignition of pulsed methane jets in a hot coflow: Influence of temperature, *Proc. Combust. Inst.* 34 (2013) 1483-1490.
- [3] M. J. Papageorge, C. Arndt, F. Fuest, W. Meier, J. A. Sutton, High-speed mixture fraction and temperature imaging of pulsed, turbulent fuel jets auto-igniting in high-temperature, vitiated coflows, *Exp. Fluids* 55 (2014) 1763.
- [4] C. M. Arndt, M. J. Papageorge, F. Fuest, W. Meier, J. A. Sutton, M. Aigner, The role of temperature, mixture fraction, and scalar dissipation rate on transient methane injection and auto-ignition in a jet in hot coflow burner. *Combust. Flame* 167 (2016), 60-71.

DNS of turbulent premixed flames at high Reynolds and Karlovitz numbers

Antonio Attili^{a,*}, Stefano Luca^a, Fabrizio Bisetti^{a,b}

^a King Abdullah University of Science and Technology (KAUST), Clean Combustion Research Center (CCRC), Thuwal 23955-6900, Saudi Arabia

^b Department of Aerospace Engineering and Engineering Mechanics, University of Texas at Austin, Austin, TX 78712-1085, USA

* Corresponding author: antonio.attili@kaust.edu.sa

A set of large scale simulations of turbulent premixed flames at different Reynolds and Karlovitz numbers is presented. The simulations feature finite rate chemistry with 16 species and 73 reactions and up to 22 Billion grid points for the case with the largest Reynolds number.

The flame configuration consists of a slot jet surrounded by a coflow of burnt gases [1]. This arrangement is similar to piloted flames used in experiments. The jet consists of a methane/air mixture with equivalence ratio $\phi = 0.7$ and temperature ranging between 500 and 800 K. The temperature and species concentrations in the coflow correspond to the equilibrium state of the burnt mixture. All the simulations are performed at 4 atm. A summary of physical and numerical parameters is given in Tab. 1.

The variation of the Reynolds number is obtained varying the jet slot width H between 0.6 and 4.8 mm and keeping the inlet velocity constant. The variation of the Karlovitz number is obtained adjusting the inlet velocity, temperature, and the size of the slot keeping the jet Reynolds number constant.

	R1-K1	R2-K1	R3-K1	R4-K4	R2-K2
Jet Reynolds Number	2800	5600	11200	22400	5600
Jet Bulk Velocity, U_{bulk}	100 m/s	100 m/s	100 m/s	100 m/s	68 m/s
Inlet temperature	800 K	800 K	800 K	800 K	500 K
Slot width, H	0.6 mm	1.2 mm	2.4 mm	4.8 mm	0.8 mm
Grid Size	720×480×256	1440×960×256	2880×1920×512	5760×3844×1024	4320×2160×512
Total number of points	88 Million	350 Million	2.8 Billion	22 Billion	4.7 Billion

Table 1: Parameters of the simulations. Four simulations with similar Karlovitz and different Reynolds numbers are presented. An additional simulation (case R2-K2) with the same Reynolds number of case R2-K1 and a nominal Karlovitz number approximately 9 times larger is included.

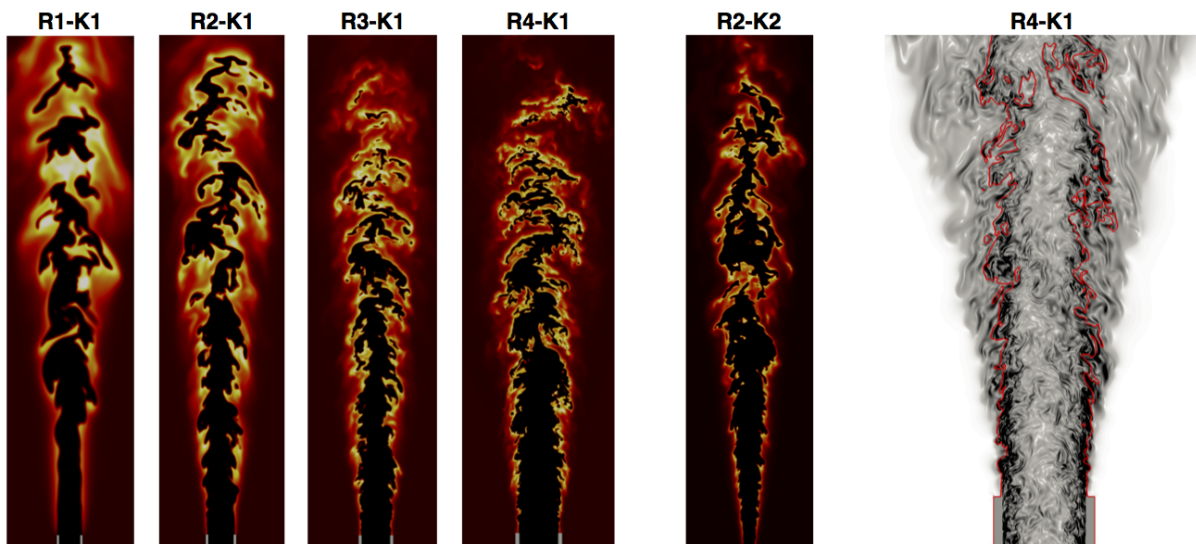


Figure 1: Two dimensional cuts of the field of the mass fraction of atomic oxygen in the five flames. The domain size in each figure is scaled differently to optimized the visualization. The figure on the right shows the vorticity and an isoline of temperature marking the flame surface for the simulation with the largest Reynolds number (only the bottom half of the flame is shown).

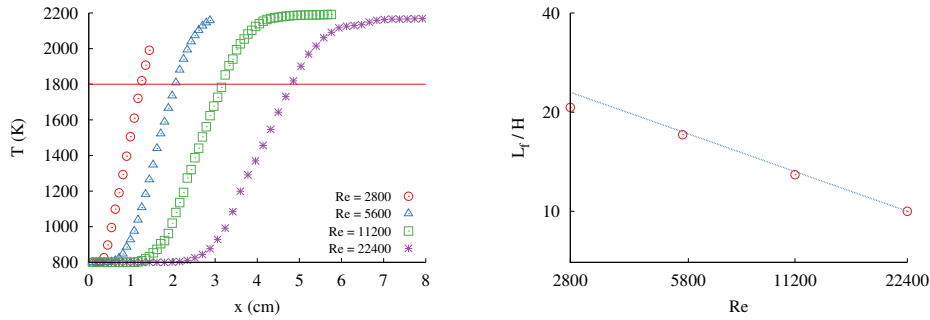


Figure 2: Left: mean temperature along the jet centerline for the four flames at different Reynolds numbers. The red horizontal line marks the temperature value used to define the flame tip and the length of the flame. Right: length of the flame for different Reynolds numbers, normalized with the slot width; the line is a power-law fit to the three cases with the highest Reynolds number with the form Re^c with $c = -0.4$.

The gas phase hydrodynamics are modeled with the reactive, unsteady Navier-Stokes equations in the low Mach number limit [2]. The species obey the ideal gas equation of state and all transport properties are computed with a mixture-average approach. The chemical mechanism employed has been derived from the GRI-3.0.

Figure 1 shows the mass fraction of oxygen in the four flames at different Reynolds number. As expected, it is evident that the range of scale characterizing the fields increases with the Reynolds number. The length of the flames, measured in terms of the slot width H , decreases as the Reynolds number increases. A quantitative assessment of the dependence of flame length L_f on the jet Reynolds number is presented in Fig. 2. The flame length, normalized with the jet width H , decreases significantly as the Reynolds number increases. Being the jet inlet velocity the same, the ratio between turbulent velocity fluctuations u' and laminar flame speed is very similar in the four cases. However, the decrease of the normalized length is consistent with an increase of the turbulent flame speed due to the increased integral scale of turbulence [3]. This behavior is typical of flames in the thin-reaction zone regime which are characterized by the important role of turbulent transport in the preheat region of the flame.

The fractal dimension of the flame, identified by the temperature isosurface $T=1800$ K, has been computed with a box counting algorithm and it is shown in Fig.3 for the flame at $Re=11200$. The analysis shows a fractal dimension of the flame surface of 2.6, in agreement with recent results obtained in different turbulent premixed flames [4]. Similar fractal dimensions have been obtained for the flames at $Re=5600$ and 22400 .

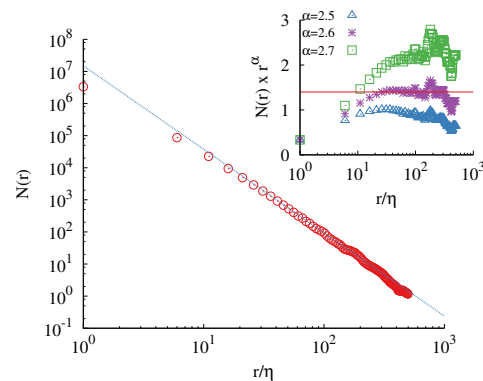


Figure 3: Application of the box counting algorithm to the flame at $Re=11200$. Number of boxes needed to cover the flame surface as function of the box size (red dots). The blue line has a slope in the log-log plot of -2.6 , corresponding to a fractal dimension of 2.6 . The inset shows the same results compensated with the scaling $r^{2.6}$ (purple star). The compensated results is shown also for a fractal dimension of 2.5 and 2.7 to assess the robustness of the results.

References

- [1] Luca S., Attili A., Bisetti F. : Direct Numerical Simulation of Turbulent Lean Methane-Air Bunsen Flame with Mixture Inhomogeneities. AIAA Paper 2016-0189, 54th AIAA Aerospace Sciences Meeting, 2016.
- [2] Attili A. *et al.*: Formation, growth, and transport of soot in a three-dimensional turbulent non-premixed jet flame. Comb. Flame 161:1849-1865, 2014.
- [3] Peters N.: The turbulent burning velocity for large-scale and small-scale turbulence. J. Fluid Mech. 384:107-132, 1999.
- [4] Chatakonda O. *et al.*: On the fractal characteristics of low Damköhler number flames. Comb. Flame 160:2422-2433, 2013.

Comparative study of RANS-EDC, LES-CSE and LES-FGM simulations of Delft jet-in-hot-coflow (DJHC) natural gas flames

H. Bao¹, X. Huang¹, J. Labahn², A. Vasavan³, D.J.E.M. Roekaerts^{1,3,*}, C. Devaud², J.A. van Oijen³

1. Department of Process and Energy, Delft University of Technology, The Netherlands

2. Department of Mechanical and Mechatronics Engineering, University of Waterloo, Canada

3. Multiphase and Reacting Flows, Eindhoven University of Technology, The Netherlands

*D.J.E.M.Roekaerts@tudelft.nl

We report on a comparative study of model predictions of jet-in-hot-coflow flames. The Delft Jet-in-Hot-Coflow (DJHC) burner was built to mimic the important characteristics of flameless combustion without the complications of a real furnace [1,2]. The DJHC burner has been used to create a turbulent diffusion flame of Dutch Natural Gas in a coflowing oxidizer stream of high temperature with low oxygen concentration. The experimental database contains the results of high speed chemiluminescence imaging, velocity statistics from LDA measurements and temperature statistics from CARS measurements. In recent years several computational studies have been made using the DJHC burner as validation database [3-9]. It has been shown before that predictions are sensitive to the coflow radial profiles of temperature and oxygen concentration, to the representation of effects of entrained air, and to turbulence-chemistry interaction and this is also the focus of the present study. Table 1 gives a summary of the models used.

TABLE 1	RANS-EDC	RANS-CSE [8]	LES-CSE [9]	LES-FGM
Domain size (mm) axial x radial; 3D Cartesian	225 x 80	225 x 80	225 x 80	43x43x250
Grid size (# cells)	27175	31250	1.5 10 ⁶	7.5 10 ⁶
Turbulence approach	RANS	RANS	LES	LES
Closure model	RSM	Realisable k- ϵ	Standard Smagorinsky	Vreman (2009) model
Kinetic scheme	DRM19	GRI-mech 2.11 TGLDM	GRI-mech 2.11 TGDLM	GRI-mech 3.0
Turb-chem-interaction	EDC $C_{\tau} = 3$	Multistream CSE (two mixture fractions)	Multistream CSE (two mixture fractions)	FGM (igniting mixing layer flamelets between fuel and coflow).
Scalar equations	Mean of species Mean of enthalpy	Mean and variance of two mixture fractions Mean of enthalpy	Resolved mixture fractions and SGS variances Resolved enthalpy	Resolved mixture fraction and resolved progress variable Resolved enthalpy
Radiation	Not included	Optically thin model. TRI not included.	Optically thin model. TRI not included.	Not included
Scalar BC coflow T coflow O ₂ (vol%) Surrounding 'Air'	Expt. Expt. Air 300K	Expt. Coupled to mean T Air 300K	Expt. Coupled to mean T Air 300K	Expt. Flat with value 0.084 Coflow comp. at 300K

In the EDC model a model constant was changed from its default value to obtain the correct lift-off height. The CSE model [8,9] uses a double conditioned conditional source term estimation (CSE) formulation of turbulence chemistry interaction including two mixture fractions. The FGM model is based on flamelets computed using one-dimensional igniting mixing layers with constant unity Le . The progress variable is based on CO_2 , H_2O and H_2 . In the FGM model, the SGS-variance of mixture fraction and progress variable are obtained from algebraic equations, but this information has not been used in calculation of subgrid scale influences on resolved properties (density, resolved temperature).

Representation of the non-uniform radial profile of scalar properties at the inflow boundary is an issue for the mixture fraction based approaches. In the LES-CSE a second mixture fraction is used to represent temperature variation and oxygen variation is coupled to the same mixture fraction. In the LES-FGM temperature variation is included via the enthalpy equation and considering flamelets with heat loss at the oxidizer side. The oxygen variation is not taken into account. This simplification is based on a separate study showing that ignition delay is much more sensitive to temperature variation than to oxygen concentration variation. Figure 1 shows snapshots of scalar fields from LES-FGM. The poster presents comparisons of predicted velocity and scalar statistics, also compared to experiments, at the heights 15, 30, 60 and 90 mm above the burner exit. Figure 2 shows the good agreement obtained for mean temperature at 30 mm but for large axial distance significant differences are observed. Overall best results are obtained with the LES-CSE model of [9].

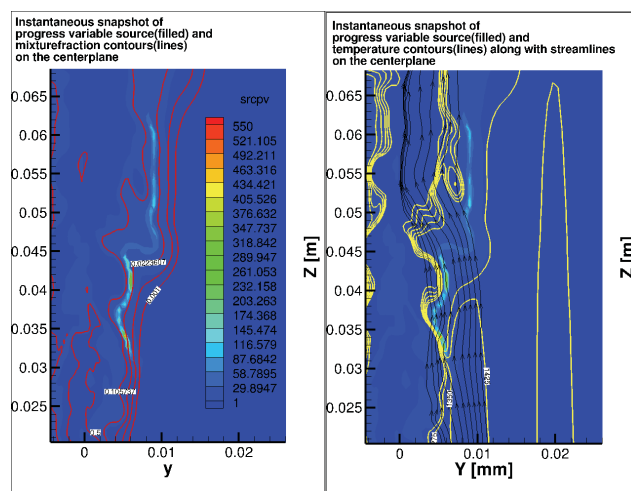


Figure 1

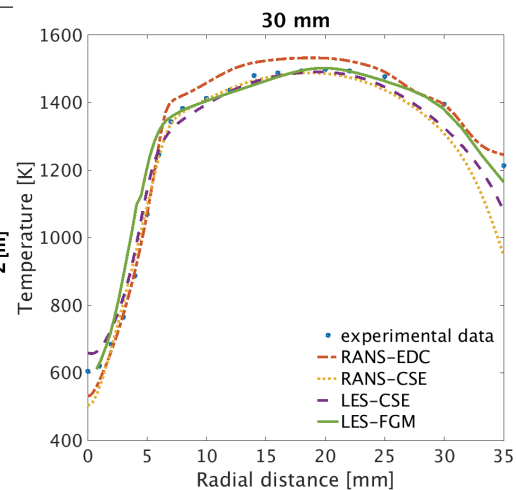


Figure 2

References

- [1] E. Oldenhof et al., *Combustion and Flame*, 2010, 157 (6), 1167 -1178.
- [2] E. Oldenhof et al., *Combustion and Flame*, 2011, 158 (8), 1553-1563
- [3] A. De et al., *Flow, Turbulence and Combustion*, 2011, 87 (4), 537-567
- [4] R.M. Kulkarni and W. Polifke, *Fuel processing technology*, 2013, 107, 138-136
- [5] Rohit Bhaya et al., *Combustion Science and Technology*, 2014, 186 (9), 1138-1165
- [6] Ashoke De and Akshay Dongre, *Flow Turbulence Combustion*, 2015, 94, 439-478
- [7] G. Sarras et al., *Flow, Turbulence and Combustion*, 2014, 93, 607-635
- [8] J.W. Labahn, D. Dovizio, C.B. Devaud, *Proc. Combust. Inst.*, 2015, 35, 3547-3555
- [9] J. Labahn and C. Devaud, *Combustion and Flame*, 2016, 164, 68-84

On defining progress variable for experiments in partially-premixed methane flames

Robert. S. Barlow¹, Gaetano Magnotti¹, Hugh C. Cutcher², Assaad R. Masri²

¹Combustion Research Facility, Sandia National Laboratories, Livermore, CA 94566

²School of Aerospace, Mechanical and Mechatronics Engineering,
The University of Sydney, Sydney 2006 NSW, Australia

Mixture fraction, Z , and progress variable, c , are central concepts in the turbulent combustion theory and in flamelet modeling of turbulent partially-premixed flames. It is common in both experimental and modeling studies to use Bilger's formulation for mixture fraction, which preserves the stoichiometric value in the presence of differential species diffusion. However, there is no such consensus on the definition of progress variable for partially-premixed flames. In flamelet modeling approaches with tabulated chemistry it is common to define progress variable as a sum of major product mass fractions, often without normalization. Examples for hydrocarbon flames include: Y_{CO_2} , $Y_{CO_2}+Y_{H_2O}$, $Y_{CO_2}+Y_{CO}$, $Y_{CO_2}+Y_{CO}+Y_{H_2O}$, and $Y_{CO_2}+Y_{CO}+Y_{H_2O}+Y_{H_2}$. Progress variable has also been defined on a molar basis as $Y_{CO_2}/w_{CO_2}+Y_{H_2O}/w_{H_2O}+Y_{H_2}/w_{H_2}$. More recently, various 'optimized' progress variables have been proposed that allow for improved efficiency and accuracy in storage and retrieval of thermochemical states from flamelet tables. These optimized progress variables can be linear combinations of many species, with weighting factors that can be positive or negative.

Experimental results on progress variable in partially premixed flames are rare the literature. Measurements of progress variable and its dissipation rate have been reported for premixed and stratified flames, based on Rayleigh scattering measurements of temperature, $c = (T - T_0)/(T_{eq}(Z) - T_0)$, where T_0 is the unburnt reactant temperature and $T_{eq}(Z)$ is the adiabatic equilibrium temperature for the local value of mixture fraction. Conditional mean values of the temperature burning index, which is similarly defined, have been reported for nonpremixed and partially premixed jet flames as an indicator of the probability of local extinction. However, a temperature-based progress variable is only appropriate for flames with negligible heat loss, and it is not favored in modeling.

The objective of the present work is to develop a species-based definition of progress variable that can be used easily in the context of Raman/Rayleigh experiments in partially-premixed methane flames and can allow for direct comparisons of experimental and computational results for such things as joint and conditional statistics of mixture fraction and progress variable, and well as gradients and dissipation rates of these quantities. Raman/Rayleigh experiments in methane-air flames yield temperature and the mass fractions of major species (N_2 , O_2 , CH_4 , CO_2 , H_2O , CO , and H_2). Therefore, an experimentally compatible progress variable should be calculated from mass fractions of a subset of these seven measured species. Furthermore, it seems preferable to define a normalized progress variable and to use a reference condition for normalization that does not depend on assumptions regarding transport. Specifically, the definition should not depend on an assumption of equal diffusivities. This means that the reference state for normalization should be calculated directly from properties of each measured sample, not from an equilibrium table or an assumed laminar flame solution. It is anticipated that a progress variable that can be calculated simply from mass fractions of the seven measured major species could also be calculated as a post-processing step from simulations, independent of the modeling approach.

Three definitions of progress variable have been considered, each based on mass fractions of the seven major species measured in Raman/Rayleigh experiments in methane flames: c_O based on oxygen; c_C based on the sum of CO_2 and CO ; and c_Y based on the sum of CO_2 , CO , H_2O , and H_2 . The progress variable based on oxygen is easiest calculate and offers some advantages. It is defined as the mass of O in the sample that is bound to fuel (C or H) divided by the mass of O that could be bound to fuel if the sample were taken fully to products, CO_2 and H_2O , consuming any deficient reactants (fully burnt state).

$$c_O = \frac{Y_{CO_2}\left(\frac{w_{O_2}}{w_{CO_2}}\right) + Y_{CO}\left(\frac{w_O}{w_{CO}}\right) + Y_{H_2O}\left(\frac{w_O}{w_{H_2O}}\right)}{\left(Y_{CO_2}\left(\frac{w_{O_2}}{w_{CO_2}}\right) + Y_{CO}\left(\frac{w_{O_2}}{w_{CO}}\right) + Y_{H_2O}\left(\frac{w_O}{w_{H_2O}}\right) + Y_{H_2}\left(\frac{w_O}{w_{H_2}}\right) + Y_{CH_4}\left(\frac{2w_{O_2}}{w_{CH_4}}\right)\right)}; \quad \phi < 1 \quad (1a)$$

$$c_O = \frac{Y_{CO_2}\left(\frac{w_{O_2}}{w_{CO_2}}\right) + Y_{CO}\left(\frac{w_O}{w_{CO}}\right) + Y_{H_2O}\left(\frac{w_O}{w_{H_2O}}\right)}{\left(Y_{CO_2}\left(\frac{w_{O_2}}{w_{CO_2}}\right) + Y_{CO}\left(\frac{w_O}{w_{CO}}\right) + Y_{H_2O}\left(\frac{w_O}{w_{H_2O}}\right) + Y_{O_2}\right)}; \quad \phi \geq 1 \quad (1b)$$

Here equivalence ratio is calculated as the oxygen required divided by the oxygen available based on the mole fractions of the same seven major species, and mixture fraction is calculated following Bilger.

$$\phi = \frac{X_{CO_2} + 2X_{CH_4} + X_{CO} + 0.5(X_{H_2O} + X_{H_2})}{X_{CO_2} + X_{O_2} + 0.5(X_{CO} + X_{H_2O})}, \quad Z = \frac{2(Y_C - Y_{C,2})/w_C + (Y_H - Y_{H,2})/2w_H - (Y_O - Y_{O,2})/w_O}{2(Y_{C,1} - Y_{C,2})/w_C + (Y_{H,1} - Y_{H,2})/2w_H - (Y_{O,1} - Y_{O,2})/w_O} \quad (2)$$

where Y_i are elemental mass fractions, w_i are molar masses, and the subscripts 1 and 2 refer to conditions in the rich (fuel) and lean (oxidizer) streams, respectively.

Figure 1 shows that the three progress variable definitions behave similarly in laminar opposed-flow partially-premixed CH_4 -air flames (Chemkin, GRI 3.0, multicomponent transport, Soret effect). A notable feature of these normalized progress variables is the existence of a “dip” near stoichiometric. Figure 2a shows that the dip exists for both equilibrium and “fully burnt” normalization. Figure 2b illustrates the problem of using equilibrium for normalization when multicomponent transport is included. Figure 2c compares progress variable and mixture fraction calculated from 18 species vs. 7. Progress variable changes by less than 1% at each point along the Chemkin solution, while mixture fraction is more strongly affected. Figure 2d illustrates a renormalization approach that removes the slope discontinuity in c_O at stoichiometric, which results from using the fully burnt state for normalization. This renormalization approximates the effect of normalizing by the local equilibrium state and avoids awkward behavior of progress variable gradients and dissipation around the stoichiometric condition. Turbulent flame results are presented in a separate poster abstract by the same authors.

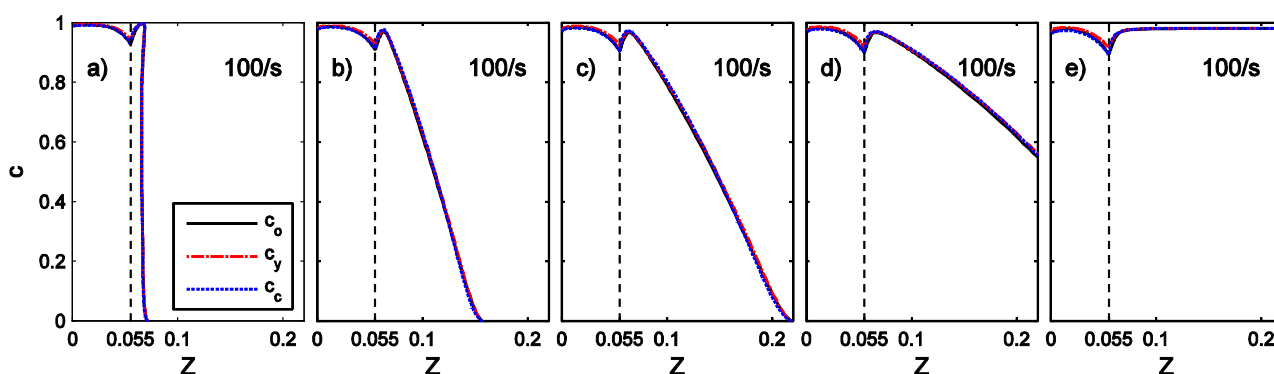


Fig. 1. Behavior of three progress variables normalized by the fully burnt state in laminar opposed-flow CH_4 -air flames with fuel-side equivalence ratios of 1.3, 3.2, 4.8, 9.5, and inf. (pure CH_4).

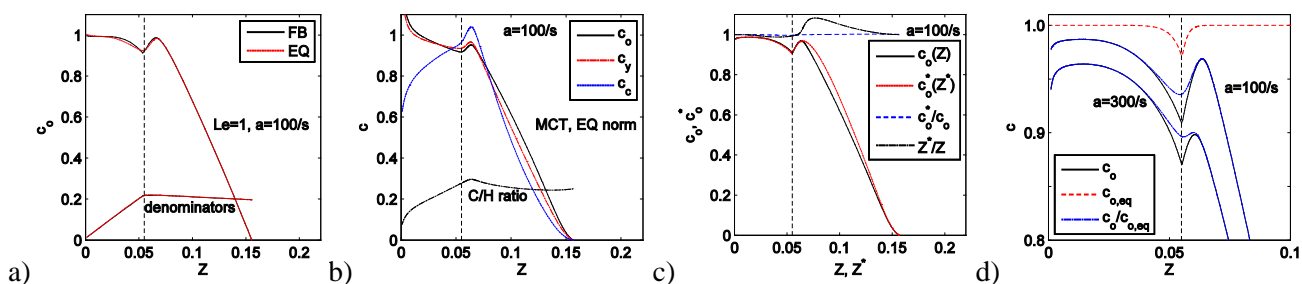


Fig. 2. a) Comparison progress variable based on normalization by the equilibrium state versus the fully burnt state for a $Le=1$ strained laminar partially-premixed flame. b) Inconsistency of results when equilibrium is used as the normalization reference for flames with multicomponent transport. c) Z and c_O calculated using 18 species (*) vs. 7 species. d) Renormalization to eliminate the slope discontinuity in c_O . The red curve, $c_{O,eq}$, is obtained by applying Eq. (1) to the equilibrium table. Note that the maximum deviation from unity is only 3 percent.

Joint Statistics of Mixture Fraction and Progress Variable in Piloted Methane Jet Flames with Inhomogeneous Inlet Flows

Robert. S. Barlow¹, Gaetano Magnotti¹, Hugh C. Cutcher², Assaad R. Masri²

¹Combustion Research Facility, Sandia National Laboratories, Livermore, CA 94566

²School of Aerospace, Mechanical and Mechatronic Engineering,
The University of Sydney, Sydney 2006 NSW, Australia

Mixture fraction, Z , and progress variable, c , are central concepts in turbulent combustion theory and in flamelet modeling of turbulent partially-premixed flames. However, experimental results on progress variable in partially-premixed flames and on the joint statistics of Z and c are rare. A progress variable based on oxygen, c_O , that can be determined from Raman/Rayleigh measurements of seven major species mass fractions (N_2 , O_2 , CH_4 , CO_2 , H_2O , CO , and H_2) in methane-air flames has been proposed. (Please see the companion abstract for the full definition of c_O and for discussion of its behavior in laminar flames.)

The joint statistics of Z and c_O are investigated using a new set of measurements from the previously described Sydney piloted partially-premixed methane-air jet flames [1,2]. These new data were acquired using methods of spatial oversampling and wavelet denoising [3,4], which provide improved spatial resolution and precision. Figure 1a shows temperature scatter plots from radial scans (positive side) at four axial locations in two flames that are TNF target cases, FJ-Lr75-80 (inhomogeneous inlet flow) and FJ-Lr300-59 (near-homogeneous inlet flow). Histograms of joint (Z, c_O) probability from the same radial scans are shown in Fig. 1b, while Fig. 1c shows results that are spatially conditioned, with a 0.3 mm window centered at the location in each profile where $\tilde{Z} = 0.065$. This value of Z was selected because it is roughly the condition where heat release rate in laminar flames calculations reaches a maximum. The Favre variances, covariance, and correlation coefficient are given for each joint distribution. The effects of local extinction on progress variable are quite obvious at downstream locations $x/D=12, 20$.

Figure 2a,b shows radial profiles of Favre average mixture fraction and progress variable, along with their variances and covariance, calculated as: $\tilde{Z} = \overline{\rho Z} / \bar{\rho}$, $\tilde{c}_O = \overline{\rho c_O} / \bar{\rho}$, $\tilde{Z}''^2 = \overline{\rho(Z - \tilde{Z})^2} / \bar{\rho}$, $\tilde{c}_O''^2 = \overline{\rho(c_O - \tilde{c}_O)^2} / \bar{\rho}$, and $\tilde{Z}''\tilde{c}_O'' = \overline{\rho(Z - \tilde{Z})(c_O - \tilde{c}_O)} / \bar{\rho}$. A complementary view of the differences between these two flames is provided in Fig. 2c by mapping the radial coordinate onto the mixture fraction coordinate and plotting \tilde{c}_O , $\tilde{Z}''\tilde{c}_O''$, and the correlation coefficient, $R_{Zc} = \tilde{Z}''\tilde{c}_O'' / (\tilde{Z}''^2\tilde{c}_O''^2)^{1/2}$, against \tilde{Z} . The near field profiles of the scalar variances in the two flames are very different. At $x/D=1$ the peaks in \tilde{Z}''^2 and $\tilde{c}_O''^2$ are aligned in flame FJ-Lr300-59 but separated in flame FJ-Lr75-80, which exhibits stratified-premixed combustion close to the jet exit. These peaks remain separated at $x/D=5$ in the inhomogeneous flame, then gradually merge with increasing downstream distance. The magnitude of the covariance is much smaller in the near field of flame FJ-Lr75-80 than in the more conventional, near-homogeneous flame, and magnitude of the correlation coefficient, R_{Zc} , is also smaller. However, the magnitude of R_{Zc} in the main heat release region of the reaction zone increases rapidly with streamwise distance as the mode of combustion evolves from stratified-premixed toward diffusion-dominated. At $x/D=5$, still within the near field of this transitioning flame, R_{Zc} reaches -0.7 just on the fuel-rich side of the stoichiometric contour, and R_{Zc} approaches -0.8 slightly farther downstream but before the onset of local extinction. This relatively high correlation in the measurements contradicts the common assumption of statistical independence of mixture fraction and progress variable. With the onset of local extinction still farther downstream, the correlation becomes weaker. Clearly, the statistical correlation of fluctuations in mixture fraction and progress variable in this type of partially premixed flame can vary significantly depending on inflow conditions, location within the flame, and the degree of local extinction. Note that the correlation coefficient within the pilot region, where gradients in Z and c are near zero and their variances are both small, is dominated by correlated noise from the measurement of Y_{O_2} . Thus, the decay of the spike in R_{Zc} near stoichiometry is actually an indicator of the entrainment of pilot products into the jet.

[1] S. Meares, V.N. Prasad, G. Magnotti, R.S. Barlow, A.R. Masri, Proc. Combust. Inst. 35 (2014) 1477–1484.

[2] R.S. Barlow, S. Meares, G. Magnotti, H. Cutcher, A.R. Masri, Combust. Flame 162 (2015) 3516–3540.

[3] M.S. Sweeney, S. Hochgreb, M.J. Dunn, R.S. Barlow, Combust. Flame, (2013) 322–334.

[4] H. Cutcher, R.S. Barlow, G. Magnotti, A.R. Masri, submitted to the 36th Combustion Symposium.

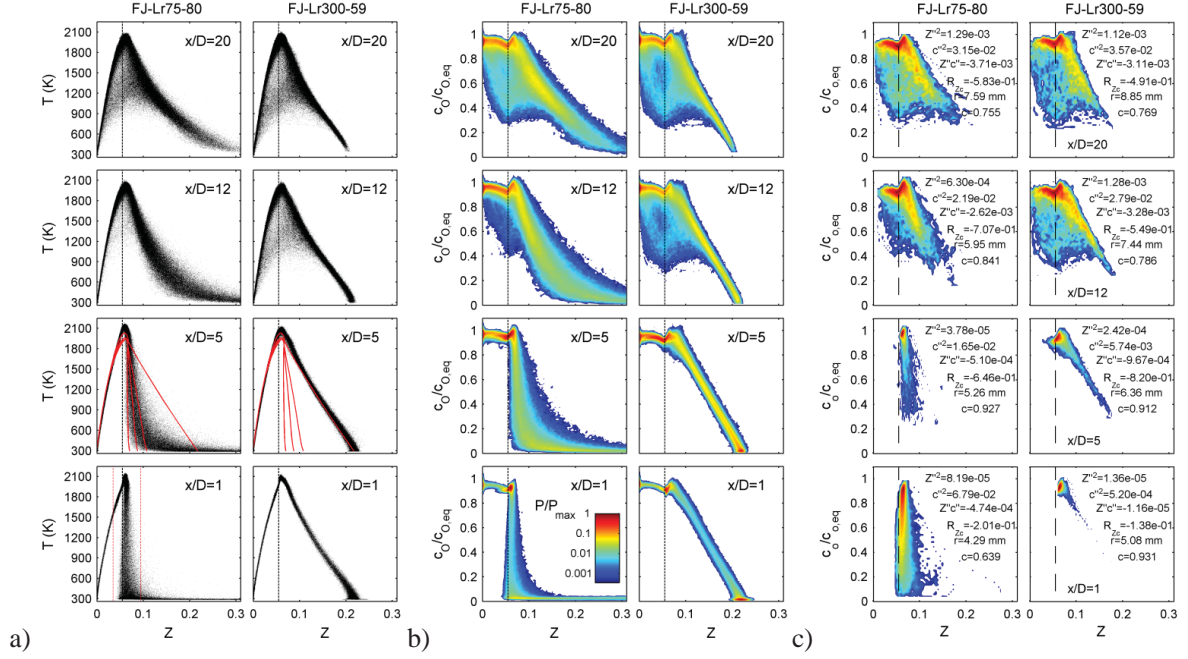


Figure 1. a) Temperature scatter data from radial profiles at the indicated downstream locations in piloted flames FJ-Lr75-80 and FJ-Lr300-59. Red curves are laminar flame calculations. b) Joint histograms of normalized progress variable and mixture fraction for the same data as in the temperature scatter plots. c) Histograms at spatial locations corresponding to $\tilde{Z} = 0.065$ and including data from a 0.3 mm window.

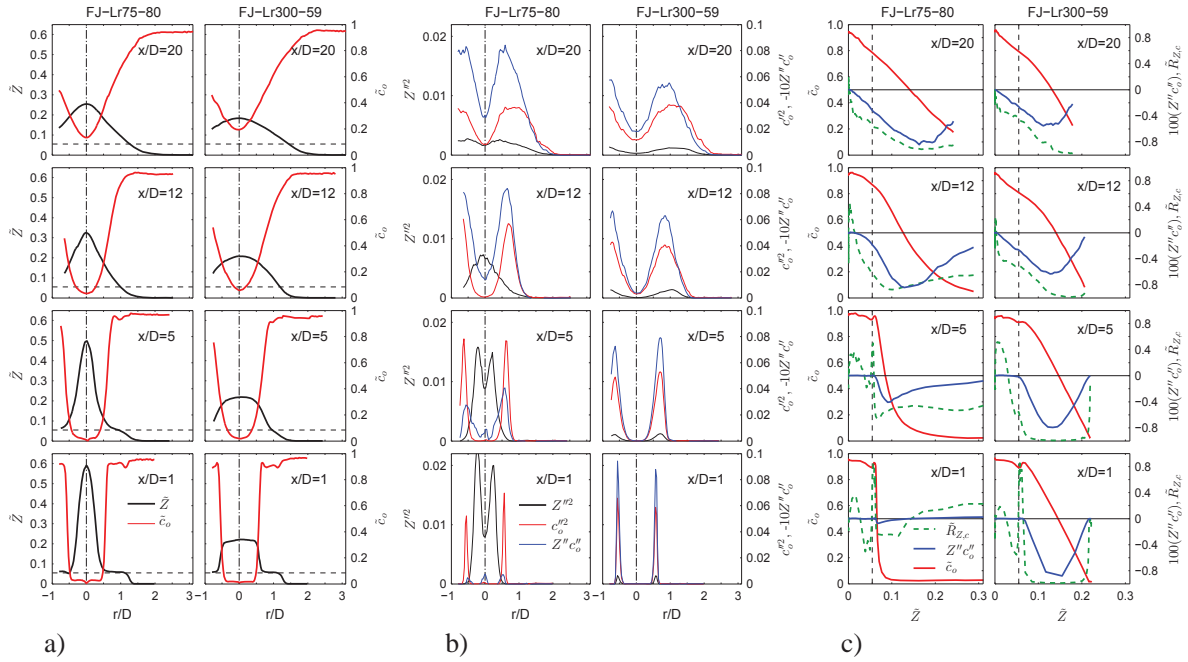


Figure 2. a) Radial profiles of \tilde{Z} and \tilde{c}_O . b) Radial profiles of the Favre variances and the covariance, $\tilde{Z}''c_O''$. c) Favre mean, \tilde{c}_O , covariance, $\tilde{Z}''c_O''$, and correlation coefficient, R_{Zc} plotted against \tilde{Z} at each point in the radial profiles (positive side only).

Pressure Effects on Flame Length in Turbulent Non-premixed Flames

Wesley R. Boyette, William L. Roberts

King Abdullah University of Science and Technology (KAUST)

wesley.boyette@kaust.edu.sa

The vast majority of experiments and simulations on turbulent non-premixed flames have considered flames only at atmospheric pressure. Brookes and Moss (1999) constructed a rig for methane-air diffusion flames at elevated pressures. However, none of the TNF workshop flames were operated in this rig. KAUST has designed and is now operating a very large rig with the explicit purpose of investigating large turbulent non-premixed flames at high pressures.

The high pressure combustion duct (HPCD) at KAUST was designed primarily for experiments on simple or piloted turbulent non-premixed flames, but is capable of supporting many other types of flames as well. The burner is positioned on a vertically translating stage within the duct, which is capable of up to 1500 mm of motion to accommodate very long flames. The HPCD is over 8 m tall to allow for visual observation of the entire flame while avoiding flame impingement on the upper surface of the duct. With an inner diameter of roughly 400 mm, the duct can accept a wide range of burner sizes. Burners may be easily replaced by lowering the bottom section of the duct from the table on which it sits. Two air inputs are available, with one typically used for the air coflow to the burner, and the other used as dilution air to limit heat transfer to the duct and its critical hardware. Four fuel inputs are available for operating piloted non-premixed flames as well as fully premixed flames. Six windows are available at the "optical plane" for laser diagnostics that require multiple lines of sight, such as stereoscopic particle image velocimetry. The HPCD's back pressure regulator is capable of pressurizing the duct up to 40 bar and a rupture disc is installed to prevent overpressurization. The lab is capable of providing dry air at up to 0.56 kg/s and 45 bar and can also provide similarly high flow rates of nitrogen for limited durations.

In this study, the high-pressure combustion duct at KAUST is used to create two series of TNFs at high pressures. In the first series, the flame is piloted and has the same geometry as Sandia target turbulent flame in the International Sooting Flame Workshop (Zhang et al 2011). The primary jet is composed of 65% nitrogen and 35% C₂H₄ and has a Re = 10,000. In the other series, the flame is identical in geometry and composition (CO/H₂/N₂) to the CHN-A flame in the TNF Workshop (Barlow et al 2000). In both cases, the Reynolds number is kept constant as the pressure is increased up to 10 atm, thus maintaining the fuel flow rates and power.

For each condition, the flame dimensions (maximum width and flame length) are calculated. This is accomplished by imaging each flame at multiple axial heights. At each height, 50 photos are taken with a very fast (1/4000 s) shutter to freeze the flame motion. Each frame is analyzed to establish the flame boundary and statistics are generated on the probability of the presence of a flame at each pixel. The sets from each height are combined to generate a profile of the full flame. This represents the first experimental study of the effect of pressure on flame length in such flames. True flame lengths decrease with pressure and the normalized lengths are found to generally agree with the predictions made by Delichatsios (1993).

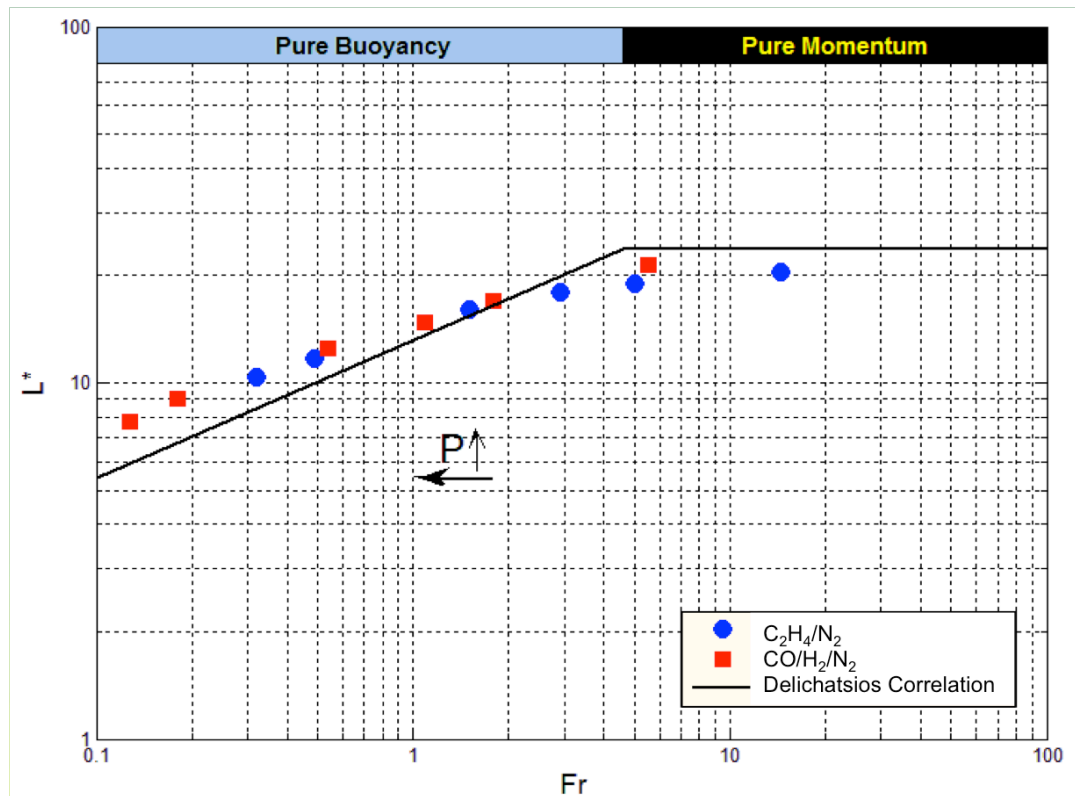


Figure 1 - Normalized flame height for each condition.

References

1. S.J. Brookes, J.B. Moss, Measurements of Soot Production and Thermal Radiation From Confined Turbulent Jet Diffusion Flames of Methane, *Combust Flame* (1999).
2. J. Zhang, C.R. Shaddix, R.W. Schefer, Design of "model-friendly" turbulent non-premixed jet burners for C_{2+} hydrocarbon fuels, *Rev Sci Instr* (2011).
3. R.S. Barlow, G.J. Fiechtner, C.D. Carter, J.-Y. Chen, Experiments on the Scalar Structure of Turbulent $CO/H_2/N_2$ Jet Flames, *Combust Flame* (2000).
4. M.A. Delichatsios, Transition from Momentum to Buoyancy-Controlled Turbulent Jet Diffusion Flames and Flame Height Relationships, *Combust Flame* (1993).

Effects of pressure on syngas/air turbulent nonpremixed flames

Pietro Paolo Ciottoli^{*†}, Bok Jik Lee^{**‡}, Hong G. Im^{**}, Mauro Valorani^{*}

^{*}Sapienza University, Rome, Italy ([†]pietropaolo.ciottoli@uniroma1.it)

^{**}Clean Combustion Research Center, KAUST, Saudi Arabia ([‡]bokjik.lee@kaust.edu.sa)

Large eddy simulations (LES) of turbulent nonpremixed jet flames were conducted to investigate the effects of pressure on the syngas/air flame behavior. This simulation campaign is aligned with the experimental effort in the Clean Combustion Research Center at KAUST, which is currently setting up high pressure combustion test facility operating at up to 40 atm. The simulations will guide the experimental operation conditions and cross-validate with the laser diagnostic measurements of various flame observables.

The software to solve the reactive Navier-Stokes equations was developed based on the OpenFOAM framework, using the the YSLFM library [1] for the flamelet-based chemical closure. The solver is based on a finite volumes pressure-based (PISO) algorithm. The LES subgrid turbulence closure relies on a Smagorinsky model, and the turbulent-chemistry interaction is modeled by means of the steady laminar flamelet model (SLFM) closure [2], which allows evaluations of the detailed reactive scalar variables at much reduced computational cost. Flamelets are generated in a pre-processing step and stored in a look-up table as a function of the mixture fraction, the mixture fraction variance, and the scalar dissipation rate. The mixture fraction and its variance are obtained from solving properly defined transport equations in the physical LES field, while the interaction between turbulent fluctuations and chemistry is taken into account by means of a presumed probability density function (PDF), in terms of the mixture fraction and of its variance. The results of the pre-processing procedure are stored in tables which are accessed during the simulation. The flamelet tabulation is obtained by means of an in-house code designed to solve unsteady flamelets of both ideal and real fluid mixtures [3].

The validation of the numerical setup is attained by comparison of the numerical results with the Sandia/ETH-Zurich experimental database of the CO/H₂/N₂ non-premixed, unconfined, turbulent jet flame, referred to as “Flame A” [4]. The experiment is operated at ambient pressure, the fuel is injected at 292 K from a straight circular tube with squared-off ends with an inner diameter of 4.58 mm, and the outer diameter of 6.34 mm. Its injection velocity is 76 m/s and the corresponding Reynolds number is 16700. The air coflow velocity is 0.75 m/s, it is wet (molar fraction of water 0.012) and has a temperature of 290 K. The fuel stream composition is 40/30/30 in volume percentage. The chemical mechanism employed is a detailed H₂/CO mechanism with 12 species and 33 chemical reactions [5].

Figure 1 shows the temperature field resulting from the simulation of the Flame A at atmospheric condition. The computational domain is cylindrical, and the axial and radial domain sizes are 1000 mm and 169 mm, respectively. The adopted computational mesh consists of approximately 6 million cells, with a resolution of about 1 mm in each direction.

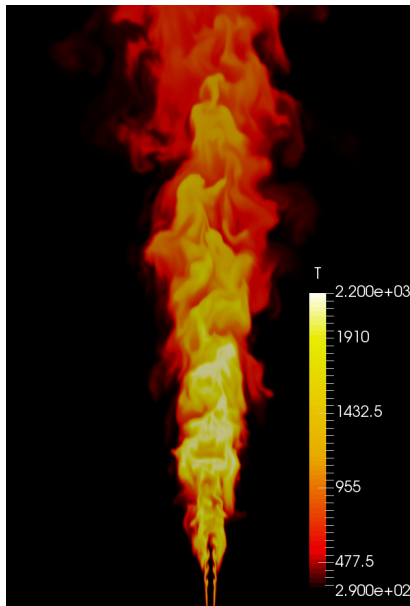


Fig 1: Temperature field of Sandia flame A at $p=1$ atm.

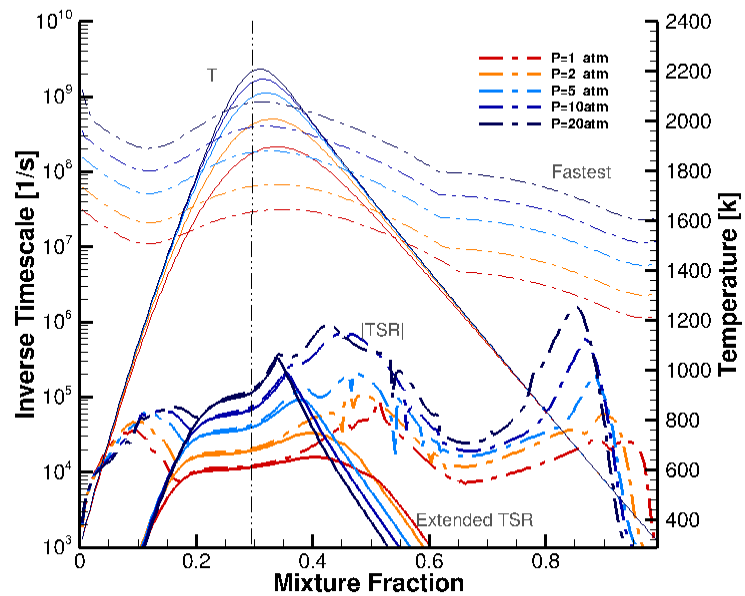


Fig 2: CSP analysis of flamelet solutions with scalar dissipation 100 s^{-1} and pressure ranging from 1 to 20 atm.

Three simulations at elevated pressure conditions up to 5 atm are compared and analyzed to unravel computational and scientific challenges in characterizing turbulent flames at high pressures.

The flamelet solutions for scalar dissipation 100 s^{-1} , and for pressure value ranging from 1 to 20 atm, are analyzed following a CSP approach. In particular, the Tangential Stretching Rate (TSR) definition, and its extension to convection-reaction systems (extended TSR), are adopted. The TSR represents the inverse of the most energetic time scale associated with the chemical source term, while the extended TSR represents the inverse of the most energetic time scale of the reaction-diffusion system [6]. The results of the CSP analysis are shown in Fig. 2 where, for each pressure value, the temperature profiles, the maximum eigenvalue associated with the chemical source term, representing the inverse of the fastest timescale, and both the TSR and the extended TSR are reported. The CSP analysis revealed that a pressure increase leads to higher temperatures and smaller timescales, as well as a shrink of the region where the system dynamics is governed by chemical kinetics, i.e. where the TSR and the extended TSR coincide. Moreover, the observation of the timescale values in the stoichiometric mixture fraction ($Z=0.295$) revealed that, while the inverse of the fastest time scale follows a power law with exponent larger than one, the most energetic chemical timescale (TSR) follows a power law with exponent smaller than one.

Bibliography:

- [1] H. Müller, F. Ferraro, M. Pfitzner, 8th Intern. OpenFoam Workshop, Jeju, Korea, 2013.
- [2] N. Peters. Turbulent Combustion. Cambridge University Press, 2000.
- [3] P.E. Lapenna, P.P. Ciottoli, M. Valorani, F. Creta, European Comb. Meeting, 2015.
- [4] R.S. Barlow, SANDIA/ETH-Zurich CO/H₂/N₂ Flame Data–Release 1.1, www.ca.sandia.gov/TNF, Sandia National Laboratories, 2002.
- [5] J. Li, Z. Zhao, A. Kazakov, M. Chaos, F.L. Dryer, J.J. Scire, Int. J. Chem. Kinet. 39, 2007.
- [6] M. Valorani, P.P. Ciottoli, R. Malpica Galassi, 36th Symposium Combustion, Seoul, Korea, 2016.

VORTICITY/STRAIN-RATE MEASUREMENTS IN TURBULENT PARTIALLY- PREMIXED METHANE/AIR JET FLAMES

Bruno Coriton and Jonathan H. Frank*

Combustion Research Facility, Sandia National Laboratories, Livermore, California 94551

*corresponding author's email: jhfrank@sandia.gov

In turbulent flows, the interaction between vorticity, ω , and strain rate, s , is considered a primary mechanism for the transfer of energy from large to small scales through vortex stretching. The development of physically accurate models of these interactions present a challenge since the vorticity-strain coupling occurs over a wide range of scales. Experimental studies of these interactions require three-component volumetric velocity field measurements. The ω - s coupling in turbulent jet flames is investigated using tomographic particle image velocimetry (TPIV) [1]. TPIV provides a direct measurement of the three-dimensional velocity field from which ω and s are determined. The effects of combustion and mean shear on the ω - s interaction are investigated in turbulent partially-premixed piloted methane/air jet flames with different probabilities of localized extinction (Sandia Flames C and F) as well as in non-reactive isothermal air jets with comparable Reynolds numbers to those of the jet flames.

Results show that combustion causes structures of high vorticity and strain rate to agglomerate in highly-correlated, elongated layers that can span the height of the probe volume, as shown in Fig. 1. In the non-reactive jets, these structures have a more varied morphology, greater fragmentation, and are not as well correlated. The enhanced spatiotemporal correlation of vorticity and strain rate in Flame C results in stronger ω - s interaction characterized by increased enstrophy and strain-rate production rates via vortex stretching and straining, respectively. The probability of preferential local alignment between ω and the intermediate principal strain rate, s_2 , which is intrinsic to the ω - s coupling in turbulent flows, is larger in the flames, as shown in Fig. 2. In the higher Reynolds number flame and air jet, preferential alignment is less pronounced and the alignment enhancement from combustion is only observed in the PDFs conditioned on high values of vorticity. The larger mean shear in the flames imposes a preferential orientation of ω and s_2 tangential to the shear layer. The extensive and compressive principal strain rates, s_1 and s_3 , respectively, are preferentially oriented at approximately 45 degrees with respect to the jet axis. The production rates of strain and vorticity tend to be dominated by instances in which ω is parallel to the \bar{s}_1 - \bar{s}_2 plane and orthogonal to \bar{s}_3 .

References

- [1] B. Coriton, J. H. Frank, *Physics of Fluids* 28 (2016) 025109.

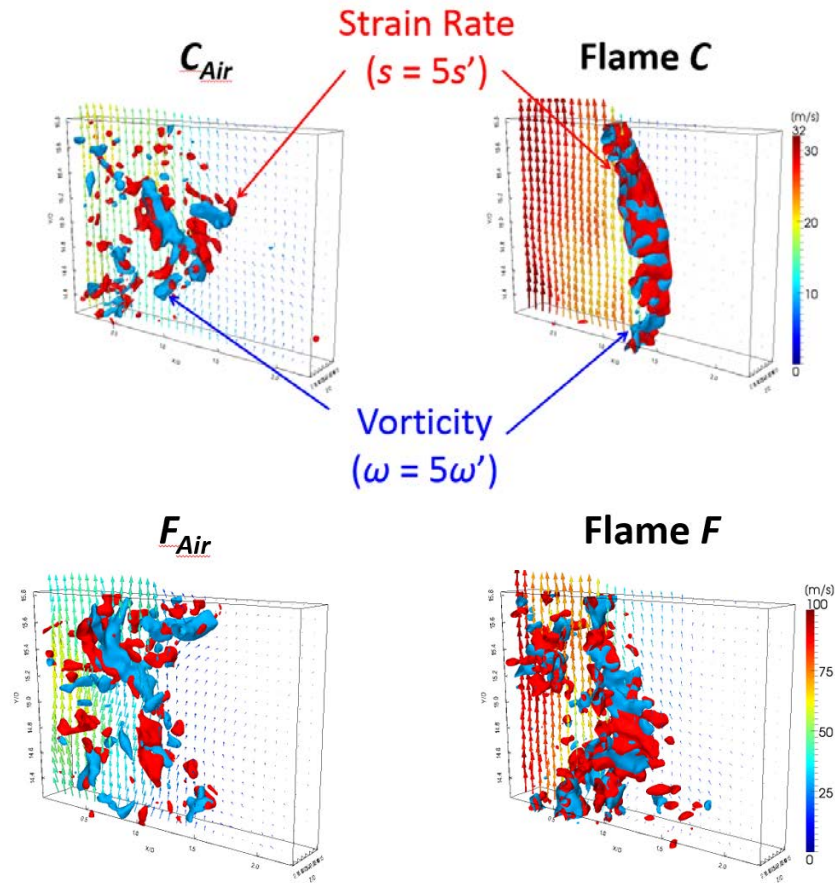


Fig. 1. Strain rate isosurfaces (red) and vorticity isosurfaces (blue) from single-shot measurements in turbulent piloted jet flames (Sandia Flames C and F) and the corresponding isothermal air jets.

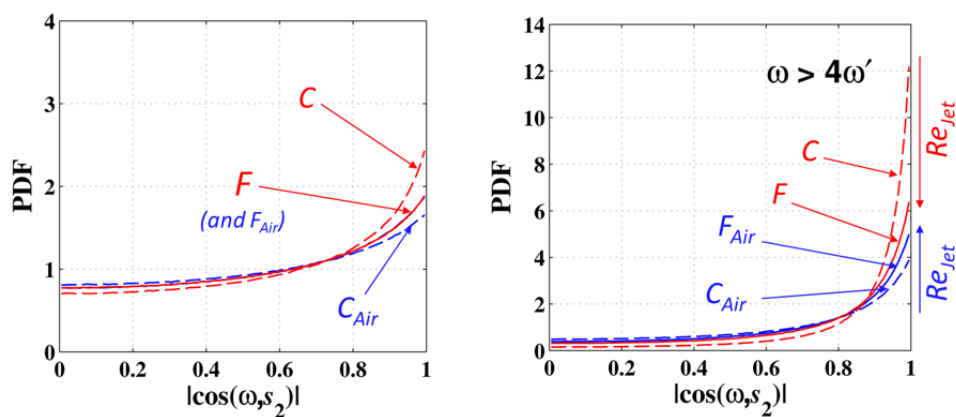


Fig. 2. Probability density functions of the alignment angle between the vorticity and the intermediate strain rate eigenvector, s_2 , in turbulent jet flames and isothermal air jets. Unconditional PDFs (left) show enhanced alignment from combustion only in Flame C. PDFs conditioned on high vorticity (right) show preferential alignment in both flames, but the enhancement is less pronounced in Flame F.

Unsteady flamelet analysis utilizing in-situ tracked mixture fraction gradient trajectories in DNS of turbulent non-premixed combustion

F. Dietzsch^{a)}, A. Scholtissek^{a)}, C. Hasse^{a)}

^{a)} Numerical Thermo-Fluid Dynamics, TU Bergakademie Freiberg, Germany
Felix.Dietzsch@vtc.tu-freiberg.de

In this work a direct numerical simulation (DNS) of a spatially evolving syngas jet is carried out to assess a recently published flamelet model including curvature-induced effects [1]. Therefore, flamelets are tracked in time and space, which is referred to as "in-situ tracking". This method allows a full reconstruction of individual flamelet histories for a detailed examination of transient effects, curvature, tangential transport (along the Z-isosurface) as well as the relations between compressive/expansive strain and scalar dissipation. For the DNS the low Mach code DINO [2] is utilized, which solves the reactive Navier-Stokes equations and an additional transport equation for the mixture fraction. Transport processes are modeled with a mixture averaged diffusion model including a correction velocity. Transport properties, as well as thermodynamic data and reaction rates, are obtained from Cantera [3], which is fully coupled to DINO. The equations are solved using a fourth-order Runge Kutta scheme for time integration and sixth-order finite differences for spatial derivatives. The coupling between continuity and momentum is achieved by a pressure-free projection method based on a spectral Poisson solver.

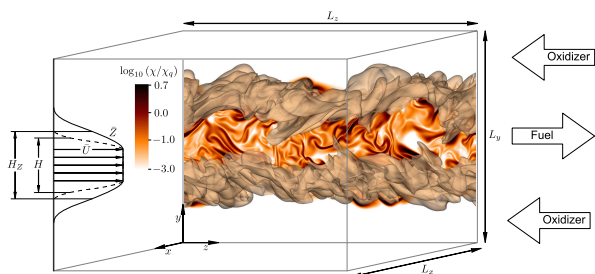


Figure 1: Setup of the DNS case according to [4]. The domain size is chosen as $L_x = 7H$ in span-wise direction, $L_y = 14H$ in cross-stream direction and $L_z = 14H$ in stream-wise direction, where H denotes the initial width of the jet.

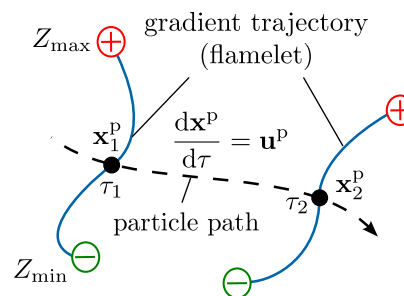


Figure 2: Schematic of the in-situ tracking algorithm for two instances in time. A gradient trajectory (blue line) is emitted from a particle (black dot). Gradient trajectories are constructed by following the mixture fraction gradient until a local maximum (Z_{\max} , red plus) or a local minimum (Z_{\min} , green minus) is reached, respectively.

The case setup, shown in Fig. 1, is based on a well-established DNS case originally proposed by Hawkes et al. [4]. The computational domain is discretized with a Cartesian grid of $512 \times 1024 \times 1024$ points. The central fuel jet (50% CO, 10% H₂ and 40% N₂) is surrounded by a counter-flowing oxidizer stream (25% O₂ and 75% N₂). Chemical kinetics are described with the mechanism by Li et al. [5]. The case is characterized by local extinction and reignition phenomena, which makes it a suitable reference for the subsequent unsteady flamelet analysis.

The in-situ flamelet-tracking algorithm combines the concept of dissipation elements by Wang and Peters [6] with the flame element tracking proposed by Sripakagorn et al. [7]. Figure 2 schematically illustrates the tracking method. Particles are initially distributed across the surface of stoichiometric mixture fraction. After positioning the particles, gradient trajectories are constructed along the ascending and descending direction of the mixture fraction gradient until the local maximum Z_{\max} or minimum Z_{\min} , see Fig. 2, is detected (thus, they represent flamelet structures). During the temporal evolution of the jet, particles are transported such that they are fixed on the respective surface using a velocity \mathbf{u}^p accounting for convective and diffusive transport. Figure 3 shows an example of tracked flamelets for one instant of the turbulent jet and their intersections with the stoichiometric mixture fraction iso-surface.

The extended flamelet model applied in this study is based on a recently published model including differential diffusion and curvature-induced flame-tangential transport [1]. Flame-tangential transport of scalar quantities, such as temperature or species mass fraction, can be differentiated into (a) curvature-induced differential diffusion and (b) transport along mixture fraction iso-surfaces (also denoted as multi-dimensional effect, MD). The model is slightly modified to describe in-situ tracked flamelets.

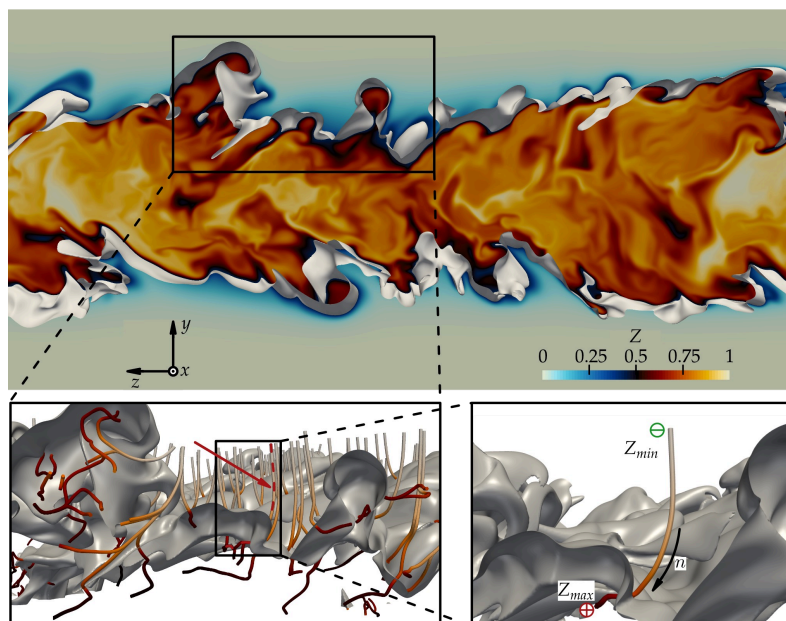


Figure 3: Top: DNS snapshot of the spatially evolving syngas jet. Bottom left: Gradient trajectories of the mixture fraction field (flamelets). Bottom right: realization of an individual flamelet with the local minimum (green) and the local maximum (red).

The flamelet equations are solved with an in-house flamelet solver and three limits are distinguished: the classical flamelet model (FLT), the flamelet model with curvature-induced differential diffusion (FLT-C) and the flamelet model with multi-dimensional effects (FLT-MD). For the flamelet calculations all relevant parameters (scalar dissipation rate, curvature and MD terms) are extracted from the DNS. Figure 3 shows the temporal evolution of the temperature at stoichiometry T_{st} for two flamelet identities F_I and F_{II} on the tracked gradient trajectory T-I. It is observed that while the flamelet solutions for F_{II} agree well with the DNS results (thus, flame-tangential transport is negligible), only the extended flamelet model FLT-MD can reproduce the flame temperature evolution for F_I . The study further examines the influencing factors for this departure from classical flamelet behavior also including the dynamic interplay of compressive strain, scalar dissipation and curvature with respect to the underlying scalar mixture fraction field.

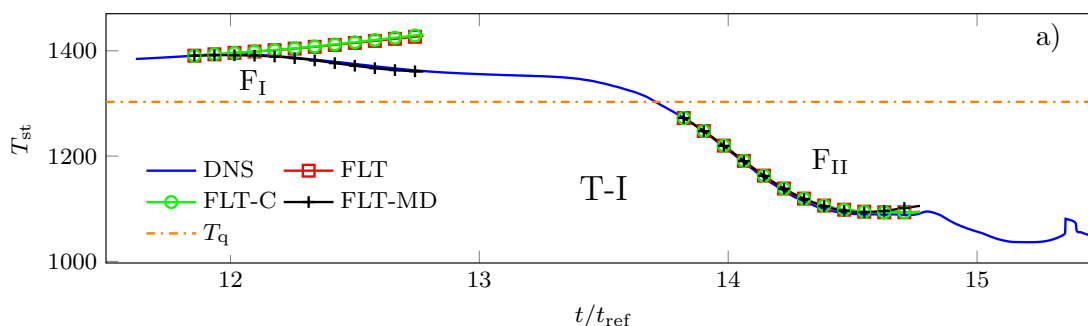


Figure 4: Evolution of the stoichiometric temperature for the gradient trajectory T-I with two exemplary flamelet realizations F_I and F_{II} . The flamelet solutions FLT, FLT-C and FLT-MD are shown in comparison to the DNS result (blue line). T_q indicates the temperature at the extinction limit for a laminar flamelet.

References

- [1] A. Scholtissek, W. L. Chan, H. Xu, F. Hunger, H. Kolla, J. H. Chen, M. Ihme, C. Hasse, *Combust. Flame* 162 (2015) 1507–1529.
- [2] A. Abdelsamie, G. Fru, T. Oster, F. Dietzsch, D. Thévenin, *Comput. Fluids* 131 (2016) 123–141.
- [3] D. G. Goodwin, H. K. Moffat, R. L. Speth, <http://www.cantera.org>, 2016. Version 1.8.0.
- [4] E. R. Hawkes, R. Sankaran, J. C. Sutherland, J. H. Chen, *Proc. Combust. Inst.* 31 (2007) 1633–1640.
- [5] J. Li, Ph.D. thesis, Mechanical and Aerospace Engineering Department, Princeton University, 2004.
- [6] L. Wang, N. Peters, *J. Fluid Mech.* 554 (2006) 457–475.
- [7] P. Sripakagorn, S. Mitarai, G. Kosály, H. Pitsch, *J. Fluid Mech.* 518 (2004) 231–259.

Applications of LES-PDF method to premixed, non-premixed and stratified flames

I. Dodoulas and S. Navarro-Martinez*

*Department of Mechanical Engineering
Imperial College, London SW7 2AZ, UK*

** Email: s.navarro@imperial.ac.uk*

Introduction

This work explores the capabilities of the Large Eddy Simulations (LES) sub-grid scale PDF to simulate a range of methane laboratory flames. The flames have been selected to cover a wide range of flame regimes (premixed, non-premixed), geometry complexity (piloted flames, single fuel stream, double fuel stream, stratified and bluff-body) and flow field complexity jet and swirl flames). Table 1 summarised the 10 flames investigated in this work. They include the premixed flames (Aachen) [1], swirl non-premixed flames (Sydney) [2], swirl and non-swirl stratified flames (Cambridge) [3] and non-premixed flames (Delft) [4]. Some of the selected flames have been extensively investigated in the literature and in previous TNF workshops. They cover a relatively wide range of conditions: Reynolds numbers from 9700 up to 52500 (based on jet diameter and bulk inlet velocities); swirl geometric ratios up to 0.79. The flames present several degrees of stratification as well as extinction levels.

Flame	Jet Reynolds	Swirl Ratio	Stratification	Extinction	Regime
F1	52500	0	No	High	Premixed
F2	40300	0	No	No	Premixed
F3	24200	0	No	No	Premixed
SwB1	5960	0	No	No	Premixed
SwB5	5960	0	Medium	No	Stratified
SwB6	5960	0.45	Medium	No	Stratified
SwB11	5960	0.79	High	Minimal	Stratified
SM1	7200	0.5	No	Low	Non-premixed
SM2	19500	0.5	No	High	Non-premixed
Delft III	9700	0	No	High	Non-premixed
Sandia D	22400	0	No	Low	Partially premixed
Sandia E	33600	0	No	Medium	Partially premixed
Sandia F	44800	0	No	High	Partially premixed

Table 1: Overview of the flames studied in this work. Sandia flames simulations from [4] are included for comparison

The objective of this work is to use the same modelling approach across all the flames: This involves the same model parameters and sub-grid closure method. The grid size also did not significantly vary from case to case, relative to the particular scales of each flame. A global error figure for CO₂ and CO (comparing LES and experimental data) was constructed for each simulation to evaluate performance across all flames.

Modelling

The LES-PDF model aims to solve the *joint sub-grid scale PDF* of the complete set of scalars. This approach is only feasible using stochastic methods, in this work the Eulerian *stochastic fields* method is used [5,6]. For the simulations, the in-house code BOFFIN-LES has been used. The calculations were performed using a grid of about 1M cells, where the grid was chosen such that the 15-20 grid points are located within the jet. The number of stochastic fields was 8/16 stochastic fields. A Smagorinsky model was used with a constant of 0.1. To represent the methane chemistry, a 19-species, 15-step augmented reduced mechanism (ARM) is used [8]

Results

Figure 1 shows the average offset between the experimental and simulation values for all test cases of this work against the inlet stream Reynolds number. To compute the offset the absolute error between experimental and numerical data plots was calculated for each axial location and the averaged over all experimental stations.

$$\Delta_{CO_2} = \frac{1}{N_s} \sum_{stations} \max \left(\frac{CO_2[LES]_i - CO_2[exp]_i}{CO_2[exp]_i} \right)$$

The previous offset provides a good indication of how accurate the prediction is compared to the experimental data. The results show a strong correlation with the Reynolds number and that flow complexity and combustion regime do not strongly affect the model. Neither do swirl or level of extinction. Except F1 and F2 flames, the results are below 10%. Similar trends are observed for CO.

Simulations with one field (neglecting sub-grid effects) were compared with the original results, providing an estimate of the effects of sub-grid modelling. The results showed that sub-grid modelling generally becomes more important as the Reynolds number increases. However below 20000, the introduction of additional stochastic fields marginally affects the results and sub-grid modelling is not important. Surprisingly, even in flames in the thin-flamelets regimes, the global improvements are small. A more detailed look at complex flames (like SwB11) reveals that in some cases, additional parameters have to be taken into account (e.g. the combination of heat losses with differential diffusion). However, overall, the LES-PDF approach performed satisfactory in a wide range of combustion regimes with virtually the same set-up of parameters.

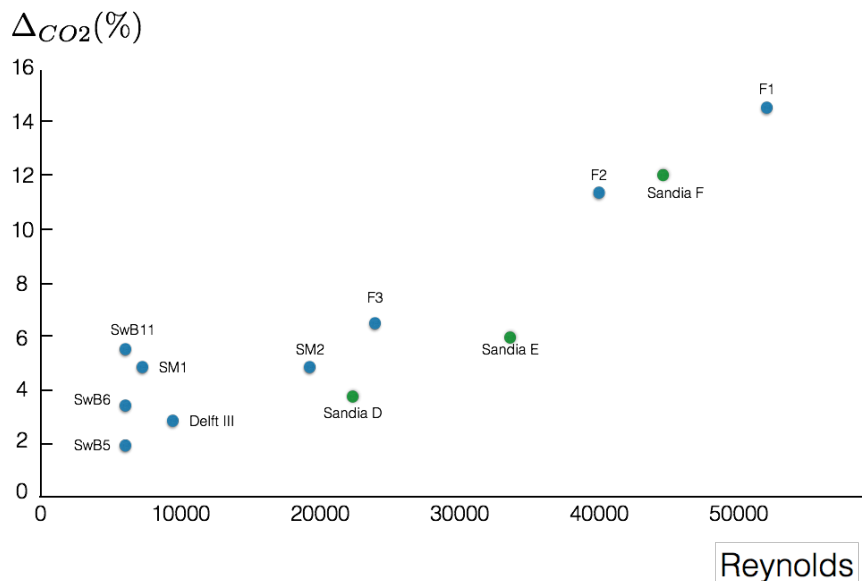


Figure 1: CO₂ offset between experimental data and LES results as a function of Reynolds number. The green symbols indicate offsets for the Sandia calculations of Jones and Prasad [7]

References

- [1] Y.C. Chen, N. Peters, G.A. Schneemann, N. Wruck, U. Renz, and M.S. Mansour, *Comb. Flame*, 107(3):223-244, (1996).
- [2] P.A.M. Kalt, Y.M. Al-Abdeli, A.R. Masri, and R.S. Barlow, *Proc. Comb. Inst.*, 29:1913-1919, 2002
- [3] M.S. Sweeney, S. Hochgreb, M.J. Dunn, and R.S. Barlow, *Comb. Flame*, 159:2896-2911, 2012.
- [4] P A Nooren, M Versluis, T H. van der Meer, R.S. Barlow, and J.H. Frank, *Appl. Phys. B-Lasers Opt.*, 71(1):95-111, 2000
- [5] R Mustata, L Valiño, C. Jimenez, W. P. Jones and S. Bondi, *Comb. Flame* 145 (2006) 88-104.
- [6] W P Jones, S Navarro-Martinez and O. Röhl, *Proc. Comb. Inst.* 31 (2007), 1765-1771.
- [7] W P Jones, V N Prasad, *Comb. Flame* 157, 1621-1636 (2006)
- [8] C J Sung, C K Law, J Y Chen, *Comb. Flame* 125 (2001) 906-919

LOCAL EXTINCTION IN A TURBULENT PARTIALLY- PREMIXED DME/AIR JET FLAME SERIES

F. Fuest^{*a}, R.S. Barlow^b, G. Magnotti^b, J.A. Sutton^c

a Lavisio GmbH, Anna-Vandenhoeck-Ring 19, D-37081 Goettingen, Germany

b Sandia National Laboratories, 7011 East Avenue, Livermore, CA, USA

c Department of Mechanical and Aerospace Engineering, The Ohio State University, 201 W. 19th Avenue, Columbus, OH, USA

Abstract

This work discusses the progress of local extinction in a turbulent partially-premixed 20%DME/air jet flame series with Reynolds numbers from 29,300 to 73,250. The flame series was first introduced at the TNF10 by Frank and coworkers [1]. It was derived in order to step towards turbulent combustion model validation with an alternative and more complex fuel following the original methane flame series D-F in the piloted Sydney/Sandia burner [2,3]. Increasing bulk flow velocities result in jet Reynolds numbers as given in the Table. The configurations are labeled DME-D, DME-E, DME-F, DME-G, and DME-G'. The additional case DME-G' was introduced to further increase the amount of local extinction by reducing the flow velocity of the pilot to 80% of the velocity of flame DME-G.

Flame	Jet bulk velocity (m/s)	Reynolds number
DME-D	45.9	29,300
DME-E	68.8	43,950
DME-F	91.8	58,600
DME-G	114.7	73,250
DME-G'*	114.7	73,250

*pilot velocity reduced to 80% of DME-G

The Figure presents scatter plots and conditional mean values of two selected major species from 1D Raman/Rayleigh/CO-LIF line measurements to show effects of local extinction at six different axial locations for five different flame configurations. Close to the nozzle exit, at axial location $x/d = 1$, a significant reaction of the jet mixture has not started yet, and scatter plots as shown for H₂O and DME+hydrocarbons conditioned on the mixture fraction are dominated by pure mixing with the hot pilot gases at all configurations (first column in the Figure). The lowest Reynolds number case DME-D shows very small amounts of local extinction at $x/d = 7.5, 10, \text{ and } 20$ as apparent from scatter which exist towards the path of unreacted mixing and the path of full reaction. Significantly increased local extinction is observed at $x/d = 5, 7.5, 10, \text{ and } 20$ towards higher Reynolds numbers. Signs of local extinction at $x/d = 40$ are negligible for all five flame configurations.

References

- [1] J. H. Frank., A. G. Hsu, J. Kuhl, Turbulent partially premixed dimethyl ether/air jet flames: A new series of target flames for experiments and modeling, Proceedings of TNF 10. URL <http://www.sandia.gov/TNF/10thWorkshop/TNF10.html>
- [2] B. Coriton, M. Zendejdel, S. Ukai, A. Kronenburg, O. T. Stein, S.-K. Im, M. Gamba, J. H. Frank, Imaging measurements and LES-CMC modeling of a partially-premixed turbulent dimethyl ether/air jet flame, Proc. Combust. Inst. 35 (2) (2015) 1251–1258.
- [3] F. Fuest, G. Magnotti, R. S. Barlow, J. A. Sutton, Scalar structure of turbulent partially-premixed dimethyl ether/air jet flames, Proc. Combust. Inst. 35 (2) (2015) 1235–1242.

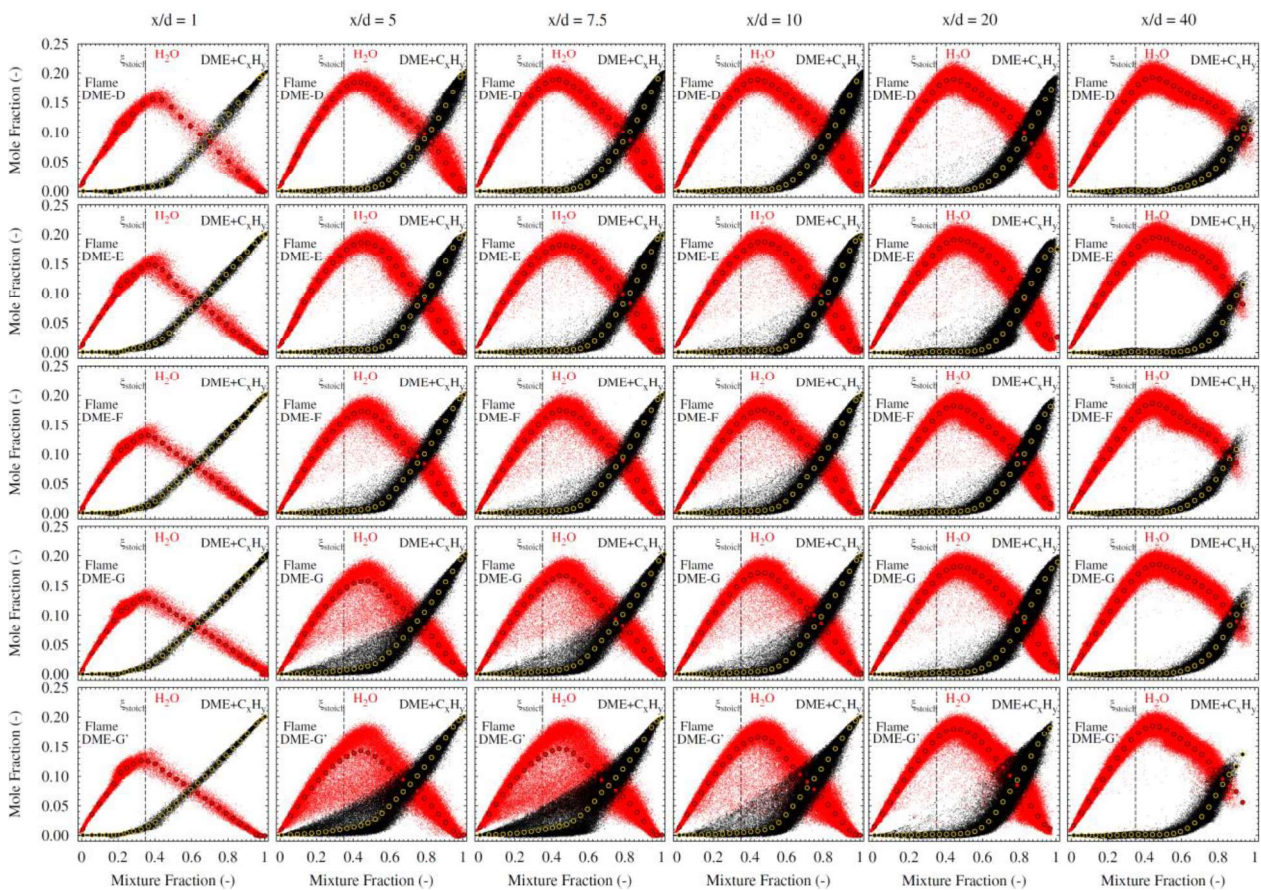


Figure: Scatter plots conditioned on the mixture fraction and conditional mean values for H_2O and DME+hydrocarbons for five flame configurations (rows) and six axial locations (columns).

SCALAR DISSIPATION RATE MEASUREMENTS IN A TURBULENT PARTIALLY-PREMIXED DIMETHYL ETHER/AIR JET FLAME

F. Fuest^a, R.S. Barlow^b, G. Magnotti^b, J.A. Sutton^c

^a Lavision GmbH, Anna-Vandenhoeck-Ring 19, D-37081 Goettingen, Germany

^b Sandia National Laboratories, 7011 East Avenue, Livermore, CA, USA

^c Department of Mechanical and Aerospace Engineering, The Ohio State University, 201 W. 19th Avenue, Columbus, OH, USA

Abstract

This work presents the gradient structure of a turbulent partially-premixed dimethyl ether (DME)/air jet flame operating at a jet Reynolds number of 29,300 (flame DME-D). Temperature and mixture fraction profiles from 1D Raman/Rayleigh/CO-LIF line measurements are used to determine one-dimensional scalar dissipation rates at six axial locations. A major focus of the current work is to assess the effects of experimental artifacts, including spatial resolution, noise, and dimensionality, on the accuracy of the derived scalar dissipation rate. Spatial averaging effects are investigated using 2D-PDFs of the mixture fraction gradients, cutoff scales determined from one-dimensional dissipation spectra (Figure 1), scaling laws, and laminar flame calculations in conjunction with optical-blur filters representing the experimental setup. The impact of noise is treated by error propagation methods. Monte-Carlo-Simulations and experimental data from laminar flames are used to verify and validate the models used to predict noise propagation for the measurements of the absolute gradients, squared gradients, and scalar dissipation rates. Scalar dissipation rate detection limits and contributions from apparent dissipation (due to noise effects) are presented as functions of measurement signal-to-noise ratios.

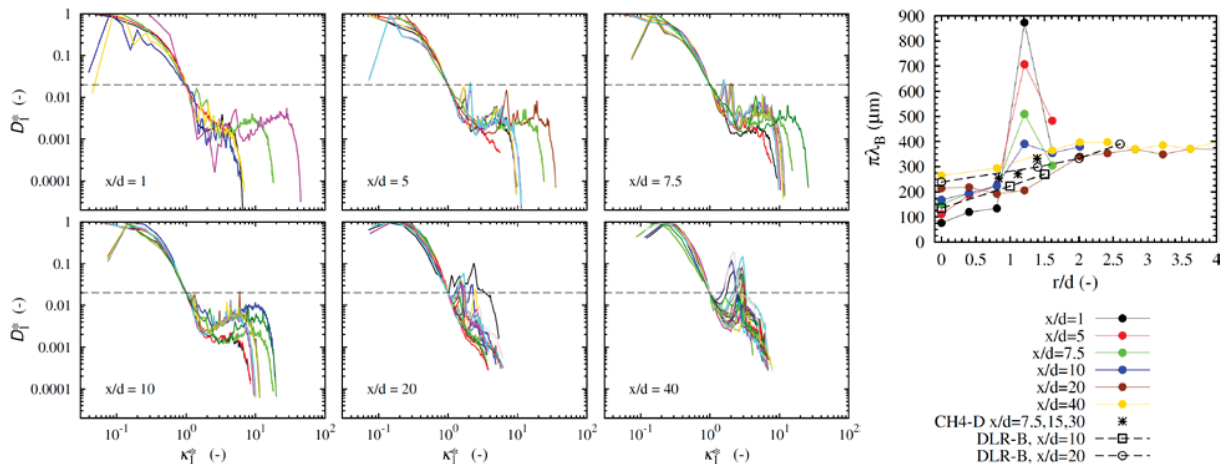


Figure 1: Left: Normalized one-dimensional dissipation spectra from inverse Rayleigh signal. Horizontal dashed lines mark the 0.02 cutoff. Right: Corresponding Batchelor scales (times π) as functions of the radial and axial location as determined from the cutoff at 0.02 in the dissipation spectra. $\lambda_B \pi$ represents the required resolution in order to resolve the dissipation until the cutoff at 0.02.

Results are presented in the form of scatter plots and conditional statistics including means (Figure 2), probability density functions (PDFs) and two-dimensional probability density functions (2D-PDFs) to examine turbulence-chemistry interaction and develop a database for model assessment. Specifically, the results are compared to laminar flame calculations over a broad range of strain rates and two transport assumptions and are used to assess the relevance of molecular diffusion effects in the turbulent flame. Potential effects from differential diffusion are found to be supported by comparing the experimental results and characteristic features of the scalar dissipation results from laminar calculations based on unity Lewis number and multi-component transport assumptions.

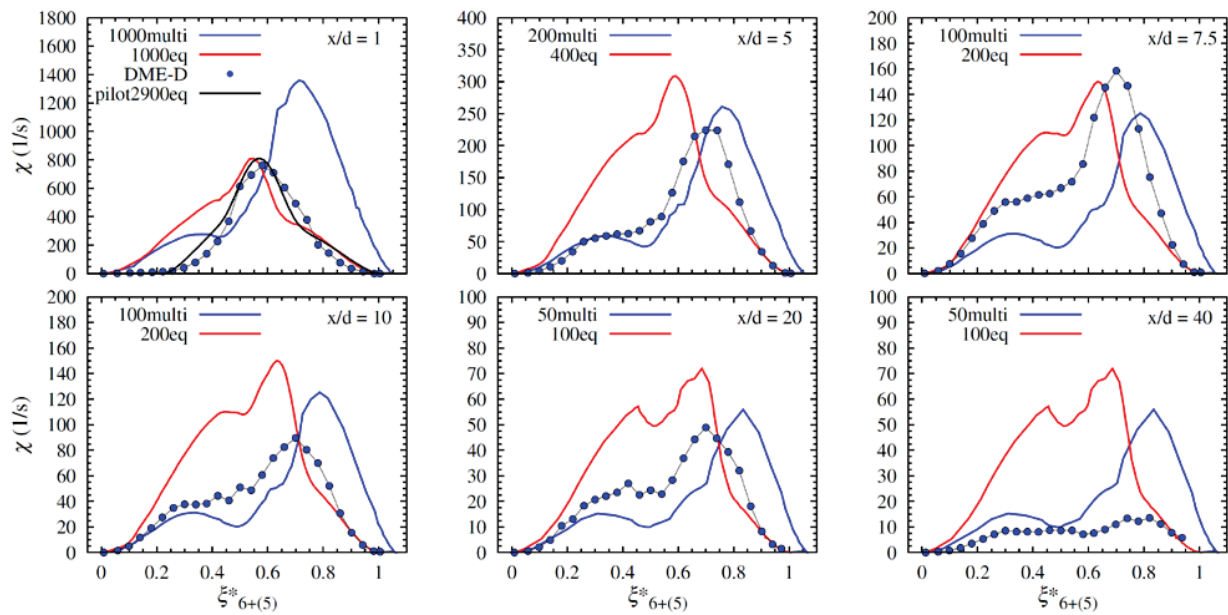


Figure 2: Radial component of conditional scalar dissipation rates in turbulent flame DME-D at six axial locations (dots) compared to scalar dissipation rates from one-dimensional laminar flame calculations at different strain rates, multi-component (multi) and unity Lewis number transport (eq) assumptions. An additional configuration with the hot pilot gas instead of cold co-flow air is shown at $x/d = 1$.

mmcFoam - A New Object-Oriented Multiple Mapping Conditioning Turbulent Combustion Code

S. Galindo-Lopez^{1*}, L.F. Zhao¹, M.N. Khan¹, A. Majbouri¹, F. Salehi¹, M.J. Cleary¹, A.R. Masri¹,
G. Neuber², S. Vo², C. Straub², J. Kirchmann², O.T. Stein², A. Kronenburg²,
Y. Ge³, B. Sundaram⁴, L. Dialameh⁴, A.Y. Klimenko⁴, A. Varna⁵, E.R. Hawkes⁵

¹ School of Aerospace, Mechanical and Mechatronic Engineering, The University of Sydney

² Institut für Technische Verbrennung, Universität Stuttgart

³ Institut für Thermodynamik LFT-10, Universität der Bundeswehr München

⁴ School of Mechanical and Mining Engineering, The University of Queensland

⁵ School of Mechanical and Manufacturing Engineering, The University of New South Wales

1 INTRODUCTION

The study of turbulence-chemistry interactions is paramount for the design of more efficient combustion devices with low pollutant emissions. The use of PDF methods in turbulent reacting flows is a powerful tool where the chemical source term appears in closed form. However, one of the difficulties of transported PDF methods is the modelling of molecular mixing. MMC in its stochastic form is a PDF model where reference variables are used to support the mixing operation complying with key mixing model principles as stated in [1].

A new code called *mmcFoam* is being developed collaboratively to develop and validate MMC for the turbulent combustion of gaseous, liquid and solid fuels in a range of configurations including non-premixed, premixed, partially-premixed and stratified configurations. The code incorporates DNS, LES and RANS solvers, various sparse and intensive MMC and conventional mixing models, alternative chemical integrators including a sectional scheme for soot and nano-particle synthesis, and submodels for evaporation and pyrolysis.

The use of object oriented programming (OPP) supports the creation of solvers for the simulation of turbulent flames in a very intuitive way as it allows for the abstraction of multiple concepts and also for great modularity. Implementation of new physics or additional aspects of the problem becomes easier using hierarchical structures and polymorphism. Secure code development in a highly collaborative environment is supported by encapsulation.

2 METHODOLOGY

2.1 The code structure

The code is split in three blocks and each is compatible with the C++ library OpenFoam [2]. The MMC block is a stochastic particle scheme for the composition PDF. The Lagrangian Fuel Parcel (LFP) block is a dispersed-phase scheme for advection and interphase heat and mass transfer with both solids and liquids. Finally, the Solver block incorporates the finite volume schemes based on DNS, LES or RANS. The development of the MMC and LFP blocks is based on OpenFOAM's Lagrangian particle tracking scheme which utilizes two base classes; the particle class and the cloud class. The cloud is a bucket class with the capability of adding, deleting and tracking particles and controlling the physical operations. The cloud class also supports parallelisation. New blocks could be introduced for alternative modelling frameworks such as conditional moment closure, provided coupling to existing blocks is also implemented.

Physics are added by means of inheritance using nested template classes which are generic classes of reusable code. New physics can be incorporated by addition of new templates while alternative methods for any given aspect of the physics may be implemented through abstract submodels. The code structure is shown schematically in Figure 1.

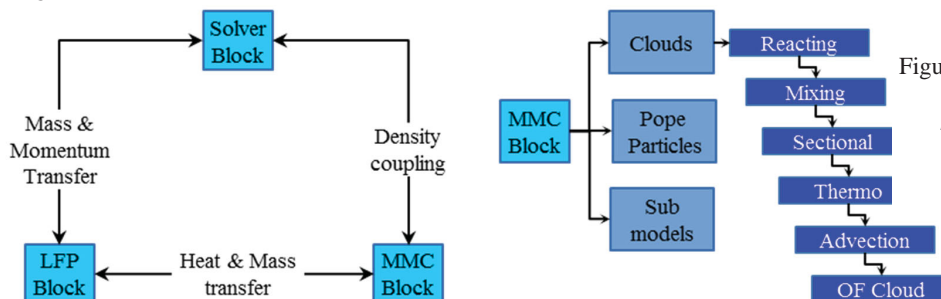


Figure 1: Schematic diagram of the *mmcFoam* code structure.

2.2 MMC block

The set of SDEs for the evolution of the transported PDF is implemented. A fractional step method is used with each layer in the nested template class structure responsible for one fraction. Currently these steps are *Advection*, *Thermochemistry*, *Mixing*, *Sectional* (for soot and particle synthesis) and *Reaction*. To make these layers more malleable to different modelling techniques submodels, which are abstract classes attached to the corresponding

*Corresponding author

E-mail: sgal8842@uni.sydney.edu.au

templates, are introduced. These abstract classes offer polymorphic behavior giving the code flexibility. Current mixing submodels include dense and sparse MMC and modified Curls model. Reaction submodels include flamesheet, finite rate and tabulation options.

2.3 LFP block

The constituents of the block implement a dispersed Lagrangian model to capture the evolution of liquid and solid fuel particles, as well as the introduction of a novel mixture fraction model for heat and mass transfer between the dispersed and carrier phases. As in the MMC block nested template classes are used. The evolutions of fuel particle velocity and position are encapsulated in the *Kinematic* template, while the transfers of thermochemical properties driven by the solid fuel pyrolysis process and liquid fuel evaporation are captured by the *Thermo* template. In the final stage of the code development, a *SurfaceReaction* template is being implemented to simulate heterogeneous reactions.

Currently the interface conditions of solid fuel pyrolysis and liquid fuel evaporation are packed into two different submodels, called *PyrolysisModel* and *EvaporationModel*, which are linked up with the *Thermo* template. A simple Arrhenius-type expression is adopted in the fuel particle *PyrolysisModel* so far to model the pyrolysis heat and mass transfer, whereas the Clausius-Claperyon phase equilibrium model is employed for the evaporation interface condition. Alternative submodels can be easily incorporated due to abstraction and polymorphism.

3 VALIDATION AGAINST EXPERIMENTAL DATA

Sample results for the three specific cases are shown in Figures 2 below.

Case 1 – flames with inhomogeneous inlets. Validation is against the Sydney inhomogeneous burner [3]. Two methane flames have been simulated with different levels of composition inhomogeneity at the burner exit plane. One is a partially premixed diffusion flame and the second exhibits mixed mode combustion.

Case2 – pulverised coal flame. The simulation set-up is based on the configuration of the CRIEPI pulverized coal burner which has been studied experimentally by Hwang et al [4]. Simulation results from various research groups regarding the same burner are shown for comparison [5].

Case3 – Sandia DME flame series. Validation is against the Sandia D, E and F flames consuming DME fuel [6]. One set of MMC-LES model parameters satisfactorily capture the series with increasing Reynolds number.

Other cases – Ongoing validation against experimental and DNS data of lifted flames, sprays, high pressure engine-like conditions, stratified flames, differential diffusion, MMC-RANS methods, soot and nano-particle formation.

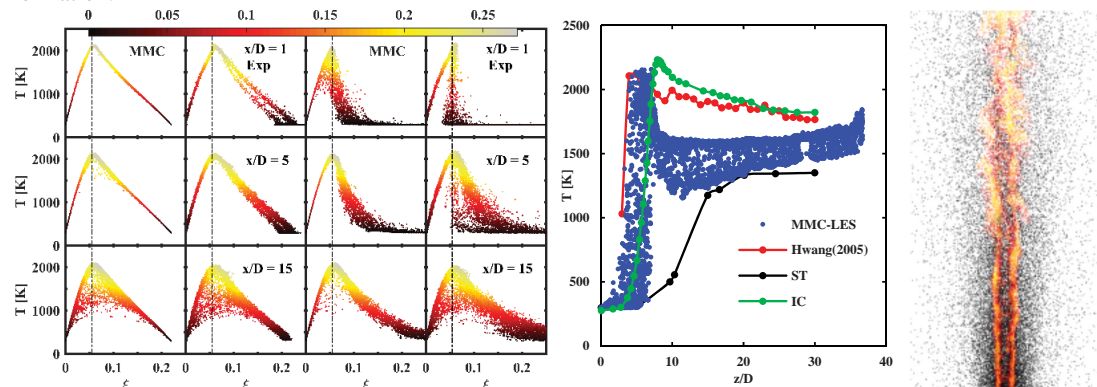


Figure 2: (left) Case 1 – temperature versus mixture fraction for homogeneous and inhomogeneous inlets coloured by reaction progress, (middle) Case 2 – gas temperature along the centre line of a pulverised coal jet, (right) instantaneous stochastic particle field of CO mass fraction in DME flame F.

4 REFERENCES

- [1] S. Subramaniam, S.B. Pope, *Combust. Flame*, 115 (1998) 487-514.
- [2] H.G. Weller, G. Tabor, H. Jasak, C. Fureby, *Comput. Phys.*, 12 (1998) 620-631.
- [3] S. Meares, A.R. Masri, *Combust. Flame*, 161 (2014) 484-495.
- [4] S.m. Hwang, R. Kurose, F. Akamatsu, H. Tsuji, H. Makino, M. Katsuki, *Energy & Fuels*, 19 (2005) 382-392.
- [5] O.T. Stein, G. Olenik, A. Kronenburg, F. Cavallo Marincola, B.M. Franchetti, A.M. Kempf, M. Ghiani, M. Vascellari, C. Hasse, *Flow, Turbul. Combust.*, 90 (2013) 859-884.
- [6] B. Coriton, M. Zendejdel, S. Ukai, A. Kronenburg, O.T. Stein, S.-K. Im, M. Gamba, J.H. Frank, *Proc. Combust. Inst.*, 35 (2015) 1251-1258.

Critical assessment of differential diffusion flamelet modeling in turbulent oxy-fuel flames

S. Gierth^{a)}, F. Hunger^{a)}, S. Popp^{a)}, C. Hasse^{a)}, M. Ihme^{b)}

^{a)}Numerical Thermo-Fluid Dynamics, TU Bergakademie Freiberg, Germany

^{b)}Centre of Turbulence Research, Stanford University, USA

Sandro.Gierth@iec.tu-freiberg.de

The present study addresses the modeling of differential diffusion effects within the flamelet/progress variable (FPV) approach using experimental data of an oxy-fuel flame [1]. For a critical assessment of the model's capability to capture the flame structure, a prior investigation of the FPV model was performed. Differential diffusion is known to decrease with increasing nozzle distance [2], an effect that was confirmed in the considered flame [1]. Thus, the flame structure close to the fuel nozzle was considered for a comparison of the experimental data and the FPV model results. The FPV approach relies on a flamelet look-up-table (FLUT), which contains the tabulated chemistry conditioned on the mixture fraction Z and the progress variable PV . Coupling to the flow solver is performed by accessing the solution of the FLUT via Z and PV , which are solved for in the flow solver. In the prior analysis the mixture fraction and the progress variable that are evaluated from the measurements are used for a table look-up. The resulting flame structure (i.e. the thermo-chemical state) is then compared to the experimental data in mixture fraction space. Figure 1 shows two non-premixed counterflow flamelet data sets, namely a unity

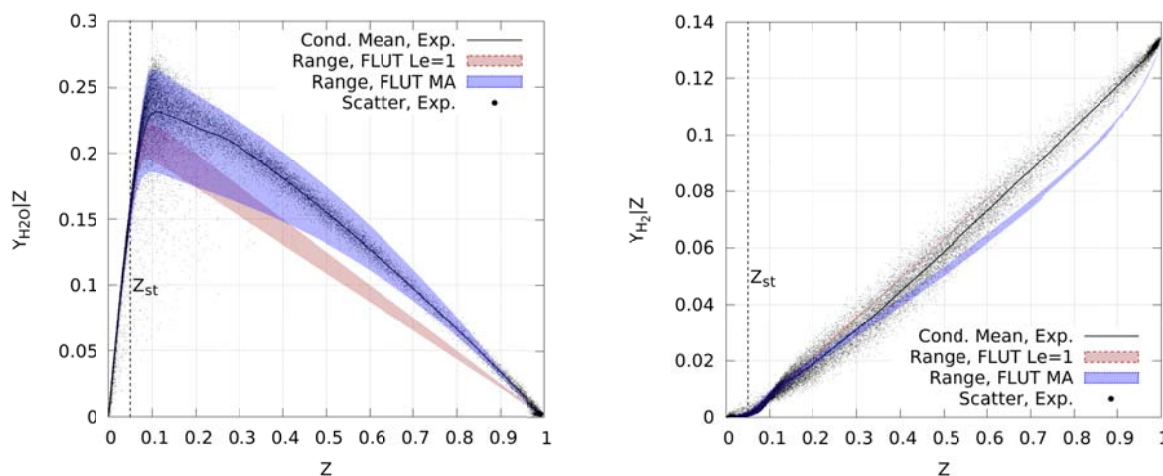


Fig. 1 Comparison of the mass fraction of H₂O and H₂ between the experimental data and two FLUTs with unity Lewis-number and mixture-averaged diffusion modeling.

Lewis-number approach ($Le = 1$) and a mixture-averaged (MA) diffusion approach, in comparison with the experimental data. Since only non-premixed flamelet data is presented here, it should be noted that stretched and unstretched premixed flame data were not suitable for this flame at all. First, when comparing the H₂O mass fraction, which is used as progress variable, a unity Lewis-number FLUT is not applicable since the range that is spanned by the flamelet (red region) is below the range of the experimental data so that the flame structure cannot be captured. In contrast, the mixture-averaged FLUT (blue range) encloses the experimental data, which is a minimum requirement for the FPV model to be applicable. However, when comparing the H₂ mass fraction, the mixture-averaged FLUT exhibits significant deviations from the experimental profiles, but the latter are captured well with a unity Lewis-number FLUT. Due to the different behavior of these two quantities showing that

a single FLUT cannot describe the flame structure sufficiently accurate, the differential diffusion parameter z according to [1] was used for further comparison. z serves as quality criterion for capturing the accurate flame structure since element mass fractions are used, which stem from the single species mass fractions. Thus, deviations in some species profiles will also be visible in the z profiles. Figure 2 shows the comparison of z between experiments and the mixture-averaged FLUT at different scalar dissipation rates on the left side. Additionally marked is the unity Lewis-number flamelet solution, where z is always zero. While in the fuel lean part z agrees well between the mixture-averaged FLUT and the experiments, a completely different evolution is obtained in the fuel rich part. The fuel rich side exhibits a straight mixing line approximately between $Z=[0.1,1]$. This analysis suggests a blending from mixture-averaged diffusion modeling in the fuel lean part to a unity Lewis-number modeling in the fuel rich part as suggested in [3]. Results of this approach are shown in Fig. 2 on the right side. It is visible that the applied blending does not reproduce the experimental structure. First, blending changes the structure on the fuel lean side and not only on the fuel rich side and second, positive z values in the fuel rich side are not created by this method.

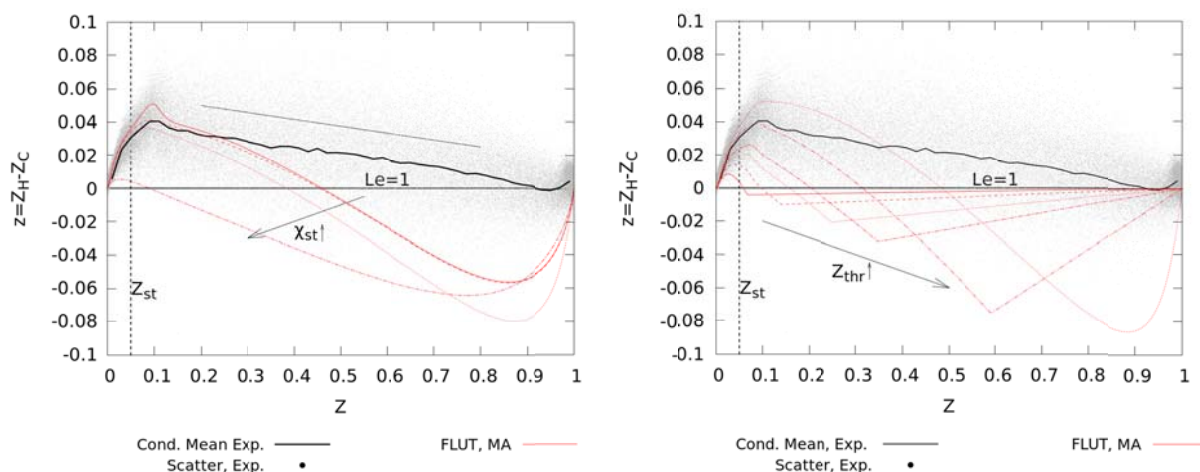


Fig. 2 Comparison of the differential diffusion parameter z between the experimental data and the mixture-averaged FLUT at different scalar dissipation rates (left) and a FLUT with Lewis-number blending at different mixture fraction values Z_{thr}

From the analysis of the experimental data, it becomes clear that none of the applied diffusion modeling approaches within the FPV model are applicable. Thus, the issue of a consistent and reliable model to describe non-unity Lewis-number effects within the FPV approach, at least for this turbulent oxy-fuel flame, is still unresolved. These observations motivate further research, which needs to address these issues.

References

- [1] A. Sevault, M. Dunn, R.S: Barlow, M. Ditaranto, *Combustion and Flame* 159 (2012) 3342-3352
- [2] G. Maragkos, P. Rauwoens, D. Fauconnier, and B. Merci, Large eddy simulations of differential molecular diffusion in non-reacting turbulent jets of H₂/CO₂ mixing with air. *Physics of Fluids*, 26(2):025102
- [3] N. Peters. *Turbulent Combustion*, Cambridge University Press, 2000.

Impact of Exhaust Gas Enthalpy on Fluid State Probabilities

F. Hampp, R. P. Lindstedt* (p.lindstedt@imperial.ac.uk)

Department of Mechanical Engineering, Imperial College London, Exhibition Road, London SW7 2AZ, UK.

Introduction and Objective

Low Damköhler number (Da) combustion has the potential to reduce NO_x emissions though stable operation under fuel lean conditions. The latter often requires thermal support to sustain the reaction progress [1]. Common enthalpy sources include exhaust gas recirculation [2] and reactant preheating via heat exchangers [3]. The current study investigates the impact of the external enthalpy on the burning mode under constant turbulent Reynolds number (Re_t) and mixture reactivity (Φ). The back-to-burnt (BTB) opposed jet configuration provides excellent parametric control including the burnt gas state temperature and composition. The evolution of the burning mode as a function of the thermal support was quantified via bimodal [4] and multi-fluid [5] probabilities and conditional velocity statistics.

Experimental Setup

The twin flame variant of the current burner (Fig. 1) was developed by Geyer et al. [6]. The current revised configuration is identical to that of Hampp et al. [7, 8] with multi-scale turbulence [9, 10] generated via a cross fractal grid (CFG; [7, 9, 10]) and with an upper nozzle bulk velocity of $U_{b,UN} = 11.0$ m/s (preheated to 320 K). The $\text{Re}_t \approx 380$ in the reactants (premixed DME/air at $\Phi = 0.60$) was based on the velocity fluctuations ($u' = 1.45$ m/s) measured via PIV and the integral length scale of turbulence ($L_I = 4.1$ mm) determined via hot wire anemometry. A Da of 1.2 was estimated from the laminar burning velocity ($S_L = 0.21$ m/s) and a flame thickness ($\delta_f = 0.44$ mm) based on the 5 – 95 % fuel consumption [11] layer obtained from strained counterflow calculations with detailed chemistry [12]. The latter also provided a value for the kinematic viscosity ($\nu_r = 17.0 \cdot 10^{-6}$ m²/s). The hot combustion products (HCP) were generated from stoichiometric H_2 /air flames for stable flame anchoring on the mesh (FSM), with a flash back arrestor (FBA) for safety. The FSM was located 100 mm upstream the LN exit to provide equilibrated HCP to the stagnation plane. The temperature ($1600 \leq T_{HCP}$ (K) ≤ 1800) was controlled by CO_2 dilution. The range covers the adiabatic flame temperature ($T_{ad} = 1760$ K) and approaches the laminar twin flame extinction temperature ($T_q = 1570$ K). The aerodynamic stabilisation of the stagnation plane in the proximity of the burner centre required a lower nozzle bulk velocity of $U_{b,LN} \approx 4.3$ m/s (at STP). Simultaneous Mie scattering, PIV and OH-PLIF was performed [13] (281.7 nm and 532 nm; height = 1D; thickness < 0.5 mm; $\Delta t = 25$ μs). The interrogation regions ($-11.6 < x < 14.1$ and $-15.0 < y < 15$ mm) were resolved by 708×829 pixels. PIV vectors were determined via adaptive [14] multi-pass cross-correlation resulting in a vector spacing and spatial resolution of $\lambda_{PIV} = 0.30$ mm.

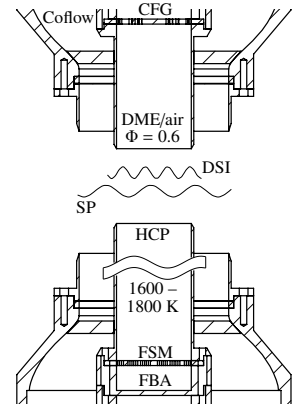


Figure 1: Burner configuration.

Post-processing and Multi-Fluid Definition

Bimodal velocity statistics are frequently inferred from PIV particle density segregation techniques (DST) [16] or on the OH-PLIF signal [17]. Comparisons can be useful. For example, the accuracy of two-fluid descriptions as a function of the Da number can be evaluated by computing the differences (Δ) for conditional reactant ($\Delta \bar{U}_r$), product ($\Delta \bar{U}_p$) and slip ($\Delta \bar{U}_s$) velocities and the scalar flux ($\Delta(\bar{c}u)$) as shown in Fig. 2. At high Da, there is good agreement as only thin interfaces separate reactants from OH rich combustion products. At $\text{Da} \leq 1$ substantial discrepancies emerge as the Mie scattering iso-contour detaches from the OH producing chemically active zones due to the need for thermal support. The current multi-fluid analysis (MFA) [7] provides a more comprehensive description of low Da flows. The purpose written algorithm permits the identification of up to five fluid states segregated by four iso-contours. The reactants were identified via DST [15]. The MFA delineates the superimposed OH and Mie images into (ii) combustion products, (iii) mixing fluid, (iv) self-sustained flames (strongly reacting fluid) and (v) mildly reacting fluid with a spatial resolution of $\lambda_{MF} = 0.25$ mm. For each condition 3000 instantaneous image pairs were recorded and processed. An example is shown in Fig. 3.

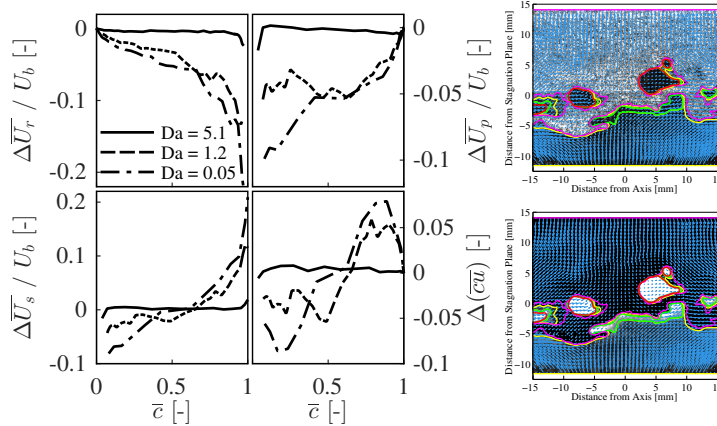


Figure 2: Limitation of the bimodal description at low Da (right).

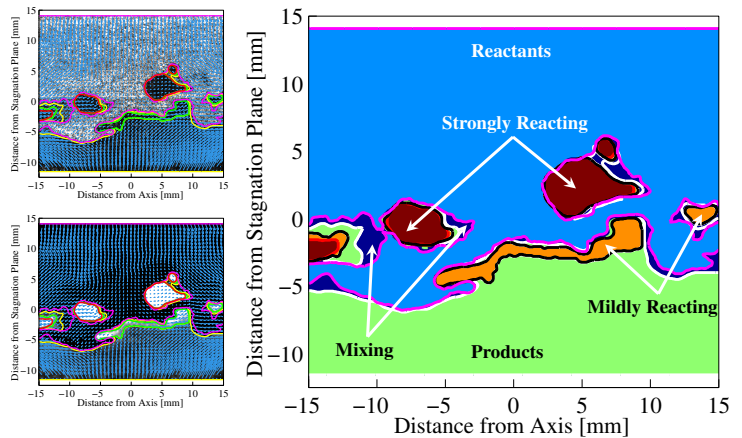


Figure 3: Mie scattering (top left), OH-PLIF (bottom left) and quinary multi-fluid (right) image.

Results and Discussion

Premixed DME/air flames at $\Phi = 0.6$ ($Da \approx 1.2$) and $Re_t \approx 380$ were stabilised against streams with varying T_{HCP} (1600, 1650, 1700, 1750, 1800 K). The multi-fluid probabilities, presented in Fig. 4, were aligned on the DST iso-contour ($x_s = 0$). Naturally, the reactant fluid probability is not affected by the HCP enthalpy, while the mixing fluid probability is slightly reduced with increasing T_{HCP} . By contrast, the reacting fluid probabilities are significantly elevated. The spatial extent of all probabilities is limited to L_I . The probabilities of encountering different adjacent fluid state pairs (i.e. interfaces between fluid states) along the burner axis through the quinary multi-fluid fields are depicted for $T_{HCP} = 1600$ and 1800 K in Fig. 5. Higher T_{HCP} yield vigorous burning more effectively, while a low T_{HCP} results in a delayed onset of strong OH production.

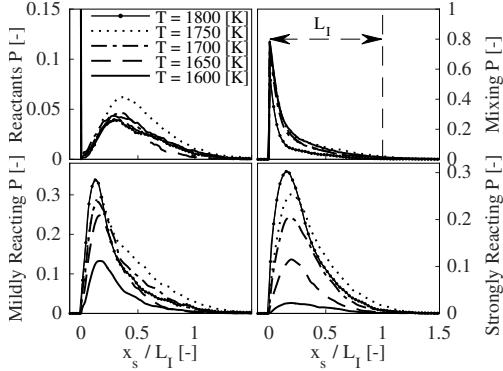


Figure 4: Multi-fluid probabilities (P): Reactants (top left), mixing (top right), mildly reacting (bottom left), strongly reacting fluid (bottom right)

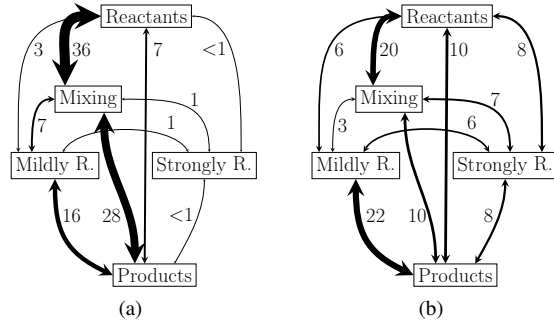


Figure 5: Multi-fluid interface statistics by traversing along the theoretical stagnation point streamline through the quinary multi-fluid image. (a) $T_{HCP} = 1600$ K and (b) $T_{HCP} = 1800$ K.

Conditional mean axial velocity and axial fluctuations for different fluid states are shown in Fig. 6. The constant Re_t leads to nearly identical reactant fluid statistics. With increasing HCP temperature, reduced mixing and mildly reacting fluid velocities are observed. This can be attributed to reduced HCP entrainment by the reactants to initiate exothermic reactions. Moreover, the resulting heat release yields stronger local dilatation with increasing T_{HCP} and a more pronounced acceleration towards the stagnation plane. The strongly reacting fluid statistics are mostly independent of the HCP enthalpy. Flames that are represented by the latter fluid state detach from the stagnation plane and are anchored in comparatively low strain regions (see Table 1) with reduced vorticity levels.

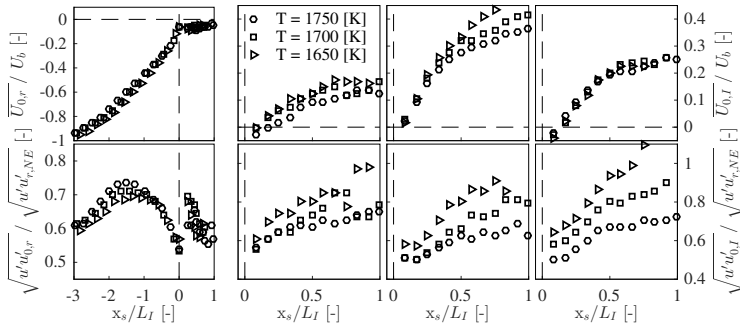


Figure 6: Conditional mean axial velocity and fluctuations aligned $x_s = 0$: Reactants (left), mixing (2^{nd}), mildly reacting (3^{rd}) and strongly reacting fluid (4^{th}).

Table 1: Mean normal (\bar{a}_n) and tangential (\bar{a}_t) strain and vorticity ($\bar{\omega}$) in $[s^{-1}]$ evaluated along the mildly (MR) and strongly reacting (SR) fluid material surface.

T_{HCP}	1750	1700	1650 K
$\bar{a}_n _{MR}$	-1248	-1450	-1534
$\bar{a}_t _{MR}$	709	737	915
$\bar{\omega} _{MR}$	2378	2690	2948
$\bar{a}_n _{SR}$	-920	-1138	-1248
$\bar{a}_t _{SR}$	660	668	778
$\bar{\omega} _{SR}$	1953	2296	2575

Conclusions and Future Work Outlook

The present work investigated the impact of exhaust gas enthalpy on fluid states for premixed DME/air flames with $Re_t \approx 380$. The analysis permits the identification of intermediate fluid states (i.e. reactants, products, mixing, mildly reacting and strongly reacting fluids) that are increasingly found in low Da flows. With increasing HCP temperature the earlier transition towards self-sustained burning was accompanied by enhanced dilatation. The interface statistics indicate that with decreasing HCP temperature the chemically active zones are increasingly separated from the reactants by an interlayer and are located in high strain and vorticity regions. By contrast, at high T_{HCP} the more vigorous flames tend to stabilise in reduced strain regions. The current data set is expected to be particularly valuable for the model development and validation that do not presume a flame structure.

Acknowledgement The authors would like to acknowledge the support of the AFOSR and EOARD under Grant FA8655-13-1-3024. The authors wish to thank Dr Chiping Li, Dr Gregg Abate and Dr Russ Cummings for encouraging the work and Dr Robert Barlow for his support. The US Government is authorised to reproduce and distribute reprints for Governmental purpose notwithstanding any copyright notation thereon.

References

- [1] E. Mastorakos, A. Taylor, J. Whitelaw, Combust. Flame 102 (1995), pp. 101–114.
- [2] J. Wüning, J. Wüning, Prog. Energ. Combust. 23 (1) (1997) 81–94.

- [3] I. B. Özdemir, N. Peters, *Exp. Fluids* 30 (2001), pp. 683–695.
- [4] K.N.C. Bray, P.A. Libby, J.B. Moss, *Combust. Flame* 61 (1) (1985) 87–102.
- [5] D.B. Spalding, *Comp. Tech. App.*, CTAC95 (1996) 59–81.
- [6] D. Geyer, A. Kempf, A. Dreizler, J. Janicka, *Combust. Flame* 143 (2005) 524–548.
- [7] F. Hampp, PhD thesis, Imperial College, May 2016 url: <http://hdl.handle.net/10044/1/32582>.
- [8] F. Hampp, R. P. Lindstedt, in Y. Sakai and C. Vassilicos (eds.) *Fractal Flow Design: How to Design Bespoke Turbulence and why*, Springer-Verlag, CISM Int. Mech. Sci. 568, 2016, DOI:10.1007/978-3-319-33310-6 3.
- [9] P. Geipel, K. H. H. Goh, R. P. Lindstedt, *Flow Turbul. Combust.* 85 (2010) 397–419.
- [10] K. H. H. Goh, P. Geipel, R. P. Lindstedt, *Combust. Flame* 161 (2014), pp. 2419–2434.
- [11] N. Peters, in W. A. Sirignano, A. G. Merzhanov, and L. de Luca, Eds, *Advances in Combustion Science: In Honor of Y. B. Zel'dovich*, Prog. Astronautics and Aeronautics 173 (1997) pp. 73–91.
- [12] S.-W. Park, Detailed Chemical Kinetic Model for Oxygenated Fuels, PhD thesis, Imperial College, March 2012, url: <http://hdl.handle.net/10044/1/9599>.
- [13] J. Kerl, T. Sponfeldner, F. Beyrau, *Combust. Flame* 158 (10) (2011) 1905–1907.
- [14] B. Wieneke, K. Pfeiffer, 15th Int. Symp. Appl. Laser Tech. Fluid Mech. (2010).
- [15] K.H.H. Goh, P. Geipel, F. Hampp, R.P. Lindstedt, *Fluid Dyn. Res.* 45 (2013), 061403.
- [16] I. G. Shepherd, R. K. Cheng, P. J. Goix, *Proc. Combust. Inst.* 23 (1991), pp. 781–787.
- [17] P. Petersson, J. Olofsson, C. Brackman, H. Seyfried, J. Zetterberg, M. Richter, M. Aldén, M. A. Linne, R. K. Cheng, A. Nauert, D. Geyer, A. Dreizler, *Appl. Optics* 46 (19) (2007) pp. 3928–3936.

blank

Flamelet modeling of differential molecular diffusion in oxy-fuel turbulent jet flames

Chao Han^a, Robert S. Barlow^b, Haifeng Wang^{a,c}

^a School of Aeronautics and Astronautics, Purdue University, West Lafayette, IN 47906, USA

^b Combustion Research Facility, Sandia National Laboratories, Livermore, CA 94551, USA

^c Corresponding author. Email: haifeng@purdue.edu

Differential molecular diffusion (DMD) is an important physical process in turbulent non-premixed flames caused by the difference of the diffusion transport rates of energy and different species. Despite the physical importance, it has not received adequate attention in modeling. Most previous models assume equal diffusion and unity Lewis number when treating molecular diffusion in turbulent non-premixed combustion. Recently, Wang [1] developed a series of consistent DMD models that can be incorporated in the flamelet models [2] to account for the effect of local Re number on DMD. The models have been examined in the Sandia piloted jet flames [3] and good performance is observed.

Table 1 the oxy-fuel jet flame conditions

Name	A-1	A-2	A-3	B-1	B-2 (A-1)	B-3
%mol H ₂	55	45	37	55	55	55
Re	15,000	15,000	15,000	12,000	15,000	18,000

A pilot exists in the Sandia piloted flames and the difficulty of imposing the DMD boundary condition for the pilot becomes another source of uncertainty in examining the DMD models in these flames. To eliminate this effect, we further examine the DMD models in a series of the oxy-fuel non-piloted turbulent jet flames [4] in this work. Two sets of the oxy-fuel flames are available, with one varying the fuel concentration ratio between CH₄/H₂ (A series) and the other varying Re (B series), as shown in Table 1. This enables us to examine the capability of the DMD model to represent the effect of the fuel concentration as well as the effect of Re on DMD.

Two types of DMD models are developed in Wang [1], linear differential diffusion (LDD) models and nonlinear differential diffusion (NDD) models. The difference between these different DMD models is found to be small in the Sandia piloted jet flames [1]. In this work, we use only one of the DMD models for the oxy-fuel jet flames, the nonlinear differential diffusion model with variance correction (NDDV) [1] along with the traditional equal diffusion (ED) model. In the NDDV model, the Lewis number in the laminar flamelet equation is modified to account for the effect of turbulence on the laminar flames

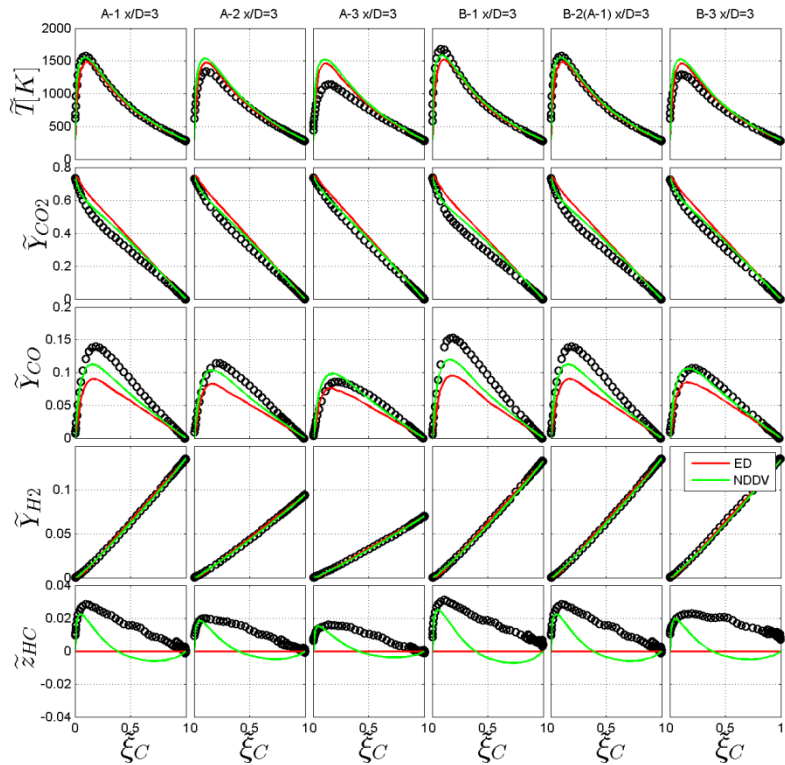


Figure 1. Predicted (lines) and measured (symbols) \tilde{T} , \tilde{Y}_{CO_2} , \tilde{Y}_{CO} , \tilde{Y}_{H_2} , \tilde{z}_{HC} against $\tilde{\xi}_C$ at $x/D = 3$ in the oxy-fuel jet flames.

$$\widehat{Le}_k = \frac{Le_k}{Le_k + \theta \cdot (1 - Le_k)}, \quad (1)$$

where Le_k is the Lewis number of the k^{th} species, \widehat{Le}_k is the modified Lewis number, and θ is the differential diffusion parameter that depends on the local Re [1].

Steady flamelet modeling combined with the Reynolds averaged Navier-Stokes (RANS) simulations are carried out to model the oxy-fuel jet flames. The details of the simulations can be found in Wang [1]. Figures 1 and 2 compare the predicted (lines) and measured (symbols) mean temperature \tilde{T} , mean mass fractions \tilde{Y}_{CO_2} , \tilde{Y}_{CO} , and \tilde{Y}_{H_2} , and $\tilde{z}_{HC} = \tilde{\xi}_H - \tilde{\xi}_C$ against $\tilde{\xi}_C$ at the different axial locations of the oxy-fuel flames. The notations $\tilde{\xi}_H$ and $\tilde{\xi}_C$ are the mixture fractions defined based on the elements H and C, respectively. From the figures, we can make the following major observations: (1) the NDDV model significantly

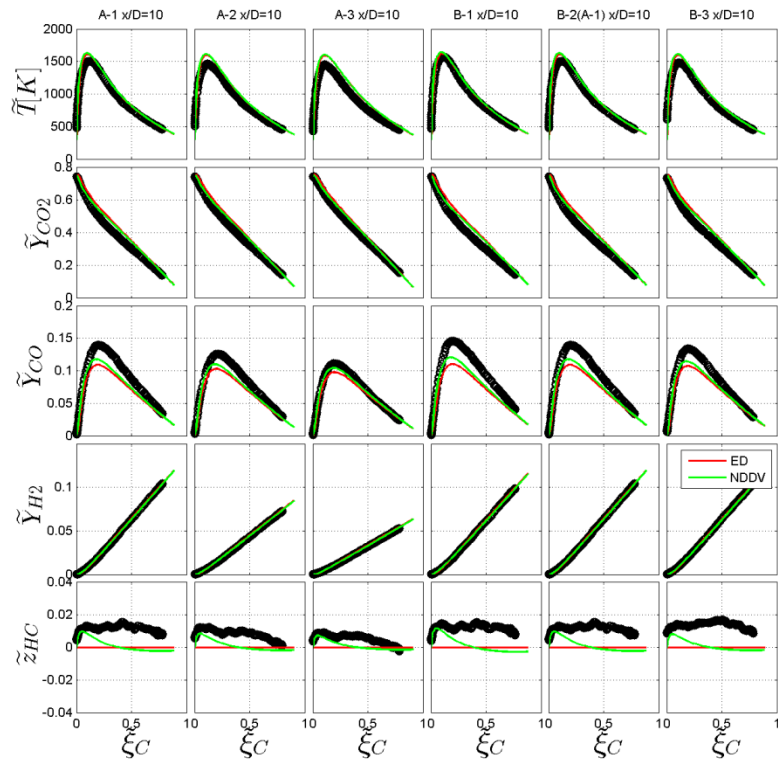


Figure 2. Predicted (lines) and measured (symbols) \tilde{T} , \tilde{Y}_{CO_2} , \tilde{Y}_{CO} , \tilde{Y}_{H_2} , \tilde{z}_{HC} against $\tilde{\xi}_C$ at $x/D = 10$ in the oxy-fuel jet flames.

improves the predictions especially for \tilde{Y}_{CO_2} , \tilde{Y}_{CO} and \tilde{z}_{HC} at the upstream location $x/D = 3$, when compared to the traditional ED model; (2) in the A flame series, the DMD is captured reasonably by the NDDV model, although the trend of increasing local extinction indicated by decreased peak temperature is not captured due to the use of the steady flamelet model; (3) in the B flame series, the DMD is also captured reasonably by the NDDV model with the local extinction also incorrectly predicted due to the steady flamelet model. The current study has not shown any significant coupling between local extinction and the behavior of DMD in the oxy-fuel jet flames.

To summarize, flamelet modeling of oxy-fuel jet flames is conducted to examine the capability of the DMD models for the prediction of DMD behaviors in these flames. The models are found to be able to capture the DMD behavior reasonably well, and the model performance in the oxy-fuel flames is found to be similar in the Sandia piloted flames reported in Wang [1]. The local extinction in these flames, however, is not captured correctly due to the usage of the steady flamelet model. This can be improved by employing more advanced flamelet models which are capable of capturing local extinction, which will be conducted in our future work.

References:

- [1] H. Wang. Consistent flamelet modeling of differential molecular diffusion for turbulent non-premixed flames. *Physics of Fluids* 28 (2016): 035102.
- [2] N. Peters. Laminar diffusion flamelet models in non-premixed turbulent combustion. *Progress in energy and combustion science*, 10 (1984): 319-339.
- [3] R.S. Barlow, J. H. Frank. Effects of turbulence on species mass fractions in methane/air jet flames. In *Symposium (International) on Combustion*, 27 (1998): 1087-1095.
- [4] A. Sevault, M. Dunn, R.S. Barlow, M. Ditaranto. On the structure of the near field of oxy-fuel jet flames using Raman/Rayleigh laser diagnostics. *Combustion and Flame*, 159 (2012): 3342-3352.

Multi-Environment PDF Modeling for Turbulent DME/AIR Pilot Jet Flames

S.T. Jeon¹, Y. Kim^{1*}

¹Hanyang University, Korea
ymkim@hanyang.ac.kr

Among oxygenated fuels, the simplest ether fuel, dimethyl ether(DME), has been attracting much attention as a clean alternative fuel for the compression-ignition engines due to its beneficial characteristics including low soot emissions as well as improved auto-ignition characteristics. However, because DME has distinctly different combustion characteristics from conventional hydrocarbon fuels in terms of oxygenate ingredient, chemical kinetics, transport properties, ignition, and heat release rate, the application of DME in practical combustion systems creates many problems. In this respect, more systematic research is needed for the combustion processes of DME fuel.

Recently, Fuest *et al.*[1, 2] carried out for 1D Raman/Rayleigh measurements[2] for the partially-premixed DME/air flames in the Sydney/Sandia piloted jet burner geometry[3]. In the present study, the multi-environment probability density function method[4] has been applied to simulate the turbulent piloted, partially-premixed DME/air jet flames[1]. The direct quadrature method of moments (DQMOM) has been adopted to solve the transport PDF equation due to its computational efficiency and robustness. The IEM mixing model is employed to represent the mixing process and the chemical mechanism is based on DME mechanism[5]. In this present study, the numerical simulation was carried out with the case of DME flame D and F using two environment PDF method. The numerical results are compared with experimental data in terms of unconditional and conditional means for scalar fields such as temperature, mixture fraction and species mass fraction.

Figure 1 shows the predicted and measured[1] radial profiles for unconditional means of temperature and mixture fraction at six axial stations. Close to the burner exit($x/d=1$), it can be clearly seen that the flame structure is mainly affected by surrounding pilot flame. And the temperature of flame D is much higher than flame F caused by lower inlet velocity and turbulent intensity. The flame structure in this region indicates there exist the pilot premixed flame and the non-premixed flame zone through the mixing process among co-flow air, pilot, and main jet. At $x/d = 5$ shortly after the burner exit, the predicted and measured flame fields indicate that the influence of the pilot flame is nearly negligible. At the fuel-lean zone($x/d=5, 10$), the mixture fraction is overestimated. This is associated with the present MEPDF approach based on the RANS especially shortcoming of standard $k-\epsilon$ model.

Figure 2 shows the predicted and measured radial profiles for rms of temperature and mixture fraction at various locations. At downstream ($x/d > 5$), the predicted results are underestimated. In the case of experiments to consist of three feeding system, two-environment PDF modeling has limitations to capture the characteristics of each feeding system. It will proceed to the three environment PDF modeling in order to further improve accurate predictions.

Figure 3 presents the conditional scatters of temperature and mole fraction of H₂O at various axial locations to account for the effects of conditional fluctuations of temperature and composition vector on the local flame structure. At the downstream region($x/d > 7.5$), DME flame D and F are very similar even if the boundary velocity is different. These similar results can be observed at the unconditional means at Fig. 1.

References

- [1] F. Fuest, R. S. Barlow, G. Magnotti, J. A. Sutton, "1D Raman/Rayleigh/CO-LIF line measurements of major and temperature in turbulent DME/air jet flame", 8th US national Combustion Meeting (2013)
- [2] F. Fuest, R. S. Barlow, J.-Y. Chen, and A. Dreizler, "Raman/Rayleigh scattering and CO-LIF measurements in laminar and turbulent jet flames of dimethyl ether", *Combust. Flame*, 159 (2012) 2533–2562.
- [3] R. S. Barlow, J. H. Frank, A. N. Karpetis, and J.-Y. Chen, "Piloted methane/air jet flames: Transport effects and aspects of scalar structure", *Combust. Flame*, 143 (2005) 433–449.
- [4] Rodney O. Fox, "Computational Models for Turbulent Reacting Flows" Cambridge Univ. Press (2003).
- [5] Z. Zhao, M. Chaos, A. Kazakov, and F.L. Dryer, "Thermal decomposition reaction and a comprehensive kinetic model of dimethyl ether", *Int. J. Chem. Kinet.*, 40 (2008) 1-18.

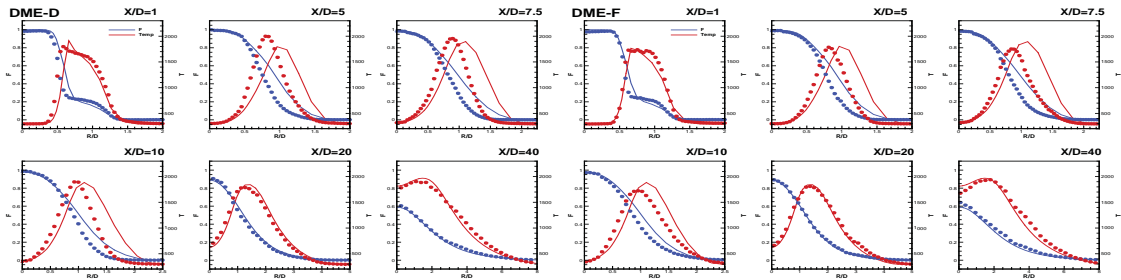


Fig. 1 Radial profiles for mean of temperature and mixture fraction for DME flame D & F.

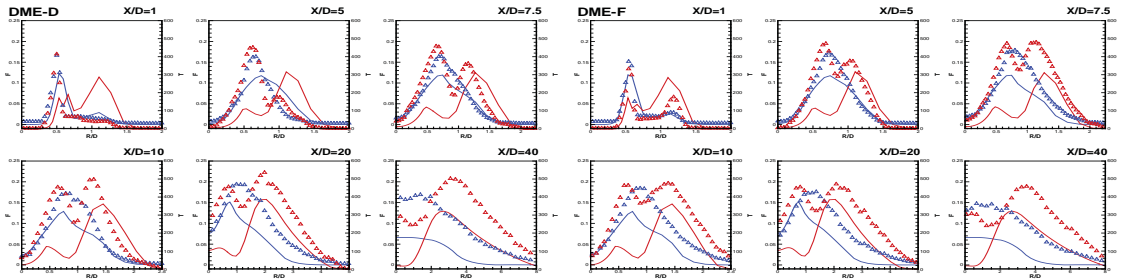


Fig. 2 Radial profiles for mean of temperature and mixture fraction for DME flame D & F.

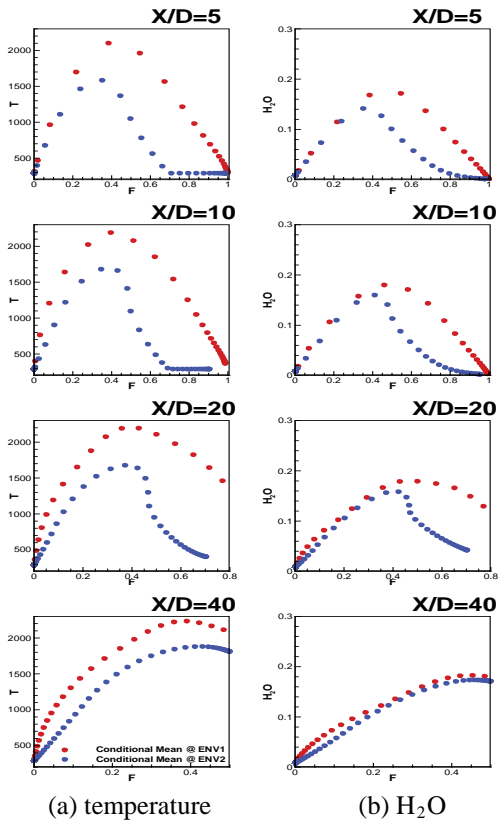


Fig. 3 Conditional means for temperature and H₂O mass fraction for DME-D

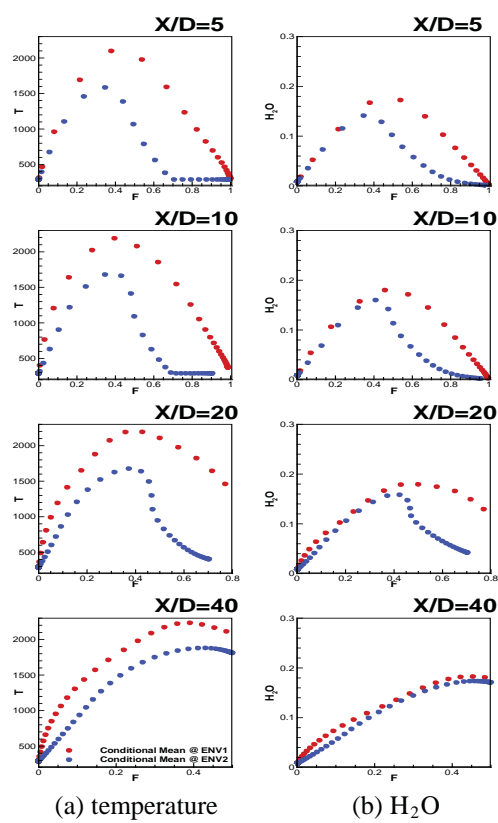


Fig. 4 Conditional means for temperature and H₂O mass fraction for DME-F

Investigation of thermoacoustic sources and their dynamics from experiments and LES

S. Kheirkhah¹, P. Saini¹, J. M. Cirtwill¹, K. Venkatesan², S. Yellapantula², A. M. Steinberg^{1*}

¹Institute for Aerospace Studies, University of Toronto, Toronto Canada

²GE Global Research Center, General Electric, Niskayuna USA

*Corresponding author: adam.steinberg@utoronto.ca

Validating the ability of large eddy simulations (LES) to predict complex dynamic phenomena, e.g. thermoacoustic oscillations, requires methodologies beyond a statistical comparison of primitive variables. This is particularly true if the simulations aim to predict non-stationary behavior, such as non-limit-cycle oscillations or thermoacoustic triggering. Here, we argue that simulations should be validated for the underlying process causing the dynamics, and we provide an appropriate (and experimentally accessible) metric for validating such non-stationary thermoacoustic oscillations. The method is then applied to a high-pressure model aeronautical gas turbine combustor.

The basic concept for the framework is motivated by the acoustic energy (\mathcal{E}) transport equation, which can be written as [1]

$$\frac{\partial}{\partial t} \mathcal{E}(\vec{x}, t) + \vec{\nabla} \cdot [p'(\vec{x}, t) \vec{u}'(\vec{x}, t)] = \frac{\gamma - 1}{\gamma \bar{p}(x)} [p'(\vec{x}, t) q'(\vec{x}, t)] + D$$

where p , q , and \vec{u} are the pressure, heat release rate, and velocity, respectively. The second term on the left represents the flux, the first term on the right is the source/sink of acoustic energy due to coupled heat release and pressure fluctuations, and D is the dissipation of acoustic energy. We assume that the pressure and heat release rate oscillations are $p'(t) = \tilde{p} \sin(\omega(t)t)$ and $q'(\vec{x}, t) = \tilde{q}(\vec{x}, t) \sin(\omega(t)t + \Delta\phi(\vec{x}, t))$, in which case the source term can be written as

$$\psi(\vec{x}, t) = \underbrace{\frac{1}{2} \tilde{p}(t) \tilde{q}(\vec{x}, t) \cos[\Delta\phi(\vec{x}, t)]}_{\psi_s} - \underbrace{\frac{1}{2} \tilde{p}(t) \tilde{q}(\vec{x}, t) \cos[2\omega(t)t + \Delta\phi(\vec{x}, t)]}_{\psi_o}$$

The instantaneous oscillation amplitudes and phase shift can be determined from space and time-resolved measurements or simulations via the Hilbert transform [2]. The first term in this equation represents the time evolving nature of the thermoacoustic source field, or its structure. This term reveals the nature of the instantaneous coupling. The second term represents oscillations in the instantaneous source due to oscillations in the underlying signals.

Here, we apply this decomposition to analyze changes in the thermoacoustic source term during self-excited non-stationary behavior. A schematic of the studied combustor is shown below. Measurements were made using 10 kHz repetition-rate OH* chemiluminescence and pressure probes.

Simulations were performed using the ANSYS Fluent LES solver with a flamelet/progress variable combustion model. The spray was treated using a Lagrangian framework. Acoustic impedance boundary conditions were applied at the combustor exit, and wall boundary conditions that accounted for heat loss were applied for the combustor confinement. The simulated domain is shown in Figure 2, and encompassed the air and fuel feed system (1), nozzle (2), combustion chamber (3), surrounding pressure vessel for the exhaust plenum (4), and outflow (5).

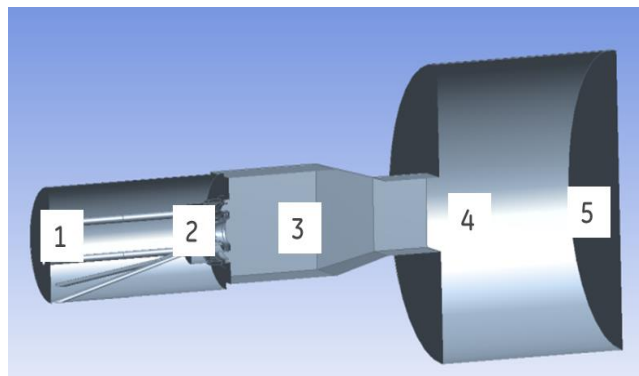


Figure 2 - Simulation domain

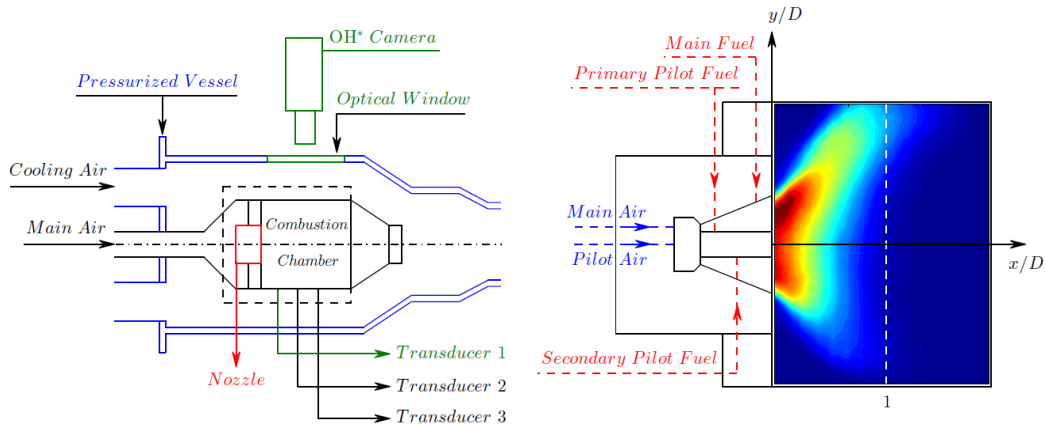


Figure 1 - Experimental layout. Left - combustion chamber in pressure vessel. Right - Nozzle detail with mean OH^* chemiluminescence field.

As shown to the right, the experimental combustor exhibited non-stationary thermoacoustic oscillations while operating at stationary conditions.

This signal has been spectrally filtered to isolate the band of the coherent dynamics. The figure below shows the evolution of the thermoacoustic source structure field from the experiments during a typical time sequence in which the pressure amplitude dropped nearly to zero and then “re-triggered” to high amplitude. This process is associated with a switch from thermoacoustic damping to driving in the upstream portion of the combustor. The poster further discusses such events from both the experiments and simulations, along with the underlying causes of these changes.

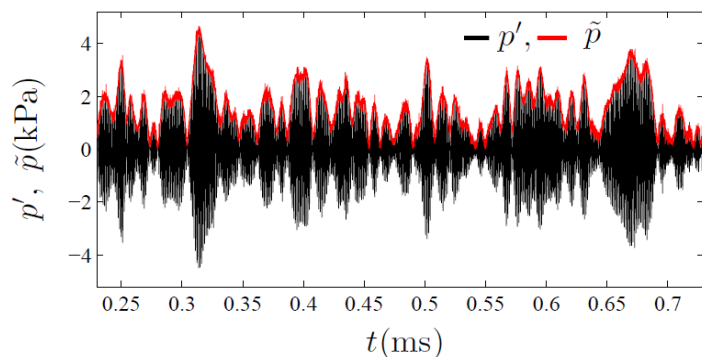


Figure 3 - Pressure signal spectrally filtered around thermoacoustic frequency.

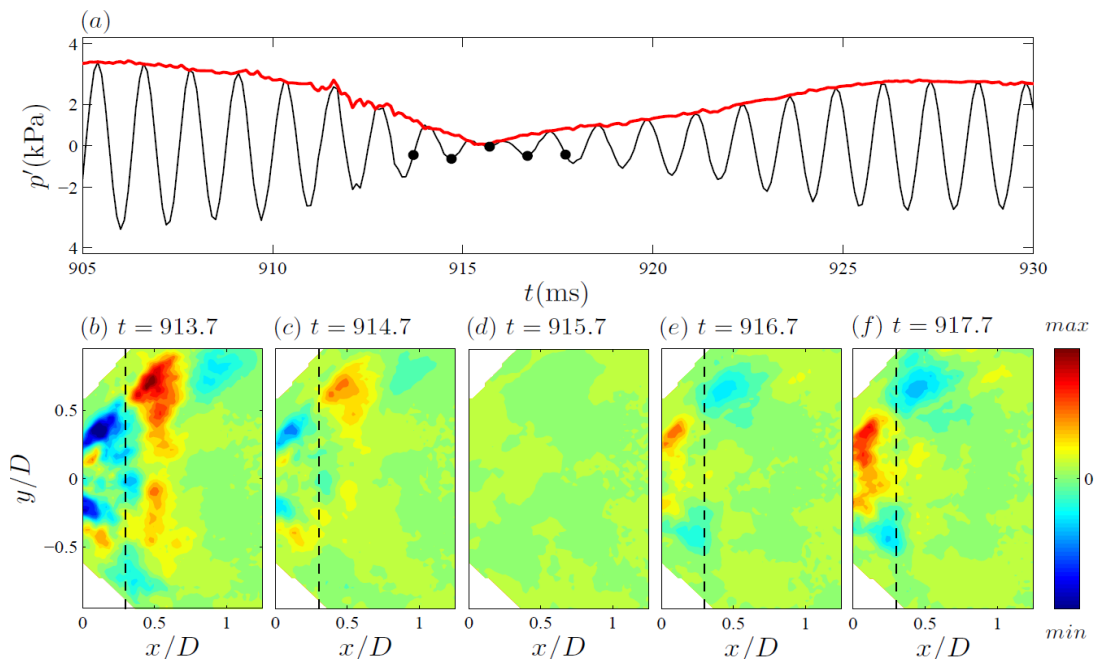


Figure 4 – (a) Pressure signal during a retriggering event. (b-f) Thermoacoustic source structure field (ψ_s) during the time sequence from (a) at the times marked by the dots.

[1] S. M. Candel, *Proc. Combust. Inst.*, 24 (1992) 1277-96

[2] R. Bracewell, “The Fourier transform and its applications”, New York: McGraw-Hill (1986)

Multi-Environment PDF Modeling for Piloted Turbulent Flame with Inhomogeneous Inlets

N.S. Kim¹, S.W. Park¹, Y. Kim^{1*}
¹*Hanyang University, Korea*
ymkim@hanyang.ac.kr

Inhomogeneous inlet is common situation for practical combustion. The inlet composition depends on the mixing process in the pre-combustor region and this mixing process is very sensitive to operation conditions. To realistically simulate the combustion processes encountered in the real combustors, the reliable turbulent combustion model with the inhomogeneous inlet is necessary. Among many turbulent combustion models, the probability density function(PDF) transport method has the inherent capability to naturally introduce the variances of composition. In this aspect, we have developed a turbulent combustion model based on the PDF transport method. In this study, in order to efficiently and realistically predict the turbulent flames with inhomogeneous inlets, the multi-environment PDF approach with IEM [2,3] model and the tabulated chemistry based on the flamelet progress variable(FPV) [4,5] has been developed. Turbulence is represented by the $k-\varepsilon$ turbulence model with $C_2 = 1.8$. The FPV library has been generated using the OPPDIF[6] code and the chemistry is based on GRI 3.0[7] mechanism. In the present tabulated chemistry, the progress variable is defined as $\gamma_c = Y_{CO} + Y_{CO_2}$. Recently, Barlow *et al.*[1] carried out for Raman/Rayleigh measurements for the CH₄/air flames in the Sydney/Sandia piloted jet burner geometry[1]. In the present study, FJ200-5GP-Lr75-57 flame has been chosen as a validation case. It is necessary to note that the recess distance of burner(L_r=75mm) is not enough to make the inlet mixture homogeneous.

Fig. 1 shows the predicted and measured [1] radial profiles for unconditional means of mixture fraction and temperature at six axial stations. Even if there exist the certain deviations with measurements, the predicted profiles of scalar fields yields the good conformity with experimental data. However, it is found that the deviations are increased in the downstream regions. These discrepancies could be attributed to the shortcomings of the RANS-based turbulence model. Fig. 2 presents radial profiles for the rms of mixture fraction and temperature. Numerical results indicate that the present approach yields the reasonably good agreement with experimental data especially for the rms of mixture fraction. However, the rms of temperature shows large discrepancies as increasing downstream distance. It is necessary to note that the predicted temperature field is very sensitive to the mixture fraction distribution near the stoichiometric mixture fraction ($Z_{st} = 0.055$). Therefore, it is quite possible that the small discrepancies of mixture fraction at $x/D > 10$ could result in the large variation of temperature profile. The overestimated progress variable could be tied with for the overestimated temperature. We think these deviations could be partly related to by the limitation of the physical submodels including the micromixing model, the turbulence model and the turbulent reaction closure.

References

- [1] R.S. Barlow, S. Meares, G. Magnotti, H. Cutcher and A. R. Masri, *Combust. Flame*, 162 (2015) 3516 – 3540.
- [2] J. Akroyd, A. J. Smith, L. R. McGlashan, M. Kraft, *Chemical Engineering Science*, 65 (2010) 1915-1924.
- [3] Q. Tang, W. Zhao, M. Bockelie, R. O. Fox, *Combustion Theory and Modelling*, 11 (2007) 889-907.
- [4] C. D. Pierce, P. Moin, *Journal of Fluid Mechanics*, 504 (2004) 73-97.
- [5] M. Ihme, H. Pitsch, *Combustion and Flames*, 155 (2008) 70-89.
- [6] A. E. Lutz, R. J. Kee (1996) A FORTRAN Program for Computing Opposed-Flow Diffusion Flames, Sandia National Laboratories Rept. No. SAND96-8243.
- [7] Gregory P. Smith, David M. Golden, Michael Frenklach, Nigel W. Moriarty, Boris Eiteneer, Mikhail Goldenberg, C. Thomas Bowman, Ronald K. Hanson, Soonho Song, William C. Gardiner, Jr., Vitali V. Lissianski, and Zhiwei Qin http://www.me.berkeley.edu/gri_mech/

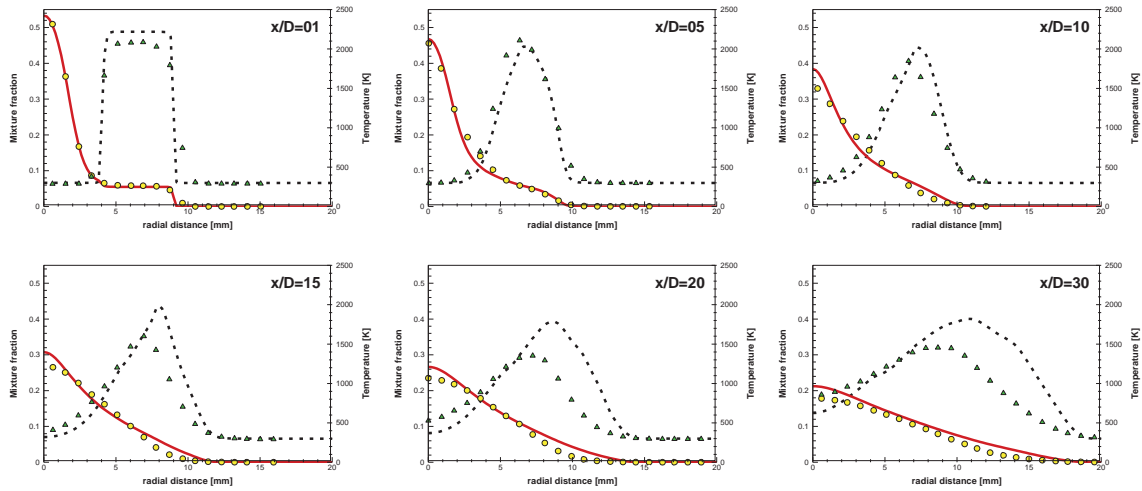


Fig. 1 Comparison of experimented (symbols) and calculated(line) mean mixture fraction and temperature at different axial locations (mixture fraction : solid, circle; temperature : dashed, delta)

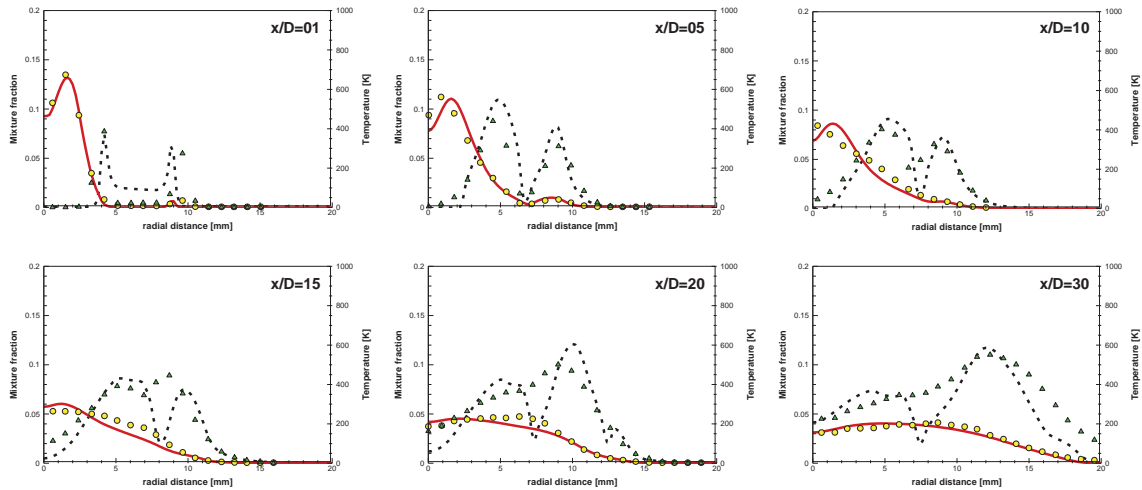


Fig. 2 Comparison of experimented (symbols) and calculated(line) rms of mixture fraction and temperature at different axial locations (mixture fraction : solid, circle; temperature : dashed, delta)

A mixing timescale model for TPDF simulations of turbulent premixed flames

Michael Kuron^a, Zhuyin Ren^{b*}, Evatt R. Hawkes^c, Hua Zhou^b,
Hemanth Kolla^d, Jacqueline H. Chen^d, Tianfeng Lu^a

^a Department of Mechanical Engineering, University of Connecticut, USA; ^b Center for Combustion Energy, Tsinghua University, China; ^c School of Photovoltaic and Renewable Energy Engineering, The University of New South Wales, Australia; ^d Combustion Research Facility, Sandia National Laboratories, USA

*Corresponding Author Email: zhuyinren@tsinghua.edu.cn

Transported probability density function (TPDF) methods are an attractive modeling approach for turbulent flames as chemical reactions appear in closed form. However, molecular micro-mixing needs to be modeled and this modeling is considered a primary challenge for TPDF methods. In the present study, a new algebraic mixing rate model for TPDF simulations of turbulent premixed flames is proposed, aiming to properly account for the transition in reactive scalar mixing rate behavior from the limit of turbulence-dominated mixing to flamelet-controlled mixing behavior in flamelets.

Timescale model development: Reactive scalar mixing rates in turbulent premixed flames depend on the local state of both the flow turbulence and the chemical reactions. For low global Damköhler number, the scalar mixing rate can be expected to be controlled by the small scale turbulent motions, which in turn are driven by large-scale motions, as is found to be a reasonable approximation in studies of passive scalar mixing. Thus in the limit of passive scalar mixing, the mixing rate of reactive scalar is proportional to the turbulence timescale according to the classical expression $\Omega_t = \tilde{\chi}/\tilde{\phi}^{\prime 2} = C_\phi \tau_{turb}^{-1}$. The constant of proportionality C_ϕ is the mechanical-to-scalar timescale ratio and is typically taken to be 2.0. In the RANS context, the turbulence timescale can be defined as the ratio of the turbulent kinetic energy, \tilde{k} , to the turbulent kinetic energy dissipation rate, $\tilde{\epsilon}$. Conversely, in the limit of large global Damköhler number, i.e., in the limit of laminar flamelets embedded in a turbulent flow field, the mixing rate is expected to be dependent on the laminar flame structure. Assuming that the premixed flamelets can be adequately described by a single reaction progress variable, c , the Favre-averaged mixing rate can be expressed in terms of the conditional scalar dissipation rate, $\langle \chi | c \rangle$, as $\Omega_f =$

$\tilde{\chi}/\tilde{c}^{\prime 2} = \int_0^1 \langle \chi | \zeta \rangle \tilde{P}_c(\zeta) d\zeta / \tilde{c}^{\prime 2}$, where $\tilde{P}_c(\zeta)$ is the Favre-averaged probability density function of the progress variable and ζ is the sample space variable. This expression is advantageous in that the PDF of the progress variable is computed naturally as a part of the TPDF solution, and thus only a model for the conditional scalar dissipation rate in the flamelet limit is required. As a first attempt, we close the model by reconstructing the conditional scalar dissipation rate from a 1D freely propagating premixed flame. The model format implies that the large variation in the mixing rate can be primarily attributed to the strong local variation in the progress variable PDF and that the local flamelets are reasonably approximated by the conditional scalar dissipation rate of the freely propagating flame at a known unburnt condition. Note that the model can in principle account for the strain/stretch effect on the flame structure by reconstructing the conditional scalar dissipation rate from a stretched premixed flame.

In practice, local mixing conditions in a turbulent premixed flame may vary such that neither of these limiting assumptions are valid for the entire flow field, and thus some intermediate local state between the two limits must be sought. To accomplish this, we define the segregation factor, $\eta = \tilde{c}^{\prime 2} / [\tilde{c}(1 - \tilde{c})]$, [22,27] to act as the blending variable between the two limiting states. As the local Damköhler number tends to infinity and the progress variable PDF becomes bimodal, the variance reaches its maximum possible value of $\tilde{c}(1 - \tilde{c})$. Conversely, in the limit of infinitely strong turbulence, the variance disappears due to perfect mixing. Accordingly, the hybrid timescale model can be constructed as [1]

$$\Omega_{hybrid} = (1 - \eta) C_\phi \tau_{turb}^{-1} + \eta \int_0^1 \langle \chi | \zeta \rangle \tilde{P}(\zeta) d\zeta / \tilde{c}^{\prime 2}. \quad (1)$$

The hybrid timescale model is constructed to take advantage of the statistical data naturally available in a TPDF simulation and to properly describe the mixing rate in the flamelet limit.

An evaluation of the timescale model using DNS: An *a priori* assessment of the new model is performed using direct numerical simulation (DNS) data of a lean premixed hydrogen-air jet flame [2], in

which two initially planar flames propagate into a slab of fresh reactants in the domain center. The temperature of the unburned reactants is 700 K, the background pressure is atmospheric, and the equivalence ratio is $\phi = 0.7$. The shear-driven flow sustains strong turbulence-flame interactions. In the hybrid mixing rate model, the scalar dissipation requires closure while the scalar variance can be computed directly from the TPDF simulation. Therefore, we compare here the spatial and temporal variation of the progress variable scalar dissipation rate extracted from the DNS as well as the scalar dissipation rate implied by the new hybrid model, $\tilde{\chi}_{hybrid} = \Omega_{hybrid} \widehat{c}^{n^2}$, which are shown in the contour plots in Fig.1. The values for both the DNS and modeled scalar dissipation rates are normalized for each DNS case by the maximum value across space and time of the DNS scalar dissipation rate. At the leading edge of the flame brush through the center of the flame, the hybrid model accurately captures the spatial and temporal variation of the scalar dissipation rate. The magnitude of the scalar dissipation rate in this region is slightly under-predicted for Case Da^- , but is accurately captured in Case Da^+ . Towards the trailing edge of the flame brush the hybrid model tends to under-predict the magnitude of the scalar dissipation rate for both cases. However, at this location in the flame brush, the mixing rate is less critical for accurate flame prediction as the burnt mixture is relaxing to chemical equilibrium. In general, the new model accurately captures the mixing timescale behavior in the DNS.

An *a posteriori* TPDF study is then performed using the same DNS data as a numerical test bed [3,4]. The DNS provides the initial conditions and time-varying input quantities, including the mean velocity, turbulent diffusion coefficient, and modeled scalar mixing rate for the TPDF simulations, thus allowing an exclusive focus on the mixing model. The new mixing timescale model is compared with the constant mechanical-to-scalar mixing timescale ratio coupled with the Euclidean Minimum Spanning Tree (EMST) mixing model, as well as a laminar flamelet closure by Pope and Anand. It is found that the laminar flamelet closure is unable to properly capture the mixing behavior in the thin reaction zones regime while the constant mechanical-to-scalar mixing timescale model under-predicts the flame speed. As shown in Fig. 2, the EMST model coupled with the new mixing timescale model provides the best prediction of the flame structure and flame propagation among the models tested, as the dynamics of reactive scalar mixing across different flame regimes are appropriately accounted for.

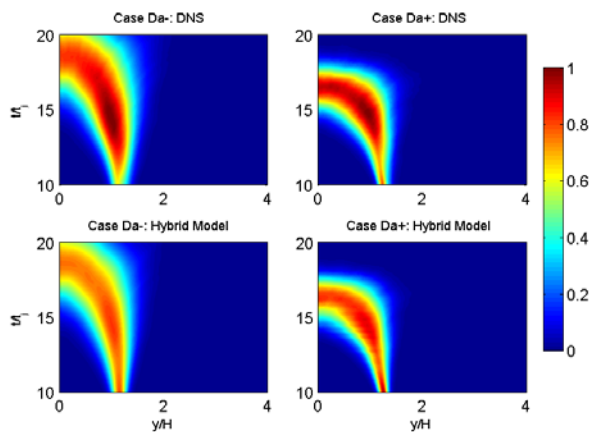


Fig. 1 Scalar dissipation rate normalized by the maximum DNS value for Case Da^- (left) and Case Da^+ (right). Top Row: DNS. Bottom Row: Hybrid Model from Eqn. (1).

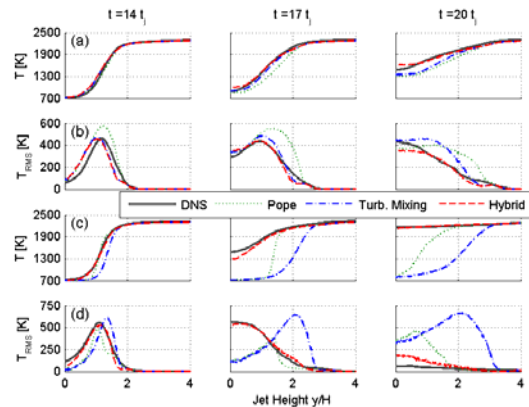


Fig. 2 Predicted mean and RMS spatial temperature profiles from the DNS and TPDF solutions. Rows (a) and (b): Case Da^- . Rows (c) and (d): Case Da^+ .

- [1] Z. Zhou, S. Li, H. Wang, Z. Ren, 68th Annual Meeting of the APS Division of Fluid Dynamics. (2015).
- [2] E.R. Hawkes, O. Chatakonda, H. Kolla, A.R. Kerstein, J.H. Chen, Combust. Flame. 159 (2012) 2690-2703.
- [3] A. Krisman, J.C.K. Tang, E.R. Hawkes, D.O. Lignell, J.H. Chen, Combust. Flame. (2014) 1-22.
- [4] M. Kuron, E. Hawkes, Z. Ren, J. Tang, H. Zhou, J.H. Chen, T. Lu, Proc. Combust. Inst. (2016), accepted for oral presentation. .

Large Eddy Simulation of Sydney Piloted Jet Flame with Inhomogeneous Inlets Using a Dynamic Second-order Moment Closure Model

Kun Luo*, Yun Bai, Wenjian Bi, Jianren Fan

State Key Laboratory of Clean Energy Utilization, Zhejiang University, Hangzhou 310027, P.R. China
zjulk@zju.edu.cn

It is a big challenge to simulate the partially-premixed flames in turbulent combustion modeling since most turbulent combustion models are separately developed in terms of premixed or non-premixed regimes. Recently Barlow et al. [1] have conducted a series of piloted CH₄/air jet flames with inhomogeneous inlets by using a modified Sydney burner to produce a partially-premixed flames. These flames can exhibit the transition from a stratified-premixed combustion mode to a diffusion-dominated combustion mode within the first ten jet diameters and also local extinction in the downstream regions, which serve as excellent benchmark for evaluating combustion models.

In the current study, one of these flames, named FJ200-5GP-Lr75-57 that has a steep gradient in mixture fraction at the jet exit, is simulated using a Dynamic Second-order Moment Closure Model in LES [2]. In this model, the chemical reaction rate is directly closed in the form of Arrhenius Law. The whole temperature exponential function is treated as a variable to avoid the Taylor series expansion. All coefficients are determined by dynamic procedures. This model does not have any assumptions on premixed or non-premixed flame regimes. It is applicable to simulate the partially-premixed flames. Previously, we have applied this model to simulate Sandia Flame series and Sydney bluff-body swirling flames and consistent results with experimental data have been achieved [2]. In the present simulation, a 4-step CH₄/air chemical reaction mechanism [3] is utilized. The computational domain is 4D × 4D × 40D, and a total of 1.5 million cells are used. The hot-temperature burnt CH₄/air mixture flow is chosen to replace the unburnt pilot flow in the experiment.

The predicted snapshot of the instantaneous temperature distribution of the flame is presented in Figure 1. The flame is stabilized by the pilot flow with some extinction events occurring in the downstream regions.

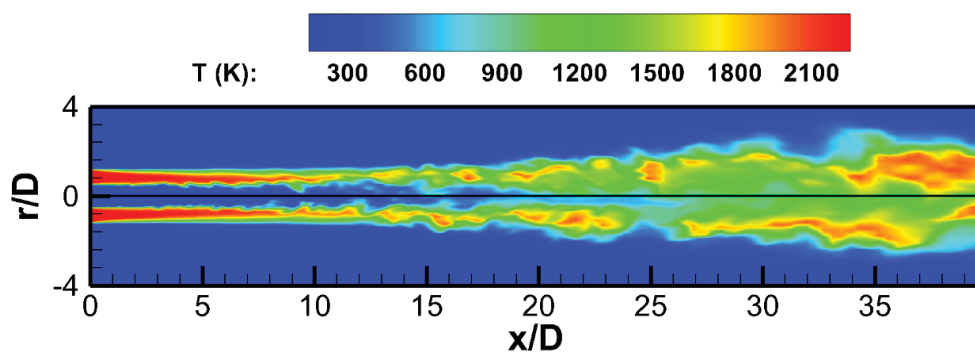


Figure 1. The snapshot of the instantaneous temperature field from LES.

Figure 2 shows the comparisons of temperature and mixture fraction at different axial locations between LES and the experiment. It can be seen that the mean temperature and mixture fraction agree well with those of the experiment, while the predicted fluctuations show deviations upstream as the boundary conditions did not match perfectly, and the deviations disappear in the downstream regions.

Figure 3 presents the experimental and predicted scatter plots for temperature versus mixture. It is found that the LES results have a similar scatter distribution. The complicated combustion patterns observed in the experiment can also be found in the current simulation, including the transition from a premixed combustion mode to a diffusion-dominated combustion mode and local extinctions in the downstream regions.

These results demonstrate that the present LES dynamic second-order moment closure model is able to reproduce the flame and have capability of predicting premixed, non-premixed and partially-premixed flames.

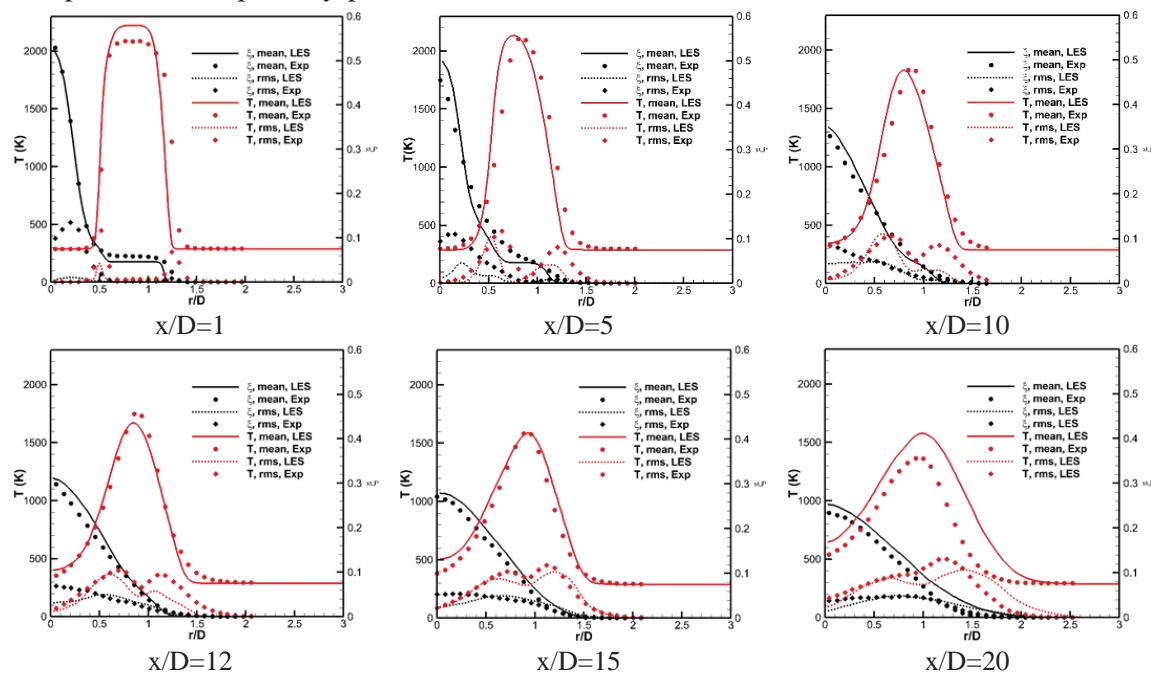


Figure 2. Comparisons of the simulated and measured radial profiles of mean and rms temperatures and mixture fractions in different axial locations.

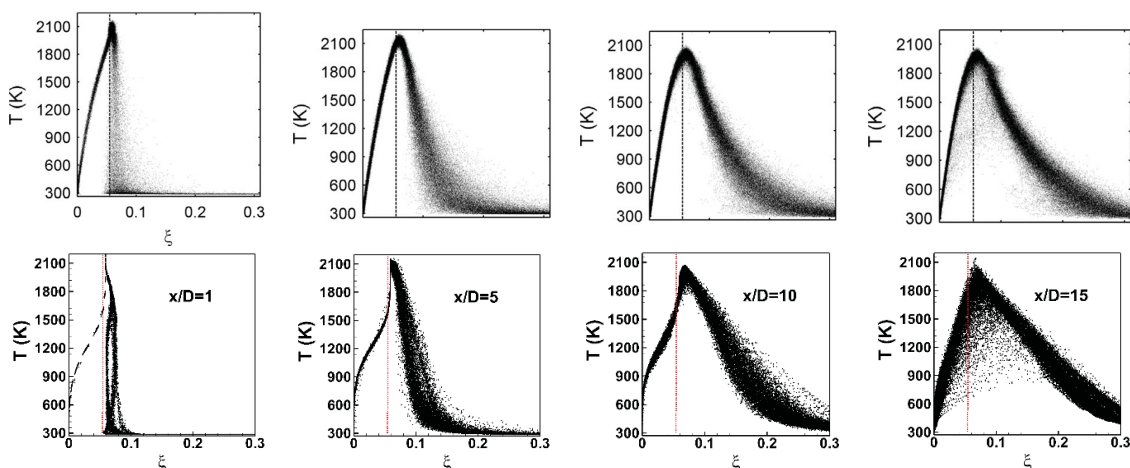


Figure 3. Scatter plots of temperature versus mixture fraction for experiment (top) and LES (bottom).

References

- [1] R.S. Barlow et al., *Combust. Flame* 162 (2015) 3516-3540.
- [2] K. Luo, J.S. Yang, J.R. Fan. *Fuel*, 2016, submitted.
- [3] W.P. Jones, R.P. Lindstedt. *Combust. Flame* 73 (1988) 233-249.

High speed 10KHz imaging of OH/CH₂O for DME issuing into a hot coflow burner with preliminary laminar calculations

A.R.W. Macfarlane*, M.J.Dunn, M.Juddoo, A.R.Masri
 School of Aerospace, Mechanical and Mechatronic Engineering,
 The University of Sydney, NSW 2006, Australia

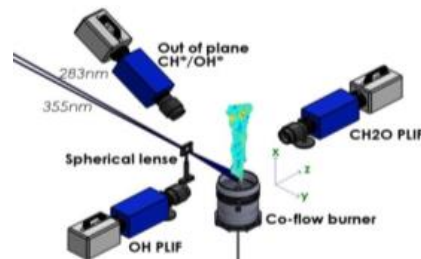
Introduction

The use of DME in a Hot Coflow burner of H₂/Air is a relatively new area of study and one of great interest; where the ratio of H₂/air alters the coflow temperature. DME's combustion nature and source of production makes it an excellent alternative as an autoignition fuel in compression engines [1], as such understanding its autoignition characteristics under turbulent conditions is of fundamental importance. The burner has been vastly explored for fuels such as methane [2] and Hydrogen [3] and is widely understood, however as DME has increased complexity and 'triple' staged autoignition the study of flame base and autoignition dynamics is important.

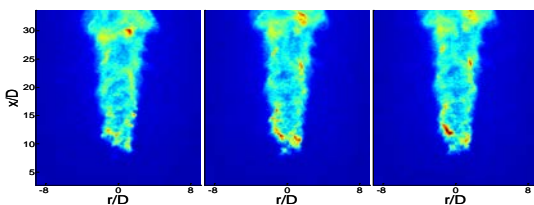
Experiments have shown the burner to be a valuable tool to explore the autoignition of DME, highlighting temporal flame base and autoignition characteristics. The focus was to explore flames with varying lift off heights, isolating kernel consumption events with upstream flame base propagation for a variety of diluents. Using a combination of highspeed Chemiluminescence, OH and CH₂O PLIF imaging the formation and growth of kernels has been explored and the product of the two radicals was used as a marker of heat release. Varying signal intensities for the spatial overlap of CH₂O onto a OH kernel were found to be highly dependent on fuel diluent and coflow temperatures. The axial position of autoignition kernels has been used to obtain delay times in an attempt to model the results with uniform autoignition and unsteady opposed flow solvers.

Burner conditions and burner setup

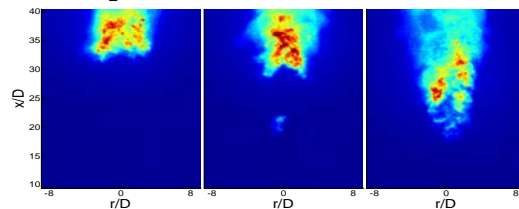
	Fuel Jet		
	Air/DME 3:1	Air/DME 1:1	Pure DME
V(m/s)	50	50	50
Re	16650	22990	38610
Q _{DME} (SLM)	11.7	23.4	46.8
Q _{air} (SLM)	35.0	23.4	0
ξ _{st}	0.2	0.107	0.064



Chemiluminescence images: DME:Air=1:3 for coflow temperatures 1400K and 1275K



1400K Coflow

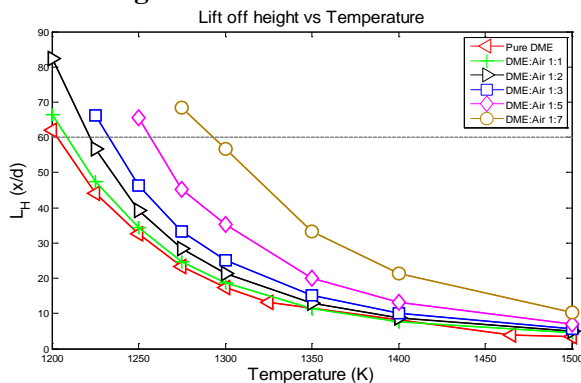


1275K Coflow

Inconsecutive 10KHz chemiluminescence images: The first and last image for a given coflow temperature indicate the highest and lowest extremes in liftoff heights while the middle image contains an autoignition kernel.

The higher 1400K coflow shows a somewhat stable flame base and only very small insignificant kernel formation and consumption. The lower 1275K coflow has large variations in Lift off height and kernels form far upstream of the main flame where they grow and advect downstream finally being absorbed by the flame body.

Lift off heights

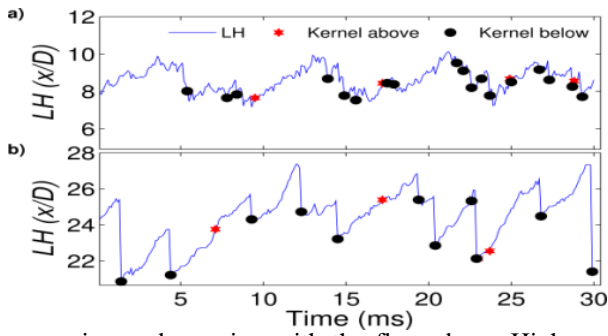


Varying diluents and their respective lift off heights were explored within this study and detailed PLIF measurements were taken for pure DME, Air:DME=3:1, Air:DME=1:1 at selected lift off height cases.

A reduction in coflow temperature for a given diluent increases the lift off height where a temperature lower than 1300K has a dramatic rise in Lift off height across all diluents. Increased diluent increases the lift off height for a given temperature where it appears to approach a linear dependence of Lift off height with coflow temperature.

*Corresponding author: amac7548@uni.sydney.edu.au

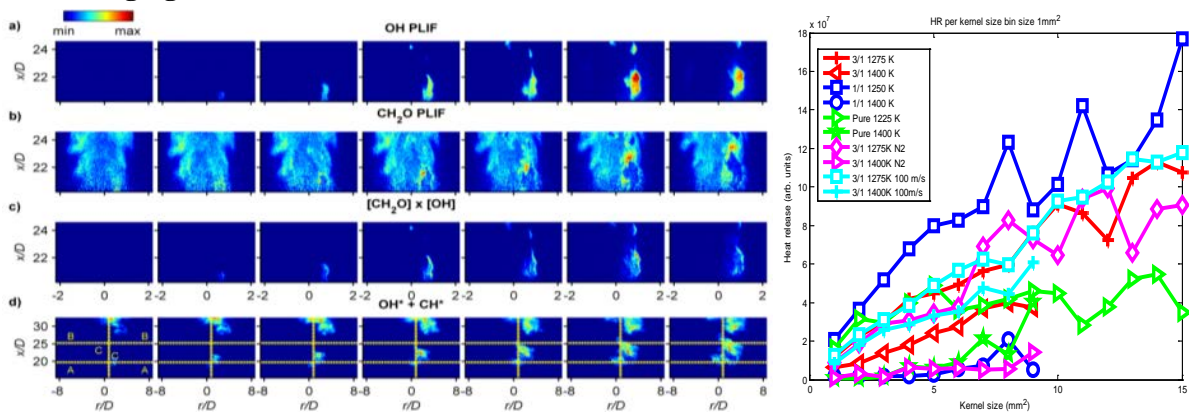
Temporal flame base dynamics: DME:Air=1:3 for coflow temperatures 1400K (a) and 1275K (b)



Temporally resolved Lift off Heights at 10 KHz was vital in understanding the interaction and necessity of kernels on the main flame base. Lift off heights were defined based on the lowest chemiluminescence signal above background threshold for the main flame base.

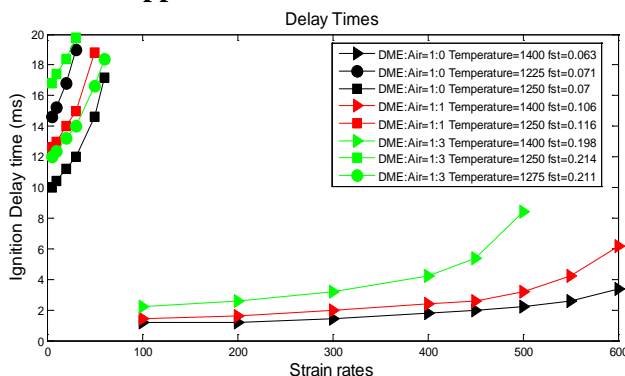
The reduction in coflow temperature does not dramatically reduce the number of kernels forming however the impact of the kernels influence on the flame base is substantially increased. A lower temperature has dramatic cliff structures occurring due to large kernels growing and merging with the flame base. Higher coflow temperatures have kernels that do not significantly propagate the flame base upstream and premixed propagation is found to occur more readily. The reduced gradient $\frac{d(LH)}{dt}$ between kernel consumption events for higher coflow temperature highlights the tendency for the flame to remain fixed in space owing to premixed propagation.

PLIF imaging and Heat release measurements



High speed imaging of OH and CH₂O radicals was used in understanding the temporal formation and growth of kernels. The spatial overlap and relative CH₂O intensities onto a kernel (defined by the OH radical) was used to identify Heat release. The integrated heat release is found to be a balance between the OHxCH₂O intensities and the amount of overlap. This compromise between spatial overlap and intensities explains the behaviour seen; where the pure kernels give of less heat than the 1:3 and 1:1 cases. There is also a distinct bimodal behaviour of heat release between high and low coflow temperatures where more heat is being released from the higher coflow temperature than the lower coflow temperature.

Transient opposed flow simulations



Through the use of the Ember transient opposed flow solver it has been possible to highlight the effect of strain on autoignition delay times. The effect of increasing strain increases the autoignition delay times, where DNS studies have indicate autoignition occurs at minimal scalar dissipation[4].

It has been found that reduced premixing has an increased resistance to strain where coflow temperature has also been found to strongly affected the resistance to strain. Finally, simulations have shown that ignition occurs in very lean regions.

References

- [1] C. Arcoumanis, C. Bae, R. Crookes, E. Kinoshita, Fuel, 87 (2008) 1014-1030.
- [2] R.L. Gordon, A.R. Masri, E. Mastorakos, Combust. Flame, 155 (2008) 181-195.
- [3] R. Cabra, T. Myhrvold, J.Y. Chen, R.W. Dibble, A.N. Karpetis, R.S. Barlow, Proc. Combust. Inst., 29 (2002) 1881-1888.
- [4] E. Mastorakos, T.A. Baritaud, T.J. Poinot, Combust. Flame, 109 (1997) 198-223.

LES Modeling of Piloted Jet Flames with Inhomogeneous Inlets Using Tabulated Chemistry Methods

Giampaolo Maio¹, Mélody Cailler^{1,2}, Renaud Mercier², Vincent Moureau³, Benoît Fiorina¹

¹Laboratoire EM2C, CNRS, CentraleSupélec, Université Paris-Saclay, Grande Voie des Vignes, 92295 Châtenay-Malabry Cedex, France

²SAFRAN Tech, Rue des Jeunes Bois, Châteaufort - CS 80112, 78772 Magny-les-Hameaux, France

³Normandie Univ, INSA Rouen, UNIROUEN, CNRS, CORIA, 76000 Rouen, France

Corresponding author: giampaolo.maio@centralesupelec.fr

I. Introduction

In many practical applications, the fuel/air mixture issuing the injection system exhibits composition inhomogeneities, promoting the development of multiple flame structures. It has been recently observed that combustion models have to account for the coexistence of both premixed and non-premixed regimes to predict pollutant such as CO [1]. The objective of the present work is to challenge over both premixed and non-premixed flame regimes the Thickened Flame model for LES (TF-LES) [2] and the Filtered Tabulated Chemistry model for LES (F-TACLES) [3] which have been already widely tested for premixed and weakly stratified premixed flames [4]. The Sydney modified piloted burner [5] recently studied experimentally both in Sandia and in Sydney laboratories is retained as test case to validate the models. This jet flame configuration is very challenging because it allows to stabilize multiple combustion regimes (stratified, premixed and diffusion mode) with simple changes to the experimental set-up.

II. Experimental set-up of the turbulent jet flame

The burner assembly shown in Figure 1 consists of two concentric tubes surrounded by a pilot annulus, centered in a wind tunnel supplying a co-flowing air stream at fixed velocity. In the configuration analyzed in this study, the central tube is fed with fuel whereas air is flowing through the outer tube. The central pipe can be recessed upstream of the burner exit plane, varying therefore the mixing between fuel and air. For sufficiently large recession distance (L_r) the mixture is nearly homogeneous at the burner exit, while intermediate recession distances lead to equivalence ratio inhomogeneities.

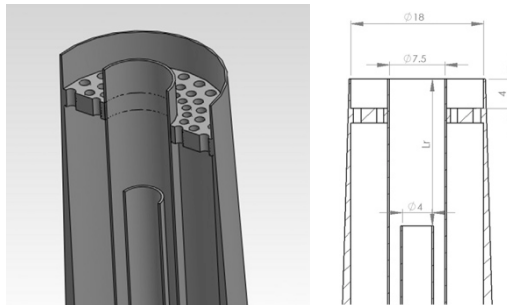


Fig 1: Isometric cutaway of the solid model of the burner and schematic of the burner [5]

III. Preliminary results

The LES simulations are performed with the finite-volume low Mach number code YALES2 [6]. A fourth order scheme in space and time is used for the numerical integration. Two configurations have been selected: the first features an homogeneous composition in equivalence ratio at the burner exit plane ($L_r = 300$ mm), while the second exhibits inhomogeneous mixture fraction profiles ($L_r = 75$ mm). In both cases the quality of the results greatly depends on the boundary conditions at the burner exit. In order to properly describe the velocity and mixture fraction profiles, the mixing within the injection tube is first calculated in a cold case simulation. The output of this simulation is used as boundary condition for the reacting geometry. Figure 2 shows the comparison of mean and RMS of axial velocity and mixture fraction for the inhomogeneous case. Comparisons are performed near the burner exit plane at $z/D=0.2$ for velocity and $z/D=0.5$ for mixture fraction.

For both mean and RMS axial velocity profiles the agreement between the LDV measurements and the LES simulation is good. However, Fig. 2 shows that the mixing in the injection tube is not well captured by the simulation. The predicted mean mixture fraction profile is more diffused than the experimental one. In order to solve this issue the authors are performing a mesh adaptation based on the combination of velocity and mixture fraction gradients [7]. The micro-mixing at the exit of the inner tube carrying fuel plays an important role to predict correctly mean and RMS mixture fraction profile at the burner exit plane. Figure 3 shows a comparison

between the initial coarse mesh and the refined one at the fuel inner tube exit plane. The simulations on the refined mesh are still in progress and updated results will be shown in the final version of the poster.

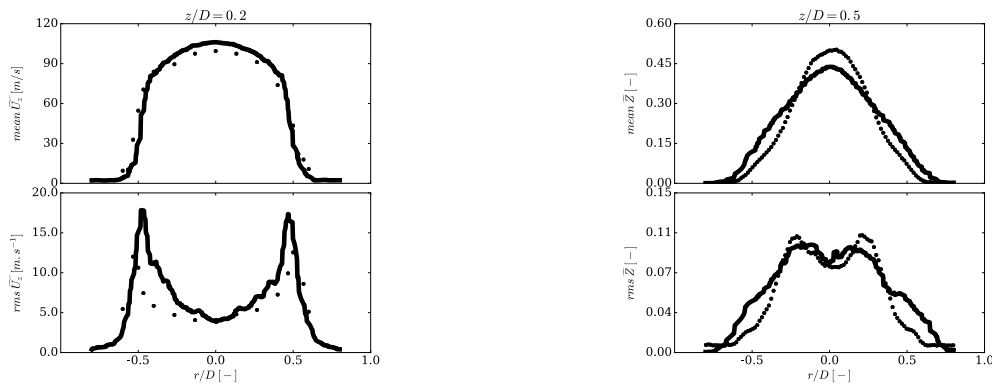


Fig 2: Velocity and mixture fraction profiles mean and RMS respectively at $z/D=0.2$ and $z/D=0.5$. Line: simulation. Symbols: experimental data.

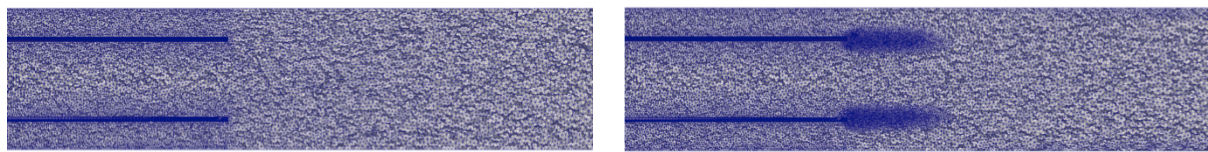


Fig 3: Comparison between the starting mesh and the refined mesh using a criterion based on the mixture fraction and velocity gradients.

Reacting simulation are also still in progress. A first reacting simulation has been performed with a 35 million cells mesh. The model that is retained is the TF-LES model using premixed flamelet look-up table. A preliminary comparison at $z/D = 1$ and $z/D = 5$ between the radial experimental profile and the simulation is shown in Figure 4 for the homogeneous configuration.

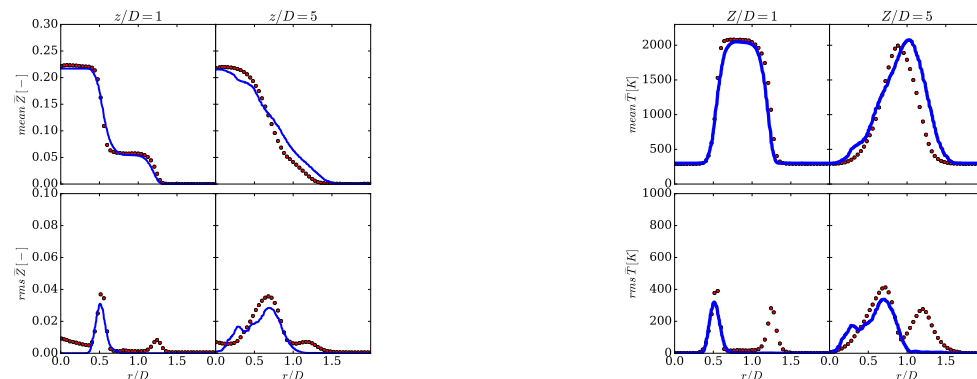


Fig 4: Mixture fraction and temperature profiles mean and RMS respectively at $z/D=0.2$ and $z/D=0.5$. Line: simulation. Symbols: experimental data.

References

- [1] Franzelli, B., Fiorina, B., and Darabiha, N., *Proceedings of the combustion institute*, Vol. 34, No. 1, 2013, pp. 1659–1666.
- [2] Colin, O., Ducros, F., Veynante, D., and Poinsot, T., *Phys. Fluids*, Vol. 12, No. 7, 2000, pp. 1843–1863.
- [3] Fiorina, B., Vicquelin, R., Auzillon, P., Darabiha, N., Gicquel, O., and Veynante, D., *Combust. Flame*, Vol. 157, 2010, pp. 465–475.
- [4] Fiorina, B., Mercier, R., Kuenne, G., Ketelheun, A., Avdić, A., Janicka, J., Geyer, D., Dreizler, A., Alenius, E., Duwig, C., et al., *Combustion and Flame*, Vol. 162, No. 11, 2015, pp. 4264–4282.
- [5] Meares, S. and Masri, A. R., *Combustion and Flame*, Vol. 161, No. 2, 2014, pp. 484 – 495.
- [6] Moureau, V., Domingo, P., and Vervisch, L., *Comptes Rendus Mécanique*, Vol. 339, No. 2-3, 2011, pp. 141–148.
- [7] Benard, P., Balarac, G., Moureau, V., Dobrzynski, C., Lartigue, G., and D’Angelo, Y., *International Journal for Numerical Methods in Fluids*, 2015.

Response of a Laminar Premixed Flame to Equivalence Ratio Oscillations

Wolfgang Meier, Holger Ax

German Aerospace Center (DLR), Institute of Combustion Technology, Stuttgart, Germany

E-Mail: wolfgang.meier@dlr.de

The mixture of fuel and oxidizer in technical combustion applications is often inhomogeneous or varies due to combustion instabilities like thermo-acoustic oscillations in gas turbines. Premixed flames can then be subject to equivalence ratio oscillations which influence the flow field, flame structure, heat release and emissions and are accompanied by pressure oscillations. A question of considerable interest concerns the response of the flame front structure to equivalence ratio oscillation, particularly when the wavelength of the oscillation is of similar order of magnitude as the flame thickness. In that case, it is expected that the flame cannot be described by sequential steady states any more due to the interaction and phase delay of convective and diffusional transport within the flame front. The limit frequencies for the non-quasi-steady behavior were given by Shreekrishna and Lieuwen [1] with 4 kHz at 10 atm and 400 Hz at 1 atm.

The experiments presented in this poster were performed in a premixed laminar CH₄/air flame at a pressure of 70 mbar. The low pressure offers the advantage of a large flame thickness that can well be resolved by optical measurement techniques. Also, the above mentioned limit frequency would be as low as approximately 30 Hz. Furthermore, the increased molecular diffusion lengths at reduced pressure help to generate a periodic flame stratification in flow direction. Figure 1 displays the experimental setup. The premixed Bunsen-flame is stabilized on a burner with 40 mm exit diameter surrounded by a matrix burner for flame anchoring. The equivalence ratio was varied by the pulsed addition of methane into the stationary premixed methane/air flow of a Bunsen-flame through 48 tubes inside the burner with an exit diameter of 1 mm each. The pulsation was triggered by a magnetic valve that was located below the burner outside the combustion chamber. By a proper choice of the dimensions a periodic variation of the equivalence ratio was achieved in flow direction while in the horizontal plane a homogenous distribution is reached upstream of the flame [2].

The flame shape and the position of the reaction zone were revealed by the detection of OH* chemiluminescence. The major species concentrations and the temperature were simultaneously measured by phase-resolved one dimensional laser Raman scattering along the center axis of the burner and flame. Thus, the concentration and temperature profiles were gained from the burner exit to the burned gas across the flame front. The flame response to equivalence ratio oscillations was investigated in a parametric study by variation of frequency and strength of the methane pulses at 70 mbar. The complex processes of convective and diffusive transport and their interaction within the flame front were investigated in detail and related to each other in terms of their length and time scales.

The results show, that in a stationary (non-oscillating) flame the temperature and species concentrations change within the flame front as expected for a low pressure flame (see Fig.2). Notably, the oxidation of CO to CO₂ reaches far up into the post-flame region and the profiles of H₂ are stretched more than those of the other species due to fast molecular diffusion. At low excitation frequencies (up to 10 Hz) the flame can follow the modulation and reaches quasi-steady states at the minimum and maximum fuel concentration. Due to the variation of the laminar flame speed during an oscillation cycle, the flame front moves periodically up and down, at a frequency of 5 Hz by approximately 7 mm. With increasing frequency, the amplitude of the flame movement becomes smaller and almost vanishes at 40 Hz. At 40 Hz, the relatively short wavelength of the modulation leads to continuous mixture fraction gradients across the flame front. The thermo-chemical state of the flame shows a significant phase dependency and the inner structure of the flame front cannot be described by quasi-steady states.

The results represent a unique data base that is suitable for the detailed description of the flame response and the validation of numerical models for combustion processes.

- [1] S.H. Shreekrishna , T. Lieuwen , Premixed flame response to equivalence ratio perturbations, *Combust. Theory Model.* 14 (5) (2010) 681–714.
 [2] H. Ax, W. Meier, *Combust. Flame* 167, 172-183 (2016).

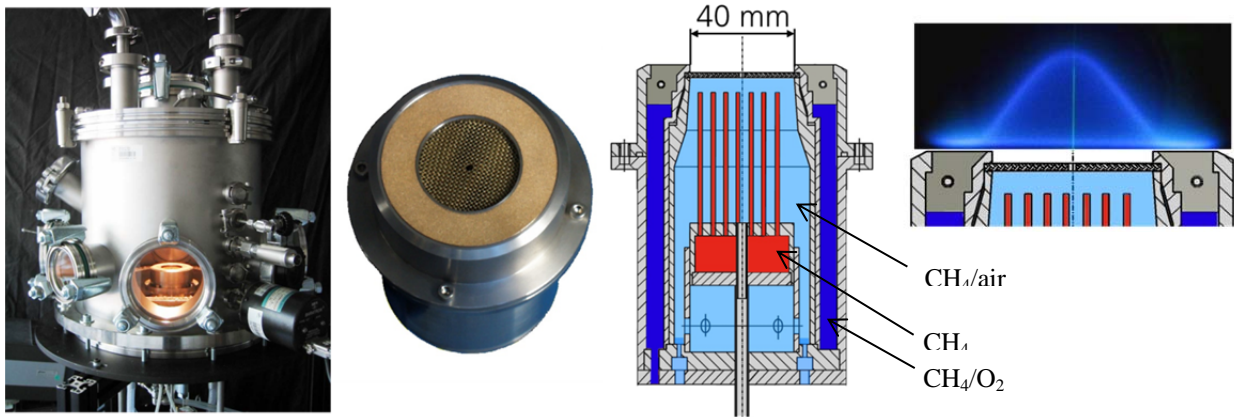


Fig.1: Low pressure burner for laminar premixed flames with periodically changing equivalence ratio.

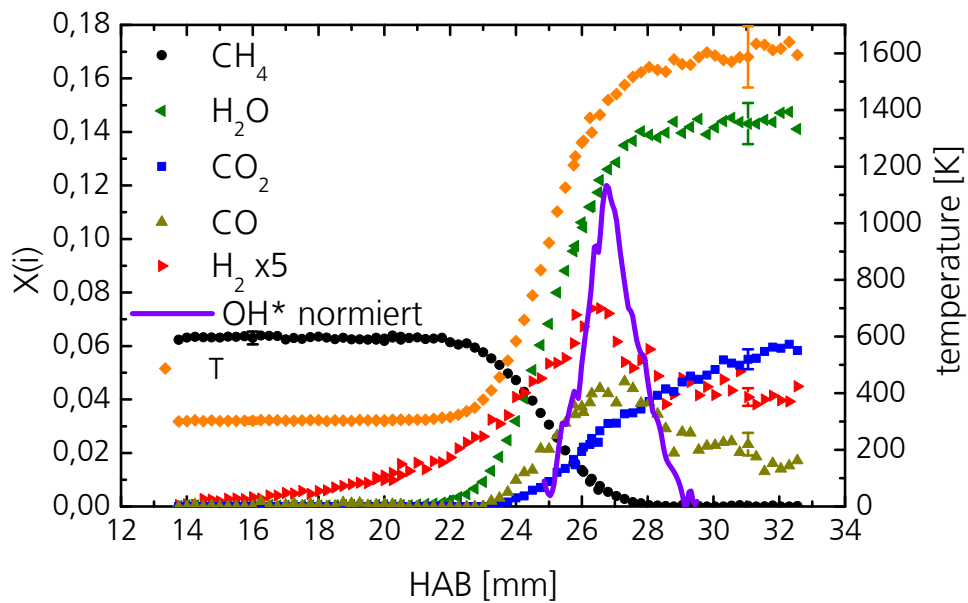


Fig.2: Axial profiles of species mole fractions, temperature and OH chemiluminescence in a stationary CH₄/air Bunsen-flame at 70 mbar.

Large-eddy simulations of a piloted jet flame with inhomogeneous inlets using a flamelet/progress variable approach and the Eulerian stochastic fields method

Hagen Müller* and Michael Pfitzner†

*Institut für Thermodynamik, Universität der Bundeswehr München
Werner-Heisenberg-Weg 39, 85577 Neubiberg, Germany*

The turbulent combustion process in practical burners often spans a wide range of scales and combustion regimes. Examples are homogeneous charge compression ignition (HCCI) engines or sequential gas turbines, where autoignition, recirculation of hot combustion products or extinction and re-ignition events may play an important role. The local composition of the fresh gases may vary throughout the turbulent flow field and affect the combustion process locally. The effect of such inhomogeneities on the stabilization of a piloted turbulent methane/air flame has recently been investigated experimentally [1]. In these experiments, the main pipe of the burner consists of two concentric tubes that separately supply methane and air. The inner tube is retractable which allows to adjust the degree of inhomogeneity at the burner inflow plane. The study demonstrates that with an optimized degree of inhomogeneity the blow-off velocity can be increased significantly compared to homogeneous inflow conditions. This test case is studied herein using Large-eddy simulations (LES).

The numerical description of turbulent combustion processes using LES has received considerable attention and much progress has been made [2]. However, especially in the light of the limited computational resources, modeling turbulent (especially hydrocarbon) combustion devices is highly challenging. Difficulties arise from the small scale interactions between reactions and turbulence as well as from the need to reduce the complex chemical kinetics. In the present contribution the piloted jet flame with inhomogeneous inlets is used as a test case for an LES combustion model that employs a flamelet/progress variable method to cut the cost of solving the finite-rate reactions during run-time. A premixed tabulation technique is used within the flammability limits to represent the thermochemical state of the flame in terms of the local mixture fraction and a progress variable. The fluid properties outside this region are represented by diffusion flamelets. This method demonstrated its capability to model piloted diffusion flames with local extinction and re-ignition events [3], which have also been observed in the present test case. The unresolved fluctuations of the thermochemical state are modeled using the Eulerian stochastic fields method [4], which has been used to simulate both premixed and non-premixed flames featuring autoignition as well as extinction and re-ignition events using finite-rate integration of the chemical reactions. Here, we use the method to describe the subgrid fluctuations of mixture fraction and progress variable that represent the composition in the present tabulated approach. A similar approach has previously been used to simulate lifted flames [5]. The LES combustion model has been implemented in the open-source CFD software OpenFOAM¹ which uses a pressure-based solution algorithm.

Preliminary results for two configurations featuring different degrees of inlet inhomogeneity are shown in Figure 1. The upper plot shows an instantaneous LES realization of temperature for the reference test case FJ200-5GP-Lr75-57, which is characterized by a high degree of inhomogeneity of the inflow composition. The result shown in the lower plot of Figure 1 corresponds

*Research Associate, hagen.mueller@unibw.de

†Full Professor, michael.pfitzner@unibw.de

¹www.openfoam.com

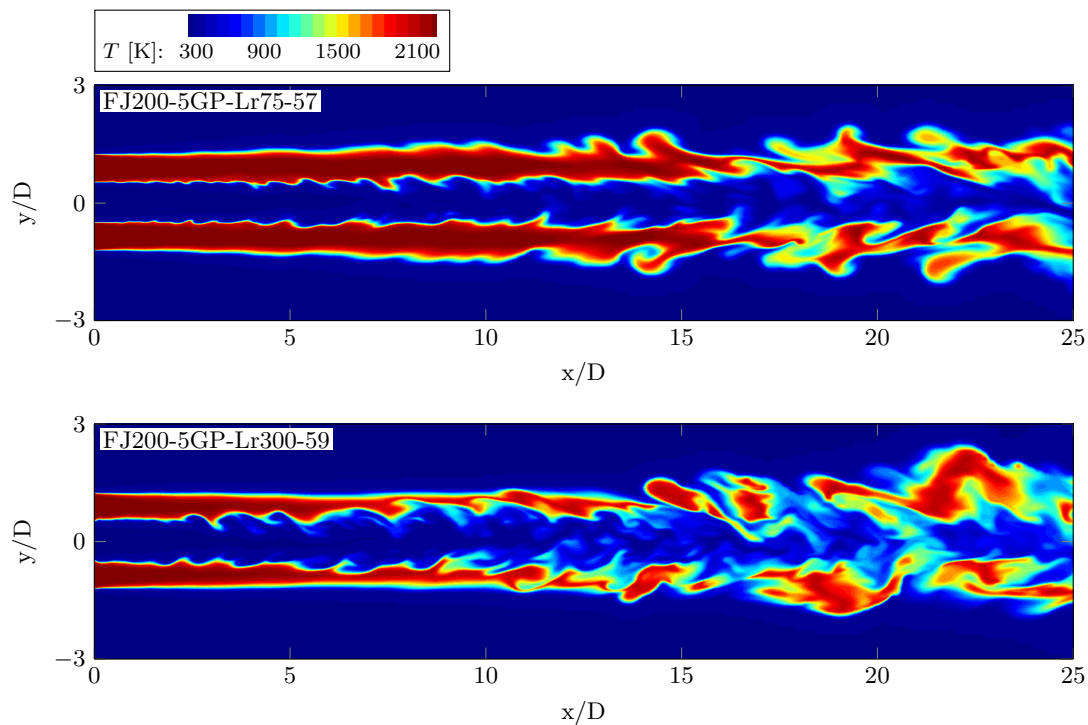


Figure 1: Instantaneous temperature field in a plane perpendicular to the inflow.

to test case FJ200-5GP-Lr300-59 in which the inflow condition is nearly homogeneous. The inflow bulk velocities are comparable in both test cases. Albeit qualitative, the instantaneous result indicates that the inhomogeneous test case is more resistant towards extinction. This is in line with the experimental observations.

The final poster will present averaged results for the two test cases and a quantitative comparison with the available experimental measurements. Furthermore, we will evaluate the role of subgrid chemistry modeling by comparing the LES results obtained with the Eulerian stochastic fields method with those obtained with a delta PDF distribution for two grid refinement levels. The results will also be submitted to the session on stratified flames organized by Benoît Fiorina and Andreas Kempf.

References

- [1] Barlow, R.S., Meares, S., Magnotti, G., Cutcher, H. & Masri, A.R., *Local extinction and near-field structure in piloted turbulent CH₄/air jet flames with inhomogeneous inlets*. Comb. Flame, 162(10): 3516-3540. 2015.
- [2] Pope S., *Small scales, many species and the manifold challenges of turbulent combustion*. Proc. Comb. Inst., 34: 1-31. 2013.
- [3] Vreman, A.W., Albrecht, B.A., van Oijen, J.A., de Goey, L.P.H. & Bastiaans, R.J.M., *Premixed and nonpremixed generated manifolds in large-eddy simulation of Sandia flame D and F*. Comb. Flame, 152(3): 394-416. 2008.
- [4] Jones, W.P. & Prasad, V.N., *Large eddy simulation of the Sandia flame series (D-F) using the Eulerian stochastic field method*. Comb. Flame, 157(9): 1621-1636. 2010.
- [5] Kulkarni, R.M. & Polifke, W., *LES of Delft-Jet-In-Hot-Coflow (DJHC) with tabulated chemistry and stochastic fields combustion model*. Fuel Proc. Tech., 107: 138-146. 2013.

Comparisons of Uncertainties from Turbulence and Chemical Kinetics Models in Turbulent Combustion Simulations

Michael E. Mueller^{1,*}, Venkat Raman^{2,+}

¹ Department of Mechanical and Aerospace Engineering, Princeton University, USA

² Department of Aerospace Engineering, University of Michigan, USA

* muellerm@princeton.edu

+ ramanvr@umich.edu

Introduction: Uncertainties in turbulent combustion simulations arise from a number of sources including operating parameters such boundary conditions, model parameters such as chemical kinetic rates, and structural uncertainties associated with the form of component models. The latter two categories represent uncertainties from models and the incomplete knowledge of the underlying physics and chemistry. An important question related to these uncertainties is the source that contributes most to the total uncertainty in a simulation. Stated differently, in even a simple configuration, which model contributes most to the total simulation uncertainty: turbulence models, chemistry models (kinetic rates), or combustion models? From a research standpoint, the source contributing most to the overall uncertainty should be the target of increased research focus and effort.

For parametric model uncertainties, formal uncertainty quantification (UQ) algorithms have begun to be applied to turbulent combustion. Mueller et al. [1] conducted the first formal UQ estimation in turbulent combustion simulations, where they considered the propagation of uncertainties in chemical kinetic rates through LES calculations of the Sandia D flame and showed that uncertainties from chemical kinetics could account for at least a substantial portion of the discrepancy between the flamelet-based LES model results and the experimental measurements. Khalil et al. [2] considered the propagation of uncertainties in turbulence model parameters through LES calculations of a turbulent bluff body flame and determined that uncertainties arising from the Smagorinsky constant were larger than uncertainties arising from the turbulent Prandtl and Schmidt numbers.

While these works are certainly novel and important, they do not address the more challenging issue of structural model uncertainty or “model form” uncertainty. This uncertainty is associated with the assumptions that lead to a model, and the challenge is providing mathematical statements of uncertainty for these assumptions. In this work, a new general notion for model form uncertainty recently developed by Mueller and Raman [3], termed “peer models”, will be applied to model form uncertainties in turbulence models, specifically the subfilter scalar dissipation rate, and this uncertainty will be compared to parametric uncertainties from chemical kinetics in the Sandia D flame.

Model Form Uncertainty Quantification: All models invoke a series of assumptions. The notion of “peer models” arrives at an *estimate* for the uncertainty associated with an assumption by deriving an “equally plausible” model with the opposite assumption. This general approach could be used to derive an estimate for the uncertainty in any assumption in any model but is applied here to the subfilter scalar dissipation rate.

The most common model for the subfilter scalar dissipation rate is the linear algebraic model between the subfilter scalar dissipation rate and the subfilter variance: $\chi_{\text{sfs}} = (C_\tau/\tau)Z_v$. For closure, this model requires a parameter and a time scale. All researchers assumes that the time scale is a turbulence time scale, often given as the ratio of the filter width squared and the subfilter diffusivity: $\tau = \Delta^2/D_{\text{sfs}}$. An alternative model could be reached by assuming that the time scale is a chemical time scale, which could be obtained from a progress variable chemical source term: $\tau = \bar{\rho}\bar{C}/\bar{m}_C$. The uncertainty with the time scale assumption can then be estimated with the difference between these two models, which is conveniently recast in a composite model using a harmonic weighting of these two time scales. The weighting parameter can be assumed to be a second model parameter, in addition to C_τ , and handled with parametric UQ methods [1].

Preliminary Results: The above approach for the uncertainty in the subfilter scalar dissipation rate model has been applied to the Sandia D flame [4]. The same flamelet-based LES model used by Mueller previously [1] is used here, and the results from that work for uncertainties from chemical kinetics are leveraged in the results shown below. Like the previous work of Mueller [1], stochastic collocation is used to propagate the uncertainties. The harmonic weighting parameter for the time scale assumption is presumed to be uniformly distributed between zero and unity, and the model constant C_τ is presumed to be lognormally distributed with a geometric standard deviation of two. As preliminary work, tensor product grid collocation is used with three points in each direction, requiring a total of nine LES calculations.

Uncertainties in the temperature from the subfilter scalar dissipation rate and chemistry model are individually shown in Fig. 1 below. At this axial location, the uncertainty in the temperature is dominated by uncertainty in the scalar dissipation rate, and uncertainty from the chemistry model is essentially negligible. Since the temperature is not a strong function of kinetics, at least far from extinction as in this flame, this result, although perhaps not the relative magnitude, is somewhat expected. Further analysis, not shown here, indicates that the uncertainty from the subfilter scalar dissipation rate is dominated by the uncertainty in the time scale assumption rather than the model coefficient C_τ .

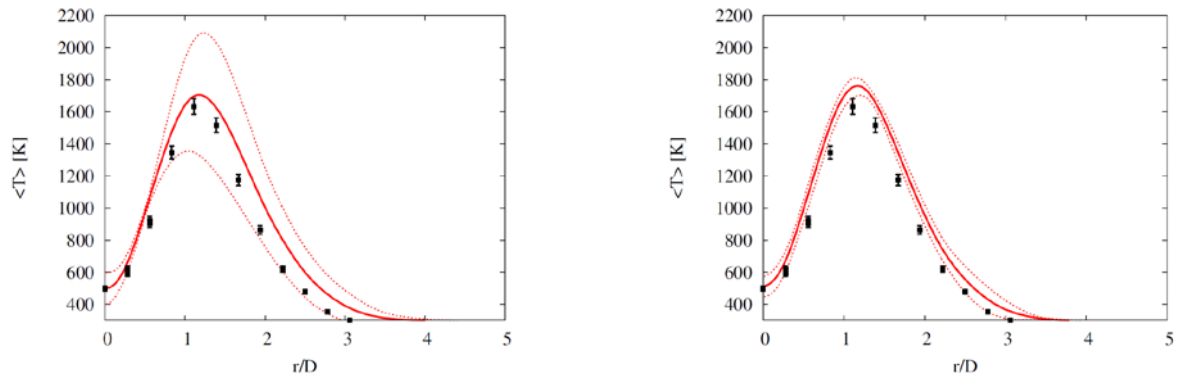


Figure 1. Comparison of uncertainties in temperature predictions arising from the subfilter scalar dissipation rate model (left) and chemical kinetics model (right). The location is $x/D = 15$. Solid lines are the mean, and the dashed lines are ± 3 standard deviations.

Uncertainties in the CO mass fraction are individually shown in Fig. 2 below. Unlike the temperature, the uncertainties in the CO prediction associated with the subfilter dissipation rate model and the chemistry model are comparable. The fact that the uncertainty from the chemistry model is larger for the CO mass fraction than for temperature is perhaps not surprising. However, the main point here is that the ranking of the sources of uncertainty is a strong function of the quantity of interest and likely also the configuration of interest.

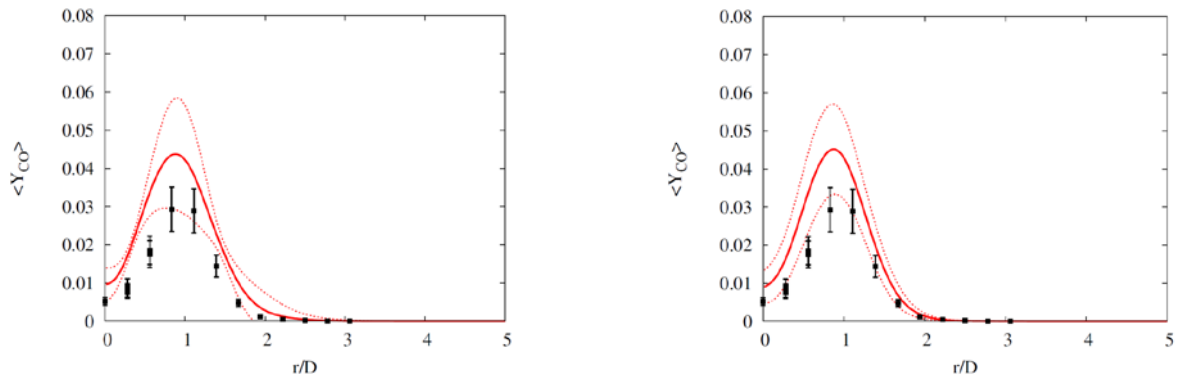


Figure 2. Comparison of uncertainties in CO mass fraction predictions arising from the subfilter scalar dissipation rate model (left) and chemical kinetics model (right). The location is $x/D = 15$. Solid lines are the mean, and the dashed lines are ± 3 standard deviations.

References:

- [1] M.E. Mueller, G. Iaccarino, H. Pitsch, Proc. Combust. Inst. 34 (2013) 1299-1306
- [2] M. Khalil, G. Lacaze, J.C. Oefelein, H.N. Najm, Proc. Combust. Inst. 35 (2015) 1147-1156
- [3] M.E. Mueller, V. Raman, 2016 Spring Meeting of the Eastern States Section of the Combustion Institute
- [4] R.S. Barlow, J.H. Frank, Proc. Combust. Inst. 27 (1998) 1087-1095

A New Mode-Switching Approach for Modeling Turbulent Flames with Inhomogeneous Partially Premixed Inlets

Bruce A. Perry^{1,*}, Michael E. Mueller¹, Assaad R. Masri²

¹ Department of Mechanical and Aerospace Engineering, Princeton University

² School of Aerospace, Mechanical, and Mechatronic Engineering, The University of Sydney, Australia

* baperry@princeton.edu

Introduction: Combustion of inhomogeneous, partially premixed fuel/air mixtures improves efficiency and reduces pollutant emissions in several emerging gas turbine and automobile engine technologies. Other systems are nominally nonpremixed or premixed but experience partial premixing due to practical limitations. For example, in aircraft combustors the vaporization of fuel droplets or the presence of multiple inlets can lead to partially premixed combustion [1]. In these systems, it is possible that there are regions of both premixed and nonpremixed combustion, as well as partially premixed regions that cannot be described by either of the limiting regimes. Therefore, improved theoretical understanding and simulation capability for multi-modal combustion are needed to accelerate the development of improved combustion systems.

To make turbulent combustion simulations computationally tractable, reduced-order models are typically employed for the underlying flame structure. In the flamelet approach, the turbulent flame is modeled as an ensemble of one-dimensional laminar premixed or nonpremixed flamelets. This allows the thermochemical state of the system to be projected onto a two-dimensional manifold parameterized by the mixture fraction (Z , representing fuel availability) and a reaction progress variable (C). However, flamelet models are only strictly applicable in the limiting regimes of premixed and nonpremixed combustion and the regime must be known *a priori*. Furthermore, premixed flamelet models require the incoming fuel/air mixture to be homogeneous, while nonpremixed models require that there be a single homogeneous fuel stream and a single homogeneous oxidizer stream.

Extended flamelet models have been developed to address these limitations. Nonpremixed models can be extended to handle cases with three inlet streams by defining an additional mixture fraction to be able to fully characterize the possible mixing states [2,3]. Alternatively, models have been developed that do not account for inlet inhomogeneity but switch between or blend the premixed and nonpremixed flamelet models based on the local value of a parameter that indicates the combustion regime. The parameter can be the flame index [4], based on the directions of gradients of fuel and oxidizer, or the combustion regime indicator [5], based on the ratio of nonpremixed and premixed terms in a two-dimensional flamelet equation.

A turbulent jet burner with controlled inhomogeneity in the central fuel/air jet has been developed at the University of Sydney and provides an excellent validation case for further partially premixed model development [6,7]. This burner features a central tube separating a fuel stream from a surrounding annulus of air that can be recessed by a variable distance from the nozzle to control the extent of premixing. At an intermediate recess distance only partial premixing occurs, resulting in a compositionally inhomogeneous inlet. Improved flame stability was observed for this inhomogeneous case and both premixed and nonpremixed combustion modes were observed in the flame. A two mixture fraction approach similar to the three stream nonpremixed flamelet models has been developed to account for the mixture inhomogeneity [8]. The objective of this work is to add the capability to switch between the premixed and nonpremixed models to account for multi-modal combustion as well.

Modeling Approach: For the case of the compositionally inhomogeneous fuel inlet of the Sydney burner, it is necessary to define two conserved scalar mixture fractions to fully characterize mixing within the system. One mixture fraction, Z , characterizes mixing between the material issuing from the nozzle and the coflowing air. A second mixture fraction, Z^* , characterizes mixing between pure fuel and air from any source. Alternatively, the fuel premixing fraction, $F = Z^*/Z$, can be used instead of Z^* . Physically, F represents the mixing of fuel with air that originated from within the jet, independent of the extent of mixing between material from the jet and coflow.

In the two mixture fraction model that was previously used to simulate this burner, the one-dimensional nonpremixed flamelet equation is solved in Z -space. The appropriate fuel side boundary condition for the flamelet calculations is variable due to the inhomogeneous fuel stream, but can be determined from the value of F . Therefore, the flamelet equations are solved with a range of fuel side boundary conditions corresponding to different values of F . The thermochemical state is then parameterized by Z , C , and Z^* or F . For LES, the flamelet solutions are calculated and convoluted with a presumed subfilter PDF *a priori* to generate a lookup table of thermochemical state information.

Here we propose an extension of the two mixture fraction nonpremixed model by implementing a new method to locally switch to a premixed model in regions where the premixed mode dominates. If the jet were a uniform flammable mixture, a propagating premixed flame front balanced by the incoming flow would be

expected. In contrast, if the jet were uniformly very rich, combustion would be essentially nonpremixed and controlled by mixing with air from the coflow. Therefore, a mode-switching approach for the inhomogeneous case can be implemented where a premixed model is applied when F , which indicates the mixing of fuel and air within the jet, is less than an upper premixed burning limit and a nonpremixed model is applied when it is greater. This approach is attractive because it is simple and does not require any new variables to be calculated. However, it introduces the upper premixed burning limit as a model parameter, initially taken to be equivalent to the upper flammability limit, and the sensitivity to this parameter will need to be assessed.

Preliminary Results: A comparison of temperature data as a function of mixture fraction for the nonpremixed LES model described above and the experimental data for the FJ200-5GP-Lr75-57 case [7] is shown in Figure 1. Near the nozzle ($x/D_j = 1$) the experimental data show a vertical drop in temperature near the stoichiometric mixture fraction, which indicates premixed combustion. The nonpremixed LES model fails to accurately predict this because it cannot account for premixed effects. At the downstream locations, the LES predictions agree well with the experiment and both follow Λ -shaped profiles, which are characteristic of nonpremixed combustion.

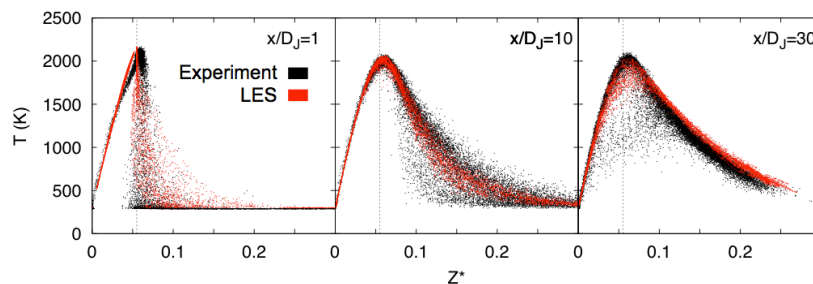


Figure 1. Comparison of scatterplots of instantaneous temperature data as a function of Z^* at three axial distances downstream of the nozzle for LES and experiment.

An *a priori* analysis based on the predictions of F using the nonpremixed two-mixture fraction model indicates that the mode-switching approach would apply the premixed model in regions where experiments indicate premixed combustion occurs and continue to apply the nonpremixed model in other regions. Mean radial profiles of F shown in Figure 2a indicate that there is a substantial region where F falls below the upper flammability limit for methane, but downstream F is uniformly above the upper flammability limit. This matches the trend of increasingly nonpremixed combustion character moving downstream that was observed experimentally. Additionally, Figure 2b shows that the scatter data points where the nonpremixed LES predictions disagree with the experiment would instead have the premixed model applied. Thus, the mode-switching approach outlined above has the potential to resolve discrepancies between the model and experiment, and this will be verified as the model is implemented.

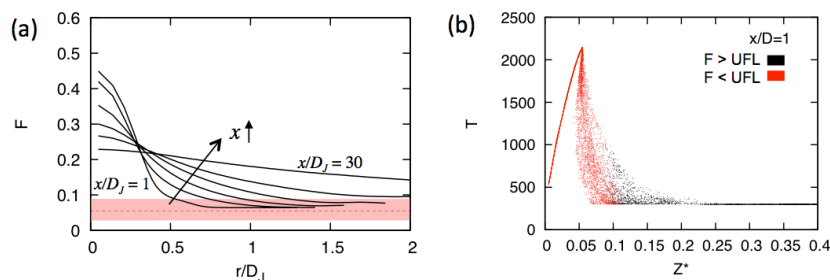


Figure 2. (a) Mean predicted profiles of F based on LES predictions with the region where F falls within the methane flammability limits highlighted in pink. (b) LES temperature scatterplot with points where F is within the flammability limits indicated in red.

References:

- [1] L.Y.M. Gicquel, G. Staffelbach, T. Poinso, *Prog. Energy Combust. Sci.* (2012) 782-817
- [2] C. Hasse, N. Peters, *Proc. Combust. Inst.* 30 (2005) 2755-2762
- [3] M. Ihme, J. Zhang, G. He, B. Dally, *Flow Turb. Combust.* 89 (2012) 449-464
- [4] P. Domingo, L. Vervisch, K. Bray, *Combust. Theory Modeling* 6 (2002) 529-551
- [5] E. Knudsen, H. Pitsch, *Combust. Flame* 156 (2009) 678-696
- [6] S. Meares, A.R. Masri, *Combust. Flame* 161 (2014) 484-495
- [7] R. Barlow, S. Meares, G. Magnotti, H. Cutcher, A.R. Masri, *Combust. Flame* 162 (2015) 3516-3540
- [8] B.A. Perry, M.E. Mueller, A.R. Masri, *Proc. Combust. Inst.* 36 (2016) submitted

Differential diffusion effects and flamelet analysis in a hydrogen jet in cross flow configuration

S. Popp^{a)}, F. Dietzsch^{a)}, A. Abdelsamie^{b)}, D. Thévenin^{b)}, C. Hasse^{a)}

^{a)} *Numerical Thermo-Fluid Dynamics, TU Bergakademie Freiberg, Germany*

^{b)} *Fluid Dynamics and Technical Flows, Otto-von-Guericke-Universität Magdeburg, Germany*

Sebastian.Popp@iec.tu-freiberg.de

As part of the changing energy landscape, the influence of hydrogen as fuel will further increase. Fuel flexibility of conventional combustion applications is a crucial issue for their development, when using e.g. blends of hydrogen and fossil fuels or even pure hydrogen. It is commonly known that conventional combustion applications cannot operate with hydrogen or hydrogen addition without adjusting the combustion chamber design, due to different combustion characteristics and flame stabilization mechanisms. Major differences occur e.g. due to an increased diffusivity. An increasing amount of hydrogen leads to differential diffusion effects, which alter the transport mechanisms towards the reaction zone. Previous studies, looking at these effects, were mainly focused on simple jet flames and concluded that detailed diffusion modeling is crucial and must be considered even for turbulent combustion modeling [1]. However, a consistent modeling approach to include differential diffusion in flamelet-based methods is still an open scientific issue.

The present study addresses differential diffusion in a more complex jet in cross flow (JICF) configuration, which is applied in systems where rapid mixing is required, e.g. aircraft and stationary gas turbines as well as recent micro gas turbine applications for hydrogen combustion [2]. Therefore, Direct Numerical Simulations (DNS) of a hydrogen JICF were conducted, using the recently developed DNS code DINO [3]. The configuration considered here is similar to a previous study [4]. The basic setup of the JICF computations is shown in Fig. 1, with an enlarged snapshot of the jet. The analysis of the JICF is focused on differential diffusion effects and their influence on the flame structure on the lee- and windward side of the jet.

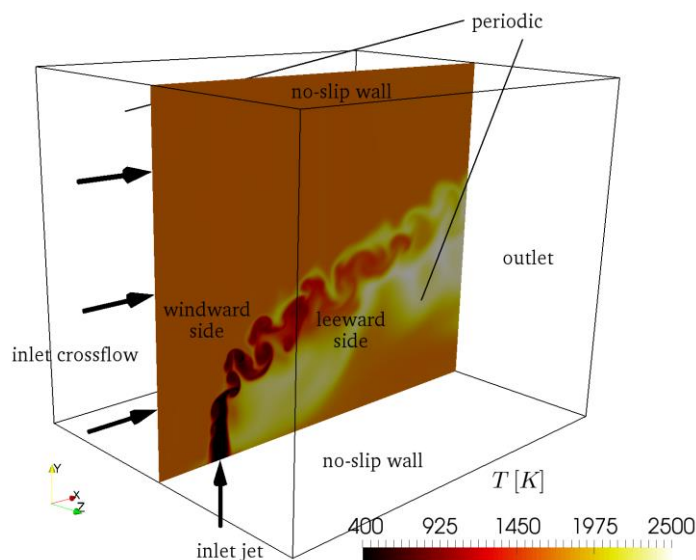
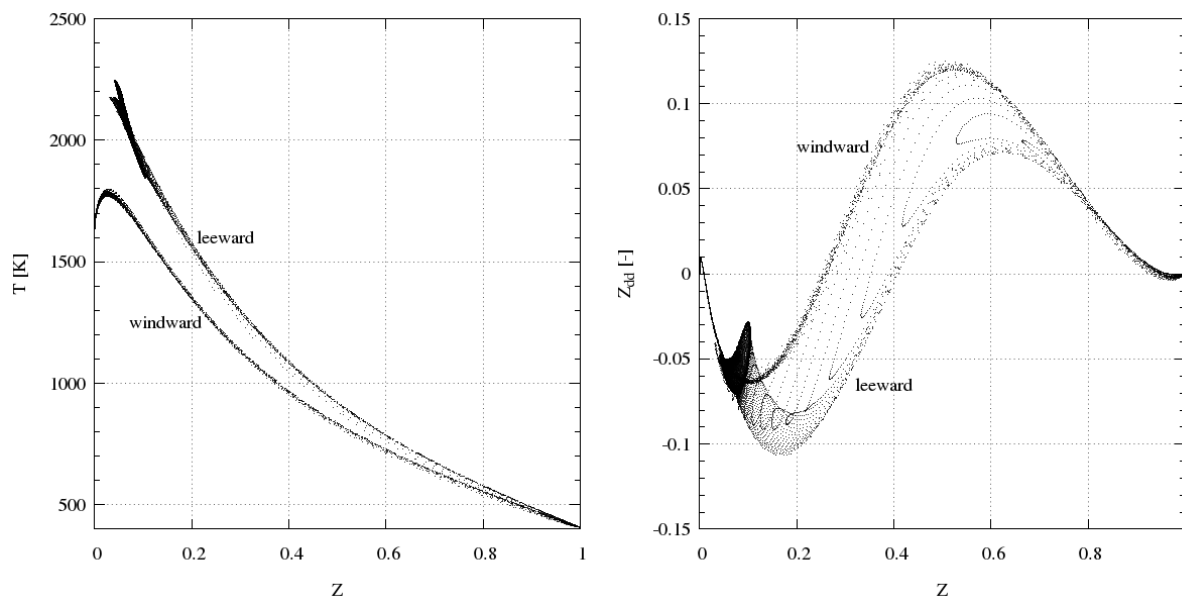


Figure 1: Setup of the JICF DNS and an instantaneous snapshot of the temperature distribution.

Figure 2 shows instantaneous results of the temperature and the differential diffusion parameter Z_{dd} , both conditioned on the mixture fraction, in a region near the jet inlet. This part of the flow field is characterized by a distinct separation of the temperature profiles. This is due to the different flow conditions on the lee- and windward side of the jet. Strong mixing

processes mainly dominate the windward side. The high shear stresses between the jet and the cross flow and the corresponding high scalar dissipation rates lead to reduced temperatures. On the leeward side, a flame is stabilized in the wake with lower strain rate as observed from the upper branch of the temperature profiles. Additionally, a significant influence of differential diffusion in this near-inlet region is found, which can be quantified by the differential diffusion parameter Z_{dd} . Again, significant differences can be observed for the lee- and windward side, see right side of Fig. 2.



TM

Figure 2: Instantaneous results of temperature (left) and differential diffusion parameter Z_{dd} (right) conditioned on the mixture fraction near the jet inlet.

The poster will show a detailed comparison of flamelet-based modeling strategies and the DNS data. The analysis will be performed for the lee- and the windward side separately and DNS data will be extracted accordingly. For the analysis, the influence of the turbulent/non-turbulent interface (T/NT), which separates the flow into turbulent and non-turbulent regions in free shear flows through a sharp vorticity increase across the interface, will be considered. Such information can be used to improve flamelet-based modeling approaches.

In addition, a DNS with unity Lewis will be performed and used for comparison, which allows quantifying the influence of differential diffusion on the overall flame structure and flame stabilization mechanisms.

References

- [1] H. Pitsch. Unsteady flamelet modeling of differential diffusion in turbulent jet diffusion flames. *Combustion and Flame*, 123(3):358–374, 2000
- [2] P. Jeschke and A. Penkner. A novel gas generator concept for jet engines using a rotating combustion chamber. *ASME. J. Turbomach.*, 137(7):071010–071010–8, 2015
- [3] A. Abdelsamie, G. Fru, T. Oster, F. Dietzsch, G. Janiga, and D. Thévenin. Towards direct numerical simulations of low-Mach number turbulent reacting and two-phase flows using immersed boundaries. *Computers & Fluids*, 131:123–141, 2016
- [4] S. Lyra, B. Wilde, H. Kolla, J. M. Seitzman, T. C. Lieuwen, and J. H. Chen. Structure of hydrogen-rich transverse jets in a vitiated turbulent flow. *Combustion and Flame*, 162(4):1234 – 1248, 2015

Large-Eddy-Simulation of Auto-ignition in a Turbulent Jet in Hot Coflow

Juliane Prause, Christoph M. Arndt, Berthold Noll, Manfred Aigner

Institute of Combustion Technology, German Aerospace Center (DLR), Stuttgart, Germany

E-mail: juliane.prause@dlr.de

Auto-ignition in a turbulent methane jet in a hot oxidizer flow is modelled with Large-Eddy-Simulation (LES). The time-averaged results are in good agreement with experimental reference data and a detailed analysis of the transient ignition process is conducted.

The combustion of fuel jets in hot turbulent flows is of relevance in many low pollution combustion systems, such as in staged gas turbine combustion, in FLOX or MILD combustion systems and in scramjet combustors. The jet-in-hot coflow configuration is a convenient generic test case for the experimental analysis of relevant flame characteristics as well as for validation of numerical models. Numerous studies have already been conducted for this configuration, which provide a good fundamental understanding of lifted jet flames in hot coflow [1, 2]. It was found that these flames are mainly stabilized by auto-ignition [3, 4]. In most test cases, a large fluctuation of the instantaneous lift-off height was observed. Separate ignition kernels are formed upstream of the flame base and the flame front can be strongly disrupted. In many applications, these ignition locations are widely scattered [2, 3]. To ensure a reliable operation of the above mentioned applications, a good prediction of the ignition distribution is essential [5]. Therefore a better understanding of the transient ignition process is required. However, the majority of the previous studies were focused on steady-state characteristics. Recently, Arndt et al. [6] conducted a detailed experimental analysis of transient ignition events in a methane jet in hot vitiated coflow. They applied high-speed planar Rayleigh scattering to measure mixture fraction and temperature simultaneously. They found that ignition occurs at the outmost periphery of large shear layer vortices at very lean mixture fractions and low scalar dissipation.

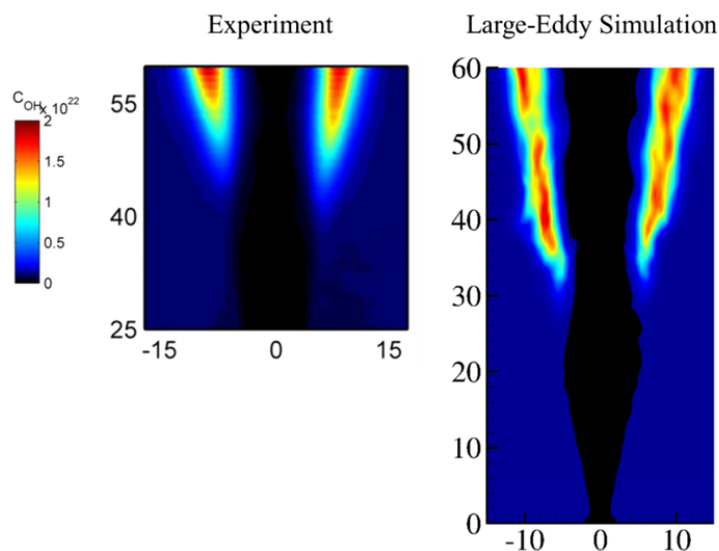


Figure 1: Time-averaged OH concentration

In the present contribution, Large-Eddy Simulation of this test case is conducted to obtain supplemental information on high resolved lean mixture fraction and pre-reaction radical species. Furthermore, a residence time model is

utilized to compare the local combustion states in the turbulent jet with calculations of enclosed homogeneous systems. In the numerical simulation, the chemical kinetics are described directly by the reduced DRM19 mechanism and additional transport equations are solved for all species (except nitrogen) and the enthalpy. The influence of sub-grid fluctuations of temperature and species on the cell-averaged chemical source term is considered by a multivariate assumed joint probability-density-function (PDF) closure [7].

First, time-averaged quantities are compared to validate the numerical simulation. Figure 1 shows the quantitative distribution of time-averaged hydroxyl concentration. A good agreement is achieved between simulation and experimental data. The lift-off height can be predicted within an accuracy of 30%. The remaining difference is mainly attributed to uncertainties in the kinetic mechanism ($\pm 25\%$ in ignition delay time) and measurement uncertainties of the coflow temperature. The coflow temperature could be assessed experimentally with an accuracy of 1-2%. Nevertheless, due to the high temperature sensitivity of auto-ignition, this results in a variation of 20-40% in ignition delay time.

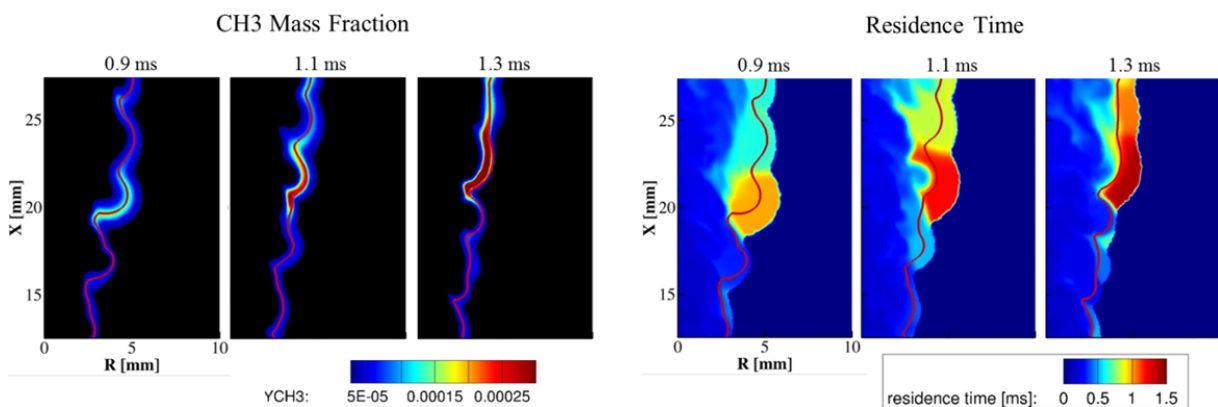


Figure 2: Transient Ignition Event

The transient evolution of an ignition kernel is presented in figure 2. The build-up of the methyl concentration marks the reaction. The red line corresponds to the isoline of the most reactive mixture fraction. In accordance with the experimental findings, the ignition takes place at the periphery of large vortical structures. The numerical results show, that ignition takes place along the most reactive mixture fraction at low scalar dissipation. Furthermore, the results reveal that these vortices have a significantly higher residence time compared to the neighbored jet fluid. The comparison with homogeneous reactor calculations shows that there is also a retarding influence of small scale turbulence on the ignition by transport processes. However, the impact is smaller compared to the large-scale effects. This shows that the spatial scatter of ignition events depends mainly on large-scale vortical structures.

References

- [1] Cabra et al., 2002, Proc. Combust. Inst. 29, pp. 1881-1888
- [2] Markides und Mastorakos, 2005, Proc. Combust. Inst. 30, pp. 883-891
- [3] Gordon et al., 2007, Combustion and Flame 151, pp. 495-511
- [4] Yoo et al., 2009, J. Fluid Mech. 640, pp. 453-481
- [5] Fleck et al., 2013, Proc. Combust. Inst. 34, Nr. 2, pp. 3185-3192
- [6] Arndt et al., 2016, Combustion and Flame, vol. 167, pp. 60-71
- [7] Girimaji, 1991, Combust. Sci. Technol., pp. 177-196

Analysis of the reaction zone dynamics in a turbulent premixed bluff-body burner based on a flame resolved simulation with tabulated chemistry

F. Proch^{1,*}, P. Domingo², L. Vervisch², A.M. Kempf¹

¹ *Chair of Fluid Dynamics, Institute for Combustion and Gasdynamics (IVG), University of Duisburg-Essen, 47048 Duisburg, Germany*

² *CORIA - CNRS, Normandie Université, INSA de Rouen, Technopole du Madrillet, BP 8, 76801 Saint-Etienne-du-Rouvray, France*

* fabian.proch@uni-due.de

Detailed analyses for the interaction of the local topology of the progress variable isosurfaces with the turbulent velocity field are presented for a lean premixed methane/air bluff body burner investigated experimentally at Cambridge University by Hochgreb and co-workers, and at Sandia National Laboratories by Barlow and co-workers [1, 2]. The analyses are carried out for a highly resolved simulation of the burner with a grid resolution of 100 μm , which enables to resolve the laminar (thermal) flame thickness of 500 μm on the computational grid [3]. The size of the computational domain was chosen as 112x120x120 mm, leading to a total number of 1.6 billion cells. The simulations were performed with the Cartesian inhouse code ‘PsiPhi’, using a third-order Runge-Kutta scheme for time integration and second order spatial discretization schemes [4, 5]. The combustion process is described by the premixed flamelet generated manifolds (PFGM) tabulated chemistry approach [6], where a non-normalized progress variable and the mixture fraction were used as control variables [5]. Visualizations of the instantaneous velocity, equivalence ratio and progress variable field are shown in Fig. 1.

The sufficient resolution of the flame- and velocity scales is carefully checked by evaluating the local Kolmogorov lengthscales and the integrated source term along the flame normal direction. It is demonstrated that all the relevant scales inside the flame have been resolved in a direct numerical simulation (DNS) sense, the small amount of under-resolved velocity scales that was still present in the fresh gas far upstream was dissipated before entering the flame zone. The simulation is validated by comparison of temporal mean and rms profiles obtained from the simulation against experimental data as shown in Fig. 2 for velocity, temperature, equivalence ratio and major species mass fractions.

The combustion process in the burner is characterized by regime diagrams [7], it is shown that the intensity of the turbulence-flame interaction depends on the distance from the burner as well as on the progress of the reaction. The local structure of the flame is compared to the laminar flame structure using ensemble-averaged and flamelet-averaged statistics. Despite the more complex burner configuration, the obtained findings are mostly comparable to the ones from DNS of canonical flame configurations – establishing a direct link that was rarely available before. A preferential alignment of the most compressive strain rate and as a consequence a slightly thinned turbulent flame compared to the laminar flame is found. It is shown that the flame displacement speed [8] takes partially negative values and is barely correlated with the flame consumption speed integrated along the flamelets. The degree of correlation can be improved if only the sum of flame normal diffusive flux and reaction source term is considered for the consumption speed. Due to the broad range of turbulence levels found in the burner the generated quasi-DNS database is a challenging test case for sub-grid scale (SGS) wrinkling factor models that enables to perform a-priori analyses under more realistic conditions.

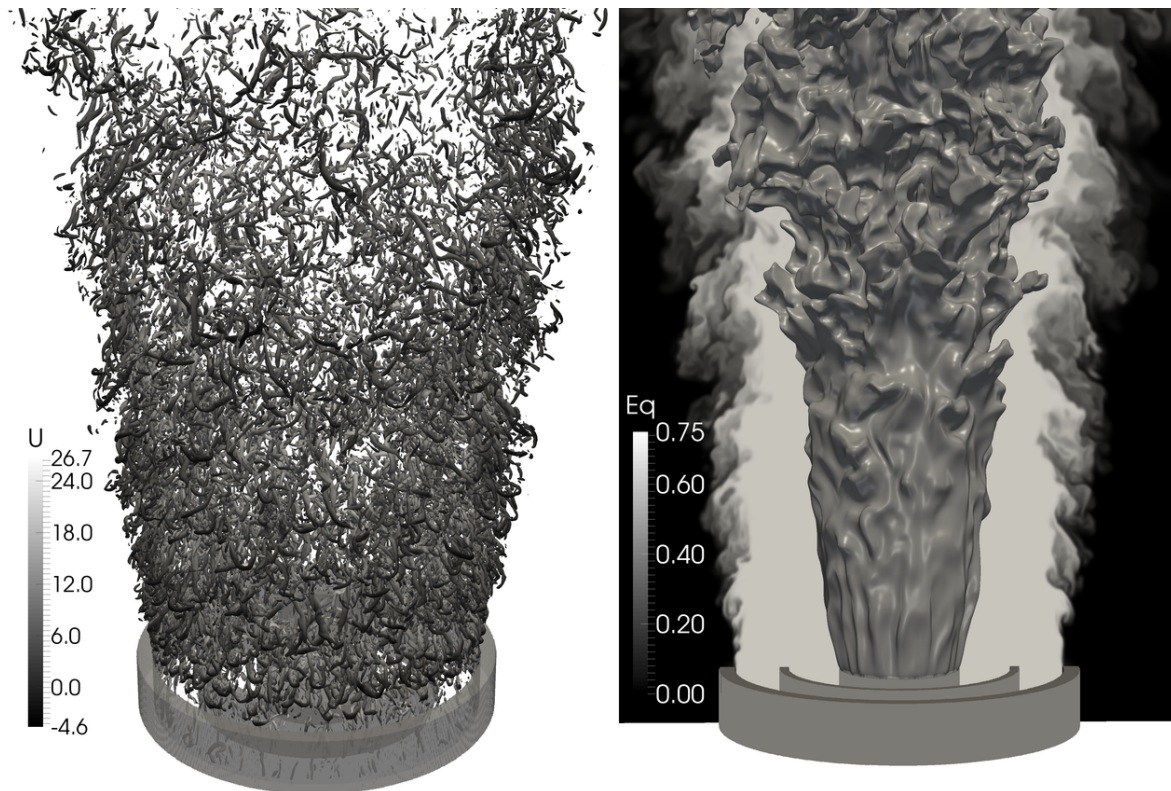


Figure 1: Iso-q-criterion colored by the axial velocity component (left) and equivalence ratio contours in the burner-mid section overlaid with the isosurface representing 50% reaction progress (right).

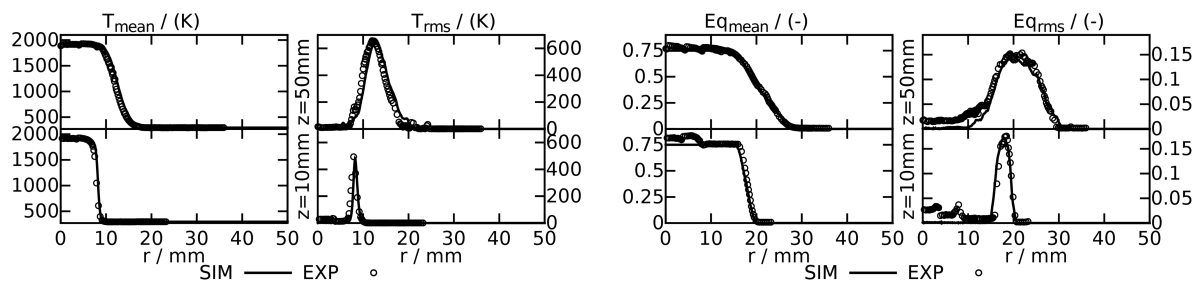


Figure 2: Comparison of radial mean and rms profiles for temperature (left) and equivalence ratio (right) obtained from the simulations with the measurements from Sweeney et al. [1] at different downstream positions.

References

- [1] M. S. Sweeney, S. Hochgreb, M. J. Dunn, R. S. Barlow, *Combust. Flame* 159 (2012) 2896 – 2911.
- [2] R. Zhou, S. Balusamy, M. S. Sweeney, R. S. Barlow, S. Hochgreb, *Combust. Flame* 160 (2013) 2017 – 2028.
- [3] F. Proch, P. Domingo, L. Vervisch, A. M. Kempf, *Combust. Flame* (under review) –.
- [4] A. M. Kempf, B. Geurts, J. C. Oefelein, *Combust. Flame* 158 (2011) 2408–2419.
- [5] F. Proch, A. M. Kempf, *Combust. Flame* 161 (2014) 2627 – 2646.
- [6] J. A. van Oijen, R. J. M. Bastiaans, L. P. H. de Goeij, *Proc. Combust. Inst.* 31 (2007) 1377–1384.
- [7] N. Peters, *Turbulent Combustion*, Cambridge University Press, 2000.
- [8] C. H. Gibson, *Phys. Fluids* 11 (1968) 2305–2315.

MIXTURE FRACTION-PROGRESS VARIABLE DEPENDENCE IN PARTIALLY-PREMIKED FLAMES

E.S. Richardson^a, T.B. Matheson^a, N.H. Meah^a, D.O. Lignell^b, C.S. Yoo^c, J.H. Chen^d

^a*Faculty of Engineering and the Environment, University of Southampton, Southampton, SO17 1BJ, UK, e.s.richardson@soton.ac.uk*

^b*Department of Chemical Engineering, Brigham Young University, Provo, UT 84602, USA*

^c*Department of Mechanical Engineering, UNIST, Ulsan 689-798, Republic of Korea*

^d*Combustion Research Facility, Sandia National Laboratories, Livermore, CA 94551-0969, USA*

It is both convenient and conventional to assume that mixture fraction and progress variable are statistically independent in turbulent partially-premixed combustion modelling. This assumption simplifies presumed-probability density function (pdf) modelling for the joint mixture fraction–progress variable pdf, implying that it can be expressed as the product of the marginal-pdf of mixture fraction and the marginal-pdf of progress variable,

$$p_{\xi,c}(\eta, \zeta) = p_{\xi}(\eta)p_c(\zeta), \quad (1)$$

where η and ζ are the sample space variables for mixture fraction ξ and progress variable c respectively. The assumption of statistical independence can give adequate model predictions in some circumstances, however there is no general theoretical basis for assuming statistical independence between mixture fraction and progress variable, and the limitations of the assumption of statistical independence are not well established. The objective of this study is to use statistical analysis of empirical joint mixture fraction–progress variable pdfs, obtained from several different Direct Numerical Simulation (DNS) datasets for partially-premixed combustion, in order to characterise the mixture fraction–progress variable dependence. Three turbulent combustion datasets shown in Fig. 1 are considered: first, data for equivalence ratio-stratified flame propagation in the thin reaction zones regime [1]; second, data for a non-premixed jet flame with significant levels of localised extinction [2]; and third, DNS data for an autoigniting slot jet flame [3].

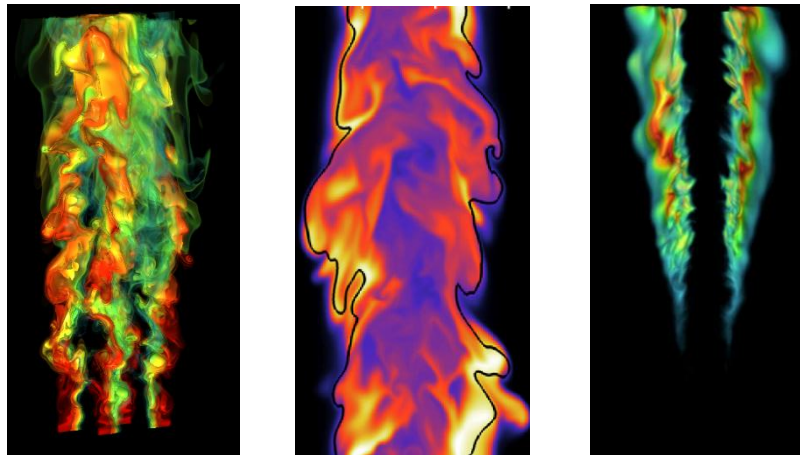


Figure 1: (left) Equivalence ratio stratified combustion DNS showing volume rendering of heat release coloured by mixture fraction [1]; (centre) Extinguishing non-premixed flame showing temperature field and stoichiometric iso-surface from Case 2 in Ref. [2]; (right) cross section through the OH mass fraction field in autoigniting ethylene jet flame DNS [3].

The statistical dependence of the two variables is visualised by defining a mathematical transformation of the data in order to remove the contributions of the marginal distributions, as illustrated in Fig. 2. The influence of the statistical dependence on the evaluation of statistical moments, such as mean reaction rates predicted in conjunction with double conditional moment closure (DCMC) modelling, are then evaluated by integrating the DCMC properties over (a) the empirical joint-pdf, (b) the independent joint-pdf based on the empirical marginal pdfs based on Eq. 1, or (c) a modelled joint-pdf with statistical dependence specified by the Plackett copula and the empirical covariance [4].

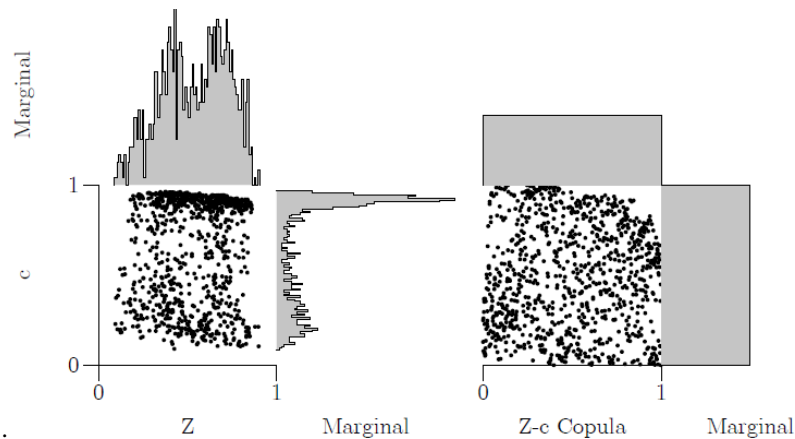


Figure 2: Illustration of the *demarginalisation* procedure, converting empirical marginal distributions (left) into uniform marginals (right) in order to reveal the underlying structure of the statistical dependence (scatter).

The lean stratified flame propagation data shows strong positive or negative mixture fraction–progress variable correlations depending on the alignment of the mean mixture fraction and mean progress variable gradients. This alignment may be introduced by the inlet boundary conditions, but analysis of the correlation transport equation shows that it is also weakly influenced by differential propagation effects due to the variation of flame speed with mixture fraction. The statistical dependence in the extinction-reignition case [2] displays correlations of different sign in richer and leaner mixture, and the signs of these correlations switch during the transition from extinction to reignition. The mechanism governing this transition is explained by considering the evolution of the progress variable (normalised as a function of mixture fraction) in extinguishing and autoigniting CMC simulations. In the lifted flame there is generally a positive correlation between mixture fraction and progress variable in the fuel-lean mixture and a negative correlation in fuel-rich mixture on account of progress variable increasing first in the vicinity of the *most reactive* mixture fraction and the peak progress variable then migrating closer to stoichiometric, seen in Fig. 3 (top row). The dependence structure (Fig. 3 middle row) is well-modelled by the Plackett copula (Fig. 3 bottom row) in the richer and leaner mixture but fails to account for the bimodal structure seen close to mean stoichiometric conditions. The analysis suggests that assumption of statistical independence gives relatively small error in the evaluation of the mean reaction rate in the lean stratified flame case, due to the generally low absolute magnitude of the mixture fraction variance, but significant errors in the extinction/reignition and lifted flame cases. While not able to represent the two-branched structure seen close to mean-stoichiometric conditions, the Plackett copula provides a relatively simple approach for including effects of statistical dependence in presumed-pdf modelling for partially-premixed flames.

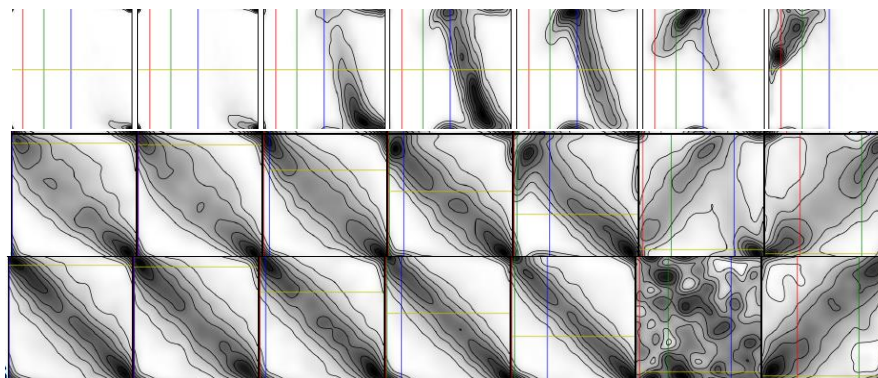


Figure 3: Lifted autoigniting ethylene jet [3] one-point kernel density estimation plots at $x/H=15$ from the centreline (left) to the edge of the jet (right), showing: (top) the empirical joint-pdf of $p_{\xi,c}(\eta, \zeta)$; (middle) the demarginalised empirical distribution; (bottom) the Plackett copula for uniform marginal distributions.

References

- [1] Richardson, E.S. and J.H. Chen (2016). “Analysis of turbulent flame propagation in equivalence ratio-stratified flow”. *Submitted to Proceedings of the Combustion Institute*.
- [2] Lignell, D.O, J.H. Chen *et al.* (2011). *Combustion and Flame* 158 (5) 949–963.
- [3] Yoo, C.S, Richardson, E.S. *et al.* (2011). *Proceedings of the Combustion Institute* 33.1, 1619–1627.
- [4] Plackett, R.L. (1965) *Journal of the American Statistical Association* 60.310, 516–522.

LES/FDF of a lean premixed methane counterflow flame

M. Rieth^a, F. Proch^a, A. M. Kempf^{a,b}

^a *Chair of Fluid Dynamics, Institute for Combustion and Gasdynamics (IVG), University of Duisburg-Essen, Duisburg, 47048, Germany*

^b *Center for Computational Sciences and Simulation (CCSS), University of Duisburg-Essen, 47048 Duisburg, Germany*

e-mail: martin.rieth@uni-due.de

A transported filtered density function (FDF) method has been implemented and used to simulate the Imperial College turbulent opposed jet (TOJ) flame [1] in a combined large eddy simulation (LES)/Lagrangian Monte Carlo (LMC) framework. The LMC particles describe the chemical composition, whereas the LES is used to solve for the flow field.

The PsiPhi code [2] solves the filtered Navier-Stokes equations in low-Mach number formulation and with an eddy-viscosity closure. The Lagrangian and Eulerian fields are consistent through coupling by a density feedback from the particles to the Eulerian field and by the interpolation of the LES velocity onto the particle positions by the parabolic edge reconstruction method (PERM) [3]. A formulation as reported in previous studies [4] is used for the FDF transport while the modified Curl's mixing model provides closure for the fluxes in composition space.

The Imperial College TOJ experiment features a back-to-back configuration with both nozzles supplied with a lean methane-air mixture with equivalence ratios of $\Phi = 0.8$ and $\Phi = 0.9$. Turbulence inside the nozzles is generated by fractal grids. Velocity and progress variable statistics are obtained by particle image velocimetry with a density segregation method.

The simulation set-up consists of both nozzles with the inlets located at the fractal grids. Particles are only used between the nozzles. The resulting load balancing issue is solved by distributing the chemistry integration across all processors such that computational expense is reduced significantly. Around 8 million particles are used to represent the region near the flame. The cell size is $(0.5 \text{ mm})^3$, which leads to an overall number of 1.7 million cells.

The simulation results show that progress variable statistics are matched well by the LES/FDF, Fig. 1. The agreement for $\Phi = 0.9$ is generally slightly better than for $\Phi = 0.8$. Velocity statistics show satisfactory agreement. Species mass fraction scatterplots in mass fraction-progress variable space (Y-C-space) are shown to illustrate the influence of turbulence on the chemistry. Minor species, such as the H-radical, are naturally affected more strongly by turbulence than the major species and hence show a larger scatter in Y-C-space, Fig. 2. In accordance to the $\Phi = 0.8$ case being closer to extinction, this case shows a lower level of H-radicals, which are necessary to sustain a stable flame.

The flame is visualized for different instants in time, illustrating a highly unsteady behavior. During some events, the two flame fronts touch and local extinction occurs while during other events the flame front is wrinkled strongly and thickened by the turbulence.

Overall, the conducted LES/FDF simulations reproduce well the Imperial TOJ methane back-to-back configuration.

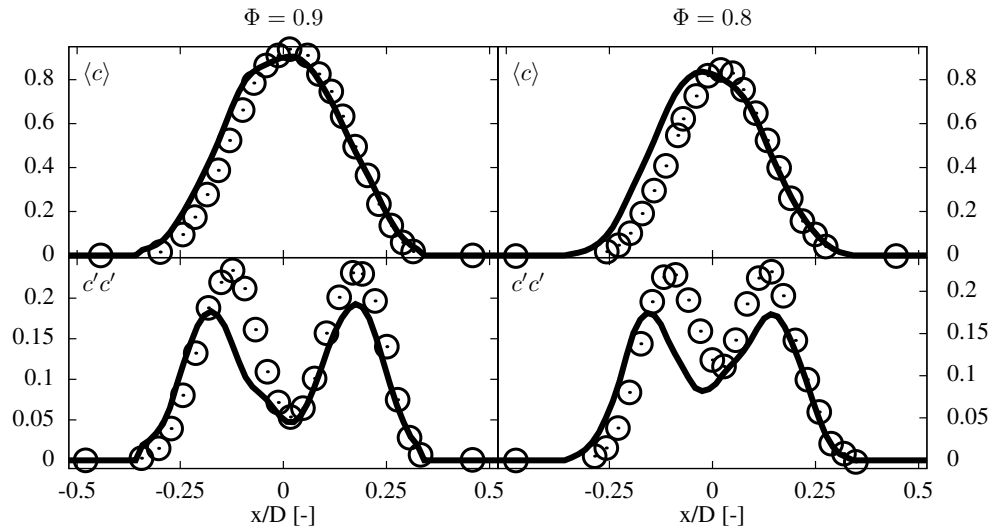


Figure 1: Normalized progress variable mean and rms values along the centerline for $\Phi = 0.9$ and $\Phi = 0.8$.

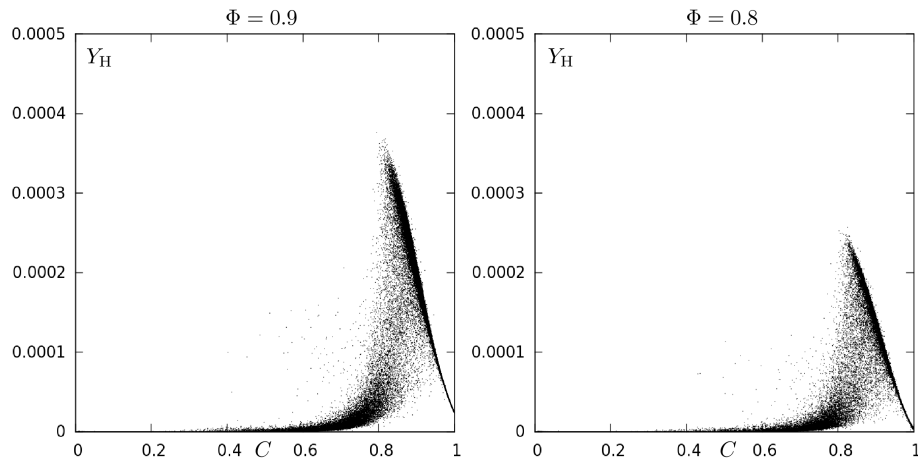


Figure 2: Scatterplot of H-radical mass fraction vs. normalized progress variable for $\Phi = 0.9$ and $\Phi = 0.8$.

References

- [1] K. Goh, P. Geipel, R. Lindstedt, *Combust. Flame* 161 (2014) 2419 – 2434.
- [2] A. M. Kempf, B. Geurts, J. C. Oefelein, *Combust. Flame* 158 (2011) 2408–2419.
- [3] R. McDermott, S. B. Pope, *J. Comput. Phys.* 227 (2008) 5447–5491.
- [4] V. Raman, H. Pitsch, *Proc. Combust. Inst.* 31 (2007) 1711 – 1719.

RAMAN/RAYLEIGH SPECTROSCOPY IN PREMIXED METHANE FLAMES INCLUDING HYDROGEN ADDITION

S. Schneider¹, N. Luciano¹, D. Geyer², A. Zschutschke³, A. Scholtissek³, C. Hasse³, A. Dreizler^{1*}

¹Technische Universität Darmstadt; ²Hochschule Darmstadt; ³TU Freiberg; Germany
dreizler@csi.tu-darmstadt.de

Addition of hydrogen to carbon-based fuels is one scenario for the progress of renewable energies. Addition of hydrogen extends the lean flammability limit and thus carries the potential for lower temperatures and subsequently a reduction in the NO_x formation rate. Combustion systems burning blends of methane and hydrogen have to be thoroughly adapted since the laminar burning velocities increase up to the factor of seven by adding hydrogen to the fuel. Therefore deeper insight into the underlying physico-chemical processes is required. On the experimental side, this can be achieved by simultaneously measuring major species concentrations and temperature by spontaneous Raman/Rayleigh spectroscopy. In combination with numerical simulations, in addition to global characteristics such as the burning velocity, the detailed flame structure can be analyzed. Two laminar flame configurations shown in Fig. 1 were investigated for lean premixed CH₄/H₂ mixtures in this joint work: a jet flame and vertical flame. The vertical flame (V-flame) closely represents a freely propagating flame.

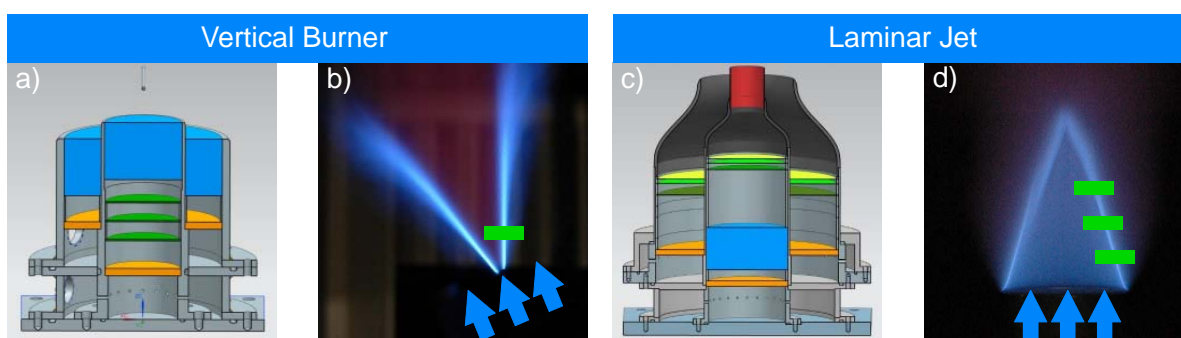


Fig. 1: Sectional drawing of the V-flame (Fig. 1a) and laminar jet flame (Fig. 1c) with flow homogenization (orange: sinter matrix, green: metal sieve, Blue: honeycomb). Fuel/air mixture from central orifice, surrounding coflow. Fig. 1b and 1d: time averaged image of the chemiluminescence of V-Flame and laminar jet flame. Green: laser probe volume, in heights of 10, 20 and 30 mm above the burner nozzle. Blue arrows: fresh gas stream lines.

The burner to stabilize the V-flame (Fig. 1a) is equipped with a honeycomb of 60 mm diameter and screens (1 mm mesh size) for flow homogenization. A 1 mm wire is utilized to stabilize the flame (Fig. 1a). In the laminar jet burner screens and a flow contraction (ratio 5.5) upstream of the nozzle (diameter 31 mm) ensure the flow homogenization. A premixed CH₄/H₂ blend with a constant equivalence ratio $\phi = 0.8$ was used in both burners. The hydrogen fraction was varied in steps of 10 % from 0 vol-% to 40 vol-%. Combined 1D Raman/Rayleigh spectroscopy was applied along a 6 mm probe volume and provides major species concentrations (CO₂, O₂, CO, N₂, CH₄, H₂O, H₂) as well as temperature. Fig. 1 shows the dependency of the intersection of the 1D probe volume with the flame front for the V-flame (Fig. 1b) and the laminar jet (Fig. 1d). First, a planar V-flame formed over the vertically tilted burner was measured in order to provide a non-stretched reference case. Secondly, measurements in the laminar jet at axial probe volume locations of 10, 20 and 30 mm downstream the burner nozzle exit allowed for different overall negative stretch rates in the flame cone in the range of -30 to -80 1/s (calculated according to [1]). A custom-made laser system (600 mJ/pulse @532 nm, 450 ns pulse length FWHM, Quantel) was used as a light source for Raman/Rayleigh scattering. A minimum spatial beam diameter of 120 μm at $1/e^2$ was achieved by focusing the laser into the probe volume using a 750 mm lens. Thus, the laser system allowed for measurements with an improved spatial resolution of $\sim 150 \mu\text{m}$.

Fig. 2 shows the experimental data for the planar V-flame and the simulation results obtained for a freely propagating flame employing detailed transport modeling including thermo-diffusion and detailed chemistry for the 40 vol% H₂ case. Experimental results and numerical data agree very well on the vertical flame for all species (equally good for the other H₂ ratios not shown here). This confirms that the V-flame configuration yields a completely unstretched (no strain, no curvature) flame. Furthermore, the approach chosen for transport and chemistry is suitable for the mixtures investigated.

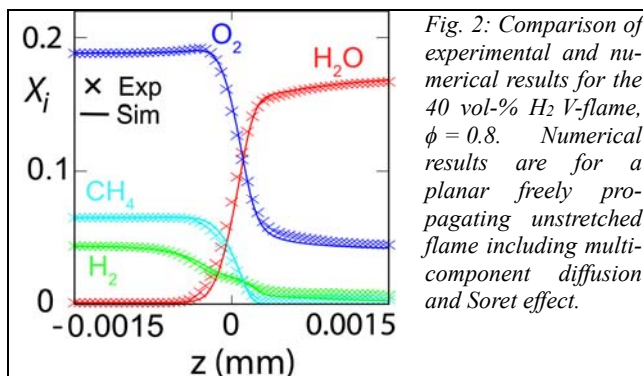
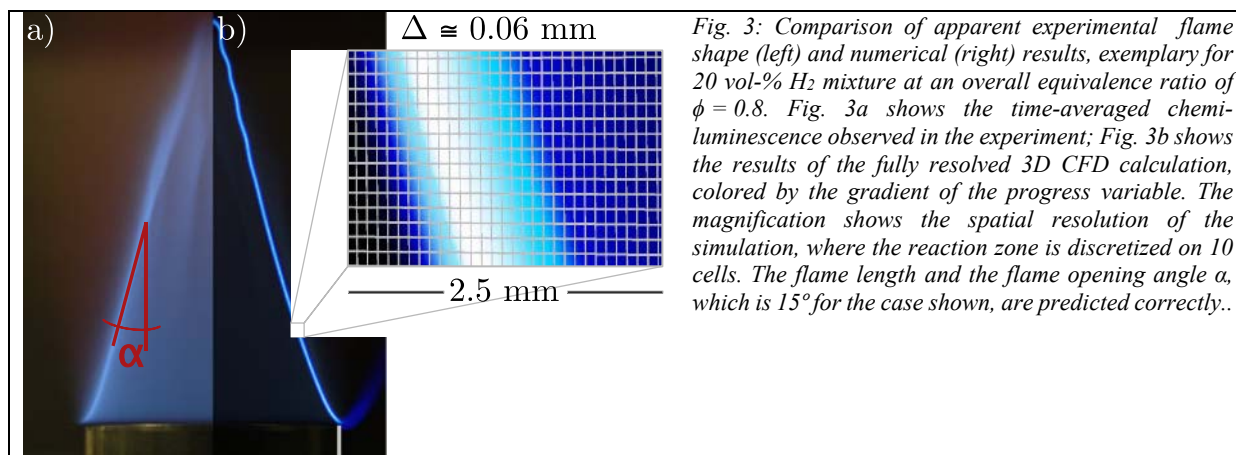
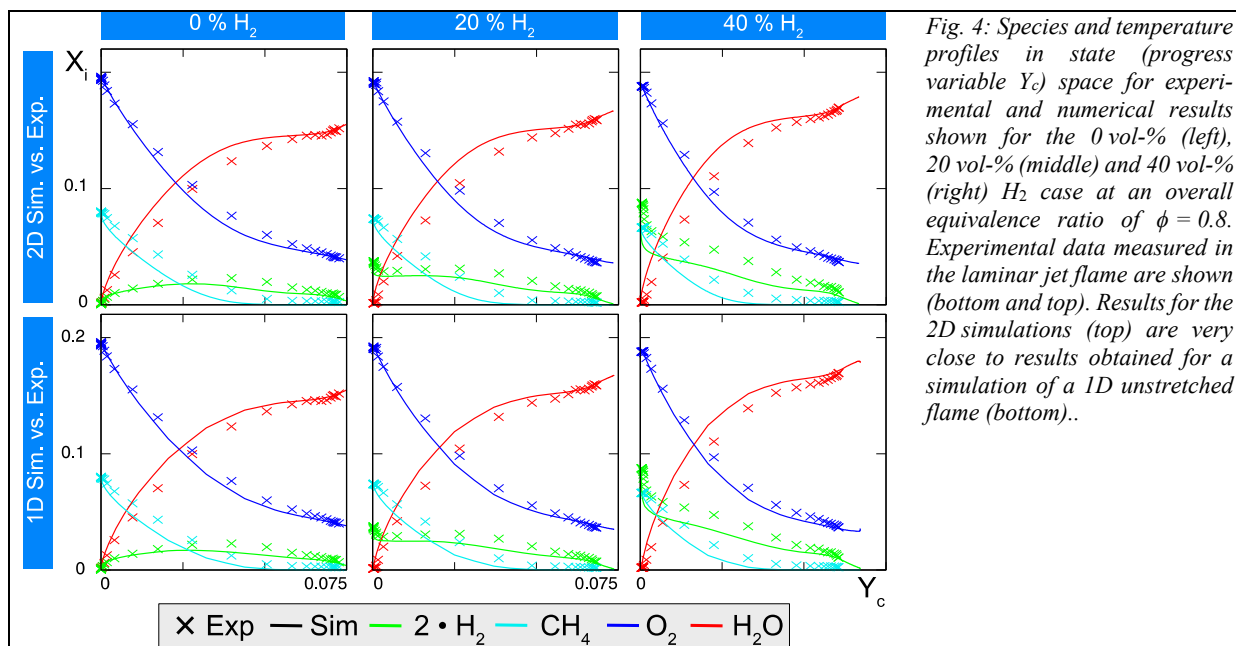


Fig. 2: Comparison of experimental and numerical results for the 40 vol-% H₂ V-flame, $\phi = 0.8$. Numerical results are for a planar freely propagating unstretched flame including multi-component diffusion and Soret effect.

For the laminar jet burner, 2D axisymmetric (quasi-3D) simulations are carried out using an OpenFOAM-based solver. The same modeling approach for transport and chemistry as for the V-Flame simulations is used. A fine mesh ($>100\,000$ cells) allows resolving the flame zone with more than 10 cells ($\Delta = 60\mu\text{m}$, see Fig. 3b). Fig. 3 compares the flame shape for the 20 vol-% H_2 mixture. On the left side, the time-averaged chemiluminescence obtained from the experiment is shown and the cone angle (as a measure of the laminar burning velocity) is marked. On the right side, the simulated gradient of the progress variable is depicted. Both the flame length and the cone angle agree for all H_2 mixtures considered.



Next, based on the Raman/Rayleigh measurements and the numerical results, the local flame structure can be analyzed in Fig. 4 showing the species profiles over progress variable (PV) for 0, 20 and 40 vol-% H_2 . Both experiment and simulation indicate an influence on the flame structure by addition of hydrogen. CH_4 and H_2 persist in higher concentrations when approaching the reaction zone. O_2 is consumed earlier in the laminar jet flame. In the upper row, the experimental data are compared to the full 2D simulation. Non-negligible differences are found for all species in the reaction zone while at maximum PV the same composition close to equilibrium is obtained. Similar differences are observed when comparing to 1D freely propagating flames. In particular, the differences between the simulations are smaller than the differences to the experimental data from either simulation. While it appears reasonable that this discrepancy is related to the negative stretch, it is not yet clear why the 2D simulation cannot recover the effect observed in the experiment. Ongoing simulation work to be presented on the poster along with the experimental data will include negative stretch effects in a 1D flame and an even further increased resolution of the 2D simulation in the flame zone.



[1] C. Law, C. Sung, *Progress in Energy and Combustion Science* **2000**, 26 (4-6), 459.

ns-CARS temperature measurements of flame quenching close to a wall

Krishna. S ^{a*}, Deanna Lacoste ^a, Jason Damazo ^b, Eddie Kwon ^b, William Roberts ^a

^a Clean Combustion Research Center, King Abdullah University of Science and Technology, Saudi Arabia

^b Boeing Research and Technology, USA

Close wall temperature measurements are essential in quenching studies. Conventional thermocouple measurements are restricted by the bead size and radiation from the flame. Similarly, Two line PLIF measurements are not suitable for close wall measurements due to reflections from the surface. Coherent Anti Stokes Raman Scattering (CARS) is a technique that has an advantage in such geometries due to the small probe volumes employed. Temperature measurements as close as 25 μm [1] and 100 μm [2] have been reported before. The wall stabilized flame configuration is similar to the one employed by Mann et al. [3]. The present CARS system employs three beams namely pump, probe and stokes beam focused at a point to obtain a coherent anti stokes signal which provides the temperature at the probe volume. A nanosecond Nd:YAG with second harmonic of 532 nm is used for the pump and the probe beam, while a modeless dye laser pumped by the Nd:YAG provides the stokes beam at ~ 607 nm. The signal is collected using a spectrometer-ICCD camera detection system and the obtained spectrum is fit against the theoretical CARS signal predicted using CARSFT [3]. The probe volume dimensions are ~ 800 μm in the direction of propagation of the beams and ~ 25 μm in the perpendicular directions. The non-resonant background is obtained from an argon environment. In this work we employ a standard premixed methane air flame close to stoichiometry in a Head-On Quenching (HOQ) configuration. A water cooled (isothermal) metal plate is placed above the conical flame and a steady flame is stabilized at a measured distance from the wall. This configuration offers a steady state temperature profile from the burner to the wall. By fixing the CARS probe volume and moving the burner and plate assembly, the temperature is measured at different locations along the axis of the burner and plotted. Time averaged temperature measurements over 500 single shots at 10 Hz are reported. Preliminary measurements as close as 200 μm to a surface have been carried out in an unconfined geometry and hence the technique offers precise measurements with high spatial resolution.

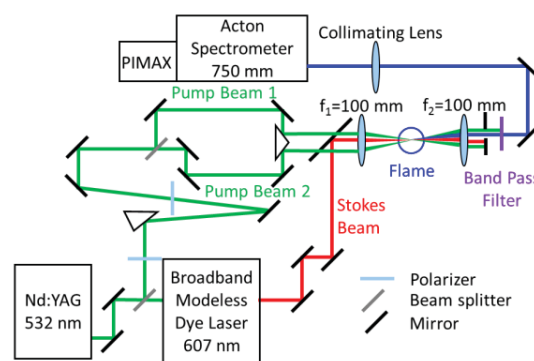


Figure 1. Schematic of Q-branch vibrational N_2 CARS system.

*Corresponding author: krishna.seshagiri@kaust.edu.sa

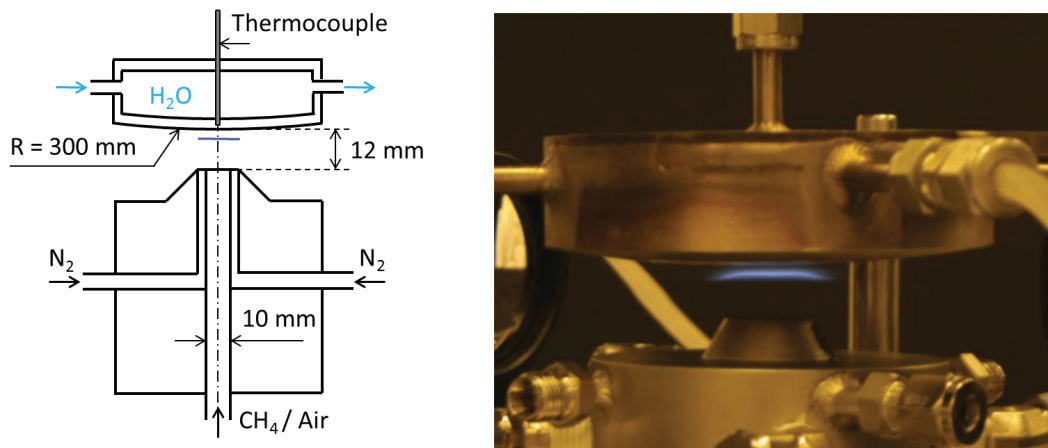


Figure 2. Schematic of burner wall assembly (left). Steady flame stabilized close to burner wall (right)

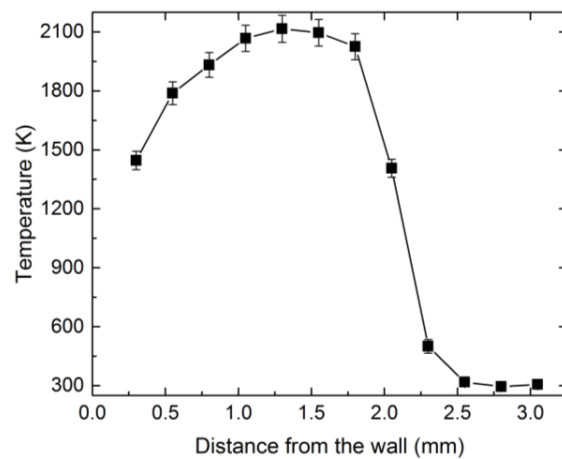


Figure 3. Axial temperature profile along centerline, the burner is located at 12 mm from the wall

References

- [1] R. Lucht, M. Maris, CARS Measurements of Temperature Profiles Near a Wall in an Internal Combustion Engine, SAE Technical Paper (1987) 870459, doi:10.4271/870459
- [2] M. Mann, C. Jainski, M. Euler, B. Böhm, A. Dreizler, Transient flame-wall interactions: Experimental analysis using spectroscopic temperature and CO concentration measurements, *Combust. Flame* 161 (2014) 2371–2386
- [3] R.E. Palmer, The CARSFT computer code for calculating coherent anti-stokes Raman spectra: user and programmer information, Sandia National Laboratories Report SAND89-8206, Livermore, CA (1989)

Simulation of Sandia Flames D, E and F with a Novel MMC Mixing Model

Achinta Varna^{a,*}, Matthew. J. Cleary^b, Evatt. R. Hawkes^a

^a*School of Mechanical and Manufacturing Engineering, University of New South Wales, Sydney, NSW 2052, Australia*

^b*School of Aerospace, Mechanical and Mechatronic Engineering, University of Sydney, Sydney, NSW 2006, Australia*

Abstract

PDF methods offer significant advantages in modeling of turbulent combustion including: chemical source terms appearing in closed form, applicability to multiple combustion modes (non-premixed, premixed, ignitions), ability to cope with both fast and slow timescale processes. Nonetheless, PDF methods still require improved mixing models. Simple models like IEM and Modified Curl do not possess the property of localness whereas EMST is too local and over-damps conditional fluctuations. Multiple mapping conditioning (MMC) is a local mixing model, but in its existing form for RANS it is difficult to comprehend, involves complex mapping functions and it is hard to determine model constants. A novel MMC mixing model has been proposed recently and has been tested under ideal and real flow conditions. In this model, the reference variable has statistics similar to that of mixture fraction and its evolution is governed by a Ornstein-Uhlenbeck process. This model is intuitive and the model constants are easy to determine. It can potentially accommodate more than one reference variable without any complications since it does not use complex mapping functions. It has all the basic characteristics of a mixing model but in addition has a tunable localness property. The model is robust and easy to implement in commercial software making it attractive to model practical combustion systems.

The two main mixing model equations are:

$$d\xi^* = -\frac{C_\xi}{\tau}(\xi^* - \bar{\xi})dt + b_o \sqrt{\frac{2C_\xi \langle \xi^2 \rangle}{\tau}} dW \quad , \text{ and} \quad (1)$$

$$d\phi_k^* = -(C_{min}/\tau)(\phi_k^* - \langle \phi_k^* | \xi^* \rangle)dt \quad , \text{ where } \xi \text{ is the reference variable, and } \phi_k \text{ is the composition state vector.} \quad (2)$$

Equation 2 can be reformulated as:

$$d\phi_k^* = -\frac{C_\xi b_o^2}{(1 - r_t^2)\tau}(\phi_k^* - \langle \phi_k^* | \xi^* \rangle)dt \quad , \text{ where } b_o, C_\xi \text{ and } r_t \text{ are model constants and } \tau \text{ is the turbulent time-scale.} \quad (3)$$

r_t is the target correlation coefficient between mixture fraction and the reference variable, which can control the localness of mixing model. Based on parametric studies, the *suggested* values are $C_\xi = 2$, $b_o = \sqrt{0.5}$, $r_t = 0.935$ ($\equiv C_{min} = 8$). $C_\xi = 2$ is due to DNS and experimental evidence that suggests the scalar mixing-to-turbulent timescale ratio is ≈ 2 and $b_o = \sqrt{0.5}$ is to ensure that the variance of reference variable and mixture fraction decay at equal rates. $r_t = 0.935$ ($\equiv C_{min} = 8$) is from [1] where it is also stated that C_{min} is case-dependent. Hence, r_t should be selected based on user experience.

In this poster, it has been shown that the novel mixing model, implemented in OpenFOAM, performs well in the context of Sandia non-premixed flames D, E and F. Figures 1 and 2 show that r_t can be effectively used to control the localness of mixing model thereby improving the predictions. Figures 3 and 4 highlight that the mixing model predictions, with $C_\xi = 2$, $b_o = \sqrt{0.5}$ and $r_t = 0.935$, are in good agreement with experiments for flames E and D respectively.

References

- [1] A. P. Wandel. Conditional dissipation of scalars in homogeneous turbulence: Closure for MMC modelling. *Combustion Theory and Modelling*, 17(4):707–748, 2013.

*Corresponding author

Email address: a.varna@unsw.edu.au (Achinta Varna)

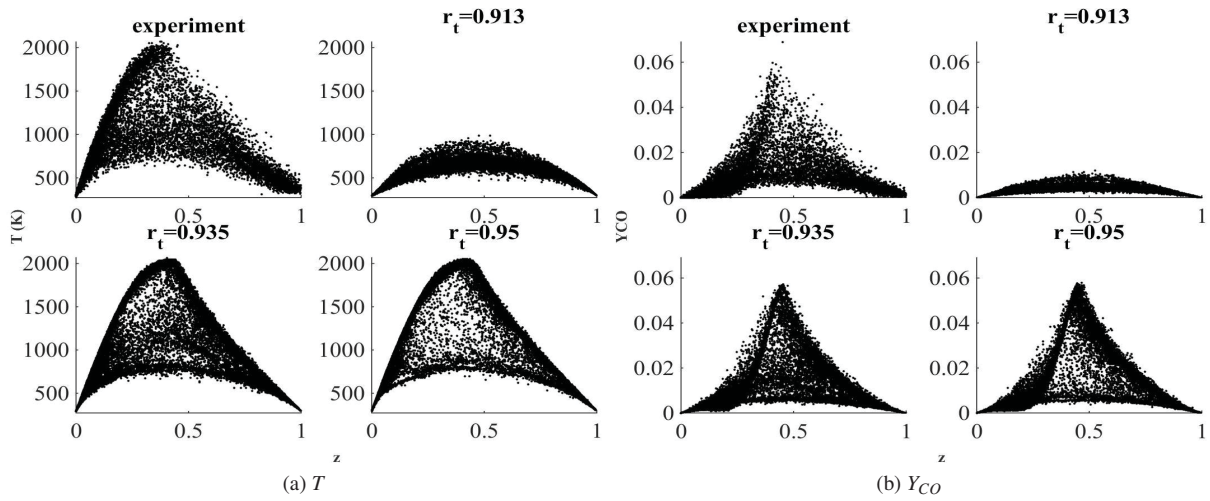


Figure 1: Flame F: Effect of r_t on scatter plot of T and Y_{CO} at $x/d=15$

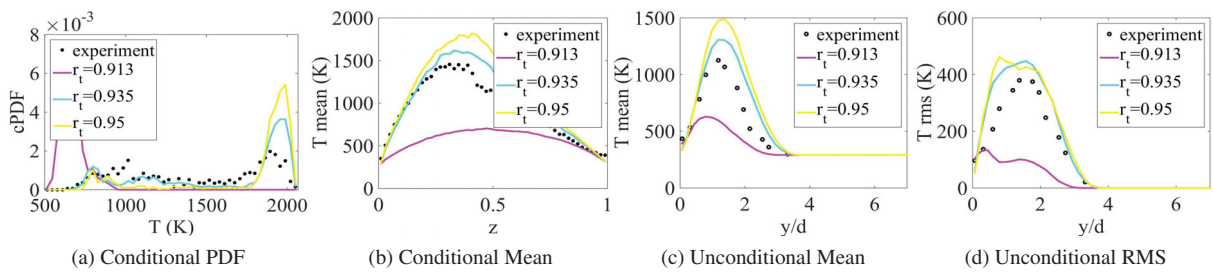


Figure 2: Flame F: Effect of r_t on conditional PDF, conditional mean, unconditional mean and RMS of T at $x/d=15$

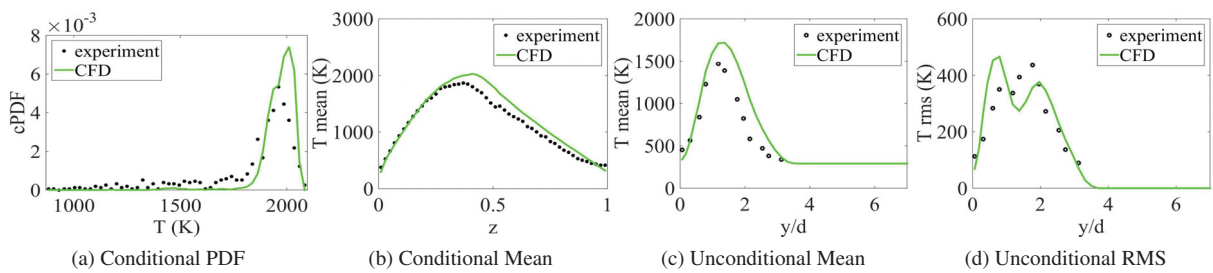


Figure 3: Flame E: Conditional PDF, conditional mean, unconditional mean and RMS of T at $x/d=15$

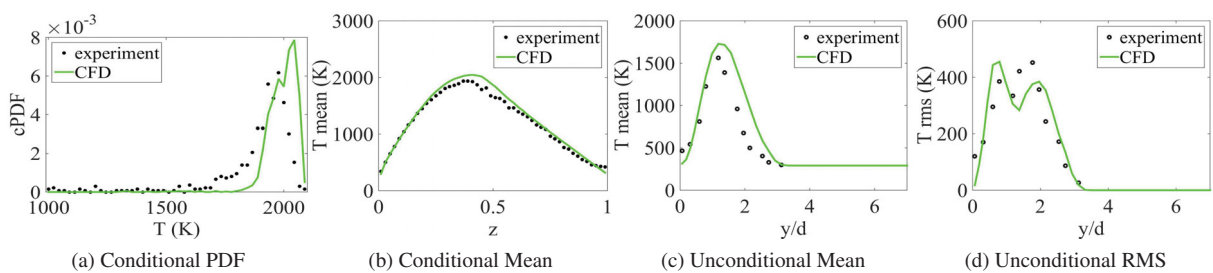


Figure 4: Flame D: Conditional PDF, conditional mean, unconditional mean and RMS of T at $x/d=15$

Use of Data Mining to Determine whether Spray Flames will Extinguish

Andrew P. Wandel

Computational Engineering and Science Research Centre, School of Mechanical and Electrical Engineering, University of Southern Queensland, Toowoomba, Qld, 4350, Australia

Direct Numerical Simulations (DNS) are performed for droplets which are evaporated and ignited using a spark [1]. The droplets of *n*-heptane are monodisperse and uniformly distributed through the middle of the domain whose initial gaseous phase is air at 500 K. The spark is modelled by a source term in the energy equation in the middle of the domain with a normal distribution in the radial direction. The droplet properties relax to the local gas-phase values and influence the gas phase through source terms in the transport equations.

Varying the turbulence, droplet number density (equivalence ratio) and droplet diameter produces different behaviours: successful burning, ignition followed by global extinction, or no ignition. This project seeks a mechanism to predict global extinction at the instant the spark is deactivated.

The data mining technique the Gaussian Mixture Model (GMM) [2,3] was used on each case separately to group data points from the DNS field. The variables analysed at each point in the field were the reaction progress variable c and its dissipation N_{cc} . GMM is a density-based method used to find clusters of arbitrary shape, where a cluster contains data points which have similar properties. Data points are assigned a probability of belonging to each cluster based on a joint-normal distribution for the distance from the centre of the cluster; the data points are assigned to the cluster with the highest probability. The cluster centre locations and variances are varied by iteration to maximize the total probability within the system.

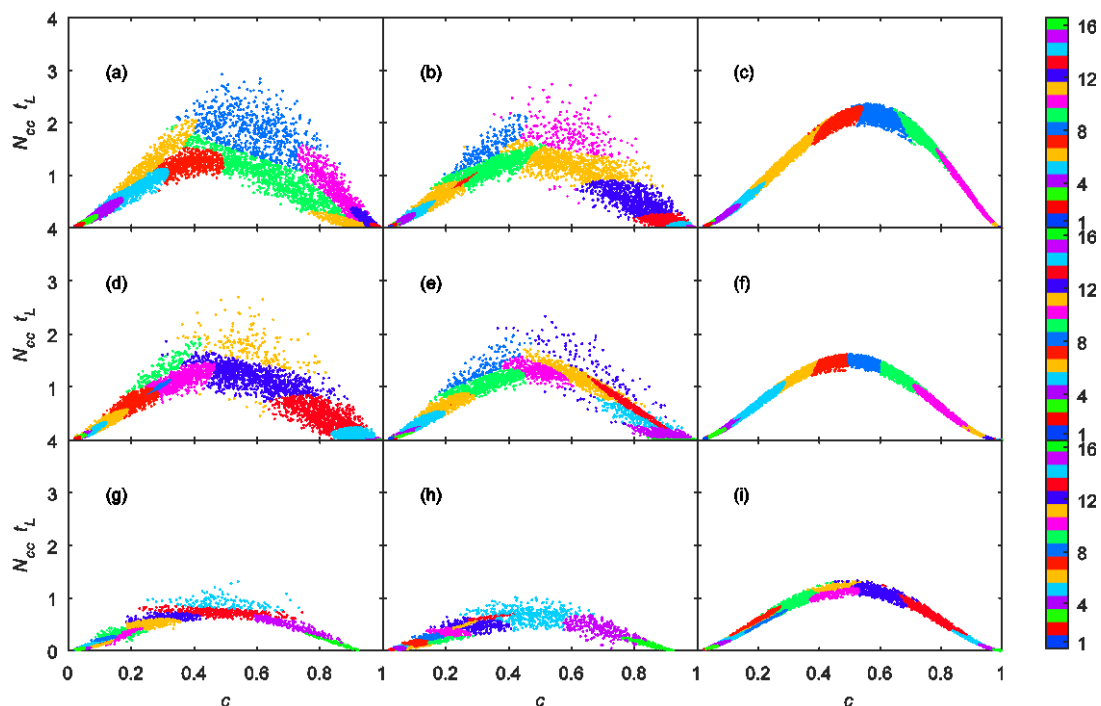


Figure 1: Cluster plots for c and N_{cc} (normalised by integral timescale) when the spark was deactivated. The colour for each cluster is shown on the right. The first two columns contain spray cases; the right column contains partially-premixed gaseous cases. Cases (a) and (c) burnt for the duration of the simulation; case (b) did not globally extinguish during the simulation, but extinction was imminent. The second row contains cases that ignited, then globally extinguished during the simulation. The third row contains cases that failed to ignite.

Figure 1 shows the analysis of the fields when the spark was deactivated, showing different behaviour in cases which successfully burn to those which globally extinguish after ignition. It is possible to distinguish between a “burning branch” and an “extinguishing branch” for the highest values of c in the cases which successfully burn (Figure 2). This split is explained physically by the extinguishing branch containing regions of space where local quenching occurred due to droplet

evaporation producing a flammable mixture ahead of the strong flame front. In cases with global extinction, the flame front was small and local quenching was part of the flame front, hence hindered the flame propagation (Figure 3).

The data mining method has enabled the prediction of future flame behaviour: based on this analysis, it is possible to prevent global extinction from commencing.

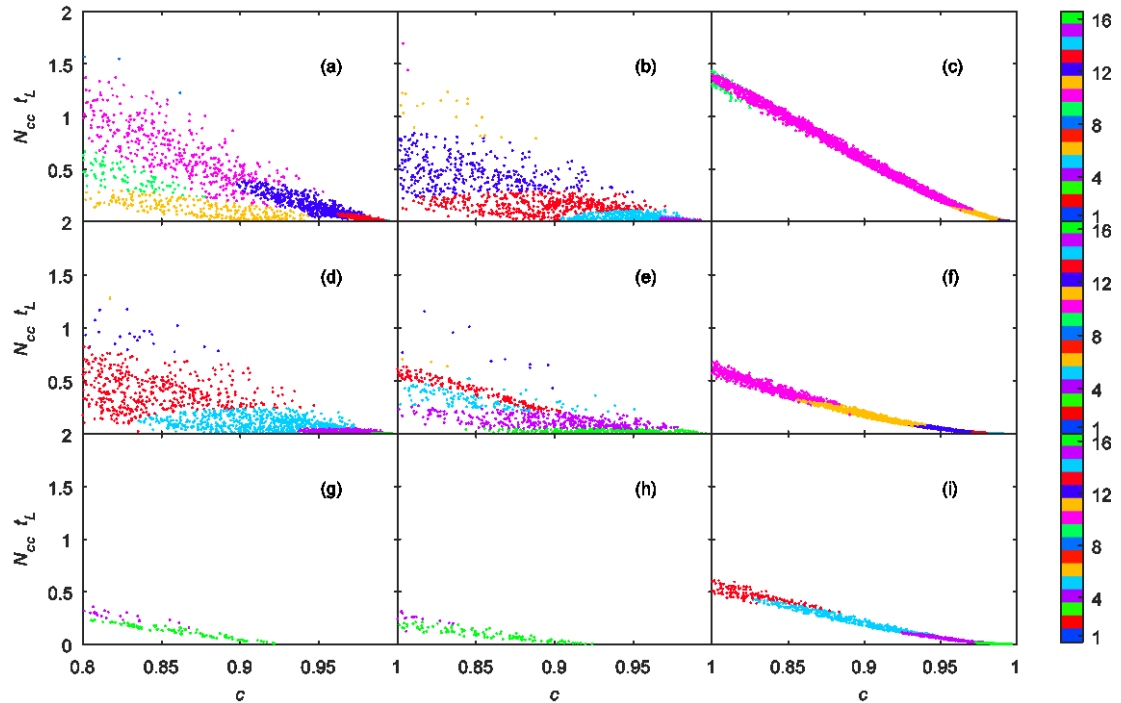


Figure 2: Figure 1 zoomed in on the bottom-right.

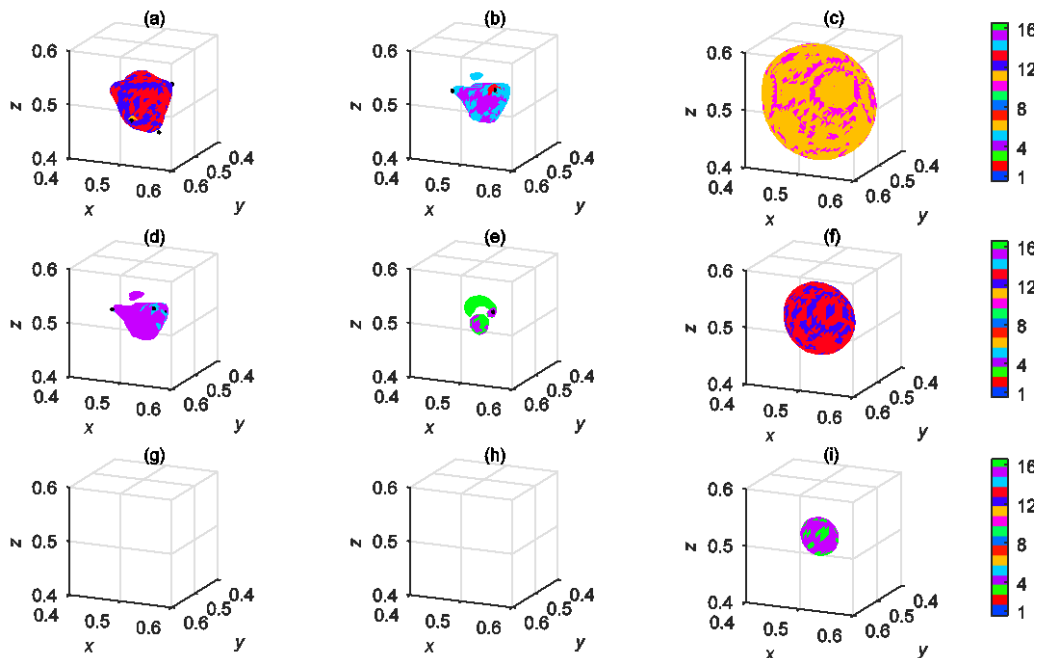


Figure 3: Isosurfaces of $c = 0.96$, coloured by cluster. Black dots represent droplets which are close to the isosurface.

References:

- [1] Wandel, AP, *Combust. Flame*, 161:2579, 2014.
- [2] Kantardzic, M, *Data Mining: Concepts, Models, Methods and Algorithms*, 2nd Ed., IEEE Press, 2011.
- [3] Reynolds, D, ‘Gaussian Mixture Models’, in: *Encyclopedia of Biometrics*, Springer, pp. 659–663, 2009.

Petascale direct numerical simulation of a high Ka laboratory premixed jet flame

Haiou Wang¹, Evatt R. Hawkes^{1,2}, Jacqueline H. Chen³

¹*School of Mechanical and Manufacturing Engineering, The University of New South Wales, NSW 2052 Australia*

²*School of Photovoltaic and Renewable Energy Engineering, The University of New South Wales, NSW 2052 Australia*

³*Sandia National Laboratories, Livermore, CA 94550, USA*

haiou.wang@unsw.edu.au.

Lean premixed combustion is usually employed in modern stationary energy gas turbines to achieve high thermal efficiencies and low NO_x emissions. However, these combustors are susceptible to operability issues including combustion instability, blowout and flashback. Also, due to enhanced turbulence and the flame being relatively weak, these devices operate at high Karlovitz numbers (Ka), where there are very strong interactions of turbulence and chemistry. In the petascale era of supercomputing, direct numerical simulations (DNS), which resolve all continuum scales of flows and chemistry, have emerged as a leading tool to examine these interactions, as some laboratory flames are now accessible.

In the present study, petascale DNS of a high Ka CH₄/air laboratory premixed flame was performed. A round jet burner employed in the experiment of Zhou et al. [1] is replicated in the DNS. The central jet operates at 1 atm and 300 K. The jet bulk velocity is $U_b = 110$ m/s and the equivalence ratio of the CH₄/air mixture is $\phi_j = 0.7$. The jet diameter is $D = 1.5$ mm and the jet Reynolds number, Re_j , based on U_b and D is 10510. A pilot flame of CH₄/air mixture at $\phi_c = 0.9$ was established surrounding the burner to provide a hot co-flow to assist with flame stabilisation. The temperature of the pilot flame is 1800 K and the velocity is 1.8 m/s. The Karlovitz number evaluated as $Ka = \tau_L/\tau_\eta$ is 253, where τ_L is the flame time scale and τ_η is the Kolmogorov time scale. The DNS is described in full in Wang et al. [2].

Figure 1a shows the volume rendering of OH radical in the entire computational domain. The instantaneous flame front is significantly wrinkled due the interactions of small-scale turbulence and the flame; the wrinkling scale of the flame surface increases downstream. Fig. 1b compares the radial profiles of the mean temperature at $x/D = 10, 24,$ and 30 . The mean temperature is predicted fairly well by the DNS at all locations. A minor discrepancy is found at $r/D = 1\sim 2$ and $x/D = 10$. In particular, the DNS slightly overestimates the mean temperature in this region, which is probably due to heat loss to the burner not being accounted for. Fig. 1c compares the radial profiles of the mean and RMS axial velocity at $x/D = 4$. Very good agreement was obtained between the DNS and the measurements for the mean axial velocity, confirming the validity of the DNS inlet velocity profile. Good agreement was also obtained for the RMS axial velocity, especially in the shear region where the RMS axial velocity peaks, whereas a minor discrepancy was found in the jet region.

Figure 2 shows instantaneous snapshots of species PLIF images of the experiment and species concentrations of the DNS. Note that the species PLIF image intensities may be interpreted qualitatively to be proportional to the species molar concentrations. While these are random realisations and not expected to agree one-to-one, it is obvious that the comparison between the DNS and experiment exhibits qualitatively similar flame structure characteristics.

Figure 3 shows the statistics of the progress variable gradient, $|\nabla c|$, which represents a reciprocal flame thickness, at the downstream location, $x/D = 20$. It is seen that $|\nabla c|$ of the DNS is considerably lower than that of the laminar flame, indicating that the flame structure is thickened in the DNS due to significant perturbations

of the flame structure resulting from small-scale turbulence in the high Ka flame. Flame thickening is most evident in highly curved and compressive tangential strain rate regions as shown in Figs. 3b and 3c.

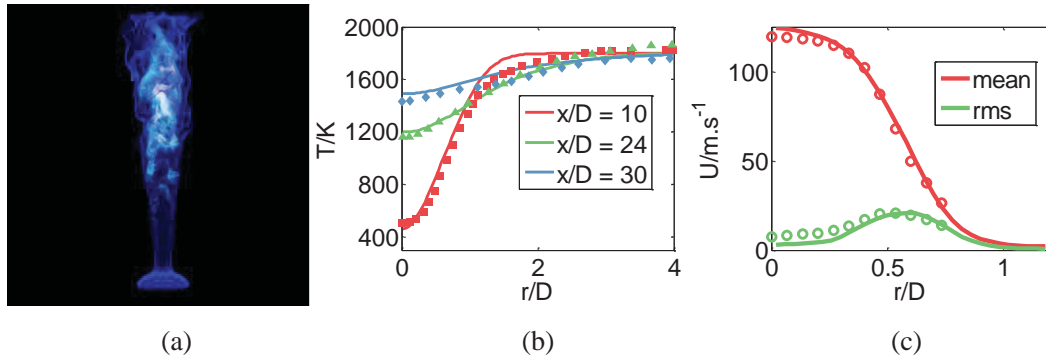


Figure 1. (a) Instantaneous volume rendering of OH radical distributions of the DNS. (b) Comparison of the mean temperature, and (c) comparison of the mean and RMS axial velocity.

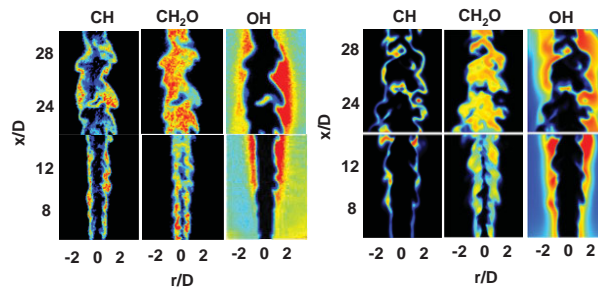


Figure 2. A typical instantaneous snapshot of (left) the simultaneous CH/CH₂O/OH experimental PLIF images and (right) the CH/CH₂O/OH molar concentration of the DNS.

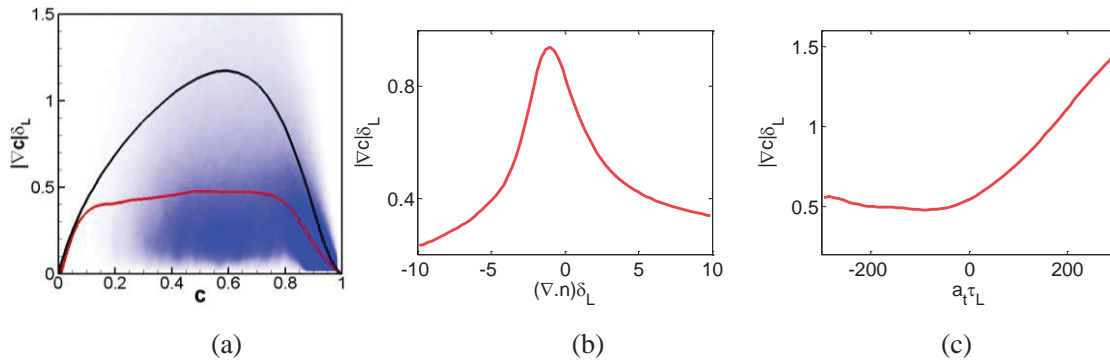


Figure 3. (a) Joint PDF of the progress variable, c , and the progress variable gradient, $|\nabla c|$, at $x/D = 20$. Black line: $|\nabla c|$ conditionally averaged on c of the unstrained laminar flame; red line: $|\nabla c|$ conditionally averaged on c of the DNS. (b) $|\nabla c|$ conditionally averaged on curvature at $x/D = 20$. (c) $|\nabla c|$ conditionally averaged on tangential strain rate at $x/D = 20$.

References:

- [1] B. Zhou, C. Brackmann, Q. Li, Z. Wang, P. Petersson, Z. Li, M. Aldén, X.S. Bai, *Combust. Flame* 162 (2015) 2937–2953.
- [2] H. Wang, E. R. Hawkes, J. H. Chen, B. Zhou, Z. Li, M. Aldén, *J. Fluid Mech.* (2016) under review.

Large Eddy Simulations of the Darmstadt Turbulent Stratified Flames with REDIM Reduced Kinetics

Ping Wang^{1,*} Cai-jun Wang² Gerd Steinhilber³ Zhi-xia He¹ Ulrich Maas³

¹Institute for Energy Research, Jiangsu University, China

²School of Energy and Power Engineering, Jiangsu University, China

³Institut für Technische Thermodynamik, Karlsruher Institut für Technologie, Germany

* pingwang@ujs.edu.cn

In stratified combustion local equivalence ratio varies significantly, which is different to idealized premixed or diffusion flames. To date, some fundamental issues are still not fully understood [1].

LES of the well-documented Darmstadt turbulent stratified flames (TSF) [2,3] are conducted to investigate the characteristics of TSF. In total, one isothermal flow case A-i2 and four reacting cases with different combinations of stratification and shear, i.e. A-r, C-r, E-r, G-r cases, are simulated. The burner consists of three concentric tubes surrounded by an air co-flow, and is sketched in Fig. 1. The inner diameters of the 3 tubes are 14.8 mm, 37 mm and 60 mm, respectively. The central tube acts as the pilot and a flame holder ring is constructed inside it.

The chemical kinetics is accounted for with a two-dimensional chemistry look-up table generated by the novel REDIM technology [4], which is generated under physical consideration for the structure of TSF. In the table, the mass fractions of CO₂ and N₂ are used as the reduced coordinates. Figure 2 shows the tabulated production rate of CO₂ as a function of CO₂ and N₂ mass fractions. The table is then combined together with the presumed filtered density function (PFDF) to model the turbulent combustion. The assumption of statistical independence of N₂ and CO₂ is employed in this work, and the PDF shapes of N₂ and CO₂ are both presumed to be of Clipped Gaussian shape. More detailed numerical methods can be found in [5].

Figures 3 and 4 show the instantaneous and time averaged streamwise velocity profiles, respectively. Snapshots of the instantaneous flame fronts, denoted by production rate of CO₂, are shown in Fig. 5 for the four reacting cases, in which the isolines of equivalence ratio are displayed as well. For the reacting case A-r, the radial profiles of H₂O mass fraction are shown in Fig. 6. The overall good agreement of the statistics of velocity, temperature and species with the experimental data demonstrates the capability of the LES/ REDIM-PFDF model to deal with TSF.

An important quantity about TSF is the alignment of mixing layer and reaction layer. The probability distribution of the alignment angle between the two gradient vectors of temperature and equivalence ratio is analyzed. Figure 7 shows the time averaged probability distribution for the four reacting cases. It is found that back-supported stratification is more likely occurring in case A-r, while for other 3 cases orthogonal alignment or normal local flame propagation is of higher probability.

[1] A.R. Masri, Proc. Combust. Inst. 35 (2015) 1115-1136.

[2] F. Seffrin, F. Fuest, D. Geyer, A. Dreizler, Combust. Flame 157 (2010) 384-396.

[3] G. Kuenne, F. Seffrin, F. Fuest, T. Stahler, et al., Combust. Flame 159 (2012) 2669-2689.

[4] G. Steinhilber, U. Maas, Proc. Combust. Inst. 34 (2013) 217-224.

[5] P. Wang, F. Zieker, R. Schießl, J. Fröhlich, U. Maas, Proc. Combust. Inst. 34 (2013) 1269-1280.

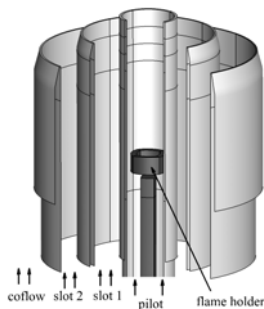


Fig. 1. Sketch of the stratified flame burner.

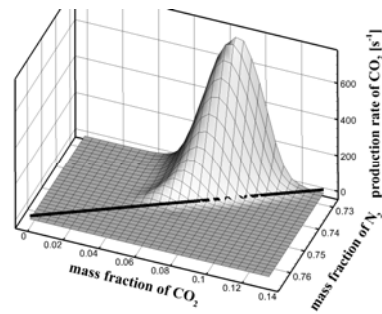


Fig. 2. Production rate of CO₂ as a function of mass fractions of CO₂ and N₂, given in REDIM table.

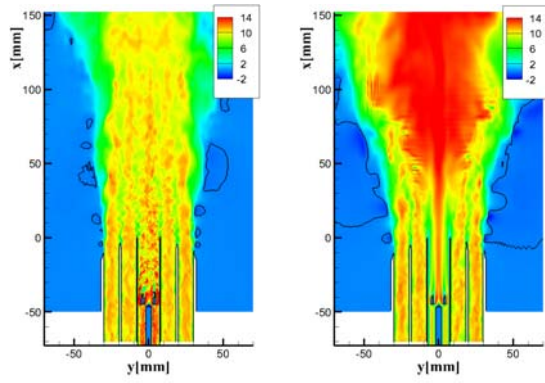


Fig. 3. Instantaneous streamwise velocity of LES for case A-i2 (left) and case A-r (right). Solid curves show the zero isolines of streamwise velocity.

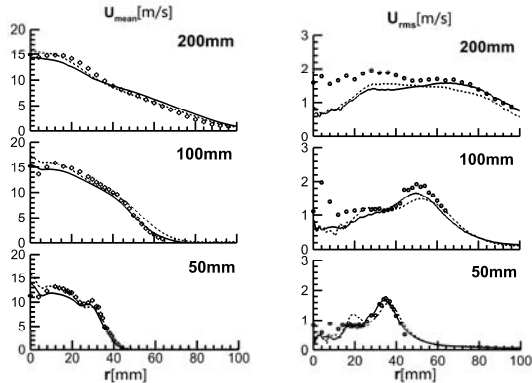


Fig. 4. Mean and rms fluctuation of streamwise velocity for case A-r. 'o': experimental data; —: results on fine grid; - -: results on coarse grid.

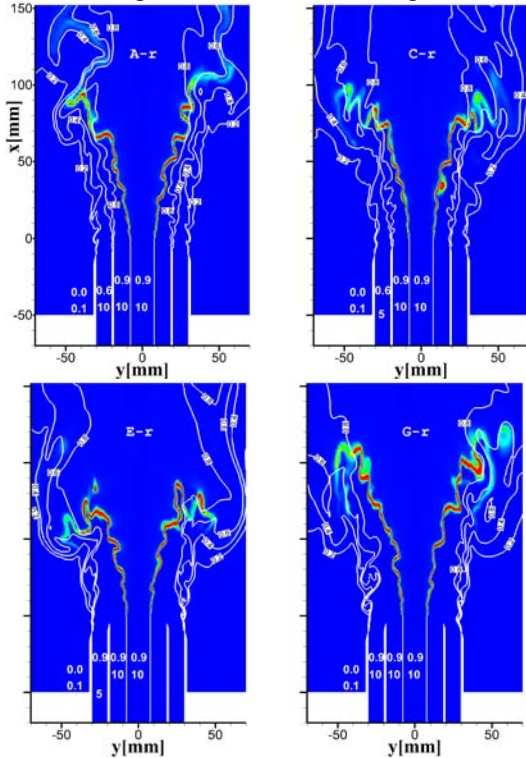


Fig. 5. Snapshots of the instantaneous contour of CO_2 production rate, with solid curves showing isolines of equivalence ratio. The numbers in the 3 inflow pipes and co-flow show the equivalence ratios (upper ones) and bulk flow speeds (lower ones).

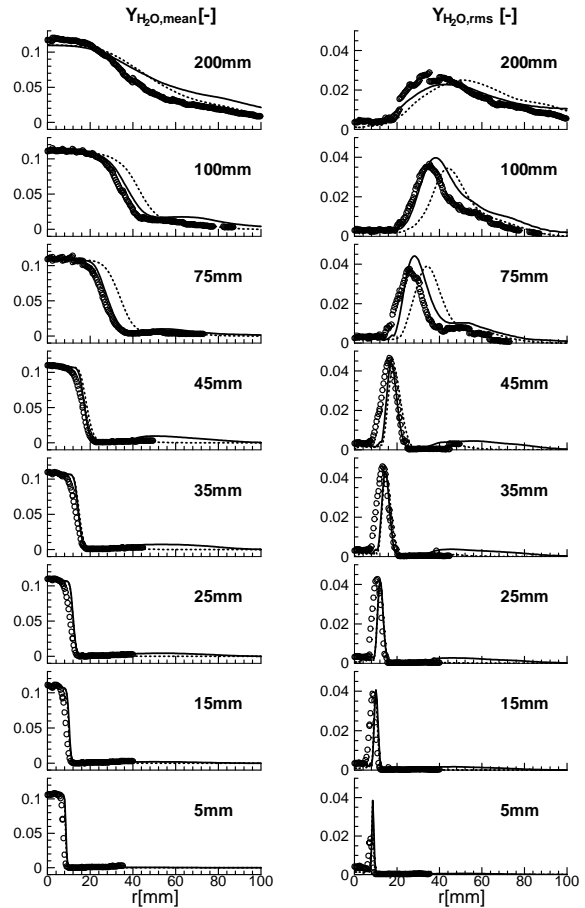


Fig. 6. Mean and rms fluctuation of H_2O mass fraction for case A-r. 'o': experimental data; —: results on fine grid; - -: results on coarse grid.

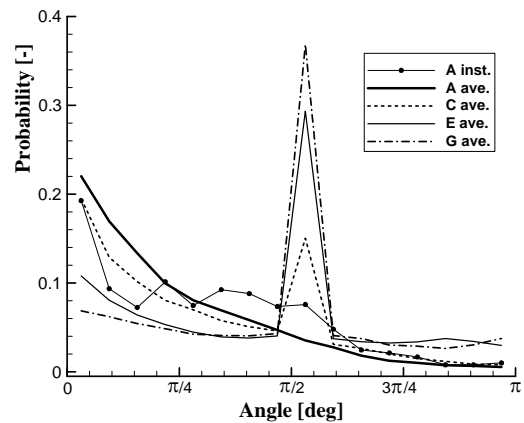


Fig. 7. Probability distribution of the alignment angle between the two gradient vectors of the temperature and the equivalence ratio. 'ave.': time averaged value, 'inst.': instantaneous value.

Compliance of flamelet models for turbulent reacting flow simulations with applications to Sydney piloted flames with inhomogeneous inlets

Hao Wu*, Matthias Ihme

Department of Mechanical Engineering,

Stanford University, Stanford, CA 94305, USA

* Corresponding author. Email: wuhao@stanford.edu

Abstract

In the application of the combustion models based on low-dimensional manifolds (for instance flamelet models) to large-eddy simulation (LES) of reactive turbulent flows, the modeling simplifications of the combustion process is a critical source of uncertainty. Therefore, the ability to quantitatively assess this uncertainty in absence of the reference result is vital to the reliable and predictive simulations of such kind. An extension of the so-called manifold drift term, D_ϕ^m , to LES is proposed to make such assessment by examining the compliance of a particular combustion model in describing a quantity of interest, ϕ , with respect to the underlying flow field representation.

The behavior of this drift term is examined in a series of test cases. LES of the Sydney partially-premixed turbulent pilot flame with inhomogeneous inlet streams is performed [1]. Both the non-premixed flamelet/progress-variable (FPV) model and the premixed filtered tabulated chemistry LES (F-TACLES) formulation are employed on the case denoted as **FJ-5GP-Lr75-57**. The drift term is shown to be capable of identifying chemically sensitive region with respect to quantities of interest (QoI). A species-specific combustion regime indicator is derived by computing the relative magnitude of the drift terms for different combustion models. The drift term was originally formulated as a key component of the Pareto-efficient combustion (PEC) framework [2], in which adaptive combustion model selection is made during the progress of the simulation and this study also serves to prepare PEC for turbulent combustion simulations.

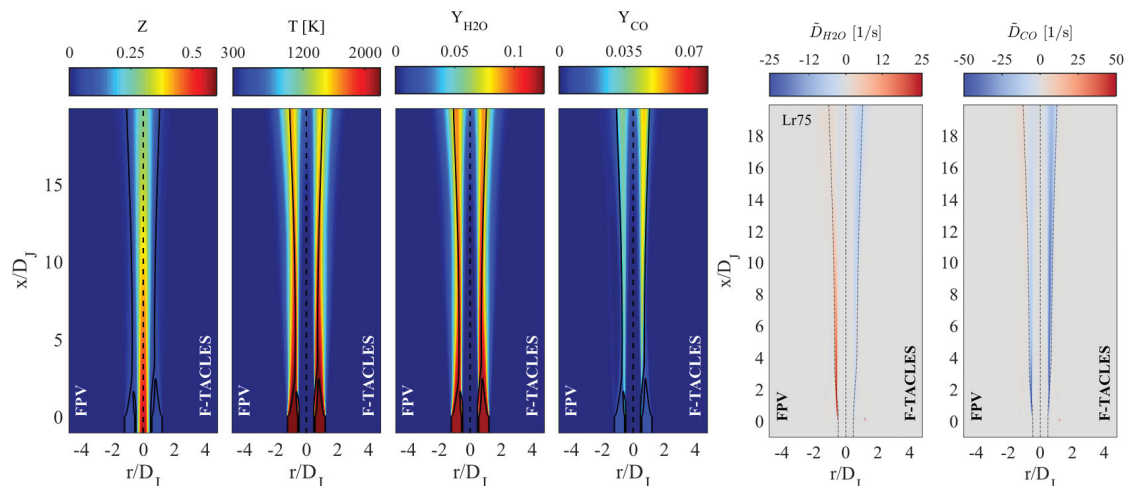


Figure 1. Favre-averaged quantities obtained from the FPV (left) and F-TACLES (right) models.

Figure 2. Drift terms for Favre-averaged for mass fraction of H₂O and CO using FPV and F-TACLES models.

Comparison of Favre-averaged mixture fraction, temperature, and mass fractions of H₂O and CO obtained from the FPV and F-TACLES models are shown in Fig. 1. Despite the drastically different modeling assumptions, good agreement is found between the FPV and F-TACLES results except the mass fractions of CO. This observation is also supported by the Favre-averaged LES drift terms evaluated for FPV and F-TACLES models are shown in Fig. 2. In general, the drift term is highly localized and is only present in the narrow region of high reactivity. The drift of CO is much larger than the corresponding values of H₂O. Furthermore, the drift for CO of the F-TACLES model is consistently negative, which suggests that the mass fraction of CO is highly likely to be over-predicted by this model.

Comparison with the measurements of the conditional Reynolds-averaged H₂O and CO mass fractions are shown in Fig. 3. In general, the mass-fractions of H₂O are predicted more

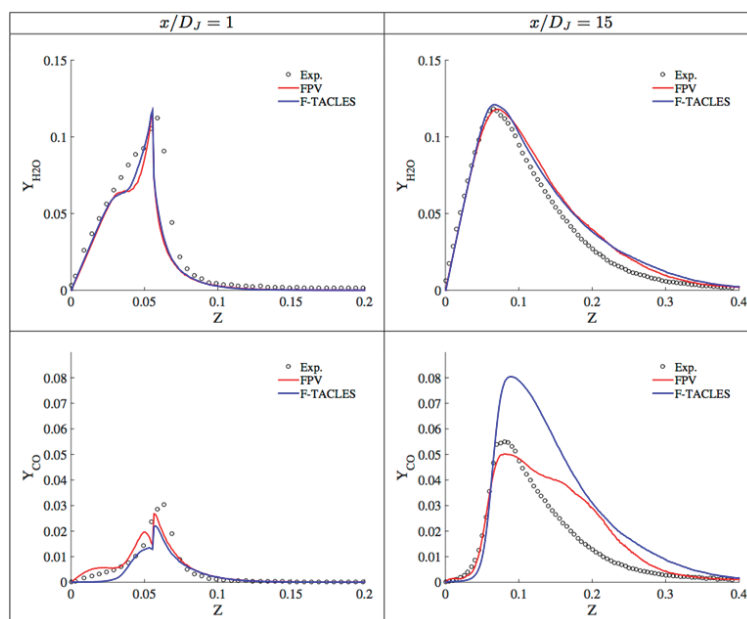


Figure 3. Conditional profile of H₂O and CO by the FPV and F-TACLES models at $x/DJ = 1$ and $x/DJ = 15$. The solid lines represent conditional Reynolds-averaged mass fractions. The results of the FPV model are in red and those of the F-TACLES model are shown in blue. The experimental results are shown as black circles.

accurately than CO, which agrees with observation made from the corresponding drift terms. Moreover, the trend of discrepancy between the modeled Y_{CO} and experimental results is also correctly indicated by the drift terms, that the F-TACLES model tends to over-predict Y_{CO} more significantly on the rich side than the FPV model and the FPV model tends to slightly under-predict Y_{CO} near the stoichiometry.

References:

- [1] S. Meares and A. R. Masri. A modified piloted burner for stabilizing turbulent flames of inhomogeneous mixtures. *Combust. Flame*, 161(2) : 484–495, 2014.
- [2] H. Wu, Y. C. See, Q. Wang, and M. Ihme. A Pareto-efficient combustion framework with submodel assignment for predicting complex flame configurations. *Combust. Flame*, 162(11) : 4208–4230, 2015.

Effects of molecular transport in LES/PDF of piloted turbulent DME/air jet flames

Jiaping You¹, Yue Yang¹, and Stephen B. Pope²

1 State Key Laboratory of Turbulence and Complex Systems, College of Engineering, Peking University, Beijing 100871, China

2 Sibley School of Mechanical and Aerospace Engineering, Cornell University, Ithaca, NY 14853, USA

yyg@pku.edu.cn

The DME flame series, including piloted partially-premixed flames at different Reynolds numbers, is developed from the canonical Sydney/Sandia piloted jet flame series. The experimental studies carried out by Coriton *et al.* [1] and Fuest *et al.* [2] provide a well-documented set of velocity fields and multi-scalar data, which serves as a testbed for developing accurate, tractable, and predictive models for turbulent combustion. In this study, two target flames DME-D and DME-F with different levels of local extinction are selected. The flame parameters are summarized in Table 1, and more details about this flame series are available in [2].

Table 1: Bulk velocities and Reynolds numbers of the DME-D and DME-F flames [2].

	U_j [m/s]	U_{pilot} [m/s]	U_{coflow} [m/s]	$Re=U_j D/\nu$
DME-D	45.9	1.1	0.9	29300
DME-F	91.8	2.1	0.9	58600

In the PDF modeling, the closure of the conditional molecular diffusion term, including molecular mixing and transport, in the PDF evolution equation is a major challenge. The effect of molecular transport is often neglected in existing Reynolds averaged Navier-Stokes simulation (RANS)/PDF calculations, because the magnitude of molecular transport is presumed much smaller than that of turbulent transport in high-Reynolds-number flows. Nevertheless, in the LES context, the molecular transport may dominate over the turbulent transport in the regions of high temperature or low turbulent intensity.

In this study, LES/PDF modeling of piloted turbulent dimethyl ether (DME)/air jet flames with a 39-species skeletal chemical mechanism [3] is reported. The PDF transport equation with three different implementations of molecular transport in the interaction-by-exchange with the mean (IEM) mixing model is solved by the NGA/HPDF code to assess their *a posteriori* performance. The three implementations considered are the classical random-walk model (IEM-RW), the mean-drift model with a single molecular diffusivity (IEM-MD), and the mean-drift model with differential diffusion (IEM-DD) [4]. Better quantitative agreement for the mean and root-mean-square profiles of mixture fraction, temperature and major species mole fractions and conditional means on mixture fraction with experimental results are obtained from the IEM-MD model than those from the IEM-RW model.

Snapshots of the instantaneous contours of temperature and mole fraction of OH for two flames are shown in Fig. 1. Flame DME-D shows continuous sheet-like structures without notable local extinctions, whereas DME-F exhibits extinction pockets and re-ignite further downstream. For quantitative comparisons, conditional mean profiles and instantaneous sample points of temperature from LES/PDF against the mixture fraction at $x/D=20$ are plotted in Fig. 2.

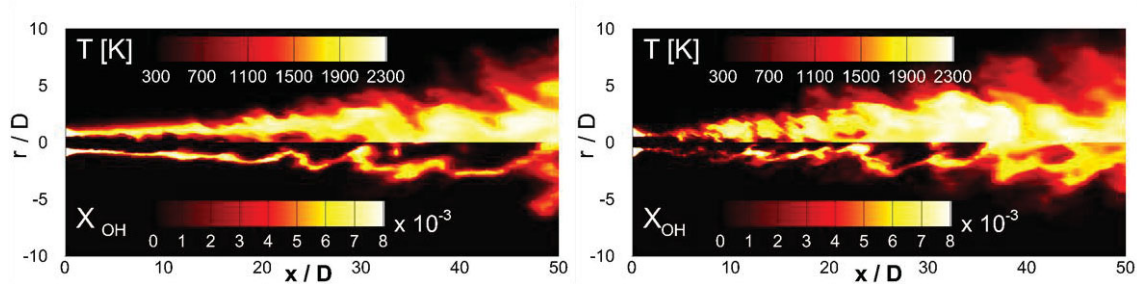


Fig. 1 Snapshots of the contour of T (upper half) and X_{OH} (lower half) on the x - r plane cut from LES/PDF of DME-D (left) and DME-F (right) flames with the IEM-MD model.

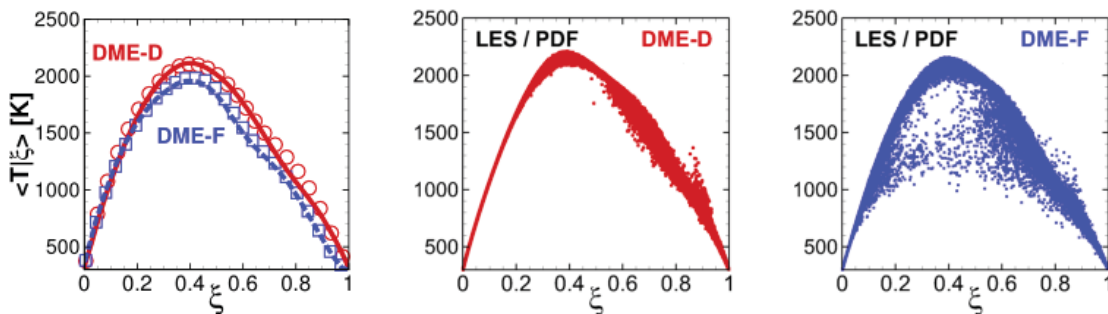


Fig. 2 Mean profiles of T (left) (symbols: experiment, lines: LES/PDF) and scatters of particle temperature conditioned on ξ -space from LES/PDF with IEM-MD for DME-D (middle) and DME-F (right) flames at $x/D=20$.

In the DME flame series, the molecular diffusivity dominates the turbulent diffusivity in the centerline region, so the accurate modeling of molecular transport plays a significant role in LES/PDF of these jet flames. Nevertheless, the IEM-DD model shows only minor effects on the model predictions compared to IEM-MD in these DME flames.

References

- [1] B. Coriton, M. Zendejdel, S. Ukai, A. Kronenburg, O. T. Stein, S. K. Im, M. Gamba, J. H. Frank, Proc. Combust. Inst. 35 (2015) 1251–1258.
- [2] F. Fuest, G. Magnotti, R. S. Barlow, J. A. Sutton, Proc. Combust. Inst. 35 (2015) 1235–1242.
- [3] Z. Luo, T. Lu, J. Liu, Combust. Flame 158 (2011) 1245–1254.
- [4] S. Viswanathan, H. Wang, S. B. Pope, J. Comput. Phys. 230 (2011) 6916–6957.

Sensitivity and Lagrangian Analysis for RANS-PDF Simulations of Turbulent Premixed Jet Flames

Hua Zhou ^a, Shan Li ^a, Zhu Yin Ren ^{a*}

^aCenter for Combustion Energy, Tsinghua University, China

*Corresponding Author Email: zhu yin ren@tsinghua.edu.cn

Turbulent lean premixed combustion has become a trend in modern combustion devices driven by ever increasingly stringent regulations on emissions. It is essential though challenging for computational models to capture complex turbulence–chemistry interactions at lean and highly turbulent conditions. The piloted premixed jet burner (PPJB) has been designed to study the lean premixed combustion under highly turbulent conditions. In this work, two PPJB flames with central jet velocity of 50 m/s and 200 m/s, i.e. PM1-50 and PM1-200, are simulated using a hybrid RANS-PDF method. The performance of two micromixing models (IEM and EMST) is investigated by analyzing the Eulerian statistics and by examining the evolution of particle composition from a Lagrangian perspective at first. Then the rate-limiting physio-chemical processes in the two simulated flames are revealed via particle-level sensitivity analysis.

Fig. 1 shows the predicted radial profiles of progress variable (C) for PM1-50 using IEM and EMST. As shown, there are good agreements between numerical prediction and experimental data, and the differences between the two mixing models are small. Lagrangian particle tracking is carried out to further investigate the performance of these two models. The compositions of a computational particle evolve according to $d\phi_i^{(n)}/dt = S_i(\phi^{(n)}) + C_\phi M^{(n)}(\{\phi_i\})$, where the terms on the right represent the contributions of reaction and micromixing. Computational particles from the central jet stream are tracked and the evolution of their particle compositions due to micromixing and chemical reaction is recorded [1]. Fig. 2 shows the contributions of reaction and mixing conditionally averaged on C for PM1-50. It is observed that when C is less than 0.5 the contribution of micromixing dominates over that of chemical reaction since chemical reaction is negligible at low temperatures. When C exceeds 0.7, the budgets of mixing and reaction from IEM and EMST are very different even though the Eulerian statistics in Fig. 1 are almost identical. For IEM, the contribution of micromixing is much smaller than that of reaction, which indicates an autoignition process for the preheated mixtures. While for EMST, a balance between micromixing and reaction is observed, which indicates flame-propagation process. This has been further confirmed in Fig. 2, which compares this observed balance with the reaction-diffusion balance from a one-dimensional laminar premixed opposed jet flame with the streams being configured with the compositions of the central jet and pilot streams in PPJB flames, respectively. These findings suggest that even though the Eulerian statistics produced by IEM and EMST model are very similar, these two models actually indicate different combustion processes, and EMST better captures the premixed combustion compared to IEM, which can be attributed to the localness feature of EMST. Similar observations are made for PM1-200 flame (not shown).

To reveal the rate-limiting processes in PM1-50 and PM1-200 flames, particle-level sensitivity analysis [2] is applied to investigate the local sensitivities of the progress variable to micromixing and reaction. The sensitivity to micromixing is represented by that to the model constant C_ϕ . To quantify the sensitivity to chemical reaction, an attenuation factor R for the overall reaction rate is introduced, so that the sensitivity to reaction is represented by that to R . The relative significance of chemical reaction and mixing is quantified by the magnitudes of sensitivities to R and C_ϕ . Fig. 3 shows the radial profiles of sensitivities at different axial positions. It can be observed that for PM1-50 flame, the sensitivities of progress variable to C_ϕ and to R are both positive, indicating that the combustion progress can be promoted by either enhancing mixing or enhancing reaction. For PM1-200 flame, in the upstream, the sensitivities of progress variable to R is positive, while sensitivities to C_ϕ is negative indicating that combustion progress may be suppressed by enhanced mixing near blow-off limit. This is consistent with previous findings from the parametric study that increasing C_ϕ alleviates the overprediction of reaction progress in PM1-200 flame [3].

By comparing the magnitude of sensitivities to C_ϕ and to R , it is found that the rate-limiting process in PM1-50 flame is mixing, while the rate-limiting process in PM1-200 flame is chemical reaction.

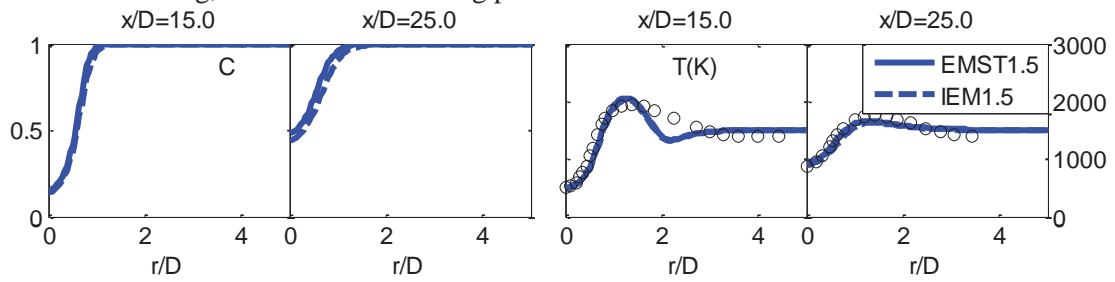


Fig. 1 Radial profiles of mean progress variable and temperature at $x/D=15$ and 25 in PM1-50 flame. Solid blue: EMST model; Dashed blue: IEM model; Circles: Experiment

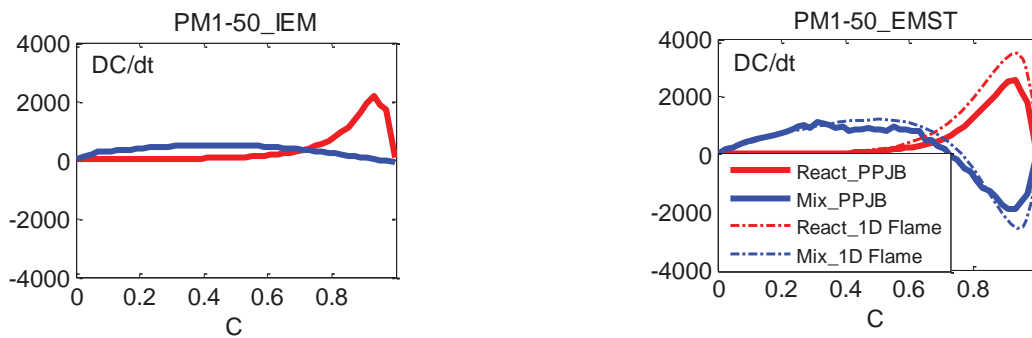


Fig. 2 Reaction–mixing budgets analysis for the composition evolution of PDF particles from the central jet stream. The results are conditionally averaged on progress variable. PM1-50 with IEM (left) and PM1-50 with EMST (right). Solid red: reaction; Solid blue: mixing. The dot dashed red and dot dashed blue lines represent reaction and molecular diffusion from a 1-D laminar premixed opposed jet flame

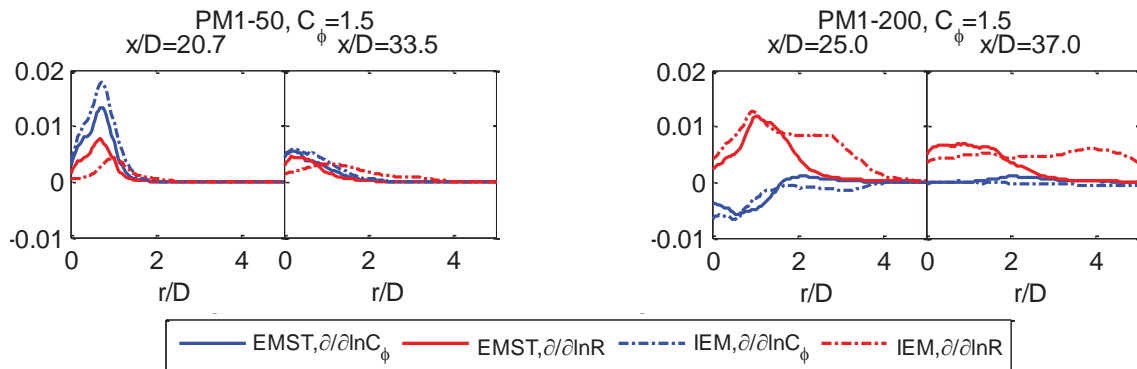


Fig. 3 Radial profiles of sensitivity coefficients, PM1-50 (left) and PM1-200 (right). Solid blue: sensitivity to C_ϕ from EMST; Solid red: sensitivity to R from EMST; Dot dashed blue: sensitivity to C_ϕ from IEM; Dot dashed red: sensitivity to R from IEM.

- [1] Wang, H. and S.B. Pope, *Combust. Theor. Model.*, 12 (2008) 857-882.
- [2] Ren, Z. and S.B. Pope, *P. Combust. Inst.*, 32 (2009) 1629-1637.
- [3] Rowinski, D.H. and S.B. Pope, *Combust. Theor. Model.*, 17 (2013) 610-656.

Acknowledgements

The work is supported by National Natural Science Foundation of China (51476087 and 91441202). The authors would like to thank Dr. David Rowinski and Professor Stephen Pope for helpful discussions.